2011
Office of Fossil Energy
Fuel Cell Program Annual Report

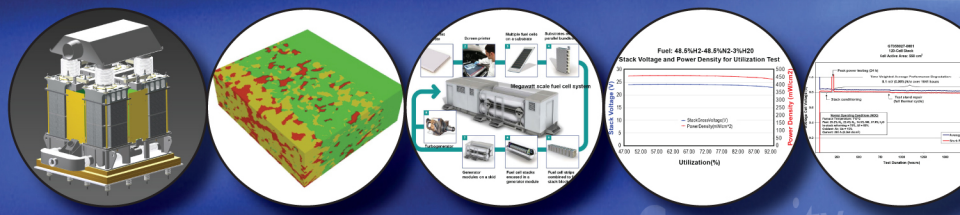

Increase Energy Security
Eliminate Carbon Footprint
Enhance Water Conservation

SECA
Solid State Energy Conversion Alliance

U.S. DEPARTMENT OF ENERGY

NETL

DOE/NETL-2012-1525

2011
OFFICE OF FOSSIL ENERGY
FUEL CELL PROGRAM ANNUAL REPORT

October 2011

Table of Contents

I. INTRODUCTION

I. Introduction

Competitive Innovation: Accelerating Technology Development

In 1999, The U.S. Department of Energy (DOE) Office of Fossil Energy, through the National Energy Technology Laboratory (NETL), founded the Solid State Energy Conversion Alliance (SECA) to develop low-cost, environmentally friendly solid oxide fuel cell (SOFC) technology.

The SECA fuel cell program is a critical element of the Office of Fossil Energy's technology portfolio. From an energy security perspective, coal is a primary resource for reducing dependence on imported oil and natural gas. More than half of the nation's electricity supply is generated from coal – developing technology to ensure environmentally clean and climate-friendly use of coal is of crucial national importance. The unique attributes of SOFC technology address environmental, climate change, and water concerns associated with fossil fuel and particularly coal use, establishing a foundation for a secure energy future in the United States.

Why SOFC Technology?

Like most fuel cell technologies, SOFCs are scalable, efficient (not heat engines and therefore not subject to Carnot cycle limitations), and produce low emissions (e.g., oxides of nitrogen [NO_x] <0.5 ppm) compared to combustion-based electrical power generation technologies (due to lower operating temperatures). However, there are a number of additional reasons why SOFCs were specifically chosen for focused development within SECA. First, relative to other fuel cell types, SOFCs are inherently fuel-flexible – they can reform methane internally, use carbon monoxide as a fuel, and tolerate some degree of common fossil fuel impurities such as hydrogen sulfide. Second, experimental data and analyses suggested that advanced SOFCs had an economically competitive cost entitlement relative to established commercial technologies and other fuel cell types. Planar SOFCs using a thin ceramic (yttria-stabilized zirconia, or YSZ) electrolyte could operate at lower temperatures (<800°C) than other SOFC topologies, thus allowing the use of lower-cost stainless steel interconnects, rather than the costly and difficult-to-process chromite interconnects required of higher-temperature SOFCs. Furthermore, the short conduction path (from the anode of one cell to the cathode of the next) results in lower (ohmic) losses and therefore higher stack efficiency and lower cost. Significantly, SOFCs are intrinsically well suited for carbon capture in that the fuel and oxidant (air) streams are easily kept separate, thereby facilitating high levels of carbon capture without substantial additional cost.

NETL, the SECA Industry Teams, and other organizations have conducted numerous system analyses for various integrated gasification fuel cell (IGFC) system configurations, with the most recent by NETL's Office of Program Planning and Analysis (OPPA) published in 2011. This work projects that SECA fuel cell technology can achieve 45% to 50% efficiency (based on higher heating value [HHV] of coal, including 99%+ CO_2 capture) with near-conventional (enhanced ConocoPhillips) gasifiers. With advanced catalytic gasification, efficiency potential is 60% HHV, with 97%+ CO_2 capture. These are near-zero emissions plants with significantly reduced water consumption relative to competing technologies due to the ability to capture and reuse the water produced within the fuel cell. The cost of electricity (COE) is competitive with or superior to (depending upon the CO_2 price) other advanced technologies under consideration (supercritical pulverized coal [SCPC], integrated gasification combined cycle [IGCC]), that include carbon capture and sequestration [CCS]. Natural gas fuel cell (NGFC) systems utilizing SECA technology are also attractive alternatives to the natural gas combined cycle (NGCC) with CCS.

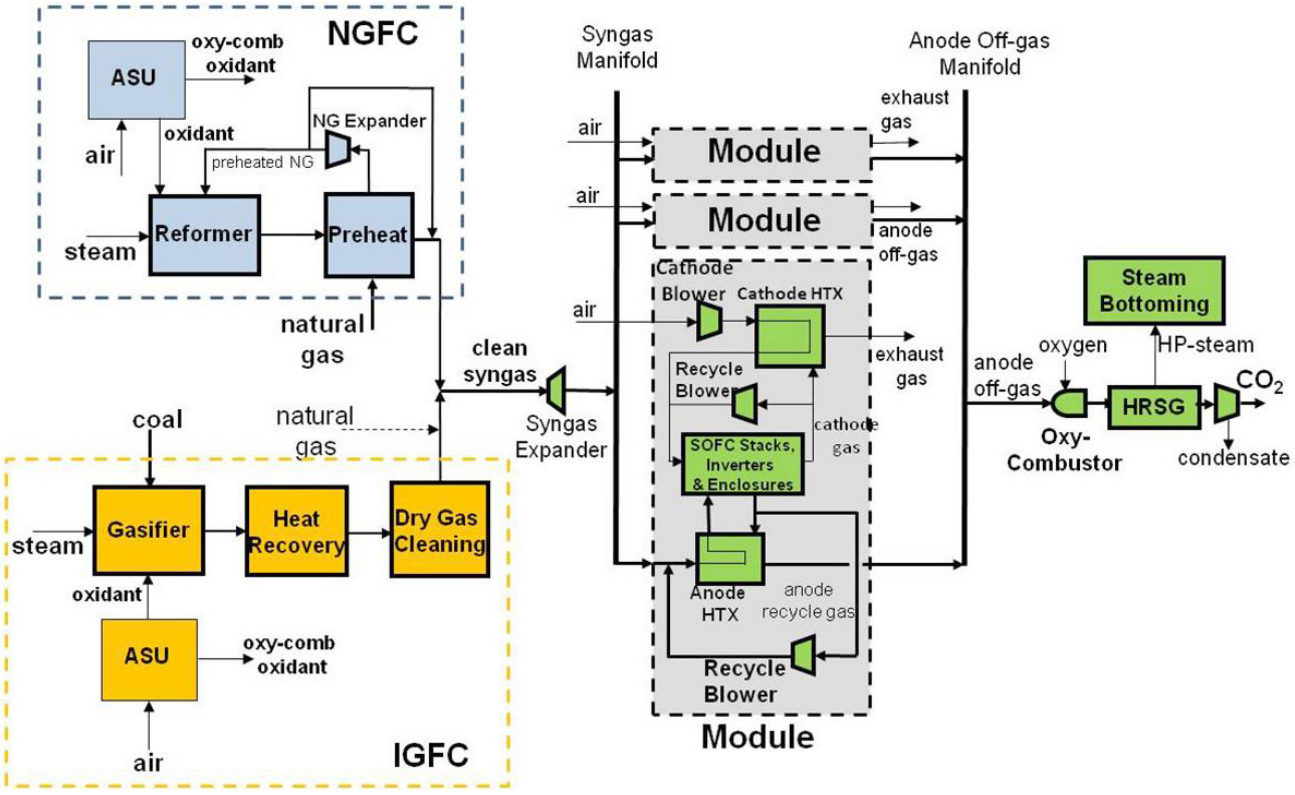

SOFC Plant Concepts

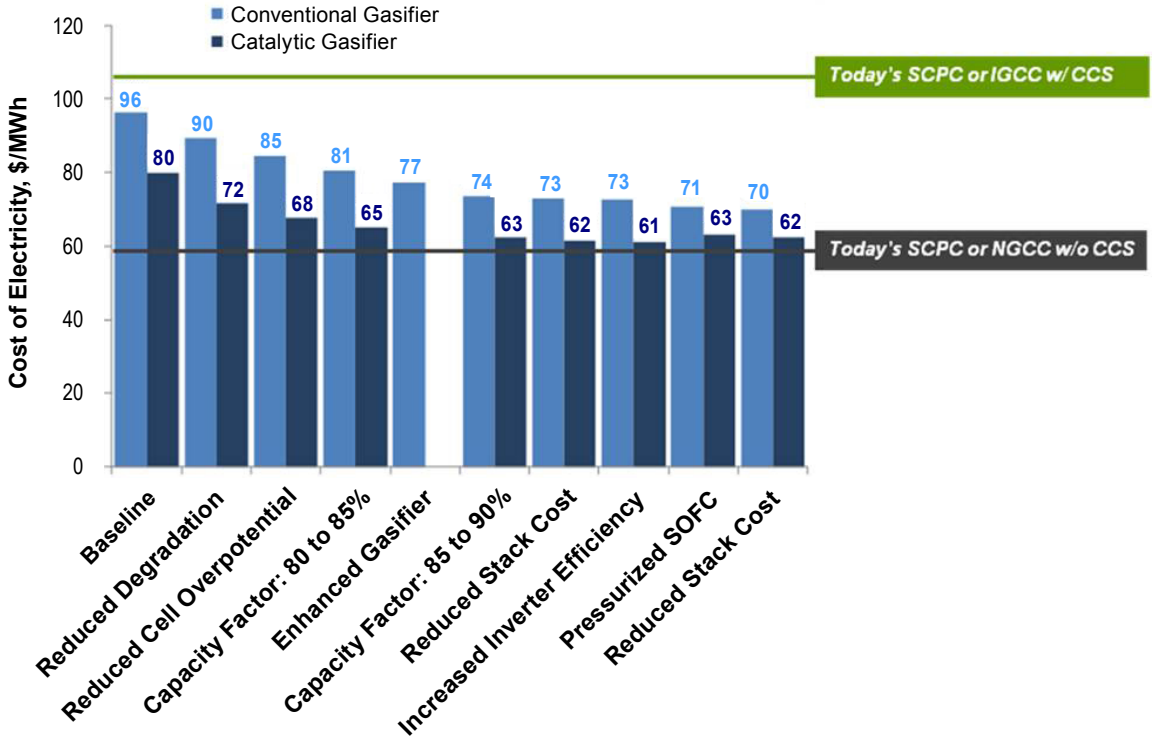

IGFC Pathway (97% - 99% CO_2 Capture)

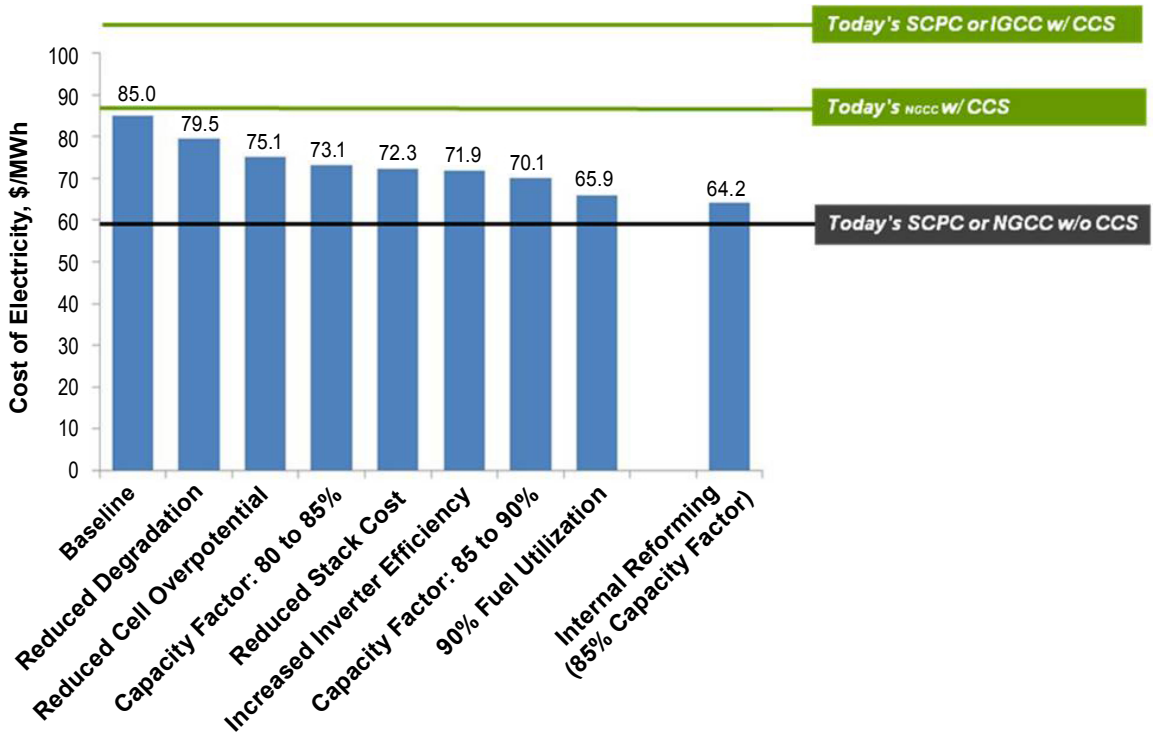

NGFC Pathway (99% CO_2 Capture)

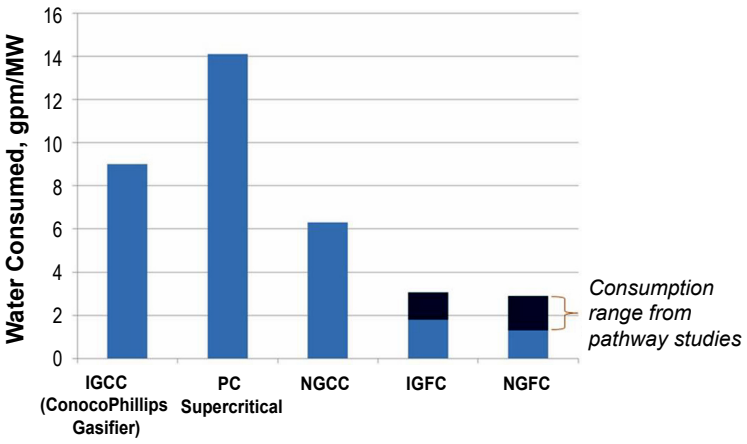

Water Consumption

History of the SECA Program

From its inception, SECA was structured as a unique alliance among government, industry and the scientific community. SECA is comprised of three groups: Industry Teams, Core Technology participants, and federal government (NETL) management. The Industry Teams design the fuel cells and handle most hardware and market penetration issues. The Core Technology program element, made up of universities, national laboratories, small businesses, and other research and development (R&D) organizations, addresses applied technological issues common to multiple Industry Teams. Findings and inventions under the Core Technology program are made available to all Industry Teams under unique intellectual property provisions (an exception to the Bayh-Dole Act) that serve to accelerate development. The federal government management facilitates interaction between Industry Teams and the Core Technology program element as well as establishes technical priorities and approaches. Program funding was established and maintained at approximately 65% for the Industry Teams and 35% for the Core Technology suite of projects. The inaugural SECA Industry Teams included General Electric (GE), Siemens Energy, Delphi Corporation, Cummins Power Generation/SOFCo, FuelCell Energy/Versa Power Systems (FCE/VPS), and Acumentrics Corp., all selected between 2001 and 2003.

At the time of its founding, SECA was part of the natural gas program, with an emphasis on distributed generation applications. The SECA concept was mass customization of a common 3-10 kW module that could address diverse markets – stationary power generation,

military applications, and the transportation sector (e.g., auxiliary power units for Class 8 trucks). Primary fuels under consideration were diesel and natural gas. Office of Management and Budget (OMB) targets were established for stack and system cost to be met in 2010, based upon a nominal production rate of 50,000 5 kW systems (250 MW total) per year - $100/kW and $400/kW, respectively, in year 2000 dollars. These 2010 targets reflected an approximately five-fold reduction in cost compared to the state of the technology that existed in 1999. Additional targets were established for other performance metrics, such as degradation (steady-state and transient). The program included rigorous periodic testing protocols to benchmark performance, with audits of the associated cost estimates.

The inaugural round of Industry Team 3-10 kW system tests was conducted between 2005 and 2007. All teams met the interim system cost ($800/kW) and steady-state degradation (4%/1,000 hours) targets over the required 1,500 hour test duration. The efficiency of these small simple cycle systems ranged from 35% to 41% (based on the lower heating value [LHV] of natural gas [NG]).

The innovative SECA program structure, as well as the aforementioned successful testing, did not go unnoticed. In 2006, the Office of Management and Budget cited the SECA program as leading the way in government-industry partnerships:

> *"The SECA program leverages private-sector ingenuity by providing Government funding to Industry Teams developing fuel cells, as long as the Teams continue to exceed a series of stringent technical performance hurdles. This novel incentive structure has generated a high level of competition between the Teams and an impressive array of technical approaches. The SECA program also develops certain core technologies that can be used by all the Industry Teams to avoid duplication of effort. The program exceeded its 2005 performance targets, and it is on track to meet its goal for an economically competitive technology by 2010."*

With the founding of SECA and its early success, the remaining legacy projects under the Vision 21 program and for less competitive fuel cell technologies (e.g., molten carbonate fuel cell-turbine hybrids and cylindrical SOFCs) were ended in the early- to mid-2000s.

In 2005, SECA transitioned from the natural gas program to the Strategic Center for Coal, with an emphasis on coal-fueled central generation with carbon capture. New solicitations in 2005 and 2007 added projects to scale up the SECA fuel cells for application in large central generation applications. Industry Team awardees included GE, Siemens, FCE/VPS, Rolls-Royce Fuel Cell Systems (RRFCS), and United Technologies Corporation (UTC)/Delphi. Along the way, Cummins withdrew from the program in 2006 as it did not have an interest at that time in the new program focus. GE scaled back from full Industry Team participation in 2006 to focus on what it saw as key SOFC technology hurdles through DOE-funded work at the Global Research Center. The Acumentrics project was transferred to DOE's Office of Energy Efficiency and Renewable Energy in 2008. By the end of 2008, there were four Industry Teams – Siemens, FCE/VPS, UTC/Delphi, and RRFCS. The year 2008 saw another round of stack metric testing, with the interim cost ($600/kW, 2000 dollars) and degradation targets met by Siemens and FCE/VPS in 5,000-hour tests. UTC/Delphi and RRFCS did not test as they were both new projects.

In 2010, FCE/VPS met the ultimate $400/kW (2000 dollars) target in testing of 120-cell 25 kW stacks comprised of scaled (550 cm^2) cells. By way of comparison, the typical planar SOFC stack at SECA's inception consisted of maximum 40 cells, each with an active area of ~100 cm^2, capable of perhaps 2 kW. At the end of 2010, Siemens made a corporate decision to end its SOFC R&D program and withdrew from SECA.

Current Status of the SECA Program

The baseline for the SECA cost goals was informally updated in 2008 to $700/kW (power block) and $175/kW (stack), in 2007 dollars. This change was formally incorporated into the OMB targets in fiscal year (FY) 2011.

As mentioned above, FCE/VPS met the cost goal in 2010. In 2011, the two later-awarded Industry Teams – UTC/Delphi and RRFCS – worked to complete SECA cost goal validation testing. In FY 2012 and beyond, all three Industry Teams will focus on improving the reliability, robustness and endurance required for commercial central generation. This work will encompass materials R&D, design, failure analysis, and manufacturing development. It will also consist of considerable stack testing, including progressively larger stacks, to validate performance and gather the required data to make further enhancements to the stack technology.

Fuel Cell Research and Development

The Office of Fossil Energy and NETL are pleased to present this FY 2011 Fuel Cell Program Annual Report, a compilation of abstracts from the fuel cell projects managed through these offices. These abstracts are divided into subsections as detailed below.

SECA Industry Teams – Coal-Based Systems

Through the Coal-Based Systems program element, SECA seeks to build upon the successes in the Cost Reduction program element by scaling SOFC cells and stacks to sizes appropriate for central power generation applications. This work includes an assessment of the integrated performance of IGFC systems. Industry Teams will focus on developing 250 kW–1 MW fuel cell module prototypes that will serve as the basis for early commercial market entry and as components in central generation plants. Key R&D topics include cell and stack scaling, manufacturing, failure analysis, system integration, materials, and pressurization (RRFCS). As the work progresses, it may extend to specialized balance-of-plant hardware, controls, and instrumentation for prototype systems.

SECA Industry Teams – Cost Reduction

The SECA Cost Reduction program element began at SECA's inception and is focused on achievement of the SECA cost goals. To achieve cost targets, Industry Teams are refining and validating advanced technology in ≥15 kW SOFC stacks that can be mass-produced, scaled and aggregated to meet a broad range of applications. This development activity is blending established manufacturing processes with state-of-the-art fuel cell technology advancements in order to leverage the advantages of economies of mass production and scale to reduce fuel cell costs. As noted previously, the scalability and fuel-flexibility permit the application of common SOFC stack technology to numerous market applications, including early adopter markets such as natural gas distributed generation (~1 MW), truck auxiliary power units, and various military applications such as unmanned undersea vehicles (UUVs). Common stack technology brought to bear in these diverse early markets will create the opportunity for the high-volume production required to reduce the real-world cost to commercially viable levels, and gather the production and operating experience desired prior to full-scale central generation deployment.

SECA Core R&D

The Core Technology Program provides comprehensive applied research support in nine focus areas. This program structure, along with special intellectual property provisions (exception to the Bayh-Dole Act), reduces R&D cost by leveraging resources so that the Industry Teams do not engage in separate, redundant applied research programs, paying multiple times for the same technical solutions. Diligent NETL management of the Core Technology Program with this approach also ensures that only major issues are addressed. SECA's goal is to raise the technology bar in large strides rather than small steps. Core Technology Program areas of research are also augmented by special topics under the DOE's Small Business Innovation Research (SBIR)/Small Business Technology Transfer (STTR) and Experimental Program to Stimulate

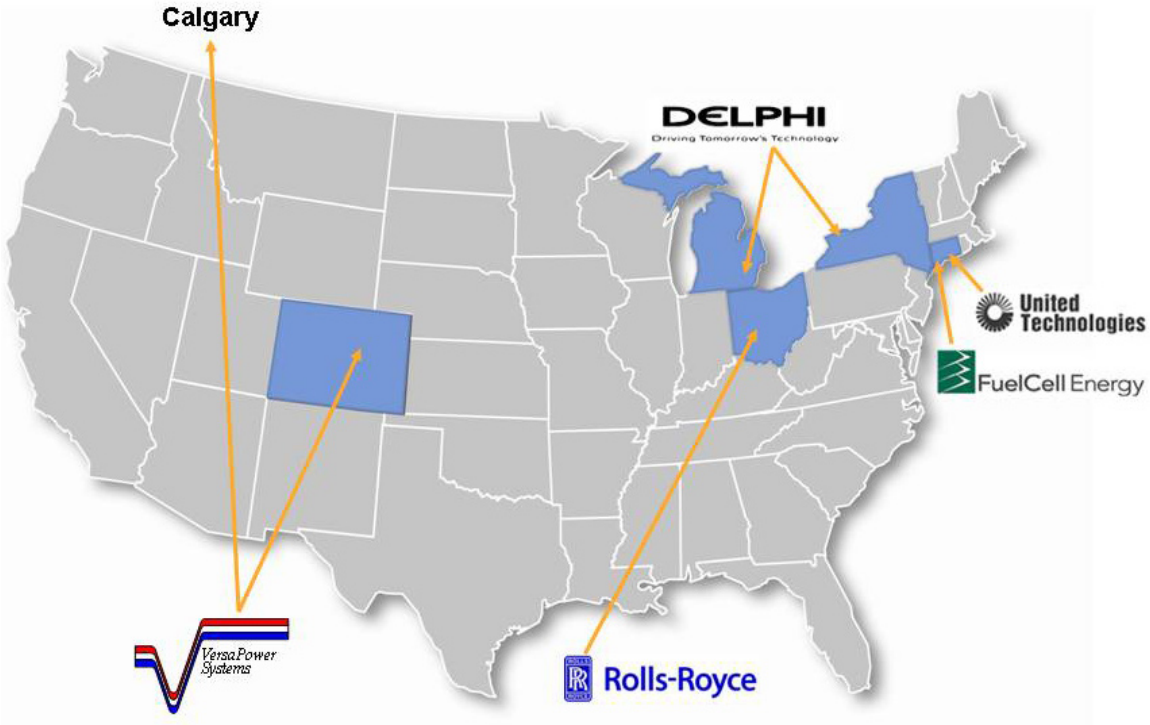

Competitive Research (EPSCoR) programs. The Core Technology Program focus areas include the following:

- **Cathodes –** Improve the stability and performance of fuel cell cathodes using state-of-the-art concepts and methodologies;
- **Anodes and Coal Contaminants –** Determine potential coal syngas contaminants and their impact on anode performance;
- **Interconnects and Contact Materials –** Develop stable, low-cost metallic interconnects and interconnect contact materials operating in the temperature range of 650 to 850ºC with acceptably low area-specific resistance (ASR) and stability over the service lifetime.
- **Seals –** Develop materials and designs exhibiting adequate sealing performance with the requisite chemical and phase stability in long-term service;
- **Cross-Cutting Materials, Testing, and Manufacturing** – Develop materials and manufacturing technologies that improve fuel cell reliability, performance, and ability to tolerate any fuel or air contaminants, and that achieve cost reductions;
- **Fuel Processing** – Develop fuel processing technologies that will meet application requirements such as zero water consumption, space and volume constraints, and transient capability;
- **Power Electronics** – Optimize efficiency and cost in conversion of fuel cell output to usable DC (direct current) and AC (alternating current) power;
- **Modeling and Simulation** – Create models to determine a reliable operating space and to guide manufacturing; and
- **Balance of Plant** – Develop high-temperature heat exchangers and blowers to enable high system efficiency and low cost.

Innovative Concepts

SECA Innovative Concepts will assess the feasibility of a coal power plant based upon a direct coal SOFC (e.g., liquid metal anode concepts) and evaluate novel planar SOFC designs (e.g., unique electrolyte support and metal support concepts). Also included are Congressionally directed projects developing novel electrochemical energy conversion and integrated technologies that advance the efficiency, reliability, and cost goals of fuel cell systems.

Key Program Accomplishments

SECA Peer Review Demonstrates Strength and Success

Seventeen projects were evaluated during the 2011 Fuel Cells Peer Review in Morgantown, West Virginia, on February 14-18, 2011. The peer review team of eight reviewers from industry and academia, assembled and led by ASME (American Society of Mechanical Engineers), assessed the projects across nine

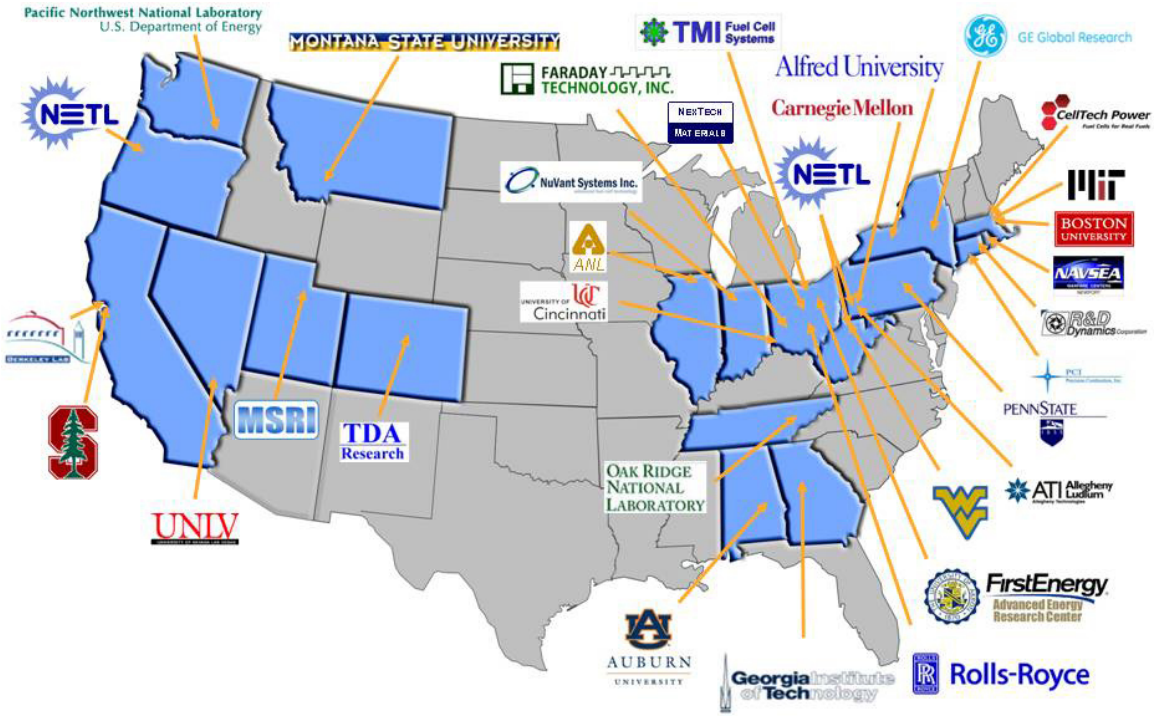

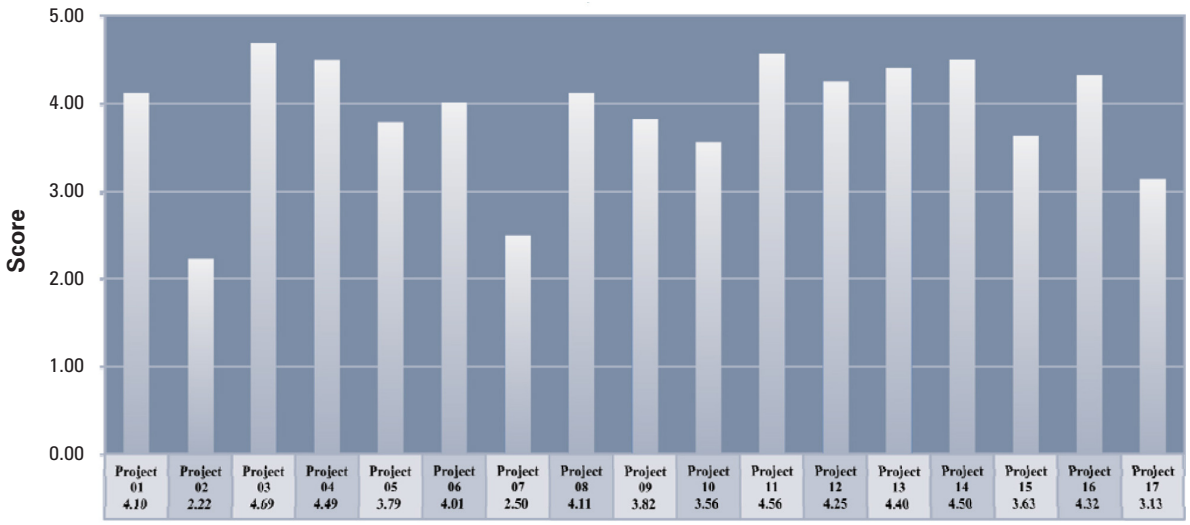

criteria: (a) scientific and technical merit; (b) existence of clear, measurable milestones; (c) utilization of government resources; (d) technical approach; (e) rate of progress; (f) potential technology risks considered; (g) performance and economic factors; (h) anticipated benefits if successful; and (i) technology development pathways. Scores were based on a whole number scale from 1 to 5, with 1 representing "results not demonstrated," 2 "ineffective," 3 "adequate," 4 "moderately effective," and 5 "effective."

Results were extremely supportive of the Fuel Cells/SECA Program and Core R&D as shown in the figure below. Fifteen of the 17 projects evaluated had average project scores ranging from 3.13 to 4.69 for the nine criteria. The overall average score for these 15 projects was an outstanding 4.09, in the top tier between moderately effective and effective. The two outlier projects, both Congressionally directed, were rated in the lower tier between ineffective and adequate. The average score across all 17 projects for each of the nine review criteria was 3.5 or higher, and five criteria had averages greater than 4.0. These results clearly demonstrate the effectiveness, strength, and success of the Fuel Cells/SECA Program.

These formal peer reviews are rigorous, documented evaluations by qualified independent reviewers using objective criteria to make judgments on a project's technical/scientific/business merit, actual or anticipated results, and productivity and management effectiveness of the project. In addition to the numerical scoring described above, reviewers are asked to provide comments on each project in four areas: Strengths, identified relative to the evaluation criteria; Weaknesses, project items or issues which might hinder a project's success, relative to the evaluation criteria; Recommendations, actions or direction that could add value to a particular project related task and/or help achieve a program goal; and Action Items, deficiencies identified by the Peer Review Panel and proposed mitigations to preclude the project from missing its stated project objectives or program goals. The comments from this year's Peer Review Panel indicate strong pursuit of relevant R&D to ensure that ambitious goals are achievable in the Fuel Cells/SECA Program.

SECA Industry Teams – Coal-Based Systems

SECA Coal-Based Systems Meet DOE's Cost and Performance Targets for IGFC Power Plants. FCE has developed an advanced coal-based SOFC baseline power plant that meets the SECA cost as well as efficiency targets. The baseline power plant, rated at approximately 672 MW, utilizes coal syngas fuel (produced by catalytic gasification and warm gas cleanup processes) in a power island consisting of an SOFC combined with a steam bottoming cycle. The system also employs oxycombustion of the fuel cell anode exhaust for CO_2 capture, using a portion of the oxygen from the air separation unit at the gasification site. A comprehensive system optimization effort resulted in achieving a system electrical efficiency of 58.7% based on HHV of coal, while capturing >99% of carbon (in the syngas) as CO_2. The baseline IGFC power plant system consumes 75% less water compared to a pulverized coal combustion plant using scrubbing technology for carbon capture and has a foot print comparable to an integrated gasification combined cycle plant. The factory equipment cost estimate has shown an SOFC power island cost of $372/kW in 2000 dollars and stack cost estimate of $85/kW, exceeding the DOE cost targets for a coal-based system. The breakthrough SOFC stack factory cost estimate was the result of a new generation of fuel cells developed by FCE's partner,

Versa Power Systems, Inc., based on improved materials and thin cell technology. The new generation of cells has demonstrated higher power density, an expanded range of operating temperature, and improved long-term stability with reduced power degradation, as compared to the previous baseline cell technology. Additionally, advances in fuel cell manufacturing, including automation and process modification combined with increased material utilization resulting from higher cell production yield, are key factors in the reduction of SOFC stack cost.

Durability of Next-Generation Rolls-Royce Fuel Cell Technology Demonstrated to Meet SECA Requirements. RRFCS has selected the next generation of its integrated planar solid oxide fuel cell (IP-SOFC) for carrying forward into ~20 kW block-scale testing. Tests will be performed within rigs able to fully duplicate the operating conditions and stack boundary conditions of high efficiency pressurized SOFC power modules projected for an integrated coal-gasification fuel cell combined cycle plant, as well as the conditions for nearer-term commercial validation through the market for natural gas fired 1 MW distributed power generation. An array of block test stands in Canton, Ohio, and Derby, United Kingdom, will serve to validate the durability and reliability of the stack technology at a repeat unit that is designed to be the building block of MW-scale power generation systems, while using balance-of-plant ejectors, insulation, and heat exchange components representative of product to accelerate commercialization. Two block test rigs were modified and commissioned during 2011 for SECA metric tests to commence in late FY 2011. The chosen cell technology has been tested to over 8,500 hours at full system relevant conditions and exhibits an average degradation rate of <0.5%/1,000 hours. Degradation mechanisms have been identified, and solutions for reducing the degradation rate to below 0.3% to meet the requirement for entry into service in 1 MW distributed generation units are being screened; the cell technology exhibits sufficiently low ASR performance levels to meet the efficiency targets for the 1 MW system. Rolls-Royce produces fuel cell modules on their protoype production line in Canton, Ohio. High volume manufacturing cost models predict systems cost meeting the SECA IGFC $700/kW target and internal Rolls-Royce targets for market entry systems.

Stack Components and IGFC Designs Meet SECA Requirements. The Delphi Gen 3 stack has successfully completed durability testing to 9,700 hrs and deep thermal cycling to 200 thermal cycles, with a degradation rate of 1.1% per 500 hours in durability testing. Delphi has developed low-cost, high-volume manufacturable processes for Gen 4 stack components and has fabricated and tested multiple Gen 4 stacks in a variety of test conditions. A 40-cell Gen 4 stack demonstrated a maximum initial power of 6.4 kW at an average power density of 398 mW/cm^2 and average cell voltage of 0.7 volts, utilizing the SECA simulated coal gas blend. When combined into a four-stack module, this will exceed the SECA requirement of 25 kW. The Gen 4 stack has completed a durability test of greater than 2,500 hours and has demonstrated a degradation rate of about 4% in the first 300 hours and no measurable power degradation thereafter. The stack has also successfully completed 60 deep thermal cycles from 750ºC operating temperature to <100ºC with a total power degradation of less than 5%. UTC Power has down-selected three power module concepts after detailed investigation of several competing designs. All three systems were designed for 400 kW net alternating current (AC) and achieve efficiency in excess of 60% based on fuel LHV. Heat-up and power ramp studies were performed on all systems to define internal and external characteristics. In addition, UTC Power developed three IGFC designs that produce greater than 100 MW net AC power at efficiency greater than 50% HHV and capture greater than 90% carbon. Sensitivity analyses were carried out, demonstrating that the designs maintained their key performance requirements over a wide range of key operating variables. A system cost analysis was completed for the baseline IGFC system. Preliminary cost analysis of the power block hardware for the IGFC power plant shows a cost of $685/kW in 2007 dollars with a 90% confidence interval, which meets the SECA cost requirement of $700/kW. UTC Power has commissioned a 50 kW capable test stand.

SECA Core R&D – Cathodes

Dynamic Lattice Parameter Changes Open New Window into SOFC Cathode Performance. Recent studies of $La_{0.6}Sr_{0.4}Co_{0.2}Fe_{0.8}O_{3-\delta}$ (LSCF) films have revealed a near instantaneous and large change in the lattice parameter of LSCF with applied electric field. Researchers at Argonne National Laboratory measured the lattice parameter of a 20 nm thick LSCF film epitaxially grown on (001) YSZ substrate (0.5 mm thick) with an intervening 50 nm gadolinium-doped ceria (GDC) (001) film. Using voltages typical of those found in SOFCs, the researchers found that the lattice parameter expanded by almost 0.5% in less than a second after a -1 V cathodic potential was applied to an LSCF film in 150 torr of oxygen at 600°C. Using an extremely small X-ray beam (20 μm in width), the lattice parameter change was mapped out as a function of distance from the Pt wire electrode. The lattice parameter change switches sign with the applied voltage, indicating that it is not a simple electrostriction effect. While the mechanism of this lattice parameter shift has not been resolved, it appears to be associated with the

injection and removal of oxygen vacancies from the LSCF film. Despite this uncertainty, since the lattice parameter shift with applied voltage is monotonically increasing, this map may be translatable into a local conductivity or potential map of the SOFC cathode, thus providing a unique, contactless method of probing the ionic processes of these important materials in a complex chemical environment at high temperatures. The presence of these large lattice parameter shifts may also be important to the thermo-mechanical design of SOFCs.

Correlations between Oxygen Exchange Kinetics and Crystallographic and Microstructural Features Effects of $La_{0.7}Sr_{0.3}MnO_3$ Uncovered. Measurements of the oxygen exchange kinetics of $La_{0.7}Sr_{0.3}MnO_3$ (LSM) thin films were made at Carnegie Mellon University (CMU). Films were prepared by pulsed laser deposition at CMU with controlled surface crystallographic and microstructural features, and these were also provided to several external collaborators at Argonne National Laboratory, Massachusetts Institute of Technology, and University of Nevada, Los Angeles. Epitaxial (100), (110), and (111) $La_{0.7}Sr_{0.3}MnO_3$ thin films with thickness of 600 nm were deposited on $SrTiO_3$ single crystal substrates. Also, 600 nm thick, (110) textured $La_{0.7}Sr_{0.3}MnO_3$ thin films were deposited on (111) YSZ (8% Y_2O_3 stabilized ZrO_2) single crystal substrates. Both the epitaxial and textured LSM films had smooth surface morphologies. The chemical surface exchange coefficients, k_{chem}, basic parameters indicative of the electrocatalytic activity of SOFC cathodes, were determined experimentally using electrical conductivity relaxation. The transient relaxation experiments were carried out from 600°C to 900°C. For the epitaxial films, k_{chem} varied from ≈1 x 10^{-6} to 65 x 10^{-6} cm/s, depending on temperature and orientation, with activation energies of ≈1.0 ± 0.2 eV. At 800°C, a four-fold variation was observed in the k_{chem} values, with (110)/(100) being the highest/lowest, explained well by the high activation energy for (110), ≈1.16 eV, and the low energy for (111) and (100), ≈0.83 eV. For the textured films, two k_{chem} values were extracted from the data, indicating that two parallel surface exchange processes occurred. These two k_{chem} values had different activation energies (E_A), which were interpreted as belonging to (1) the native surface response of individual grains/variants and (2) the variants boundaries/grain boundaries of the textured films. The first (native surface) process had an activation energy of $E_{A,1} \approx 1.5$ eV, while the second (extended defect) process had an activation energy of $E_{A,2} \approx 0.75$ eV. These observations indicate that a range of k_{chem} values and limiting processes are important in different regions of the SOFC microstructure; they also indicate methods for improved surface exchange properties.

Catalyst Infiltration Enhances Cathode Performance and Stability. Georgia Institute of Technology has developed an optimized solution infiltration process to fabricate high quality continuous LSM coatings on porous LSCF cathodes and demonstrated that the performance and stability of an LSCF cathode can be enhanced by infiltration of a catalyst such as LSM and praseodymium strontium manganite. Comparative microanalyses of the structure, composition, and morphology of LSM and LSCF surfaces as well as LSM/LSCF interfaces annealed at 850°C for 900 hours reveal that the presence of Mn is able to effectively suppress the formation of a surface layer consisting of La and Sr oxides on LSCF, which is likely related to the degradation of blank LSCF cathodes. Considering the improvement in performance and stability achieved by infiltration, it is anticipated that the implementation of catalyst-infiltrated cathode may help to meet the DOE cost goals for solid oxide fuel cells.

Promising Cathode Contact Materials Identified and Assessed. Lawrence Berkeley National Laboratory (LBNL) is focused on cathode contact material selection and development. The primary challenge addressed during FY 2011 concerns electrical connection and bonding between the interconnect and SOFC cathode layers. Historically, cathode materials such as LSM is used as a cathode contact material (CCM) paste to bond the cell to the interconnect. High temperature is typically required to achieve good bonding, however, leading to rapid oxidation of the stainless steel interconnect. If a temperature low enough to avoid oxidation of the steel (<1,000ºC) during the bonding step is employed, poor bonding and eventual delamination of the contact material occur. The goal of the work at LBNL is to identify candidate cathode materials displaying adequate properties after bonding at <1,000°C. During FY 2010, candidate cathode contact compositions were purchased from Praxair or fabricated by glycine-nitrate process. The properties of primary relevance, including conductivity, sintering behavior, coefficient of thermal expansion, and reactivity with manganese-cobalt spinel (MCO) and LSCF, were then determined. The summary of this screening effort suggested that the most promising candidates are LSCF and lanthanum strontium copper ferrite (chosen for extensive sintering at low temperature) and strontium samarium cobalt oxide (SSC) and lanthanum strontium cobalt oxide (LSC) (chosen for high conductivity). In FY 2011, these four materials were incorporated into ASR specimens in which electrical resistances of the individual LSCF/CCM and 441-MCO/CCM interfaces and LSCF/CCM/MCO junction were monitored over time. LSC and SSC are the most promising compositions tested to date. They provided low and stable ASR for 200 hours at 800ºC. In situ testing of these CCM candidates has commenced,

using anode-supported button cells and coated 441 steel interconnect coupons.

Lattice Strain Shown to Be Important to Cathode Surface Chemistry and Electronic Structure. Massachusetts Institute of Technology demonstrated the effects of epitaxial strain on the surface cation chemistry and the surface electronic structure of LSM as a model system, both at room temperature and at elevated temperatures. A larger tendency for Sr enrichment is prevalent for the tensile-strained LSM surface, owing to the relatively larger space available for the Sr cation on the surface compared with that in the bulk with increasing tensile strain. Tensile strain also facilitates oxygen vacancy formation on LSM. While the electronic structure exhibits the presence of an energy gap between the occupied and unoccupied states at room temperature, favoring a smaller band gap for the compressively strained LSM, the picture reverses at elevated temperatures. At 500ºC in 10^{-3} mbar of oxygen, both LSM film surfaces exhibit metallic-like behavior, and the tensile-strained LSM has enhanced density of states near the Fermi level compared with the compressively strained LSM. These results illustrate the importance of lattice strain in controlling the high-temperature surface chemistry and electronic structure for oxygen reduction activity on SOFC cathodes. In-depth probing and analysis of such correlations on a broad range of materials and conditions are essential toward advancing understanding of how the surface state, including the presence of strain, relates to the oxygen reduction activity on oxide cathodes.

Strategies for Mitigating Degradation of SOFC Cathode Materials Identified. One of the major concerns of long-term viability of SOFC systems is degradation of cathode materials. One identified problem is how elements are redistributed at surfaces and interfaces during normal and atypical SOFC operation. Sr out-diffusion to the surface as Sr oxide has been determined by Montana State University as a function of electrochemical environment in $La_{0.6}Sr_{0.4}Co_{0.2}Fe_{0.8}O_{3-\delta}$ using Cr as a tracer in X-ray absorption spectroscopy to distinguish the segregated Sr from the bound Sr in the bulk. Oxygen vacancy concentration variations, caused by bias potentials existing during operation, have been identified as the driving mechanism for the Sr out-diffusion. Cathodic bias potentials have been found to reduce the oxygen vacancy concentration resulting in Sr segregation, while anodic bias potentials inhibit Sr segregation. Possible mitigation strategies have been suggested.

Collaboration between NETL Regional University Alliance (RUA) and Advanced Institute for Science and Technology (AIST) of Japan Kicked Off. NETL RUA researchers hosted visitors on August 21 and 22, 2011, from the AIST for a research collaboration kickoff meeting between the organizations. Discussions focused on detailed research planning associated with the recent award made by the New Energy Development Organization (NEDO, Japan) to the AIST group to investigate novel SOFC anodes that are resistant to poisoning by sulfur and phosphorus. The project includes a formal collaboration with West Virginia University (WVU) and an informal research collaboration with NETL that allows researchers to engage in a no-cost informational exchange. The parties formalized the details of the research collaboration, which will require WVU to provide cathode materials innovation and testing, while NETL will provide consultative advice on test parameters and testing methods. As possible, NETL may also deliver exposed specimens for investigation at AIST by a sensitive materials analysis technique known as secondary ion mass spectrometry. WVU and NETL researchers have been invited to deliver lectures and tour SOFC research facilities in Japan as part of the research collaboration.

Researchers Engineer High Porosity Cathode with In Situ Foaming Technique. NETL RUA fuel cell researchers at WVU have recently engineered and demonstrated an in situ fabrication method that generates highly porous SOFC cathodes. The technique utilizes a gas-evolving reaction to create a porous foam structure in a conventional $(La,Sr)(Co,Fe)O_3$ cathode that can be applied to any type of SOFC. By controlling the composition of the precursor cathode solution and the foaming reaction rate, the researchers control critical microstructural features such as pore size distribution and total porosity. Control over microstructure is critical in cathode engineering, as researchers attempt to make the most porous, highest surface area cathode that still retains sufficient mechanical strength to withstand fuel cell operating conditions. Recent experiments on an electrolyte supported button cell have shown that the engineered porous structure enhances power density by 30% compared to a cell possessing a conventionally processed cathode. A presentation describing the complete results was accepted to the Electrochemical Society Meeting held in Boston in October 2011.

SOFC Cathode Performance Enhanced through Infiltration of Samaria-Doped Ceria. WVU researchers successfully infiltrated $Ce_{0.8}Sm_{0.2}O_{1.9}$ (SDC) into a conventional SOFC cathode composed of $La_{0.8}Sr_{0.2}MnO_3$ (LSM) as part of the NETL RUA collaboration to develop advanced SOFC cathode materials. The infiltrated material is applied to the conventional cathode as a liquid, but subsequent thermal processing deposits a homogeneously distributed array of sintered nano-particles onto the surface of the cathode backbone. Addition of infiltrated material is expected to improve cathode performance (or decrease cathode inefficiency)

by enhancing the cathode catalytic activity towards the oxygen reduction reaction or by providing additional surfaces for exchange of oxygen. Experimental results obtained on LSM cathodes infiltrated with SDC indicate that polarization resistance can be reduced significantly compared to uninfiltrated cathodes, and that the portion of the cathode that is active towards oxygen reduction is increased by at least three times. The complete results have been published in the *Journal of Power Sources* in an article titled "Electrochemical characteristics of SDC infiltrated LSM cathodes with varied thickness for yttria-stabilized zirconia electrolytes."

Stable Cathode Suitable for Infiltration in Solid Oxide Fuel Cell Developed. NETL RUA researchers have recently completed a total of 800 hours performance testing of a SOFC with customized cathode structure prepared by solution infiltration. The infiltration technique introduces precursor solution into a backbone cathode to tailor nano-structured composite for improved electrode activity. The three-layered backbone cathode composed of Sr- and Co-doped $LaFeO_3$ and Sm-doped CeO_2 was fabricated using a screen-printing method on an anode-supported electrolyte. The baseline cell produced 440 mW/cm^2 under 0.7 V at 750°C for 500 hours with only 0.7% degradation. Cell tests were continued for another 300 hours at 750°C after Sr-doped $LaCoO_3$ infiltration on the same cell. The infiltration demonstrated a 53% increase in power density (675 mW/cm^2 under 0.7 V) and 40% decrease in polarization resistance compared to the baseline test. The research demonstrates that a new SOFC cathode backbone has been successfully designed for solution infiltration.

Novel SOFC Cathode Material Generated Using Electro-Spinning Technique. WVU researchers have recently fabricated an SOFC cathode material known as LSCF using a novel electro-spinning technique developed through a collaborative Regional University Alliance research activity. The electro-spinning technique and subsequent processing generate ceramic fibers with aspect ratios exceeding 40:1 (diameter of 240 nm, length of 10-20 μm), which are suitable for application to SOFCs as cathodes. X-ray diffraction and scanning electron microscopy results indicate that the material possesses the proper crystallographic phase and microstructure, and the fibers have demonstrated stability under typical SOFC operating temperatures of 800°C. LSCF nano-fibers produced by this technique are coated with a thin film of $Gd_{0.2}Ce_{0.8}O_2$ in subsequent processing steps. The thin coating provides a stabilizing barrier on the LSCF and increases the fiber diameter to approximately 400 nm. Efforts are presently underway to compare the electrochemical performance of cathodes composed of nanofibers generated using this technique to that of cathodes generated using more traditional cathode fabrication processes. The project published a related paper describing generation of YSZ nanofibers coated with $La_{0.8}Sr_{0.2}MnO_3$ in the journal *Energy and Environmental Sciences*.

Operating SOFC Cathodes Analyzed by In Situ High Temperature X-Ray Diffraction Technique. A test stand has been developed at Pacific Northwest National Laboratory that allows anode-supported SOFCs to be operated in the heating chamber of a high temperature X-ray diffractometer, thereby allowing for collection of X-ray diffraction (XRD) spectra of SOFC cathodes under actual operating conditions. During FY 2011, further improvements were made to the in situ test fixture, and XRD spectra were continuously obtained for a working lanthanum strontium cobalt ferrite cathode over several hundred hours of operation. Computational software was used to analyze the collected XRD patterns. This analysis, involving a combination of correlation coefficients, determined that a statistically significant time-dependent change (i.e., expansion of the perovskite lattice) occurred through the duration of the test.

SECA Core R&D – Anodes and Coal Contaminants

Syngas Contaminant Partitioning Evaluated for Gasifiers Equipped with Low-Temperature Cleanup Systems. NETL researchers recently completed a thermodynamic evaluation of the partitioning of gasification-derived trace contaminant materials in a process stream subjected to conventional low temperature gas cleanup technology. In the theoretical study, synthesis gas compositions typical of deployed gasification technology are equilibrated at temperature (35-50°C) and pressure (300 psia) conditions typical of conventional gas cleanup technologies based on Selexol and amine gas treatment processes. The study quantifies the partitioning of volatile trace materials between sour water streams and gaseous streams passing to downstream process equipment, and the results are pertinent to coupled gasification fuel cell systems expected for near-term, large-scale demonstrations. The results indicate that relatively smaller magnitudes of trace material pass through low temperature gas cleanup systems compared to high temperature (>300°C) systems, but volatile elements including Hg, P, Sb, and Se remain in gas phase under certain conditions. The concentration of trace materials passing through the low temperature cleanup systems is sensitive to water content in the process gas. The full study and results were published as an NETL Technical Note, which appears in the SECA reference shelf on the NETL website.

Remedies Found for Poisonous Effects of Coal Syngas Impurities on SOFC Anodes. Researchers from the National Institute for Fuel Cell Technology at West Virginia University have combined multiple expertises in

experimentation and modeling to address the problems associated with impurities in coal syngas and other complex fuels when used in SOFCs. Comprehensive ex situ and in situ experiments have been performed to identify the effects of phosphine, hydrogen sulfide, and other coal syngas impurities on the Ni/YSZ-based SOFC anodes. Recent observations of phosphine contaminant indicate faster degradation in the presence of steam and reaction of phosphine with YSZ along with nickel. Nickel- and iron-based prefilters have been shown to remove phosphine from syngas fuel effectively to levels which are not harmful to the Ni-YSZ anode. With proper filter design, the Ni-YSZ SOFC can operate on contaminated coal syngas without degradation over a prescribed period of time. Novel anode materials and coatings have been designed and demonstrated to be effective in resisting the degradation due to common syngas contaminants. Computational modeling has been used to study the effect of low concentrations of contaminants on performance and structural degradation of SOFCs, to find correlations for cell lifetime predictions, and to aid experimental work.

SECA Core R&D – Interconnects and Contact Materials

Surface Blasted American Iron and Steel Institute (AISI) 441 Improves SOFC Interconnect Performance. ATI Allegheny Ludlum studied post-processing surface modifications as methods for increasing metallic interconnect performance. Samples from a production coil of AISI 441 underwent various post-processing treatments, including desiliconization, surface blasting, surface grinding, and temper rolling, while an acid pickled mill surface served as a control. These modifications sought to modify the sub-surface or near-surface grain structure or chemistry in order to suppress electrically resistive phases from forming at the scale metal interface during exposure to SOFC operating conditions. They were used in conjunction with the application of an external oxidation-resistant and electrically conductive coating. These surface modifications neither substantially improved nor deteriorated the electrical resistance of AISI 441. Long-term isothermal oxidation testing at elevated temperature revealed that surface blasted material had improved resistance to scale delamination, while temper rolled material suffered from oxide spallation. Results agree with similar testing performed at the Pacific Northwest National Laboratory. Surface blasted AISI 441 should help achieve SOFC electrical interconnect requirements for lifetimes of 40,000 hours or more and should be further evaluated in SOFC test cells.

Chromium Content in Interconnect Alloy and Reaction Layer Critical to SOFC Performance. Auburn University has shown that the high chromium content in the reaction layer formed at the alloy-coating interface will likely dominate the electrical resistance between the interconnect and the cathode in a SOFC, and that the ferritic stainless steel alloy used for the interconnect should contain at least 17% chromium to minimize the thickness of the reaction layer.

Manufacturing Process for Electrodepositing Mn-Co Alloy Meets DOE Targets. Faraday Technology and West Virginia University are developing a cost-effective manufacturing process for application of $(Mn,Co)_3O_4$ spinel coatings onto SOFC interconnects to minimize chromia scale growth and chromium evaporation that can cause unacceptable degradation in the SOFC electrochemical performance. The manufacturing process involves using pulse reverse electrodeposition for application of a Mn-Co alloy coating onto the interconnect surface and subsequent conversion to the $(Mn,Co)_3O_4$ spinel. Faraday Technology and West Virginia University previously demonstrated that the electrodeposition process could produce uniform, dense, crack-free, well-adhered Mn-Co alloy coatings of various compositions on a 5 cm x 5 cm T441 stainless steel interconnect surface. A post-deposition thermal treatment converted the Mn-Co alloy coatings to $(Mn,Co)_3O_4$ spinels in which a coating thickness of ~3 µm was shown to be sufficient to mitigate chromia diffusion after 500 hours of thermal exposure at 800ºC. Further revision of the previously reported economic assessment based on using batch manufacturing for the pulse reverse electrodeposition process demonstrated that the innovative coating technology can meet DOE's high volume target of 1,600,000 plates per annum for 250 MW fuel cell stacks at a cost of ~$1.23 per 25 cm x 25 cm coated interconnect.

Long-Term Evaluation of Protective Interconnect Coatings Exceeds 2 Years. In previous work, Pacific Northwest National Laboratory systematically investigated and applied $(Mn,Co)_3O_4$ (MC) spinels as protection layers on a variety of candidate SOFC interconnect steels. Recently, the primary emphasis has been on the application of spinel coatings to AISI 441 ferritic stainless steel, which is being investigated as an interconnect alloy. A Ce-modified version of the coating has been developed to improve the interfacial adhesion between the steel substrate and the oxide scale that grows beneath the spinel coating. In long-term tests (still in progress), Ce-modified manganese cobalt (Ce-MC) spinel coatings on AISI 441 ferritic stainless steel have exhibited low, stable ASR for over 18,000 hours at 800ºC. To further improve oxide scale adhesion and spallation resistance, a series of surface treatments (performed by Allegheny Ludlum) is under investigation. Ce-MC coatings were applied to the surface-treated AISI 441 and then subjected to oxidation testing at

800 and 850ºC. Over 12,000 hours of testing at 800ºC, and 6,000 hours of testing at 850ºC, the spinel-coated, surface-treated coupons have exhibited improved spallation resistance compared to spinel-coated mill reference coupons. The surface treatment oxidation tests are also still in progress.

New Cathode-Interconnect Contact Materials for SOFCs Offer High Electrical Conductivity and Improved Mechanical Strength. The interconnect is one of the key components in a SOFC stack. Stainless steels are typically chosen as interconnect materials for intermediate temperature SOFCs. However, metallic interconnects can cause power loss and performance degradation during operation due to the continuous growth of oxide scales and contact resistances. Therefore, optimization of interconnect materials and coatings is a necessary, but not sufficient, condition for obtaining stable stack performance. The complete solution to interconnect-related challenges must also take into account the electrode/interconnect interfaces. Thus, it is necessary to develop a complete materials system, which includes not only the interconnect, but also stable, high-performance contact materials for cathode/interconnect interfaces. Many conductive oxides, such as those commonly used as cathodes, demonstrate high electrical conductivity and chemical compatibility, but these oxides usually have low sintering activity at typical intermediate temperature SOFC stack sealing temperatures (825-950°C). As a result, the cathode/interconnect contact zone tends to have low mechanical strength and durability. During FY 2011, Pacific Northwest National Laboratory developed new cathode contact materials based on a novel reaction-sintering process. This reaction-sintering approach, which utilizes the energy released from the chemical reactions of metallic precursors with oxygen molecules in air to assist in situ solid-state sintering of the contact material, was used to fabricate Ni-Co-O and Mn-Co-Cu-O based cathode contact materials. After process optimization, these cathode contacts exhibited the required low electrical resistance, as well as tensile strength on the order of 5-10 MPa, which was much higher than the strength of conventional cathode contacts (<1 MPa).

Optimization of Composition and Processing of Yttrium Chromite Results in Improved Densification under Constrained Sintering Conditions. Yttrium chromite-based perovskites exhibit several attractive features for SOFC interconnect applications over lanthanum chromites, such as stability with respect to formation of hydroxides, low chemical expansion in reducing environments, and chemical compatibility with YSZ electrolyte. In recent work at Pacific Northwest National Laboratory, electrical, thermal, and structural properties of yttrium chromite were improved through A-cation site doping with Ca, and B-cation site doping with Co, Ni, and/or Cu. In addition, studies were performed to improve the density of screen-printed, sintered chromite interconnects. Screen printing is a simple, low-cost process for ceramic SOFC interconnect fabrication. However, in general, densification of the screen-printed layer is difficult, and modification of the process is necessary to increase the density of the film. In addition, application of the thick film to a pre-sintered substrate results in sintering constraint in lateral directions, which can further retard densification. Densification at 1,300ºC of screen-printed films under constrained sintering conditions was substantially improved through the development and optimization of a fabrication process based on infiltration of pre-sintered layers with water/alcohol solutions containing nitrate precursors and complexing agents.

SECA Core R&D – Seals

Several Viable Gallio-Silicate Glasses for Viscous Sealing at Intermediate Temperatures Identified. Alfred University identified two main compositional ranges of gallio-silicate glasses as candidate viscous sealants for specific operating temperatures. The first glass system is alkali-free and fuses with SOFC stack components at temperatures as low as 750°C. Powdered samples of these glasses crystallize at 850°C but remain mostly amorphous after 500 h at 750°C and are applicable for operation at 700 to 750°C. The second glass system incorporates a few mol% alkali with glass transition temperatures near 600°C. Bulk crystallization occurs at 850°C, but ~60% glass phase remains even after 1,500 h to sustain viscous sealing. These glasses are stable against 8 mol% YSZ electrolytes after 1,500 h at 850°C. Stability was also observed with aluminized stainless steel interconnect materials after 500 h at 850°C where the Al_2O_3 coatings remain 1 to 5 µm thick in contact with the glasses. Viscous sealing behavior was observed via crack healing near 810°C. The glasses remain completely amorphous after 500 h at 650°C, and reactions with electrolytes are minimal. This glass system can sustain viscous sealing behavior with operating temperatures throughout the entire range of 650 to 850°C.

Durable Glass-MgO Sealing Composition for High Temperature Fuel Cells Evaluated by Helium Leak Testing and In-Stack Testing. Materials & Systems Research, Inc. (MSRI) has formulated two glass-magnesium oxide sealing compositions for high temperature SOFCs. The sealing compositions consist of base-glasses into which specific amounts of nanosize magnesium oxide are added. The compositions have been tailored to yield specific phases on crystallization, resulting in significant reduction in the variability

of their thermal expansion over time, at elevated temperatures. Thermal expansion and crystallization data over 2,500 hours at 800°C indicate that Comp.-5 has the best stability over time while Comp.-3, though not as stable, is better than barium-calcium-aluminum-boron silicate (BCAS) glass. The compositions were fabricated into flexible gaskets by tape-casting, and the gaskets were used for helium leak testing. The leak tests on glass/stainless steel seal interfaces suggest that compositions 3 and 5 display short-term sealing characteristics that are at par with or better than those of BCAS glass at 800°C. Data obtained from a three-cell stack (sealed with gaskets made from Comp.-5) tested at MSRI that uses Nd-doped $LaCrO_3$ coating on the sealing area of the stainless steel interconnects indicates satisfactory sealing performance. The glass-magnesium oxide sealing compositions, when used in combination with the protective interconnect coatings, provide sealing options that are chemically, thermally, and mechanically stable over long durations of operation at the operating temperature of the SOFC stack.

Innovative Self-Repairable Composite Seals Developed for SOFCs. A functioning SOFC requires high temperature seals that prevent the mixing of fuel and oxidant streams as well as prevent reactant escape to the surrounding environment. In previous years, the University of Cincinnati advanced a novel in situ self-healing sealing glass concept. Glasses were fabricated and characterized to advance this concept, and seal testing was done to demonstrate in situ self-repair capability of the glass seals. Seal tests displayed excellent seal performance, including in situ self-repair of cracked/leaking seals. The self-healing concept requires glasses with low viscosity at the SOFC operating temperature of 800°C, but this requirement may lead to excessive flow of the glass under load in areas forming the seal. To address this challenge, a modification to glass properties such as creep via addition of particulate fillers is now being pursued by the University of Cincinnati. The underlying idea is that non-reactive ceramic particulate filler is expected to form glass-ceramic composite and increase the glass transition/glass softening temperatures and seal viscosity, thereby increasing the creep resistance of the glass-composite seals under load. In addition, the incorporation of an appropriate filler can affect the coefficient of thermal expansion of the glass-ceramic, thereby providing additional flexibility for developing composite sealing glasses with the optimum expansion mismatch among materials forming the seal, reducing mismatch stresses and improving seal reliability. The University of Cincinnati has successfully identified filler materials, fabricated glass-ceramic composites, and demonstrated stability for making seals for SOFCs.

SECA Core R&D – Cross-Cutting Materials, Testing, and Manufacturing

Solid Oxide Fuel Cells Tested and Evaluated under Extreme Conditions. The Naval Undersea Warfare Center, Division Newport (NUWCDIVNPT) conducted demonstrations in 2009-2010 focused on evaluation of fuel reforming of various fuels for UUV applications. In these experiments, simulated reformate was fed into a SOFC stack, and the hot anode exhaust was used to facilitate steam reforming of S-8, JP-10, and methane. This configuration allowed reformer operation using the waste heat and steam supply from the SOFC stack. In this way, half the anode recycle loop could be verified while protecting the stack from reformate that was not yet qualified and might contain species detrimental to the stack. These firsthand demonstrations unveiled the limitations of relying on waste heat alone to drive the steam reforming process. While the SOFC exhaust exited at over 700°C, by the time this stream reached the reformer inlet, the temperature had dropped to 400°C, which was too low to activate the steam reforming catalyst. Therefore, the burner was used in the Delphi fuel processor to add additional heat to the reformer. This was valuable for the purposes of reformer demonstration but not practical for an actual UUV system, which cannot afford continual burner or catalytic partial oxidation operation that consumes considerably more oxygen and lowers fuel efficiency as compared to steam reforming. Delphi's fuel processor is designed to operate with a continuous combustor channel; thus, its thermal mass is quite large and radiates heat away from the catalyst bed. Another aspect is fuel vaporization, which must be precisely controlled for liquid fuel feeds in order to minimize carburization and respond to power transients. A gaseous fuel such as methane is easier to throttle, and its reforming could be accomplished in a variety of locations within the reformer bed (and stack). This reduces concern over the issues of fuel vaporization and sooting. NUWCDIVNPT has hence turned its attention towards first generation SOFC power systems for UUVs that utilize methane as the primary fuel. Methane offers similar energy metrics to liquid fuels because of its higher hydrogen to carbon ratio, which minimizes oxygen consumption and carbon dioxide sequestration per unit energy generated. Methane could also be widely utilized across other military platforms while meeting many of the Navy's energy goals regarding carbon emissions, energy security, and renewable fuels.

Aerosol Spray Deposition Shows Promise as SOFC Component Coating Technique. NexTech Materials, Ltd. has made significant progress in the continuing development of commercially viable protective coatings for SOFC components. Aerosol

spray deposition (ASD) has been identified as being amenable to large-scale manufacturing and capable of enabling low cost (<$2/part) at 400 MW annual stack production volumes. Refined cost and manufacturing models have been developed to encompass volumes from prototyping through pilot-scale production and full-volume production, with strategies identified to reduce volume manufacturing costs within each regime. Key process limits have been defined, and ongoing lifetime stability testing of MCO coatings is in progress to demonstrate the effectiveness of the ASD coating approach. By correlating coating behavior with microstructural evolution within the coating/scale during high temperature oxidation, predictive lifetime models based on the mechanical and electrical degradation of the coating have been developed. These oxidation-based models have been continuously validated against the long-term stability experiments. Initial efforts have shown that the oxidation resistance of the coatings is sufficient to allow more than 40,000 hours operation. Accelerated testing protocols have been identified for expeditious evaluation of oxidation kinetics and prediction of coating lifetime.

SECA Manufacturing Cost Targets Validated for SOFC Stacks through Bottoms-Up Manufacturing Cost Analysis. A detailed, process-driven assessment of manufacturing costs of 20 kW-scale planar SOFC stacks was performed for an annual manufacturing volume of 500 MW. Leveraging existing cell and stack component cost models, high-volume process and component design investigations, and analysis support from collaborative partners, NexTech Materials, Ltd. developed a manufacturing system design and cost analysis for its SOFC stack. First, a cell cost model was established for both NexTech's electrolyte-supported *FlexCell* and anode-supported cells. Manufacturing costs of other stack components (endplates, coated interconnects, current collectors, and seals) were then determined, with endplate analysis activities led by investment casting experts BuyCastings.com. Working with automation experts Xigent Automation Systems, stack components, processes, and labor requirements were evaluated to determine appropriate levels of automation and process control methods. Particular attention was given to handling requirements of individual stack materials to ensure component integrity and quality throughout the assembly process. From these inputs, a stack assembly process was defined and all equipment identified in order to determine accurate cost contributions to the stack manufacturing process. A facilities layout was then created for the stack assembly operation, showing all unit operations and material transport systems between stations. Utilizing its manufacturing system design and cost analysis process, finally, NexTech established a comprehensive cost model for its 20 kW-scale SOFC stack, forecasting a total stack manufacturing cost of $166 per kilowatt, validating SECA's cost target of $175 per kilowatt at high-volume production scale.

SECA Core R&D – Fuel Processing

Exclusive Patent License Signed with Pyrochem Catalyst Corporation. Pyrochem Catalyst Company will commercialize two NETL catalysts that reform diesel fuel to hydrogen and enable other chemical and refining processes. The licensing agreement marks the first time a start-up company has been established using NETL technologies. NETL research has focused on converting heavy hydrocarbons, such as diesel and coal-based fuels, into hydrogen-rich synthesis gas, a necessary step for fuel cells and other applications. The high sulfur and aromatic content of these fuels poses a major technical challenge, since these components can deactivate reforming catalysts. The first of NETL's patent-pending technologies relates to using catalysts with a pyrochlore-type structure to reform hydrocarbon fuels, while the second involves a method for designing a reforming catalyst. Together, these inventions help overcome limitations of current catalysts by efficiently reforming diesel fuel while maintaining thermal stability and resistance to sulfur, aromatics, and carbon formation.

Fuel Processing Book Published. NETL researchers have edited a book entitled Fuel Cells: Technologies for Fuel Processing. The book, published by Elsevier in April 2011, is available in hardcover and a Kindle version. Several of the chapter authors are affiliated with NETL, while others are well-known global contributors from industry, academia, government research laboratories, and foreign institutes. Despite the increasing technical and commercial importance of fuel cells, few books have addressed the critical subject of fuel reforming technology in a comprehensive fashion. This book provides an overview of the most important aspects of fuel reforming to the generally interested reader, researcher, technologist, teacher, student, or engineer. The coverage includes all aspects of fuel reforming: fundamental chemistry, modes of reforming, catalysts types, catalyst deactivation, fuel desulfurization, reaction engineering, thermodynamics, heat and mass transfer, system design, and recent research and development. This book will serve as an excellent self-instruction book for those new to fuel cells or as a comprehensive resource for experts in the area of fuel processing. The material is presented in such a way that it can also serve as a reference for graduate level courses, fuel cell developers, and fuel cell researchers.

Molten Catalytic Coal Reactor to Produce High Methane Content Syngas for SOFC Power Plants. NETL will generate a high methane content syngas via the steam gasification of coal with molten alkali salts

as catalysts. The high methane content syngas is an ideal fuel for generating electricity in a SOFC because it significantly reduces the parasitic cooling loads of the SOFC. The integration of a molten catalytic gasifier or a fluidized bed catalytic gasifier with a SOFC is one of only a few ways to reach an overall electrical efficiency of 60% while allowing the co-production of hydrogen and/or methane during times of off-peak electricity demand. The goal of NETL's research is to expand the operating range of molten catalytic gasifiers. The operating temperature of the reactor has been lowered by using mixed alkali salts, and the pressure of the reactor has been lowered, while maintaining sufficient production of methane, so as to improve integration with SOFCs that operate at or near atmospheric pressures. NETL has successfully operated a new design of the molten catalytic reactor. Tests that study the effect of both pressure and temperature have been completed, and tests on the effect of coal-to-catalyst and carbon-to-steam ratios are nearing completion. NETL also conducted exergy analyses of two power plant configurations that integrate a catalytic gasifier with a pressurized SOFC. In both cases, the power plants were ~62% efficient in converting the exergy of the coal into electricity.

Cost-Effective Diesel Reformer Operation Demonstrated for Water Neutrality. Precision Combustion, Inc. (PCI) has successfully demonstrated efficient, durable, fuel flexible autothermal reformer (ATR) operation under water neutral condition. The parasitic losses related to the operation of the fuel processor unit were minimized by utilizing a novel low pressure nozzle for the introduction of fuel, air, and steam to the catalyst in the reformer unit. This low pressure nozzle was further developed, optimized, and tested for turndown and cold-start capability. The durability of the nozzle has been evaluated for over 100 hours by integrating it with an ATR fuel processor and operating it with Tier II diesel and sulfur-containing distillate fuel. The test demonstrated stable catalyst and nozzle performance under water neutral condition. This result is significant because it permits reduction in parasitic power requirements of an auxiliary power unit system while providing uniform flow and reliable performance over a wide operating range. To date, the operating conditions of the low pressure ATR unit have been optimized and the reactor performance has been characterized and evaluated. Additionally, through the Phase II supplemental effort awarded in 2010, PCI has successfully scaled up the preparation method for an alternative, cost-effective catalyst and performed multiple tests to determine the applicability, effectiveness, and durability of this material for practical, low-cost, stand-alone diesel fuel ATR operation. Finally, preliminary testing of PCI's fuel reformer using biodiesels was successfully performed to demonstrate the fuel flexibility of the reformer system.

SECA Core R&D – Modeling and Simulation

Micro-Scale Model Developed to Describe Oxygen Reduction on LSM-YSZ Cathodes in SOFCs. NETL RUA fuel cell researchers at West Virginia University have recently completed a one-dimensional micro-scale model describing oxygen reduction in a LSM-YSZ cathode system that is standard in SOFCs. The model assumes a detailed oxygen reduction mechanism featuring competitive oxygen adsorption pathways split broadly between surface and bulk oxygen transport. Assumption of competitive oxygen transport pathways allows evaluation of oxygen distribution between two-phase boundary and three-phase boundary routes as a function of the assumed cell power output and concomitant global overpotential. Knowledge of the oxygen distribution and associated local overpotential (local resistances to transport) is necessary to inform more complex models of cathode degradation that are needed to accurately predict long-duration SOFC performance. This initial version of the model will be extended over coming months to three dimensions, will include real cathode microstructural information, and will be used to make electrochemical impedance predictions. The model was the subject of a conference paper presented at the Twelfth International Symposium on Solid Oxide Fuel Cells (SOFC-XII) during the Electrochemical Society's 219th Annual Meeting in Montreal, Québec, Canada, May 1–6, 2011.

Sintering of Cathode Contact Materials in SOFC Stacks Simulated. Pacific Northwest National Laboratory has developed modeling tools to evaluate the effects of material volume change on mechanical stress during formation of the cathode contact layer in SOFC stacks. Volumetric changes resulting from contact material sintering are important to determine residual stresses and reliability for the cell components. The previously developed constitutive model was used with experimental sintering data for a candidate material (LSCF with 3 mol% CuO as a sintering aid) to simulate cathode contact densification in a five-cell planar stack during a two-hour 930°C heat treatment. Contact layer stresses after sintering and during electrochemical operation were generally within the estimated 15 MPa allowable strength, but large regions exceeded the allowable strength after stack shutdown. The final relative density reached a maximum of only 72% and exhibited significant variation across each cell, but this density distribution was similar for all cells in the stack and attributed to the stiffness of the cell support frame. A beneficial effect on final relative density of the contact

layer was observed for a smaller initial grain size or thermal expansion coefficient.

Official Software Package, User Manual, and Example Cases for Two-Dimensional (2D) SOFC-MP Modeling Tool Released. The SOFC Multi-Physics (SOFC-MP) 2D modeling tool developed by Pacific Northwest National Laboratory was documented and released. This simulation tool is used to quickly evaluate the distributions of current density, voltage, species, and temperature in tall symmetric SOFC stacks. A user manual for 2D SOFC-MP was published and includes instructions for software installation, model input creation, solution, and results evaluation. The manual also includes several example cases to demonstrate usage of the software. An official software package, including the installation files, utilities, documentation, and example cases, was released.

Multi-Physics Computer Code Developed and Tested. RRFCS has developed a multi-physics SOFC computer code (MPC) for performance calculations of the RRFCS fuel cell structure to support fuel cell product design and development. The MPC is based in the STAR-CCM+ (from CD-adapco) computational fluid dynamics software package, which has been enhanced with new models that allow for coupled simulations of fluid flow, porous flow, heat transfer, chemical, electrochemical, and current flow processes in SOFCs. Simulations of single-cell, five-cell, and substrate models have been successfully validated against experimental data obtained by RRFCS. The MPC includes a set of Java (from Oracle) macros to automate STAR-CCM+ tasks and an Excel (from Microsoft) spreadsheet to store model inputs. These features have been extended to fully automate all activities within STAR-CCM+ (mesh generation, model installation, and running and post-processing simulations), which greatly reduces the time to build new models and will facilitate MPC use outside of the code development team.

SECA Core R&D – Balance of Plant

Reliable High Temperature Recycle Cathode/ Anode Blowers Made Possible for Large SOFC Power Plants. R&D Dynamics Corporation has proved the feasibility of a reliable high temperature recycle blower. The blower is designed such that it can be dually used as a cathode or anode recycle blower. It is high temperature capable (up to 850°C), efficient, reliable, oil-free, maintenance free, and easily scalable. The recycle blower will increase the overall plant efficiency of large SOFC power plants. The blower was manufactured and tested at ambient temperature conditions.

Low Cost, Regenerable Sorbent Developed to Enable 100% CO_2 Capture on Fuel Cell Power Generation Systems. To achieve efficient power production from domestic coal with CO_2 capture, technologies are needed to oxidize the residual fuel from the anode exhaust of SOFCs so that the CO_2 can be isolated. To economically oxidize residual fuel in the SOFC anode exhaust, TDA Research, Inc. has developed an oxygen sorbent which can burn the residual fuel. Thus, the fuel is oxidized without being diluted with nitrogen and without requiring an air separation unit. Recently, experiments have shown that TDA's oxygen sorbent can reduce the residual anode fuel rapidly to very low levels (10 ppmv CO and <80 ppmv H_2). This means the process will be extremely effective at completely oxidizing the residual fuel, allowing all energy remaining in the anode-off gas to be utilized and maximizing the efficiency of the plant. FuelCell Energy carried out a preliminary system design (using the methodologies and guidelines of the SECA program) to assess how the technology best integrates into an integrated gasification combined cycle system. This work showed that TDA's fuel oxidizer increases the net system efficiency (based on coal higher heating value). The system efficiency when integrated with TDA's anode exhaust fuel oxidizer is 59.25%, compared to 58.50% with the SECA baseline oxy-combustion fuel oxidizer (exclusive of CO_2 compression) at normal operating conditions. The factory power island cost with TDA's fuel oxidizer was also 6% lower at $350/kW versus $372/kW for the baseline SECA system with oxy-burner.

Innovative Concepts

Direct Conversion of Coal to Power Demonstrated Using Liquid Tin Anode Fuel Cell Operating on Illinois #6 Coal. The direct conversion of fuel to energy in a fuel cell is highly efficient. A new concept for direct generation of power from a variety of fuels, including coal and biomass, called ElectroChemical Looping[1] (ECL) has been proposed by CellTech Power LLC. ECL combines a new type of fuel cell that uses a liquid tin anode and the direct conversion of fuel with the liquid tin to simplify multiple processes, which reduces inefficiency and lowers capital cost compared to other advanced baseload technologies. For instance, there is no oxygen plant or gasifier required. CellTech Power has demonstrated the feasibility of direct coal conversion to electricity in a liquid tin anode solid oxide fuel cell (LTA-SOFC) in a laboratory-scale prototype by continuously feeding Illinois #6 coal onto a surface of molten tin for 24 hours. The prototype achieved

[1] The electrochemical aspect refers to the highly efficient production of power without combustion while the looping concept refers to the shuttling or "looping" of oxygen by the liquid tin anode.

adequate gravimetric separation of reaction products (ash and exhaust gas) from the molten tin anode. This provides additional proof-of-concept validation for the use of LTA-SOFC in a direct coal environment.

The core fuel cell technology for ECL has been demonstrated in small scale on complex liquid fuels. The commercialization for small power applications provides an important link to development of large-scale generation technologies. The current plan of action to accelerate ECL development includes further work on key risk items at the cell level. Key risk items such as coal ash, contaminant solubility in liquid tin, and the impact of contaminants on the performance and durability of the fuel cell components are under investigation. Early results indicate that molten tin is able to separate, reduce, and remove some key contaminants under various conditions, thus demonstrating the technical feasibility of direct coal conversion in a liquid tin anode. The preliminary system analysis of a 250 MW coal power plant using liquid tin shows a system level fuel efficiency of 61% with carbon dioxide separation at comparable cost. The ECL roadmap incorporates early revenue from markets such as portable power and distributed generation, providing near-term reliability improvement while reducing the time and risk associated with development of baseload applications.

Liquid Tin Anode Solid Oxide Fuel Cell Demonstrates Ability to Withstand High Amounts of Sulfur. The most challenging volatile impurity in coal for use in a fuel cell is sulfur. CellTech Power LLC is exploring the technical merit and feasibility of incorporating an LTA-SOFC in an in situ gasification configuration. The target fuel for this evaluation is Illinois #6 coal, which is the highest sulfur content coal (5 wt%) in the United States. The technical approach includes testing the LTA-SOFC cell using a simulated gas stream of H_2S in H_2 with concentrations comparable with and exceeding the total sulfur content in Illinois #6 coal. CellTech has demonstrated stable performance of the LTA-SOFC operating on H_2 with a higher sulfur content (3.6 wt% at high flow rate) than the sulfur content in Illinois #6 coal, thus demonstrating technical feasibility of the "In Situ Gasification" concept.

Low Degradation, High Performance of LSCF-Based SOFCs Successfully Demonstrated. GE Global Research has made significant progress in mitigating performance degradation of LSCF-based SOFCs. A high-performance LSCF-based cathode architecture and processing route was demonstrated to have no measurable performance degradation over 1,000 hours at 800°C measured at 0.7 V using a gold cathode current collector. Subsequent test results using 441HP ferritic stainless steel current collectors with protective spinel coatings, operating at ~1 W/cm^2, yielded a 1.9%/1,000 h power density degradation rate that decreased with time and approached an asymptotic value over the 1,500 hour test. The observed resistance increase was purely ohmic, with no loss in catalytic activity. Further, the resistance change could be directly attributed to the resistance associated with the anticipated growth of chromium oxide on the stainless steel current collector. This accomplishment contributes to the overall SECA goals of <2%/1,000 h degradation and <$100/kW stack cost.

Fuzzy Logic Schemes Applied to Control a Fuel Cell Turbine Hybrid Power Plant. A novel fuzzy logic control methodology was developed to regulate and track turbo machinery synchronous speed and fuel cell cathode mass flow rate of a SOFC gas turbine (GT) hybrid. Data from the NETL Hyper hardware simulation facility were used to evaluate performance of such control with the sole use of airflow bypass valves. The work utilized empirically derived transfer functions as the system model and applied a fuzzy logic control algorithm that was tested in a numerical environment for various perturbations of turbine load and fuel cell heat exhaust. Theoretically, fuzzy logic control algorithms could be applied over non-linear regions of operating space, or even to scaled systems of similar configurations. The results of the numerical study showed that, for a pressurized SOFC/GT hybrid system, it is possible to simultaneously track and regulate fuel cell airflow and turbo machinery speed with the sole use of airflow bypass valves when the perturbations remain near the nominal operating point. The use of a nonlinear controller combined with linear decoupling and disturbance compensation techniques can facilitate the realization of a fuel cell power generating system under synchronous operation of the gas turbine system. An article detailing this work was accepted for publication in the conference proceedings of the 2011 Energy Sustainability and Fuel Cell Science, Engineering and Technology conference.

Robust, Real-Time Spatial SOFC Model Developed for Hardware-Based Simulation of Hybrid Power Systems. A one-dimensional, real-time operating SOFC model has been developed and integrated into the Hyper facility at the NETL. The model is capable of characterizing operation of an SOFC and driving hardware used to simulate the SOFC operating in a hybrid arrangement. Hardware used to simulate the fuel cell has been physically integrated with significant process equipment, including turbo machinery and heat exchangers. The SOFC model is also coupled to a real-time gasifier model so that fully coupled integrated gasification fuel cell dynamics can be evaluated and control strategies can be developed. The capabilities of the model were demonstrated through case studies investigating SOFC internal dynamics during inert heat-up and a step change in fuel cell current demand. Spatio-temporal plots of SOFC solid and oxidant stream

temperature; spatial temperature gradients; and temporal temperature derivatives, Nernst potential, current density, species concentrations, and electrochemical losses were all presented, analyzed, and discussed as well. The model algorithms and results were verified using benchmarks provided by the International Energy Agency and National Fuel Cell Research Center. An article detailing this work was accepted for publication in the conference proceedings of the 2011 Energy Sustainability and Fuel Cell Science, Engineering and Technology conference. The integrated model in the Hyper facility is the only hardware-in-the-loop simulation of a fuel cell hybrid anywhere in the world.

NETL RUA Electrochemically Characterizes Liquid Metal Anode SOFC. NETL RUA researchers have developed an experimental apparatus and measurement techniques that facilitate performance evaluation of a novel SOFC concept featuring a liquid metal anode made of tin. The liquid metal anode systems operate between 800 and 1,000ºC and are being investigated for their ability to directly receive processed and unprocessed fuels including hydrogen, synthesis gas, coal, and graphitic carbon. The specialized apparatus and testing methods developed in this research have been used to complete electrochemical impedance spectroscopy investigations, which reveal the mechanistic processes by which the solid fuel reacts with oxygen to produce electricity. Recently completed experiments on hydrogen have collected repeatable, low-noise impedance data that exhibit a decrease in the mass transfer resistances as temperatures increase. The data are fit by electrochemical impedance models with high accuracy, and results are compared to a virtually identical reactor at NETL in Morgantown, West Virginia, to ensure data quality. Kramers-Kronig transformations have been performed to validate quality of the obtained data, and all observed data have been determined to be internally consistent. Equivalent circuit models using Gerischer or Warburg elements have been developed to describe electrochemical and transport processes in the cell. A full description of the testing apparatus and recently collected results was accepted for presentation at the 220th Electrochemical Society meeting in Boston, Massachusetts, October 9–11, 2011.

NETL RUA Characterizes Oxygen Transport in Liquid Tin Using *ab initio* Techniques. NETL RUA researchers have recently completed *ab initio* molecular dynamics simulations describing the diffusion of oxygen through pure liquid tin, and subsequently extended the method to screen a series of binary and ternary tin alloys for enhanced oxygen diffusion performance. This first known computational chemistry study of a liquid tin/oxygen system supports development of the liquid metal anode solid oxide fuel cell, an advanced fuel cell concept designed for direct fueling with materials such as hydrogen, synthesis gas, coal, and biomass. Initial research focused on proper formulation of the research problem, and the computational methods were tuned by comparing with experimental data for liquid tin properties (density, structure, diffusion constant) and binary tin oxides (lattice parameter, enthalpy of formation, phase diagram) until close agreement was obtained. Based on the proven computational algorithms and model assumptions, predictions were then made for the oxygen diffusion in the liquid tin system. Models predict an oxygen diffusion coefficient of $9.0*10^{-5}$ cm^2/sec at 800ºC, and compare very favorably with the NETL RUA experimentally measured value of $9.2*10^{-5}$ cm^2/sec at 800ºC. The excellent agreement in the tin/oxygen system has permitted identification of promising binary and ternary alloys, accelerating anode development by limiting the number of alloys that must be experimentally investigated. The computational methodology and initial results were accepted for presentation at the MS&T ‘11 Conference in Columbus, Ohio, October 16-20, 2011.

Advanced Electrolyte-Supported Planar SOFCs Demonstrated. NexTech Materials, Ltd. is validating an advanced planar SOFC design for megawatt-scale power generation systems. This design, termed the FlexCell, offers intrinsic scalability to large areas, as well as other important attributes that translate to high performance and efficiency. The overall goal of the project is to demonstrate these promising attributes with electrolyte-supported FlexCells made with YSZ. NexTech has demonstrated high performance in YSZ-based FlexCells and has scaled their fabrication to 500 cm^2 areas. A manufacturing cost analysis confirmed that full-scale (250 MW) production costs of FlexCells will be less than $50/kW, and paths were identified to reduce costs to less than $40 per kilowatt. Since this project was initiated in 2008, NexTech has transitioned all of its stack fabrication and testing work to YSZ-based FlexCells and has fabricated more than 700 FlexCells of varying sizes.

Improved Flowfield Structures for Direct Methanol Fuel Cells Developed. NuVant Systems, Inc. has developed a novel configuration for direct methanol fuel cells (DMFCs) that offers the use of highly concentrated fuel streams with reduced fuel crossover within the fuel cell. This reduced crossover improves the performance characteristics of the fuel cell while simultaneously increasing the fuel efficiency and power generation per unit volume of fuel solution (also known as gross fuel energy density). This configuration required a design of a porous graphite barrier plate that would regulate the delivery of methanol fuel (which can be synthesized from gasified coal) to the cell electrodes while also acting to normalize the fuel concentration across the surface of the electrode. The design of this

plate, referred to as an integrated flowfield diffusion layer (IFDL), was evaluated and optimized using Fluent computation fluid dynamic modeling software. Graphite IFDL plates were fabricated and placed within a single-cell assembly for testing with DMFC membrane electrode assemblies. These cells were able to achieve gross fuel energy densities of up to 781 Wh/L with fuel utilizations of over 79% for periods of up to 80 hours. Work is continuing with the objectives of increasing the gross fuel energy densities to over 1,000 Wh/L and demonstrating operation for several hundred hours with little or no decrease in power output. A multi-cell stack (several fuel cells electrically connected in series in one piece of hardware) has been constructed, and testing and evaluation is currently underway to verify the performance levels observed in the single-cell mode and to identify cell-to-cell variations.

Multifuel Small Scale SOFC Distributed Generation System Demonstration Sites Selected and Design Completed. Technology Management, Inc. (TMI) has completed site selection and system design for a demonstration at end-user sites of the TMI residential scale prototype SOFC system. The TMI system is expected to provide the basis for a new paradigm for power production and integration to utility smart grids – massively distributed generation. These small scale systems would operate 24 hours a day, 7 days a week on either conventional or renewable biofuels, producing cost-effective, uninterruptible electric power for on-site use and grid export with the option for recovered heat for cogeneration, thereby transforming today's residential power grid. Small on-site generation provides a critical missing component to the smart grid equation – intelligent on-site power generation that can adapt to user loads.

Highly Active Cu-Ni/YSZ Anodes Demonstrated for Direct Electrochemical Oxidation of Hydrocarbons and Solid Carbon Fuels. The University of Akron has synthesized and characterized Cu-Ni/YSZ anode catalysts for their activity towards direct electrochemical oxidation of hydrocarbons and solid carbon fuels. The catalysts were prepared by electroless deposition of copper (i.e., Cu^0) over conventional Ni/YSZ anodes. The activity of the Cu-Ni/YSZ and Ni/YSZ anodes was investigated by measuring the performance of the fuel cell (i.e., the voltage-current polarization curves) in H_2, CH_4, and carbonaceous materials (i.e., pet coke, coal, and biomass). The microstructure and chemical composition of the anode electrodes prior to and after testing experiments were studied by scanning electron microscopy and energy dispersive spectroscopy. Initial results from this study show that electroless deposition of Cu over the Ni/YSZ anode can lead to dramatic improvements in the activity and resistance of the fuel cell to deactivation by coking during exposure to hydrocarbons. The development of materials that increase the carbon-surface reaction/conversion and extend the resistance of the fuel cells to deactivation constitutes a key step toward demonstrating the technical and economic viability of a coal-based fuel cell.

SECA Adds SBIR Projects

Two new Phase I projects were selected in 2011 under SBIR solicitations. FCE will develop a catalytic heat exchanger for oxidizing residual fuel to provide heat for cathode air streams (FE funded), and Materials and Systems Research, Inc. will develop catalysts for cathode infiltration to increase cell power density (BES funded). Mo-Sci Corporation will reactivate work on a compliant seal based on a promising viscous glass as a Phase II project.

2011 Annual SECA Workshop in Pittsburgh, Pennsylvania

The SECA program held its 12th annual workshop July 26-28, 2011, in Pittsburgh, Pennsylvania. Ram Sastry, the Director of Research & Technology, Customer & Distribution Services from American Electric Power was the featured speaker. Principal investigators of projects made oral and/or poster presentations on recent findings, conclusions, and recommendations, which will be used by DOE to guide future work and by to make programmatic and funding decisions for the upcoming fiscal years. The workshop proceedings can be found on the program's website at http://www.netl.doe.gov/seca.

R&D 100 Award

A coating for SOFC interconnects developed collaboratively by NETL was recognized by R&D Magazine as among the 100 most technologically significant products to enter the marketplace in the past year. These prestigious annual awards, known as the "Oscars of Invention," are selected by an independent panel of judges and the editors of R&D Magazine. A manganese-cobalt (Mn-Co) spinel coating was specifically tailored for interconnects of SOFCs. The coating was designed to prevent the evaporation of chromium from the ferritic stainless-steel-based interconnect while maintaining the electrical conductivity of the interconnect system. The coating was co-developed with West Virginia University and was transferred to Faraday Technology Inc., which has continued to develop and optimize the coating.

Summary

SECA met its final power block cost goal of $400/kW (2000 dollars) in 2010. Driven by Industry Team feedback and extensive systems analyses, SECA is now aggressively pursuing R&D to address remaining commercialization hurdles, with particular emphasis on SOFC stack robustness, reliability and endurance. The near- to mid-term goal is the validation of scaled, low-cost entitlement stacks in a system configuration, up to and including modules suitable for use as the building blocks of multi-MW systems.

SECA will ultimately enable fuel cell-based near-zero emission coal plants with greatly reduced water requirements and capable of capturing 99% of carbon at costs not exceeding the typical cost of electricity available today. Achievement of this goal will have significant impact for the Nation, given the size of the market, expected growth in energy demand, and the age of the existing power plant fleet. This is particularly important to the Nation's energy security, given that coal is our most abundant domestic energy resource. Federal funding support of this research is appropriate given the game changing nature of the technology, accompanied by risks higher than the private sector initially can accept. In parallel, SECA Industry Teams will take advantage of the inherent scalability and fuel flexibility of SOFCs in seeking nearer-term, smaller-scale commercial applications for this efficient, environmentally friendly technology which have less risk than a first-of-a-kind full-scale IGFC (or NGFC) system. Success in these spin-off applications (e.g., distributed generation, military, etc.) will further SOFC technology advancement and widespread commercial deployment through the resultant manufacturing and operational experience.

II. SECA INDUSTRY TEAMS

A. Coal-Based Systems

II.A.1 SECA Coal-Based Systems – FuelCell Energy

Hossein Ghezel-Ayagh
FuelCell Energy, Inc.
3 Great Pasture Road
Danbury, CT 06813
Phone: (203) 825-6048; Fax: (203) 825-6273
E-mail: hghezel@fce.com

DOE Project Manager: Travis Shultz
Phone: (304) 285-1370
E-mail: Travis.Shultz @netl.doe.gov

Subcontractors:
Versa Power Systems, Inc., Littleton, CO
WorleyParsons Group, Inc., Reading, PA

Contract Number: NT41837

Start Date: February 27, 2004
End Date: September 30, 2012

Fiscal Year (FY) 2011 Objectives

- Improve anode supported solid oxide fuel cell (SOFC) components to enhance cell performance, lower performance degradation rate, and decrease cost.
- Incorporate the cell component improvements in fabrication of scaled-up cells and stacks.
- Enhance stack robustness and reliability during assembly, conditioning, transport and operation (steady-state and transient) at system representative conditions.
- Conduct a 5,000 h test of a 96-cell, scaled-up (15 kW) stack to demonstrate a steady-state degradation of <2%/1,000 h.
- Verify factory cost of SOFC stack is ≤$175/kW (2007 United States dollars [USD]) at high production volumes.
- Design, fabricate and test an assembly of 60 kW stack module hardware to demonstrate fit, finish and functionality of the components design and assembly procedures.
- Develop the preliminary design of a ~250 kW proof-of-concept module (PCM) unit, including SOFC stack module and balance-of-plant (BOP) equipment, for future demonstrations.

FY 2011 Accomplishments

- Improvements in cell materials have reduced performance degradation at 750°C to <0.3%/1,000 h (at 500 mA/cm^2, over ~16,000 h period), in an 81 cm^2 active area cell. Cell performance degradation rates at 650°C and at 800°C have also been reduced to <0.5%/1,000 h (at 500 mA/cm^2, over 5,000-11,800 h test periods), in 81 cm^2 active area cells.
- Thin anode substrate cells with increased mechanical strength have been developed for cost reduction and improved operating performance. These cells, scaled up to 550 cm^2 active area (25 cm x 25 cm cell size) and implemented in 16-cell stacks, have shown a performance improvement of up to 8% at high fuel utilization conditions compared to baseline cells (Phase I). These cells offer cost reductions of 20-30% through material reduction and processing time optimization, corresponding to a savings of ~$20/kW.
- Manufacturing processes were developed for scaled-up (25 cm x 25 cm) cells based on the third generation of high-performance technology using tape-casting, screen-printing and co-firing (TSC-3) process, optimized to take advantage of the new cell materials and thin cell technology. Over 1,000 thin cells have been fabricated.
- A 120-cell stack built for the Phase II metric test, using thin TSC-3 cell technology, generated 25.2 kW of peak power (over 22 h test period). The stack generated a direct current (DC) power output of 20.2 kW during long-term steady-state testing at normal operating conditions. The 120-cell stack metric test successfully met DOE's requirement of completing 1,500 h of testing before end-of-Phase II, with an average power degradation rate of 0.9%/1,000 h which is well below DOE's requirement of ≤2%/1,000 h.
- The first 96-cell stack block, representative of the manufactured building blocks for large-scale modules (>250 kW), was fabricated and tested. Test procedures were developed for the final quality control and check of the assembled stacks prior to integration in the stack modules.
- Design of the 60 kW SOFC power module, an intermediate step in module development, has been completed. The bill of material and engineering drawings for the 60 kW module have been prepared. Components for the 60 kW module were fabricated. Tests of the assembled components, including four mock stacks, are planned for the last quarter of FY 2011.
- Design of the system configuration for the 250 kW SOFC PCM, offering an electrical efficiency of 61% (based on lower heating value of natural gas), was further developed. As part of the BOP component related testing, performance testing of the pre-reformer monolithic catalyst has been conducted, showing that the catalyst meets process requirements.

- A baseline integrated gasification fuel cell (IGFC) system (~670 MW nominal) utilizing catalytic gasification and capturing >99% of carbon (as CO_2) in the syngas was developed with an electrical efficiency of 58.7% (high heating value [HHV] of coal), surpassing the U.S. Department of Energy (DOE) target for an atmospheric pressure SOFC plant. The baseline system was designed to consume 75% less water compared to pulverized coal combustion plants utilizing scrubbing technology for carbon capture.
- Factory cost estimates for both the stack and power island of the baseline IGFC power plant were developed and audited by a third party auditor. The SOFC stack cost estimate is $85/kW and the power island (IGFC plant) factory equipment cost is $372/kW ($287/kW BOP cost). The cost numbers are based on the peak power output of 671.8 MW net alternating current (AC) and 2000 USD, and assume annual production level of two plants per year. The cost estimated exceeded the Solid State Energy Conversion Alliance (SECA) Phase II targets of ≤$100/kW (2000 USD) and ≤$400/kW (2000 USD) for stack and power island costs, respectively.

Introduction

FuelCell Energy, Inc. (FCE) is in Phase III of a multi-phase project to develop SOFC modules and power blocks for application in coal-based IGFC power plants. The primary objective of the project is to develop affordable and highly efficient multi-MW SOFC systems that have near-zero emissions of oxides of sulfur and nitrogen, low water consumption, and capture >90% of greenhouse gases (carbon dioxide).

FCE utilizes the SOFC technology of its partner, Versa Power Systems, Inc. (VPS), in the development of IGFC power plants. VPS has well-established processes, quality control procedures, and equipment for the manufacturing of fuel cells. Key research and development activities for the project include: improving cell and stack operating range, improving stack reliability and robustness, reducing cell and stack costs, and reducing cell performance degradation. System development activities consist of completing conceptual design and factory cost estimation for the SOFC cell stack and power island of the multi-MW baseline power plant, and developing the preliminary design for a 250 kW PCM unit power plant.

Approach

Fuel cell development work has been focused on key cell issues related to cost reduction, endurance improvement and performance enhancement. The main technical approach includes extension of the operating temperature window, reduction of average operating temperature, thermo-mechanical strength improvement, and scaled-up cell stack fabrication process development. The emphasis is placed on the development of a thin anode substrate with increased thermo-mechanical strength. Material solutions with enhanced electrochemical properties have been evaluated. Various cell component design considerations, such as anode substrate thickness and porosity, have been evaluated to identify the optimum cell configuration for operation at high power density on coal syngas. Parameters such as performance (power, thermal management, and efficiency), design simplicity, technical risk, manufacturability, and cost have been considered in the design selection process.

Baseline power plant conceptual design focused on evaluation of process alternatives that increase power plant efficiency, meeting carbon capture requirements, and minimizing cost of the power plant's power island. Various process configuration analyses and parametric studies were conducted considering voltage, current density, fuel utilization, stream recycle levels, and process components. Concurrent with the baseline power plant design work, conceptual design of a PCM test unit continued with process configuration evaluations and operating parameter studies.

Results

The on-going endurance tests of the improved cathodes and modified anodes in single cells (81 cm^2 active area) continue to demonstrate very low performance degradation rates at 750°C. A cell test has accumulated over ~16,000 h with an average performance degradation rate of less than 0.3%/1,000 h (at 500 mA/cm^2), as shown in Figure 1. To expand the operating temperature window (for stack implementation of the cell technology), the performance degradation rate at temperatures other than 750°C, in the range 650-800°C is also being reduced. Based on better understanding of the degradation mechanism and material improvements, the performance degradation rates at 650°C and at 800°C have been reduced to <0.5%/1,000 h (at 500 mA/cm^2), over 5,000 h test periods. The test at 650°C has accumulated over 11,800 h.

A major advancement in the SOFC technology area was the development of thin anode substrate cells for cost reduction. Improving intrinsic anode substrate strength is one of the key strategies for implementing thinner cells in a stack. A new set of anode substrate materials were developed which imparted mechanical strength to the thin structure. The research and development efforts were also focused on increasing the hydrothermal stability of the new anode substrate

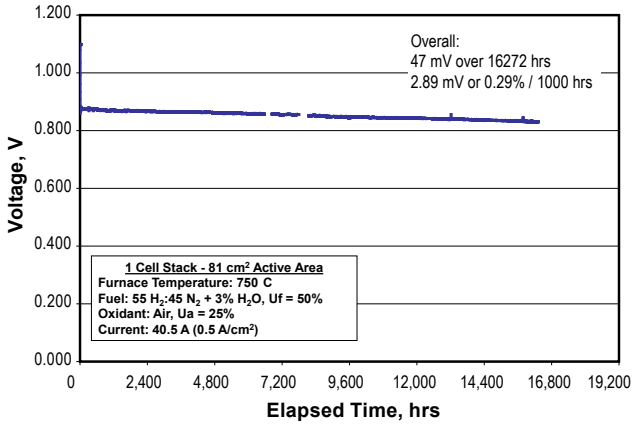

FIGURE 1. Long-Term Steady-State Test of a TSC-3 Cell (with Alloy Coating) at 750°C

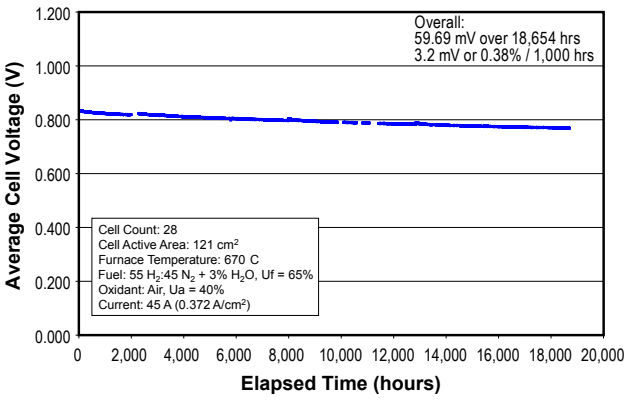

FIGURE 2. Stack Test GT056019-0132 Evaluating Advanced Pre-Coated Interconnects

material to resolve the issues related to the crystal phase transformation in the presence of moisture. Scaled-up thin cells with 40% reduction in anode substrate thickness and 25 cm x 25 cm cell size (550 cm^2 active area) were produced using the TSC-3 process. Thin cells offer cost reductions of 20-30% through material reduction and processing time optimization. This corresponds to a cost reduction of ~$20/kW. Cell manufacturing process development effort has been focused on 25 cm x 25 cm thin cells. Over 1,000 thin cells have been fabricated. The overall process yield has been improved as the advanced thin cell technology is moved from the research and development stage to the pilot manufacturing stage.

Long-term endurance tests of advanced pre-coated interconnects and cathode corrugations (flow media) in stacks have shown very low performance degradation rates. The 28-cell (121 cm^2 cell active area) stack test evaluating the pre-coated interconnect material has accumulated over 18,000 h of operation with a degradation rate of 0.4%/1,000 h, as shown in Figure 2. The 32-cell (550 cm^2 cell active area) multi-metal stack test featuring TSC-3 cells and alternating layers of the advanced pre-coated alloy and baseline stainless steel cathode corrugations (contact/flow media) has accumulated over 10,000 h with a degradation rate of 1.06%/1,000 h for the advanced pre-coated alloy cell group compared to that of 1.96%/1,000 h for the stainless steel cell group.

A stack tower (SO-30-4) was assembled consisting of two 92-cell stacks utilizing the 550 cm^2 active area TSC-3 cells. The tower was tested in a module enclosure environment, with fuel compositions representative of the system (simulated baseline power plant fuel gas). The peak power test achieved 30.2 kW DC output at 200 A and 151.0 V, with a fuel utilization of 54% and an air utilization of 12.6%. Following the peak power test, under the NOC (normal operating condition) steady-state hold, the stack tower produced an output of 27.0 kW of power at 185 A and 146.0 V, with a fuel utilization of 70% and an air utilization of 13.5%. Overall, the stack tower operated for >1,900 hours with a power degradation of 1.89%/1,000 h, based on linear regression for the NOC portion of the test, exceeding the targeted value of 2%/1,000 h. The tower tests verified the building block approach, i.e., using factory stack blocks to assemble large arrays of towers in MW-scale modules.

A 120-cell stack, using the latest TSC-3 cell technology (550 cm^2 active area), was built for Phase II metric tests. The stack featured thin TSC-3 cell design with thin interconnects. Over a 22-h peak power test period, the stack generated 25.2 kW. This corresponded to an average cell voltage of 831 mV at 459 mA/cm^2 and a power density of 381 mW/cm^2. Following the peak power test, NOCs were established for the long-term steady-state test. The stack performance at NOC corresponded to an average cell voltage of 835 mV at 367 mA/cm^2 and a DC power of 20.2 kW. The 120-cell stack metric test successfully met DOE's requirement of completing 1,500 h of testing before the end of Phase II, as shown in Figure 3. The steady-state average power degradation rate of the stack is 0.9%/1,000 h which is well below the Phase II DOE requirement of ≤2%/1,000 h.

Subsequent to the 120-cell stack tests, the next generation of 96-cell stack block was designed utilizing the advances in the TSC-3 cell and stack technology developed in Phase II of the project. A picture of 96-cell stack installed in the test stand after the assembly is shown in Figure 4.

The SOFC module concept development focused on the design of a 250 kW module, based on a stack tower array of eight towers, each tower containing two 96-cell stack blocks. The towers are arranged in two quads of four towers, with each quad assembled on a single fixed-

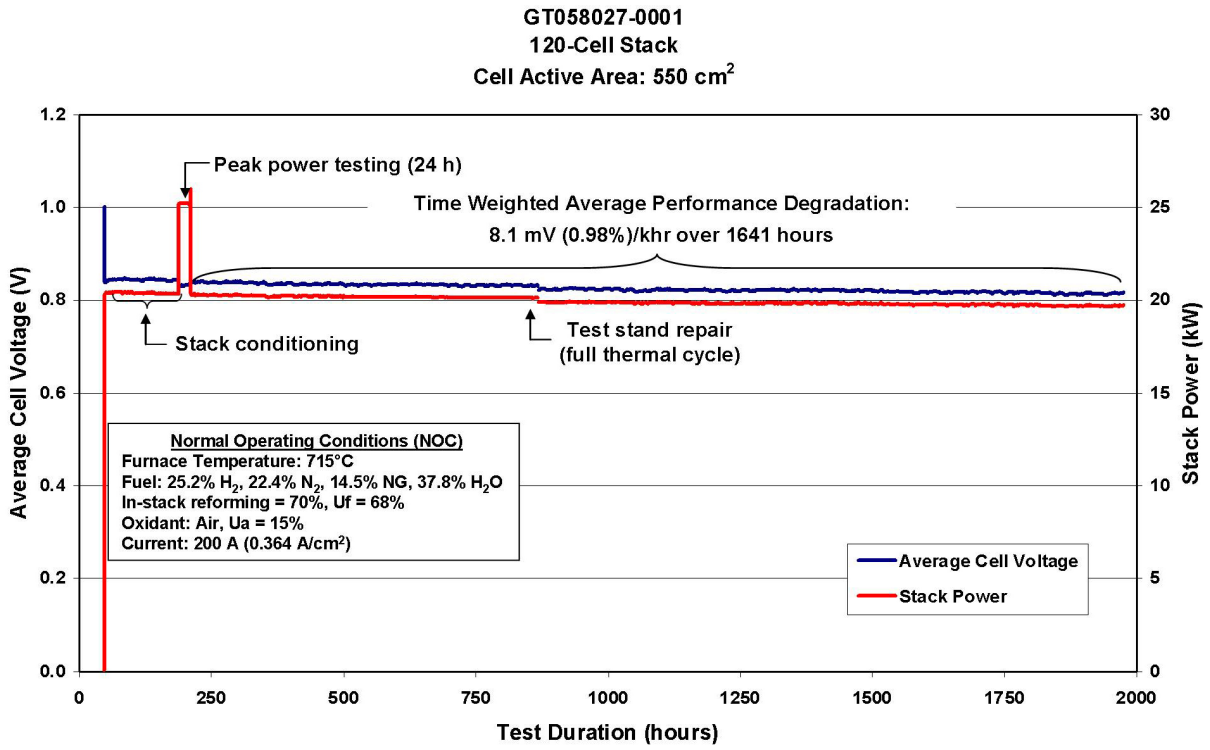

FIGURE 3. Performance Stability of 120-Cell Stack (Average Cell Voltage and Stack Power)

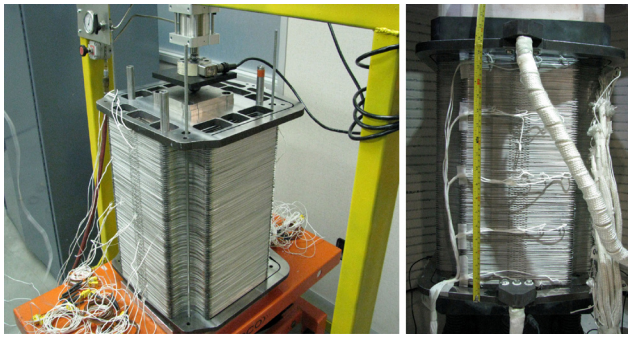

FIGURE 4. 96-Cell Stack Assembly and Stack Installed in Test Stand

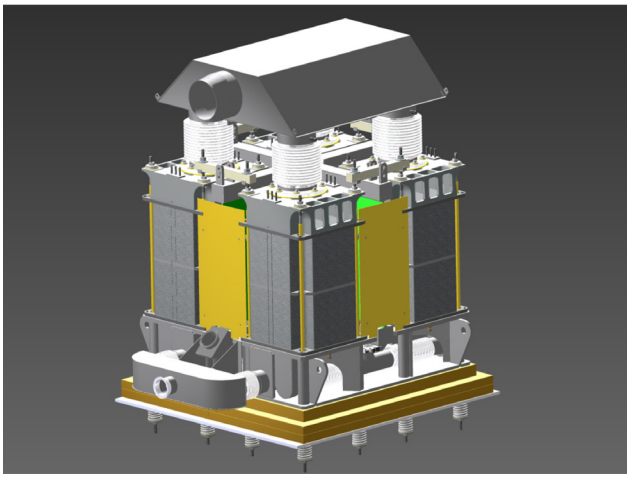

FIGURE 5. 60 kW SOFC Stack Module Assembly

end base. The quad base design, providing the support structure and facilitating the gas flow distribution to towers, is in progress.

The SOFC power module development path from the current 30 kW (two-stack tower) size to the 250 kW (two, four-tower quads) size includes a 60 kW size module as the next intermediate step (for validation testing before continuation of module scale up). Design of the 60 kW module was completed. Engineering drawings for major non-repeat components have been prepared for manufacturability review. Module components have been fabricated, including: vessel base and enclosure shell, module internal bellows, fuel gas heat exchanger, tower quad base, buss bar and combined compression plate. Figure 5 shows the three-dimensional view of the 60 kW stack assembly including 4 x 96 cell stacks arranged on a quad base.

The conceptual design for the PCM test unit is progressing with equipment sizing and selection ongoing. A heat-up plan was developed to guide design of necessary plant start up equipment. BOP equipment related testing has also been performed. Test results from performance testing of pre-reformer monolithic

catalyst have shown that the catalyst meets the process operating temperature requirements while providing the necessary level of reforming.

Advanced Baseline System configuration development and analysis resulted in a highly efficient coal-based power plant. The system employs catalytic gasification and warm gas cleanup to provide syngas fuel for the SOFC. The system also employs oxycombustion of the anode exhaust for CO_2 capture using a portion of the oxygen from the air separation unit at the gasification site. The power plant is estimated to have an electrical efficiency of 58.7% based on HHV of coal, while capturing >99% of carbon (in the syngas) as CO_2. The conceptual layout of the baseline system's power island is shown in Figure 6. The power island consists of eight sections, with 42 fuel cell modules per section. The SOFC module sections are grouped with four sections on each side of the central syngas expander, oxy-combustor, HRSG (heat recovery steam generator), and steam turbine. Piping from the centralized system equipment to the fuel cell modules is located between groups of fuel cell clusters. Clean syngas is distributed and anode exhaust is collected by the centralized power island equipment. The SOFC system consumes 75% less water compared to pulverized coal combustion plants (using scrubbing technology for carbon capture), due to the ease of water recovery from the anode exhaust. A Phase II factory cost analysis for the fuel cell stack and the baseline power island was performed. The power island factory equipment cost is $372/kW including SOFC stack cost of $85/kW and BOP cost of $287. The cost numbers are based on a peak power output of 671.8 MW net AC, assuming a production of two power plants per year. This requires the production of 43,008 stacks (stack building blocks) per year. The factory cost estimates are less than the SECA goals of $100/kW and $400/kW for stack and power island costs, respectively.

Conclusions and Future Directions

Advances in thin cell technology, combined with improvements in cell material, have resulted in leap-frogging developments in both reduction of stack cost and increased cell performance. A new generation of cells (TSC-3), combining the improved cathodes and modified anodes with thin cell technology, have been scaled up to 550 cm^2 active area. Stacks made from these cells have been operated successfully at fuel utilizations in excess of 80% and system representative gas compositions. New ground was also broken in stack scale up technology. The stack building block, based on the 550 cm^2 active area cells, was scaled up successfully from 64 to 92 cell count in a cell stack. Performance characterization tests at system representative conditions have demonstrated the 92-cell block DC power output of 18 kW. The large cell area in combination with increased stack cell count is aimed at the reduction of the overall stack cost. Cost analysis for the baseline power plant system (>400 MW) has shown that the DOE cost target of $400/kW (2000 USD) was met by the system developed.

The recently initiated Phase III of the SECA project will focus on design and fabrication of a PCM power plant unit with a beginning-of-life capacity of ~250 kW, paving the way to future multi-MW power plant demonstration and commercialization opportunities. Research and development activities will focus on supporting improvements in stack fabrication for increased reliability, better materials-of-construction, scaled-up cell manufacturing processes, and BOP equipment design. Future cell development efforts are focused on expanding the operating temperature window to accommodate larger temperature gradients in a stack while focusing on reliable, robust operation. Fabrication, testing, and post-test analyses of the fuel

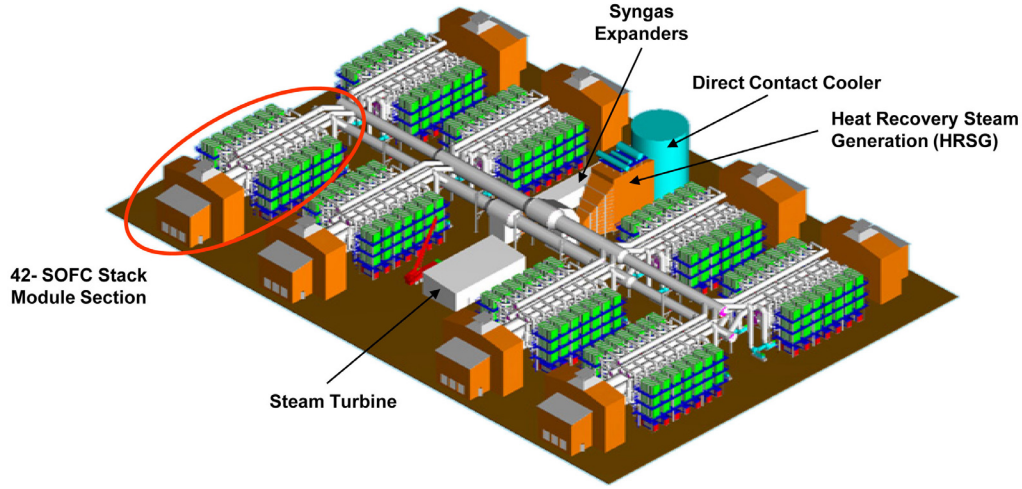

FIGURE 6. 672 MW Coal-Based SOFC Power Island Layout

cells and fuel cell stacks, culminating in the test of a ≥30 kW stack tower for 3,000 h or more, is also planned for Phase III. The stack tower test shall meet DOE cost goal of ≤$175/kW stack (2007 USD) and endurance goal (≤1.5%/1,000 h steady-state degradation). A 60 kW module, an intermediate step in module development, will be assembled for validation testing required for continuation of module scale up. The test of the thermally self-sustaining 60 kW module will be conducted for >1,500 h using system process conditions and gases.

FY 2011 Publications/Presentations

1. Hossein Ghezel-Ayagh, Richard Way, Peng Huang, Jim Walzak, Steven Jolly, Dilip Patel, Carl Willman, Keith E. Davis, David Stauffer, Vladimir Vaysman, Sunitha Asapu, Brian Borglum, Eric Tang, Michael Pastula, Randy Petri, and Mark Richards, "Advances in Development of Coal-Based Integrated Gasification Fuel Cell Systems Utilizing Solid Oxide Fuel Cell Technology," Electrochemical Society Transactions – 2010 Fuel Cell Seminar & Exposition, Editor(s): M. Williams, N. Garland, Volume 30, Issue 1, pp. 157-165.

II.A.2 SECA Coal-Based Systems - Rolls-Royce

Richard Goettler (Primary Contact), Greg Rush, Ted Ohrn, Mark Scotto
Rolls-Royce Fuel Cell Systems (U.S.) Inc. (RRFCS)
6065 Strip Avenue NW
North Canton, OH 44720
Phone: (330) 491-4821; Fax: (330) 491-4808
E-mail: richard.goettler@rrfcs.com

DOE Project Manager: Patcharin Burke
Phone: (412) 386-7378
E-mail: Patcharin.Burke@netl.doe.gov

Subcontractors:
- Rolls-Royce Fuel Cell Systems Limited, Loughborough and Derby, UK
- Case Western Reserve University, Cleveland, OH
- University of Connecticut, Storrs, CT
- Matrix Innovations, Lynchburg, VA
- Oak Ridge National Laboratory, Oak Ridge, TN
- Pacific Northwest National Laboratory, Richland, WA

Contract Number: FE0000303

Start Date: September 1, 2009
End Date: September 30, 2011

Fiscal Year (FY) 2011 Objectives

- Select the next generation active cell layers to carry forward into metric stack testing.
- Demonstrate through subscale testing that the Rolls-Royce cell/stack technology can meet the Solid State Energy Conversion Alliance (SECA) Phase I power degradation targets of <2%/1,000 hours.
- Complete modification and commissioning of block-scale pressurized test rigs for running the metric stack tests.
- Commence the metric stack test that will run 5,000 hours.
- Prepare a Factory Cost Report that estimates the high volume manufactured cost of the solid oxide fuel cell (SOFC) power module for a 100 MW integrated gasification fuel cell (IGFC) plant.

FY 2011 Accomplishments

- A next generation cell technology having an area specific resistance (ASR) of 0.29 ohm-cm^2 was selected for the ~10 kW to ~20 kW block-scale durability and reliability metric tests. The cumulative power density improvement of single cells has been 73% since the beginning of the project.
- Durability testing of the selected cell technology under system relevant conditions is showing an average power degradation rate of <0.5%/1,000 hours at the 8,500-hour mark, with testing continuing. Key degradation mechanisms have been identified with candidate optimized cell layers being screened for further reduction in the degradation rate.
- A new pressurized block test rig in Canton, Ohio, has been commissioned and a second rig in the United Kingdom (UK) has been modified to accommodate the next generation stack technology. The rigs will be used for the metric tests to commence in late FY 2011.
- A draft Factory Cost Report incorporating all the subsystems for the 100 MW power modules of the IGFC power plant was submitted and projects costs at <$700/kW for peak power densities expected from the metric test.

Introduction

The Rolls-Royce Fuel Cell Systems (U.S.) Inc. (RRFCS) SECA Program is aimed at demonstrating the viability of the RRFCS integrated-planar solid oxide fuel cell (IP-SOFC) technology, which is being developed for the distributed energy market, for eventual scale up to a megawatt scale system suitable for incorporation into centralized power generation facilities employing coal gasification and carbon sequestration. IGFC systems offer efficiencies of >50% (higher heating value), inclusive of CO_2 capture. The RRFCS stack concept is based on thin planar cells which are series-connected on a fuel-carrying porous ceramic support substrate [1-3]. These active substrates are the elemental building blocks of the fuel cell stack and are grouped together to form a megawatt-scale IP-SOFC system as shown in Figure 1. These cells are applied onto the substrates using well established thick film screen printing techniques. Contrary to other SOFC developers who seek ever larger single cell active areas, RRFCS desires smaller cells to reduce current levels and achieve lower ohmic (I^2R) losses. RRFCS currently prints 60 cells of ~1.3 cm^2 on each side of the substrate. This represents a switch in design philosophy from a low voltage, high current fuel cell to a high voltage, low current approach. Substrates having the narrow 60-cell design (adopted pre-SECA) allow the use of lower conductivity and lower cost-basis materials to meet in-plane conductance requirements which has been an important materials substitution for achieving the DOE costs targets of

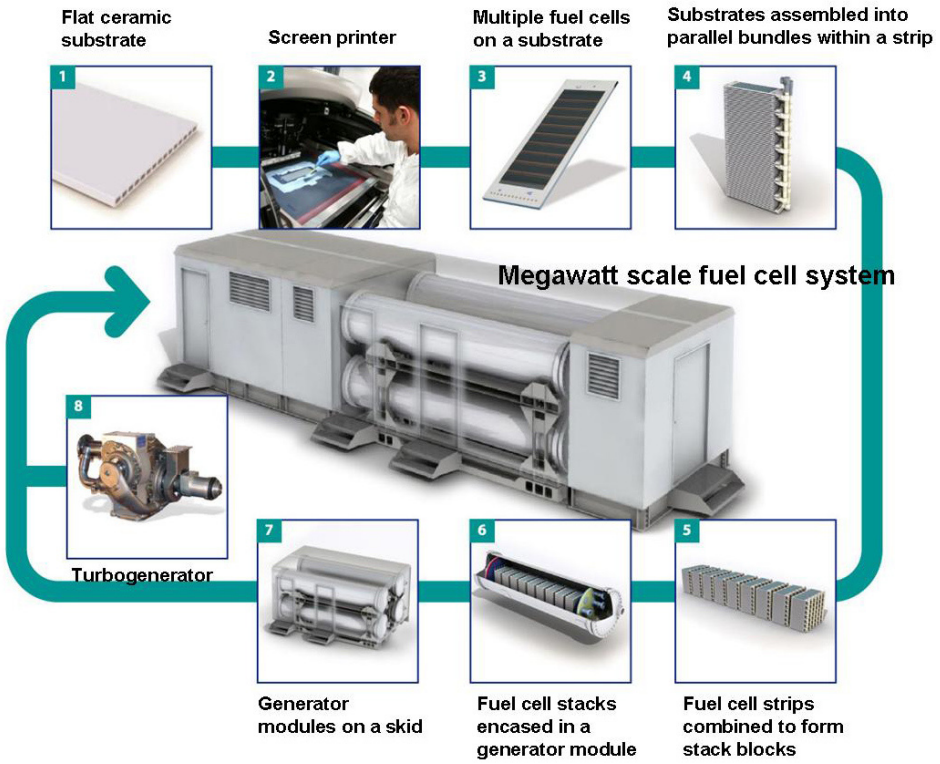

FIGURE 1. Schematic of the Planned RRFCS 1 MW Distributed Power Generation System

<$700/kWe (in 2007$). FY 2011 activities were focused on durability testing of the selected lower cost and optimized active cell layers of the 60-cell IP-SOFC technology to demonstrate meeting the SECA Phase 1 degradation targets of <2%/1,000 hours.

Approach

The RRFCS SOFC system operates at pressures up to 7 bar. Benefits of pressurized operation are improved IGFC system efficiency (DOE system models predicting 57% efficiencies inclusive of CO_2 capture) [4] with higher volumetric power densities allowing smaller footprint. RRFCS has developed in-house designed pressurized test stands ranging from subscale substrates for testing single and 5-cell articles, bundle rigs (~350 W) which tests the fundamental stack assembly unit, stack block rigs (~20 kW) and tier rigs (~125-250 kW). All scales of test rigs can duplicate the operating conditions planned for the commercial power systems and thus serve as the source of initial pre-commercialization verification of the long-term durability of the cell and stack technology. Subscale test units are highly instrumented to allow detailed breakdown of ASR between ohmic versus polarization contributions and to identify degradation sources between that of the anode, cathode and interconnect cell layers. These subscale tests are run at the extremes and mid-points of block temperature and fuel utilization to bracket degradation trends and provide estimates of the degradation trends for larger scale tests. Cell technologies meeting target degradation rates in subscale test are then tested at bundle then block level. Electrochemical models are used to analyze the performance results at all scales.

The stack block is the heart of the RRFCS SOFC power system. It contains the fuel cell stack and components of the fuel and air sub-systems that establish the thermal, flow and compositional boundary conditions for the stacks. The stack block is the basic repeat unit which will be packaged into the generator module illustrated in Figure 1. Testing at the block-scale provides representative durability and reliability testing of future product and such tests will provide the foundational database validating the commercial readiness of the RRFCS SOFC cell and stack technology. Product representative balance-of-plant components and features such as the insulation system, ejectors, and heat exchangers are included in the block test rigs to provide crucial system-level qualification as necessary to shorten the path to commercialization. The block rigs achieve product level heat balancing including representative fuel and air recycle loops and provide for thermal self-sustaining block tests. The University of Connecticut is performing assessments of the alloys selected by RRFCS for the balance-of-plant components, with particular emphasis on chromium release rates and alternate alloys and/or coatings for mitigating chromium

volatility to minimize long-term degradation associated with chromium poisoning of the cathode.

Manufacturing of the fuel cell stacks are performed on the Process Verification Line (PVL) located in Canton, Ohio, and includes a screen printing line representative of that required for a high volume factory. Current substrate/cell sizes and stack architecture are that planned for market entry product. The experience on the PVL along with the current stack assembly operations have guided the inputs for the activity-based cost model that was developed for estimating the high volume manufacturing costs for the SOFC power module. Projected power module costs meet the <$700/kW SECA target; the final cost estimate will be based on the peak power output derived from the metric stack test.

Not only must the fuel cell stack meet electrochemical performance and durability targets, it must demonstrate structural integrity to meet reliability/mean-time to failure necessary for commercial launch. Stack mechanical reliability is being investigated in collaboration with Oak Ridge National Laboratory where detailed mechanical characterization of the substrate is being performed. Substrates with the permeability characteristics for low diffusive losses are being supplied to RRFCS, and the as-received substrate and fully processed active substrates meet the specified strength requirements supported by finite element analysis. Further validation of the stack reliability will be obtained by thorough residual property measurements of stack components following long-term block-scale testing.

Results

Based on subscale-level testing and post-test analysis results, RRFCS made a final selection of the cell layers to carry forward into more exhaustive durability testing up through stack-block metric testing. The selected cell technology incorporated an optimized primary interconnect between adjacent cells of the substrate that mitigated a significant materials migration degradation mechanism that had resulted in accelerating interconnect ohmic ASR degradation in the first 1,000 hours. The primary interconnect has now shown stable ASR at <0.05 ohm-cm^2 out to nearly 9,000 hours of testing. The overall durability of the selected cell technology is highlighted in Figure 2 where power degradation rates of <0.29%/1,000 hours at stack-block midpoint conditions (860°C, mid-stack fuel composition) and <0.34%/1,000 hours for the most aggressive 925°C and 80% fuel utilization boundary condition have been demonstrated for subscale tests. These tests provide confidence in the ability of the cell technology to deliver the <2%/1,000-hour Phase I target degradation rate.

Electrochemical impedance spectroscopy (EIS) is routinely performed on the subscale test and the results of that analysis suggest that the dominant

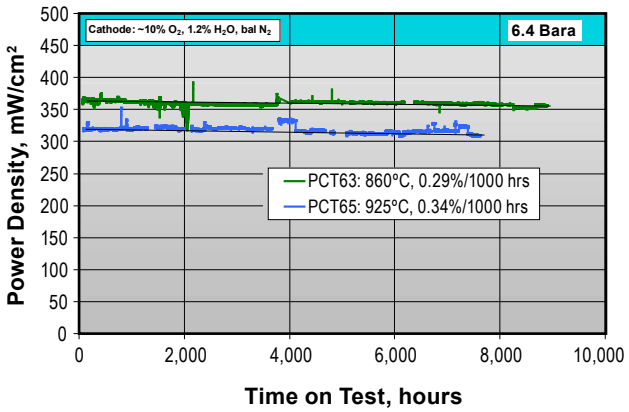

FIGURE 2. Subscale Test Article Degradation Rate of Cell Technology Selected for Phase 1 Metric Stack-Block Test

degradation mechanism is associated with the cathode. Detailed transmission electron microscopy and electron energy loss spectroscopy reveals some cathode phase segregation and optimized lanthanum strontium manganite-based cathode compositions are currently being screened to further lower the cell degradation to the levels required by DOE SECA and RRFCS for SOFC products exhibiting service life of greater than 40,000 hours. Anode degradation mechanisms, although not identified by EIS as significant for testing out to 8,000 hours, are a focus area of cell development for longer service life. Optimized and alternate anode technologies are being screened to limit microstructure coarsening and nickel volatility.

The selected cell technology is being qualified in a pressurized bundle test. The performance curves for a bundle operating at 6.4 bar$_a$ and 860°C is shown in Figure 3. The ASR at this representative average block temperature and fuel composition is 0.28 ohm-cm^2. The stack technology was optimized last year to achieve improved fuel flow uniformity throughout the bundle to allow operation at high (greater than 80%) fuel utilization while avoiding regions of local fuel starvation that could adversely impact long-term degradation rates. Figure 3 shows that the outlet substrate 6 of the bundle reached 90% fuel utilization with only limited diffusion losses. The experimental data matches closely that predicted from electrochemical models providing confidence in the accuracy of the models and their use in assessing performance of larger scale tests. Bundles running at 80% fuel utilization, corresponding to a stack direct current electrical efficiency of ~64%, show degradation rates very similar to that obtained on subscale test articles.

Over the past years, RRFCS has been operating pressurized block-scale test stands in the UK with stacks comprised of an earlier stage cell technology. These test rigs have shown reliable operation. A block test

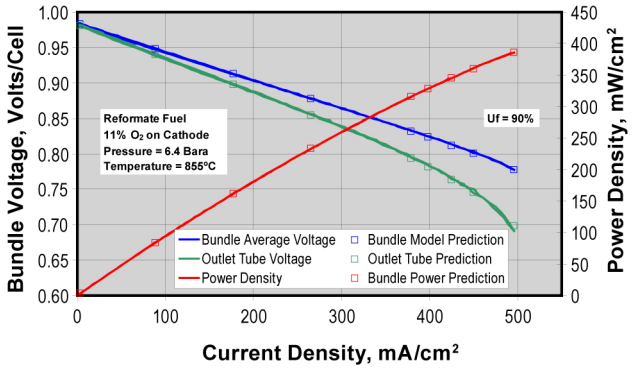

FIGURE 3. Bundle (6-Substrate) Performance to High Fuel Utilization Conditions

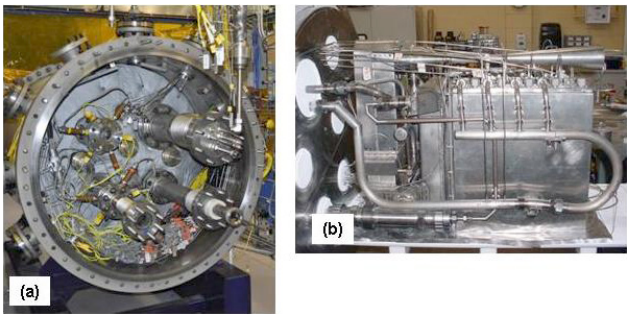

FIGURE 4. Block Test Stand Modified and Commissioned for Performing a Phase 1 Metric Stack Test; (a) Pressure Vessel with Inserted Block Chamber and (b) Block Arrangement

stand (Figure 4) has been installed in Canton, Ohio, funded by both the Ohio's Third Frontier program and RRFCS capital. The test stand has been modified under the SECA program to achieve the required IGFC system cycle configuration allowing separation of anode and cathode gas streams as is required for CO_2 sequestration. The IGFC system now closely matches the RRFCS revised natural gas cycle achieving commonality in the SOFC power module systems for both coal-fired centralized and natural gas-fired distributed power generation markets and allowing nearer-term demonstration of distributed generation system to provide validation of the technology for future IGFC plants. As shown in Figure 4b, the assembled block for these tests have a high level of system thermal integration incorporating cathode and anode recycle loops and including key product component features. The strips for the Phase I metric test are completing assembly and the test is scheduled to start Q4-FY 2011.

Conclusions and Future Directions

In FY 2011 RRFCS has made significant progress in validating the durability of its cell technology. Subscale articles tested from 7,000 to 9,000 hours at average and extreme stack conditions have exhibited degradation rates well below the SECA Phase I requirement of <2%/1,000 hour over a 5,000-hour testing period. Block tests at 10-15 kW in scale will commence in the late FY 2011 timeframe. The test rigs for the metric tests already incorporate generator module product features that provide for thermal self-sustaining metric tests that are not required until SECA Phase II, hence these Phase 1 tests will provide an accurate assessment of the performance and durability of the RRFCS technology under conditions highly representative of future power modules for both IGFC and distributed power systems. Fuel flow optimization within the stack has been achieved to insure reaching 80% fuel utilization in the metric tests while avoiding excessive diffusive losses. RRFCS is acquiring a detailed understanding of the sources of ASR degradation of its current cell technology that is undergoing long-term durability testing now exceeding one year in duration. Promising degradation rates are being measured for the current technology, and EIS and post-test analysis results has guided the selection of optimized cathode and anode layers to further reduce the degradation rate of the IP-SOFC technology towards meeting the ultimate commercialization goal of 5-year service life. The RRFCS stack is comprised entirely of ceramic substrates and manifolds with glass-ceramic based seals and joints. Validating the long-term structural reliability of the stack is a top priority. Residual property measurements from long-term block tests will provide the volume of test data required for Weibull-based ceramics analysis and reliability evaluation of structures analysis.

FY 2011 Publications/Presentations

1. B. Haberman, C. Martinez Baca, and T. Ohrn, "IP-SOFC Performance Measurement and Prediction," Proc. 219th ECS Meeting, Montreal, Quebec, Canada, May 1–6, 2011.

2. Presentation at 2011 SECA Workshop, Pittsburgh, Pennsylvania, July 26–28, 2011.

References

1. U.S. Patent 7,422,820.

2. G. Agnew, M. Bozzolo, R.R. Moritz, and S. Berenyi, *Proc. ASME Turbo Expo*., **2**, 801 (2005).

3. G. Agnew, R. Collins, M. Jorger, S. Pyke, and R. Travis, *ECS Trans*. **7**(1), 105 (2007).

4. National Energy Technology Laboratory Report DOE/NETL 40/080609, August 6, 2009.

II.A.3 SECA Coal-Based Systems – UTC Power

Praveen Narasimhamurthy (UTC Power, Primary Contact), Jodi Vecchiarelli (UTRC), Toby Junker (UTRC), Peles Slaven (UTRC), Handa Xi (UTRC), Dan Hennessy (Delphi), Andrew Rosenblatt (Delphi), Rick Kerr (Delphi), Subhasish Mukerjee (Delphi)
UTC Power
195 Governors Highway
South Windsor, CT 06074
Phone: (860) 727-2667; Fax: (860) 998-9236
E-mail: praveen.narasimhmaurthy@utcpower.com

DOE Project Manager: Joseph Stoffa
Phone: (304) 285-0285
E-mail: Joseph.Stoffa@netl.doe.gov

Subcontractors:
- Delphi, West Henrietta, NY
- United Technologies Research Center (UTRC), East Hartford, CT
- Battelle/Pacific Northwest National Laboratory, Richland, WA

Contract Number: NT0003894

Start Date: October 1, 2010
End Date: September 30, 2011

Fiscal Year (FY) 2011 Objectives

- Complete evaluation of material sets for long-term stability.
- Implement low-cost balance-of-stack components.
- Complete cell cost reduction analysis.
- Complete the stack cost analysis.
- Complete the design model for a 25 kW stack module.
- Deliver stacks for the 25 kW stack module to UTC Power.
- Initiate testing of stack module.
- Initiate layout work for 100+ kW stacks.
- Procure, build and commission a test stand capable of testing a stack up to 50 kW.
- Develop a test plan for the 25 kW stack test consistent with the Solid State Energy Conversion Alliance (SECA) minimum requirements.
- Complete a detailed system analysis of a 250-1,000 kW solid oxide fuel cell (SOFC) power module operating on either pre-reformed natural gas or coal syngas with respect to performance and operability.
- Complete the conceptual design of a 5 MW proof-of-concept (POC) system.
- Complete the system cost analysis for the baseline integrated gasification fuel cell (IGFC) system.
- Complete 1,500-hour test of Delphi ≥25 kW stack.

FY 2011 Accomplishments

- The Gen 3 stack successfully completed durability testing to 9,700 hours and deep thermal cycling to 200 thermal cycles, with a degradation rate of 1.1% per 500 hours in durability testing.
- Developed low-cost, high-volume manufacturable processes for Gen 4 stack components. Fabricated and tested multiple Gen 4 stacks in a variety of test conditions.
- A 40-cell Gen 4 stack demonstrated a maximum initial power of 6.4 kW at an average power density of 398 mW/cm^2 and average cell voltage of 0.7 volts, utilizing the SECA simulated coal gas blend. When combined into a four-stack module, this will exceed the SECA requirement of 25 kW.
- The Gen 4 stack has completed a durability test of greater than 2,500 hours and has a degradation rate of about 4% in the first 300 hours and no measurable power degradation thereafter. The successful stack test results provide confidence that the stacks have the potential to meet SECA durability goals.
- The Gen 4 stack has successfully completed 60 deep thermal cycles from 750ºC operating temperature to <100ºC with a total power degradation of less than 5%. The successful stack test results provide confidence that the stacks will survive periods of maintenance and shutdowns in larger power plants.
- Completed the design and fabrication of a 25 kW test article for the SECA peak power and steady-state tests.
- Down-selected three Power Module concepts after detailed investigation of several competing designs. All three systems were designed for 400 kW net alternating current (AC) and achieve efficiency in excess of 60% based on fuel lower heating value (LHV). Heat-up and power ramp studies were performed on all systems to define internal and external characteristics.
- Developed three IGFC designs that produce greater than 100 MW net AC power at an efficiency greater than 50% higher heating value (HHV) and capture greater than 90% carbon. Sensitivity analyses were carried out demonstrating that the designs

maintained their key performance requirements over a wide range of key operating variables.

- Commissioned the 50 kW capable test stand at UTC Power. A debug Gen 4 stack was installed into the test stand and operated to confirm test system operation.
- Completed system cost analysis for the baseline IGFC system. Preliminary cost analysis of the power block hardware for the IGFC power plant shows a cost of $685/kW in 2007 dollars with a 90% confidence interval, which meets the SECA cost requirement of $700/kW.

Introduction

In addition to its high power density, a key advantage of the SOFC system is its high system efficiency, particularly when its high temperature co-product heat can be used in combination with its electrical output. The other advantage of the SOFC is that the system could potentially be very simple with minimal requirement for external fuel processing. SOFC is also tolerant to some fuel contaminants that are known to cause degradation in stacks of other technologies such as PEM (proton exchange membrane).

Delphi has been developing SOFC systems since 1999. After demonstrating its first generation SOFC power system in 2001, Delphi teamed with Battelle under the SECA program to improve the basic cell and stack technology, while Delphi developed the system integration, system packaging and assembly.

Current and prior generation Delphi stacks have demonstrated performance that shows strong potential to meet SECA durability goals. The focus in Phase 1 of this SECA project has been on further improving the overall durability of the stack while lowering cost and improving manufacturability. In addition to large stationary applications, the same SOFC stacks can be used in other applications which are good fits for the technology, including transportation. In transportation, SOFC stacks will initially be used in auxiliary power units (APUs) to provide hotel load power to heavy-duty trucks during periods of rest and idle.

UTC Power is a world leader in developing and producing fuel cells that generate energy for buildings and for transportation, space and defense applications. UTC Power has successfully completed multiple installations of its newest generation fuel cell system, the 400 kW Phosphoric Acid PureCell, for the commercial combined heat and power market. UTC Power and UTRC developed conceptual process designs for a wide range of SOFC power systems ranging from 250 kW up to 100+ MW with a focus on meeting the system efficiency and carbon separation targets specified in the SECA minimum requirements. In support of the design of a 250–1,000 kW SOFC power module, UTC Power has designed, built and commissioned a test stand capable of testing a stack up to 50 kW, and will subsequently test a Delphi stack module for at least 1,500 hours in Phase I on a simulated coal syngas.

Approach

Delphi utilized a staged approach to develop a modular SOFC system for a range of fuels and applications. Major subsystems and individual components were developed and tested as building blocks for applications in targeted markets. These were then integrated into a “close-coupled” architecture for integrated bench testing, as well as a stationary power unit and an APU for the stationary and transportation markets, respectively.

UTRC developed first principles-based steady-state models to prepare mass and energy balances and to predict the performance of the concept designs for the power module. Results from the mass and energy balances are used for trade studies and concept viability, component sizing and costing. To design low cost and highly efficient SOFC systems, UTC is working closely with vendors to establish performance models for critical components such as turbines, heat exchangers and fuel reformers. Using these models, both atmospheric and pressurized SOFC designs are being developed. Final designs are selected to meet the desired cost, performance and efficiency targets.

Results

The SECA Coal-Based Systems (CBS) project is a continuation of the core hardware development activities begun in the SECA Cost Reduction project. The efforts in SECA CBS are more application-driven as Delphi and UTC move this technology closer to pilot and production releases. The SECA CBS project will support and address the development of fuel cells for central generation applications. This market has unique demands, and development tasks must address specific issues that are economic drivers of the design and application.

Delphi continues to make progress with improved cell fabrication techniques by focusing on material and process improvements. A key element is Delphi’s partnership with commercial suppliers of production materials to develop a consistent supply of production grade material and optimize the material properties to provide robust performance in the SOFC stack and ultimately the fuel cell system. The principles of the Delphi Manufacturing System Design are continuously applied to develop control and quality standards for each

step of the manufacturing process. By focusing efforts in these areas early in the development process, Delphi has been able to scale up the fabrication process to mass quantities while maintaining high quality standards.

The Gen 3 stack successfully completed durability testing to 9,700 hours and deep thermal cycling to 200 thermal cycles, with a degradation rate of 1.1% per 500 hours in durability testing. Stack design efforts have focused on further optimizing the current design and adding features such as a cassette containing thermocouples in the center of the stack to get better temperature feedback. Development also focused on investigating different concepts for scaling up the active area footprint to achieve increased power while retaining low-cost, high-volume manufacturing designs, materials, and processes from Gen 3. Figure 1 shows both Gen 3 and Gen 4 stack configurations.

Delphi fabricated and tested multiple Gen 4 stacks in a variety of test conditions. A 40-cell Gen 4 stack demonstrated a maximum initial power of 6.4 kW at an average power density of 398 mW/cm^2 and average cell voltage of 0.7 volts, utilizing the SECA simulated coal gas blend. When combined into a four stack module, this will exceed the SECA requirement of 25 kW. The Gen 4 stack has completed a durability test of greater than 2,500 hours and had a degradation rate of about 4% in the first 300 hours and no measurable power degradation thereafter. The Gen 4 stack has successfully completed 60 deep thermal cycles from 750ºC operating temperature to <100ºC with a total power degradation of less than 5%. The successful stack test results provide confidence that the stacks have the potential to meet SECA durability goals and will survive periods of maintenance and shutdowns in larger power plants.

UTC Power and UTRC explored a wide variety of system designs and down-selected three power module designs for potential work in the next contract phase, two designs operate on natural gas and one design operates on coal gas. All three systems were designed for 400 kW net AC and achieve efficiency in excess of 60% based on fuel LHV. In addition, analysis of off-design conditions such as start-up and shut-down were also performed using quasi steady-state simulation models. Ultimately, these studies shall be performed with dynamic models; however, dynamic models require a significant amount of component design specs not available at this early design stage. Because start-up of this type of system is expected to be slow, steady-state models still provide meaningful results to investigate additional hardware requirements.

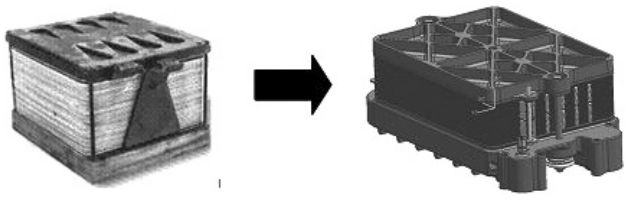

Gen 3 stack Gen 4 stack

FIGURE 1. Gen 3 to Gen 4 Stack – Power Increased while Retaining High-Volume Manufacturing Designs, Materials, and Processes from Gen 3

UTRC has completed conceptual designs of three IGFC systems that produce greater than 100 MW net AC power at efficiency greater than 50% HHV and capture greater than 90% carbon. Two of the systems were designed to operate at atmospheric pressures while the third was a pressurized system. The simpler of the two atmospheric systems uses an air blower to feed fresh air and has a steam bottoming cycle. The second atmospheric system uses a gas turbine (GT) instead of an air blower. Using the same GT, a pressurized system was designed that achieves approximately 40% higher current density and a slightly higher efficiency than the atmospheric GT design. The basic steam turbine design has the lowest efficiency but the highest technology readiness level and lowest capital cost. Since it meets the performance requirements it is the preferred final design for future project phases. Figure 2 shows the entire process flow diagram of this system.

UTC Power has successfully commissioned the 50 kW capable test stand. A debug stack was installed into the test stand and operated on various gas compositions and at various temperatures and pressures to confirm test system operation. Some limited stack diagnostics were performed to verify data acquisition systems and test stand controls. The test stand is ready for installation of the larger stack module and will be used to demonstrate 5,000 hours of durability, 1,500 hours of which will occur in Phase I. Development of a test plan for the 25 kW stack test, consistent with the SECA minimum requirements, has been completed and submitted to DOE.

UTC Power completed a preliminary cost analysis of the power block hardware for the IGFC power plant excluding the coal handling and gasification, syngas clean-up and CO_2 separation subsystem that shows a cost of $685/kW in 2007 dollars. A sensitivity analysis of the cost estimate was performed using Monte Carlo simulation to assess the uncertainty around the mean cost estimate. The simulation resulted in a 90% confidence interval showing that the true cost lies within -10% to +12% of the actual factory cost estimate which is well within the required ±25% SECA requirement for this cost analysis (the uncertainties in the process design are not included in the 90% confidence interval).

Conclusions and Future Directions

SECA CBS is focused on the stationary markets, with Delphi leading stack development for a coal

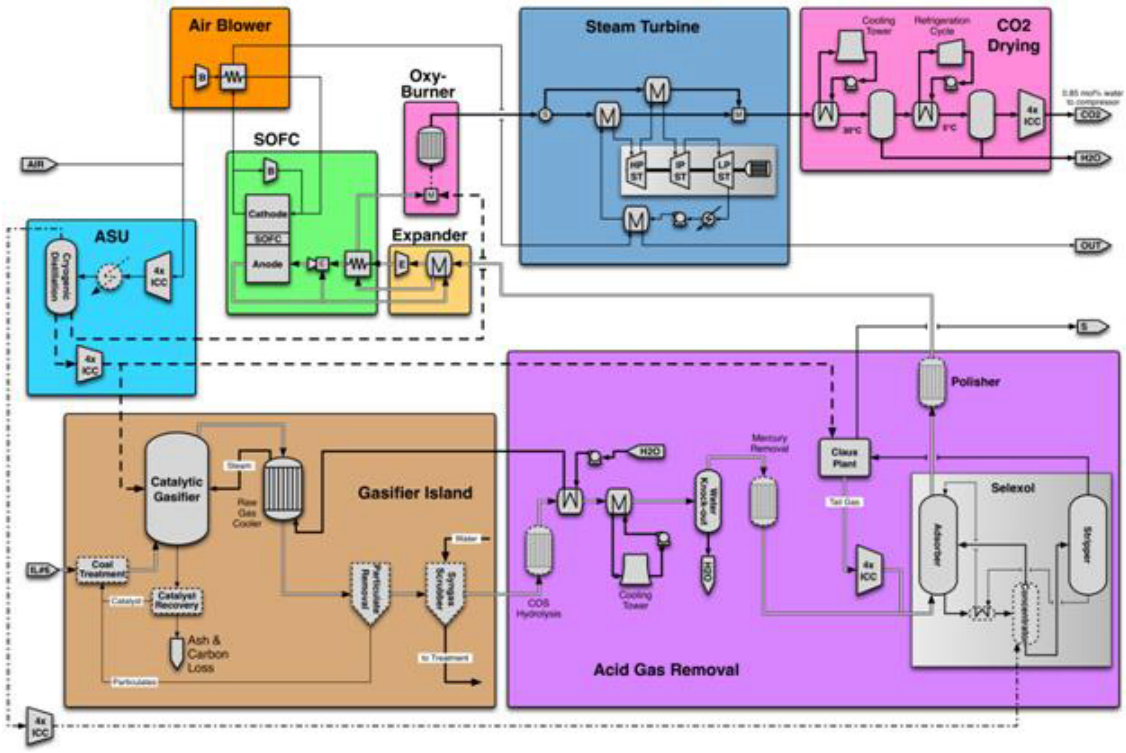

FIGURE 2. Process Flow Diagram of the Selected Atmospheric SOFC/Steam Turbine Design

syngas-based MW-scale power module. Development will continue to improve the electrochemical performance stability, durability, and reliability of the Gen 4 stack while continuing cost reduction activities through manufacturing enhancements, cell and stack design and materials development.

UTC is leading the systems development work. The present sub-MW power module design meets all design specifications. Current and future work efforts are directed at developing a packaged system design with improved reliability and cost. The scaled stacks developed and tested during Phase I shall be integrated into a thermally self-sustaining 15-25 kW demonstration breadboard power plant. The breadboard shall be tested in accordance with guidance provided in the DOE-approved test plan and the SECA minimum requirements, and the performance and cost evaluated with respect to the metrics specified therein. This power plant shall form the basis for larger power plants to be fabricated and tested in subsequent project phases.

FY 2011 Publications/Presentations

1. Rick Kerr, "Delphi SOFC Development Update," 11th Annual SECA Workshop, Pittsburgh, Pennsylvania, July 28, 2010.

2. Steven Shaffer, "Solid Oxide Fuel Cell Development at Delphi," 2010 Fuel Cell Seminar, San Antonio, Texas, October 20, 2010.

3. Rick Kerr, "Cell and Stack Technical Progress," SECA Peer Review, Morgantown, West Virginia, February 14, 2011.

4. Dan Hennessy, "Solid Oxide Fuel Cell Diesel Auxiliary Power Unit Demonstration," DOE Hydrogen Program Peer Review, Arlington, Virginia, May 12, 2011.

5. Rick Kerr, "Solid Oxide Fuel Cell Development at Delphi," 21st Century Truck Partnership and National Academy of Sciences Review Committee, Washington, D.C., January 31, 2011.

6. Subhasish Mukerjee, "Latest Update on Delphi's Solid Oxide Fuel Cell Stack for Transportation and Stationary Applications," SOFC XII, Montreal, Quebec, Canada, May 1, 2011.

II. SECA INDUSTRY TEAMS
B. Cost Reduction

II.B.1 Solid State Energy Conversion Alliance Delphi SOFC

Daniel Hennessy (Primary Contact),
Andrew Rosenblatt, Karl Haltiner,
Subhasish Mukerjee, David Schumann,
Gail Geiger, Larry Chick, Ellen Sun
Delphi Automotive Systems LLC
5725 Delphi Drive
Troy, MI 48098
Phone: (248) 732-0793
E-mail: daniel.t.hennessy@delphi.com

DOE Project Manager: Maria Reidpath
Phone: (304) 285-4140
E-mail: Maria.Reidpath@netl.doe.gov

Subcontractors:
- Battelle/Pacific Northwest National Laboratory, Richland, WA
- Electricore, Inc., Valencia, CA
- United Technologies Research Center, East Hartford, CT

Contract Number: NT41246

Start Date: July 1, 2002
End Date: December 31, 2011

Fiscal Year (FY) 2011 Objectives

- Fabricate two 30-cell Gen 3.2 stacks and a catalytic partial oxidation (CPOx) reformer.
- Deliver stacks and reformer to the National Aeronautics and Space Administration (NASA) for testing.

FY 2011 Accomplishments

- Successfully fabricated the two Gen 3.2 30-cell stacks.
- Successfully fabricated the CPOx reformer.
- Completed baseline testing with the hardware.
- Delivered the hardware to the customer (NASA) and provided assistance in testing.

Introduction

Delphi has been developing solid oxide fuel cell (SOFC) systems since 1999. After demonstrating its first generation SOFC power system in 2001, Delphi teamed with Battelle under the Solid State Energy Conversion Alliance (SECA) program to improve the basic cell and stack technology, while Delphi developed the system integration, system packaging and assembly, heat exchanger, fuel reformer, and power conditioning and control electronics, along with other component technologies. Compared to its first generation system in 2001, the Delphi-led team has reduced system volume and mass by 75 percent. By January 2005, the Delphi team was able to demonstrate test cells with power density more than required to meet the SECA 2011 goals.

Approach

Two 30-cell Gen 3 stacks and a CPOx reformer were successfully fabricated and characterized in-house before being shipped to the customer as per the U.S. Department of Energy's (DOE's) requirement. Testing is ongoing at the customer site with encouraging results.

Stack Summary Results

Two 30-cell Gen 3.2 stacks were fabricated for NASA (stack 883 and 884). Stack 883 produced 1,477 Watts at a power density of 468 mW per cm^2 with 48.5% H_2, 3% H_2O, rest N_2 (Figure 1). The average voltage was 0.82 Volts. Utilization evaluation at 570 mA per cm^2 also demonstrating very encouraging results (Figure 2). The stack showed minimal lowering of power going from low utilizations to 80% + fuel utilization.

The second NASA stack (884), similarly, produced 1,499 Watts at a power density of 476 mW per cm^2 with 48.5% H_2, 3% H_2O, rest N_2. The average voltage was 0.83 Volts. The stack also showed minimal lowering of power going from low utilization to 80% + fuel utilization. Both stacks were delivered and initial testing conducted. A CPOx reformer was also assembled, characterized and delivered for NASA testing. Initial testing is complete and further testing is planned at NASA.

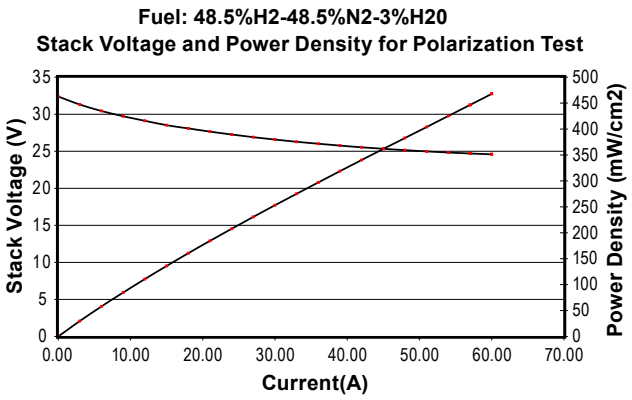

FIGURE 1. Current-Voltage Curve for Stack 883

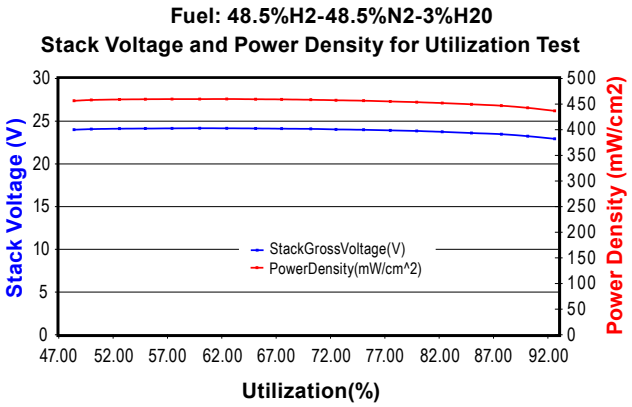

FIGURE 2. Power Density and Voltage Versus Fuel Utilization

Future Directions

The project is currently on hold.

FY 2011 Publications/Presentations

1. Rick Kerr, "Delphi SOFC Development Update," 11th Annual SECA Workshop, Pittsburgh, Pennsylvania, July 28, 2010.

2. Steven Shaffer, "Solid Oxide Fuel Cell Development at Delphi," 2010 Fuel Cell Seminar, San Antonio, Texas, October 20, 2010.

III. SECA CORE RESEARCH & DEVELOPMENT

A. Cathodes

III.A.1 Synchrotron X-Ray Studies of SOFC Cathodes

P.H. Fuoss (Primary Contact), K.-C. Chang, J.A. Eastman, B.J. Ingram, E. Perret, H. You
Argonne National Laboratory (ANL)
9700 S. Cass Ave.
Argonne, IL 60439
Phone: (630) 252-3289; Fax: (630) 252-7777
E-mail: fuoss@anl.gov

DOE Project Manager: Briggs White
Phone: (304) 285-5437
E-mail: Briggs.White@netl.doe.gov

Contract Number: FWP49071

Start Date: June 2007
End Date: May 2012

Fiscal Year (FY) 2011 Objectives

- Perform in situ X-ray scattering measurements of the structure and atomic scale chemistry in $La_{0.6}Sr_{0.4}Co_{0.2}Fe_{0.8}O_{3-\delta}$ (LSCF) as a function of temperature, oxygen partial pressure (pO_2) and electrochemical potential.
- Perform feasibility studies examining the use of atomic layer deposition (ALD) techniques to enhance the performance of SOFC cathodes by depositing thin layers or nanoparticles into cathode materials and measuring: 1) the thermal and chemical stability of the structure, and 2) the electrochemical performance of the cathode.
- Establish the surface electrochemical potential on LSCF and $La_{1-x}Sr_xMnO_3$ (LSM) thin films as well as model infiltration systems.
- Correlate in situ X-ray measurements with ex situ determinations of area specific resistance and fuel cell performance.

FY 2011 Accomplishments

- Determined the lattice parameter and electrical conductance of thin LSCF films as functions of temperature, pO_2, and electrochemical potential.
- Developed a detailed model of the surface polarization and position dependent current for thin film LSCF with wire electrodes.
- The effects of long-term applied electrochemical potential on the surface structure and chemical state of pulse laser deposited thin-film cathodes were measured.
- A symmetric solid oxide fuel cell (SOFC) cell for ultra-small angle X-ray scattering studies was designed and constructed. The cell was used to determine the baseline porosity of sintered cathodes in preparation for ALD infiltration studies.

Introduction

The performance of SOFCs is strongly influenced by the nanoscale structure and chemistry of electrode materials under operating conditions. However, because SOFCs are operated at elevated temperatures and at near atmospheric pressure, the utilization of traditional surface science techniques, which typically involve vacuum conditions near room temperature, requires validation. The studies being performed in this project provide the needed understanding of in situ-ex situ correlations. The results also enable the development of molecular-level models for stimulating the rational design and development of high-performance cathode materials.

Approach

We employ in situ X-ray scattering and spectroscopy technologies developed at ANL to both measure equilibrium structures of SOFC cathode materials at elevated temperatures and under controlled oxygen partial pressures. We examine the dynamic structural and chemical changes that occur at the cathode side of a fuel cell under conditions that simulate actual operating conditions. This work, particularly sample preparation, microscopy measurements, ultra-high vacuum-based surface characterizations, and theoretical studies, is performed in collaboration with investigators at several universities including Carnegie Mellon, Stanford, and Massachusetts Institute of Technology.

Results

Last year, we reported initial measurements demonstrating that the lattice parameter of LSCF exhibited a surprisingly large change in lattice parameter when a typical sample stack (see Figure 1) was biased with typical SOFC voltages. These measurements have been extended with a larger parameter space, better spatial and time resolution, and more samples. These studies have shown that a large lattice parameter change occurs quickly upon the application of an electrochemical potential.

The new experiments were performed on LSCF thin films grown on (001) yttria-stabilized zirconia (YSZ) with a gadolinia-doped ceria (GDC) interlayer.

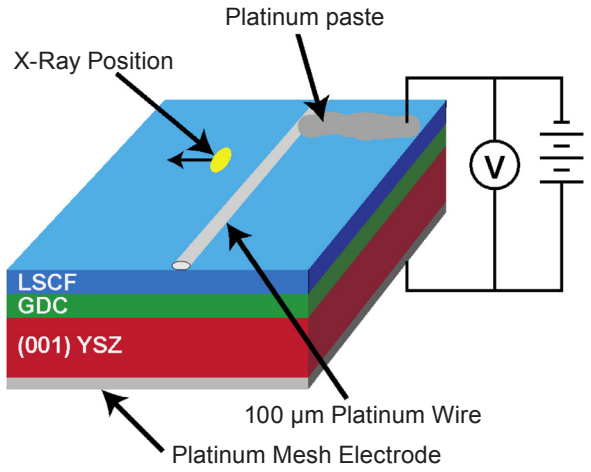

FIGURE 1. A schematic diagram showing details of the sample geometry. The incident X-ray beam was ~20 μm wide and was positioned at various distances from the Pt-wire electrode.

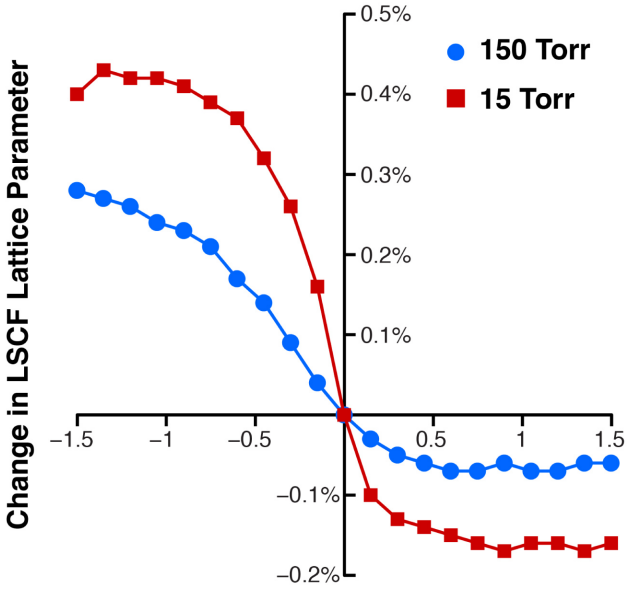

FIGURE 2. The shift of the LSCF lattice parameter as a function of applied electrochemical potential at 600°C and 1.3 mm away from the electrode for pO_2 of 15 and 150 Torr.

The thickness of the LSCF layers was determined to be approximately 20 nm using X-ray reflectivity. An LSCF sample (shown schematically in Figure 1) was mounted on a sample stage capable of achieving temperatures up to 1,000°C in pure oxygen. A chamber with X-ray transparent beryllium windows was designed specifically for use at the Advanced Photon Source and used to control pO_2 levels while maintaining a total pressure of 150 Torr. Experimental temperatures were maintained ≤700°C to limit physical changes in the sample such as surface roughening and phase segregation. Changes in the LSCF film lattice parameter were measured by monitoring the LSCF (004) Bragg peak while changing temperature, pO_2, and electrochemical polarization. The Bragg peak position was monitored using a Dectris 100K pixel array detector at a sample-detector distance where one pixel corresponds to 0.0126° (2θ).

Data were collected at 700, 600 and 500°C and pO_2 values of 150, 15, and 0.15 Torr. Figure 2 compares the changes in the LSCF c-lattice parameter for two pO_2 values at 600°C as a function of applied electrochemical potential. The incident beam intersected the LSCF film 1.3 mm from the Pt-wire electrode. Under a cathodic potential, a c-lattice parameter expansion was observed. Since the a- and b-lattice parameters remained fixed due to the epitaxial relationship with the underlying GDC layer, changes in the c-axis corresponded to changes in the lattice volume. The reversal of strain with applied field eliminated electrostriction (which shows a quadratic dependence on electric field) as the source of the lattice parameter change. Reducing the pO_2 increases the effect, and the absolute magnitudes of the lattice contractions at the most anodic (positive) potentials are smaller than the expansions at the most cathodic (negative) potentials: -0.18% vs. 0.42% and -0.06% vs. 0.3% at 15 and 150 Torr, respectively.

The typical time dependent behavior of the LSCF (004) Bragg peak (shown in Figure 3) indicates a sudden (i.e., <1 s) response upon application of 1 V (cathodic) potential. The response is stable over the time period of experimental observations. It should also be noted that the GDC and YSZ (006) Bragg peaks (not shown) were simultaneously monitored and did not shift in response to electrochemical potential. Additionally, upon removing the electrochemical load, the LSCF Bragg peak position returned to the original equilibrium value (i.e., 2θ = 46.532°).

Bishop et al have related LSCF oxygen non-stoichiometery (i.e., oxygen vacancies) with lattice expansion [1]; whereas, Lubomirsky has alternatively described lattice changes with association/dissociation reactions of defects [2,3]. The reversal of strain with applied field appears to support an interpretation based on injection and removal of vacancies instead of association/dissociation defect reactions. The very large magnitude of the effect compared to the applied potential on the LSCF film (most of the potential drop is across the YSZ substrate) argues against a piezoelectric effect.

The change in LSCF c-lattice parameter with application of 1 V cathodic electrochemical potential (relative to equilibrium) is shown in Figure 4 as a function of position from the Pt-wire electrode. The estimated extent of residual Pt-paste is indicated by the shaded region and may contribute to the observed behavior within 200 µm of the wire. The variation of lattice parameter with position can be used to guide models of electrical transport in the LSCF thin film.

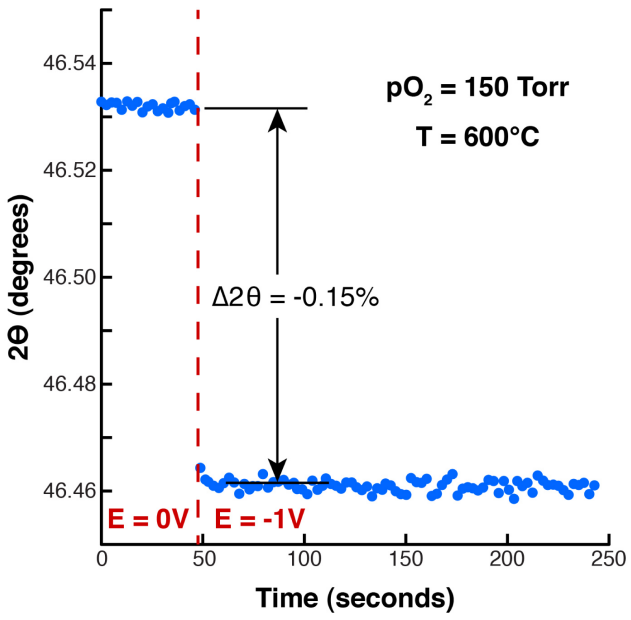

FIGURE 3. The time response of the shift of the LSCF (004) Bragg peak with the application of a -1 V bias at 600°C.

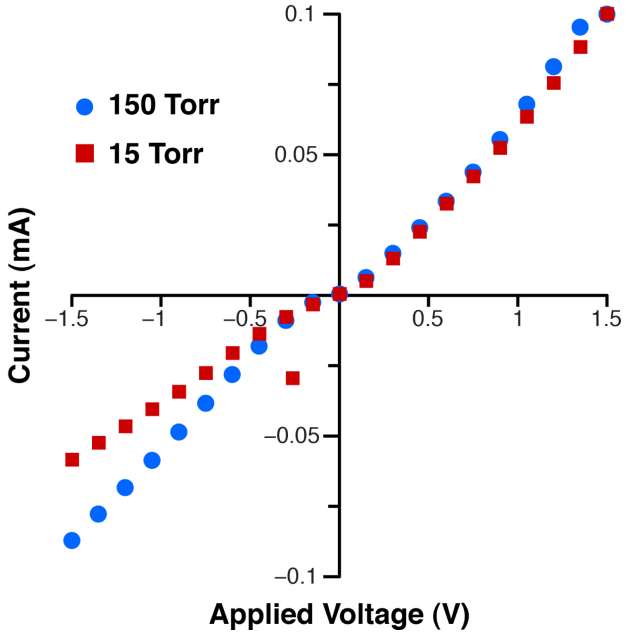

FIGURE 5. The i-V curve of LSCF/GDC/YSZ(001) at 600°C for different oxygen partial pressures. This data shows that oxygen reduction reactions are the limiting mechanism.

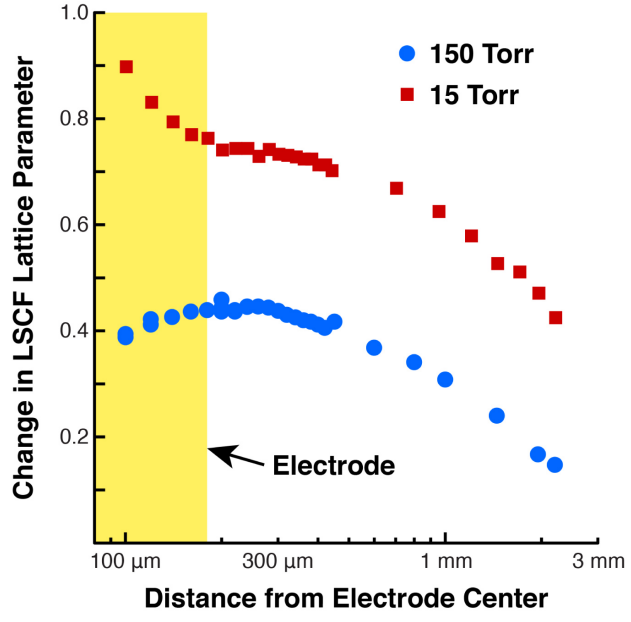

FIGURE 4. The LSCF lattice parameter change observed with the application of electrochemical polarization of -1 V at 600°C and pO_2 =150 Torr as a function of distance from the electrode.

Current-voltage (i-V) curves corresponding to Figure 2 are shown in Figure 5. The oxygen partial pressure does not affect the anodic (positive) response but a decreased pO_2 reduces the magnitude of the resultant currents for cathodic potentials. The cathodic and anodic behavior described in Figure 2 and Figure 5 indicates that oxygen reduction reactions at the surface, not bulk oxygen transport, is the limiting mechanism in cell performance. The decrease in current flow at cathodic potentials at low pO_2 is due to concentration overpotential losses associated with limited availability of molecular oxygen. If the rate of oxygen reduction is limiting relative to $V_O^{\cdot\cdot}$ transport, an increase in $[V_O^{\cdot\cdot}]$ would be expected as the cathodic potential is increased. The equilibrium (i.e., zero potential) oxygen stoichiometry of LSCF has been shown to be relatively constant at 600°C over the pO_2 range investigated for this experiment; therefore, injection of oxygen vacancies will be greater at lower pO_2 values. This is consistent with the results in Figure 2 and Figure 3.

Conclusions and Future Directions

Large changes in the lattice parameter of LSCF in response to applied electrochemical potentials are observed at temperatures and oxygen partial pressures that correspond to normal operating conditions for a SOFC. From the potential dependence of this result, it appears to arise from a change in the number density of oxygen vacancies in the LSCF film. Such a large, current-dependent lattice parameter change is important for the design of fuel cells. It also provides an opportunity to understand the mechanisms of oxygen conduction in these materials and a method to probe the local current in an operating fuel cell. Through exploration of this mechanism, advances have been made

in understanding the electrochemical performance and current flow through model thin film cathode materials.

Future experiments will continue to investigate the mechanisms and consequences of this lattice volume expansion. Structural studies of the atomic arrangements on the low index LSCF surfaces will be completed with the goal of providing insight into the catalytic mechanisms on those surfaces. Further investigations of LSM/LSCF thin films will be performed to identify how the LSM layer chemically and structurally enhances the stability of the underlying LSCF film. The possible enhancement of the oxygen reduction activities due to the LSM overlayer, reported in literature, will be examined by measuring the chemical states of the interfacial elements. Finally, improved cell configurations will improve the sensitivity of X-ray signals to the electrochemical conditions of LSCF films with or without a LSM overlayer and allow for a clearer understanding of the functioning of these important materials in the operating environment of a SOFC.

FY 2011 Publications/Presentations

1. T.T. Fister, D.D. Fong, J.A. Eastman, H. Iddir, P. Zapol, P.H. Fuoss, M. Balasubramanian, R.A. Gordon, K.R. Balasubramaniam, and P.A. Salvador, "Total-Reflection Inelastic X-Ray Scattering from a 10-nm Thick $La_{0.6}Sr_{0.4}CoO_3$ Thin Film," Physical Review Letters, **106**, 037401(2011).

2. P.H. Fuoss, T.T. Fister, M.J. Highland, D.D. Fong, and J.A. Eastman, "X-Ray Scattering Studies of Dynamic Surface Processes: Materials for Energy Conversion," 11th International Conference on Surface X-Ray and Neutron Scattering, Evanston, Illinois, July 13–17, 2010.

3. Kee-Chul Chang, Brian Ingram, Hui Du, Daniel Hennessy, Paul Salvador, and Hoydoo You, "In Situ X-Ray Studies of $La_{0.6}Sr_{0.4}Fe_{0.8}Co_{0.2}O_3$ Thin Films as Model Solid Oxide Fuel Cell Cathodes," 11th International Conference on Surface X-ray and Neutron Scattering, Evanston, Illinois, July 13–17, 2010.

4. P.H. Fuoss, T.T. Fister, Hoydoo You, K.-C. Chang, D.D. Fong, J.A. Eastman, M.J. Highland, B. Ingram, H. Du, and P.A. Salvador, "Synchrotron X-Ray Studies of SOFC Cathodes," 11th Annual Solid State Energy Conversion Alliance (SECA) Workshop, Pittsburgh, Pennsylvania, July 27–29, 2010.

5. B.J. Ingram, M. Krumpelt, K.-C. Chang, Hoydoo You, H. Du, and P.A. Salvador, "The Effect of Electrical Polarization on Solid Oxide Fuel Cell Cathode Thin Films," 11th Annual Solid State Energy Conversion Alliance (SECA) Workshop, Pittsburgh, Pennsylvania, July 27–29, 2010.

6. P.H. Fuoss, M.J. Highland, S.O. Hruszkewycz, D.D. Fong, J.A. Eastman, S.K. Streiffer, G.B. Stephenson, M.-L. Richard, and Carol Thompson, "Real-Time X-Ray Studies of the Effect of Chemical Transients on Oxide Thin Film Surface Structure," European Crystallographic Meeting, Darmstadt, Germany, August 29 – September 2, 2010.

7. T.T. Fister, G. Seidler, M. Balasubramanian, R.A. Gordon, S. Heald, K. Nagle, J. Bradley, J. Cross, P.H. Fuoss, and P. Fenter, "The LERIX User Facility: Extending X-Ray Raman Scattering across the Periodic Table," The 16th Pan-American Synchrotron Radiation Instrumentation Conference, Argonne, Illinois, September 21–24, 2010.

8. T.T. Fister, G. Seidler, K. Nagle, J. Bradley, M. Balasubramanian, R.A. Gordon, P.H. Fuoss, and P. Fenter, "Extending X-Ray Raman Scattering across the Periodic Table," 7th International Conference on Inelastic X-ray Scattering, Grenoble, France, October 11–14, 2010.

9. T.T. Fister, P.H. Fuoss, and P. Fenter, "In Situ Characterization of Surfaces and Buried Interfaces Using Total Reflection Inelastic X-Ray Scattering," Materials Science & Technology 2010 Conference and Exhibition, Houston, Texas, November 17–21, 2010.

References

1. S.R. Bishop, K.L. Duncan, and E.D. Wachsman, J. Am. Ceram. Soc. **93** (2010) 4115-4121.

2. I. Lubomirsky, Phys. Chem. Chem. Phys. **9** (2007) 3701.

3. I. Lubomirsky, Monatsh. Chem. **140** (2009) 1025-1030.

III.A.2 Solid Oxide Fuel Cell Cathodes: Unraveling the Relationship Among Structure, Surface Chemistry and Oxygen Reduction

Srikanth Gopalan
15 St. Mary's Street
Department of Mechanical Engineering
Boston University
Boston, MA 02215
Phone: (617) 358-2297
E-mail: sgopalan@bu.edu

DOE Project Manager: Patcharin Burke
Phone: (412) 386-7378
E-mail: Patcharin.Burke@netl.doe.gov

Contract Number: NT0004104

Start Date: September 1, 2008
End Date: September 30, 2011

Fiscal Year (FY) 2011 Objectives

- Continue deposition of high quality epitaxial and polycrystalline cathodic thin films.
- Use in situ X-ray chamber to obtain high temperature surface structure and composition analysis
- Obtain kinetics data on oxygen exchange on cathode thin films using impedance spectroscopy.

FY 2011 Accomplishments

- We have continued to deposit high-quality lanthanum strontium manganite (LSM) thin films as evidenced by high-resolution transmission electron microscopy (TEM) and roughness measurements using atomic force microscopy.
- Ex situ measurements using X-ray emission spectroscopy (XES) and X-ray adsorption spectroscopy (XAS) have continued on lanthanum strontium cobalt ferrite (LSCF).
- Total reflection X-ray fluorescence data clearly show diminished A/B ratios at the surface of LSM thin films.
- Oxygen adsorption, surface diffusivity, and incorporation reaction rate coefficients have been measured on polycrystalline thin films.

Introduction

Many of the specific details of the oxygen reduction reaction in a solid oxide fuel cell (SOFC) remain poorly understood. Surface chemistry directly influences the nature of oxygen reduction reaction pathways on the SOFC cathodes and the rates at which the individual processes proceed. From semi-empirical correlations between the chemistry and structure of oxide surfaces and their electrocatalytic performance, the true cause-and-effect relationships in the oxygen reduction processes at the cathode could be elucidated. This would provide valuable guidance in improving cathode performance.

Approach

In this work, we aim to acquire such surface-specific chemical and structural data on heteroepitaxial thin films of LSM and LSCF cathodes on single crystals of yttria-stabilized zirconia (YSZ) and YSZ coated with a barrier layer of rare-earth doped ceria (e.g., Y_2O_3-doped CeO_2 or YDC) electrolytes. This is being accomplished using a combination of analytical spectroscopic techniques and TEM. Further, we also aim to employ soft X-ray spectroscopies, namely XES/XAS, to correlate changes in the thin film polarization resistance to the surface chemical composition and the charge state of the Mn ion. The overall goal is to understand the role of surface atomic and electronic structure on the oxygen exchange reaction.

Results

We have performed total reflection X-ray fluorescence (TXRF) measurements on LSM thin films in the as-deposited, annealed in air at high temperature, and quenched states. The results are shown in Figure 1. The results show that for our LSM thin films of composition:

- There is manganese enrichment at the surface during annealing.
- The quenched and cooled samples are similar.
- This suggests surface composition developed at high temperature is preserved.

Figure 1 shows the A/B ratio of lattice-matched LSM films on $NdGaO_3$ (neodymium gallate, NGO) substrates and columnar grained LSM on YSZ

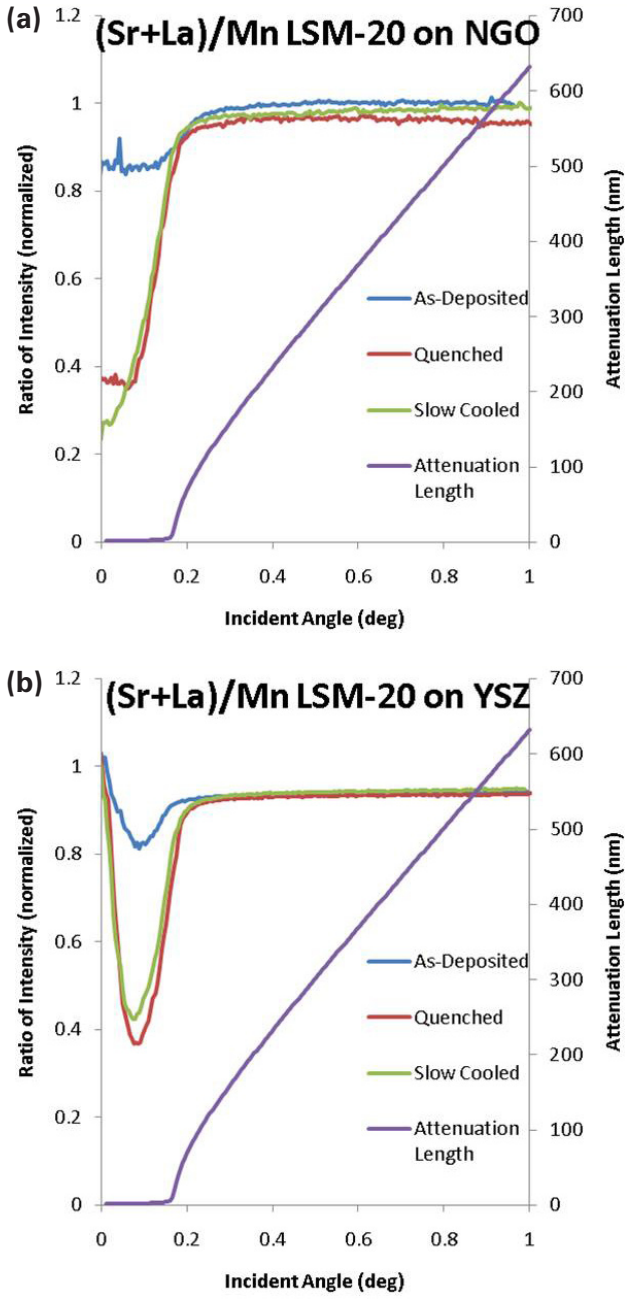

FIGURE 1. (a) A/B ratio measured by TXRF on lattice-matched LSM thin films on NGO. (b) A/B ratio measured by TXRF on columnar thin film of LSM on polycrystalline YSZ.

substrates. The results show that in both cases there is a decrease in the A/B ratios of the films closer to the surface which is present in annealed, quenched and slow cooled films.

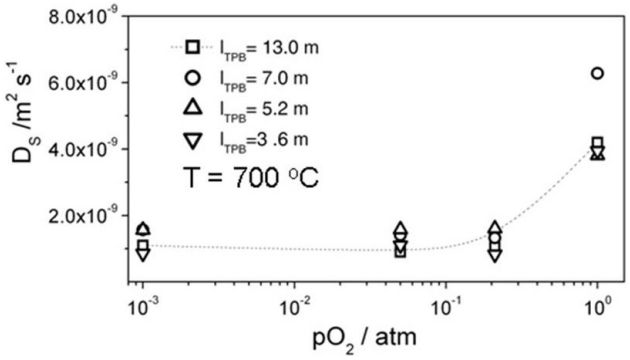

FIGURE 2. Surface Diffusivities of Oxygen on LSM Measured as a Function of Oxygen Partial Pressure

Concurrent with the TXRF measurements we have also performed impedance experiments and the surface diffusivities of oxygen on polycrystalline thin films have been measured using a suitable transport model (Figure 2). The measurements show *inter alia* that surface diffusivities are constant as a function of oxygen partial pressure (pO_2) over a wide range, but increase at very high pO_2s. The increase in pO_2 is consistent with the filling up of surface oxygen vacancies and increase in charge compensation by Mn^{4+} which are thought to be the sites of oxygen adsorption. These results tie in very well with prior results of the detection of Mn^{4+} valence state on the surface of LSM thins films. Mn^{4+} are thought to be the adsorption sites for oxygen ad-atoms.

Conclusions and Future Directions

In prior year work we concluded that subjecting LSM thin films to cathodic conditions leads to formation of Mn4+ ions on the surface.

In current work we have shown that the A/B ratio on the surface of LSM thin films decreases from the bulk values towards the surface.

Further analysis of impedance spectroscopy results shows an increase of surface diffusivities of oxygen as a function of oxygen partial pressures which can be attributed to filling up of oxygen vacancies and increase in the number of Mn^{4+} sites.

Future work will involve obtaining a more accurate picture of the surface defect chemistry of LSM and LSCF by combining the surface cation segregation data obtained by TXRF with a defect thermodynamic model.

III.A.3 SOFC Cathode Surface Chemistry and Optimization Studies

Paul A. Salvador (Primary Contact), Lu Yan, Philip Tsang
Carnegie Mellon University (CMU)
Department of Materials Science and Engineering
5000 Forbes Avenue
Pittsburgh, PA 15206
Phone: (412) 268-2703; Fax: (412) 268-3113
E-mail: paul7@andrew.cmu.edu

Drs. Paul Fuoss,[a] Jeff Eastman,[a] Brian Ingram,[a] Hoydoo You,[a] Kee-Chul Chang,[a] Bilge Yildez,[b] and C. Heske[c]
[a] Argonne National Laboratory (ANL)
9700 South Cass Avenue
Argonne, IL 60439-4837
[b] Massachusetts Institute of Technology (MIT)
Department of Nuclear Science and Engineering
77 Massachusetts Avenue, Rm: 24-210
Cambridge, MA 02139
[c] University of Nevada, Las Vegas (UNLV)
Department of Chemistry
4505 Maryland Parkway, Box 454003
Las Vegas, NV 89154

DOE Project Manager: Patcharin Burke
Phone: (412) 386-7378
E-mail: Patcharin.Burke@netl.doe.gov

Contract Number: NT0004105

Start Date: March 1, 2010
End Date: August 31, 2011

Fiscal Year (FY) 2011 Objectives

- Develop samples of cathode materials having specific surface structures and chemistries using thin film preparation methods, as requested by collaborators.
- Provide lanthanum strontium manganese oxide (LSM), lanthanum strontium cobalt oxide (LSC), and lanthanum strontium cobalt iron oxide (LSCF) samples for surface characterization to collaborators at ANL's Advanced Photon Source (ANL-APS), MIT, and UNLV.
- Determine the activation energy of the chemical surface exchange coefficient (k_{chem}) for LSM (100), (110), and (111) at different thicknesses and on different substrates.
- Refine investigations into the oxygen uptake kinetics in thin film samples, specifically to make correlations between the extended defect populations and oxygen exchange for (110) textured LSM films on yttria-stabilized zirconia (YSZ) (111).
- Determine the oxygen exchange kinetics for high index samples, such as (621) LSM.

FY 2011 Accomplishments

- Further developed single-crystal, epitaxial, textured, and polycrystalline thin films of LSM, LSC, and LSCF with low roughness values on both insulating and electrolytic substrates of various geometries that were used in both in-house and collaborators' experimental facilities to understand the nature of the surface chemistry/reactivity of cathode materials.
- Thin film samples were characterized at the APS as a function of temperature (T), pressure (P), and electrochemistry for their surface compositions, structures, and charge states; at MIT for their local electronic properties using scanning tunneling spectroscopy and electrochemical properties with electrochemical impedance spectroscopy; at UNLV with Auger electron spectroscopy and X-ray photoelectron spectroscopy, and at CMU with X-ray diffraction (XRD), atomic force microscopy (AFM), electrical conductivity relaxation (ECR), and Kelvin probe spectroscopy.
- Demonstrated that the activation energy of 600 nm thick LSM films were between ≈0.8 and ≈1.2, depending on the orientation of the crystal.
- Demonstrated that relaxed films of the (110) orientation had the largest k_{chem} value in solid oxide fuel cell (SOFC) conditions owing to their high activation energy (and their large high-temperature intercept value on an Arrhenius plot).
- Demonstrated that the activation energy of 600 nm thick LSM films were between ≈0.75 and ≈1.5, depending on the crystal quality and strain state of the film, as well as the temperature itself.
- Demonstrated that the strained (100) films had the highest exchange rate of all measured (100) films, indicating strain can be an important enhancing factor in SOFCs.
- Strained films had significantly different and greater activation energies than relaxed films.
- Two surface exchange values were used to fit the response of textured (110) films, with the area each contributed being a function of temperature and with the large activation energy contributing the most to the high temperature SOFC response.
- Extended defects play a major role in the oxygen exchange at intermediate temperatures.

Introduction

The cathode in SOFCs is responsible for the reduction of O_2 gas and its incorporation into the electrolyte. When SOFCs are operated at specific current densities/voltages, the oxygen incorporation (or uptake) process can contribute significantly to the losses of the cell, thereby limiting the performance of the SOFC system. Two major options exist for improving the cathode performance by specifically targeting the oxygen incorporation process: changing the component solid materials or adding yet another material (a catalyst) to the existing frameworks [1,2]. We aim to address both approaches in this work by (1) developing an experimental program that allows us to probe the nature of atomic scale surface chemistry and its role in oxygen incorporation in LSM, LSC, LSF (lanthanum strontium iron oxide), and LSCF (and related cathode materials) and (2) determining the optimal catalyst chemistry from both an activity and stability perspective [3-7]. Realizing these goals will lead to improved cathode performance in SOFCs and an acceleration of introduction of new materials into SOFCs to allow for the U.S. Department of Energy's Solid State Energy Conversion Alliance (DOE-SECA) program to meet performance metrics.

Generally speaking, the limitations in designing highly active cathodes for oxygen incorporation arise from the general lack of direct correlations between surface/interface chemistry/structure and performance of SOFC cathode materials over the appropriate ranges of SOFC operational conditions [8]. In this work, we aim to fill this need by (1) developing experimental protocols that will provide a sensitive measure of activity/stability in operational conditions and by (2) determining key correlations between structure (solid state atomic, electronic, crystallographic, and chemical) and electrochemical performance (mass and charge transfer) parameters in surface engineered samples. At CMU, we are generating surface engineered samples and providing them to a range of collaborators who characterize the samples [3-7,9-14]. Several groups at ANL have investigated samples using high-energy synchrotron X-ray techniques at the APS [3,4,10]. A group at MIT uses scanning-tunneling spectroscopy and electrochemical impedance spectroscopy to determine electrical characteristics of the films [14]. A group at UNLV carries out experimental electronic structure determination of thin film surfaces. Separate reports are provided by these collaborators. In this report, we describe the progress at Carnegie Mellon on sample preparation, especially on correlating the oxygen uptake kinetics of LSM with microstructural defects.

Approach

Thin film samples are prepared using pulsed laser deposition [5,6,9,11-13,15]. By calibrating the growth rate using X-ray reflectivity (XRR), films of specific thicknesses are fabricated. Using XRD, the orientation relationship between the film and substrate can be determined. Using AFM, the film surface topography can be determined. By correlating the results of XRR, XRD, and AFM to growth parameters, we fabricate high quality films with controlled microstructural and surface features. Specifically, (1) epitaxial (100) and (110) films of LSM were prepared on $SrTiO_3$ (STO) and $NdGaO_3$ (NGO) substrates, which allowed for the isolation of strain and dislocation effects, and (2) textured (110) films of LSM were prepared on (111) YSZ, which allowed for the control of extended boundaries.

ECR measurements [9,11,15] were made on a variety of films. The oxygen pressure (PO_2) was changed between 50 mTorr and 500 mTorr, using the mass flow controller. All ECR data was modeled on the basis of a surface exchange model [11,16-20], using one or two surface exchange coefficients [9,11,15]. k_{chem} was obtained based on fitting the data of the relaxation curves and corrected by taking account of the chamber flush time [11]. The mathematical relationships are given as follows:

$$g(t) = \frac{\sigma_t - \sigma_{final}}{\sigma_{final} - \sigma_{initial}} = 1 - A\exp(-\frac{k_{1,chem}t}{L}) - (1 - A)\exp(-\frac{k_{2,chem}t}{L})$$

where g(t) is the normalized conductivity, σ_t is the conductivity at time t, σ_{final} is the conductivity at re-equilibrium and $\sigma_{initial}$ is the conductivity at the initial equilibrium state A is a constant and L is the sample thickness.

Results

As indicated in past publications [3,4,7,9,10,11,14,15] and reports [5,6,12,13] and in forthcoming publications, we have been providing high quality surface engineered thin films to collaborators, who are working on identifying surface chemistries and properties that lead to improved electrocatalytic performance. It is essential to characterize the details of the thin film structure to interpret properly experimental observations. At Carnegie Mellon, we carry out the necessary processing and characterization to ensure samples have the characteristics requested from collaborators. Reports from collaborators are given elsewhere.

Only one time constant (or A = 1) was needed for all ECR data registered for the epitaxial LSM on STO substrates [11,15]. Figure 1 [9] shows how a two time constant fitting was carried out for the (110) film on (111) YSZ at 600°C. The data is given in open symbols, while the fitted fast (slow) time constant is shown in

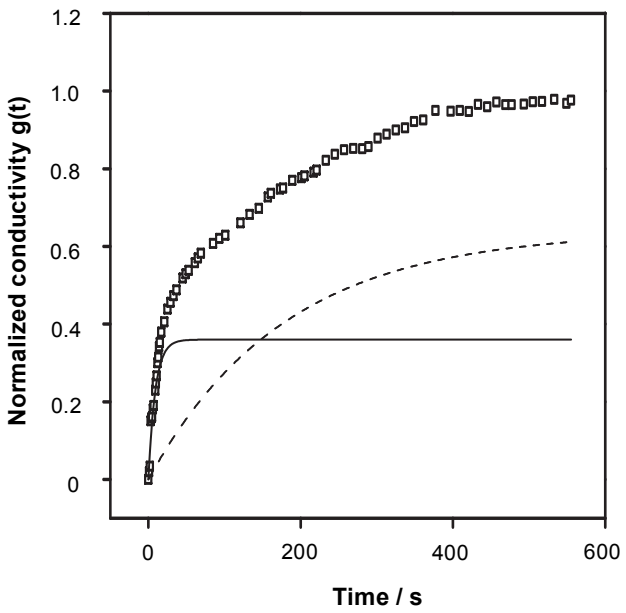

FIGURE 1. ECR normalized conductivity curve and data fitting for a textured LSM film. Data measured at 600°C (open square) and the corresponding data fitting with a fast (solid line) and a slow (dashed line) processes. Adapted from reference [9].

a solid (dashed) line. The sum of the two fitted lines gives the observed data with A ≈0.4. This will be further discussed.

As we discussed in past reports [6,12], a single k_{chem} value was capable of describing the response of epitaxial LSM samples. In this period we focused on determining the relative importance of microstructural features such as strain and extended defects, in addition to surface properties such as orientation, on the overall performance metrics, such as the oxygen exchange coefficient (k_{chem}) and its activation energy. During this time we focused on LSM and now have a broad understanding of its surface properties.

Epitaxial (100), (110), and (111) oriented LSM films were fabricated on STO. The LSM films exhibited bulk-like steady-state electrical properties and exhibited surface dominated responses in ECR [11,15]. The chemical surface exchange coefficients (k_{chem}) were determined and varied from ≈1 x 10^{-6} to 65 x 10^{-6} cm/s, and depended on temperature and orientation [15]. Figure 2 shows ln k_{chem} for (100), on left, and (110), on right, surfaces [15]. At 800°C, a four-fold variation is observed in the k_{chem} values, with (110)/(100) being the highest/lowest, explained by the activation energy for (110), ≈1.16 eV, compared to that energy for (111) and (100), ≈0.83 eV. Note that both the activation energy and the high temperature intercept (1/T ≈0) are different on these surfaces, indicating that the mechanisms must be explored for many surfaces. Also, the oxidation and reduction processes are approximately equal for these samples. Most importantly for understanding the important surface chemistry for SOFCs, these results indicate that investigating (100) surfaces, as is widely done in the literature, is only an important start; at SOFC temperatures, this orientation is the slowest oxygen exchange surface. We also investigated the (111) and (621) surfaces, and these have activation energies and intercepts larger than the (100) surface. For SOFCs, this indicates that the local activity of relaxed surfaces may range by a factor of 5.

Relaxed epitaxial films have large quantities of dislocations, much larger than typically observed in ceramic microstructures. As such, one interpretation of the prior observations is that dislocations on different surfaces behave differently, if the surface exchange is dominated by the behavior around dislocations. To

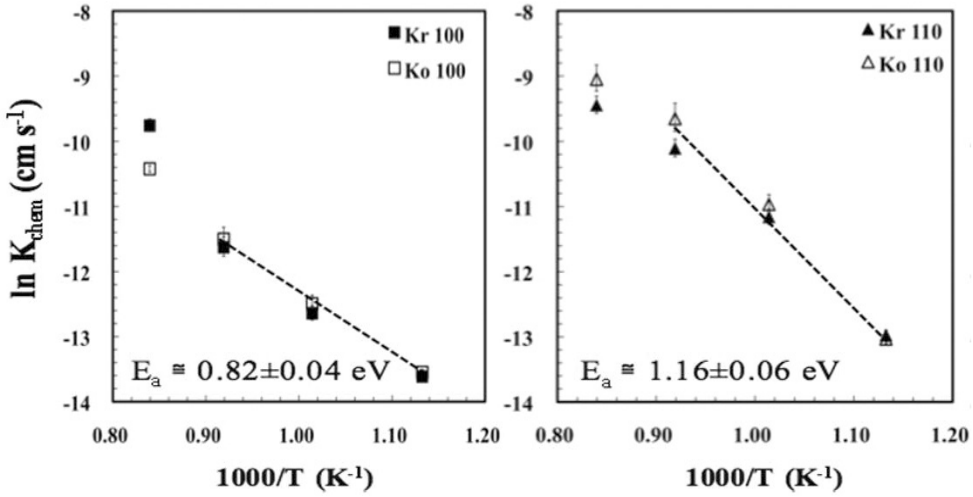

FIGURE 2. Temperature dependence of surface exchange coefficient k_{chem} for the (100) and (110) oriented $La_{0.7}Sr_{0.3}MnO_3$ films. The activation energies (E_a) are given in the plot. Adapted from reference [15].

explore this, we prepared films of different thicknesses. Also, we prepared films on different substrates. In this fashion, we could disentangle the effects of substrate strain and dislocations, since the strain is controlled by the lattice mismatch and the dislocation content is controlled by both the substrate quality and lattice mismatch. Figure 3 shows k_{chem} measured for epitaxial films on STO (main panel) and NGO (inset panel) substrates at different thicknesses, plotted as ln k_{chem} vs. 1/T. What we observed was that the activation energy was a strong function of thickness and a weaker function of substrate. On the other hand, k_{chem} itself was a strong function of substrate.

In Figure 3, we plotted solid lines that represent the approximate activation energy limits: ≈1.5 eV for the thinnest films (50 nm) that are coherently strained and ≈0.75 eV for the thickest films (>600 nm). On STO, the absolute value of k_{chem} crosses over in the middle of the temperature range (≈700°C). On NGO, the same crossover is expected at higher temperatures than 800°C. At low temperatures, all the thicker films on STO exhibited nearly identical k_{chem} values, while the values varied on NGO substrates. At high temperatures the opposite was observed; all the thicker films on NGO exhibited nearly identical k_{chem} values, while the values varied on STO substrates. Most importantly, the thinnest strained (100) films on STO have the highest k_{chem} values. This observation indicates that strain plays a major role of the surface exchange. On the other hand, the thinnest strained (100) films on NGO have the lowest k_{chem} values, indicating again that strain can either enhance or degrade properties. As such, it is important to understand the local strains in SOFCs if we are to properly model local properties, which contribute strongly to degradation.

In Figure 3, the activation energy depends on the number of dislocations (thickness and substrate) and temperature, which indicates that there is a crossover between the two processes observed. The low activation energy is assigned to heavily dislocated surfaces at intermediate temperatures. The high activation energy is assigned to the native surfaces, which are active at high temperatures and at much lower temperatures, depending on the strain and dislocation content. This will be explored more deeply in the remaining time and published soon.

To explore further the role of extended boundaries, we prepared textured (110) films on YSZ (111) [9]. As shown in Figure 1, two time constants were observed in the ECR measurements of the textured films. Figure 4 shows the two k_{chem} values versus inverse temperature. The reduction process was observed to be slightly faster than the oxidation process over the entire temperature range; $k_{chem,red}$ was greater by slightly less than a factor of two. In either oxidation or reduction, the fast process does not completely oxidize/reduce the films and, therefore, one can extract $k_{chem,1}$ of the slower

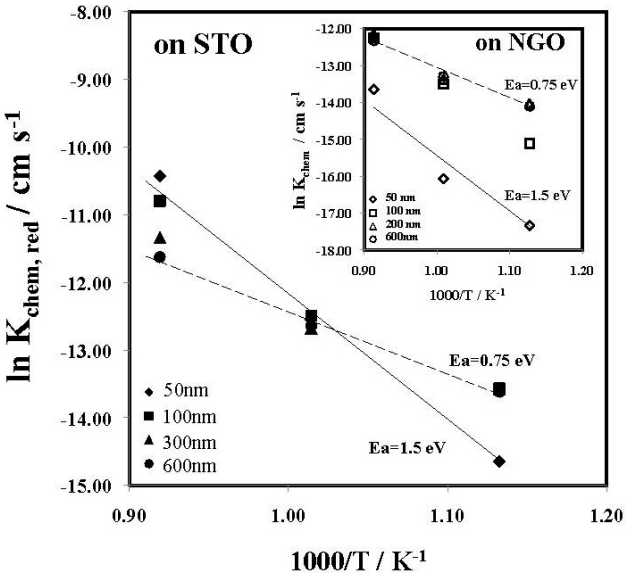

FIGURE 3. k_{chem} values (in reduction process) as a function of temperatures for films of various thicknesses on STO in closed markers; inset shows films on NGO in open markers. Activation energies were fitted with solid line for 50 nm thick films (=1.5 eV), dotted lines for 600 nm thick films (= 0.75 eV).

process. At higher temperatures, on the other hand, only one k_{chem} was needed: $k_{chem,1}$. The activation energy for the two processes (based on the low T data) are $E_{a,1} = 1.57$ eV and $E_{a,2} = 0.87$ eV. The value measured at the highest temperature is on the order of our ability to measure and was not used. Extrapolation from low temperatures indicates that $k_{chem,1}$ approaches $k_{chem,2}$ at high temperatures (see Figure 4). Furthermore, A increases with increasing temperature, indicating the relative contribution of $k_{chem,1}$ to the overall response increases at higher temperatures, while the parallel contribution of $k_{chem,2}$ decreases.

We assign these two values to (1) the native grain surfaces and (2) the variant boundaries (which can be considered as highly defective regions). These activation energies are similar to those observed for the epitaxial (100) films, which were also assigned to native surfaces (strained though) and defects (dislocations). On the textured films, we see both processes because (1) they are parallel processes, (2) the grain boundaries are interconnected along the current path (unlike the dislocations), (3) the grain centers are not interconnected, and (4) the grain boundaries are unable to exchange the entire volume. The lower plot of Figure 4 shows this schematic process. As the temperature increases, the higher activation energy process plays an increasingly important role and the surface area over which it plays the most important role expands, leading to a decreased surface area over which exchange is dominated by the extended boundaries. As such, at higher temperature the native

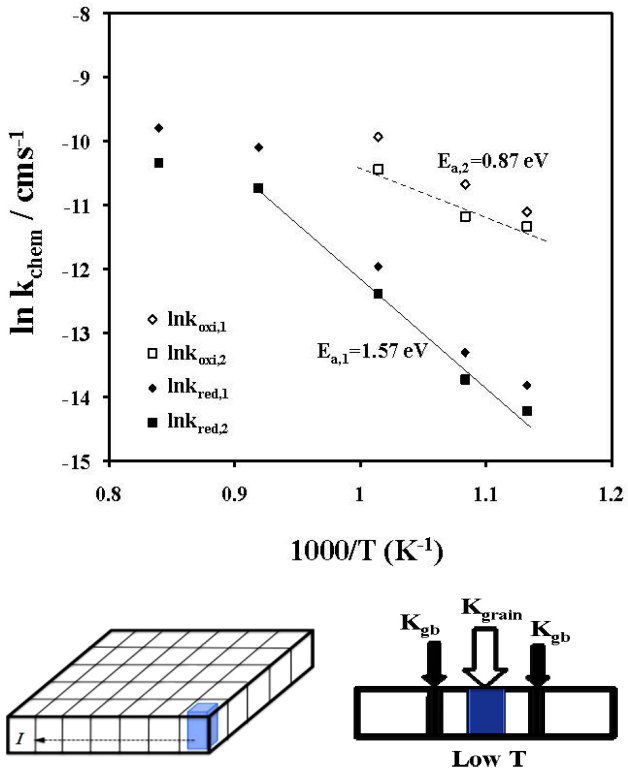

FIGURE 4. (Top) Temperature dependence of surface exchange coefficients k_{chem} for textured LSM films: open markers are for the faster process, closed markers are for the slow process; oxidation process is shown as square markers, reduction process is shown as diamond markers. (Bottom left) schematic of grain boundaries networks inside textured film. The grain centered is filled in the lower right grain. The dashed line indicates in plane current direction, indicating the parallel pathes. (Bottom right) schematic of two possible oxygen flux pathways on the surface, one through intrinsic surface/grain, the other through variant/grain boundaries. Adapted from reference [9].

surface plays the most important role. What needs to be better understood is if this stays true for all orientations. We will determine this in the future.

Conclusions and Future Directions

We have demonstrated that surface engineered films of cathode materials can be produced and characterized in detail for the structural and chemical properties. Crystallographic anisotropies were observed for epitaxial LSM single crystal films in their oxygen uptake kinetics, where low index orientation vary by a factor of 4 in SOFC conditions of temperature and effective pressure. We showed that this is a function of the activation energies and pre-exponential factors, which vary with orientation. Furthermore, we showed that the activation energy is a strong function of the thickness of the films, indicating that strains and dislocations compete in importance for surface exchange. On textured (110) films, we showed that two processes occur in parallel and can be distinguished in a single ECR measurement. We assigned them to the native surface and to the extended defects (variant boundaries). At low temperatures, the extended boundaries dominate the response - more than three orders of magnitude greater than the native surfaces. We will continue to produce a series of surface engineered films and will investigate (1) their structural properties, (2) their stabilities, and (3) their oxygen uptake kinetics using ECR, especially focusing on LSCF films. By continuing to fabricate a matrix of related materials and carrying out these measurements, we will be able to provide a large amount of data to determine the key parameters that correlate surface structure to surface activity, with the aim of providing information to the DOE-SECA program to improve cathode activity by design. In the next year, we aim to provide a comprehensive report of the state of surface science on SOFC cathodes.

FY 2011 Publications/Presentations

1. L. Yan, K.R. Balasubramaniam, S. Wang, H. Du, and P.A. Salvador, "Effects of Crystallographic Orientation on the Oxygen Exchange Rate of $La_{0.7}Sr_{0.3}MnO_3$ Thin Films," *Solid State Ionics,* **194**, 9-16 (2011). doi: 10.1016/j.ssi.2011.05.004

2. L. Yan, K.R. Balasubramaniam, K.-C. Chang, H. You, and P.A. Salvador, "Microstructural Effects on the Oxygen Exchange Kinetics of $La_{0.7}Sr_{0.3}MnO_3$ Thin Films," *Electrochemical Society Transactions,* **35**, (2011). doi: 10.1149/1.3570197

3. T.T. Fister, D.D. Fong, J.A. Eastman, H. Iddir, P. Zapol, P. Fuoss, M. Balasubramanian, R.A. Gordon, K.R. Balasubramaniam, and P.A. Salvador, "Total Reflection Inelastic X-ray Scattering from a 10 nm Thick $La_{0.6}Sr_{0.4}CoO_3$ Thin Film," *Physical Review Letters,* **106**, 037401 (2011). doi: 10.1103/PhysRevLett.106.037401

4. L. Yan, B. Kavaipatti, S. Wang, H. Du, and P. Salvador, "Electrical Conductivity Relaxation Study of Solid Oxide Fuel Cell Cathodes Using Epitaxial (001)-Oriented Strontium-Doped Lanthanum Manganite Thin Films," *Mat. Res. Soc. Symp. Proc.,* **1255**, 1255-M02-02 (2010). doi: 10.1557/PROC-1255-M02-02

5. Paul Salvador, "Thin Films of SOFC Cathode Materials: Understanding Surface Chemistry and Design of Improved Cathodes," Invited Presentation, Laboratoire CRISMAT at the University of Caen, Lower Normandy, Caen, France, June, 2011.

6. "Microstructural Effects on the Oxygen Exchange Kinetics of Strontium-Doped Lanthanum Manganite Thin Films," SOFC-XII Symposium at the Electrochemical Society Meeting, Montreal, Canada, May 4, 2011.

7. Paul Salvador, "Surface Chemistry and Activity of SOFC Cathodes," Invited Presentation, American Chemical Society, 241st American Chemical Society National Meeting, Anaheim, California, March 30, 2011.

8. "Investigation of Cathode Electrocatalytic Activity Using Surfaced Engineered Thin Film Samples and High Temperature Property Measurements," SECA FY11 Fuel Cells Peer Review, Morgantown, West Virginia, February 16, 2011.

9. "Effects of Substrate and Thickness on the Oxygen Exchange Kinetics of $La_{0.7}Sr_{0.3}MnO_3$ Films," presented by Lu Yan (CMU) at ECS 218th Meeting, Las Vegas, Nevada, October 2010.

10. P.A. Salvador, L. Yan, S. Wang, K.R. Balasubramaniam, P. Fuoss, J. Eastman, D. Fong, T. Fister, P. Baldo, H. You, K.-C. Chang, B. Yildiz, K. Katsiev, C. Heske, and S. Krause, "SOFC Cathode Surface Chemistry and Optimization Studies," *FY 2010 Office of Fossil Energy Fuel Cell Program Annual Report*, U.S. Department of Energy, Paper III.A.3 (2010).

11. "SOFC Cathode Surface Chemistry and Optimization Studies," presented by Paul Salvador (CMU) at 11th Annual SECA Workshop, Pittsburgh, Pennsylvania (July 2010).

12. "Crystallographic Anisotropy of Oxygen Surface Exchange in (La,Sr)MnO_3 Thin Films," poster presented by Lu Yan (CMU) at 11th Annual SECA Workshop, Pittsburgh, Pennsylvania (July 2010).

13. "Crystallographic Anisotropy of Oxygen Surface Exchange in (La,Sr)MnO_3 Thin Films," poster presented by Lu Yan (CMU) at Gordon Research Conference on Solid State Studies in Ceramics, New London, New Hampshire (July 2010).

References

1. E. Maguire, B. Gharbage, and F.M.B. Marques, "Cathode Materials for Intermediate Temperature SOFCs," *Solid State Ionics*, (2000).

2. N.Q. Minh and T. Takahashi, Science and Technology of Ceramic Fuel Cells, Elsevier Science (1995).

3. K.-C. Chang, B. Ingram, K.R. Balasubramaniam, B. Yildiz, D. Hennessy, P.A. Salvador, N. Leyarovska, and H. You, "In situ Synchrotron X-ray Studies of Dense Thin-Film Strontium-Doped Lanthanum Manganite Solid Oxide Fuel Cell Cathodes," *Mat. Res. Soc. Symp. Proc.*, **1126**, 1126-S08-10 (2009).

4. T.T. Fister, D.D. Fong, J.A. Eastman, P.M. Baldo, M.J. Highland, P.H. Fuoss, K.R. Balasubramaniam, J.C. Meador, and P.A. Salvador, "In situ Characterization of Strontium Surface Segregation in Epitaxial $La_{0.7}Sr_{0.3}MnO_3$ Thin Films as a Function of Oxygen Partial Pressure," *Applied Physics Letters,* **93**, 151904 (2008). doi: 10.1063/1.2987731

5. P.A. Salvador, J. Meador, K.R. Balasubramaniam, P. Fuoss, J. Eastman, D. Fong, and P. Baldo, "SOFC Cathode Surface Chemistry and Optimization Studies," *FY 2007 Office of Fossil Energy Fuel Cell Program Annual Report*, U.S. Department of Energy, Paper IV.A.4 (2007).

6. P.A. Salvador, L. Yan, S. Wang, K.R. Balasubramaniam, P. Fuoss, J. Eastman, D. Fong, T. Fister, P. Baldo, H. You, K.-C. Chang, B. Yildiz, and I.B. Misirlioglu, "SOFC Cathode Chemistry and Optimization Studies," *FY 2008 Office of Fossil Energy Fuel Cell Program Annual Report*, U.S. Department of Energy, Paper III.A.2 (2008).

7. K. Katsiev, B. Yildiz, K.R. Balasubramaniam, and P.A. Salvador, "Electron Tunneling Characteristics on $La_{0.7}Sr_{0.3}MnO_3$ Thin-Film Surfaces at High Temperature," *Applied Physics Letters,* **95**, 092106 (2009). doi: 10.1063/1.3204022

8. J. Fleig, H. Kim, J. Jamnik, and J. Maier, "Oxygen Reduction Kinetics of Lanthanum Manganite (LSM) Model Cathodes: Partial Pressure Dependence and Rate-Limiting Steps," *Fuel Cells*, **8**, 330-337 (2008).

9. L. Yan, K.R. Balasubramaniam, K.-C. Chang, H. You, and P.A. Salvador, "Microstructural Effects on the Oxygen Exchange Kinetics of $La_{0.7}Sr_{0.3}MnO_3$ Thin Films," *Electrochemical Society Transactions,* **35**, (2011). doi: 10.1149/1.3570197

10. T.T. Fister, D.D. Fong, J.A. Eastman, H. Iddir, P. Zapol, P. Fuoss, M. Balasubramanian, R.A. Gordon, K.R. Balasubramaniam, and P.A. Salvador, "Total Reflection Inelastic X-ray Scattering from a 10 nm Thick $La_{0.6}Sr_{0.4}CoO_3$ Thin Film," *Physical Review Letters,* **106**, 037401 (2011). doi: 10.1103/PhysRevLett.106.037401

11. L. Yan, B. Kavaipatti, S. Wang, H. Du, and P. Salvador, "Electrical Conductivity Relaxation Study of Solid Oxide Fuel Cell Cathodes Using Epitaxial (001)-Oriented Strontium-Doped Lanthanum Manganite Thin Films," *Mat. Res. Soc. Symp. Proc.*, **1255**, 1255-M02-02 (2010). doi: 10.1557/PROC-1255-M02-02

12. P.A. Salvador, L. Yan, S. Wang, K.R. Balasubramaniam, P. Fuoss, J. Eastman, D. Fong, T. Fister, P. Baldo, H. You, K.-C. Chang, B. Yildiz, K. Katsiev, C. Heske, and S. Krause, "SOFC Cathode Surface Chemistry and Optimization Studies," *FY 2010 Office of Fossil Energy Fuel Cell Program Annual Report*, U.S. Department of Energy, Paper III.A.3 (2010).

13. P.A. Salvador, L. Yan, S. Wang, K.R. Balasubramaniam, P. Fuoss, J. Eastman, D. Fong, T. Fister, P. Baldo, H. You, K.-C. Chang, B. Yildiz, K. Katsiev, C. Heske, and S. Krause, "SOFC Cathode Surface Chemistry and Optimization Studies," *FY 2009 Office of Fossil Energy Fuel Cell Program Annual Report*, U.S. Department of Energy, Paper III.A.3 (2009).

14. K. Katsiev, B. Yildiz, K. Balasubramaniam, and P.A. Salvador, "Correlations of Electronic and Chemical State on $La_{0.7}Sr_{0.3}MnO_3$ Dense Thin-Film Cathode Surface," *Electrochemical Society Transactions,* **25**, 2309-2318 (2009).

15. L. Yan, K.R. Balasubramaniam, S. Wang, H. Du, and P.A. Salvador, "Effects of Crystallographic Orientation on the Oxygen Exchange Rate of $La_{0.7}Sr_{0.3}MnO_3$ Thin Films," *Solid State Ionics,* **194**, 9-16 (2011). doi: 10.1016/j.ssi.2011.05.004

16. M. Burriel, G. Garcia, J. Santiso, J.A. Kilner, J.C.C. Richard, and S.J. Skinner, "Anisotropic Oxygen Diffusion Properties in Epitaxial Thin Films of $La_2NiO_{4+delta}$," *J. Mater. Chem.,* **18**, 416-422 (2008). doi: 10.1039/b711341b

17. G. Kim, S. Wang, A.J. Jacobson, and C.L. Chen, "Measurement of Oxygen Transport Kinetics in Epitaxial $LaNiO_{4+delta}$ Thin Films by Electrical Conductivity Relaxation," *Solid State Ionics,* **177**, 1461-1467 (2006).

18. L. Chen, C.L. Chen, and A.J. Jacobson, "Electrical Conductivity Relaxation Studies of Oxygen Transport in Epitaxial $YBa_2Cu_3O_{7-d}$ Thin Films," *IEEE Transactions on Applied Superconductivity,* **13**, 2882-2885 (2003).

19. X. Chen, S. Wang, Y.L. Yang, L. Smith, N.J. Wu, B.-I. Kim, S.S.P.A.J. Jacobson, and A. Ignatiev, "Electrical Conductivity Relaxation Studies of an Epitaxial $La_{0.5}Sr_{0.5}CoO_{3-d}$ Thin Film," *Solid Sates Ionics,* **146**, 405 (2002).

20. A. Rivera, J. Santamarı, and C. Leo, "Electrical Conductivity Relaxation in Thin-Film Yttria-Stabilized Zirconia," *Applied Physics Letters*, **78**, 610 (2001).

III.A.4 Theory, Investigation and Stability of Cathode Electro-Catalytic Activity

Meilin Liu (Primary Contact), Dong Ding, Wentao Qin, Matt Lynch, Xingbao Zhu, Mingfei Liu, Xiaxi Li
Georgia Institute of Technology
School of Materials Science and Engineering
771 Ferst Drive
Atlanta, GA 30332-0245
Phone: (404) 894-6114; Fax: (404) 894-9140
E-mail: meilin.liu@mse.gatech.edu

DOE Project Manager: Briggs White
Phone: (304) 285-5437
E-mail: Briggs.White@netl.doe.gov

Contract Number: NT0006557

Start Date: September 1, 2008
End Date: August 31, 2011

Fiscal Year (FY) 2011 Objectives

- Characterize the surface composition, morphology, and electro-catalytic properties of a catalyst infiltrated $La_{0.6}Sr_{0.4}Co_{0.2}Fe_{0.8}O_{3-\delta}$ (LSCF) cathode.
- Establish the scientific basis for rational design of high-performance cathodes by combining a porous backbone (such as LSCF) with a thin catalyst coating.

FY 2011 Accomplishments

- Developed a semi-empirical phenomenological model for studying the mechanism of performance enhancement of the $La_xSr_{1-x}Mn_8O_{3-\delta}$ (LSM)-coated LSCF cathode.
- Optimized LSM solution infiltration process further on LSCF pellets by a variety of parameters including solution pH value, surfactant addition, thermal treatment conditions as well as ambient humidity.
- Quantified the correlation among performance, infiltration concentration and operation condition (polarization current density) of LSM-coated LSCF cathode. Characterized porous LSCF and LSM-coated LSCF cathode electrochemically as a function of the time of polarization and relaxation under different oxygen partial pressures.
- Characterized the detailed structure, composition, and morphology of pure LSCF surfaces, the LSM/LSCF interfaces in LSM-coated LSCF at 850°C annealed for 900 hours.
- Developed new Mn-based materials infiltration into LSCF cathode, and demonstrated that the infiltration of $Pr_xSr_{1-x}MnO_{3-\delta}$ (PSM) with lanthanum in A site replaced by Pr could lead to much more performance improvement over LSM in symmetrical cell and full cell configurations.

Introduction

One of the reasons that LSCF-based cathodes show much better performance than those based on LSM is that LSCF has much higher ionic and electronic conductivity than LSM, significantly extending the active sites beyond the triple-phase boundaries (TPBs) [1]. One obvious downfall for LSCF is that it reacts adversely with YSZ, which can be mitigated by the use of a buffer layer of doped-CeO_2 between LSCF and YSZ [2]. However, the catalytic activity of the stand-alone LSCF cathodes is likely to be limited by the surface catalytic properties. Further, the long-term stability of LSCF cathodes is a concern. Thus, it is hypothesized that the *performance* and *stability* of a porous LSCF cathode may be improved by the application of a catalytically active coating though infiltration. The selection of the catalytic materials as well as the detailed microstructures of the porous LSCF and the catalyst layer may critically impact the performance of the proposed cathodes. The objective of this project is to optimize the composition and morphology of the catalyst layer and microstructure of the LSCF backbone for better performance.

Approach

A semi-empirical method based on continuum modeling was developed for interpretation of electrochemical testing results regarding the performance enhancement of the LSM coated LSCF cathode. Two kinds of infiltration solutions, non-aqueous-based and water-based, were used for deposition of LSM films on LSCF pellets to optimize the infiltration process and to examine the microstructure evolution during annealing at high temperatures. The optimized LSM infiltration process was applied to porous LSCF cathodes which were electrochemically examined under steady-state polarization using symmetrical cells with three-electrode configuration. The PSM infiltration process is as the same as for the LSM infiltration. The effects of LSM and PSM coating on performance of the LSCF cathode were determined using symmetrical and anode-supported button cells. The detailed structure, composition, and morphology of the LSCF surface, the LSM/LSCF interfaces in LSM-coated LSCF were characterized using electron microscopy and spectroscopy. The microscopic

details of the cathodes are also correlated directly with their electrochemical performance.

Results

A Semi-Empirical Phenomenological Model for Mechanism of LSM-coated LSCF Cathode

We extended our model of the phenomenon of LSM-coated LSCF cathode. Figure 1(a) shows the trend of the area normalized interfacial resistance modeled as a function of oxygen vacancy concentration dependent upon cathodic bias. LSCF clearly has a different trend from LSM, as it is suspected that the trend of LSM leads to improved performance under large bias when the LSM is coated with LSCF. Figure 1(b) shows the trend of interfacial resistance as oxygen vacancy formation is made less favorable by modifying the free energy of reaction. The trend shows an increasing tendency toward larger activation at more severe cathodic bias. Figures 1(c) and (d) show how the trend of the area specific resistance is affected by making adsorption and dissociation of oxygen more favorable. These results indicate that the LSM coating is less active at open circuit voltage because it has fewer oxygen vacancies, however its activation under large cathodic bias due to larger relative increase in vacancy concentration as well as its suspected more favorable adsorption properties make it more active at mild cathodic bias. These modeling trend agree with our experiments in both thin-films and porous, operational cathodes.

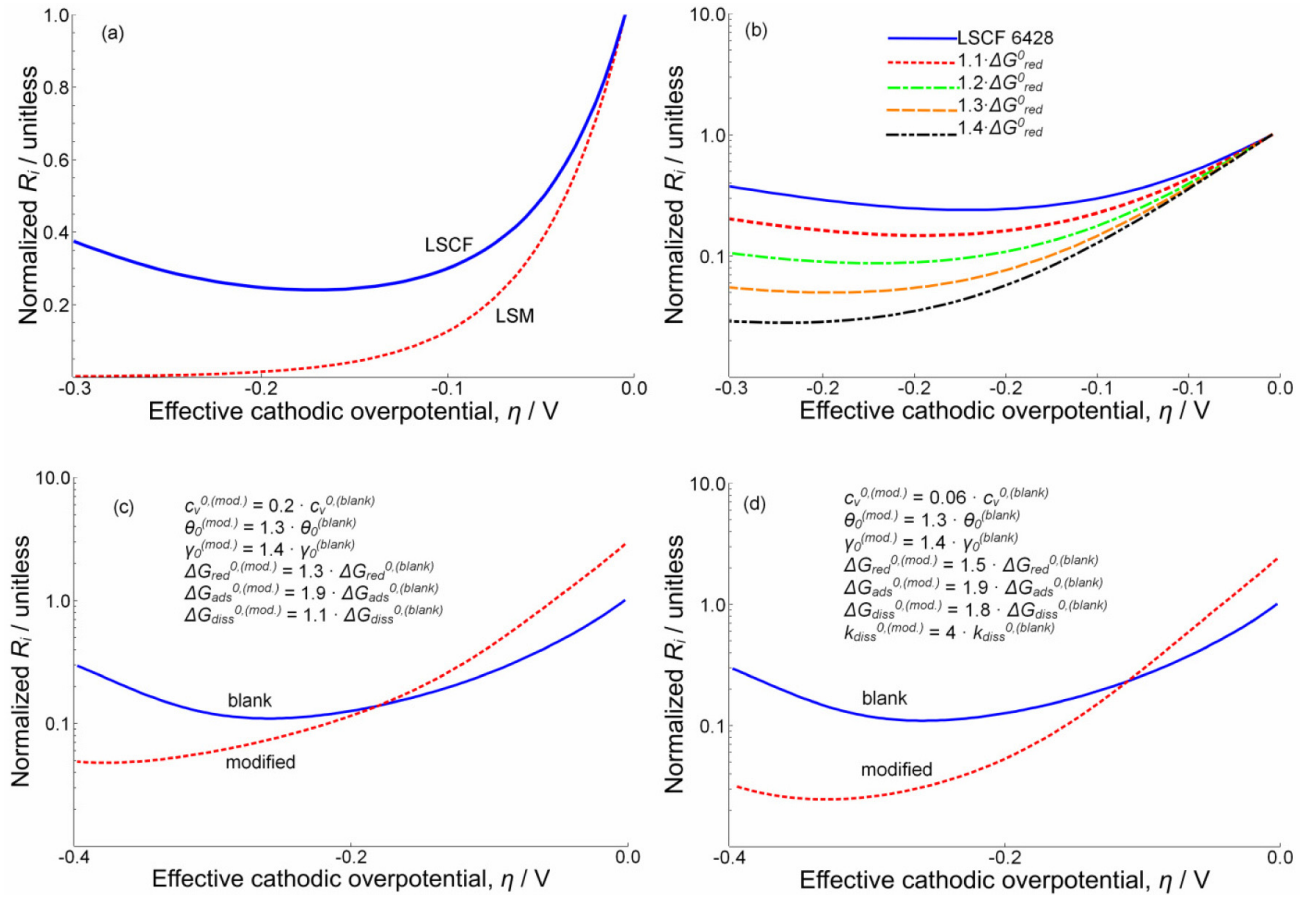

FIGURE 1. a) Normalized interfacial resistance of LSCF and LSM films assuming that the current at the effective overpotential is described by Equation

$$i \propto \left(\frac{C_v}{C_v^0} - 1 \right)$$

normalized to their respective values at open circuit voltage (OCV). b) Normalized interfacial resistance associated with tighter oxygen binding associated with lower free energy of oxygen reduction assuming current proportional to oxygen vacancy concentration. c) Simulated normalized interfacial resistance versus effective cathodic overpotential for blank LSCF and LSCF with modified surface properties when $\Delta G_{red}^{0(surface)} < \Delta G_{red}^{0(LSCF)}$, $\Delta G_{diss}^{0(surface)} < \Delta G_{diss}^{0(LSCF)}$, and $\Delta G_{ads}^{0(surface)} < \Delta G_{ads}^{0(LSCF)}$. R_i is normalized to the value of the blank LSCF at OCV. d) Simulated normalized interfacial resistance versus effective cathodic overpotential for blank and LSCF with modified surface properties when $\Delta G_{red}^{0(surface)} < \Delta G_{red}^{0(LSCF)}$, $\Delta G_{diss}^{0(surface)} < \Delta G_{diss}^{0(LSCF)}$, $\Delta G_{ads}^{0(surface)} < \Delta G_{ads}^{0(LSCF)}$, $k_{diss}^{0(surface)} > k_{diss}^{0(LSCF)}$.

LSM Coating on Porous LSCF Cathode

We have successfully fabricated dense continuous LSM films with desired structure, composition, morphology, and thickness on the LSCF surface by two kinds of infiltration solutions: non-aqueous and water-based. The infiltration process parameters, including solution pH value, surfactant addition, thermal treatment conditions (thermal history of substrate), and ambient humidity (drying time), have been demonstrated to have critical effects on the ultimate quality of LSM films.

Surface and Interface Study of LSCF and LSM/LSCF

Optimized solution infiltration was applied to LSCF pellets and LSM pellets to prepare LSM films on different substrates. Subsequently the samples were annealed at 850°C for 900 hours to examine microstructure evolution. As a comparison, a blank LSCF substrate was thermally treated under the same condition. Figure 2(a) presents a transmission electron microscope (TEM) image of the surface of an LSCF pellet after annealing at 850°C for 900 hours. The sample was coated with a thin layer of Cr to provide delineation of the sample surface. The image shows presence of crystalline oxide particles on the LSCF, and the particles have a maximum thickness of 0.17 μm. A high-resolution (HR)TEM image taken in the interfacial area (marked by the yellow square in Figure 2(a)) between the surface oxide particle and the LSCF is displayed in Figure 2(b). The HRTEM image reveals lattice fringes of both the LSCF and the surface oxide particle. Fourier-filtered images of the surface oxide and LSCF in the green and red rectangular areas in the two phases are presented in Figures 2(c) and (d), respectively. The structural coherence is better manifested by alignments of the two pairs of lattice fringes of these two phases. The spacings of one of these two pairs of lattice fringes with the least mistmatch of about 1.8% are labeled in the images. Sr, La and O were identified by energy dispersive X-ray spectroscopy from the crystalline particle with thickness labeled in Figure 2(a). With standardless quantification, the atomic ratio of Sr/La is 1.4.

Figure 2(e) is a TEM image of an LSCF grain boundary in the sample of LSM-coated LSCF pellet

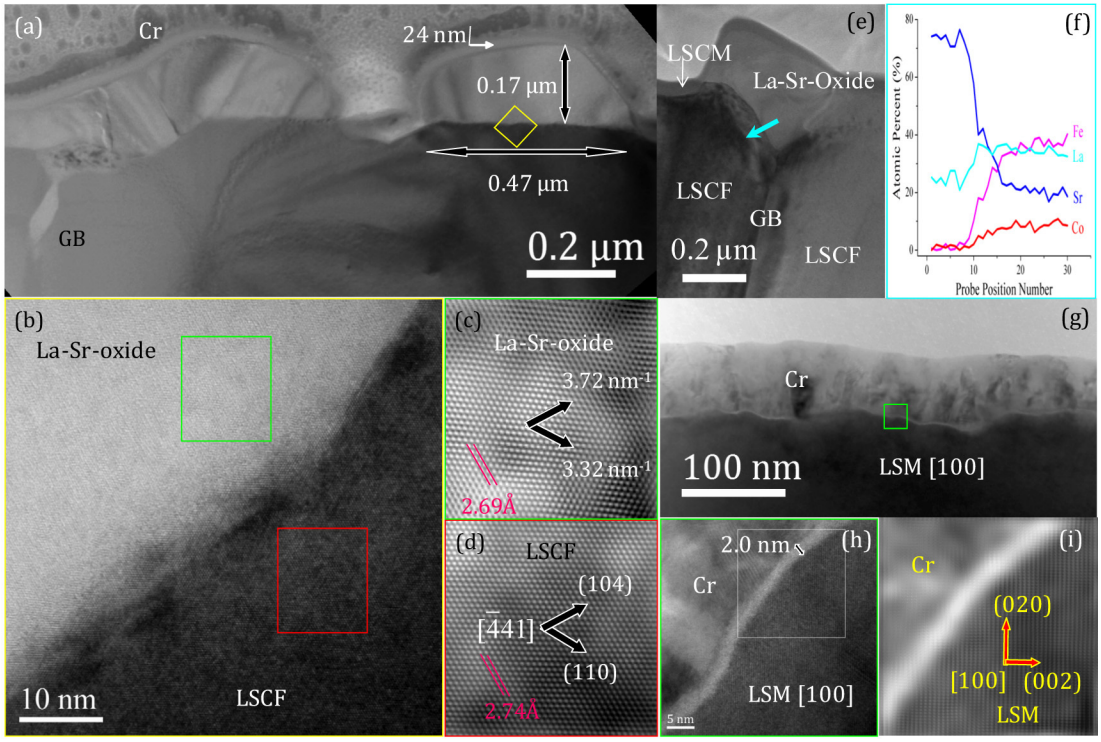

FIGURE 2. (a) TEM image of surface of LSCF pellet annealed at 850°C for 900 hours. A thin layer of Cr coating was used to delineate the sample surface. (b) HRTEM image of the interface between an oxide particle and the underlying LSCF pellet in the yellow square marked in (a). (c) and (d) Fourier-filtered images of the green and red rectangles marked in the surface oxide and the LSCF in (b). (e) TEM image of LSCF grain boundary of LSM-coated LSCF pellet after annealing at 850°C for 900 hours. (f) Profiles of atomic percents along the line marked by the blue arrow in (e). (g) TEM image of LSM-coated LSM pellet after annealing at 850°C for 900 hours. The sample received sequential depositions of C and Cr for the purpose of protection and delineation of the surface. (h) HRTEM image of the green rectangular area highlighted in (g). (i) Fourier-filtered image of the white recgangular area marked in (h).

after the annealing. Mn has been found to have diffused along the LSCF grain boundary and is absent near the surface of the LSCF grain boundary as shown in Figure 2(f), which presents profiles of atomic percents along the line marked by the blue arrow in Figure 2(e). A sub-micron particle that consists of La, Sr and O is located on top of the LSCF grain boundary. With the absence of Mn near the surface of the LSCF grain boundary, the finding of the La-Sr-oxide particle here is consistent with that on the blank LSCF pellet after the annealing. Figure 2(g) displays a TEM image of the surface of LSM-coated LSCF pellet after the annealing. C and Cr were deposited in sequence to protect and delineate the sample surface. The figure shows an LSM grain oriented with [100] zone axis along the electron transmission direction. An interfacial layer with a thickness on the order of 1 nm exists between Cr and LSM. A high-resolution image of the Cr/LSM interface within the green square area highlighted in Figure 2(g) is presented in Figure 2(h). The Cr/LSM interfacial layer appears as amorphous, and the LSM [100] zone-axis lattice fringes are clearly visible and labeled in the Fourier-filtered image displayed in Figure 2(i). There is not a discrete LSM layer on the sample surface, either. The absence of such a discrete LSM layer is believed to be due to the LSM layer coated on the LSM pellet assumed an epitaxial relationship with respect to the underlying LSM pellet.

TEM observation suggests that formation of thick oxide of La and Sr after annealing both on the blank LSCF pellet, and possibly along the LSCF grain boundaries on the LSM-coated LSCF pellet where Mn is insufficient due to its diffusion. As a sharp contrast, there is no such thick oxide on the LSM-coated LSM after annealing. Such thick surface oxide particles that are expected to severely hamper electrochemical activities have not emerged after annealing.

Cathode Performance and Stability Improvements by LSM Coating on LSCF Surface

To investigate the electrochemical behavior of LSM infiltrated porous LSCF cathodes under different cathodic polarization conditions and correlate the performance with the LSM infiltration solution concentration (to which the coating thickness should be proportional), a series of direct current (DC) passage treatments were employed to symmetrical cells with a three-electrode configuration and relevant steady polarization behavior was examined [3]. Shown in Figure 3 is a comparison in interfacial polarization resistance (R_p) for a blank LSCF and an LSM-infiltrated LSCF cathode with different concentrations of LSM solutions measured at different cathodic current densities. Obviously, R_p of all infiltrated LSCF cathodes are larger than that of the blank LSCF under the open circuit voltage condition, and it increases with solution

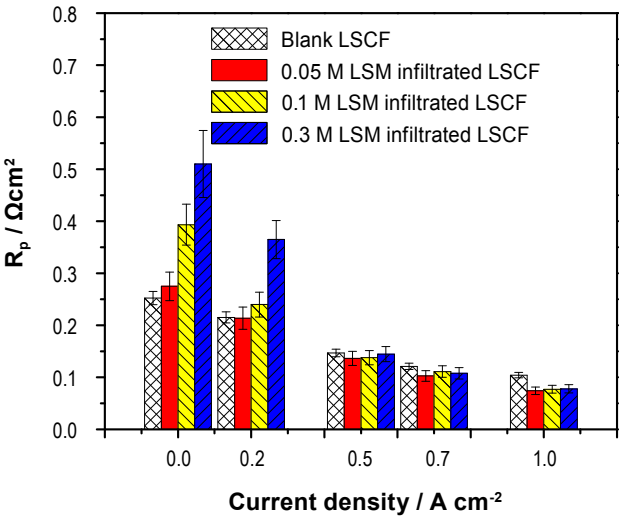

FIGURE 3. Interfacial polarization resistance versus cathodic current density for LSCF cathodes without/with 0.05, 0.1 M, and 0.3 M of LSM infiltration measured at 750°C. Impedance spectra were obtained under a steady state polarization with a constant cathodic current passage.

concentration. When a cathodic current passed through the cell, R_p in all cases decreased. The higher the infiltration solution concentration, the larger the decreasing rate. As the current density is high enough (e.g., 1 A cm^{-2}), R_p for all infiltrated LSCF cathode show similar values which is visibly lower than that of blank LSCF cathode under the same conditions. Accordingly, it seems that there is a compromise between performance improvement and solution concentration under different operation conditions.

A typical comparison for the overpotential dependence of interfacial polarization resistance (R_p) for the LSCF cathode with/without LSM infiltration was shown in Figure 4(a). Clearly there is an intersection at an overpotential of 0.08 V. R_p for LSM infiltrated LSCF cathode decreases much faster than that for blank LSCF cathode with η, leading to smaller R_p at higher η in spite of the initially larger value in the former. This is the reason that the performance of an LSM-infiltrated LSCF cathode is enhanced under typical fuel cell operation conditions.

Exploration of Mn-Based Perovskite Similar to LSM as a Catalyst Material

The main objective of the project is to develop a catalytically active coating onto LSCF backbone to improve the performance and stability of a porous LSCF cathode. Based on our knowledge for LSM infiltration, a new Mn-based perovskite material, PSM, was developed using a similar film preparation technique [4]. Presented in Figure 4(a) are R_p versus overpotential for blank LSCF and LSCF infiltrated with the identical concentration PSM and LSM solution. The

initial R_p of PSM is lower than blank LSCF and LSM infiltrated LSCF cathode, implying that it has more catalytic activity for oxygen reduction. Under cathodic polarization, the PSM infiltrated LSCF cathode also showed significant activation behavior, making the enhancement in performance more evident. However, long-term stability is more important, especially for highly active materials. PSM infiltrated LSCF cathode was applied to our homemade button cells and long-term stability was tested at a constant voltage of 0.7 V and 750°C. Figure 4(b) showed lifetime of the full cells with different cathodes. As a comparison, the performance of the cells with the baseline and LSM infiltrated LSCF cathodes were presented as well. Clearly, the cells with PSM infiltration cathode showed better performance and was even still increasing with 250-hour operation. Compared with LSM infiltration, the improvement in performance is around 5%. Due to possible degradation of the pure LSCF cathode during operation, more significant difference in performance would be expected over blank cells with operation.

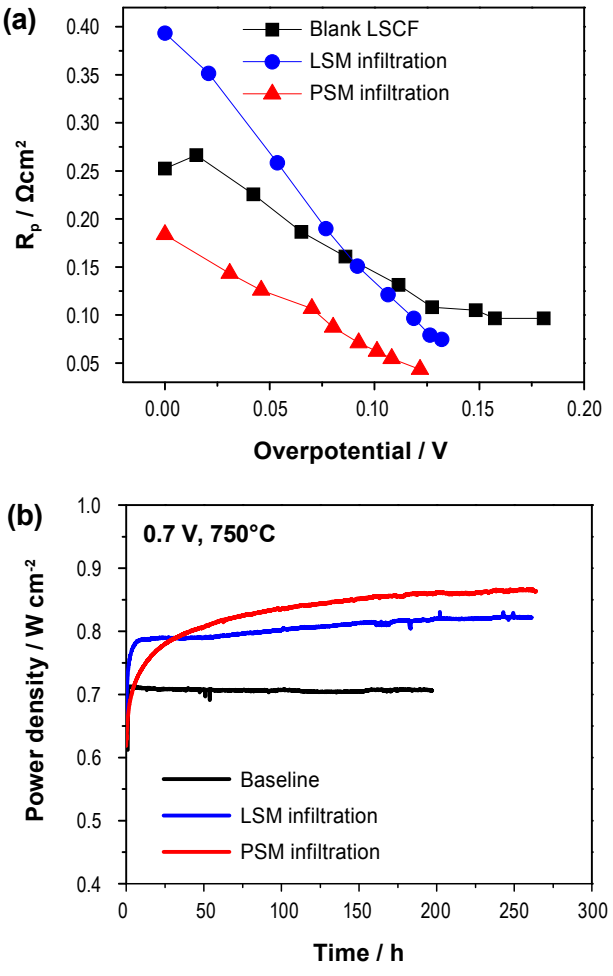

FIGURE 4. (a) Interfacial polarization resistance versus overpotential for LSCF cathodes without/with 0.1 M of PSM and LSM infiltration measured at 750°C. (b) Typical power outputs of the homemade button cells with PSM and LSM infiltrated LSCF cathodes (compared with baseline LSCF cathode) at a constant voltage of 0.7 V at 750°C.

Conclusions

A semi-empirical method based on continuum modeling was developed for interpretation of electrochemical testing results regarding the performance enhancement of the LSM coated LSCF cathode. The dense continuous LSM films with desired structure, composition, morphology, and thickness on LSCF surface were developed by a series of infiltration parameters optimization. The correlation between performance improvement, infiltration solution concentration, and operation condition (polarization condition) shows the performance improvement can be achieved in the LSCF cathode with 0.05, 0.1 and 0.3 M LSM infiltration at a relatively high cathodic current passage. It also demonstrated that a Mn-based perovskite material, PSM, could lead to more performance improvement for LSCF cathodes. Microanalysis revealed that presence of Mn is able to effectively suppress the formation of thick oxide of La and Sr on blank LSCF pellets during annealing at 850°C for 900 hours, which may be related to the degradation of LSCF cathodes.

FY 2011 Publications/Presentations

1. M. Lynch, L. Yang, W.T. Qin, J.J. Choi, M.F. Liu, K. Blinn, and M.L. Liu, "Enhancement of $La_{0.6}Sr_{0.4}Co_{0.2}Fe_{0.8}O_{3-\delta}$ Durability and Surface Electrocatalytic Activity by $La_xSr_{1-x}Mn_8O_{3-\delta}$ Investigated Using a New Test Electrode Platform," *Energy and Environmental Science*, 4, 2249-2258, 2011.

2. J.J. Choi, W.T. Qin, M.F. Liu, and M.L. Liu, "Preparation and Characterization of $(La_{0.8}Sr_{0.2})_{0.95}MnO_{3-\delta}$ (LSM) Thin Films and LSM/LSCF Interface for Solid Oxide Fuel Cells," *Journal of the American Ceramic Society*, DOI: 10.1111/j.1551-2916.2011.04614.x.

3. M. Lynch and M. Liu, "Investigation of Sheet Resistance in Thin-Film Mixed-Conducting SOFC Cathode Test Cells," *J. Power Sources*, 195(16), 5155-5166, 2010.

4. X. Lou, Z. Liu, S. Wang, Y. Xiu, C.P. Wong, and M. Liu, "Controlling the Morphology and Uniformity of a Catalyst-Infiltrated Cathode for SOFCs by Tuning Wetting Property," *J. Power Sources*, 195, 419–424, 2010.

5. L.F. Nie, M.F. Liu, Y.J. Zhang, and M. Liu, "$La_{0.6}Sr_{0.4}Co_{0.2}Fe_{0.8}O_{3-\delta}$ Cathodes Infiltrated with Sm-Doped CeO_2 for SOFCs," *J. Power Sources*, 195(15), 4704-4708, 2010.

6. Z. Liu, Z.W. Zheng, M.F. Han, et al., "High Performance SOFCs Based on Tri-Layer YSZ by Low Temperature Sintering Process," *J. Power Sources*, 195, 7230-7233, 2010.

7. L.F. Nie, Z. Liu, M.F. Liu, L. Yang, Y. Zhang, and M. Liu, "Enhanced Performance of $La_{0.6}Sr_{0.4}Co_{0.2}Fe_{0.8}O_{3-\delta}$ Cathodes with Graded Microstructure Fabricated by Tape Casting," *Journal of Electrochemical Science and Technology*, 1(1), 50-56, 2010.

8. M. Lynch, X. Li, L. Yang, D. Mebane, and M. Liu, "Investigation of SOFC Cathode Kinetics by Means of Continuum Modeling and Well-Defined Electrodes," 217th Meeting of The Electrochemical Society, Vancouver, British Columbia, Canada, April 2010.

9. X. Li, M. Lynch, M.F. Liu, X. Lou, and M. Liu, "Investigating Catalytic Properties of Cathode Materials Using Patterned Electrodes," 217th Meeting of The Electrochemical Society, Vancouver, British Columbia, Canada, April 2010.

References

1. S.P. Jiang, "A Comparison of O_2 Reduction Reactions on Porous (La,Sr)MnO_3 and (La,Sr)(Co,Fe)O_3 Electrodes," *Solid State Ionics*, 2002. **146**(1-2): p. 1-22.

2. D. Stover, H.P. Buchkremer, and S. Uhlenbruck, "Processing and Properties of the Ceramic Conductive Multilayer Device Solid Oxide Fuel Cell (SOFC)," *Ceramics International*, 2004. **30**(7): p. 1107-1113.

3. D. Ding, M.Y. Gong, C.C. Xu, N. Baxter, Y.H. Li, J. Zondlo, K. Gerdes, and X.B. Liu, "Electrochemical Characteristics of Samaria-Doped Ceria Infiltrated Strontium-Doped $LaMnO_3$ Cathodes with Varied Thickness for Yttria-Stabilized Zirconia Electrolytes," *Journal of Power Sources*, 2011. **196**(5): p. 2551-2557.

4. S.J. Skinner, "Recent Advances in Perovskite-type Materials for Solid Oxide Fuel Cell Cathodes," *International Journal of Inorganic Materials*, 2001. **3**(2): p. 113-121.

III.A.5 Cathode Contact Materials for Anode-Support Cell Development

Michael C. Tucker (Primary Contact),
Lutgard DeJonghe, Lei Cheng
Lawrence Berkeley National Laboratory (LBNL)
MS 62-203
1 Cyclotron Rd.
Berkeley, CA 94720
Phone: (510) 486-5304; Fax: (510) 486-4881
E-mail: mctucker@lbl.gov

DOE Project Manager: Joseph Stoffa
Phone: (304) 285-0285
E-mail: Joseph.Stoffa@netl.doe.gov

Contract Number: MSD-NETL-01

Start Date: October 1, 2010
End Date: September 30, 2011

Fiscal Year (FY) 2011 Objectives

- Identify and develop candidate materials, architectures and concepts to solve issues related to delamination and degradation of cathode contact material.
- Initiate in situ testing using commercially available lab-scale fuel cells.
- Target high-risk/high-benefit strategies and novel technical approaches.

FY 2011 Accomplishments

- Screened a long list of candidate cathode materials for suitability as cathode contact pastes. Determined conductivity, sintering behavior, coefficient of thermal expansion (CTE), reactivity with lanthanum strontium cobaltite ferrite (LSCF) and $Mn_{1.5}Co_{1.5}O_4$ (MCO) neighbor materials and bonding.
- Determined area specific resistance (ASR) of most promising candidates at 800°C for 200 h.
- Conducted post-mortem analysis of ASR specimens to determine extent of reaction between layers.
- Identified novel cathode contact schemes and materials. Determined feasibility of novel approaches, and selected most promising candidates for further development.
- Initiated in situ testing of cathode contact material (CCM) candidates using anode-supported lab-scale cells and MCO-coated 441 interconnect coupons.

Introduction

The main focus of the LBNL project is to support industrial Solid State Energy Conversion Alliance (SECA) teams in their effort to commercialize solid oxide fuel cell (SOFC) technology that meets the SECA performance and cost targets. In order to achieve this goal, it is necessary to improve the performance of SOFC components through selection of appropriate materials and development of novel yet inexpensive alternative materials, architectures and concepts. The primary challenge addressed by LBNL during FY 2011 concerns electrical connection and bonding between the interconnect and cathode layers, shown in Figure 1. Historically, cathode materials such as lanthanum strontium manganate are used as a CCM paste to bond the cell to the interconnect. High temperature is typically required to achieve good bonding, however, leading to rapid oxidation of the stainless steel interconnect. If a temperature low enough to avoid oxidation of the steel (<1,000ºC) during the bonding step is employed, poor bonding and eventual delamination of the contact material occur. The goals of the work at LBNL are to: 1) screen known candidate cathode materials to ascertain whether they can be used as CCMs displaying adequate properties after bonding at <1,000ºC; and 2) identify and develop novel materials, architectures, and approaches to solving this issue.

Approach

Accordingly, in FY 2011 the LBNL core effort has been focused on the following issues:

- Identification of cathode materials from the existing literature that offer promise as candidate cathode-interconnect contact materials.
- Synthesis and characterization of candidate materials, including determination of sintering

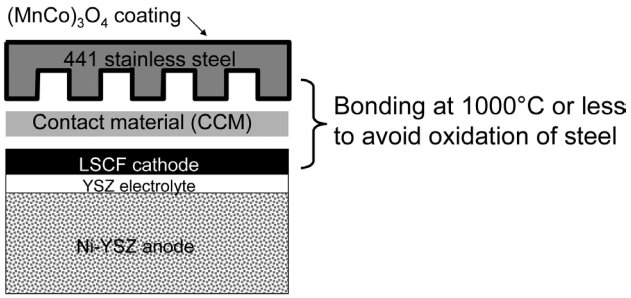

FIGURE 1. Schematic of CCM Placement in Cell Stack

behavior, conductivity, bonding, CTE, and reaction with neighbor materials.
- Down-selection of the most promising candidates, and determination of the long-term stability of their ASR in relevant test geometries using model cathode and interconnect layers.
- Demonstration of the best materials in lab-scale cells operating under realistic conditions.
- Novel materials and architectures have also been pursued, wherein the bonding and electronic connection functions of the CCM material are separated, and composite materials are used to provide the dual functionality.

Results

Screening of Candidate CCM Materials

A long list of cathode compositions were identified as candidates for application as CCM materials. The compositions were purchased from Praxair or fabricated by GNP. The properties of primary relevance, including conductivity, sintering behavior, CTE, and reactivity with MCO and LSCF were then determined. The summary of this screening effort suggested that the most promising CCM candidates are LSCF and lanthanum strontium copper ferrite (LSCuF), chosen for extensive sintering at low temperature and strontium samarium cobalt oxide (SSC) and lanthanum strontium cobaltite (LSC), chosen for high conductivity.

Testing of Most Promising Candidates

These four materials were then incorporated into ASR specimens in which electrical resistances of the individual LSCF/CCM and 441-MCO/CCM interfaces and LSCF/CCM/MCO junction were monitored over time. Figure 2 shows a schematic of the sample geometry and ASR results. LSC and SSC are the most promising compositions tested to date. They provided low and stable ASR for 200 h at 800°C.

After testing, the ASR specimens were cross-sectioned and analyzed with scanning electron microscope (SEM) and energy dispersive X-ray analysis (EDAX). Figure 3 shows SSC on MCO-coated 441 substrate. The layers are well-bonded and homogeneous. EDAX indicated minimal interdiffusion across the CCM/LSCF interface. Some interdiffusion between MCO and LSC, SSC, and LSCuF did occur. We speculate that this may alter the electrical and oxygen transport properties of the MCO, thereby influencing the growth rate of the underlying chromia scale.

In situ tests are now under way. The CCM candidates are used to bond MCO-coated 441 interconnect coupons to anode-supported lab-scale cells. Total ASR and high-temperature bonding will be assessed.

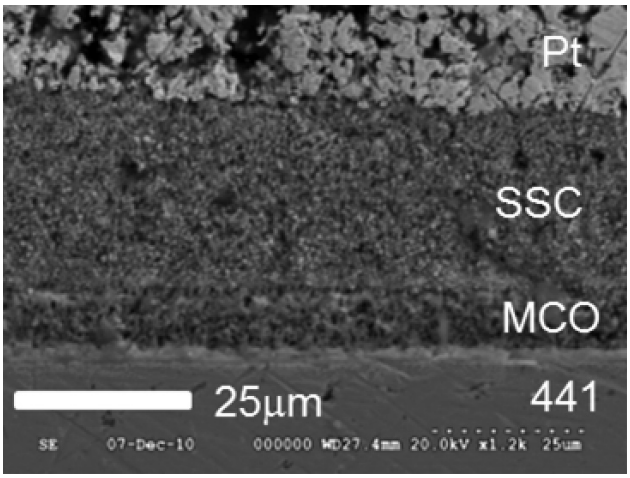

FIGURE 3. Post-Mortem Cross Section SEM Image of SSC on MCO-441 Substrate

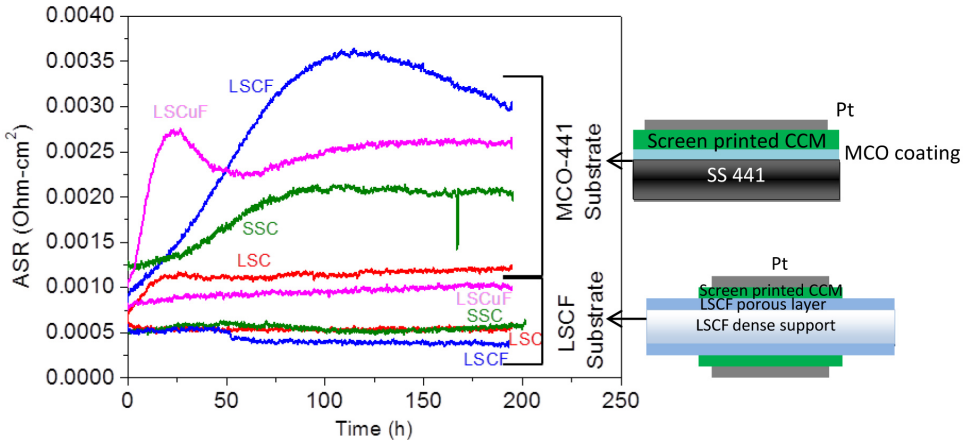

FIGURE 2. ASR for Various CCM Compositions at 800°C

Conclusions and Future Directions

- Many candidate CCM compositions were synthesized and screened for relevant physical properties.
- LSCF, LSCuF, SSC, and LSC were chosen as the most promising candidates, and ASR testing was conducted with these compositions. Initial results indicate that SSC and LSC provide low, stable ASR. Post-mortem analysis indicated minimal interdiffusion between the CCM and neighbor materials.
- Assessment of mechanical properties, tolerance to thermal cycling, and in situ testing are under way.
- Novel solutions to the CCM issue were assessed and developed.

Special Recognitions & Awards/Patents Issued

1. Patent application: Improved electrical contact material

FY 2011 Publications/Presentations

1. M. Tucker and L. Cheng, "Integrated Thermal Management Strategy and Materials for Solid Oxide Fuel Cells," *J. Power Sources*, in review.

2. M. Tucker, L. Cheng, and L. DeJonghe, "Glass-Containing Composite Cathode Contact Materials for Solid Oxide Fuel Cells," *J. Power Sources*, in review.

3. M. Tucker, L. Cheng, and L. DeJonghe, "Selection of Cathode Contact Materials for Solid Oxide Fuel Cells," *J. Power Sources*, in review.

III.A.6 Electronic Structure and Chemical State on $La_{0.7}Sr_{0.3}MnO_3$ Dense Thin-Film Cathode Surfaces – Correlations to Thin-Film Strain

Bilge Yildiz (Primary Contact), Wonyoung Lee, Helia Jalili
Massachusetts Institute of Technology
Department of Nuclear Science and Engineering
77 Massachusetts Avenue, 24-210
Cambridge, MA 02139
Phone: (617) 324-4009; Fax: (617) 258-8863
E-mail: byildiz@mit.edu

DOE Project Manager: Briggs White
Phone: (304) 285-5437
E-mail: Briggs.White@netl.doe.gov

Subcontractor:
Clemens Heske
University of Nevada, Las Vegas (UNLV), Las Vegas, NV

Contract Number: NT0004117

Phase I Start Date: October 1, 2008
Phase I End Date: March 31, 2010
Phase II Start Date: April 1, 2010
Phase II End Date: September 30, 2011

Fiscal Year (FY) 2011 Objectives

- Observation of local electronic structure, electron tunneling properties, and chemical characteristics on $La_{0.7}Sr_{0.3}MnO_3$ (LSM) dense thin-film model cathodes at elevated temperatures and reactive gas environment with oxygen.
- Identify correlations between surface chemical state and electron transfer characteristics on LSM as a function of temperature and thin film strain state that is of relevance to infiltrated cathode microsctructure.

FY 2011 Accomplishments

- We demonstrated the effects of epitaxial strain on the surface cation chemistry and the surface electronic structure of LSM as a model system, both at room temperature and at elevated temperatures.
- X-ray photoelectron spectroscopy (XPS) results showed that a larger tendency for Sr enrichment is prevalent for the tensile-strained LSM surface, owing to the relatively larger space available for the Sr cation on the surface compared with that in the bulk with increasing tensile strain.
- Scanning tunneling spectroscopy (STS) results showed that the electronic structure exhibits the presence of an energy gap between the occupied and unoccupied states at room temperature, favoring a smaller band gap for the compressively strained LSM. At 500ºC in 10^{-3} mbar of oxygen, however, both LSM film surfaces exhibit metallic-like behavior, and the tensile-strained LSM has enhanced density of states near the Fermi level compared with the compressively strained LSM.

Introduction

The relation of surface cation chemistry and surface electronic structure to oxygen reduction reaction (ORR) kinetics remains an outstanding question to this day in the search for highly active cathodes for solid oxide fuel cells (SOFCs). While traditionally perovskite-type transition-metal oxides have been extensively investigated as SOFC cathodes, more recent studies highlight the potential of layered oxide cathodes. On the surface of the perovskite-structured $La_{1-x}Sr_xMnO_3$, a widely used and studied SOFC cathode material, the fractional presence of constituent cations can deviate from the nominal bulk stoichiometry significantly because of an enrichment of Sr or La cations on the surface. It has been possible to control the bulk magnetic and electronic properties of perovskite thin films by manipulating their lattice parameters with different growth conditions, hydrostatic pressure, or use of substrates with a different lattice mismatch to the films. Furthermore, the impact of the lattice strain on the surface electronic structure and reactivity has been long demonstrated for low-temperature noble metal electrocatalysts. On the other hand, the role of lattice strain on the surface cation and anion chemistry, electronic structure, and ionic transport, which all influence the ORR activity of SOFC related oxides, is attracting its due interest only recently.

We have recently demonstrated, from first principles-based calculations, that the epitaxial strain up to a critical tensile strain value favors oxygen-vacancy formation as well as oxygen adsorption on another widely studied SOFC cathode, $LaCoO_3$. Experiments validating the direct role of strain on the reactivity with oxygen and oxygen transport in SOFC materials have been yet scarce. Sase *et al.* [1] showed that the oxygen surface exchange rate at the heterointerface of $La_{0.6}Sr_{0.4}CoO_3/(La,Sr)_2CoO_4$ thin films is larger by three orders of magnitude compared with the single-phase cobaltite surfaces. A reasonable hypothesis that could explain the enhanced oxygen exchange at that interface

region is the role of local strains. Studies on fluorite systems have suggested strong coupling of biaxial strain also to the oxygen ion diffusion. Here, we report our results on the strain-induced changes in the surface chemical and electronic state of LSM as a model system. We assessed two key parameters for reactivity with oxygen as a function of strain: (1) chemical environment on the LSM surface, in particular, the segregation of Sr cations and oxygen vacancy formation, experimentally probed with angle-resolved XPS and (2) surface electronic structure, experimentally probed using scanning tunneling microscopy and spectroscopy (both at ambient and in situ at elevated temperatures).

Approach

X-ray diffraction (XRD) measurements were performed employing a PANalytical Expert Pro MPD diffractometer to determine the phase purity and the strain states. Scanning tunneling microscopy/spectroscopy (STM/STS) at room temperature as well as at elevated temperatures was used to investigate the surface morphology and electronic structure of the strained films. The measurements were performed in a modified ultra-high vacuum (UHV) system designed by Omicron Nanotechnology, with a variable temperature scanning tunneling microscope. The chemical state of the surfaces was probed using angle-resolved XPS using a five-channel hemispherical electron analyzer, equipped in the same chamber with the STM. CasaXPS 2.3.15 software was used to assess the spectra and calculate the relative intensity of each constituent by employing the Shirley background. The total intensity of each constituent was normalized by their corresponding cross section values from Scofield's table. We removed carbon contamination from the surfaces of the air-exposed LSM films by heating them in oxygen pressure of 5×10^{-5} mbar at 500°C for at least 30 min in the UHV chamber. All STM, STS, and XPS results reported here were obtained after the cleaning process. A pyrolytic boron nitride (PBN) heater was used to evenly heat the LSM films during the cleaning process as well as during the STM experiments at high temperatures. STM measurements were performed in the constant-current mode using Pt/Ir tips, with a bias voltage of 1 to 2 V applied to the tip and a tunneling current of 200-500 pA.

Results

Epitaxial 10 nm thick LSM films, grown by pulsed laser deposition [2] on (001) $SrTiO_3$ (STO) and (001) $LaAlO_3$ (LAO), are the model materials in this study. The XRD results indicate that both films are fully strained with the (001) out-of-plane orientation. The film on STO has 0.8% in-plane tensile strain, whereas the film on LAO is under -2.1% in-plane compression at room temperature. The expected strain in LSM films at the deposition temperature of 850°C is +0.6 and -2.3% based on the differences of the thermal expansion coefficients of LSM, STO, and LAO. The surface of LSM films grown on both substrates, hereafter denoted as LSM/LAO and LSM/STO, has well-resolved and atomically smooth terraces with different lateral sizes (Figure 1a,c). The height profiles on these terraces show that the height difference between each layer is 4.0 ± 0.3 Å (Figure 1b,d), in good agreement with the lattice parameter of the LSM (3.88 Å). The overall morphology on these two substrates is similar, whereas the size of these terraces on LSM/LAO is smaller.

To assess the strain dependence of Sr content and its chemical environment on/near the surface, La 4d and Sr 3d emissions in XPS were analyzed for LSM/STO and LSM/LAO. The La 4d and Sr 3d emissions have similar kinetic energies, with a mean free path (MFP) of 20 Å [3,4] in LSM. These spectra were measured at two emission angles, 0 and 70°, between the surface normal and the detector position; measurements at 70° are more surface-sensitive, with a mean probing depth of 7 Å from the surface. The Sr/(Sr + La) ratio is taken as a first measure of Sr enhancement near the surface and was quantified using the total La 4d and Sr 3d emissions normalized by their corresponding cross-sectional values from the Scofield table. The Sr/(La + Sr), evaluated at 70° in Figure 2a, is almost the same, 0.36 to 0.37, on both LSM/LAO and LSM/STO and is larger than the bulk nominal value of Sr/(La + Sr) = 0.3. This result implies that the near-surface region of both LSM films is Sr-rich, and the total Sr fraction on the A-site (A = La, Sr) of LSM within the top nearly 7 Å depth is the same regardless of the sign or magnitude of strain.

To obtain quantitative information about the differences in the chemical environment on LSM surfaces as a function of strain, the Sr 3d core level photoemission line shapes were analyzed. As shown in Figure 2b, the Sr 3d emission deviates from the theoretical line shape and was deconvoluted to show that it has two Sr core level binding environments on both LSM/LAO and LSM/STO. These are represented by one doublet of Sr 3d located at the lower binding energy, LBE (132.0 ± 0.2 eV) [5], and a second doublet located at the higher binding energy, HBE (133.4 ± 0.2 eV) [5]. The LBE component has a larger contribution in the total Sr 3d emission and is attributed to the Sr cations fully coordinated within the bulk of the perovskite lattice ($Sr_{lattice}$). As the emission angle increases from 0 to 70°, the contribution of the HBE component increases, implying that the HBE binding environment is related to the Sr cations on the surface ($Sr_{surface}$) of LSM [4,5,6]. The $Sr_{surface}$ contribution is different among the Sr 3d emissions on LSM/LAO and LSM/STO, as evident from the different line shapes of the spectra in Figure 2b. Figure 2c shows the intensity ratio of the $Sr_{surface}$ to $Sr_{lattice}$ on LSM/STO relative to that on LSM/LAO, quantified as the ratio $[(Sr_{surface}/Sr_{lattice})_{LSM/STO}]/[(Sr_{surface}/Sr_{lattice})_{LSM/LAO}]$,

as a function of the emission angle. The increase in the surface Sr component with the increasing emission angle is more pronounced on LSM/STO compared with that on LSM/LAO. This ratio changes from 0.93±0.05 at 0° emission to 1.23±0.06 at 70° emission and shows that the $Sr_{surface}$ binding environment has a larger presence on LSM/STO. The exact nature of this HBE $Sr_{surface}$ component of the Sr 3d emission varies in different reports. Two major possibilities for the origin of the HBE component in our results are the SrO or Sr-OH phase formation on the surface [7,8] and the under-coordinated Sr cations on the perovskite LSM surface with an AO-termination layer [7,9]. Our STM measurements (Figure 1) do not show a significant variation in the morphology or in the step heights that could be correlated to a discernible presence of SrO or Sr-OH surface phase. Therefore, we believe that the HBE intensity in the Sr 3d emission more likely originates from the presence of the under-coordinated Sr on the perovskite surface. Therefore, the enhanced presence of the $Sr_{surface}$ on LSM/STO suggests a further enrichment of surface Sr driven by the tensile strain state of the LSM film. However, the relative changes in $Sr_{surface}$ constitutes only about 4 to 5% difference within the total Sr 3d, which is beyond the resolution of the Sr/(Sr + La) quantification in Figure 2a.

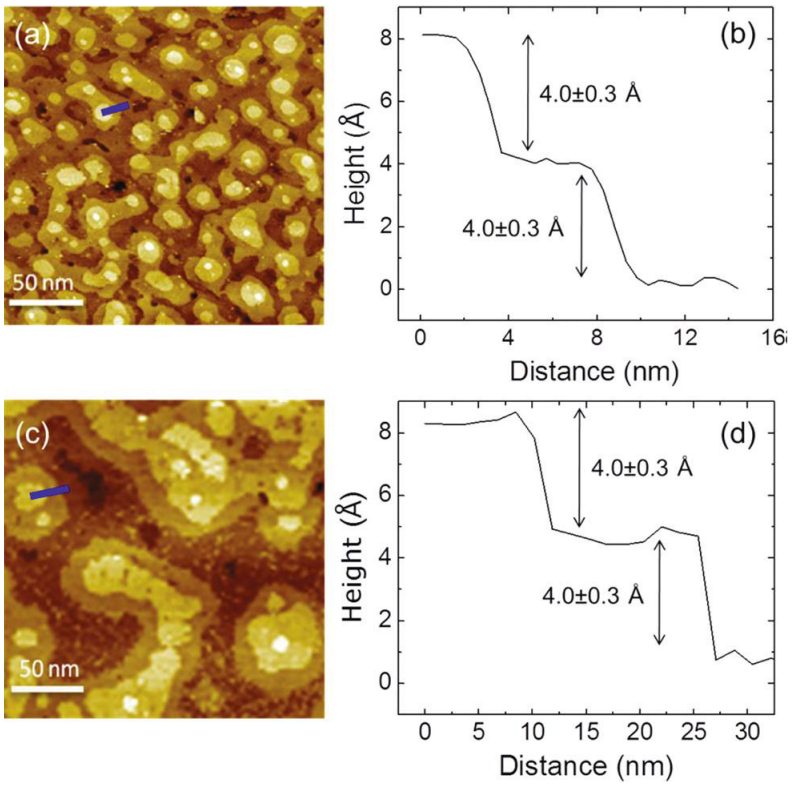

FIGURE 1. (a,c) Surface morphology and (b,d) height profile of the 10 nm thick (a,b) LSM/LAO and (c,d) LSM/STO films at room temperature. Blue bars in panels (a) and (c) show the position of the line profiles in panels (b) and (d).

Electronic structure is strongly coupled to the surface reactivity of the material [10]. Here we compare the electronic density of states using tunneling spectroscopy, probing the occupied and unoccupied states on LSM surfaces near the Fermi level both at room temperature and at an elevated temperature in oxygen. LSM surfaces at room temperature exhibited an energy gap between the occupied (negative sample bias) and unoccupied (positive sample bias) states (Figure 3), with a smaller gap of 0.9 ± 0.2 eV on LSM/LAO compared with 2.1 ± 0.2 eV on

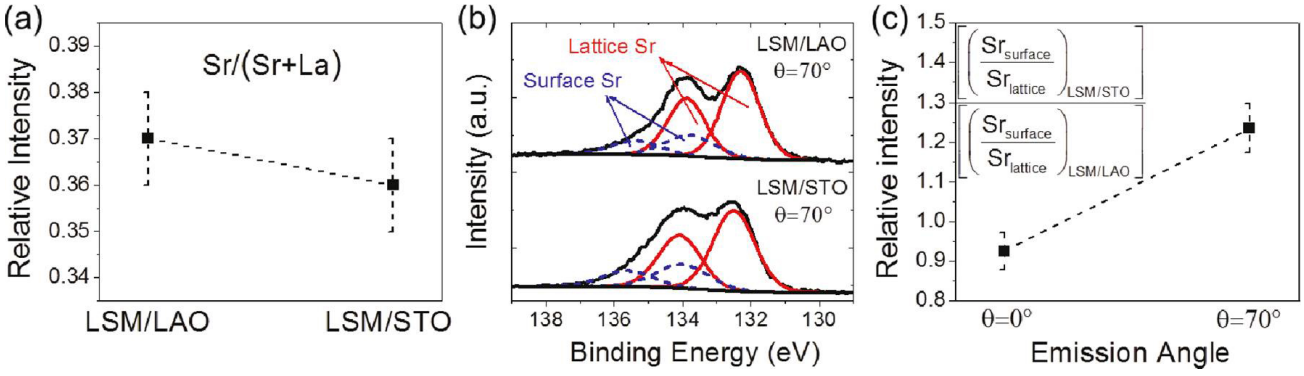

FIGURE 2. (a) Relative intensity of Sr/(La+Sr), (b) Sr 3d spectra and the two curve-fitted doublets at the high binding energy for $Sr_{surface}$ (blue/dashed line) and at the low binding energy for $Sr_{lattice}$ (red/solid line), shown for LSM/LAO and LSM/STO at 70° emission angle, and (c) the relative increase in the $Sr_{surface}$ component of the Sr 3d spectra from 0 to 70° emission angle on LSM/STO with respect to that on LSM/LAO.

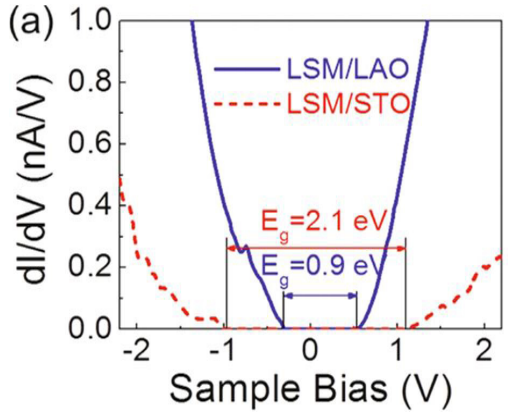

FIGURE 3. Tunneling spectra on LSM/LAO (blue, solid line) and LSM/STO (red, dashed line), showing the energy gap, E_g, for both samples at room temperature in ultra-high vacuum.

LSM/STO. In prior tunneling studies on LSM and related perovskite thin films, differences in electronic characteristics at room temperature or below were attributed to the coexistence of paramagnetic insulating and ferromagnetic metallic regions on the surface and were related to the differences in the local Mn-O bond lengths, nanoscopic disorder, [11] oxidation, [12] and formation of oxygen vacancy defects [13]. We note that our LSM films of ~10 nm thickness are fully strained, and the observation of semiconducting-like energy gap at room temperature is in good agreement with previous reports on fully strained manganite films [12,15] and with our recent work [15,16] on textured LSM films on zirconia substrates with a large lattice mismatch to LSM. The larger band gap found on LSM/STO compared with that on LSM/LAO may partially be related directly to the strain state differences (both magnitude and sign) on these films. On the basis of our experimental observation, we conclude that the biaxial lattice strain can induce direct changes in the surface electronic structure of LSM, determined here as the differences in the energy gap between the occupied and unoccupied states.

The picture, however, reverses for the tunneling conductance and density of states at elevated temperatures, presented in Figure 4 at 500°C. Both of the above-mentioned films exhibit no gap between the occupied and unoccupied states (Figure 4c) at 500°C, but a significantly larger tunneling conductance and density of states (represented by dI/dV) prevails on LSM/STO surface. The transition from the presence of an energy gap to a metallic-like electronic structure may arise from the delocalization of the charge carriers at elevated temperatures, possibly accompanied by a transition from the ferromagnetic insulator to a paramagnetic metal (for $x > 0.3$) structure [17] or due to the formation of oxygen vacancies on the surface that create defect states in the band gap [13,18]. The thermal excitations at 500°C are not sufficient to enable the closure of 0.9 to 2.1 eV energy gap. Moreover, and importantly for the focus of this report, this transition at high temperature is stronger with a larger density of states near the Fermi level for the tensile-strained LSM/STO compared with the compressively strained LSM/LAO. Taking the density of states near the Fermi level (0 V sample bias) as a measure of reactivity [10], our results suggest that tensile strain state on LSM may favor electron transfer to and reactivity with oxygen at elevated temperatures in solid oxide fuel cells. We hypothesize that this difference in the electronic

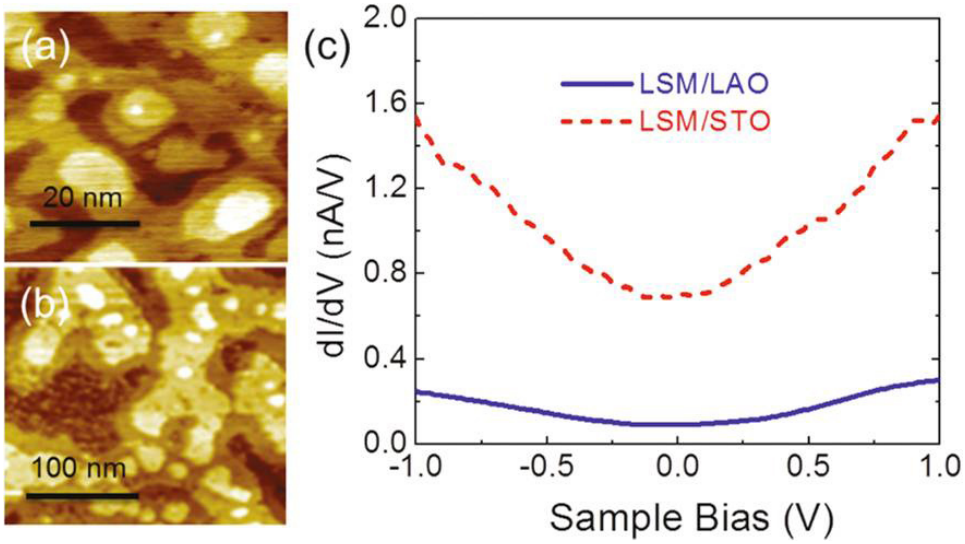

FIGURE 4. Surface structure on (a) LSM/LAO and (b) LSM/STO was stable at 500°C in 10^{-3} mbar oxygen, with no evident change in morphology. (c) Tunneling spectra (dI/dV, proportional to the density of states) on LSM/LAO (blue, solid line) and LSM/STO (red, dashed line), taken at 500°C in 10^{-3} mbar of oxygen.

structure on LSM surface, directly or indirectly due to the strain state, could arise from the following two possible mechanisms. The first mechanism is associated with the formation of oxygen vacancies on the surface [19], which modifies the d band structure of the neighboring transition metals and can induce states in the gap [20,21]. More facile formation of oxygen vacancies on the tensile-strained LSM/STO, and thus, an increase in the defect states that enhances the density of states near the Fermi level is a reasonable explanation. The second mechanism is related to the possible phase changes or restructuring on LSM [12] as a function of temperature and Sr content [17]. The precise role of surface defects and restructuring in governing the high-temperature electronic structure and reactivity of strained LSM requires further experimental and theoretical investigation.

Conclusions and Future Directions

In summary, we demonstrated the effects of epitaxial strain on the surface cation chemistry and the surface electronic structure of LSM as a model system, both at room temperature and at elevated temperatures. A larger tendency for Sr enrichment is prevalent for the tensile-strained LSM surface, owing to the relatively larger space available for the Sr cation on the surface compared with that in the bulk with increasing tensile strain. Tensile strain also facilitates oxygen vacancy formation on LSM. While the electronic structure exhibits the presence of an energy gap between the occupied and unoccupied states at room temperature, favoring a smaller band gap for the compressively strained LSM, the picture reverses at elevated temperatures. At 500°C in 10^{-3} mbar of oxygen, both LSM film surfaces exhibit metallic-like behavior, and the tensile-strained LSM has enhanced density of states near the Fermi level compared with the compressively strained LSM. These results illustrate the importance of lattice strain in controlling the high-temperature surface chemistry and electronic structure for oxygen reduction activity on SOFC cathodes. In-depth probing and analysis of such correlations on a broad range of materials and conditions are essential toward advancing our understanding of how the surface state, including the presence of strain, relates to the oxygen reduction activity on oxide cathodes. Integration of surface-sensitive in situ techniques and first principles-based simulations, as demonstrated here, is a necessary approach for this goal.

FY 2011 Publications/Presentations

Conference Presentations

1. April-May 2011, *"Strain Effects on the Surface Chemistry and Electronic Structure of $La_{0.7}Sr_{0.3}MnO_3$,"* 2011 Spring Meeting of the Materials Research Society, Symposium Frontiers of Solid State Ionics, San Francisco, California, United States; 219th Meeting of the Electrochemical Society, Solid Oxide Fuel Cells XII, Montreal, Canada.

2. July 2011, *"Strain Effects on the Surface Chemistry, Electronic Structure, and Reactivity of $La_{1-x}Sr_xMnO_3$ and $La_{1-x}Sr_xCoO_3$,"* 18th International Conference on Solid State Ionics, Warsaw, Poland.

3. May 2011, *"Strain Effects on the Surface Chemistry, Electronic Structure, and Reactivity of Solid Oxide Fuel Cell Cathodes,"* E-MRS 2011 Spring Meeting, E-MRS / MRS Bilateral Conference on Energy, Symposium X - Fuel Cells Energy Conversion, Nice, France.

Journal Publication

4. Helia Jalili, Jeong Woo Han, Yener Kuru, Zhuhua Cai, and Bilge Yildiz, *"New Insights into the Strain Coupling to Surface Chemistry, Electronic Structure, and Reactivity of $La_{0.7}Sr_{0.3}MnO_3$,"* The Journal of Physical Chemistry Letters, 2011, 2, 801-807.

References

1. M. Sase, K. Yashiro, K. Sato, J. Mizusaki, T. Kawada, N. Sakai, K. Yamaji, T. Horita, and H. Yokokawa, Solid State Ionics **2008**, 178, 1843.

2. K.R. Balasubramaniam, S. Havelia, P.A. Salvador, H. Zheng, and J.F. Mitchell, Appl. Phys. Lett. **2007**, 91, 232901.

3. H. Dulli, P.A. Dowben, S.H. Liou, and E.W. Plummer, Phys. Rev. B **2000**, 62, R14629.

4. R. Bertacco, J.P. Contour, A. Barthelemy, and J. Olivier, Surf. Sci. **2002**, 511, 366.

5. P.A.W. van der Heide, Surf. Interface Anal. **2002**, 33, 414.

6. G. Vovk, X. Chen, and C.A. Mims, J. Phys. Chem. B **2005**, 109, 2445.

7. P.A.W. van der Heide and J.W. Rabalais, Chem. Phys. Lett. **1998**, 297, 350.

8. J.-C. Dupin, D. Gonbeau, P. Vinatier, and A. Levasseur, Phys. Chem. Chem. Phys. **2000**, 2, 1319.

9. L.T. Hudson, R.L. Kurtz, S.W. Robey, D. Temple, and R.L. Stockbauer, Phys. Rev. B **1993**, 47, 10832.

10. A. Gross, Theoretical Surface Science: A Microscopic Perspective, 2nd ed.; Springer-Verlag: Berlin, 2009.

11. M. Bibes, L. Balcells, S. Valencia, J. Fontcuberta, M. Wojcik, E. Jedryka, and S. Nadolski, Phys. Rev. Lett. **2001**, 87, 067210.

12. K. Fuchigami, Z. Gai, T.Z. Ward, L.F. Yin, P.C. Snijders, E.W. Plummer, and J. Shen, Phys. Rev. Lett. **2009**, 102, 066104.

13. K. Szot, W. Speier, R. Carius, U. Zastrow, and W. Beyer, Phys. Rev. Lett. **2002**, 88, 075508.

14. N. Okawa, H. Tanaka, R. Akiyama, T. Matsumoto, and T. Kawai, Solid State Commun. **2000**, 114, 601.

15. K. Katsiev, B. Yildiz, K. Balasubramaniam, and P.A. Salvador, Appl. Phys. Lett. **2009**, 95, 092106.

16. K. Katsiev, B. Yildiz, B. Kavaipatti, and P. Salvador, ECS Trans. **2009**, 25, 2309.

17. A. Urushibara, Y. Moritomo, T. Arima, A. Asamitsu, G. Kido, and Y. Tokura, Phys. Rev. B **1995**, 51, 14103.

18. U. Diebold, S.-C. Li, and M. Schmid, Annu. Rev. Phys. Chem. **2010**, 61, 129.

19. Y.-L. Lee and D. Morgan, ECS Trans. **2009**, 25, 2769.

20. M.V. Ganduglia-Pirovano, A. Hofmann, and J. Sauer, Surf. Sci. Rep. **2007**, 62, 219.

21. Y.S. Kim, J. Kim, S.J. Moon, W.S. Choi, Y.J. Chang, J.G. Yoon, J. Yu, J.S. Chung, and T.W. Noh, Appl. Phys. Lett. **2009**, 94, 202906.

III.A.7 Synchrotron Studies of SOFC Cathode Materials

Y.U. Idzerda
Dept. of Physics
Montana State University
Bozeman, MT 59717
Phone: (406) 994-7838; Fax: (406) 994-7838
E-mail: Idzerda@physics.montana.edu

DOE Project Manager: Patcharin Burke
Phone: (412) 386-7378
E-mail: Patcharin.Burke@netl.doe.gov

Contract Number: NT0004115

Start Date: September 3, 2008
End Date: September 2, 2011

Fiscal Year (FY) 2011 Objectives

- Characterize atomic variations and modifications occurring in the nanometer range, in the cathode/electrolyte interface region of solid oxide fuel cell (SOFC) related materials.
- Correlate these modifications to electric potential, ion current, gaseous environment, and possible synergistic effects between them.
- Identify degradation mechanism for Sr segregation in $La_{0.6}Sr_{0.4}Co_{0.2}Fe_{0.8}O_{3-\delta}$ (LSCF) materials.

FY 2011 Accomplishments

- Observations of the power curves for LSCF/gadolinia-doped ceria (GDC) sandwich structures driven with potentials ranging from 350 mV to 500 mV at 800°C for 100 hours of operation, shows a slight performance degradation. The mechanism underlying the degradation is determined to be Sr out-diffusion onto the LSCF surface.
- Determined that the Sr segregation is dependent on a reduction in oxygen vacancy concentration in the near surface region.
- Outlined mitigation strategy by increasing and stabilizing oxygen vacancy concentrations through co-doping in the near surface region or matching oxygen vacancy concentrations.
- Periodic reverse SOFC operation serves to prolong SOFC lifetimes.

Introduction

Oxygen vacancies are responsible for some of the exciting properties exhibited by perovskites, including magnetism [1], two-dimensional electron channels in otherwise insulating materials [1], and oxygen ion transport in mixed ionic/electronic conductors which are essential for oxygen production (solid oxide electrolyzer cells [2]), separation (oxygen separation membranes [3]) and as electrodes in hydrogen-based energy technologies (SOFCs) [4]. Unfortunately, a critical lack in understanding of material degradation under operational conditions (e.g., ion flux, bias potential and high temperature) remains a barrier to their broad implementation.

The success of LSCF as a mixed ionic/electronic conducting electrode in these applications stems from its high oxygen vacancy concentration, generated by the substitution of Sr^{2+} for La^{3+}. However, long-term performance degradation, attributed to decomposition of the perovskite structure induced by Sr out-diffusion [5] which compromises oxygen dissociation at the surface [6] remains a concern for this class of materials. An understanding of the segregation mechanism, and the electrochemical environment's influence on it, remains elusive, with some work suggesting that the driving factor is the variation in oxygen vacancy concentration [7].

In this work we demonstrate that cation segregation in perovskite electrodes has its origin in the variation in oxygen vacancy concentration induced by the existing bias potential during operation by utilizing X-ray absorption spectroscopy (XAS) to directly investigate the secondary phase formation. Due to the difficulty of differentiating between surface segregated and bulk Sr, we introduce gaseous Cr which reacts with out-diffused Sr to form $SrCrO_4$ because of the favorable [8] acid-base reaction of Sr with hexavalent chromium (Cr^{6+}). In the absence of segregated Sr, Cr deposits in the reduced form of Cr_2O_3 (Cr^{3+}). The ex situ measured Cr^{6+}/Cr^{3+} ratio enables us to quantify the relative Sr segregation and allows us to explore the influence of the electrochemical environment on this degradation mechanism.

Approach

In our experimental setup, we first perform four-probe conductivity measurements of symmetric-half-cells [2,9] consisting of a GDC electrolyte with LSCF porous electrodes on *both* sides. The symmetrical nature of the samples allows us to study how oxygen dissociation

and recombination affect Sr segregation dynamics. The GDC powder was uniaxially pressed in 0.5 inch diameter disks with thicknesses of 1-3 mm. A thin LSCF paint was applied to both sides and co-sintered at 1,200°C for 10 hours in air. The LSCF electrode thicknesses were measured by cross section field emission scanning electron microscope and found to range from 40 to 50 µm with uniform porosity. Silver mesh contacts are pressed on each side of the sample with Inconel™ disks, held together with alumina fasteners. The discs are perforated to allow ambient air access and serve as the gaseous Cr source.

The sample current was measured for 48 hours with an applied constant direct current voltage (potentiostatic method) with the sample and holder in a quartz tube furnace at 800°C in air. Various GDC thicknesses were run with bias voltages from 0.1 to 0.6 V allowing us to independently assess the effects of ion current and bias potentials. One sample was disconnected from the power source 1 hour prior to cool down to verify that our results are independent of the presence of a bias voltage during the cooling process. After cooling at a rate of 4°C/min to room temperature, the samples were stored in a dessicator and subsequently the Cr L_{23}-edge XAS was measured in total electron yield mode at beamlines 4.0.2 and 6.3.1 of the Advanced Light Source of the Lawrence Berkeley National Laboratory. Reference L_{23}-edge XAS spectra for Cr^{3+} and Cr^{6+} from powders consisting of Cr_2O_3 (99% purity) for the trivalent chromium, CrO_3 (99.99% purity) and $SrCrO_4$ (99.9% purity) for the hexavalent chromium were also measured. The Sr M_{45}-edge XAS spectra for all samples (not shown) were nearly identical and, as previously noted, could not be used to distinguish Sr in the $SrCrO_4$ from Sr in LSCF.

Since the electrolyte is an electrical insulator, the measured current is due to the oxygen ion flow across the GDC electrolyte, originating from oxygen molecule dissociation at the negative LSCF contact (cathode) and terminating in molecular recombination at the positive LSCF contact (anode). The ion current of each sample samples (with a specific bias potential and GDC thickness) was recorded over a 48 hours period. After the heating transient, a sharp but brief initial degradation was observed followed by slower long-term degradation. A plot of the ending current density as a function of bias potential for each GDC electrolyte thicknesses (not shown here), a linear behavior of the ion current with potential was observed, indicating that the heterostructures are in a regime where the total ion flux resistance is dominated by the GDC electrolyte.

Results

To quantify the Sr surface segregation, the Cr L_{23}-edge XAS of both sides of each heterostructure were measured. In Figure 1 top panel, the reference

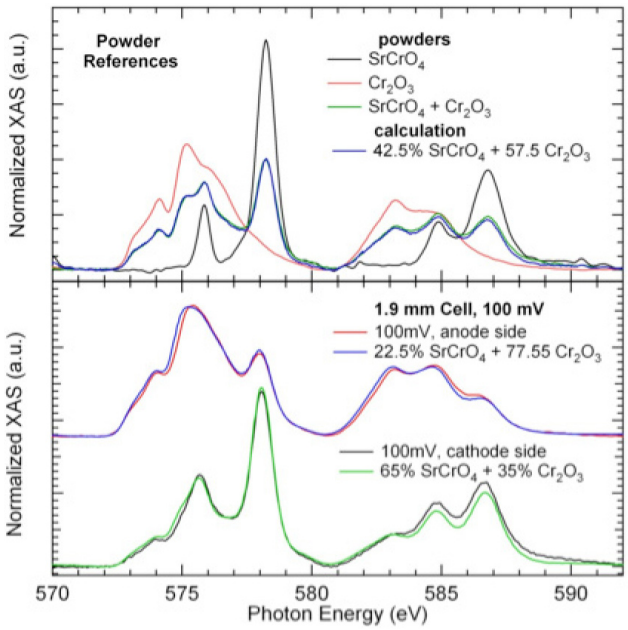

FIGURE 1. (top) XAS Reference Powder Spectra for Cr^{3+} and Cr^{6+}, with a Measured Powder Mixture and the Best Fit; (bottom) Cr Precipitate Spectra and Fits for Both Sides of a Representative Sample

spectra for hexavalent chromium ($SrCrO_4$, black line) and trivalent chromium (Cr_2O_3, red line) and a mixture of both powders (green line) are displayed. XAS spectra for the less stable CrO_3 did not resemble any of the spectra. After energy referencing the main Cr_2O_3 peak to 575.20 eV, the spectra were area normalized to the integrated L_3 peak and subsequently normalized to the number of d-holes; seven for Cr_2O_3 in [Ar] $3d^3$ configuration and 10 for $SrCrO_4$ in [Ar] $3d^0$ configuration [10]. The mixed powder spectra can be accurately reproduced with a least-squares-fit linear sum of the two reference spectra (blue line), allowing for a quantitative determination of the relative concentrations of Cr^{6+} and Cr^{3+}.

Representative spectra of the cathode and anode side of the 1.9 mm thick GDC structure with 100 mV bias voltage and their associated fits are shown in Figure 1 bottom panel. The only free parameter for fitting the Cr spectra is the ratio of the contributions of the d-hole normalized Cr^{3+} and Cr^{6+} reference spectra. This ratio can be used to determine the variation in the $SrCrO_4$ concentration as a function of bias voltage and is shown in Figure 2 for each side of 1.1, 1.9 and 2.7 mm thick samples. The open symbols represent the oxygen dissociation side (cathode) and the solid symbols the oxygen recombination side (anode).

The anode side unambiguously displays an increase in $SrCrO_4$ with increasing bias potential. This trend is not observed on the cathode side where a high and nearly constant $SrCrO_4$ concentration is observed. This discrepancy is a clear demonstration of the

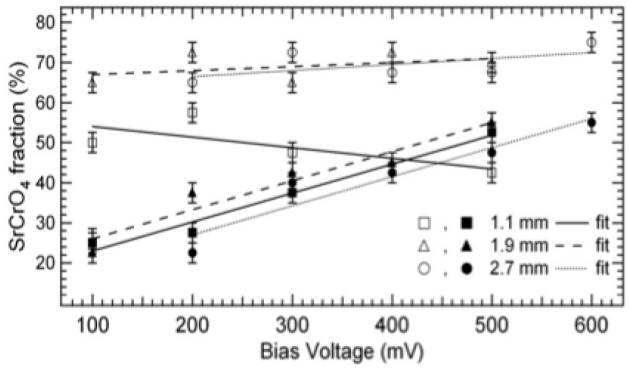

FIGURE 2. Cr Precipitate Composition for Both Sides of All Samples with Open Markers for the Oxygen Dissociation Side (Cathode), and Solid Markers for the Oxygen Recombination Side (Anode)

electrochemical environment affecting the composition of the Cr precipitates. Changing the contact material from silver to gold, or eliminating the bias potential before cool-down results in no change in the Cr^{3+} to Cr^{6+} ratio. Finally, in comparing samples with different bias potentials and electrolyte thicknesses but similar current densities, we find that the $SrCrO_4$ concentration showed no correlation to the current density while samples at the same bias potential, but different GDC thickness and current density, had very similar $SrCrO_4$ concentrations demonstrating that the bias potential controls the segregation kinetics of Sr out-diffusion of the LSCF electrodes.

The mechanism of Sr segregation and its variability with bias voltage can now be understood in the context of oxygen vacancy concentrations in the cathode and anode. At the cathode, the dissociation of oxygen molecules occurs at a high rate due to the abundance of oxygen molecules and the catalytic activity of LSCF [11,12]. With an applied bias potential, the oxygen ion concentration in the LSCF cathode increases, as thermodynamic modeling for electrochemical systems similar to ours have shown [13]. Conversely, the oxygen *vacancy* concentration drops dramatically.

To maintain overall charge neutrality with the decrease in oxygen vacancy concentration, the transition metal ions can increase their oxidation state and/or the Sr ions can out-diffuse from the LSCF, effectively reducing their concentration from the initial stoichiometry. (Recall that Sr addition in LSCF generates the initial oxygen vacancy concentration.) Although transition metal valency changes occur, our results in combination with the previously shown diffusivity of Sr in LSCF [5] clearly demonstrate that Sr segregation is an important contributor to the compensation, as directly monitored through the formation of $SrCrO_4$. Since the rate limiting step is the oxygen ion transport through the electrolyte, the oxygen vacancy concentration at the cathode will be relatively low over a range of bias potentials, which results in significant Sr out-diffusion as experimentally observed in Figure 2 for the cathode sides of the samples (open markers).

On the anode side, the bias potential drives the drives oxygen ion flux which controls the re-association of oxygen ions. Since the ion flux is limited by the GDC interlayer for low bias potentials, the oxygen vacancy concentration is higher in the anode than in the cathode. As the bias potential is increased, the oxygen vacancy concentration in the anode is reduced. This leads to a variable Sr segregation at the anode, which increases with bias potential, as observed in Figure 2 (solid markers). At high bias potentials, the re-association of oxygen ions becomes the limiting process and the oxygen vacancy concentration becomes higher in the cathode than in the anode. For a given GDC thickness, at some bias point the oxygen vacancy concentrations are equal in the cathode and anode LSCF, and we expect the same Sr segregation and the same composition of the Cr precipitates. This is indicated by the crossing point of the fitting curves at 410 mV for the 1.1 mm GDC sample in Figure 2. Extrapolating the linear fits for the 1.9 and 2.7 mm GDC thicknesses suggest crossovers at 760 mV and 890 mV, respectively.

Conclusions and Future Directions

In conclusion, the advantage of XAS in studying porous surfaces was clearly demonstrated. The bias potential dependency of dopant segregation in mixed ionic/electronic conductors such as $La_{0.6}Sr_{0.4}Co_{0.2}Fe_{0.8}O_{3-\delta}$ determined using the chemical signatures of low concentrations of surface Cr by XAS. By determining the relative concentrations of hexavalent Cr in $SrCrO_4$ and trivalent Cr in Cr_2O_3, the surface concentration of segregated Sr at the anode and cathode of symmetric LSCF/GDC/LSCF heterostructures as a function of bias potential and electrolyte thickness identified the driving factor for Sr out-diffusion to be the oxygen vacancy concentrations in the near-surface regions of the cathode and anode.

With this understanding of the Sr out-diffusion mechanism, multiple mitigation strategies can be pursued. Baumann et al. [5] showed that short, reverse-bias direct current pulses during operation lead to a performance increase of LSCF. Similarly, maintaining a high oxygen vacancy concentration in the electrodes, or stabilizing the Sr ions within the LSCF through additional co-doping (perhaps only in the near surface region) should lead to lower degradation of the cathode. Reducing the initial imbalance of oxygen vacancies in the electrolyte in comparison to the electrode (e.g., higher doping of the electrolyte or lower doping of the electrodes) or matching the catalytic activity of the electrode to the ion transport rate of the electrolyte should also lead to a more stable concentration

of oxygen vacancies. Sr stabilization could be accomplished by increased multi-valent transition metal doping into the B-site which further promotes reversible valency change rather than irreversible Sr out-diffusion. In either case, overall performance need not be sacrificed for improved lifetime.

FY 2011 Publications

1. A.L.M. Finsterbusch, J.A. Schaefer, and Y.U. Idzerda, "Oxygen Vacancy Induced Sr Segregation in $La_{0.6}Sr_{0.4}Co_{0.2}Fe_{0.8}O_{3-\delta}$," Appl. Phys. Lett. (submitted) (2011).

References

1. J.N. Eckstein, Nature Materials **6,** 473-474 (2007).

2. V.I. Sharma and B. Yildiz, Journal of the Electrochemical Society **157,** B441-B448 (2010).

3. M. Burriel, C. Niedrig, W. Menesklou, S.F. Wagner, J. Santiso, and E. Ivers-Tiffee, Solid State Ionics **181,** 602-608 (2010).

4. Z.P. Shao, S.M. Haile, J. Ahn, P.D. Ronney, Z.L. Zhan, and S.A. Barnett, Nature **435,** 795-798 (2005).

5. F.S. Baumann, J. Fleig, M. Konuma, U. Starke, H.U. Habermeier, and J. Maier, Journal of the Electrochemical Society **152,** A2074-A2079 (2005).

6. S.P. Simner, M.D. Anderson, M.H. Engelhard, and J.W. Stevenson, Electrochem. and Solid-State Letters **9,** A478-A481 (2006).

7. T.T. Fister, D.D. Fong, J.A. Eastman, P.M. Baldo, M.J. Highland, P.H. Fuoss, K.R. Balasubramaniam, J.C. Meador, and P.A. Salvador, Applied Physics Letters **93,** - (2008).

8. D. Oh, E.N. Armstrong, D. Jung, C.C. Kan, and E.D. Wachsman, ECS Transactions **25 (2),** 2871 (2009).

9. S.P. Jiang and Y. Zhen, Solid State Ionics **179,** 5 (2008).

10. E. Riedel, *Anorganische Chemie*, 5th ed. (de Gruyter, Berlin, New York, 2002).

11. H. Kusaba, Y. Shibata, K. Sasaki, and Y. Teraoka, Solid State Ionics **177,** 2249-2253 (2006).

12. Z.P. Shao and S.M. Haile, Nature **431,** 170-173 (2004).

13. S.B. Adler, J.A. Lane, and B.C.H. Steele, Journal of the Electrochemical Society **143,** 3554-3564 (1996).

III.A.8 NETL RUA Cathode Materials R&D

Kirk Gerdes
U.S. Department of Energy
National Energy Technology Laboratory (NETL) –
Regional University Alliance (RUA)
3610 Collins Ferry Rd.
Morgantown, WV 26507
Phone: (304) 285-4342; Fax: (304) 285-4469
E-mail: Kirk.Gerdes@netl.doe.gov

Contract Number: 10-220621 6923
(NETL RUA Cathode Materials R&D)

Start Date: October 1, 2010
End Date: September 30, 2011

Fiscal Year (FY) 2011 Objectives

- Synthesize and characterize at least one perovskite and perovskite-related structure modified by catalytic metals (e.g., (LaSr)(CoPt)O_3) suitable for infiltration. Setup infiltration technical parameters for optimized wetting and microstructure of infiltrate.
- Generate Evaporation Induced Self Assembly (EISA) infiltrated commercial fuel cells ((LaSr)MnO_3 [LSM] on (LaSr)(CoFe)O_3 [LSCF]) characterized for particle distributions and mesoporosity and measured for performance enhancement.
- Demonstrate (make at least five attempts) doped $LaFeO_3$ porous cathode architectures (30-60 vol% porosity level) through controlled in situ pore formation strategies.
- Demonstrate operation of anode supported, thin electrolyte solid oxide fuel cell (SOFC) with cathodes composed of LSCF nanofibers; generate basic estimate of cathode materials and processing costs.
- Generate public report on the key conclusions from the work.

FY 2011 Accomplishments

- Developed cathode infiltrate materials including (LaSr)CoO_3, (LaSr)(CoPt)O_3, and (LaSr)FeO_3. Completed detailed evaluation of infiltrate material wetting of cathode backbone. Demonstrated 30-40% reduction in electrode polarization resistance and 35-40% power performance improvement over uninfiltrated baseline cells.
- Generated mesoporous infiltrate materials with particle size of 20-100 nm and pore sizes on the order of 1 nm, and demonstrated thermal stability at SOFC operating temperatures. Demonstrated performance in 200 hour cell operations showing more than 20% performance improvement with mesoporous LSM coating than baseline cells. All infiltrated cells have slower degradation rates than the baseline cells.
- Demonstrated generation of 30-60% porous LSCF and praseodymium-containing perovskite (PSCF) cathodes applied to standard anode supported button cells and tested cell performance in comparison to traditionally formed cathode. LSCF showed 40% performance improvement over the baseline cell and PSCF was still better.
- Demonstrated generation of four different LSM/yttria-stabilized zirconia (YSZ) composite nanofibers, and verified proper phase formation achieved for samples sintered at 1,000°C.
- Reported the detailed technical results of cathode materials development in six published reports and four conference presentations.

Introduction

A SOFC is a device which generates electrical energy by exchanging oxygen ions between an oxygen containing process stream such as air and a process stream containing an oxidizeable material such as hydrogen. The SOFC cathode facilitates the reduction of oxygen to an ionic form in preparation for transport across the impermeable electrolyte membrane. This electrochemical oxygen reduction process is sensitive to the material composition and physical structure of the cathode, and the oxygen reduction reaction (ORR) efficiency can be impacted by chemical or structural alterations.

Methods to improve the efficiency of the ORR typically focus on addition of electrocatalytic material into the porous cathode or focus on control of the cathode microstructure to increase the presence of beneficial structural features. Proposed changes to cathode materials and microstructure must be carefully evaluated according to four principal criteria: 1) the magnitude of achievable performance enhancement under relevant SOFC operating conditions; 2) the chemical compatibility of materials with unaltered components in the fuel cell; 3) long-term stability of new materials and engineered structures; and 4) the cost associated with implementation of the new methods.

Although a SOFC cathode is typically composed of a 60 μm thick porous ceramic, the cathode is particularly

active at the locations within 1-10 μm of the interface between cathode and electrolyte, and material deposition is therefore preferred at the solid interface. Cathode infiltration is therefore attempted to deposit highly active material at specific locations inside the cathode at difficult-to-reach interfaces. The primary challenges of cathode infiltration are: 1) ensuring that the desired infiltrate material phase is deposited; 2) achieving proper distribution of infiltrate into the active regions of the cathode; 3) ensuring that the material is stable as evaluated by electrochemical, thermochemical, and thermomechanical performance metrics. Achievement of targeted cathode infiltration resulting in improved cathode activity and long-term stability are the objectives of the present infiltration research effort.

Another approach to enhancement of cathode performance is exercise of control over the cathode microstructure using techniques of ceramics engineering. Control of microstructure allows a ceramicist to tailor the cathode for enhancement of desirable features such as increasing cathode porosity, improvement of mechanical strength, or to increase the total number of active boundaries within the cathode. The challenges to microstructural engineering are: 1) engineering the cathode microstructure using a practical and inexpensive process; 2) ensuring that the engineered structures remain thermally stable at relevant operating conditions; and 3) verifying that the resulting cathode demonstrates a sufficient performance enhancement to justify cost. The target of the present research effort is to demonstrate a practical method for engineering microstructure that results in improved and stable cathode performance.

Approach

In the infiltration portions of the project, a porous ceramic SOFC cathode of standard composition ($La_{1-x}Sr_xMnO_3$ or $La_{1-x}Sr_xFe_{1-y}Co_yO_3$) is infiltrated with materials intended to enhance the chemical activity of the cathode and enhance the oxygen reduction reaction. Materials suitable for infiltration into the cathode are identified, the materials are generated and infiltrated, and the impact on cathode performance is electrochemically evaluated. Materials demonstrating improved cathode performance are also screened through extended testing to ensure that long-term stability will be adequate to meet lifetime performance metrics.

Infiltrate materials are developed using two principal methods. Method 1 produces widely dispersed, dense nanoparticles of diameters approximately 20-50 nm and surface areas of approximately 2-5 m^2/g. Method 2, known as EISA, produces widely dispersed particles possessing inherent mesoporosity. The mesoporous materials feature increased particle size at 50-100 nm, but also 10 times enhanced surface area at 20-50 m^2/g. Method 1 is used to screen constituent materials for performance, wettability, and chemical stability. Several novel infiltrate materials are generated by Method 1 and include $(LaSr)CoO_3$, $(LaSr)(CoPt)O_3$, and $(LaSr)FeO_3$. Method 2 is restricted to more conventional materials, in order to concentrate research on the EISA process and evaluation of material stability. Materials include $(LaSr)MnO_3$ and $(LaSr)CoO_3$.

In the cathode microstructural engineering efforts, the objective is to develop engineered SOFC cathode microstructures that are tailored to provide a high triple-phase boundary (TPB) concentration, low resistance to gas diffusion, and optimal architecture for nano-catalyst impregnation. Structural engineering may focus on specific phases within the cathode, or on the overall cell architecture. Efforts to engineer the phases are intended to enhance the ionic and electronic conductivity of the cells, while architectural engineering is intended to enhance gas flow, mechanical strength, and connectivity of phases.

Two methods are used to control cathode microstructure. Method 1 produces a foam-like cathode structure with engineered porosity from the electrolyte surface to the interconnect. Efforts are made to engineer submicron pores (nanopores) within the open foam structure to enhance the TPB concentration while retaining porosity for optimal gas flow and infiltration of the cathode active area. Method 2 generates high aspect ratio nanofibers of traditional cathode materials ($(LaSr)MnO_3$, YSZ), which will then be applied as microstructurally novel cathodes. Nanofibers are generated through an electrospinning method, which ejects a precursor fluid containing the component materials through a high voltage electric field.

Cells possessing novel microstructure or infiltrated with electrocatalytically active materials are then operated electrochemically for at least 200 hours at 750-800°C using hydrogen as the fuel source. Long duration tests lasting 1,500+ hours have also been completed to assess the stability of infiltrated specimen. Cells under test are also periodically probed with electrochemical impedance spectroscopy, and results are used to examine changes in the electrode polarization and cell ohmic resistance. The quality of structure and infiltration is evaluated visually and spectroscopically on the basis of structural features, particle size, and uniformity of infiltrate coverage. The battery of results are used to evaluate the performance of all candidate materials in order to identify the infiltrate materials and structures demonstrating the greatest performance improvement and/or greatest stability.

Results

Throughout FY 2011, substantial success has been achieved in both infiltration and microstructural engineering efforts. Generation of lanthanum strontium

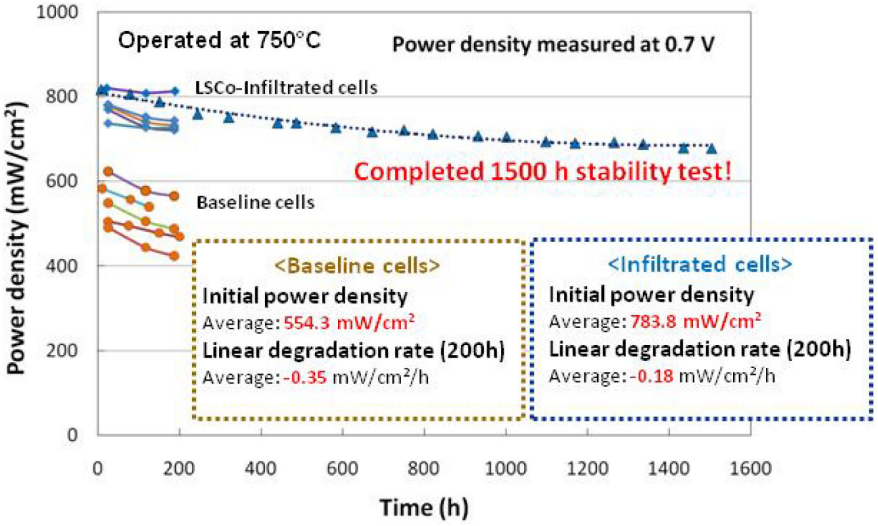

FIGURE 1. Comparison of SOFC power performance tests conducted on baseline and LSCo-infiltrated cathodes. Data for a 1,500-hour stability test are also shown.

cobalt oxide (LSCo) nanoparticle material and an infiltration vehicle sufficient to penetrate to the active regions of the SOFC cathode were proven in multiple direct cell tests. Figure 1 depicts the observable performance enhancement of LSCo infiltrated cathodes compared to an identical (but uninfiltrated) baseline cell. Duplicate tests of baseline and infiltrated systems have established average performance values of approximately 550 and 780 mW/cm^2, respectively, for cells operated at 750°C and loaded to 0.7 V. The infiltrate material generating this greater than 40% increase in average power density also stabilizes the base cell, and suppresses degradation, as demonstrated in repeat testing. A 1,500-hour test also indicates that performance remains stable for industrially relevant time periods.

Cells infiltrated with materials generated by the EISA process demonstrated similarly enhanced performance. Figure 2 compares performance of a conventional baseline cell to cells infiltrated by LSM nanoparticles (NP), LSM mesoporous particles (MP), and LSCo MP. The data reported are average values acquired for multiple cell tests of each material, and confirm a statistically relevant enhancement in cell performance for all infiltrates over the time period of operation. Polarization tests for the infiltrated cells indicated an increase in relative power density of up to 40% after 200 hours of operation, and impedance tests indicated a decrease in polarization resistance of up to 28%. As observed with the nanoparticle materials, infiltration of the mesoporous materials enhanced the stability of the SOFC, as shown by a depression of the measured degradation rate compared to the baseline cells.

Cathodes generated using the in situ foaming process were shown to be well controlled and highly porous. Figure 3 shows scanning electron microscope

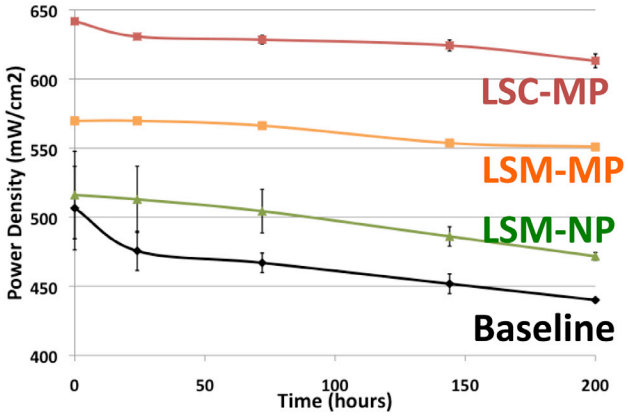

FIGURE 2. Comparison of SOFC power performance tests conducted on baseline and cathodes infiltrated with mesoporous (MP) and nanoparticle (NP) materials. Mesoporous materials are generated by the EISA process.

(SEM) micrographs of a typical foamed structure produced by the in situ foaming technique. Image a) is a zoomed view of a narrow section showing the pore shapes and particle morphology. Image b) depicts a wider view of the cathode and demonstrates the distribution of pores throughout the structure. Initial electrochemical performance testing on the foamed cathodes indicates peak power densities on electrolyte supported cells of 400 mW/cm^2, when operated at 800°C. This compares favorably with similarly composed commercial cells, and further innovations resulting from continued research are expected to enhance this result still further.

Nanofiber materials formed by the electrospinning methods are generated for a variety of materials and

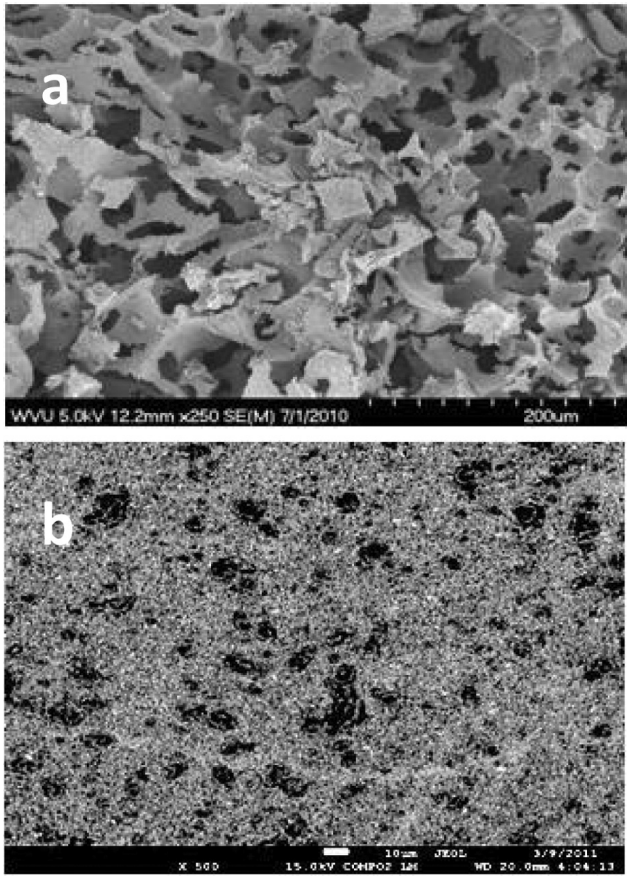

FIGURE 3. SEM image of an SOFC cathode generated by the foaming process. Image a) shows a close-up of the porous structure. Image b) shows a wider view of the whole cathode indicating the distribution of pores throughout. The images clearly show the high porosity inherent to cathodes fabricated using the technique.

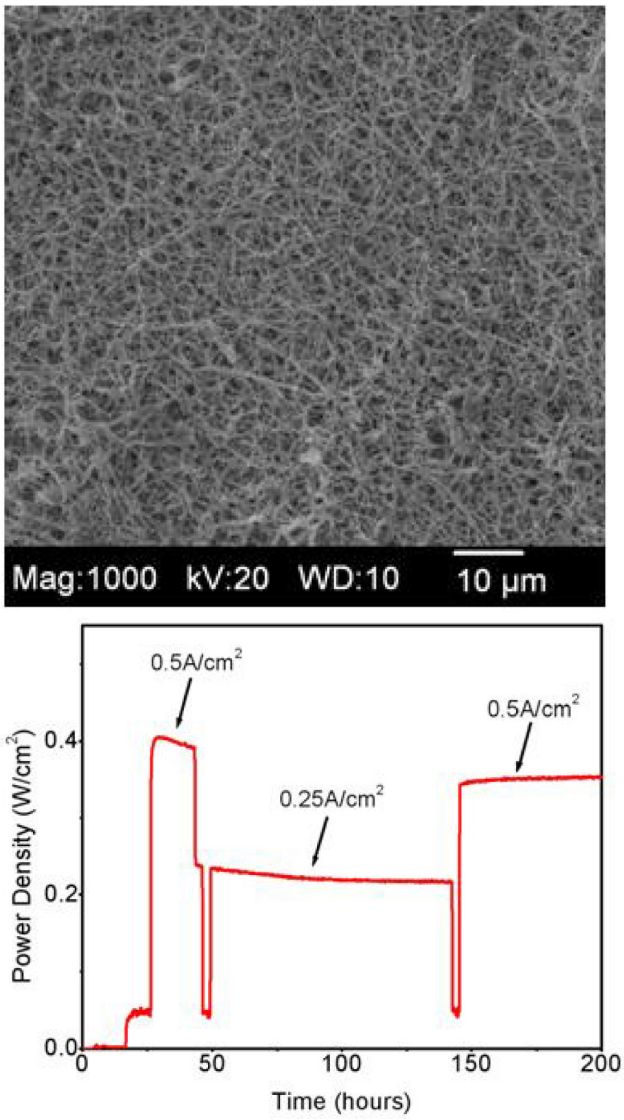

FIGURE 4. SEM image of an SOFC cathode fabricated from nanofibers and electrochemical performance data. The SEM image clearly shows the high aspect ratio of the fibers generated from the electrospinning technique, while the performance data indicate the promise of the method.

phases. Figure 4 depicts a SEM micrograph of the nanofiber cathode structure, and accompanying data indicating electrochemical performance. The high aspect ratio fibers (200 nm diameter by 2-10 microns long) are generated in an effort to enhance the cathode performance by engineering interconnected and highly conductive pathways for ionic and electronic transport. Data from initial electrochemical performance tests are shown in the bottom portion of the figure, and indicate that power performance is sufficiently high to pursue further process optimization. Efforts in FY 2011 have focused primarily on demonstration of the engineering technique to create fibers from several different SOFC relevant materials, and focused methods to improve cathode performance will be pursued in future efforts.

Conclusions and Future Directions

The FY 2011 cathode materials effort has provided valuable data confirming the potential of specific cathode microstructural engineering and infiltration techniques to substantially improve the cathode performance. In particular, the present effort has generated infiltrate materials and mesoporous structures demonstrating substantial performance increases when applied to commercially available SOFC cathodes of conventional microstructure. The infiltrate systems have been verified for stability, and methods are documented for infiltration techniques capable of penetrating to the cathode active layer and distributing infiltrate uniformly throughout. The dense $(LaSr)CoO_3$ infiltrate and the mesoporous LSM infiltrate generated by EISA in particular demonstrated significantly positive impacts, and will be pursued with industrial partners for full scale up.

Efforts to engineer microstructure were shown to be effective in enhancing the cell power performance. The highly porous foam cathode specifically demonstrated promising increases in peak power output, and methods for controlling the foam structure are well documented. The foamed cathode technique was demonstrated with materials typical of current cathodes, and the method could be transferred directly to industrial partners. The techniques used to produce nanofiber structures demonstrated generation of a variety of individual and mixed phases, of both ionic conductors and mixed ionic electronic conductors. Materials were structurally characterized and shown to be stable.

Future efforts will include generation of a final infiltrate material combining the approaches used here to produce a high surface area infiltrate with high electrocatalytic activity and superior thermochemical stability. The foamed microstructural engineering technique will be further proven and foamed structures will be produced for infiltration with the advanced infiltrate materials developed here. Efforts will also be made to scale the techniques for industrial applicability.

FY 2011 Publications/Presentations

1. Shiwoo Lee, Nicholas Miller, Harry Abernathy, Kirk Gerdes, and A. Manivannan, "Effect of Sr-Doped $LaCoO_3$ and $LaZrO_3$ Infiltration on the Performance of SDC-LSCF Cathode," J. Electrochem. Soc., 158 (2011) B735.

2. Shiwoo Lee, Nicholas Miller, Margo Staruch, Kirk Gerdes, Menka Jain, and A. Manivannan, "$Pr_{0.6}Sr_{0.4}CoO_3$- Catalyst for SOFC Cathode Introduced by Infiltration," Electrochemica Acta, submitted.

3. R. Chao, "Synthesis and Characterization of Mesoporous, High Specific Surface Area Strontium-doped Lanthanum Manganate Using Evaporation-Induced Self-Assembly," Microporous and Mesoporous Materials (submitted).

4. R. Chao, "High Surface Area, Mesoporous Catalysts in Solid Oxide Fuel Cell Cathodes," ECS SOFC-XII Symposium.

5. N.Q. Wu, "Nanofibers for Solid Oxide Fuel Cell Cathode," SOFC-XII, Montreal, Canada, May 1–6, 2011.

6. M. Zhi, N. Mariani, R. Gemmen, K. Gerdes, and N.Q. Wu, "Nanofiber Scaffold for Cathode of Solid Oxide Fuel Cell," Energy & Environmental Science, 4 (2011), 417-420.

7. M. Zhi, G. Zhou, Z. Hong, J. Wang, R. Gemmen, K. Gerdes, A. Manivannan, D. Ma, and N.Q. Wu, "Single Crystalline $La_{0.5}Sr_{0.5}MnO_3$ Microcubes as Cathode of Solid Oxide Fuel Cell," Energy & Environmental Science, 4 (2011), 139-144.

8. Shiwoo Lee, Nicholas Miller, and A. Manivannan, "Microstructural Control of Composite Cathode by Wetting Nature of Infiltrated Solutions," ECS Transaction, 35 (2011) 2401.

9. Shiwoo Lee, Nicholas Miller, Harry Abernathy, Kirk Gerdes, and A. Manivannan, "Modification of SDC-LSCF Cathode Functional Layer by Solution Infiltration," 35th ICACC, Daytona Beach, Florida, January 23–28, 2011.

10. E. Sabolsky, "Microstructural Engineering of Porous Cathodes for SOFC Applications," ECS, Boston, Massachusetts, October 9–14, 2011.

III.A.9 Development of SOFC Cathodes

J.S. Hardy (Primary Contact), J.W. Templeton, Z. Lu, J.W. Stevenson
Pacific Northwest National Laboratory
P.O. Box 999, MS K2-44
Richland, WA 99352
Phone: (509) 375-2627; Fax: (509) 375-2186
E-mail: john.hardy@pnnl.gov

DOE Project Manager: Briggs White
Phone: (304) 285-5437
E-mail: Briggs.White@netl.doe.gov

Contract Number: FWP40552

Start Date: October 1, 2010
End Date: September 30, 2011

Fiscal Year (FY) 2011 Objectives

- Investigate the effects of A-site non-stoichiometry on the performance of lanthanum strontium cobalt ferrite (LSCF) cathodes.
- Measure the performance of LSCF / strontium-doped ceria (SDC) composite cathodes fabricated by co-synthesis and mechanical mixing after heat treating at various temperatures.
- Perform in situ X-ray diffractometry (XRD) on the LSCF cathodes of anode-supported solid oxide fuel cells (SOFCs) during electrochemical performance testing.

FY 2011 Accomplishments

- Demonstrated that all but one of the A-site deficient LSCF cathode compositions exhibited over 10% improvement in power density over stoichiometric LSCF.
- Determined that adding SDC to the LSCF cathode did not provide an improvement in performance regardless of the method used to fabricate the LSCF-SDC composite or the heat treatment temperatures.
- Measured lattice expansion in an operating LSCF cathode over 60 hours of operation.

Introduction

It is generally accepted that the cathode is a major contributor to internal losses in the SOFC, so improvements in the cathode can lead to higher SOFC power density and efficiency, which will help SOFC manufacturers achieve the long-term Solid State Energy Conversion Alliance goals in terms of cost and power stability. As LSCF is currently a leading candidate amongst cathode materials due to its ability to conduct both electrons and oxygen ions, both of which are essential to cathodic performance in the SOFC, work in this task in FY 2011 was focused on investigating potential modifications to the composition of the LSCF cathode in order to obtain potential improvements in electrochemical performance. Meanwhile, in order to investigate the underlying causes of the degradation that occurs in cathodes during fuel cell operation, a new research capability has been developed that allows XRD measurements to be performed on the cathode of an operating SOFC. It is anticipated that this will provide additional insight into any chemical reactions and/or changes in the crystal lattice of the cathode over time while the fuel cell operates.

Approach

The effects of compositional modifications of LSCF cathodes were determined through electrochemical performance testing of anode-supported button cells at 750°C. The tests were carried out under constant current conditions at the current that was obtained from the cell when operation was initiated at 0.8 V. An additional set of tests was also performed on A-site non-stoichiometric cathodes in which all compositions were tested at the same constant current. The current to be employed was determined by taking the average of the currents measured when cell operation was initiated at 0.8 V for all of the cells included in the test that had been operated up to that point, including the cells to be tested at this current. The A-site non-stoichiometric LSCF cathode compositions were all A-site deficient, but deficiency was instituted in two distinct ways. Three compositions were formulated in which the La:Sr ratio was maintained at 3:2, while three other compositions were formulated in which deficiency was achieved by decreasing only the Sr content. The Sr-deficient compositions adhered to the general chemical formula, $La_{0.6}Sr_{0.4-x}Co_{0.2}Fe_{0.8}O_{3-\delta}$, and the compositions with the proportional A-site deficiency adhered to the formula, $(La_{0.6}Sr_{0.4})_{1-x}Co_{0.2}Fe_{0.8}O_{3-\delta}$, where x = 0.02, 0.05, and 0.10 for both groups of compositions. The screen printed A-site deficient LSCF cathodes were sintered at 1,100°C. The other compositional modification of the LSCF cathode to be investigated was the addition of $Ce_{0.8}Sm_{0.2}O_{2-\delta}$ (SDC) to $(La_{0.6}Sr_{0.4})_{0.95}Co_{0.2}Fe_{0.8}O_{3-\delta}$ to form a composite cathode. Two different methods were also employed to make the composite cathodes.

First, composites were fabricated in the conventional manner by mechanically mixing two commercially supplied powders together. The mechanically mixed compositions contained 30, 40, or 50 vol% SDC and were sintered at 900, 1,000, or 1,100°C. The second method to produce the composites was glycine nitrate combustion co-synthesis. This method creates an intimate mixture of nanoscale particles of both materials. The resulting powders were calcined at 600, 800, 900, 1,000, 1,100, or 1,200°C and sintered at 900, 1,000, or 1,100°C.

XRD analysis of operating LSCF cathodes was performed using a Bruker D8 Advance XRD fitted with an Anton Paar HTK 1200 heating chamber. A small scale button cell test fixture that is compatible with the heating chamber was developed to operate 13 mm diameter anode-supported button cells. XRD patterns were measured while electrochemical performance data was simultaneously being collected at ~0.8 V. Upon completion of the tests, the Cluster Analysis add-on module for Jade [v9.3; Materials Data, Inc., Livermore, California] XRD analysis software was used to calculate the similarity index of each XRD pattern to the first pattern measured. To improve statistics, patterns taken within sequential intervals of time (e.g., 1 hour or 20-hour periods) were integrated together and similarity indices for those intervals were also compared to the first in the series. Once it was established that the XRD patterns were generally becoming less similar to the original pattern as a function of time, the patterns were plotted together to evaluate what specific changes were occurring in the spectra.

Results

Electrochemical tests determined that all of the A-site deficient LSCF cathodes outperformed stoichiometric LSCF. This is illustrated in Figure 1, which plots the power densities of cells operated under constant currents corresponding to an operating voltage of 800 mV. These tests compared various A-site deficient LSCF cathode compositions to stoichiometric LSCF. In the legend of Figure 1, the non-stoichiometric compositions are designated "A -*x*" or "Sr -*x*" where *x* is a number representing the percent A-site deficiency arising from the depletion of proportional amounts of La and Sr or from the depletion of Sr only, respectively. Due to the variability in performance for different cells with the same cathode composition, it was not possible to resolve a significant trend in performance as a function of composition, except that the 10% Sr-deficient composition (designated "Sr -10" in the legend) underperformed the other non-stoichiometric compositions while still outperforming the stoichiometric composition. These results were confirmed in tests in which all compositions were operated at a constant current of 1.937 A.

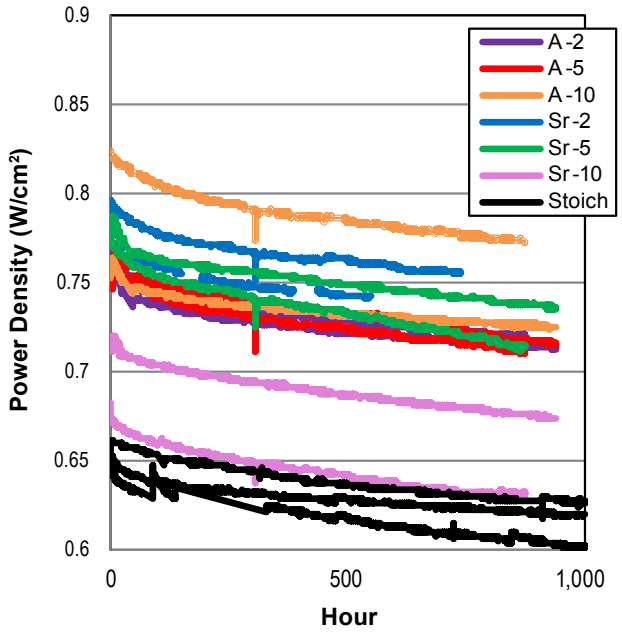

FIGURE 1. The power densities of anode-supported SOFCs with A-site deficient LSCF cathodes are compared to those of cells with stoichiometric LSCF cathodes as a function of time.

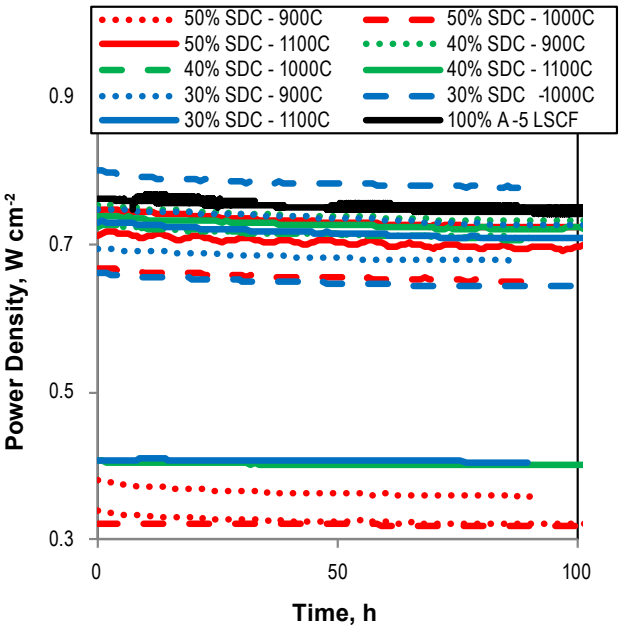

FIGURE 2. Power density is plotted as a function of time for SOFCs with mechanically mixed SDC-LSCF composite cathodes containing 30-50 vol% SDC that were sintered at 900, 1,000, or 1,100°C.

Unlike A-site deficiency, the introduction of SDC into the LSCF cathode did not produce an improvement in performance. Figure 2 shows the performance of mechanically mixed composites with black lines representing the performance of cells with cathodes

made using only the LSCF for comparison. The legend for the chart provides the composition and sintering temperature. Only a single test conducted with a composite cathode performed better than the single phase cathode and its duplicate performed much worse. Additionally, the variability in the performance of the composite cathodes was much higher than that of the single phase cathodes and it was found that composites made using the glycine-nitrate process did not provide an improvement over those that were mechanically mixed.

Figure 3 is a plot showing the performance of an anode-supported cell with a stoichiometric LSCF cathode as a function of time. Also plotted is the similarity index of XRD patterns collected at various times during cell operation compared to the initial pattern in the series. The general decreasing trend in the similarity index of the individual 10-minute scans and in the 1 hour and 20-hour integrals of these scans indicates that the XRD patterns are becoming less and less similar to the initial pattern in the series as time progresses. Therefore, something is progressively changing in the LSCF lattice as a function of time. In Figure 4, the 20-hour integral XRD patterns are overlaid for nine of the major LSCF peaks to illustrate the changes that are occurring in the cathodes. The black pattern is from the scans taken between 0-20 hours, the red is from 20-40 hours, and the blue is from 40-60 hours. For each peak, there is a slight shift to lower angles over time, indicating an expansion in the crystal lattice. It was also noted that peaks from the underlying SDC interlayer did not exhibit a consistent change in position or intensity as a function of time, therefore acting as an internal control. Additional work is underway to determine the cause of the lattice strain. Possible causes include compositional changes such as oxygen depletion or strontium segregation.

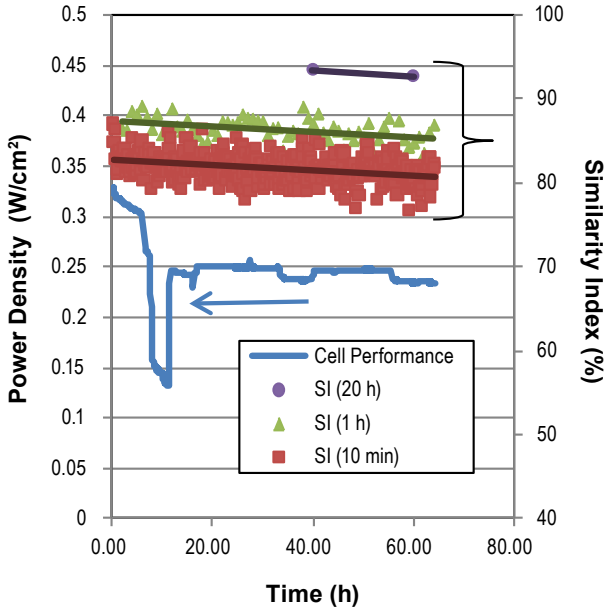

FIGURE 3. Power density and LSCF cathode XRD pattern similarity index are plotted as a function of cell operation time for an anode supported cell operated at ~0.8 V.

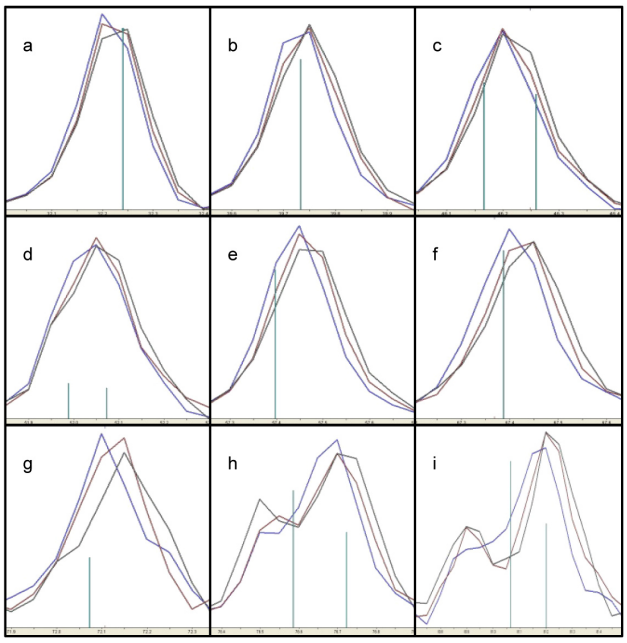

FIGURE 4. The XRD patterns resulting from integrating the patterns collected from the LSCF cathode during the intervals 0-20 hours (black line), 20-40 hours (red line), and 40-60 hours (blue line) of cell operation are shown in the regions of nine LSCF peaks including (a) 32-32.4°, (b) 39.6-39.9°, (c) 46.1-46.4°, (d) 51.9-52.3°, (e) 57.3-57.7°, (f) 67.2-67.6°, (g) 71.9-72.3°, (h) 76.4-76.9°, and (i) 80.8-81.5° 2θ.

Conclusions and Future Directions

- LSCF cathodes with up to 10% A-site deficiency significantly outperformed stoichiometric LSCF. However, when 10% of the A-site deficiency was due solely to Sr, performance began to decline but still outperformed the stoichiometric composition.
- The effect of A-site deficiency in the LSCF cathode on the amount of Sr that diffuses into the SDC interlayer and YSZ electrolyte will be examined using wavelength dispersive spectroscopy.
- The addition of SDC to LSCF to form a composite cathode did not benefit performance and led to a higher degree of cell-to-cell variability in performance.
- The capability for simultaneously performing electrochemical testing of anode-supported SOFCs and collecting XRD patterns from the cathodes has been demonstrated.

- During 60 hours of cell operation, the crystal lattice of the LSCF cathode gradually expanded.
- The cause of the lattice expansion is currently being investigated.

FY 2011 Publications/Presentations

1. Z. Lu, J.S. Hardy, J.W. Templeton, and J.W. Stevenson, "New Insights in the Polarization Resistance of Anode-Supported Solid Oxide Fuel Cells with $La_{0.6}Sr_{0.4}Co_{0.2}Fe_{0.8}O_3$ Cathodes," *Journal of Power Sources* 196(1):39-45 (2011).

2. J.W. Templeton, J.S. Hardy, Z. Lu, and J.W. Stevenson, "The Effect of A-site Stoichiometry on LSCF Cathode Performance and Stability," *35th International Conference and Exposition on Advanced Ceramics and Composites*, (2011) – In press.

3. Z. Lu, J.S. Hardy, J.W. Templeton, and J.W. Stevenson, "On Pursuit of High Performance Solid Oxide Fuel Cells for Intermediate Temperature Applications," MS&T 2010, Houston, Texas, October 18, 2010.

4. J.W. Templeton, J.S. Hardy, X.D. Zhou, and J.W. Stevenson, "Optimizing LSCF Sintering Temperature for SOFC Performance and Stability," MS&T 2010, Houston, Texas, October 20, 2010.

5. J.W. Templeton, J.S. Hardy, X.D. Zhou, Z. Lu, G.D. Maupin, and J.W. Stevenson, "Effect of Potential Contaminants from Glass Seals on SOFC Cathodes," MS&T 2010, Houston, Texas, October 20, 2010.

6. J.S. Hardy, J.W. Templeton, Z. Lu, and J.W. Stevenson, "In-situ XRD of Operating Cathodes," 35th International Conference & Exposition on Advanced Ceramics & Composites, Daytona Beach, Florida, January 25, 2011.

7. Z. Lu, J.S. Hardy, J.W. Templeton, and J.W. Stevenson, "Densification of $Sm_{0.2}Ce_{0.8}O_2$ (SDC) Interlayer in Solid Oxide Fuel Cell (SOFC)," 35th International Conference & Exposition on Advanced Ceramics & Composites, Daytona Beach, Florida, January 26, 2011.

8. J.S. Hardy, J.W. Stevenson, J.W. Templeton, and Z. Lu, "The Effect of A-site Stoichiometry on LSCF Cathode Performance and Stability," 35th International Conference and Exposition on Advanced Ceramics and Composites, Daytona Beach, Florida, January 25, 2010.

III.A.10 Electronic Structure of Cathode Materials

Walter A. Harrison
GLAM/McCullough Bldg.
Stanford University
Stanford, CA 94305-4045
Phone: (650) 723-4224
E-mail: walt@stanford.edu

DOE Project Manager: Briggs White
Phone: (304) 285-5437
E-mail: Briggs.White@netl.doe.gov

Contract Number: PPM 300.02.08

Start Date: January 7, 2008
End Date: September 30, 2011

Fiscal Year (FY) 2011 Objectives

- Carry out Madelung calculations for the electrostatic potentials and energies associated with manganite surfaces.
- Use these studies in support of the experimental projects at the University of Nevada, Las Vegas, and Carnegie Institute in Pittsburgh.
- Explore the role of these potentials in fuel cell operation.

FY 2011 Accomplishments

- Discovered the origin of strontium segregation to the surfaces of $La_{1-x}Sr_xMnO_3$ (LSM).
- Extended the theory to $La_{1-x}Sr_xCo_{0.8}Fe_{0.2}O_{3-\delta}$ (LSCF) and interfaces.
- Explored the consequences of the segregation concerning fuel cells.

Introduction

We undertook the planned Madelung calculations and in the course of this realized their relevance to the segregation of strontium ions to the surface of lanthanum-strontium manganite, LSM. This segregation had been observed experimentally by Dulli, et al. [1] (Figure 1) and had been followed up in studies at Argonne National Laboratory by members of our group. Fortunately we were able to set aside the objectives we had been required to provide last year and follow up on this opportune finding. Though this segregation had been found experimentally before 2000, there had been no clue as to its cause. It became quite clear in our work that it arose directly from the electrostatic effects of polar surfaces special to perovskite structures. We followed this up, completed the related Madelung calculations, and in the end described the theory of the segregation in a paper in the Physical Review [2]. Much of our effort after that was centered on exploring the diverse consequences of this segregation which was now understandable.

The fact that this segregation arose from electrostatic effects, which would be the same in LSCF, meant that the same segregation should occur there, and further that it should arise at the interface between the LSCF cathode and the yttria-stabilized zirconia (YSZ) electrolyte in an oxide fuel cell. Neither of these had been observed experimentally. However, it would have the effect of making the cathode *insulating* just in the regions where electron transfer is needed in order for oxygen vacancies to move through the system. It would thereby hinder the operation of fuel cells which depends directly on this flow of oxygen vacancies.

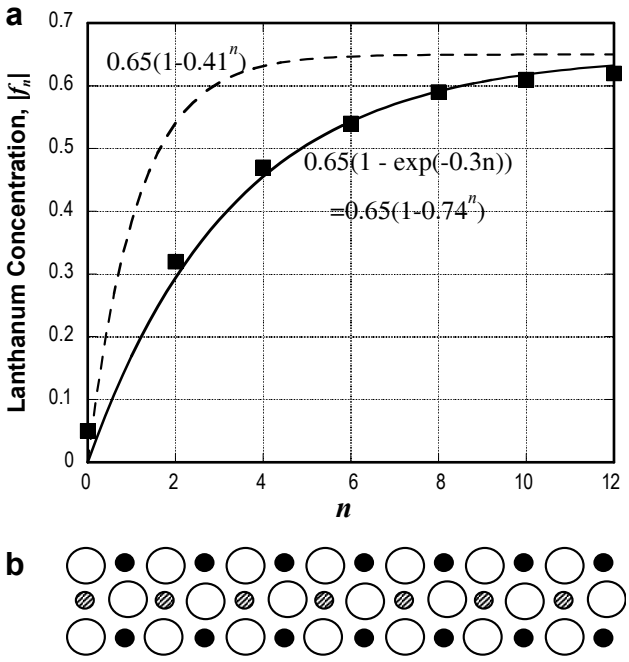

FIGURE 1. The squares in Part a are the fraction f_n of A sites occupied by La in (100) planes of $La_{0.65}Sr_{0.35}MnO_3$, as measured by Dulli, et al. [1], for planes numbered n (starting with $n = 0$ for the surface AO plane). The solid line is a fit to the data. The dashed line is the exponential which gave lowest electrostatic energy. Part b represents the lattice; shaded circles are A (Sr or La) atoms, black circles are Mn and open circles are oxygen.

Finally it appeared likely that this effect of segregation has been inhibiting the operation of these systems, though there still remains no direct experimental evidence for the segregation at the interface, nor for its adverse effects. We sought, and found, possible methods for eliminating the segregation. We plan to present these ideas at the annual Solid State Energy Conversion Alliance Workshop in Pittsburgh in July, 2011.

Approach

The theoretical basis for these electrostatic effects is the existence of polar surface on perovskite crystals. These are ion arrangements which effectively give the surfaces net surface charge and divergent electrostatic energy. These are always avoided in real systems, but by different means in different systems. We had always assumed that the divergences were eliminated in LSM and LSCF by changing the charge states of Mn, Co, or Fe ions near the surface, as it corrects for different doping in the bulk. However, it turned out here that a different mechanism actually occurs, based on segregation of the Sr ions to the surface.

The nature of the strontium segregation is most clearly seen in the experiments of Dulli, et al. [1], which we showed in Figure 1. Indeed the concentration of La drops very nearly to zero at the surface, replaced entirely by strontium. In many ways it would be more appropriate to regard this as lanthanum depletion, rather than strontium segregation. This concentration then rises to its bulk value along an exponential curve, as indicated by the solid line in Figure 1. It is quite possible to calculate the electrostatic energy for such an arrangement of ions of charge +3 (La) and of charge +2(Sr), neutralized by reversed charges on the intervening planes, using the simplified approach for performing Madelung calculations which we had developed earlier [3]. That we did, and found it to be minimum for an exponential decay shown as the dashed line in Figure 1. This included *only* the electrostatic contributions to the energy though there are additional effects of electronic structure. Thus we cannot expect complete agreement between the two curves, but it provided convincing evidence that this was indeed the origin of this remarkable experimental finding.

Results

The consequences of knowing the origin of the lanthanum depletion at the surfaces turned out to be very far-reaching. First we consider other systems to see whether the same effect might occur there. A very important system for fuel cells is the electrolyte, YSZ. We look first at pure zirconia in the same cubic structure, a face-centered-cubic lattice of Zr^{4+} ions, with O^{2-} ions at the center of each of the eight "cubies", making up the face-centered cube (the fluorite structure). (100) faces would be highly charged, made entirely of Zr ions or made entirely of O ions, and such surfaces would not be expected to occur. However, (110) faces would each contain one Zr for every two O ions and would be neutral. We expect (110) surfaces to be the natural cleavage and growth surfaces. Replacing a fraction of the Zr ions with Y^{3+} ions is equivalent to removing a single proton from some of the Zr nuclei, a view sometimes called *theoretical alchemy* [4]. The system is known to maintain charge neutrality by forming one oxygen vacancy, V_O^{2+}, for every two yttrium substitutions. Then for a uniform distribution of yttrium ions and oxygen vacancies each (110) plane acquires on average one vacancy for each two yttrium ions and remains neutral. The difference from LSM is that each plane has the full crystal stoichiometry, so bulk charge neutrality leads to planar neutrality. The same would be true of ceria which also occurs in the fluorite structure. It would seem that this segregation only occurs in more complex structures such as the perovskite structure of LSM. In this structure there seem not to be planes containing the ABO_3 (a general perovskite composed of AO and BO_2 planes of ions) stoichiometry (at least no low-index planes, which are favored). With any substitution of different valence, such as Sr and La on the A site, another case of theoretical alchemy [4], charged planes arise and segregation of the same form as for LSM may be expected. The most important such case for fuel cells is lanthanum-strontium cobalt ferrite, LSCF, since it is the other principal fuel cell cathode. Thus we are anticipating that such segregation is present in all of the important cathode materials. Further, the same polar surface will arise at an interface between LSCF and YSZ since, as we just saw, the surface of YSZ is not polar, and therefore behaves electrostatically the same as the vacuum, or air, at an LSCF surface.

Perhaps the most important consequence of the depletion concerns the conductivity. These systems are polaronic conductors, fundamentally different from semiconductors as we emphasized in reference [5]. This fact for LSCF was unambiguously demonstrated in the experiments of Tai, et al. [6], shown in Figure 2. This temperature dependence bears no resemblance to that of band conductors such as semiconductors. One such negatively charged polaron is generated for every La ion substituted in $SrCo_{1-y}Fe_yO_3$ crystal. As the number of La ions increases the conductivity increases until most of the ions are La. Then the conductivity decreases and is usually interpreted in terms of positively-charged polarons, decreasing toward zero as it becomes pure $LaCo_{1-y}Fe_yO_3$, as seen in Figure 2. Further, local charge neutrality requires that these polarons remain in the region where the La is substituted. Thus the region closest to the interface, which has no La ions becomes insulating and no longer effective as a cathode.

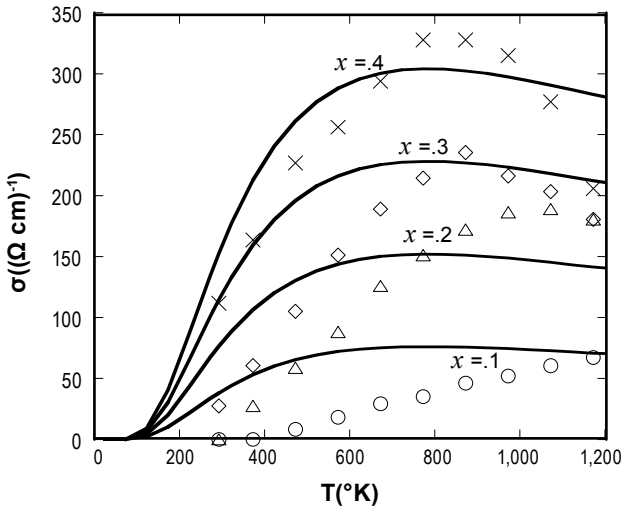

FIGURE 2. Points are experimental conductivities for $La_{1-x}Sr_xCo_{0.8}Fe_{0.2}O_{3-\delta}$ from Tai, et al. [5]. Lines are directly from small-polaron theory.

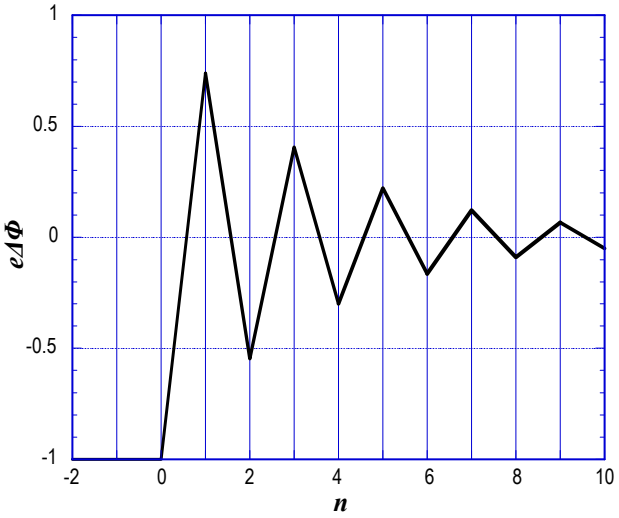

FIGURE 3. The electrostatic potential, relative to bulk sites for LSM, at the oxygen sites in planes numbered from the surface as in Figure 1. Even planes are of AO type.

We found a second, unexpected consequence of the lanthanum depletion, a segregation of oxygen vacancies toward the surface. This was unanticipated since we had shown that oxygen vacancies form neutral complexes [6] and would not be expected to be affected by these electrostatic effects. The double positive charge of the vacancy is balanced by two B ions being modified from 4+ to 3+ charge states. The states for these added electrons turn out to be lower by 0.5 eV next to the vacancy so that they will form, and diffuse as, neutral complexes. However, the potentials which were generated by the depletion actually fluctuated near the surface, as shown in Figure 3. Since the A-site ions are all on even-numbered planes, the *fluctuation* did not play a role in the La depletion calculation. On the other hand, an oxygen vacancy (itself positively charged) on an AO plane has its potential energy lowered, and the two electrons which neutralize the vacancy complex lie in the adjacent BO_2 planes with opposite potential and are therefore also lowered in energy, attracting the vacancy to the surface. Oxygen vacancies on the BO_2 planes had the associated electrons in the same plane, with no shift in the energy of the complex.

The direct calculation of electrostatic potentials gave much larger than realistic attraction, and we scaled it by a factor γ in our calculations for this effect. We then modeled the diffusion of the vacancies in the presence of such a potential, following it until equilibrium was reached, leading to distributions of oxygen vacancies shown in Figure 4. The very large reductions in the bulk for γ more than 0.01 were quite inconsistent with observed bulk concentrations so the true effects must correspond to the small-γ regime. We could carry out the corresponding diffusion calculations, in the same way but with different surface concentrations on the two sides, to see that it did not seriously affect the diffusion

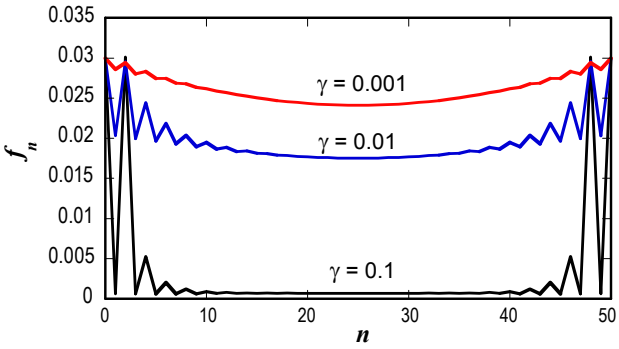

FIGURE 4. The fraction of oxygen sites vacant as a function of plane number in a symmetric 50-plane slab of LSCF, with surface concentrations of $f(n)$ of 0.03, for three choices of the scaling parameter γ.

properties important to fuel cells. The fact that the vacancy complexes are neutral remains important. It means that oxygen incorporation does not occur by ionization of oxygen at the surface, but occurs by the transfer of neutral oxygen atoms or molecules filling neutral vacancies. No charge transfer occurs at the cathode surface. It occurs at the interface between the cathode and electrolyte.

We turned finally to seeking methods for enhancing the operation of the fuel cell by eliminating the La depletion at that interface. This depletion was of electrostatic origin and we may hope to eliminate it by electrostatic means. The segregation came because of a polar surface of $La_{1-x}Sr_xCo_{1-y}Fe_yO_3$, where each (100) plane has a charge of $\pm(1-x)/a^2$ (with a the perovskite cube edge). This gives an effective surface charge of $(1-x)/2a^2$, if we terminate the crystal at an AO

surface, which we have seen can be neutralized by the segregation profile. If we could replace a quarter of the La ions in this interface plane by alkali atoms, maybe potassium, that would eliminate the effective surface charge and presumably the segregation.

There are other ways in which this depletion might be eliminated. One that comes to mind is forcing a polar surface on the YSZ. If equal and opposite to that on the LSCF it would eliminate the cause for segregation, but that would seem more difficult to accomplish. In any case, once the depletion barrier is removed we may expect that the oxygen vacancies could flow freely between the electrolyte and the cathode, eliminating this last roadblock, as illustrated in Figure 5.

Conclusions and Future Directions

The principal activity during the year has been first discovering that the origin of the segregation of strontium, which has been known to occur in LSM, is the presence of polar surfaces in perovskite crystals, such as LSM. We had not recognized earlier that this segregation was an important effect, but this origin suggested that it would occur in all important cathode materials, and produce insulating surfaces – and also insulating interfaces. We explored this effect, and the possibility of associated effects on the oxygen vacancies which are central to fuel cell operation. We found that only the insulating aspect would seem to be important, but that it may be seriously affecting fuel cell capacity. Knowing the origin, we could also seek ways to eliminate this detrimental feature of the perovskite cathodes, and selected on approach which seems most promising.

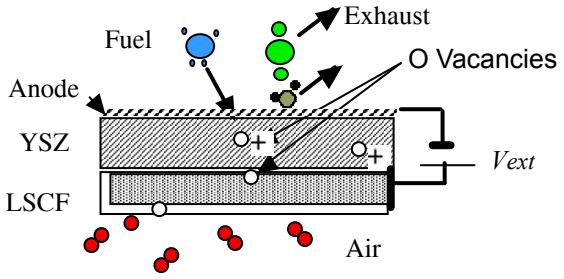

FIGURE 5. An idealized fuel cell. The depletion area, white in LSCF, remains at the surfaces, but is eliminated between the cathode and the electrolyte. Then the complete process is uninhibited.

These findings associated with segregation were based on the original experimental discovery of the effect, but the intermediate conclusions such as segregation at interfaces, remain to be verified experimentally. The best theoretical approach for the coming year may be to leave the segregation behind and make a systematic study of the existing experiments on diffusion of oxygen in YSZ and LSCF and oxygen permeation experiments, reinterpreting them in terms of the more complete understanding of the electronic structure of these systems which we have developed. We have begun such an effort and hope to continue it during the coming year to obtain a clearer picture of each aspect of the fuel cell system, and then maybe a complete picture of an ideal fuel cell such as that in Figure 5.

FY 2011 Publications/Presentations

1. Walter A. Harrison, *Theoretical Alchemy,* World Scientific Publishing Company (Singapore, 2010).

2. Walter A. Harrison, "The Origin of Sr Segregation at $La_{1-x}Sr_xMnO_3$ Surfaces," Phys. Rev. B **83**, 155437 (2011). (arXiv:1101.5414).

References

1. Hani Dulli, P.A. Dowben, S.-H. Liou, and E.W. Plummer, "Surface Segregation and Restructuring of Colossal-Magnetoresistant Manganese Perovskites, $La_{0.65}Sr_{0.35}MnO_3$," Phys. Rev. B **62**, R14629 (2000).

2. W.A. Harrison, "The Origin of Sr Segregation at $La_{1-x}Sr_xMnO_3$ Surfaces," Phys. Rev. B **83**, 155437 (2011). (arXiv:1101.5414).

3. W.A. Harrison, "Simple Calculation of Madelung Constants," Phys. Rev. B **73**, 212103 (2006).

4. W.A. Harrison, *Theoretical Alchemy,* World Scientific Publishing Company (Singapore, 2010).

5. L.-W. Tai, M.M. Nasrallah, H.U. Anderson, D.M. Sparlin, and S.R. Sehlin, "Structure and Electrical Properties of $La_{1-x}Sr_xCo_{1-y}Fe_yO_3$. Part 1. The System $La_{0.8}Sr_{0.2}Co_{1-y}Fe_yO_3$," Solid State Ionics **76**, 259 (1995).

6. W.A. Harrison, "Tight-Binding Theory of Lanthanum Strontium Manganate," arXiv:0807.2248, submitted to Phys. Rev., but not accepted.

III. SECA CORE RESEARCH & DEVELOPMENT

B. Anodes and Coal Contaminants

III.B.1 NETL RUA Anode Contaminants R&D

Kirk Gerdes
U.S. Department of Energy
National Energy Technology Laboratory (NETL) –
Regional University Alliance (RUA)
3610 Collins Ferry Rd.
Morgantown, WV 26507
Phone: (304) 285-4342; Fax: (304) 285-4469
E-mail: Kirk.Gerdes@netl.doe.gov

Contract Number: 10-220621 6923
(NETL RUA Anode Contaminants R&D)

Start Date: October 1, 2010
End Date: September 30, 2011

Fiscal Year (FY) 2011 Objectives

- Complete 500-hour ethylene exposure tests on a typical Ni-based anode supported solid oxide fuel cell (SOFC). Generate a comprehensive report detailing ethylene exposure tolerances.
- Generate a thermodynamic analysis predicting the presence of trace material in syngas cleaned using a typical cold gas cleanup process.
- Generate a detailed report describing the gas chromatograph (GC) inductively coupled plasma/mass spectrometer (ICP/MS) analytical method including the previously developed calibration procedure.
- Perform detailed microstructural analysis in support of Ni/yttria-stabilized zirconia (YSZ) anode SOFC exposed to higher hydrocarbons such as naphthalene and ethylene. Compare results to cells fuelled with hydrogen gas.

FY 2011 Accomplishments

- Completed ethylene exposure tests and generated performance analysis describing exposure tolerance. Completed a detailed engineering effort to improve data quality.
- Completed a detailed report describing the scrubbing efficiency of a traditional low-temperature cleanup system for trace metals in coal-derived syngas.
- Completed a detailed report describing the GC-ICP/MS method and finalized a report describing the gas phase calibration procedure.
- Completed detailed analysis of anode microstructure, particularly concentrating on intergranular phase evolution in syngas and hydrogen environments.
- Reported results in four publications and three presentations.

Introduction

High efficiency electricity producing systems containing SOFCs are the subject of substantial research. Many of the system designs considered include a coal gasification unit coupled to a gas processing system that provides synthesis gas to the SOFC. The coal gasification process may volatilize some of the naturally occurring trace materials found in the coal. Nickel-based SOFC anodes have been theoretically and experimentally shown to negatively interact with trace metal species contained in synthesis gas derived from coal gasification.

In order to operate an SOFC on coal fuel sources, the trace materials that are reactive with the fuel cell anode must first be identified. Trace material exposure limits acceptable for maintaining SOFC performance must also be determined as a function of operating conditions. Results of this research effort are used to design cleanup systems that will reduce the trace material content of the fuel stream to operationally acceptable levels.

Approach

Research is focused on evaluating deleterious performance effects observed from exposing a Ni-based SOFC anode to trace species present in SOFC fuel (syngas) that is derived from coal gasification. In general, trace materials negatively impact performance by blocking active reaction sites within the anode or reacting with the anode to produce undesirable secondary phases. The key technology gap for all trace material interaction characterizations is an absence of well controlled, long-term (500-hour) test data for the trace materials of interest. Steady control of all test parameters through a 500-hour experiment is difficult to maintain, and comparison to repeatable baseline cell results is necessary. To address the identified gap in knowledge, research continues in which SOFC anodes are exposed to simulated and direct coal syngas containing trace materials while performance is recorded through an extended duration test (typically 500 hours). In particular, trace metals such as Hg, Se, and As, and trace hydrocarbons such as benzene, naphthalene, and ethylene will be exposed to the SOFC anodes. The performance data are used to determine the rate of contaminant related deactivation, which is then used to

support prediction of cleanup targets for integrated coal gasification fuel cell applications.

Performance testing is supported directly by concerted spectroscopic analysis. This activity is initiated to supply high resolution microstructural and chemical information pertinent to chemical interactions with trace materials in direct and indirect coal-fuelled SOFCs. The comprehensive microstructural analysis of materials in a scale ranging from microns to atoms complements expertise in materials and devices design and performance evaluation. The comprehensive microstructure information facilitates the correlation between the anode electrocatalysis, microstructure, and chemistry degradation mechanisms attributable to various contaminants. This information provides understanding of relevant materials parameters, microstructure, and performance, in order to identify and develop materials with improved resistance to degradation. In SOFC possessing Ni-YSZ anodes, efforts are initiated to apply scanning electron microscopy, high resolution transmission electron microscopy, scanning transmission electron microscopy, and energy dispersive X-ray spectroscopy to conduct comprehensive chemical and microstructural analysis. The analysis coupled with cell testing efforts elucidates the mechanisms of contaminant interactions causing changes to the atomic structure and chemistry of anode materials at the triple phase boundary region. Parallel multi-scale transmission electron microscopy (TEM) microstructure analysis is carried out on as-received and contaminant exposed cells in order to provide a baseline for assessment of trace material induced degradation.

Another key gap in the area of trace metal analysis is the absence of established methods and technical data describing the operation, calibration, and quality control procedures for direct GC-ICP/MS analysis of gas phase industrial process streams. A research project continues to develop methods for GC-ICP/MS that are equivalent to the established liquid phase ICP/MS methods that have been widely reported and tested. The first known calibration procedure applicable to direct gas phase analysis has been developed, and the calibration procedure will be combined with a comprehensive method generating a repeatable, reliable process for conducting analysis. The method will be validated through a battery of performance tests including analysis of a multi-element, mixed-phase unknown sample to produce an accuracy of analysis approaching that of the established ICP/MS methods for liquid samples. The research develops reliable techniques and protocols for transmission of gas phase samples from the process stream to the analytical system for analysis.

Results

Substantial progress in evaluation of anode degradation processes has been made. Estimates of permissible ethylene exposure have been generated for tests conducted at ethylene exposures of 1,000 ppm. Figure 1 depicts the recorded degradation in cell performance as a function of ethylene exposure over the course of 450 hours. The image at the top shows data for a button cell operated at 0.25 A/cm^2 at 800°C. Cell voltage is observed to decrease throughout the period of exposure, from a starting voltage of approximately 0.857 V to a final voltage of approximately 0.835 V. The degradation may be fit by an exponential decay model, which predicts an initial degradation of 4.8% per 1,000 hours. The image at the bottom shows results from an electrochemical impedance spectroscopy experiment. The curves measured indicate more specific details of the process of degradation. In this case, curve shapes remain roughly stable, but greater impedance is observed as time elapses. This indicates that real ohmic resistance is the primary source of performance degradation in this system, and the ability of the cell to transfer charge is degrading.

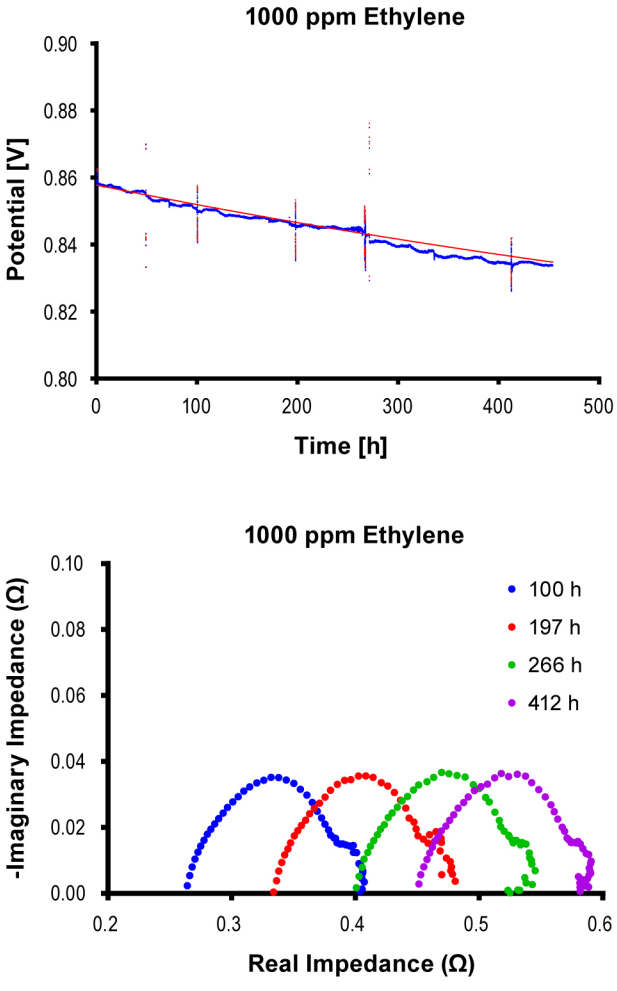

FIGURE 1. (Top) Temporal plot of SOFC performance for 1,000 ppm ethylene exposure. (Bottom) Evolution of impedance data for cell exposed to ethylene for 500 hours.

Experimental results demonstrating degradation may be further investigated in post-operation cell analysis, typically using advanced spectroscopic methods. A technique known as TEM can be applied to investigate features of the anode that may correspond to the observed degradation. Figure 2 shows images collected by TEM of an intergranular phase that grows between the nickel (Ni) and YSZ particles. The intergranular nickel oxide (NiO) phase appears to grow according to the conditions of cell operation, from approximately 30 nm after 45 hours of operation to approximately 65 nm after 500 hours of operation. The NiO phase appears to grow more strongly in the presence of certain fuels, especially those containing greater carbon-based species. Carefully controlled tests are presently underway to ensure that the phase growth occurs during cell operation, and to determine the root cause of growth.

In addition to providing high resolution, TEM can also detect differences in crystal structure over very small domains of a few nanometers in width. Figure 3 depicts a TEM image generated for an intergranular region between anode constituents Ni and YSZ. In the image, a localized zone of altered structure is detectable in the YSZ at the Ni/YSZ interface. Typical YSZ possesses a cubic structure (c-YSZ), but

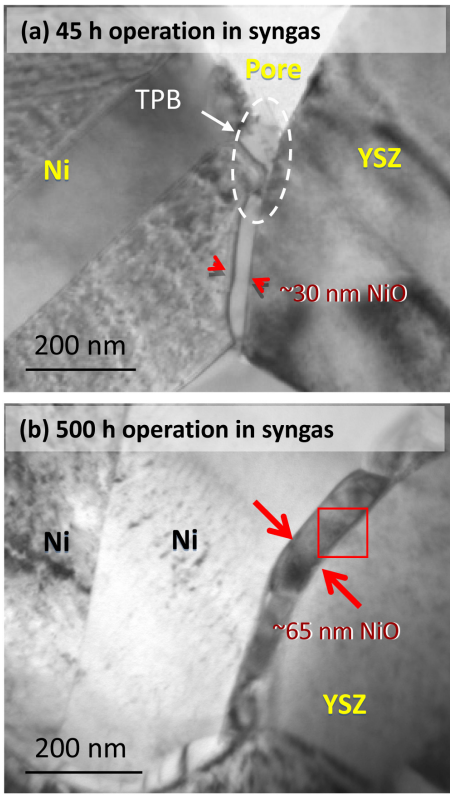

FIGURE 2. Intergranular phases of NiO appearing at interface between Ni and YSZ. The phase only appears for polarized cells, and grows with duration of exposure to synthesis gas.

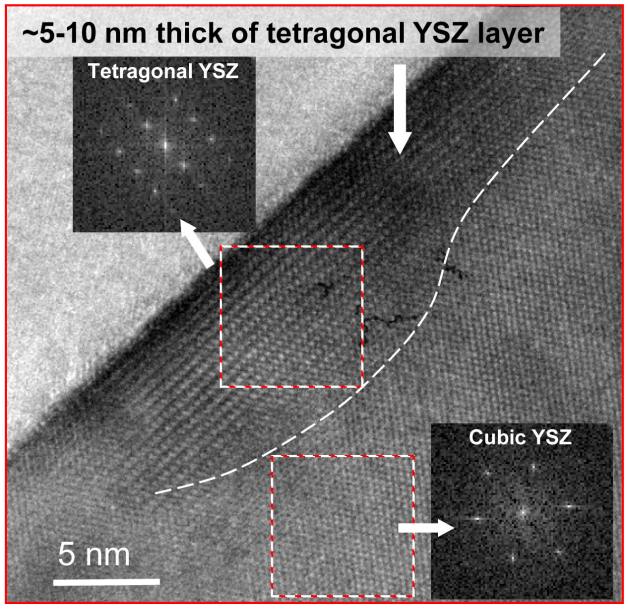

FIGURE 3. TEM image of intergranular t-YSZ zone developing between YSZ and Ni in SOFC anodes exposed to naphthalene. Degradation of c-YSZ to t-YSZ is only observed for polarized samples exposed to hydrocarbon fuel.

in the intergranular region of this cell exposed to hydrocarbons, a region of tetragonal YSZ (t-YSZ) is detected. The t-YSZ is typically found in a band parallel to the grain interface. This observation is important, as t-YSZ possesses a lower ionic conductivity than c-YSZ, and ionic transport through the anode may be impeded at these critical interfaces. Further investigations are presently underway to prove that the t-YSZ phase is generated from operation of the SOFC in the presence of hydrocarbon fuel.

The hydrocarbon components in syngas are present in the greatest relative fractions, but trace materials may also be present that will cause more rapid and pronounced degradation in a nickel-based fuel cell. Many of these materials are present in trace amounts, and specialized detection methods must be developed to quantify their relative abundance. Figure 4 shows exemplary results of a trace gas analysis for a single element, mercury (Hg). The figure shows that the actual concentration of 0.055 μg/L of mercury present in a gas stream is well approximated using the analytical technique of GC-ICP/MS. The quantification generated is the result of an intensive effort to develop a unique technique capable of providing rapid trace metal analysis of gas phase samples derived from chemical process streams. The technique is based on a single element calibration procedure and has been demonstrated for accuracy in semi-quantitative evaluations of trace metal concentration. The corresponding method can analyze trace metal content at gas phase concentrations of 1 ppb or less, and can assess the presence of every metal in the periodic table.

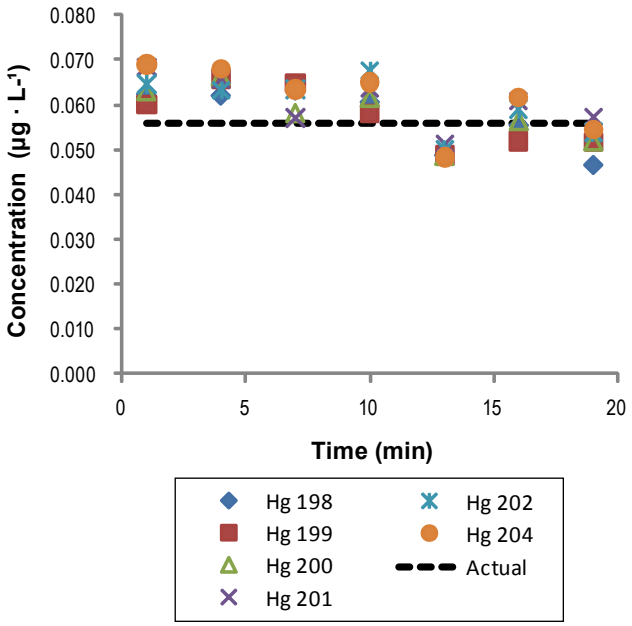

FIGURE 4. GC-ICP/MS measurements of gas phase mercury quantified using semi-quantitative, gas-phase calibration and evaluation processes developed in this research. Predictions for mercury concentration compare favorably to actual concentration of mercury.

Conclusions and Future Directions

Investigation has generated substantial progress in understanding anode degradation mechanisms associated with the most common fuel constituents (hydrocarbons) and trace metals present in coal derived syngas. In particular, carefully controlled hydrocarbon exposure experiments are completed to provide information on the impact to electrochemical performance, and ultimately to assess the permissible thresholds for hydrocarbon exposure in the systems. The specimens generated are observed with high resolution techniques such as TEM in order to correlate the electrochemical performance degradation with specific microstructural features that appear especially in the intergranular regions. First-of-their-kind techniques have been developed to semi-quantitatively assess the trace metal content in gas phase chemical process streams, and the methods have demonstrated accuracy.

Future investigations will be conducted in anode degradation associated with exposure to hydrocarbon species in order to elucidate the exact mechanisms of interaction. The sensitivity of the observed degradation rate will be assessed relative to the operating conditions of the cell, and prescriptions for cell operation will be generated. Threshold material exposure levels will also be generated using the data collected for the cell degradation response as a function of exposure. The GC-ICP/MS system will be deployed to support testing that requires analysis of trace metal, including efforts in gasification, membranes, catalysts, sorbents, and sensors.

FY 2011 Publications/Presentations

1. G. Hackett and K. Gerdes, "Trace Species Partitioning as Affected by Dry (Cold) Gas Cleanup Conditions: A Thermodynamic Analysis," NETL Reference Shelf, June 2011.

2. K. Gerdes, "Impact of Minor Species from Coal Syngas on SOFC Performance," FY11 Fuel Cells Peer Review, February 14–18, 2011.

3. K. Gerdes and K. Carter, "Calibration Method for Direct GC-ICP/MS Analysis of Gas Phase Samples," submitted to Spectrochemica Acta B.

4. S. Chen, Y. Chen, et al., "Crystal Defects of Yttria-Stabilized Zirconia in Solid Oxide Fuel Cells and Their Microstructural Evolution upon Cell Operation," submitted to Solid State Ionics.

5. Y. Chen, Y. Chen, et al., "Microstructural and Chemical Evolution near Anode Triple Phase Boundary in Ni/YSZ Solid Oxide Fuel Cells," submitted to Solid State Ionics.

6. X. Song, C Song, et al., "Crystal Defects of YSZ in Solid Oxide Fuel Cells and Their Microstructure Evolution upon Cell Operation," Submitted to the 220th ECS Meeting, Boston, Massachusetts, October 9-14, 2011.

7. X. Song, Y. Chen, et al., "Evolution of Microstructure and Chemistry of Solid Oxide Fuel Cells upon Operation," MRS Fall Meeting, GG10.19, Boston, Massachusetts, December 2010.

III.B.2 Utilization of Coal Syngas in High Temperature Fuel Cells: Degradation Mechanisms and Lifetime Prediction

Ismail Celik
West Virginia University (WVU)
P.O. 6106
Morgantown, WV 26506
Phone: (304) 293-3209; Fax: (304) 293-6689
E-mail: ismail.celik@mail.wvu.edu

DOE Project Manager: Briggs White
Phone: (304) 285-5437
E-mail: Briggs.White@netl.doe.gov

Contract Number: ER46299

Start Date: August 1, 2009
End Date: July 31, 2012

Fiscal Year (FY) 2011 Objectives

- Implement new characterization methods.
- Develop remedies for impurity effects.
- Identify the tolerance limits of solid oxide fuel cell (SOFC) anode for specific impurities.
- Predict the lifetime of the anode for a given impurity level.

FY 2011 Accomplishments

- It was found that hydrogen fuel mixed with steam including 10 ppm PH_3 lead to faster degradation when compared to dry fuel condition.
- The surface temperature of button cells was measured under to different operating conditions using the new in situ technique.
- PH_3 impurity was successfully removed from the coal syngas using nickel and iron-based filters before it got into the cell.
- Transmission electron microscopy (TEM) characterization revealed new nano-scale phenomena in the SOFC anodes exposed to impurities.
- A mass spectrometer was acquired and tested to monitor in situ forms of impurity species and their concentrations, before and after passing through the cell.
- Cell lifetimes and tolerance limits for impurities are estimated using the new degradation model.
- The synergistic effects of multiple impurities were simulated including H_2S, AsH_3 and PH_3 and it was found that mixture of impurities leads to faster degradation compared to single impurity.
- In-house modeling code was used to simulate button cells operating on biogas with both dry and wet reforming.
- Numerical simulations showed that the co-flow arrangement in a planar SOFC resulted in longest structural life.
- It was found that at low PH_3 concentrations the anode structural degradation may be as significant as electrochemical degradation.
- The mechanism responsible for sulfur tolerance of lanthanum-doped ceria (LDC) impregnated anodes was studied.
- Ni/galladium-doped ceria (GDC) anode was shown to be a suitable material for syngas contaminated with H_2S.
- New $Sr_2MgMoO_{6-\delta}$ (SMM)/GDC anodes were prepared in-house and are shown to be tolerant to PH_3 in syngas.

Introduction

This project is supported under the U.S. Department of Energy Experimental Program to Stimulate Competitive Research (EPSCoR), a program designed to enhance the capabilities of EPSCoR states in energy research and economic development through the support of advanced research at academic institutions. The long-term goal is to establish an internationally recognized, sustainable fuel cell research center for coal-based clean power generation which serves as a technology resource for the emerging fuel cell industry in West Virginia. Towards this goal, we formed a multidisciplinary team of research professionals who have worked together for several years and have strong credentials in their respective areas of expertise. Our strengths are in applying nano-technology to develop and fabricate materials for advanced coal-based fuel cells; state-of-the-art material characterization and fuel cell testing facilities involving both ex situ and in situ measurement techniques; and multi-dimensional modeling of fuel cells at various scales using high-performance computing. During the first phase of the project, we developed a laboratory infrastructure, solidified interactive working relationships, and attained national recognition for the work conducted by the center in the area of coal-based clean power generation via fuel cells. The research cluster has proven itself to be sustainable with team

members working together on other related projects. Based on the progress made, we obtained a three-year continuation of funding from DOE EPSCoR with cost share from the National Energy Technology Laboratory, West Virginia State, and WVU. The goal under this project is to further expand the infrastructure for fuel cell research at WVU, to increase our reputation as a centre of excellence and thus ensure continued funding. The proposed technical objectives of the project are to establish the tolerance limits of contaminant levels in the coal syngas for SOFCs and to predict the lifetime of the cells for a given contaminant levels.

Approach

The research cluster is based on a multi-scale, multi-disciplinary approach conducted by eight faculty members in four departments at WVU. The work is organized under three integrated projects: 1) characterization of contaminant effects; 2) multi-scale continuum modeling; and 3) anode material development. The knowledge base gained from experiments (Projects 1 and 3) will be used in multi-scale computational models (Project 2) to establish the tolerance limits for the impurities and to predict the life time of SOFCs operating on coal syngas with the impurities.

Results

Characterization of Contaminant Effects

Tests were conducted in which button cells were exposed to ppm levels of PH_3 in dry and moist hydrogen to study the PH_3 poisoning effect on SOFC performance at 800°C. Along with electrochemical measurements, in situ infrared (IR) temperature measurements were made at the anode surface with and without PH_3 contaminant to investigate the polarization effects under different operating conditions. During the PH_3 exposure, Ni-ytrria-stabilized zirconia (YSZ) reacted with PH_3 and generated the P-based secondary phases, which would cause the fuel cell performance degradation and alter the IR emissivity of electrode. The secondary phase formation and microstructure change were confirmed via the post-term characterization (i.e., scanning electron microscopy [SEM], and X-ray diffraction [XRD]). The button cell exposed to H_2/3 vol% H_2O with the same 10 ppm PH_3 showed more degradation and higher surface temperature than exposure to dry H_2 at the same current densities.

The electrochemical performance of the Ni-YSZ anode operating in PH_3 contaminated coal syngas with different current loadings was also investigated using symmetric cell experiments. It is confirmed that the Ni-YSZ anode degraded more severely with electrical current and the presence of the water content in the syngas accelerates the degradation. A series of tests at 10 ppm PH_3 in syngas showed that the dominant species of Ni_xP_y detected on the cell anode are Ni_5P_2 with H_2O present, and $Ni_{12}P_5$ without H_2O present. Further, the appearance of Ni_xP_y phases is independent of the electrochemical reactions in the cell. In addition, Ni patterned electrodes on YSZ substrate were prepared using photo lithography, and a well-defined Ni\YSZ interface (triple phase boundary, TPB) is achieved. These structures will be further used to study the fundamental mechanism of the Ni-YSZ degradation due to coal syngas contaminants.

As a remedy to reduce the impact of PH_3 on the cell performance, Ni- and Fe-based prefilters were investigated. These filters were shown to remove PH_3 impurity from syngas fuel effectively to levels which are not harmful to the Ni-YSZ anode. Iron is a cost-effective material for efficient PH_3 removal, but the sintered ferrous phosphate layer can block the fuel diffusion channels and reduce fuel transport. The addition of nickel to the iron-based filter was shown to inhibit the formation of the coherent iron product layer, thus maintaining a porous structure in the filter. Figure 1 shows the SOFC exposed to syngas with PH_3 under a 0.5 Acm^{-2} constant current load at 800°C. Both H_2S and PH_3 were fed to the cell with Ni-based (phase (c) & (d)) and Fe/Ni-based (phase (f) & (d)) filters (Figure 1) during an 1,100-hour test. The results showed

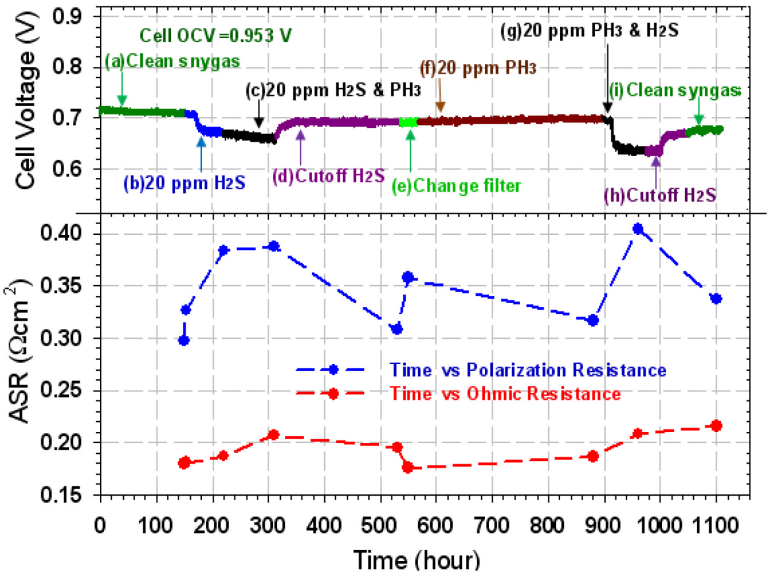

FIGURE 1. The cell voltage and area specific resistance versus time during the entire 1,100-hour test under constant 0.5 Acm^{-2} current load at 800°C. The cell ohmic resistance remained almost constant and the polarization resistance increased when 20 ppm H_2S was added to the fuel.

that the interaction between these two impurities did not significantly impact the filter performance. With proper filter design, the Ni-YSZ SOFC can operate on contaminated coal-syngas without degradation over a prescribed period of time.

The microstructure and chemistry of the SOFCs, which were run with syngas plus 10 ppm PH_3 for 120 hours, were investigated using TEM. Three major phenomena were observed in the anode of the cell: 1) an external reaction layer of ~20 µm containing Ni and P. Near this reaction layer, the content of the Ni grains decreases dramatically, which suggests that Ni migrates out to react with PH_3 and forms a new surface layer. 2) An extra tetragonal YSZ layer at the Ni/YSZ interface (Figure 2a). Energy dispersive X-ray spectroscopy (EDS) results show that there is Y/Zr ratio variation along the Ni/YSZ interface from 8.7 atom% to 55.1% accompanied with the variation of the tetragonal and cubic YSZ, which indicates the Y could migrate along the Ni/YSZ interface. 3) A new cubic phase (red oval in Figure 2b) forms at the Ni/YSZ interface in the anode active layer. The EDS showed this new cubic phase contains Y, P and O, which indicates that the PH_3 may react not only with Ni, but also with YSZ. With SOFC running on pure H_2, the thickness of this layer is only about 10 nm and does not change up to 600 hours of operation time. There was no structural change of the YSZ grain near the Ni/YSZ interface.

A Cirrus MKS mass spectrometer was connected to the exhaust gases of a test stand to monitor phosphine gas (mass 34) or a P fragment ion (mass 31) in either a syngas mixture or pure nitrogen. This attempt was unsuccessful. This lack of changes at mass 34 or mass 31 that correlated with the presence or absence of phosphine is tentatively attributed to loss of phosphine within the furnace due to a combination of reactions at 800°C. In syngas mixtures, addition of 100 ppm hydrogen sulfide led to increased signals at mass 34 and mass 33 (for H_2S and HS ions), but the rise in the (uncalibrated) partial pressures at these masses was very slow, taking about 20 hours to reach a near steady-state value. Subsequent changes in the concentration of H_2S resulted in more rapid responses of the signal at mass 34. Mass 33 signals responded in a similar manner. These data suggest that hydrogen sulfide or its reaction products are adsorbing onto interior surfaces of the tubes inside the furnace until the surfaces are saturated. When the hydrogen sulfide is added to a syngas mixture, increases in partial pressures of mass 60 and mass 64 were observed. These changes were attributed to oxidation of H_2S to SO_2 (mass 64) and COS (mass 60).

Continuum Level Modeling

The anode degradation model is extended to simulate effects of several new syngas contaminants and also simultaneous exposure to multiple impurities. The

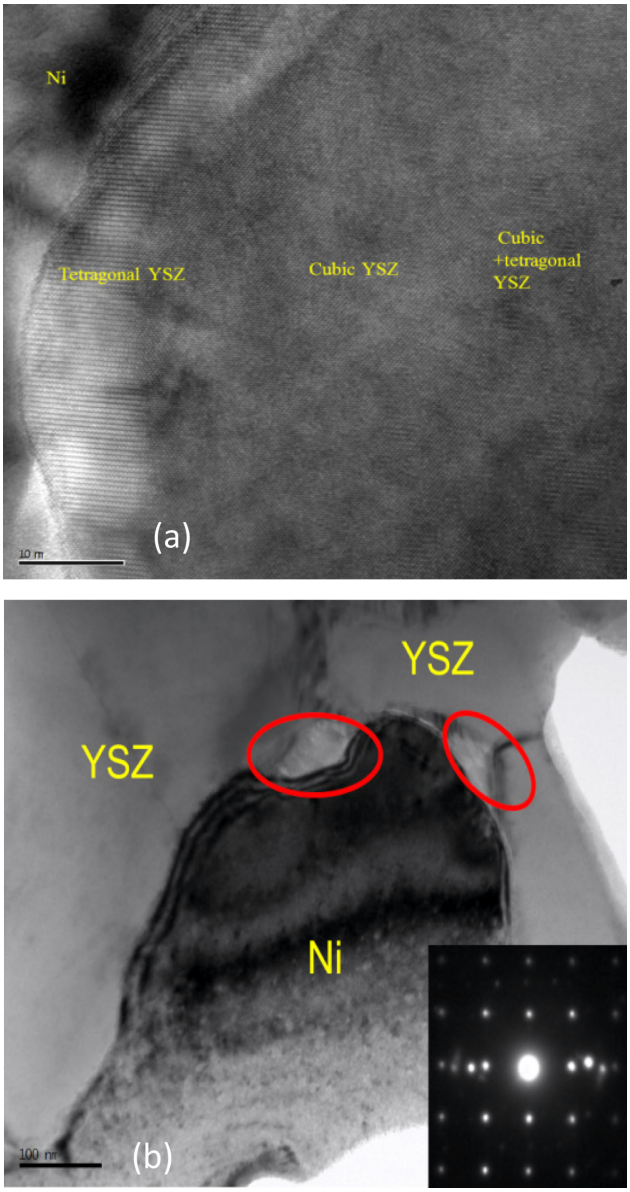

FIGURE 2. (a) Formation of the tetragonal YSZ layer by the interface of Ni/YSZ, from the anode of SOFC operated using syngas with PH_3 contamination. (b) Formation of the Y-P-O phase (circled) by the Ni/YSZ interface, from the anode of SOFC operated using syngas with PH_3 contamination.

model parameters were calibrated for contaminants such as hydrogen sulfide (H_2S) and hydrogen selenide (H_2Se) using experimental data obtained from accelerated testing conditions (Figure 3a). The synergistic effect of various impurities including AsH_3, PH_3 and H_2S was also examined and it was concluded that the mixture of impurities leads to faster degradation and thus shorter lifetime of the cell when compared to that of a single impurity.

A summary of predicted cell lifetimes for electrolyte-supported cells with an anode thickness of

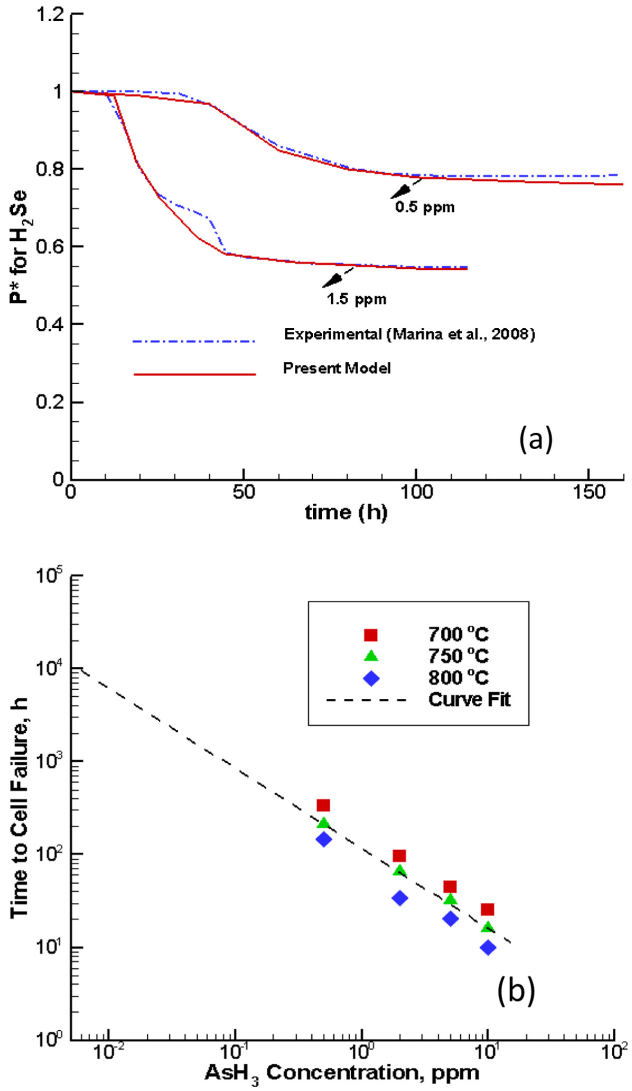

FIGURE 3. (a) Calibration of modified power density against experimental data adopted from Ref. [1] for 1.5 ppm H_2Se in coal syngas at 800°C. (b) Time to cell failure for electrolyte-supported cells exposed to simulated coal syngas with varying concentrations of arsine at different operating temperatures.

30 μm operated in simulated coal syngas containing 23% CO, 30% H_2, 21% CO_2 and 26% H_2O and varying concentrations of AsH_3 impurity is shown in Figure 3b. The criterion for cell failure is taken as the time when 60% of power loss occurs. Extrapolation of the fitted curve to lower impurity concentrations shows that for 10,000 hours of operation, the minimum allowable arsine concentration is estimated to be about 5 ppb. The minimum allowable phosphine concentration is estimated to be less than 0.5 ppb. Coal syngas containing 1 ppb PH_3 resulted in 1% degradation in 600 hours for an anode supported cell with 1 mm thickness. It was also found that there is a linear relationship between the cell failure time and the anode thickness.

The anode structural durability model, incorporating both the thermo-mechanical and fuel contaminants effects, is enhanced to predict the long-term structural behavior of planar-SOFC anodes. Co-flow, counter-flow and cross-flow cells are simulated under similar operating conditions (Figure 4). The model predicts that the co-flow arrangement yields the longest anode structural life. It was also shown that, under lower PH_3 concentration, the anode structure degradation may be significant as compared to the electrochemical degradation.

New sub models and numerical techniques were introduced in our three-dimensional in-house code, DREAM-SOFC, to account for dry reforming reaction and to handle zero hydrogen and steam concentrations in biogas. Good agreement between the predicted and measured (Project 1) voltage-current (VI) curves was obtained. The results from the computations shed light on critical reaction rates and thermal management required for smooth operation of SOFCs on biogas fuel.

Anode Materials Development

The aim of this project is to fabricate SOFCs with high performance for syngas operation and to improve stability of the SOFC anode in sulfur and phosphorous containing syngas. Our previous results have identified LDC as an effective sulfur-tolerant SOFC anode material. Sulfur tolerance achieved by impregnated LDC has a dramatic impact on Ni-YSZ/stabilized scandium zirconia anode degradation. The Pt current collector reacts with Ni to form Ni-Pt intermetallic phase, causing Ni to migrate toward anode outlayer.

The observed recovery of a Ni-based anode under 20 ppm of H_2S thus indicates LDC can actively "gather" sulfur in the anode outlayer, reducing the amount of sulfur reaching active reaction sites and in this case, transferring Ni back into the anode interlayer.

The fundamental reaction mechanism between the LDC-impregnated SOFC anode and H_2S was studied by morphological and structural characterization techniques of SE), X-ray photoelectron spectroscopy (XPS) and XRD. Thermodynamic calculations were also carried out using Factsage software. XRD analysis results for anodes after H_2S-containing syngas exposure show that the LDC oxide decomposed as a result of the reaction with H_2S. This finding for LDC is in sharp contrast to other doped ceria systems like GDC and SDC, whose phases will typically not change after exposure to a relatively low concentration of H_2S. Such comparison suggests LDC may be a better sulfur-adsorption candidate than GDC and SDC systems especially for preventing poisoning from lower concentration of sulfur.

Test results also showed that the Ni/GDC anode has tolerance of up to 1,000 ppm of H_2S in both wet

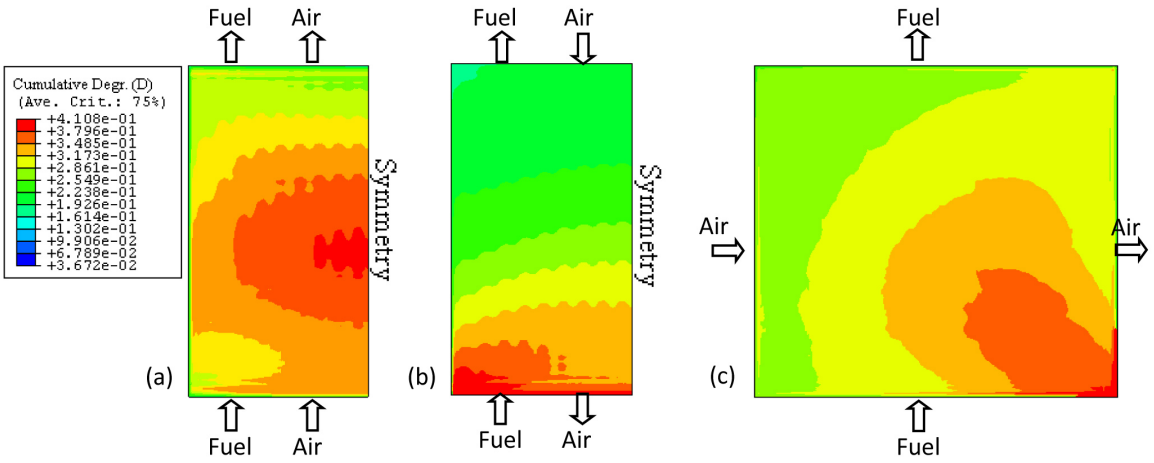

FIGURE 4. Anode structure failure locations comparison: (a) co-flow: 19,920 h; (b) counter-flow: 16,310 h; (c) cross-flow: 18,450 h.

hydrogen and syngas fuels. The cell also exhibits long-term stability upwards of 250 hours in 100 ppm H_2S (Figure 5a), which has not been reported in previous literature.

The use of a double-perovskite SMM anode in coal syngas in the presence of hydrogen sulfide and phosphine was investigated. The B and B'-sites are also being doped with Ni and Co (B-site) and W, Nb, and Ta (B'-site) to control electrocatalytic nature and to control the electronic and ionic conduction mechanisms. The pure SMM and SMW ($Sr_2MgWO_{6-\delta}$) anode was synthesized via a solid-state method and GDC was incorporated into the anode for improved ionic conductivity. Figure 5b shows the results of the SMM/GDC anode operating in 3% wet H_2 with 10 ppm PH_3. Tests have shown that the cell degrades slowly over an extended period of time (>70 hrs in 10 ppm PH_3), but that the degradation appears not to be due to phosphorus reaction in the active or bulk of the anode. XPS and EDS do not detect phosphorus chemical reaction with the anode, and thus, this data leads to the conclusion that the cell degradation is likely to be due to anode delamination. These new findings present a path for the development of new ceramic anodes that are resistant to phosphine degradation.

In addition, the materials group has been fabricating large-area, planar fuel cells in an effort to conduct experiments more applicable to commercial fuel cell devices. Electrolytes 100 cm^2 in area and electrode active areas ranging from 16-64 cm^2 have been manufactured and are going to be tested in the coming months.

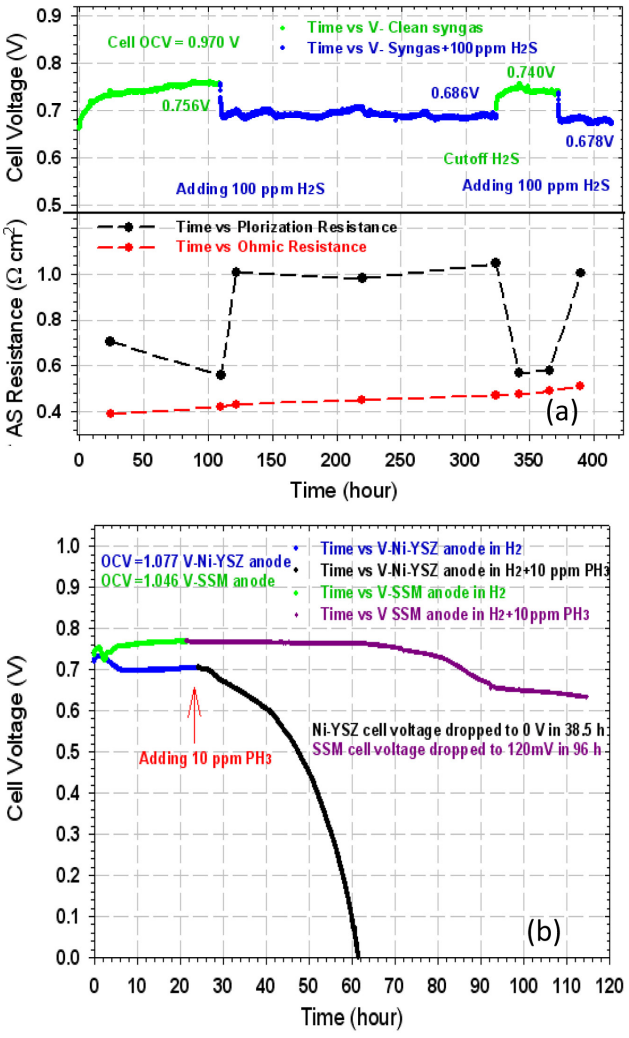

FIGURE 5. (a) Ni/GDC performance in clean syngas with/without 100 ppm H_2S. (b) SMM/GDC anode comparison to Ni/YSZ anode in 3% wet H_2 and 10 ppm PH_3.

Conclusions and Future Directions

Long-term exposure tests under PH_3 will be carried out and out-of-plane surface deformations would be measured at specified time intervals to quantify the

PH_3 effects on the anode structural properties. The test results will facilitate the development of the long-term anode structural durability and electrochemical degradation models under coal syngas utilization. Kinetics of PH_3/Ni reaction will be measured using thermogravimetric analysis. Investigations of the P penetration rate into the Ni-YSZ anode will continue. A model will be built based on the experimental data to determine the influence of the electrical current and the water content on the degradation rate and the Ni migration. Such a model will be used to predict the lifetime of the anode operated in PH_3 contained in coal syngas. The Ni patterned electrode will be used to study the influence of the PH_3 on the TPB sites. The data will be integrated with the electrochemical measurements to verify TPB length change during PH_3 attacking.

The mass spectrometer will be connected to the point at which contaminant gases are mixed with the fuel stream to confirm the composition of gases going into the hot zone of the tube furnace. A sampling tube will be constructed for gases to be sampled and analyzed at a point just above the anode surface. These gas analyses will be correlated to determine the fate of contaminants (phosphine, hydrogen sulfide, etc.) inside the furnace as a function of the initial composition of the fuel, the temperature and the current flow through the SOFC.

In developing contaminant tolerant materials, the focus will be on the design and development of alternative ceramic anode components for operation in sulfur- and phosphor-containing coal syngas. The materials of interest are ionically and electronically conductive ceramic oxides with perovskite structure (ABO_3). This type of anode material has been proven to tolerate higher concentration of sulfur. Our previous research indicated PH_3 can degrade the perovskite anode even at the ppm level. The challenge is to design and synthesize the anode materials which are able to mitigate both sulfur and phosphorus poisoning. The group's research experiences on SOFC manufacturing, mixed oxides impregnation, together with atmospheric high-temperature instrument will be utilized to overcome these technical barriers. Large planar fuel cells in co-flow configuration will be tested, to investigate how fuel utilization and delivery affects degradation and fuel poisoning mechanisms in fuel cell stacks. Initially, the standard Ni/YSZ anode will be used, and later work will focus upon the new alternate anodes described previously. Poisoning and fuel utilization as a function of displacement will be emphasized once baseline testing is completed. Work on the Ni/GDC anode will continue for other fuels such as bio-gas and natural gas. The degradation mechanism of the SMM/GDC cell in the presence of PH_3 will be further studied to help develop new ceramic anodes that are resistant to degradation in fuels containing the combined H_2S and PH_3 contaminants.

The modeling efforts will continue to extend the electrochemical degradation model to three-dimensions, multi-component contaminants using the DREAM-SOFC, the in-house code. Results will be validated against planned large planar cell experiments. Simulations will be performed to predict the lifetime of planar cells running on coal syngas and biogas. The existing LBM code will be extended to three-dimensional multi-component flow simulations in porous medium and will be applied to a typical fuel cell anode.

Based on the knowledge gained from SOFC testing in this research project, we will extend our work to CO_2/NO_x decomposition. We propose an integration of metal oxide electrodes with solid oxide electrolyzer cell to: 1) decompose CO_2 into C/CO and oxygen for further processing; and 2) decompose NO_x into N_2, and O_2. Preliminary exploratory tests show very promising results in achieving a high percentage of CO_2 decomposition into C/CO and O_2. These preliminary results will be used to strengthen our research proposal for securing future funding.

Special Recognitions & Awards/Patents Issued

1. Patent disclosure: "Pre-Filter for Removal of Trace Contaminants from Gaseous Fuels for Use in Solid Oxide Fuel Cells," U.S. Patent & Trademark Office, August 2010, Pending.

2. Dr. Edward Sabolsky received the 2010-2011 Weaver Award within the WVU Mechanical and Aerospace Engineering department for outstanding teaching in the area of Mechanics of Materials.

FY 2011 Publications/Presentations

1. H. Guo, G. Iqbal, and B.S. Kang (2011), "Effects of PH_3 Contaminant on SOFC Performance and Related Anode Surface Temperature Measurements," International Journal of Applied Ceramic Technology, v. 8, p. 68-73.

2. D. Ding, M. Gong, C. Xu, N. Baxter, Y. Li , J. Zondlo, K. Gerdes, and X. Liu (2011), "Electrochemical Characteristics of Samaria-Doped Ceria Infiltrated Strontium-Doped $LaMnO_3$ Cathodes with Varied Thickness for Yttria-Stabilized Zirconia Electrolytes," Journal of Power Sources, v. 196, p. 2551-2557.

3. C. Xu, J. Zondlo, M. Gong, F. Elizalde-Blancas, X. Liu, and I.B. Celik (2010), "Tolerance Tests of H_2S-laden Biogas Fuel on Solid Oxide Fuel Cells," Journal of Power Sources, v. 195, p. 4583-4592.

4. C. Xu, J. Zondlo, M. Gong, and X. Liu (2011), "Effects of PH_3 Poisoning on a Ni-YSZ Anode-Supported SOFC under Various Operation Conditions," Journal of Power Sources, v. 196, p. 116-125.

5. Fatma N. Cayan , Suryanarayana R. Pakalapati, Ismail Celik, Chunchuan Xu, and John Zondlo (2011), "A Degradation Model for Solid Oxide Fuel Cell Anodes Due

to Impurities in Coal Syngas: Part I. Theory and Validation," submitted to Fuel Cells.

6. Chunchuan Xu, John Zondlo, and Edward Sabolsky, "A Prefilter for Mitigating PH_3 Contamination of a Ni-YSZ Anode," Journal of Power Sources, accepted for publication.

7. Huang Guo, Gulfam Iqbal, and Bruce S. Kang, "Investigation of Secondary Phases Formation Due to PH_3 Interaction with SOFC Anode," American Society Ceramics Transaction, accepted for publication.

8. Gulfam Iqbal, Raju Pakalapati, Huang Guo, Ismail Celik, and Bruce Kang, "PEN Structure Thermal Stress Analysis for Planar-SOFC Configurations," American Society Ceramics Transaction, accepted for publication.

9. Gulfam Iqbal and B.S. Kang, "Elastic Brittle Damage Model for Ni-YSZ and Predicted Stress-Strain Relations as a Function of Temperature and Porosity," ASME Journal of Fuel Cell Sciences and Technology, accepted for publication (2011).

10. F. Elizalde-Blancas, S.R. Pakalapati, F.N. Cayan, C. Xu, I.B. Celik, H.O. Finklea, and J.W. Zondlo, "A Computational Model for SOFC Running on Syngas," submitted to Journal of Power Sources.

11. Y. Chen, S. Chen, H. Finklea, X. Song, G. Hackett, and K. Gerdes, "Microstructure and Chemistry Evolution of Triple Phase Boundaries in the Anode of Solid Oxide Fuel Cells," submitted to Solid State Ionic.

12. C. Xu, J.W. Zondlo, M. Gong, X. Liu, and I.B. Celik, "Tolerance Tests of Co-feeding Cl_2 and H_2S Impurities in Biogas on a Ni-YSZ Anode-Supported Solid Oxide Fuel Cell," Proceeding of ASME 2010 8th Fuel Cell Science, Engineering & Technology Conference, Brooklyn, New York, June 14–16, 2010.

13. C. Xu, J. Zondlo, and E. Sabolsky, "Exploring Remedies for PH_3 Poisoning of a Ni-YSZ Anode SOFC in Coal-Syngas Fuel," Proceeding of ASME 9th Fuel Cell Science, Engineering and Technology Conference, Washington, D.C., August 7–10, 2011.

14. F.N. Cayan, S.R. Pakalapati, and I. Celik, "A Degradation Model for Solid Oxide Fuel Cell Anodes Due to Impurities in Coal Syngas," Proceeding of ASME 9th Fuel Cell Science, Engineering and Technology Conference, Washington, D.C., August 7–10, 2011.

15. S.R. Pakalapati, Y. Vural, C. Xu, J. Zondlo, and I. Celik, "Three-Dimensional Modeling of a SOFC Operating on Biogas," Proceeding of ASME 9th Fuel Cell Science, Engineering and Technology Conference, Washington, D.C., August 7–10, 2011.

16. H. Guo, G. Iqbal, and B.S. Kang, "Phosphine Effects on Ni-based Anode Material and Related SOFC Button Cell Performance Investigation," Proceeding of ASME 2010 8th Fuel Cell Science, Engineering & Technology Conference, Brooklyn, New York, June 14–16, 2010.

17. G. Iqbal, R. Pakalapati, H. Guo, I. Celik, and B. Kang, "Anode Structure Degradation Model for Planar-SOFC Configuration under Fuel Gas Contaminants," Proceeding of ASME 2010 8th Fuel Cell Science, Engineering & Technology Conference, Brooklyn, New York, June 14–16, 2010.

18. P. Gansor, C. Xu, J. Zondlo, K. Sabolsky, and E. Sabolsky, "Investigation of Phosphine Tolerant Anodes for Solid Oxide Fuel Cells," Presented at 34th International Conference and Exposition on Advanced Ceramics and Composites (ICACC), Daytona Beach, Florida, January 24–29, 2010.

19. M. Zhi and N. Wu, "Degradation Mechanism of Nickel –Yttria Stabilized Zirconia Anode Materials in PH_3 containing Coal Syngas," 218th ECS Meeting, Las Vegas, Nevada, October 12, 2010.

20. M. Zhi, J. Yan, A. Manivannan, and N. Wu, "Degradation Mechanism of Nickel –Yttria Stabilized Zirconia Anode Materials in PH_3 Containing Coal Syngas," 219th ECS Meeting, Montreal, Canada, May 2011.

21. R. Bajura, I. Celik, H. Finklea, B. Kang, X. Liu, E. Sabolsky, X. Song, N. Wu, J. Zondlo, S. Pakalapati, C. Xu, and Y. Vural, "Effect of Syngas Trace Contaminants on SOFC Anode Performance," Poster presented at the 11th Annual SECA Workshop, Pittsburgh, Pennsylvania, July 27, 2010.

22. X. Song, Y. Chen, S. Chen, H. Finklea, G. Hackett, and K. Gerdes, "Evolution of Microstructure and Chemistry of Solid Oxide Fuel Cells upon Operation," Poster presented at Materials Research Society Symposium on Next-Generation Fuel Cells – New Materials and Concepts, Boston, Massachusetts, December 1, 2010.

References

1. O.A. Marina, L.R. Pederson, C.A. Coyle, E.C. Thomsen, D.J. Edwards, C.D. Nguyen, and G.W. Coffey, "Interactions of Ni/YSZ Anodes with Coal Gas Contaminants," in 9th Annual SECA Workshop, Pittsburgh, Pennsylvania, August 7, 2008.

III. SECA CORE RESEARCH & DEVELOPMENT

C. Interconnects and Contact Materials

III.C.1 Evaluation of a Functional Interconnect System for SOFCs

Matthew D. Bender
ATI Allegheny Ludlum
1300 Pacific Avenue
Natrona Heights, PA 15065
Phone: (724) 226-6575
E-mail: Matt.Bender@ATImetals.com

DOE Project Manager: Robin Ames
Phone: (304) 285-2078
E-mail: Robin.Ames@netl.doe.gov

Contract Number: NT42513

Start Date: July 1, 2005
End Date: December 31, 2010

Fiscal Year (FY) 2011 Objectives

- Identify compositional modifications that lead to improved oxidation resistance and enhanced electrical conductivity in commercial ferritic stainless steel alloys.
- Evaluate surface treatments to maximize performance of ferritic stainless steel in solid oxide fuel cell (SOFC) environments by completing oxidation experiments and electrical resistance testing.
- Complete project by finishing experiments, analyzing data, and summarizing the improvement in critical SOFC-related properties for interconnect systems that incorporate modified alloy compositions and surface modifications.

FY 2011 Accomplishments

- Area-specific resistance (ASR) testing of cerium-modified $(Mn,Co)_3O_4$ (Ce-MC) spinel coated, third generation experimental alloy coupons was completed for exposure times beyond 3,000 hours at temperature. The rate of increase in ASR once the test systems reached steady-state conditions was observed to be as low as 0.8 mΩ·cm^2/1,000 hours for a Ce-MC spinel coated Fe-17Cr alloy coupon and 1.4 mΩ·cm^2/1,000 hours for a Ce-MC spinel coated Fe-26Cr alloy coupon.
- ASR testing of Ce-MC spinel coated, surface-modified ATI 441HP™ alloy coupons was completed. The surface modifications neither improved nor deteriorated the electrical resistance substantially.
- Long-term oxidation testing at 800°C for 5,000 hours was completed on Ce-MC spinel coated, experimental alloy coupons and Ce-MC spinel coated, surface-modified ATI 441HP™ alloy coupons. Surface blasting was found to be effective, while temper rolling was not.

Introduction

This project was focused on evaluating the performance of affordable materials integrated into systems for use as SOFC interconnects. Interconnects can be a source of degradation of fuel cell stack performance by the formation and growth of electrically resistive surface oxide layers. It is critical for SOFC performance to control which types of oxides form and to minimize layer growth over an extended period of time.

The reference points for this project were two monolithic ferritic stainless steels: ATI 441HP™ alloy (UNS S44100) and ATI E-BRITE® alloy (UNS S44627). These were chosen for their combination of low cost, general availability, and performance characteristics. Functionality was added to these basic interconnect materials at the cost of increased complexity. Material modifications – including minor chemistry modifications, special processing, surface treatments, and applied coatings – were aimed at tailoring the relevant properties of a ferritic stainless steel surface to its local environment in a fuel cell.

Approach

Two methods for increasing metallic interconnect performance were studied. The first was to incorporate minor but impactful modifications to the composition of commercially available alloys. Seven experimental alloy compositions were designed, melted, rolled, and evaluated, to explore the compositional space around two top performing alloys identified earlier in the project.

The second method was to alter the surface of a stainless steel by post-fabrication processing. Samples from a production coil of ATI 441HP stainless steel underwent various post-processing treatments including desiliconization, surface blasting, surface grinding, and temper rolling. An acid pickled mill surface served as a control. Some post-fabrication methods sought to modify the sub-surface or near-surface grain structure to improve initial oxide formation. A different post-fabrication technique sought to selectively remove silicon from the material surface to prevent electrically resistive phases from forming at the scale metal interface

® Registered Trademark of ATI Properties, Inc.
™ Trademark of ATI Properties, Inc.

during exposure to SOFC operating conditions. These post-processing techniques were used in conjunction with the application of an external oxidation-resistant and electrically conductive coating to remove the stainless steel surface from direct contact with the SOFC environment.

ASR testing was used to evaluate the impact of minor compositional variations and surface-modifications on electrical performance. ASR test parameters were typical of those used in the industry – 800°C test temperature, lanthanum strontium manganate ceramic contact layer, and a constant current density of 0.5 A/cm^2 of contact area. Isothermal oxidation testing in air at 800°C was used to evaluate the evolution of the oxide scale and the interaction between external regions of the oxide and an applied spinel coating. Based on previous results, all testing was done on substrates coated with an external oxidation-resistant and electrically conductive Ce-MC spinel, which was developed by researchers at the Pacific Northwest National Laboratory. [1]

Results

A set of seven experimental alloys, listed in Table 1 and designated 'EXP', were designed, melted, and processed to sheet in order to study relatively minor modifications to the commercially available ATI E–BRITE and ATI 441HP alloy compositions. The experimental alloys were further modifications of experimental EXP. 580-6 and EXP. 580-5 alloys, which had good performance in earlier testing. Table 2 compares the coating and oxide thicknesses after 5,000 hours of oxidation testing. ASR test results for these experimental alloys were previously reported.

ASR evolution rates determined from ASR test data – shown in Figure 1 – for the surface-modified ATI 441HP alloy coupons are summarized in Table 3. Figure 2 shows the ASR evolution rates for the coupons in the surface blasted and mill reference states. In these half-cell experiments, the critical metric for comparison was the steady-state rate of ASR increase as a function of time, made specific to an interval of 1,000 hours for ease of interpretation. A good target for fuel cell performance is an ASR of less than 0.1 Ω·cm^2 after 40,000 hours.

The results of oxide and coating thicknesses after long-term oxidation testing, performed on coupons of surface-modified ATI 441HP alloy in air at 800°C, are

TABLE 1. Third Generation Experimental Alloy Compositions (Weight Percent)

Alloy	Cr	Nb	Si	Others
ATI 441HP™ alloy	17.5	0.3	0.4	0.3 Mn, 0.2 Ti
EXP. 580-6	17	0.3	0.15	0.3 Mn, 0.2 Ti
EXP. 580-6 MOD1	17.3	0.5	0.15	0.3 Mn, 0.2 Ti
EXP. 580-6 MOD2	17.3	0.7	0.15	0.3 Mn, 0.2 Ti
EXP. 580-6 MOD3	17.3	0.7	0.35	0.3 Mn, 0.2 Ti
EXP. 580-6 MOD4	17.3	0.3	0.35	0.3 Mn, 0.0 Ti
EXP. 580-6 MOD5	17.3	0.3	0.35	0.8 Mn, 0.2 Ti
E-BRITE® alloy	26	0.2	0.3	1 Mo
EXP. 580-5	26	0.2	0.3	1 Mo, 0.3 Mn, 0.1Ti
EXP. 580-5 MOD1	26	0.5	0.35	1 Mo, 0.3 Mn, 0.2 Ti
EXP. 580-5 MOD2	24	0.3	0.35	1 Mo, 0.3 Mn, 0.2 Ti

TABLE 2. Coating and Oxide Thicknesses (Units: Microns) for the Third Generation Experimental Alloys after 5,000 Hours in Air at 800°C

Alloy	Coating	Oxide underneath coating	Oxide on uncoated side	Inner oxide layer on uncoated side
ATI 441HP™ alloy	44.2 / 5.9	3.6 / 4.3	7.8	3.9
EXP. 580-6 MOD1	9.5	2.8	7.0	4.0
EXP. 580-6 MOD2	13.9	3.1	7.4	4.1
EXP. 580-6 MOD3	6.9	3.2	8.5	4.3
EXP. 580-6 MOD4	3.9	6.3	6.9	3.5
EXP. 580-6 MOD5	5.6	4.6	10.2	4.7
EXP. 580-5 MOD1	7.4	1.1	4.8	2.1
EXP. 580-5 MOD2	24.9	5.8	6.1	2.0

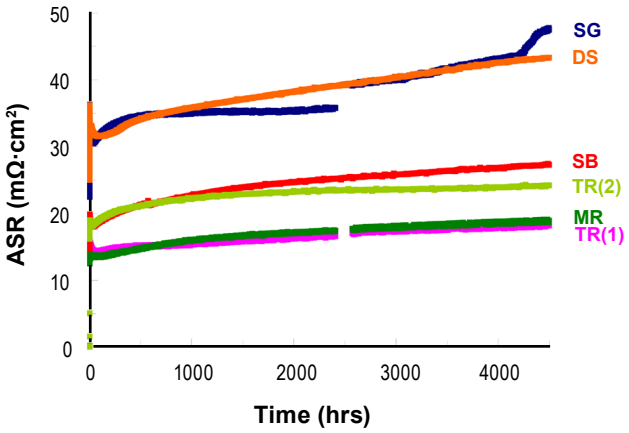

FIGURE 1. Compilation of ASR Test Results versus Time of All Ce-MC Spinel Coated, Surface-Modified ATI 441 HP™ Alloy Coupons for Comparison (DS = desiliconized, SG = surface ground, SB = surface blasted, TR = temper rolled, MR = pickle annealed mill reference)

TABLE 3. ASR Evolution Rate Results for Surface-Modified ATI 441 HP™ Alloy Coupons

Condition (ATI 441HP™ alloy)	ASR Evolution Rate (mΩ·cm^2/1,000h)	
	Uncoated	Coated
Mill Reference	no test	0.6
Surface Ground	no test	0.3 / 2.9
Surface Blasted	no test	1.0
Temper Rolled	no test	0.5
Desiliconized	no test	2.2

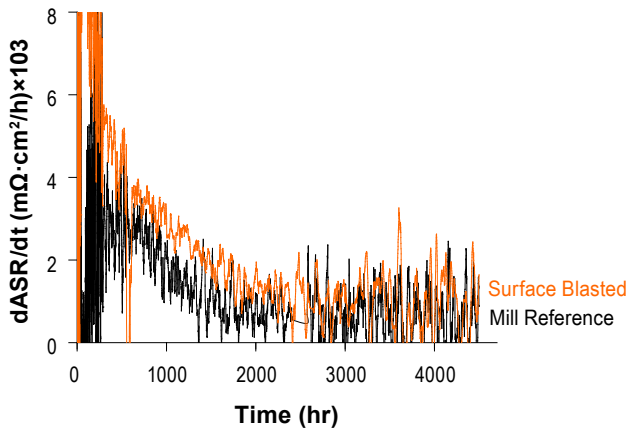

FIGURE 2. ASR Rate of Change Measurement versus Time for ATI 441HP™ Alloy Coupons in the Surface Blasted and Mill Reference Conditions

TABLE 4. Coating and Oxide Thicknesses (Units: Microns) for Pickle Annealed Mill Reference (MR), Desiliconized (DS), Surface Ground (SG), Surface Blasted (SB), and Temper Rolled (TR) ATI 441HP™ Alloy Coupons

	MR	DS	SG	SB	TR
Remaining coating	5.8	12.3	8.7	12.9	4.8
Oxide beneath coating	4.0	1.8	5.3	6.7	4.8
Entire oxide on uncoated region	5.7	9.1	12.5	12.1	8.1

listed in Table 4. Micrographs that show the oxides and coatings in cross-section for these samples are presented elsewhere.

Conclusions and Future Directions

- When tested at 800°C in air, many of the Ce-MC spinel coated experimental Fe-17Cr alloys exhibited ASR evolution rates below 2.5 mΩ·cm^2/1,000 hr, which corresponds to a 40,000 hour lifetime goal of a fuel cell stack; however, the Ce-MC spinel coated ATI 441HP alloy was the lowest at 0.8 mΩ·cm^2/1,000 hr. Because Ce-MC spinel coated ATI 441HP alloy also performed well in oxidation testing, it was identified as a robust material for SOFC interconnect fabrication.
- The applied Ce-MC spinel coating may have obscured the performance variations due to the alloy chemistry modifications; however, it helped the tested coupons to meet the SECA goal for interconnect lifetime. Testing the experimental alloys in an uncoated condition may provide better insight into the effect of minor chemistry modifications.
- Addition of manganese to the commercial ATI E-BRITE composition may be a robust alternative to ATI 441HP alloy if the oxidation resistance and ASR properties of lower-chromium alloys are found to be insufficient during scale up of SOFC technology. These higher-chromium, Mn-containing alloys exhibited relatively low rates of ASR evolution, with a trend towards decreasing rates as a function of increasing chromium content. The best performance of a Ce-MC spinel coated, higher-chromium experimental alloy substrate achieved an ASR evolution rate of 1.4 mΩ·cm^2/1,000 hr. This is an order of magnitude better than Ce-MC spinel coated ATI E-BRITE alloy, which does not have the added manganese.
- Surface modifications neither improved nor deteriorated the electrical resistance of ATI 441HP alloy substantially. Surface blasting prevented scale delamination and is a promising surface modification for further research. Temper rolled material suffered from oxide spallation after long exposure to elevated temperatures. Additional research could be done on combinations of post-processing surface modifications (i.e., both cold deformation and surface blasting) or on combinations of minor compositional modifications with applied post-processing surface modifications.
- No additional work is planned as this project was concluded in December 2010. It would, though, be interesting to verify these experimental results by testing in an SOFC stack.
- The primary goal of this project was realized: Ce-MC spinel coated ATI 441HP alloy was identified as an optimized low-cost, high-performance material capable of mass production of interconnects that can achieve SOFC electrical interconnect requirements for lifetimes of 40,000 hours or more.

FY 2011 Publications/Presentations

1. M.D. Bender and J.M. Rakowski, "Investigating the Effect of Chemistry Modifications on SOFC Interconnect Alloy Performance," 2010 Fuel Cell Seminar, San Antonio, Texas, October 19, 2010.

2. Quarterly status report for Project 42513, January 2011.

3. Final Scientific / Technical Report for Project 42513, March 2011.

References

1. Zhenguo Yang, Guanguang Xia, Zimin Nie, Joshua Templeton, and Jeffry W. Stevenson, "Ce-Modified (Mn, Co)$_3$O$_4$ Spinel Coatings on Ferritic Stainless Steels for SOFC Interconnect Applications," *Electrochem. Solid-State Lett.*, Volume 11, Issue 8, 2008: B140-B143.

III.C.2 Effect of SOFC Interconnect-Coating Interactions on Coating Properties and Performance

Jeffrey W. Fergus
Auburn University
Materials Research and Education Center
275 Wilmore Laboratories
Auburn, AL 36849
Phone: (334) 844-3405; Fax: (334) 844-3400
E-mail: jwfergus@eng.auburn.edu

DOE BES Project Manager: Timothy Fitzsimmons
Phone: (301) 903-9830
E-mail: Tim.Fitzsimmons@science.doe.gov

DOE NETL Project Manager: Briggs White
Phone: (304) 285-5437
E-mail: Briggs.White@netl.doe.gov

Contract Number: ER46497

Start Date: June 15, 2008
End Date: June 14, 2012

Fiscal Year (FY) 2011 Objectives

- Identify the electrical resistance of the reaction layer formed at the alloy-coating interface.
- Evaluate the effect of reducing the chromium content in the ferritic stainless steel.

FY 2011 Accomplishments

- The high electrical resistance portion of the reaction layer has been identified as the chromia scale and the spinel phase with a high chromium content.
- Ferritic stainless steels with the alloying contents of AISI 441 but with lower chromium contents generally behave similarly in oxidation tests to those with higher chromium contents. However, the reaction layer for lower chromium contents is thicker, which suggests that at least 17% Cr is needed for alloys used in solid oxide fuel cells (SOFCs) for long operating times.

Introduction

The high operating temperature of SOFCs, which provides their excellent fuel flexibility, can lead to degradation of individual fuel cell components. One form of degradation is chromium poisoning of the cathode, which results from volatilization of chromium from the chromia scale formed on alloys used for the interconnect. The amount of chromium volatilization, and thus the associated cell poisoning, can be minimized by applying a ceramic coating to the alloy surface. One promising coating material systems is the spinel $(Mn,Co)_3O_4$ [1-4], which has been shown to reduce chromium volatilization [5,6].

Although chromium can form a spinel phase with other transition metals, chromium has not been observed in the coating during use in a SOFC [7,8]. However, with time, interaction of the coating with the chromia scale or with other SOFC components can lead to changes in the coating composition, which can affect properties and thus performance. This purpose of this work is to study the interaction between chromia and potential interconnect coating materials to provide information needed to design effective coatings for long-time SOFC operation.

Approach

The project addresses three aspects of coating properties and performance: 1) thermodynamics; 2) transport properties; and 3) physical properties. The thermodynamic aspects include phase equilibria, crystal structure stability and chemical activity. The transport properties to be evaluated include conductivity and diffusion rates. The physical properties are those that are important for coating performance, such as the coefficient of thermal expansion. These aspects will be evaluated for the original coating composition and for compositions resulting from interaction of the coating with other fuel cell components by preparing bulk analogues of the compositions expected after the interaction occurs. Characterization of these bulk analogues will provide valuable information for evaluating any changes in the performance after interaction with other components. Finally, the results will be used to identify compositions with potentially improved performance and these promising compositions will be similarly evaluated. This knowledge and understanding will allow coatings to be designed so that the expected compositional changes during operation increase the conductivity in an amount that offsets the increase in resistance due to growth the chromia scale. In this case, the coating electrical resistance, and thus the associated overpotential, would be constant with time, so fuel cell performance would not degrade during operation.

Results

The results presented in the previous report showed that iron and titanium additions to $(Mn,Co)_3O_4$ could reduce the degree of reaction with Cr_2O_3 with little or no decrease in electrical conductivity. However, electrons flowing from interconnect to the cathode must pass through the reaction layer formed at the alloy-coating interface, so the electrical properties of this interlayer are important for understanding the performance of the coated interconnect. To evaluate the properties of the interlayer, bulk analogues of the compositions observed in the interlayer were prepared and evaluated using 4-point direct current conductivity measurements. The results in Figure 1 show that the conductivity of the spinel phase decreases as the chromium content increases and for the highest chromium content, $Mn_{0.5}Co_{0.5}Cr_2O_4$, is even lower than Cr_2O_3. Figure 2 shows that the activation energy for conduction increases with the increase in chromium content beginning with 0.5-1.0 chromium per formula unit. These results suggest that the reaction layer and the chromia scale will likely dominate the resistance between the interconnect and the cathode. However, the overall resistance will depend on the thickness of the layer as well as the conductivity of the phase.

The other area for investigation this past year has been evaluating the possibility of using lower chromium content in the alloy. A spinel oxide is typically present on the scale formed during oxidation of ferritic stainless steels containing manganese as an alloying addition and when the alloy is coated with a $(Mn,Co)_3O_4$ the scale and coating merge together. To evaluate if this structure will allow for a lower chromium content in the alloy, a series of experimental alloys containing the alloying additions in AISI 441 with varying chromium contents were prepared by Allegheny Technologies Inc. The compositions of these experimental alloys are summarized in Table 1. Some of the alloys were coated with $Mn_{1.5}Co_{1.5}O_4$ at Pacific Northwest National Laboratory using a slurry coating process.

The oxidation resistances of coated and uncoated alloys were evaluated with both cyclic and isothermal exposures to air at 800°C. The results of 25-hour cyclic exposures are shown in Figure 3. The coated alloys exhibited a large initial weight gain, which was

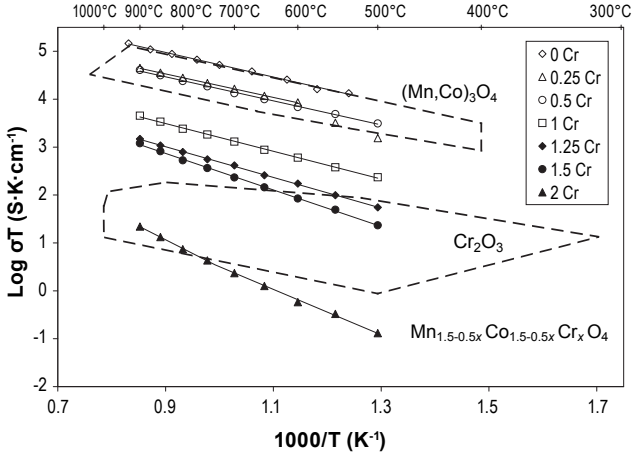

FIGURE 1. Conductivity of $Mn_{1.5-0.5x}Co_{1.5-0.5x}Cr_xO_4$ in Air

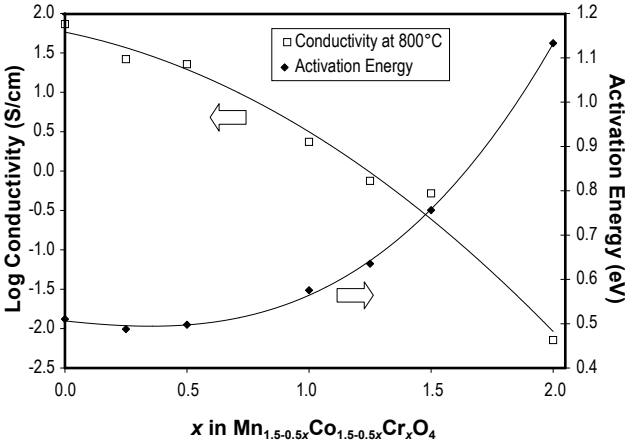

FIGURE 2. Conductivity and Activation Energy of $Mn_{1.5-0.5x}Co_{1.5-0.5x}Cr_xO_4$ in Air

TABLE 1. Composition of Alloys

Alloy	Concentration (wt%)					
	Fe	Cr	Mn	Si	Ti	Nb
H52	Bal.	13	0.3	0.4	0.2	0.4
H53	Bal.	15	0.3	0.4	0.2	0.4
H54	Bal.	17	0.3	0.4	0.2	0.4
H55	Bal.	18	0.3	0.4	0.2	0.4
AISI 441	Bal.	18	0.4	0.3	0.2	0.5

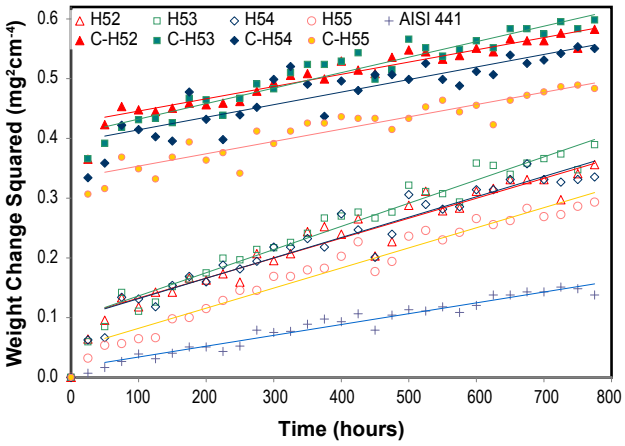

FIGURE 3. Cyclic Oxidation Behavior of Coated and Uncoated Experimental Alloys in Air at 800°C

presumably due to re-oxidation of cobalt that was formed during the final sintering of the coating in a reducing atmosphere. The parabolic rate constants were determined by fitting the results beginning with 50-hour exposures and are summarized in Figure 4. The parabolic rate constant does not appear to vary significantly with chromium content. However, the parabolic rate constants for the experimental alloys are significantly higher than that measured for AISI 441. These differences are presumably related to the small production sizes in the experimental alloys, as compared to commercial steels, but the specific cause for the difference is not clear.

A scanning electron microscope (SEM) micrograph of the cross-section of coated H52 after an isothermal exposure of 800 hours at 800°C in air is shown in Figure 5a. The concentration gradients as determined by energy dispersive X-ray spectroscopy are shown in Figure 5b. Figure 5 is for the alloy containing 13% Cr (H52), but the features were similar for other chromium contents. As the chromium content increased in the spinel phase, the Co:Mn ratio increased, which is presumably related to site occupancy preference as chromium and manganese have stronger preference for the octahedral site as compared to cobalt. Titanium was sometimes observed at the alloy-scale interface, while niobium was typically not present in the reaction layer.

The general features of the reaction layer were similar for different chromium contents, but there were differences in the amount of the reaction. Figure 6 shows the reaction layer thickness as determined by the average of 50 measurements. Although the standard deviations of the measurements overlap, the student t-test indicates that the thicknesses for 13-15%Cr were statistically different from those of 17-18%Cr to greater than 99% confidence.

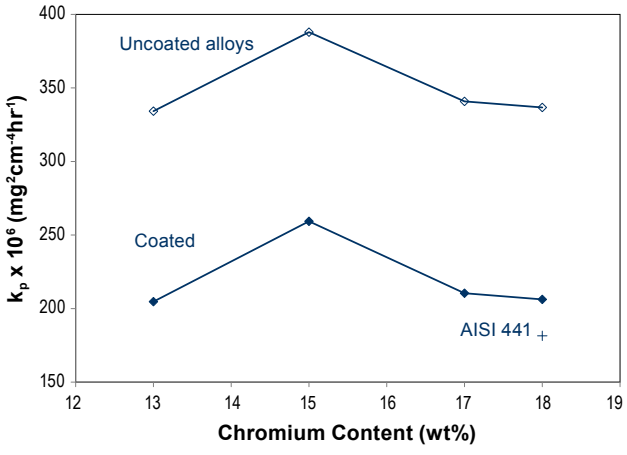

FIGURE 4. Parabolic Rate Constants for Cyclic Oxidation of Coated and Uncoated Experimental Alloys in Air at 800°C for Data Shown in Figure 3

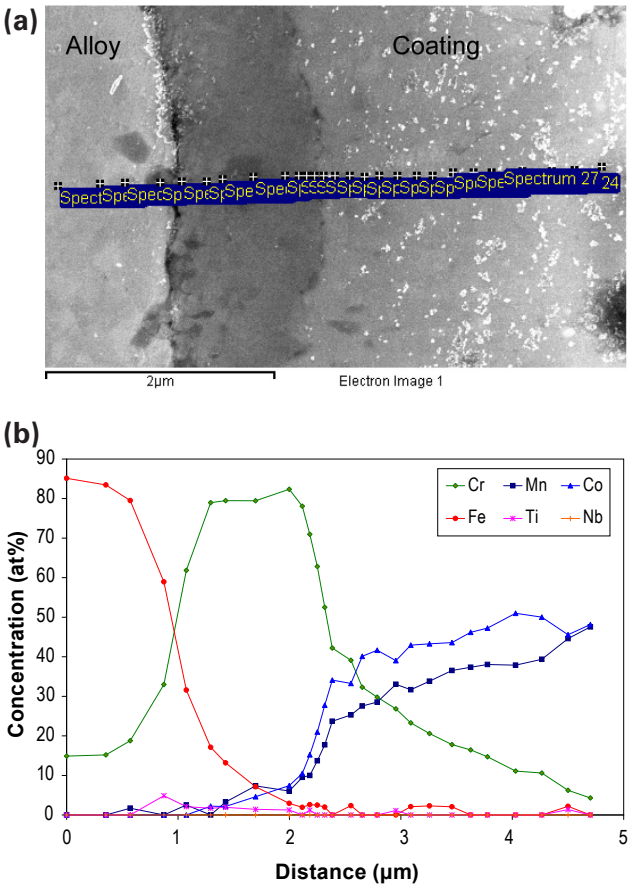

FIGURE 5. SEM Cross Section and Concentration Gradients at the Interface between H52 (13% Cr) and the $Mn_{1.5}Co_{1.5}O_4$ Coating after 800 Hours at 800°C in Air

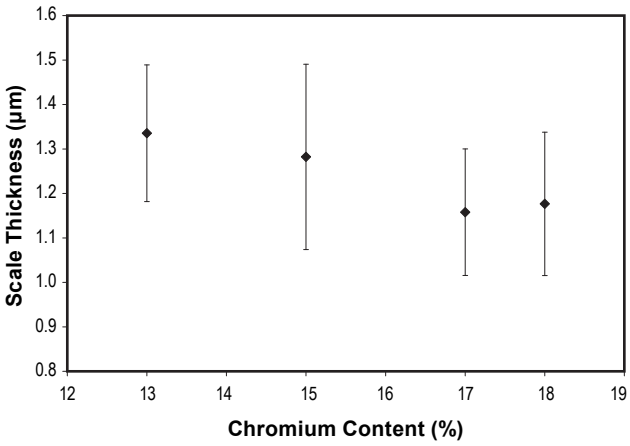

FIGURE 6. Thicknesses of reaction layers between experimental alloys and $Mn_{1.5}Co_{1.5}O_4$ coatings after 800 hours at 800°C in air. The error bars represent the standard deviation of 50 measurements.

Conclusions and Future Directions

The conductivity of $(Mn,Co,Cr)_3O_4$ spinel phase decreases with increasing chromium content, which suggests that the electrical resistance between the cathode and interconnect will be dominated by the reaction layer. Work is underway to identify coating dopants, such as Ni and Cu, that might be incorporated into the reaction layer and increase its conductivity. In addition, neutron diffraction studies are being used to characterize the cation site occupancies, which will help in understanding the transport properties.

The initial results on the reduction of the chromium content in the stainless steel alloys indicate that the general behavior is similar for the lower chromium contents, but that the reaction rate, as measured by the reaction layer thickness, is higher for low chromium contents. Additional analysis of samples exposed to longer exposures is underway.

FY 2011 Publications/Presentations

1. J.W. Fergus, "Synergism in the Design of Interconnect Alloy-Coating Combinations for Solid Oxide Fuel Cells," *Scripta Materialia* **65** (2011) 73-77.

2. J.W. Fergus and Y. Zhao, "Low-Chromium Alloys for Solid Oxide Fuel Cell Interconnects," *Electrochemical Transactions* **35**[1] (2011) 2447-2453.

3. J.W. Fergus, K. Wang, and Y. Liu, "Transition Metal Spinel Oxide Coatings for Reducing Chromium Poisoning in SOFCs," *Electrochemical Transactions* **33**[40] (2011) 77-84.

4. Y. Liu, K. Wang, and J.W. Fergus, "Effect of Chromium Doping on the Crystal Structure, Electrical Conductivity and Thermal Expansion of Manganese Cobalt Spinel Oxides," in N.P. Bansal, P. Singh, S. Widjaja, and D. Singh, *Advances in Solid Oxide Fuel Cells VII: Ceramic Engineering and Science Proceedings* **32**[4] (2011) in press.

5. J.W. Fergus, K. Wang, and Y. Liu, "Effect of Titanium and Iron Additions on the Transport Properties of Manganese Cobalt Spinel Oxide," *Ceramics Transactions,* in press.

References

1. Y. Larring and T. Norby, "Spinel and perovskite functional layers between Plansee metallic interconnect (Cr-5 wt% Fe-1 wt% Y_2O_3) and ceramic $(La_{0.85}Sr_{0.15})_{0.91}MnO_3$ cathode materials for solid oxide fuel cells," *J. Electrochem. Soc.* **Vol. 147**, 2000, pp. 3251-3256.

2. Z. Yang, G.-G. Xia, G.D. Maupin, and J.W. Stevenson, "Conductive protection layers on oxidation resistance alloys for SOFC interconnect applications," *Surf. Coating Tech.* **Vol. 201**, 2006, pp. 4476-4483.

3. M.R. Bateni, P. Wei, X. Deng, and A. Petric, "Spinel coatings for UNS 430 stainless steel interconnects," *Surf. Coating Tech.* **Vol. 201**, 2007, pp. 4677-4684.

4. M.J. Garcia-Vargas, M. Zahid, F. Tietz, and A. Aslanides, "Use of SOFC metallic interconnect coated with spinel protective layers using the APS technology," *ECS Trans.* **Vol. 7**, 2007, pp. 2399-2405.

5. H. Kurokawa, C.P. Jacobson, L.C. DeJonghe, and S.J. Visco, "Chromium vaporization of bare and of coated iron-chromium alloys at 1073 K," *Solid State Ionics* **Vol. 178**, 2007, pp. 287-296.

6. C. Collins, J. Lucas, T.L. Buchanan, M. Kopczyk, A. Kayani, P.E. Gannon, M.C. Deibert, R.J. Smith, D.-S. Choi, and V.I. Gorokhovsky, "Chromium volatility of coated and uncoated steel interconnects for SOFCs," *Surf. Coating Tech.* **Vol. 201**, 2006, pp. 4467-4470.

7. Z. Yang, G.-G. Xia, H.-H. Li, and J.W. Stevenson, "$(Mn,Co)_3O_4$ spinel coatings on ferritic stainless steels for SOFC interconnect applications," *Int. J. Hydrogen Energy* **Vol. 32**, 2007, pp. 3648-3654.

8. Z. Yang, G. Xia, and J.W. Stevenson, "$Mn_{1.5}Co_{1.5}O_4$ spinel protection layers on ferritic stainless steels for SOFC interconnect applications," *Electrochem. Solid-State Lett.* **Vol. 8**, 2005, pp. A168-A170.

III.C.3 Electrodeposited Mn-Co Alloy for Solid Oxide Fuel Cell Interconnects

Heather McCrabb (Primary Contact), Tim Hall
Faraday Technology, Inc.
315 Huls Drive
Clayton, OH 45315
Phone: (937) 836-7749; Fax: (937) 836-9498
E-mail: heathermccrabb@faradaytechnology.com

DOE Project Manager: Briggs White
Phone: (304) 719-5116
E-mail: Briggs.White@netl.doe.gov

Subcontractor:
West Virginia University, Morgantown, WV

Contract Number: FE0006165

Start Date: October 1, 2010
End Date: September 30, 2012

Fiscal Year (FY) 2011 Objectives

- Design/modification of FARADAYIC Electrodeposition Cell.
- Completion of 2,000-hour soak test at 850°C.
- Process development for 100 mm x 100 mm planar interconnects.

FY 2011 Accomplishments

- Completion of the design and modification of the large FARADAYIC Electrodeposition Cell for interconnect substrates ranging in size from 2.5 cm x 2.5 cm to 28 cm x 35 cm.
- Refinement of the original preliminary economic analysis.

Introduction

Commercialization of solid oxide fuel cells (SOFCs) requires low-cost components, materials and manufacturing processes. Specifically, the interconnect material and coating used in SOFCs represent 45% of the total material cost for the typical stack [1]; therefore it is desirable that new materials and manufacturing technologies be developed that effectively increase system durability while decreasing production costs. The decrease in the SOFC operating temperatures from 1,000ºC to between 650 and 850ºC has enabled the use of less expensive chromia-forming ferritic stainless steels as interconnects instead of ceramic interconnects. However, even newly developed ferritic alloys such as SS441 and Crofer 22 APU, cannot completely eliminate the chromia scale growth and chromium evaporation into cells that can cause unacceptable degradation in the SOFC electrochemical performance. One attractive method to resolve the chromia scale growth and diffusion issues is to electrodeposit a Mn-Co alloy coating onto the interconnect surface and subsequently convert it to a $(Mn,Co)_3O_4$ spinel.

Faraday and West Virginia University are working to develop, optimize, and validate the FARADAYIC Electrodeposition Process as an effective and economical manufacturing method for coating stainless steel interconnects used in SOFC stacks with Mn-Co alloys. The FARADAYIC Process utilizes pulse and pulse reverse waveforms and simple electrolyte solutions for manufacturing the interconnect coatings. A preliminary economic analysis based on using batch manufacturing suggests that the innovative coating technology can meet DOE's high volume target of 1,600,000 plates per annum for 250 MW of fuel cell stacks at a cost of ~$1.23 per 25 cm x 25 cm coated interconnect.

Approach

The FARADAYIC Electrodeposition Process is a pulse/pulse reverse plating process that controls the electric field and the boundary layer to reduce gradients (composition, thickness, or morphological) in the formed coating. The novel aspect of this technology is the manner in which the electric field and double layer are controlled and how these parameters can inherently control the properties of the coating. For instance, when using a direct current overpotential for deposition, the composition, thickness, and morphology of the deposit is controlled by the surface texture of the substrate/electrode. With the use of the FARADAYIC Electrodeposition Process the electric field can be tuned to reduce effects of the substrate and obtain better overall control of the deposit's properties. In addition, the cell geometry, plating bath flow, and shape of the applied electric field influence the current distribution that develops on the surface of the substrate. The main advantages of the proposed technology, as compared to conventional, direct current electrodeposition, are:

- Enhanced process control: Since the process proceeds only under the influence of an electric field, the processing time is exact and uniform across the plate.
- Enhanced surface structure and thickness control: The FARADYAIC Process parameters can be selected to minimize the diffusion boundary layer,

decreasing the effect of substrate surface morphology on the deposit properties across an area.

Results

In order to demonstrate the coating process on industrial scale interconnects that will be inserted into single fuel cell test stands, Faraday modified an existing electrodeposition cell located in its pilot scale facility to coat patterned interconnect substrates ranging in size from 2.5 cm x 2.5 cm to 28 cm x 35 cm. The modified plating system was designed to enable many of the electrodeposition cell's original parts and controls to be used including digital laminar flow velocity control, anode to cathode spacing as well as oscillation and vibration control, which made the modification process more cost efficient. The enhanced control that this cell enables allows for optimization of the FARADAYIC Electrodeposition Process for uniform deposition of Mn-Co alloy onto the patterned interconnect substrates of interest to industrial members in the fuel cell community.

The computer-aided design drawings for the modifications to the cell are shown in Figure 1 while the completed cathode, anode and flow assemblies are shown in Figure 2. The double-sided flow assembly shown in Figure 2 allows the Mn-Co electrolyte to be pumped into two side-by-side chambers, where the flow is directed in an upward vertical direction by quarter-pipe ramps. Separating the two flow streams is a pair of baffles (shown in the Figure 1 cathode assemblies) and the interconnect substrate, which acts as the cathode in the electrodeposition cell. Opposing the surface of the interconnect substrate is the electrodeposition cell anode support assemblies. The supports are suspended on rails, which allow for the adjustment of the spacing between the electrodeposition cell anode and cathode for a distance of up to 11.4 cm. A thin rectangular titanium sheet coated with an oxide coating that serves as the anode is bolted to the backing plate. Electrical contact to the anode is made by two copper bars that fit within grooves on the backing plate, and the bars are connected by a welded cross bar.

As shown in Figure 1, the cathode assemblies were designed with the flexibility to adapt to the size of the interconnect substrate of interest to industry. The interconnect substrate and rack is mounted to the original oscillation assembly on the electrodeposition cell. The default substrate position is at the median between the two flow channels, and the baffles along the sides will maintain the vertical channel wall. If desired, the oscillatory and vibrational motion capabilities of the electrodeposition cell will be exploited if it is determined that this is necessary to obtain a more uniform Mn-Co alloy coating on grooved/patterned interconnect surfaces. This cell is based upon Faraday's electrochemical cell design that facilitates uniform flow across the surface of a flat substrate (U.S. patent #7,553,401). A photograph of the modified electrocell for this project is provided in Figure 3.

Faraday continues to refine the preliminary manufacturing throughput and cost analysis of the FARADAYIC Electrodeposition Process for high volume manufacturing of Mn-Co spinel interconnect coatings. The cost analysis is based upon an annual production volume of 250 MW of fuel cell stacks

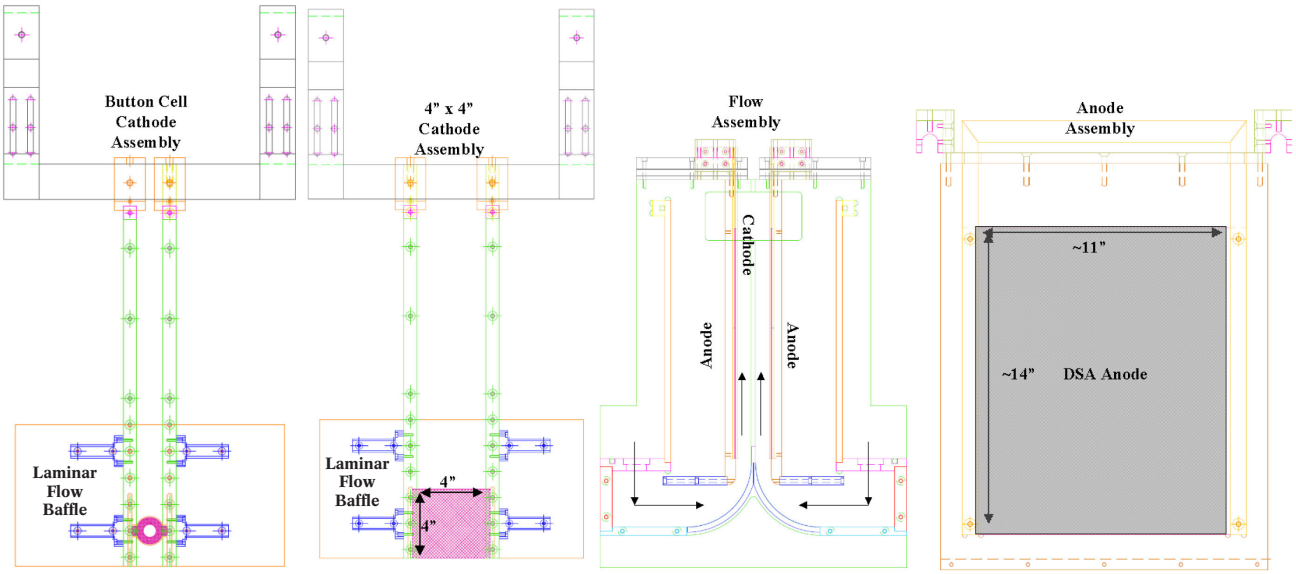

FIGURE 1. The As-Designed Cathode, Flow, and Anode Assemblies That Demonstrate the Flexibility of the Cathode to Fit Various Size Parts and the Total System Capacity of 28 cm x 35 cm Substrates

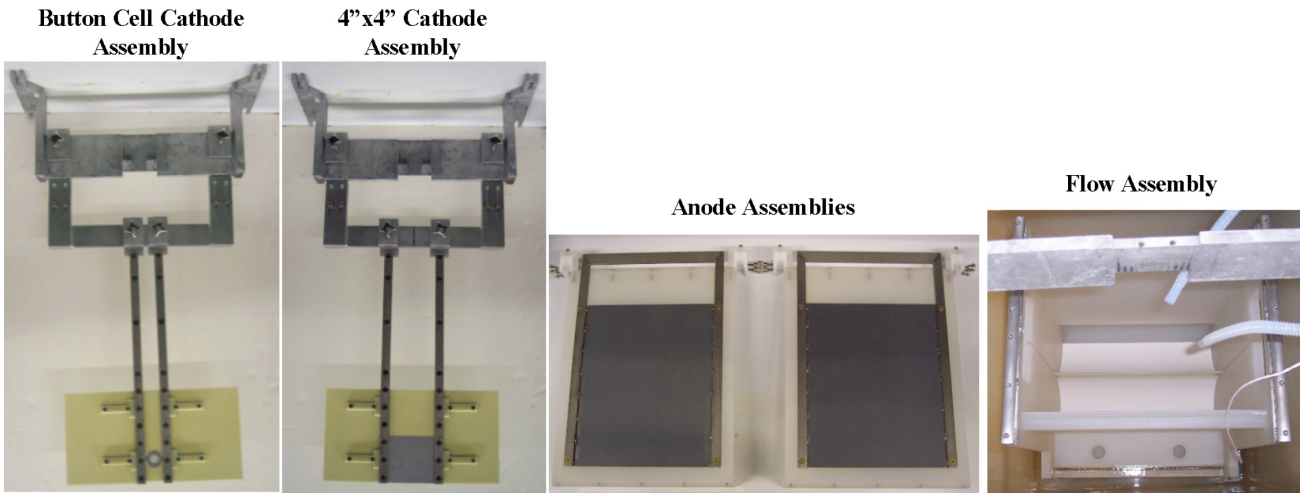

FIGURE 2. The As-Built Cathode and Anode Assemblies and the Flow Assembly in Which They Are to be Installed

FIGURE 3. Photograph of Modified FARADAYIC Electrodeposition Cell for Mn-Co Alloy Deposition onto SOFC Interconnects

for which approximately 1,600,000, 25 cm x 25 cm interconnect plates would need to be coated per year. The throughput assessment considers the FARADAYIC Electrodeposition Process as a batch manufacturing process. The original, preliminary cost analysis drafted during the initial phase of the project indicated that the process could coat interconnects at $1.87/interconnect. The largest cost contributor to the process is the plating bath chemicals, which originally comprised 66% of

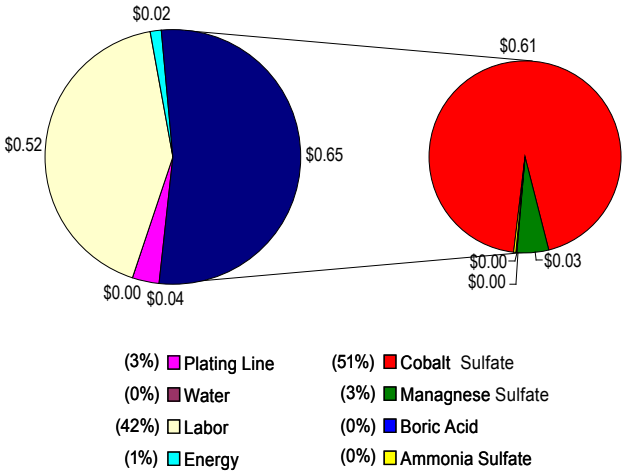

FIGURE 4. Current Cost Analysis of Coating Process Based upon Batch Manufacturing of 1,600,000 Plates Per Annum at a Cost of ~$1.23 Per 25 cm x 25 cm Coated Interconnect

the cost to coat each interconnect. After consultation with chemical vendors, Faraday has negotiated reduced prices for the chemicals necessary for the plating bath. Specifically, the cobalt sulfate and manganese sulfate prices have been reduced by 44% and 73%, respectively. Figure 4 provides the current cost analysis of the FARADAYIC Electrodeposition Process based upon batch manufacturing of 1,600,000 plates per annum at a cost of ~$1.23 per 25 cm x 25 cm coated interconnect.

Conclusions and Future Directions

A cost-effective process to apply high-quality coatings to SOFC interconnects in a mass production scenario is being developed. The FARADAYIC

Electrodeposition Process can be used to deposit a Mn-Co alloy with a controlled composition and thickness that can subsequently be converted to a spinel by thermal exposure at high temperatures in an oxidizing environment. In order to demonstrate the process capability on full-size industrial-scale SOFC interconnects, Faraday implemented design modifications to an existing electrodeposition cell located in its pilot-scale facility. Further analysis and refinement of the original preliminary economic analysis suggests that the FARADAYIC Electrodeposition Process is cost competitive with other industrial manufacturing processes under consideration for these types of interconnect coatings, including physical vapor deposition and spraying processes.

Development of the FARADAYIC Electrodeposition Process is still in progress with the following activities planned:

- Development, optimization and validation of the FARADAYIC Electrodeposition Process for 10 cm x 10 cm single- and dual-sided grooved interconnect materials.
- Mitigation of chromium diffusion by determining the controlling mechanism through in situ high temperature X-ray diffraction measurements and X-ray photoelectron spectroscopy depth profiling.
- Continued development of a more comprehensive economic assessment of the electrodeposition coating process as it relates to interconnect manufacturing.

FY 2011 Publications/Presentations

1. H. McCrabb, "Electrodeposited Mn-Co Alloy Coatings for SOFC Interconnects," Poster presentation at the Department of Energy's 2011 Annual Merit Review and Peer Evaluation Meeting, Washington, D.C., May 2011.

2. T. Hall, H. McCrabb, J. Wu, H. Zhang, X. Liu, and J. Taylor, "Electrodeposition of CoMn onto Stainless Steels Interconnects for Increased Lifetimes in SOFCs," ECS Trans. 35 (1), 2489 (2011).

3. T. Hall, H. McCrabb, J. Wu, H. Zhang, X. Liu, and J. Taylor, "Electrodeposition of CoMn onto Stainless Steels Interconnects for Increased Lifetimes in SOFCs," Oral presentation presented at the 219th Meeting of the Electrochemical Society, Montreal, Quebec, Canada, May 2011.

4. H.A. McCrabb, T.D. Hall, J. Wu, H. Zhang, and X. Liu, E.J. Taylor, "Electrodeposited Mn-Co Alloy Coating for SOFC Interconnects," Oral presentation presented at TMS 2011 Annual Meeting and Exhibition, San Diego, California, March 2011.

References

1. Eric J. Carlson, Suresh Sriramulu, Peter Teagan, and Yong Yang, "Cost Modeling of SOFC Technology," First International Conference on Fuel Cell Development and Deployment, University of Connecticut, Storrs, Connecticut, March 10, 2004.

III.C.4 Development of SOFC Interconnects and Coatings

Guan-Guang "Gordon" Xia (Primary Contact), Ryan Scott, Xiaohong Li, Zimin Nie, Jung-Pyung Choi, and Jeff Stevenson
Pacific Northwest National Laboratory
P.O. Box 999, MS K2-44
Richland, WA 99352
Phone: (509) 371-6261; Fax: (509) 375-2186
E-mail: Guan-Guang.Xia@pnnl.gov

DOE Project Manager: Briggs White
Phone: (304) 285-5437
E-mail: Briggs.White@netl.doe.gov

Contract Number: FWP40552

Start Date: October 1, 2010
End Date: September 30, 2011

Fiscal Year (FY) 2011 Objectives

- Develop cost-effective, optimized materials for intermediate temperature solid oxide fuel cell (SOFC) interconnect applications.
- Identify, understand, and mitigate degradation processes in interconnects and at interconnect interfaces.

FY 2011 Accomplishments

- Evaluated long-term performance of spinel-coated ferritic stainless steel interconnect materials at 800 and 850ºC.
- Evaluated performance of MnCo oxide coatings with reduced Co content.

Introduction

In previous work, $(Mn,Co)_3O_4$ (MC) spinels have been systematically investigated and applied as protection layers on a variety of candidate SOFC interconnect steels. In recent years, the primary emphasis has been on the application of spinel coatings to AISI 441 ferritic stainless steel, which is being investigated as an interconnect alloy by Pacific Northwest National Laboratory (PNNL) in collaboration with Allegheny Ludlum and the National Energy Technology Laboratory (NETL). AISI 441 is prepared via conventional melt metallurgy and is therefore less expensive than other candidate steels, such as Crofer22APU, which utilize vacuum processing to reduce the Si content to very low levels. Additions of Nb and Ti to the AISI 441 tie up residual Si in Laves phase at grain boundaries, eliminating the need for expensive processing. To mitigate scale adhesion issues, a Ce-modified MC (Ce-MC) coating (e.g., $Ce_{0.02}Mn_{1.49}Co_{1.49}O_4$) was developed, which combines the advantages of rare earth (RE) surface treatment or additions with those of the MC spinel coating. The stability and electrical performance of AISI 441 coated with Ce-MC protection layers were validated in short-term and long-term (1 year) testing. These tests indicated that the spinel protection layers helped minimize the interfacial electrical resistance and mitigate the scale growth beneath the spinel coatings on AISI 441. In addition, the Ce-modified coatings improved the scale adherence and overall interconnect surface stability.

Approach

To supplement and confirm previous test results, long-term area specific resistance (ASR) tests are being carried out to evaluate the long-term performance and structural stability of Ce-MC coatings on AISI 441. The AISI 441 was manufactured by Allegheny Technologies, Inc. MC and Ce-MC spinel powders were applied to selected alloy coupons using a slurry-based approach, and heat-treated to form protective coatings. The electrical resistance of bare and coated AISI 441 is measured by applying a four-probe direct current measurement technique to simulated interconnect/coating/contact material/cathode structures. In addition to baseline testing of spinel-coated AISI 441 at 800°C, the effects of: a) physical surface modifications to the AISI 441, and b) higher exposure temperature (850°C) are being studied. Alternative protective coating compositions are also being developed and evaluated, with an emphasis on reduction of coating cost (e.g., reduction of Co content).

Results

Figure 1 shows long-term ASR test results of bare AISI 441 and Ce-MC coated AISI 441 at 800°C. The tests are still in progress. In contrast to the bare (uncoated) AISI 441, the ASR of the Ce-MC coated AISI 441 has remained low and essentially unchanged over time, indicating good stability of the coated steel coupons. Oxidation studies have also been performed on coated AISI 441 coupons at 800 and 850°C. As expected, the oxidation rates were faster at the higher temperature, and spallation was observed at the scale/alloy interface of some coated AISI 441 coupons after ~1,500 hours at 850°C. No obvious differences in

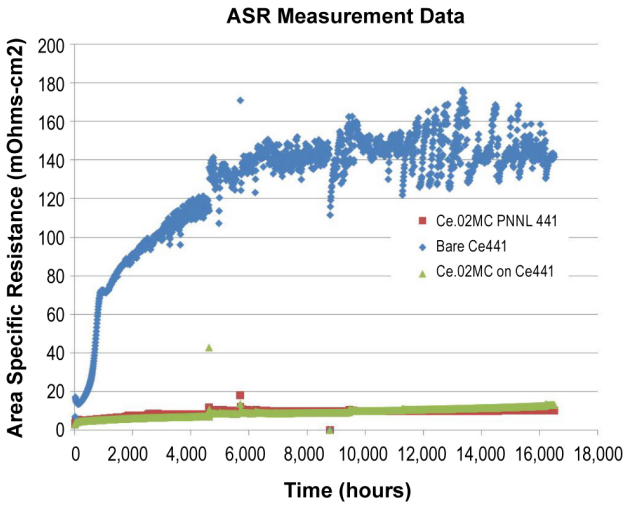

FIGURE 1. ASR of Bare and Ce-MC Coated AISI 441 at 800°C in Air

coating/scale/alloy chemistry were observed during post-test scanning electron microscopy (SEM)/energy dispersive spectroscopy analysis, suggesting that the spallation may have been primarily related to increased thermal stresses (due to coefficient of thermal expansion mismatch) resulting from increased oxide scale thickness at the higher temperature.

To mitigate possible spallation issues, a variety of physical surface modifications to the AISI 441 are being investigated. Allegheny Ludlum provided sheet stock (0.02" thick) of AISI 441with the following five surface conditions:

1. Mill reference (as would be provided to a customer without any additional modifications)
2. De-siliconized (a treatment to sequester silicon from the near surface of the sheet; an alternative to decreasing the Si content of the alloy)
3. Surface blasted (a grit/shot blast process resulting in surface deformation)
4. Surface ground (rough surface abrasion resulting in surface deformation)
5. Temper-rolled (a cold rolling process)

Coupons of the surface-treated steel were coated with Ce-MC spinel and subjected to oxidation testing in air at 800°C. At 2,000 hour intervals, the coupons were cooled down to room temperature and examined. One coupon from each surface treatment was removed from the study for SEM evaluation, while the rest of the coupons were reheated to 800°C for continued testing. After 2,000 hours, no spallation was observed on any of the specimens. After another 2,000 hours (total oxidation time of 4,000 hours), the coupons were again cooled to room temperature and examined. Spallation was observed on only one coupon (1 of the 14 mill reference coupons). After another 2,000 hours (total oxidation time of 6,000 hours), the coupons were again cooled and examined. Extensive spallation was observed on the mill reference coupons, while only one of the surface-treated coupons (a de-siliconized AISI 441 coupon) exhibited spallation. SEM montages of the 6,000-hour coupons are shown in Figure 2. While no spallation was observed during visual examination of the temper-rolled coupon, SEM analysis revealed complete debonding of the oxide scale from the alloy substrate, possibly due to stresses occurring during the metallographic preparation of the sample. After another 2,000 hours (total oxidation time of 8,000 hours), the last of the mill reference coupons exhibited spallation, but no spallation was observed on any of the surface-modified coupons. In summary, all of the surface treatments resulted in improved spallation resistance compared to the mill reference material, although the post-test debonding observed for the cold-rolled coupons suggests inferior protection compared to the other surface treatments.

Average scale thicknesses as a function of time at 800° for the coated, surface treated coupons are shown in Figure 3. Oxidation testing is also being performed at 850°C; after 2,000 hours, no spallation was observed on any of the coated coupons.

As mentioned above, alternative protective coating compositions are also being developed and evaluated, with an emphasis on reduction of coating cost. One cost reduction approach involves reduction of the Co content of the coating. A series of ASR tests were conducted on coatings prepared from mixtures of Mn and Co powders covering a range of Mn/Co ratios. Figure 4

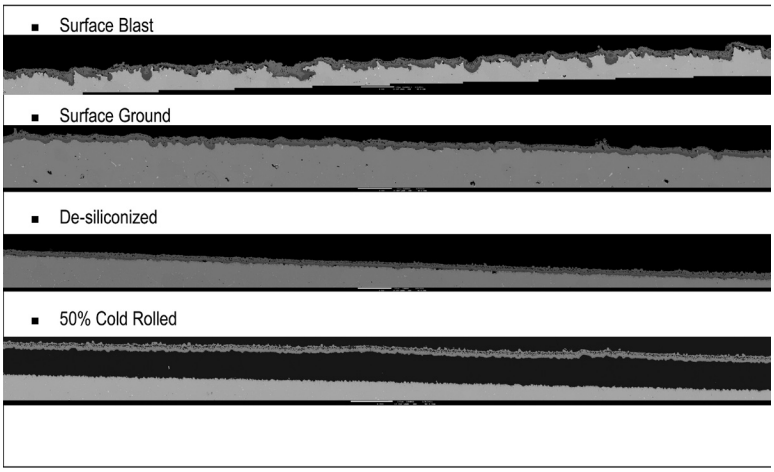

FIGURE 2. Cross-Section SEM Images of Ce-MC Coated, Surface Treated AISI 441 after Oxidation at 800°C for 6,000 Hours in Air

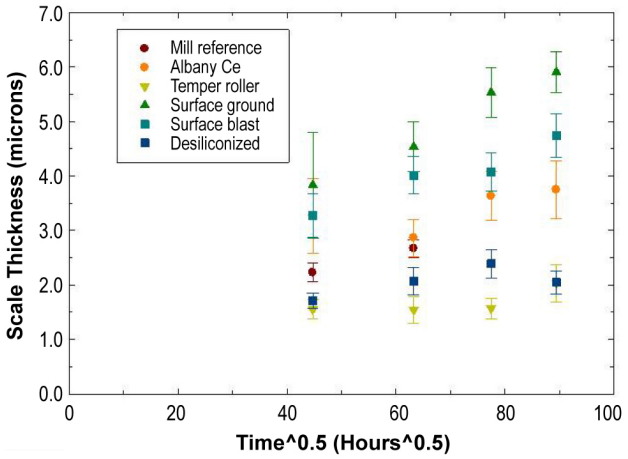

FIGURE 3. Average Scale Thicknesses as a Function of Time at 800°C for the Ce-MC Coated, Surface Treated AISI 441 Coupons

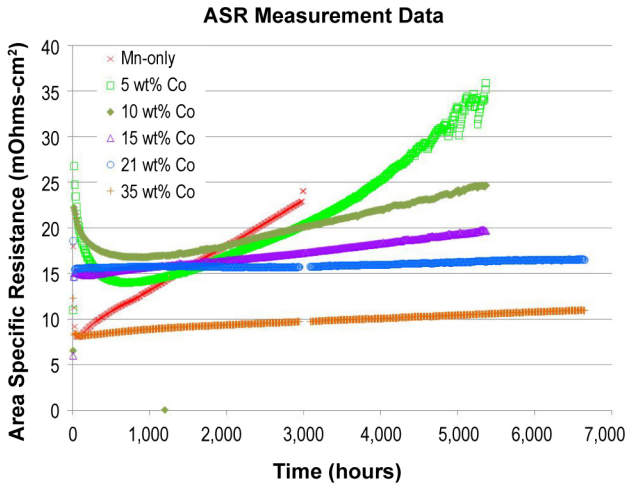

FIGURE 4. ASR of AISI 441 with MnCo oxide coatings with varying Co content. The measurements were carried out at 800°C in air.

shows the ASR results at 800°C in air for Mn-Co based protection coatings with various Co contents. In all cases, after reaching a minimum during the early stages of the test, the ASR increased over time, although the rates of increase were not the same. Figure 5 shows a plot of the ASR slope (i.e., rate of ASR increase) vs. Co content, taken from the linear range for each ASR plot in Figure 3. The ASR slope decreased with increasing Co content in the Mn-Co oxide coatings. The results suggest that a value of Co/(Co+Mn) somewhat less than 0.5 may produce satisfactorily stable ASR, although none of the alternative compositions produced the essentially zero ASR slope which has been repeatedly observed with coatings having Co/(Co+Mn) equal to 0.5.

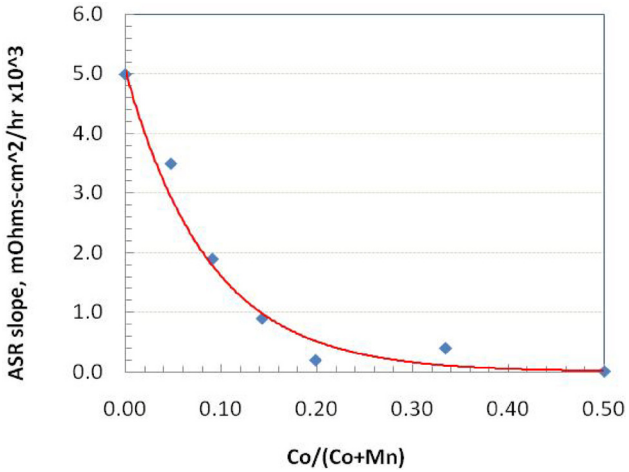

FIGURE 5. Slope of ASR of AISI 441 with MnCo Oxide Coatings with Varying Co Content, as Determined from Linear Portions of Figure 4

Conclusions and Future Directions

Spinel-coated AISI 441 is a promising alloy/coating combination for intermediate temperature SOFC interconnect applications. Surface modifications to AISI 441 appear to be a means of extending interconnect life by delaying the onset of scale/substrate de-bonding. Although spinel coatings with Co/(Co+Mn) equal to 0.5 offer the best performance (in terms of stability of ASR), coatings with reduced Co content have also demonstrated encouraging stability, at least in the 6,000-hour time frame.

Future research directions include long-term testing in realistic stack environments (using PNNL's Solid State Energy Conversion Alliance Core Technology Program stack test fixture), continued long-term oxidation testing at 800 and 850°C to determine upper service limits for the coated AISI 441, continued efforts to reduce coating cost, and further optimization/implementation of spray-based fabrication processes.

FY 2011 Publications/Presentations

1. J.P. Choi, J.W. Stevenson, R.C. Scott, and Y.S. Chou, "The Effect of MnCoO-CeO Spinel Coating Thickness on Electrical Conductivity at Long-term SOFC Operating Condition," Materials Science & Technology Conference & Exhibition, Columbus, Ohio, October 2010.

2. G.G. Xia, X.S. Li, J.D. Templeton, Z. Lu, T. Oh, Z. Nie, Z.G. Yang, and J.W. Stevenson, "Development of Protection Coatings and Contact Materials for Metallic Interconnects in SOFCs," 218th Electrochemical Society Meeting, Las Vegas, Nevada, October 2010.

3. G.G. Xia, X.S. Li, J.D. Templeton, Z. Nie, Z. Lu, R.C. Scott, Z.G. Yang, and J.W. Stevenson, "Development of Low Cost Protection Coatings for SOFC Interconnect,"

35th International Conference & Exposition on Advanced Ceramics & Composites (ICACC), Daytona Beach, Florida, January 2011.

4. J.P. Choi, J.W. Stevenson, and Y.S. Chou, "Optimized Spray MnCoO Spinel Coating for SOFC Application with Design of Experiment Method," 35th International Conference & Exposition on Advanced Ceramics & Composites (ICACC), Daytona Beach, Florida, January 2011.

5. G.G. Xia, X.S. Li, Z. Lu, R.C. Scott, Z.G. Yang, and J.W. Stevenson, "Development of Low Cost Protection Coatings for SOFC Interconnect Applications," 38th International Conference on Metallurgical Coatings and Thin Films, San Diego, California, May 2011.

III.C.5 Development of Cathode-Interconnect Contact Materials for SOFCs

Guan-Guang "Gordon" Xia (Primary Contact), Xiaohong Li, Zigui Lu, Zimin Nie, Ryan Scott, Joshua Templeton, and Jeff Stevenson
Pacific Northwest National Laboratory
P.O. Box 999, MS K2-44
Richland, WA 99352
Phone: (509) 371-6261; Fax: (509) 375-2186
E-mail: Guan-Guang.Xia@pnl.gov

DOE Project Manager: Briggs White
Phone: (304) 285-5437
E-mail: Briggs.White@netl.doe.gov

Contract Number: FWP40552

Start Date: October 1, 2010
End Date: September 30, 2011

Fiscal Year (FY) 2011 Objectives

- Develop and investigate cost-effective contact materials and fabrication processes for cathode/interconnect interfaces that demonstrate strong bonds and low electrical resistance with long-term chemical, electrical, and structural stability.
- Identify, understand, and mitigate degradation processes at cathode/interconnect interfaces.

FY 2011 Accomplishments

- Identified several high performance candidate cathode contact materials, including Ni-Co oxide and $Mn_{2.7-x}Co_xCu_{0.3}O_4$.
- Studied relevant parameters such as the form of precursor, particle size distribution, composition, process temperature, etc. to optimize the properties and processing of candidate cathode contact materials.
- Demonstrated excellent performance of candidate contact materials including strong bond strength (tensile strength up to 10 MPa), low electrical contact resistance (area specific resistance [ASR] as low as $5x10^{-3}$ ohm-cm^2 over 2,000 hrs at 800°C), and long-term stability.

Introduction

The interconnect is one of the key components in a solid oxide fuel cell (SOFC) stack. Stainless steels are typically chosen as interconnect materials for intermediate temperature (IT-)SOFCs (650-850°C). However, metallic interconnects can contribute a significant portion of power loss and performance degradation during operation due to the continuous growth of oxide scales and contact resistances. Optimization of interconnect materials and coatings is a necessary, but not sufficient, condition for obtaining stable stack performance. The complete solution to interconnect-related challenges must also take into account the electrode/interconnect interfaces. Thus, it is necessary to develop a complete materials system, which includes not only the interconnect itself, but also stable, high-performance contact materials for electrode/interconnect interfaces to ensure good stack performance for meeting the U.S. Department of Energy technical targets and achieving the Fuel Cell Program goals.

Requirements for successful development of cathode contact materials include:

- High electrical conductivity to minimize the resistance of the contact layer and the contact interfaces.
- Chemical compatibility with the interconnect and the perovskite cathode. If reaction occurs, the resulting reaction products should be stable and conductive.
- Appropriate thermal expansion behavior and high thermo-chemical and structural stability in the SOFC operating environment.
- Appropriate bond-forming ability and sintering activity for increased contact area, decreased contact resistance, and adequate interfacial structural stability and strength.
- Low cost.

Finding suitable materials for electrical contact layers at the cathode interface can be especially challenging, particularly in intermediate temperature SOFCs where high-temperature oxidation-resistant alloys are used as interconnects. The contact layer must provide a low-resistance contact between a conductive oxide cathode (e.g., lanthanum strontium manganese oxide [LSM], lanthanum strontium iron oxide [LSF], or lanthanum strontium cobalt iron oxide [LSCF]) and the interconnect (probably coated, if alloy-based). Therefore, there always exists a ceramic/metal interface, and possible additional ceramic/ceramic interfaces as well, all of which potentially contribute to high contact resistance and power loss. Many conductive oxides, such as those commonly used as cathodes, demonstrate high electrical conductivity and chemical compatibility, but these oxides usually exhibit low sintering activity at typical IT-SOFC stack sealing temperatures (825-950°C). On the other hand, many

conductive oxides with a low sintering temperature are highly reactive and demonstrate poor compatibility and stability. Consequently, there is a pressing need for optimized, cost-effective contact materials for cathode-side applications.

Approach

During FY 2011, the primary focus was on the development of a novel reaction-sintering process and the selection of proper candidate cathode contact materials. The reaction-sintering approach is a processing technique which utilizes the energy released from the chemical reactions of metallic precursors with oxygen molecules in air to assist solid-state sintering of a contact material in situ. A similar approach has been successfully developed for protective MC spinel coatings on IT-SOFC interconnects.

Composition-microstructure-property relationships were determined for SOFC-relevant properties including sintering activity, coefficient of thermal expansion (CTE), electrical conductivity, and bond strength. Evaluation of the electrical resistance and chemical stability of simulated cathode/contact material/interconnect structures was performed using interfacial electrical resistance tests followed by post-test analysis (scanning electron microscopy [SEM], energy dispersive spectroscopy, transmission electron microscopy, X-ray diffraction analysis, etc.). Bond strength was evaluated through tensile testing of simulated cathode/contact material and interconnect/contact material interfaces.

Results

Several metal oxides, including Mn-Co, Mn-Fe, Ni-Co oxides as well as Mn-Co oxides with Cu addition, were evaluated as potential cathode contact materials, based on their high electrical conductivity and good CTE match to other SOFC components. Although preliminary studies indicated that these oxide powders used as cathode contact materials could yield reasonably low ASRs, weak bond strengths between cathode/contact layer and interconnect coating/contact layer caused unstable ASR during thermal cycling. It is believed that the weak bond strength resulted from insufficient sintering activity and minimal interfacial interaction when oxide powders were used as the contact material precursors.

Recently, a new approach - in situ reaction sintering - was developed to improve contact layer bond strength by employing metal powder mixtures instead of oxide powders as the contact material precursors. Such contact pastes can be prepared by simply mixing appropriate amounts of fine metal powers with a binder vehicle. Two types of metallic mixtures, Ni-Co and Mn-Co-Cu systems were found to be very promising. For the former system, a Ni:Co ratio of 1:2 provided more stable ASR values than other ratios, such as 2:1 or 1:1. For the $Mn_{2.7-x}Co_xCu_{0.3}O_4$ system, Cu content was kept at 10 mol% (metal basis) to minimize phase segregation upon oxidation.

In order to quantify the bulk and interfacial mechanical properties of cathode/contact material/interconnect structures, a tensile stress fracture measurement method has been developed. Figure 1

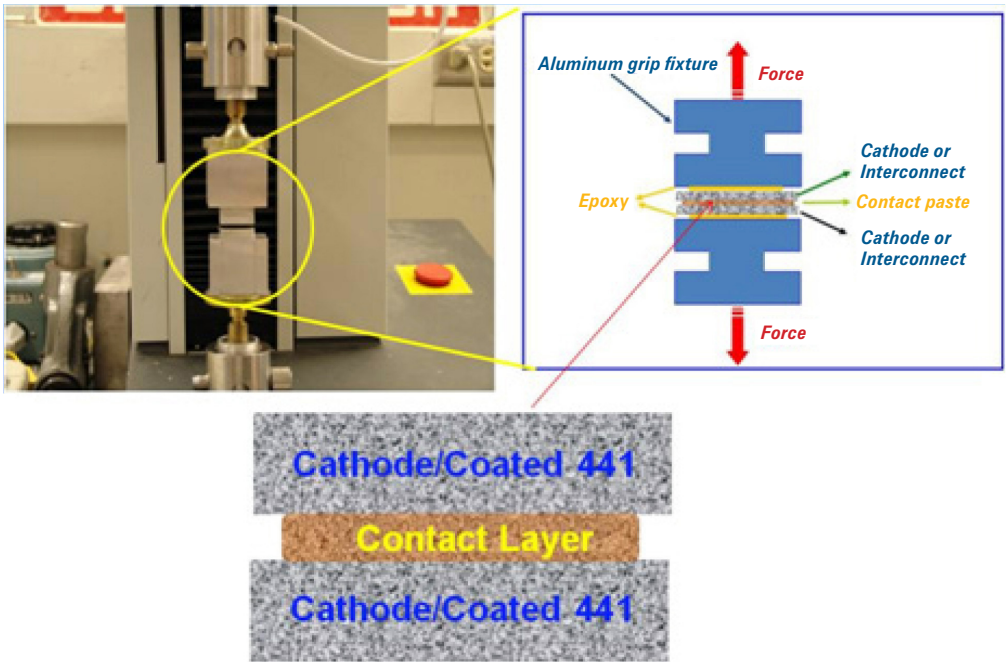

FIGURE 1. Tensile Strength Measurement Setup

illustrates the setup for mechanical tensile strength measurements. These tests allow for determination of the effects of contact material composition, cathode and interconnect surface morphology, and processing variables on the mechanical properties of the cathode contact zone. As shown in Figure 1, the contact paste was applied between two simulated cathode bars or two coated interconnect coupons. Test specimens were heated from room temperature at 3°C/min in air up to 850-950°C for 30 min, then kept at 800°C for 50-100 hrs before cooling down to room temperature under ~12 psi compressive load. The specimens were then glued onto two aluminum test fixtures using fast-setting epoxy. The assembly was then tested in uniaxial tension using a mechanical tensile stress tester (MTS Bionix 400, MTS Canton, MA) with a cross-head speed of 0.02 inch min^{-1} in ambient conditions. The fixture had a self-alignment joint to minimize bending or twisting during tensile testing. For each condition, more than five specimens were tested.

Figure 2 summarizes the tensile strength data for different contact materials that were used for bonding Ce-MC coated AISI441 coupons or simulated cathode bars (LSM or LSCF). Yttria-stabilized zirconia (YSZ) fibers were added to some contact pastes for the purpose of contact layer reinforcement. The data in Figure 2 demonstrate that the mechanical bond strengths for all cases were quite strong (over 3~8 MPa) as compared to conventional perovskite contact materials previously tested at Pacific Northwest National Laboratory (PNNL) (less than 0.6 MPa). The resulting bond strengths are comparable to that of glass seals used in SOFC research and development, although the YSZ fibers did not enhance the bond strength during these tests. Post-mortem analysis of specimens after the tensile bond strength measurements using optical microscopy and SEM techniques were conducted to determine where the failures occurred. For the cathode/contact layer/cathode configuration, the fractures occurred primarily at the contact/cathode interfaces, but failures through the contact layers and even through the porous LSCF layer were also observed. For the interconnect coating/contact layer/interconnect coating configuration, failure also occurred at the contact interface and through the contact layer, and, in some cases, at the oxide scale/alloy interface.

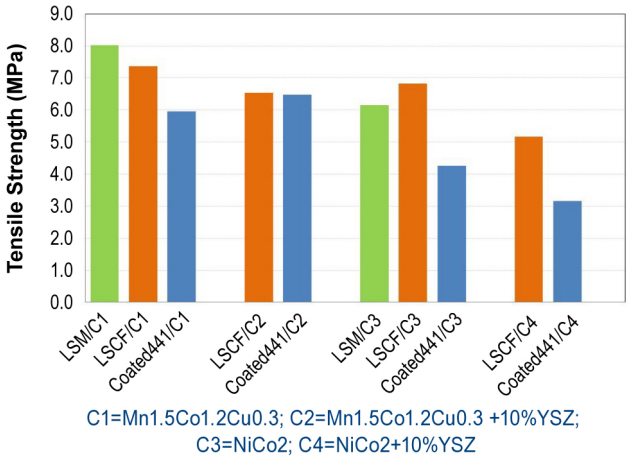

FIGURE 2. Tensile Strength Results for Various Contact Materials

Figure 3 shows strength results for a series of $Mn_{2.7-x}Co_xCu_{0.3}$ compositions prepared from metallic powder precursors. The average fracture stresses vs. Co composition ranged from 3 to 10 MPa. Figure 4 displays ASR results for a $Mn_{1.5}Co_{1.2}Cu_{0.3}O_4$ contact layer from metal precursors that was applied between a simulated LSCF cathode and Ce-MC coated AISI441 coupons. An isothermal ASR measurement was conducted at 800°C in air for over 2,400 hours, then thermal cycling ASR was measured between ~70-800°C with a hold at 800°C for 24 hours for every thermal cycle; the thermal cycle ASR is depicted in the inset. Although the ASR jumped from ~5 mOhm-cm^2 to ~8 mOhm-cm^2 at the starting point of the thermal cycling measurements, relatively stable ASR was retained for more than 35 thermal cycles.

In order to further evaluate the performance of candidate cathode contact materials, button cell tests were conducted with the following configuration: an anode (Ni+YSZ) supported cell (1" in diameter) with thin layers of YSZ electrolyte, scandia doped ceria interlayer, and LSCF cathode was glass-sealed onto an alumina tube; a perforated AISI441 interconnect (1/2" in diameter and 20 mil thick) that was coated with Ce-MC spinel and pre-treated in 2.5% H_2/Ar at 850°C for 4 hours was placed on top of the porous cathode layer with the contact paste applied between them; the interconnect was pushed against the cathode using a spring-loaded ceramic fixture; and Pt wires were used for

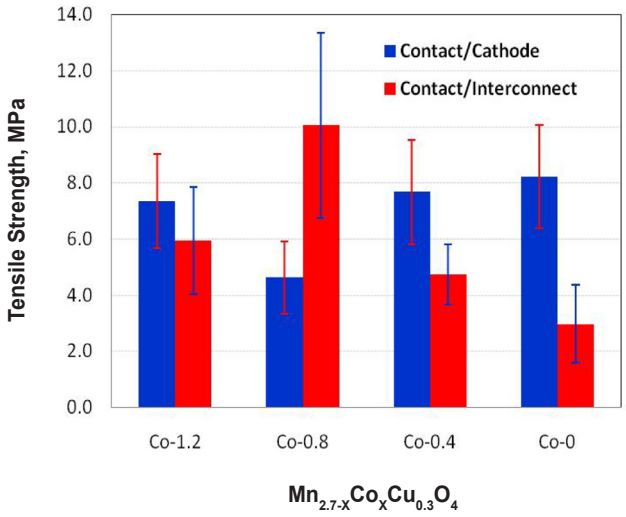

FIGURE 3. Tensile Strength Results for Mn-Co-Cu Contact Materials with Various Co Contents

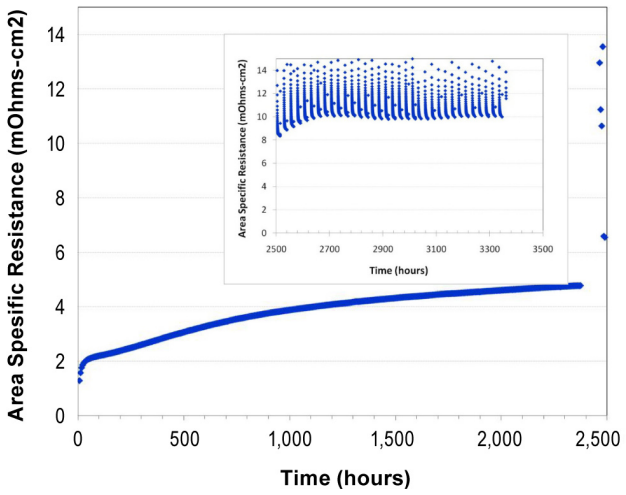

FIGURE 4. Static and Cycling ASR Results of $Mn_{1.5}Co_{1.2}Cu_{0.3}$ Contact Material

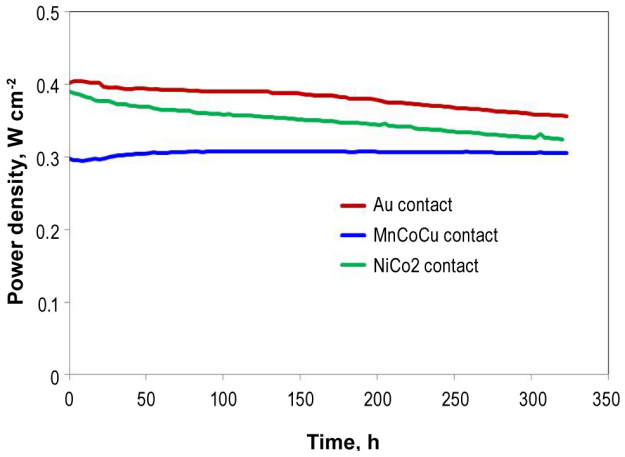

FIGURE 5. Button Cell Performance of Different Contact Materials

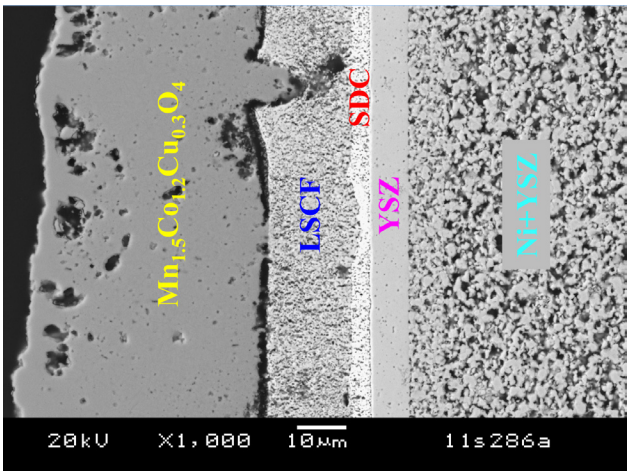

FIGURE 6. Cross-Section SEM of a Button Cell with $Mn_{1.5}Co_{1.2}Cu_{0.3}O_4$ Contact Layer

electrical current collectors. Moisturized H_2 and ambient air were used as fuel and oxidant.

Two candidate cathode contact materials, based on metal powder stoichiometries of $NiCo_2$ and $Mn_{1.5}Co_{1.2}Cu_{0.3}$, were studied, along with Au as a baseline contact material, in the button cells. Preliminary results are plotted in Figure 5. Initial power density using Au or $NiCo_2$ as the contact paste was higher than that of Mn-Co-Cu contact paste. However, the later exhibited superior stability over time. Cell impedence data show that the initial ohmic resistances and total polarization resistances of the three cells have the order of Mn-Co-Cu>$NiCo_2$>Au as contact pastes in the early stage of the tests. As the tests continued over time, the total polarization resistance for Mn-Co-Cu system decreased while the other two systems exhibited increasing resistance. This observation agrees with the ASR data. These results indicate that the Mn-Co-Cu contact materials may have played an additional role in protecting Cr migration from the metallic interconnect into the cathode, helping to maintain a stable power density output. The reason for its overall low power density of Mn-Co-Cu as the contact material may be dense $Mn_{1.5}Co_{1.2}Cu_{0.3}O_4$ layer formation due to the reaction sintering process that impedes oxygen molecule transport to the cathode. Figure 6 shows the very dense $Mn_{1.5}Co_{1.2}Cu_{0.3}O_4$ contact layer that formed on top of the porous cathode. The Ni-Co and Au contact layers were porous (images are not shown here). Further optimization of the formulas and processes for making high performance contact pastes is in progress at PNNL.

Conclusions and Future Directions

A newly developed reaction sintering process for making robust contact layers with increased bond strength appears to be a promising approach for SOFC stack assembly. Both Ni-Co and Mn-Co-Cu systems show good performance, especially in terms of enhanced bond strength. Future research directions include optimizing the reaction sintering approach as a means of increasing intrinsic and interfacial bond strengths, and the determination of preferred contact material compositions.

FY 2011 Publications/Presentations

1. Z. Lu, G. Xia, J.D. Templeton, X. Li, Z. Nie, Z. Yang, and J.W. Stevenson, "Development of $Ni_{1-x}Co_xO$ as the Cathode/Interconnect Contact for Solid Oxide Fuel Cells," Electrochemistry Communications, 13, 642 (2011).

2. G. Xia, X.S. Li, J.D. Templeton, Z. Lu, T. Oh, Z. Nie, Z. Yang, and J.W. Stevenson, "Development of Protection Coatings and Contact Materials for Metallic Interconnects in SOFCs," 218th Electrochemical Society, Las Vegas, Nevada, October 12, 2010.

3. G. Xia, X.S. Li, Z. Lu, J.D. Templeton, R.C. Scott, Z. Nie, and J.W. Stevenson, "Development of Cathode/Interconnect Contact Materials at PNNL," 35th International Conference and Exposition on Advanced Ceramics and Composites (ICACC'11), Daytona Beach, Florida, January 27, 2011.

III.C.6 Development of Ceramic Interconnect Materials for SOFCs

Kyung Joong Yoon (Primary Contact),
Jeffry W. Stevenson, Olga A. Marina
Pacific Northwest National Laboratory
902 Battelle Blvd.
Richland, WA 99354
Phone: (509) 372-4255; Fax: (509) 375-2186
E-mail: kyungjoong.yoon@pnnl.gov

DOE Project Manager: Briggs White
Phone: (304) 285-5437
E-mail: Briggs.White@netl.doe.gov

Contract Number: FWP40552

Start Date: October 1, 2010
End Date: September 30, 2011

Fiscal Year (FY) 2011 Objectives

- Evaluate thermal and electrical properties of yttrium chromite doped with Ca on the A-site and various transition metals on the B-site.
- Investigate constrained and co-sintering behavior of screen-printed doped yttrium chromite.
- Suggest optimum composition and processing parameters consistent with an integrated planar solid oxide fuel cell (SOFC) design.

FY 2011 Accomplishments

- 10 at% Co, 4 at% Ni, and 1 at% Cu substitution on the B-site of 20 at% Ca-doped yttrium chromite led to a close match of thermal expansion coefficient (TEC) with that of 8 mol% yttria-stabilized zirconia (YSZ).
- Relative density of $Y_{0.8}Ca_{0.2}Cr_{0.86}Co_{0.1}Ni_{0.04}O_3$ sintered at 1,300°C was measured to be ~98% of theoretical density.
- Ni dopant improved both electrical conductivity and dimensional stability in reducing environments.
- Electrical conductivity of 57 S cm^{-1} in air and 11 S cm^{-1} in fuel (pO_2=5×10^{-17} atm) environment was achieved with $Y_{0.8}Ca_{0.2}Cr_{0.85}Co_{0.1}Ni_{0.04}Cu_{0.01}O_3$ at 900°C.
- Chemical compatibility of doped yttrium chromite with other cell components was verified at the relevant processing temperatures.
- Densification of screen-printed films was improved for both co-sintering and constrained sintering conditions by the use of an infiltration process.

Introduction

For SOFC stack designs which utilize higher operating temperatures, ceramic interconnects are required. Currently, acceptor-doped lanthanum chromite is the predominant ceramic interconnect material due to its relatively good stability, electrical conductivity, and thermal expansion match. However, it exhibits inferior sintering behavior, and is susceptible to hydration in moist environments. In addition, it undergoes a phase transition from orthorhombic to rhombohedral symmetry upon heating, and is reactive with YSZ electrolyte at high temperatures. Therefore, an alternate interconnect material is needed to overcome these technical limitations of acceptor-doped lanthanum chromite.

Yttrium chromite-based perovskites exhibit several attractive features for interconnect applications over lanthanum chromites, such as stability with respect to formation of hydroxides, low chemical expansion in reducing environments, and chemical compatibility with YSZ electrolyte. The electrical conductivity of yttrium chromite is known to be relatively low, but can be improved by multiple doping on A- and B-sites. Electrical and thermal properties of yttrium chromite are strongly influenced by transition metal doping on B-site, and the basic properties of yttrium chromite can potentially be tailored by a wide variety of dopants to satisfy the rigorous requirements for SOFC interconnect applications. During FY 2011, Pacific Northwest National Laboratory investigated the effect of Co-, Ni-, and Cu-doping on thermal and electrical properties of yttrium chromite. Co-firing and constrained sintering behavior of doped yttrium chromite was evaluated, and densification of screen-printed layer was improved by the addition of infiltration steps. Based on the results, an optimized composition for SOFC interconnect application was proposed.

Approach

Powders of yttrium chromite doped with 20 at% Ca on the A-site and various transition metal elements on the B-site were synthesized using the glycine nitrate process. After calcination at 1,200°C in air, the phase purity was verified using X-ray diffraction (XRD) analysis. The phase stability up to 1,100°C was investigated using a high temperature XRD. The chemical stability in reducing atmosphere was examined by XRD after annealing the powders at 900°C in humidified hydrogen ($pO_2 = 4.7\times10^{-20}$ atm) for 24 hours. Rectangular specimens were prepared by uniaxial pressing at 35 MPa

followed by isostatic pressing at 200 MPa. Sintering shrinkages were measured up to 1,400°C in a dilatometer using 3×3×14 mm bars. The relative density after sintering was determined using the Archimedes method. The sintered samples were used to measure TECs in the temperature range of 25-900°C in air. Isothermal "chemical" expansions were measured in a controlled-atmosphere dilatometer at 900°C by varying the oxygen partial pressure from 1.0 to 5×10^{-17} atm. Electrical conductivity measurements were performed by a four-probe direct current method using 3×3×30 mm dense rectangular bars. The electrical contacts were made using Pt wires and Pt paste, and conductivity was measured in the temperature range 600-900°C in air. Electrical conductivity was also measured as a function of oxygen partial pressure at 900°C by varying the oxygen partial pressure from 1.0 to 5×10^{-17} atm. Chemical compatibility of doped yttrium chromite with other cell components was studied by mixing doped yttrium chromite powders with 8 mol% YSZ, NiO, and $(La_{0.8}Sr_{0.2})_{0.95}MnO_3$ (LSM) powder in a 50:50 weight ratio separately, ball-milling for 24 hours and heating in air at 1,400, 1,400, and 1,200°C, respectively, for 12 hours. The resulting specimens were crushed and the powders were analyzed by XRD.

Inks for screen printing were prepared by mixing $Y_{0.8}Ca_{0.2}Cr_{0.85}Co_{0.1}Ni_{0.04}Cu_{0.01}O_3$ powders with a commercial binder in a three-roll mill. Bi-layers of Ni-YSZ anode and YSZ electrolyte were used as substrates. For the infiltration process, 1 M nitrate solution was used. Sample cross-sections were examined with scanning electron microscopy (SEM) after the co-sintering, constrained sintering, and infiltration process.

Results

In XRD analysis of $Y_{0.8}Ca_{0.2}Cr_{0.85}Co_{0.1}Ni_{0.04}Cu_{0.01}O_3$ powders after calcination at 1,200°C in air, all the peaks were indexed to a single phase orthorhombic perovskite structure with space group *Pbnm* (62), and no impurity phase was observed. After exposure to a reducing environment ($pO_2 = 4.7\times10^{-20}$ atm) at 900°C for 24 hours, no phase segregation or decomposition product was found. Moreover, phase analysis performed in situ using high temperature XRD while heating the calcined powder up to 1,100°C in air confirmed the single orthorhombic phase. Therefore, the doped yttrium chromite is stable under the SOFC operating conditions. Lanthanum chromites typically experience a first order phase transition from orthorhombic to rhombohedral symmetry at 250~300°C upon heating, which causes a loss of mechanical strength. Therefore, improved mechanical reliability is expected for doped yttrium chromite interconnects due to the absence of the phase transformation.

The TEC of $Y_{0.8}Ca_{0.2}CrO_3$ is 9.7×10^{-6} K^{-1}, which is substantially lower than that of 8 mol% YSZ, 10.8×10^{-6} K^{-1}. TEC increased with transition metal substitution, and $Y_{0.8}Ca_{0.2}Cr_{0.85}Co_{0.1}Ni_{0.04}Cu_{0.01}O_3$ (11.0×10^{-6} K^{-1}) gave the closest match to 8 mol% YSZ. Without B-site doping, the TEC of chromite-based perovskite increases with the amount of alkaline earth element on the A-site, and typically, more than 30% substitution is required to match TEC of YSZ. However, when the total calcium content exceeds 25%, calcium chromate ($CaCrO_4$) exsolves from the perovskite structure as a secondary phase, and reacts with YSZ to form $CaZrO_3$ as a reaction product during the co-firing process. In addition, $CaCrO_4$ dissociates into α and β phases of $CaCr_2O_4$ under reducing environments, which causes a large volume expansion. The results of this study suggest that thermal expansion of Ca-doped yttrium chromite can be controlled by B-site substitution while keeping the calcium content below the solubility limit.

Figure 1 illustrates the effect of partial substitution of Co, Ni, and Cu for Cr on sintering shrinkage ($\Delta l/l_o$) of $Y_{0.8}Ca_{0.2}CrO_3$. Without B-site doping, the shrinkage began at about 1300°C, and only 3% of sintering shrinkage was observed at 1,400°C, which is comparable to the sintering behavior of acceptor-doped lanthanum chromite. The sintering curve showed gradual shrinkage over a wide temperature range, which is a characteristic of solid-state sintering. With 10 at% Co and 4 at% Ni doping on B-site, the sintering curve exhibited more rapid shrinkage above 1,200°C, and 20% of sintering shrinkage was observed at 1,340°C. With the addition of 1 at% Cu, sintering behavior was remarkably improved, showing 20% sintering shrinkage at 1,240°C. The relative density of $Y_{0.8}Ca_{0.2}Cr_{0.86}Co_{0.1}Ni_{0.04}O_3$ sintered at 1,300°C was measured to be ~98% of theoretical density. Thus, it is suggested that adequately dense yttrium chromite-based interconnects can be fabricated at a

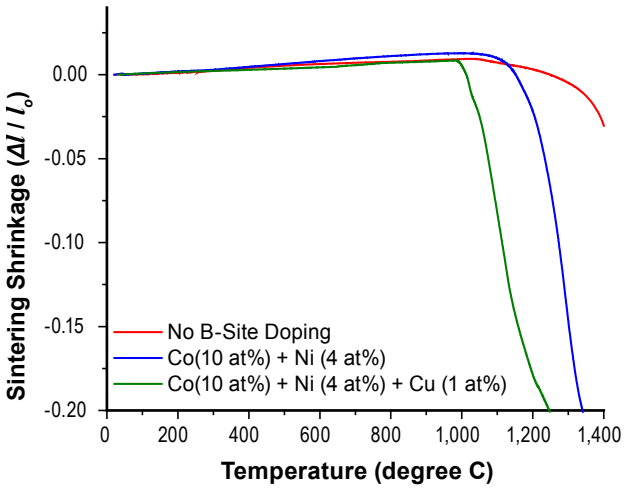

FIGURE 1. Linear Sintering Shrinkage ($\Delta l/l_o$) of $Y_{0.8}Ca_{0.2}CrO_3$, $Y_{0.8}Ca_{0.2}Cr_{0.86}Co_{0.1}Ni_{0.04}O_3$, and $Y_{0.8}Ca_{0.2}Cr_{0.85}Cu_{0.01}Co_{0.1}Ni_{0.04}O_3$ as a Function of Temperature

processing temperature as low as 1,300°C, and common problems accompanied by high sintering/processing temperatures, such as undesired chemical interactions, migration of elements, and excessive sintering of other cell components can be avoided.

The volume of chromite-based perovskite materials expands upon reduction due to the loss of lattice oxygen. Figure 2 shows the effect of B-site dopants on the isothermal chemical expansion of Ca-doped yttrium chromite in the oxygen partial pressure range of 5×10^{-17}–0.21 atm at 900°C. In all samples, no significant expansion was observed until the ambient oxygen partial pressure reached 10^{-10} atm, and the onset of the expansion occurred at $pO_2 = 10^{-12}$ atm. Without B-site doping, $Y_{0.8}Ca_{0.2}CrO_3$ showed an expansion of 0.09% on reduction at pO_2=5×10^{-17} atm. Co- and Cu-doped yttrium chromite, $Y_{0.8}Ca_{0.2}Cr_{0.89}Co_{0.1}Cu_{0.01}O_3$, exhibited very similar behavior to $Y_{0.8}Ca_{0.2}CrO_3$. When 4 at%Ni was added, the isothermal expansion of $Y_{0.8}Ca_{0.2}Cr_{0.85}Co_{0.1}Ni_{0.04}Cu_{0.01}O_3$ decreased to 0.055% under the same condition. Importantly, all samples exhibited good reversibility when cycled between oxidizing and reducing environments, which indicates that no microcracks from internal stress were generated. The chemical expansion of chromite-based materials could be reduced by decreasing the concentration of alkaline earth metal dopant (Ca or Sr) because the low initial concentration of Cr^{4+} allows less oxygen to be removed from the lattice before all of the Cr^{4+} is reduced to Cr^{3+}. However, the charge carriers for electrical conduction in the chromites are electron holes associated with Cr^{4+}, and, thus, the electrical conductivity is also lowered by reducing the concentration of alkaline earth metal dopant. The acceptor-doped yttrium chromite shows a chemical expansion about 40% less than that of similarly doped lanthanum chromite because the reduced unit cell size of yttrium chromite suppresses the oxygen evolution in reducing atmosphere. The results of the current study indicate that the chemical expansion of the yttrium chromites can be further reduced by Ni substitution on B-site without loss of electrical conductivity.

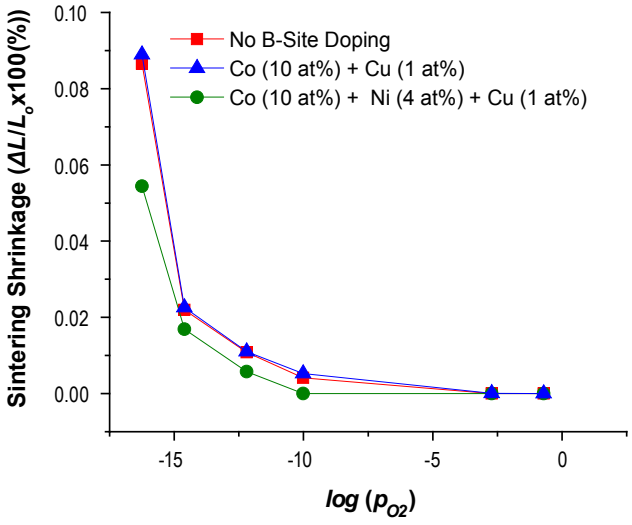

FIGURE 2. Isothermal Linear Expansion of $Y_{0.8}Ca_{0.2}CrO_3$, $Y_{0.8}Ca_{0.2}Cr_{0.89}Co_{0.1}Cu_{0.01}O_3$, and $Y_{0.8}Ca_{0.2}Cr_{0.85}Co_{0.1}Ni_{0.04}Cu_{0.01}O_3$ at 900°C as a Function of Oxygen Partial Pressure

Despite other superior properties, the yttrium chromites possess lower electrical conductivity than similarly doped lanthanum chromites, but doping with alkaline earth metal on the A-site and/or transition metal on the B-site generally improves the electrical conductivity of chromite-based materials. The effect of Co, Ni, and Cu partial substitution on the electrical conductivity of Ca-doped yttrium chromite in the temperature range between 600 and 900°C in air is shown in Figure 3(a). For all compounds, the conductivity increased with temperature, as expected for a thermally activated conduction process. The conductivity increased with Ni doping, but even more so with Co doping. The conductivity values at 900°C were 10 S cm^{-1} for $Y_{0.8}Ca_{0.2}CrO_3$, 21 S cm^{-1} for $Y_{0.8}Ca_{0.2}Cr_{0.85}Ni_{0.14}Cu_{0.01}O_3$, and 57 S cm^{-1} for $Y_{0.8}Ca_{0.2}Cr_{0.85}Co_{0.1}Ni_{0.04}Cu_{0.01}O_3$. Ni doping increases the electrical conductivity because most of the nickel ions are divalent and act as acceptor dopants in chromite-based oxides. Substitution of Cr with Co likely leads to an increase in both charge carrier density and hopping mobility. Charge carrier population increases due to the disproportionation among the Co sites: Co^{4+} becomes energetically favorable and populated at high temperatures. Hole mobility also increases because of the low small polaron site energy of Co and rapid electron transfer between Co^{3+} and Co^{4+}. The activation energies obtained from the slopes of Figure 3(a) were 0.24 eV $Y_{0.8}Ca_{0.2}CrO_3$, and around 0.15 eV for both $Y_{0.8}Ca_{0.2}Cr_{0.85}Ni_{0.14}Cu_{0.01}O_3$ and $Y_{0.8}Ca_{0.2}Cr_{0.85}Co_{0.1}Ni_{0.04}Cu_{0.01}O_3$.

The electrical conductivity of doped yttrium chromites during the oxygen partial pressure change from 1 atm to 5×10^{-17} at 900°C is given in Figure 3 (b). The conductivities were independent of pO_2 in the high oxygen partial pressure region and decreased below a critical oxygen partial pressure, in agreement with the *p*-type conduction mechanism. At high oxygen partial pressure, the charge imbalance caused by doping is compensated by the formation of holes, and the number of charge carriers is determined by the amount of dopants. Thus, the electrical conductivity is independent of oxygen partial pressure. Below the critical oxygen partial pressure, lattice oxygen is released to the atmosphere and the loss of oxygen creates positively charged oxygen vacancies that consume positively charged holes to maintain the charge neutrality. Therefore, the conductivity develops a strong dependence on oxygen partial pressure and

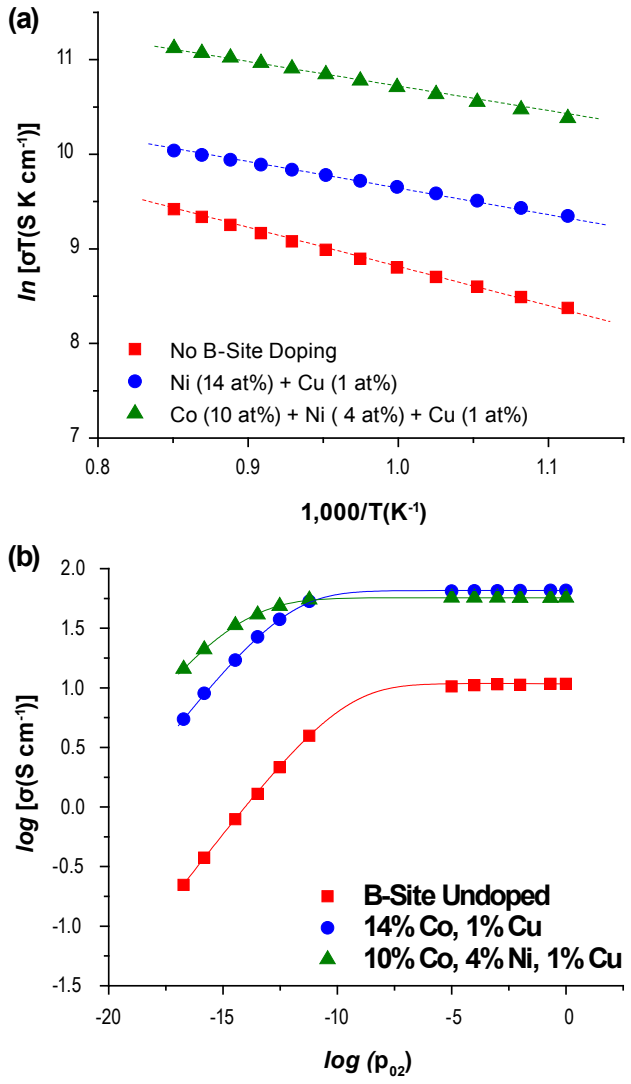

FIGURE 3. Plots of (a) $ln(\sigma T)$ Versus 1000/T for $Y_{0.8}Ca_{0.2}CrO_3$, $Y_{0.8}Ca_{0.2}Cr_{0.85}Ni_{0.14}Cu_{0.01}O_3$, and $Y_{0.8}Ca_{0.2}Cr_{0.85}Co_{0.1}Ni_{0.04}Cu_{0.01}O_3$ in Air, and (b) $log(\sigma)$ Versus $log(pO_2)$ for $Y_{0.8}Ca_{0.2}CrO_3$, $Y_{0.8}Ca_{0.2}Cr_{0.85}Co_{0.14}Cu_{0.01}O_3$, and $Y_{0.8}Ca_{0.2}Cr_{0.85}Co_{0.1}Ni_{0.04}Cu_{0.01}O_3$ at 900°C

decreases with decreasing pO_2 as the ionic charge compensation becomes important. Also, as shown in Figure 3(b), $Y_{0.8}Ca_{0.2}Cr_{0.85}Co_{0.14}Cu_{0.01}O_3$ showed slightly higher conductivity than $Y_{0.8}Ca_{0.2}Cr_{0.85}Co_{0.1}Ni_{0.04}Cu_{0.01}O_3$ in the oxidizing atmosphere. Since the total amounts of B-site dopants were identical, Co-doping is more effective in increasing the conductivity in an oxidizing environment, as suggested above. In reducing environments, the sample containing Ni showed higher electrical conductivity compared to that without Ni. The slopes of the $log(\sigma)$ versus $log(pO_2)$ for the sample without B-site dopants and with Co and Cu dopants were close to 0.25. This $pO_2^{1/4}$ dependence of electrical conductivity indicates predominantly ionic charge compensation and negligible hole concentration. The slope for the sample containing Ni was 0.162, which indicates that the system did not reach the extreme reducing conditions, and that both ionic and electronic compensation mechanisms were operative. An absolute conductivity value of 11 S cm^{-1} was measured for the $Y_{0.8}Ca_{0.2}Cr_{0.85}Co_{0.1}Ni_{0.04}Cu_{0.01}O_3$ at 900°C at the partial oxygen pressure of 5×10^{-17} atm. Because the value of 1 S cm^{-1} is a well-accepted minimum conductivity for the interconnect materials to be used in SOFCs, the electrical conductivity of $Y_{0.8}Ca_{0.2}Cr_{0.85}Co_{0.1}Ni_{0.04}Cu_{0.01}O_3$ in both oxidizing and reducing environments satisfies this requirement.

The chemical compatibility of $Y_{0.8}Ca_{0.2}Cr_{0.85}Co_{0.1}Ni_{0.04}Cu_{0.01}O_3$ with 8 mol% YSZ, NiO, and LSM was evaluated using XRD analysis. The chromite-YSZ (50:50 wt%) mixture was heated in air for 24 hours at 1,400°C (above the densification temperature), as was the chromite-NiO (50:50 wt%) mixture. The chromite-LSM (50:50 wt%) mixture was heated at 1,200°C, the typical cathode sintering temperature. In XRD analysis, all peaks of the composites corresponded to the individual constituents only, and no reaction product was observed. Therefore, detrimental secondary phase formation is not expected between the doped yttrium chromite interconnect and standard cell components under normal processing and operating temperatures.

Screen printing is a simple, low-cost process for SOFC interconnect fabrication. However, in general, densification of the screen-printed layer is difficult, and modification of the process is necessary to increase the density of the film. In addition, application of the thick film to a pre-sintered substrate results in sintering constraint in lateral directions, which can further retard densification. Figure 4(a) and (b) shows the screen-printed layers after constrained sintering and co-sintering at 1,300°C, respectively. They show limited densification, so an infiltration process was used to further improve the film density. For infiltration, ethanol was added (40 vol%) to a water-based nitrate solution to improve the wetting of the solution, and urea was used as a complexing agent. As a result, significantly improved densification was observed for both constrained sintering and co-sintering processes (Figure 4(c) and (d)).

Conclusions

Electrical and thermal properties of Ca-doped yttrium chromite were improved through multiple transition metal doping (Co, Ni, and Cu) on the B-site for SOFC interconnect applications. Sintering was facilitated by Cu substitution. Co substitution effectively enhanced the electrical conductivity in oxidizing atmosphere and Ni substitution improved stability toward reduction, lowering the chemical expansion

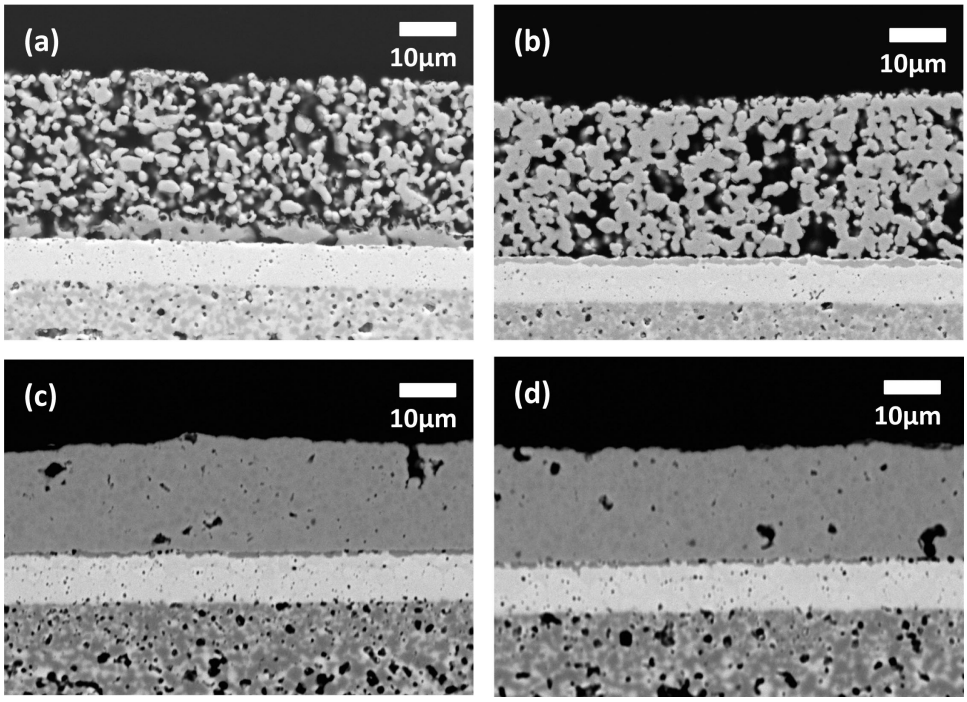

FIGURE 4. SEM Images of Screen-Printed $Y_{0.8}Ca_{0.2}Cr_{0.85}Co_{0.1}Ni_{0.04}Cu_{0.01}O_3$ Layer after (a) Constrained Sintering, (b) Co-Sintering, (c) Infiltration in Constrained Sintered Layer, and (d) Infiltration in Co-Sintered Layer

and enhancing the electrical conductivity in reducing atmospheres. With optimized amounts of Co, Ni, and Cu dopants, a good match in thermal expansion coefficient with 8 mol% YSZ was achieved. Chemical compatibility of doped yttrium chromite with YSZ, NiO, and LSM was confirmed at the standard cell processing temperatures. Densification of screen-printed layers was significantly improved by the use of infiltration after constrained or co-sintering. Based on the improved stability and thermal and electrical properties, an optimized composition of yttrium chromite, $Y_{0.8}Ca_{0.2}Cr_{0.85}Co_{0.1}Ni_{0.04}Cu_{0.01}O_3$, is recommended for use as a ceramic interconnect material for SOFCs.

FY 2011 Publications/Presentations

1. "Calcium- and Nickel-Doped Yttrium Chromite as an Advanced Ceramic Interconnect Material for Solid Oxide Fuel Cells (SOFCs)," 218th ECS Meeting, Las Vegas, Nevada, October 2010.

2. K.J. Yoon, J.W. Stevenson, and O.A. Marina, "Effect of Nickel Substitution on Defect Chemistry, Electrical Properties, and Dimensional Stability of Calcium-Doped Yttrium Chromite," *Solid State Ionics*, accepted (2011).

III. SECA CORE RESEARCH & DEVELOPMENT

D. Seals

III.D.1 Viscous Glass/Composite SOFC Sealants

Scott Misture (Primary Contact), James Shelby
NYS College of Ceramics at Alfred University
2 Pine St., Binns-Merrill Hall
Alfred, NY 14802
Phone: (607) 871-2438; Fax: (607) 871-2354
E-mail: misture@alfred.edu

DOE Project Manager: Joseph Stoffa
Phone: (304) 285-0285
E-mail: Joseph.Stoffa@netl.doe.gov

Contract Number: NT0005177

Start Date: October 1, 2008
End Date: September 30, 2011

Fiscal Year (FY) 2011 Objectives

- Understand interfacial reactions of viscous sealants with solid oxide fuel cell (SOFC) stack electrolytes and interconnects after extended times at operating temperatures.
- Identify ideal operating temperatures for individual sealants.
- Monitor effects of operating conditions on physical and chemical stability of sealants.

FY 2011 Accomplishments

- Identified four candidate glass compositions for an operating temperature (OT) of ~850°C, 11 compositions for an OT of ~750°C, and six compositions for an OT of ~650°C.
- Demonstrated stability of viscous sealants with 8 mole% yttria-stabilized zirconia (8YSZ) electrolytes. Select glasses dissolve ~5 µm of the electrolyte and penetrate ~5 µm into the remaining grain boundaries, but interact no further even up to 1,500 h at 850°C.
- Demonstrated stability of viscous sealants with Al_2O_3 coated stainless steel (SS) interconnect materials. The glasses are stable against the 1 to 5 µm alumina coatings after 500 h at 850°C.
- Observed crack healing and viscous flow of sealants below 850°C even after ~40% crystallization.

Introduction

Large scale production of SOFC laminate stacks is complicated by difficulties of sealing the stack components using a reliable method that is robust over the lifetime of the device. Candidate sealants should exhibit high coefficient of thermal expansion (CTE) values near 12 ppm/K, gas impermeability, minimal interaction with SOFC stack components for 40,000 h between 600 and 850°C, and a maximum processing temperature of ~950°C [1]. Glass, glass-ceramic, and glass-ceramic composite seals are the best candidates for forming seals due to ease of manufacture and ability to control CTE, viscosity, and sealing temperatures with composition.

Many sealants currently being studied contain large amounts of alkaline earths such as barium or strontium which aids in seal formation below 1,000°C, yet form undesirable crystals when held at temperatures within the SOFC target operating temperature range [2-3]. Some contain undesirable amounts of boron which partially vaporizes during SOFC operation [4]. The current project centers on developing new viscous oxide glass sealants that will flow at the operating temperature to reduce mechanical stresses between components but maintain the required hermeticity. By using glasses with lower alkaline earth content and reduced alkali content as well, we hope to avoid known reactivity issues. Compositions with gallium and germanium additions to silicate based compositions appear to be promising candidates.

Approach

Initial candidate glass sealants were researched in the literature. Glass compositions containing low alkali concentrations and exhibiting properties described above were surveyed using the SciGlass® database to identify initial SOFC sealant compositions. These glasses were melted and screened by measuring thermophysical properties such as CTE, glass transition temperature, viscosity, and crystallization behavior. Quantitative crystallization behavior and weight loss studies were performed via heat treatment for 504 h. Compositional modifications were used to optimize properties that were undesirable in relation to the target properties.

An iterative approach of screening, down-selection and optimization is in process. Some of the down-selected glasses from the initial matrices were also evaluated for stability in glass composite seals. Optimized compositions were fritted and

mixed with Al_2O_3 or 8YSZ powders to characterize interactions between the glass and substrate materials and properties of the glass-ceramic composite material. Heat treatments of ~500 h, followed by extensive characterization, are currently underway.

Results

Modified gallio-silicate glasses were studied thoroughly to understand beneficial glass chemistry for further compositional developments. Chemical substitutions resulted in alkali-free gallio-silicate (GBS1) glasses. Previously, extreme crystallization was noted in GBS1 glasses at 850°C. These glasses do not crystallize dramatically at 750°C after 500 h and are excellent non-alkali candidate viscous sealants for OTs between 700 and 750°C. Another series of gallio-silicate glasses (GBS2) were developed and studied in detail. These glasses retain ~60% remnant glass to sustain viscous flow even after 1,500 h at 850°C. These glasses also exhibit little or no interaction with SOFC stack components at 850 and 650°C and thus allow flexibility for use within the entire OT range of 650 to 850°C.

Bulk crystallization of GBS2 glasses at 850°C depends on original glass chemistry, and the crystalline content is ~40% after 500 h, which remains largely unchanged after 1,500 h with two more thermal cycles to and from room temperature as shown in Figure 1. The glasses do not crystallize when held at 650°C for 500 h followed by an initial treatment at 850°C for 30 minutes. Furthermore, crystallization of the glasses is minimal when heated to 750°C and held for 500 h.

The GBS2 sealant is stable against 8YSZ electrolytes at 850°C up to 1,500 h. GBS2 glasses dissolve the initial ~5 µm of the electrolyte and incorporate yttrium and zirconium ions ~60 to 80 µm from the interface. Electron microprobe studies indicate presence of each glass component within the grain boundaries of the 8YSZ within 10 µm from the original 8YSZ surface. The glass does not continuously dissolve the electrolyte, demonstrating viability of GBS2 glasses with 50 µm thick electrolytes up to at least 1,500 h at 850°C. Some glasses partially crystallize at the 8YSZ interface, while others exhibit an entirely amorphous interface, as shown in Figure 2. As might be expected, interactions are

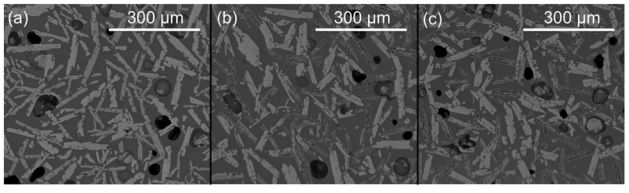

FIGURE 1. Bulk Crystallization of a GBS2 Glass Frit Heat Treated at 850°C (a) for 500 h, (b) for 1,000 h, and (c) for 1,500 h

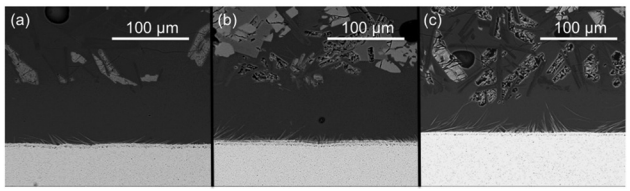

FIGURE 2. Mostly Amorphous Interface within a GBS2 Glass Frit on 8YSZ Substrate Heat Treated at 850°C (a) for 500 h, (b) for 1,000 h, and (c) for 1,500 h

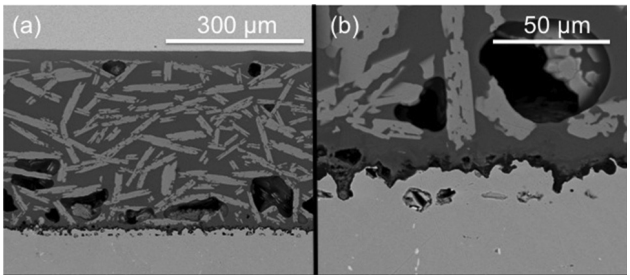

FIGURE 3. Test seal of a GBS2 glass frit heat treated at 850°C for 500 h showing (a) the microstructure with no fracture and (b) the glass to Al-SS interface with the Al_2O_3 coating intact. The Al-SS substrate is on the bottom of the image and the 8YSZ is on top.

minimal after 500h at 650°C and interfaces remain sharp with no dissolution of the 8YSZ substrate.

GBS2 glasses in contact with Al_2O_3 coated SS substrates do not dissolve the protective coating after 500 h at 850°C. The coating helps to inhibit iron and chromium diffusion into the glass. Some glasses exhibit interfacial crystallization of K-Ga-Si-O phases. Test seals of GBS2 glasses with 8YSZ/glass/SS test cells suggest the glasses do not fracture on cooling as shown in Figure 3.

Viscous sealing behavior of GBS2 glasses was observed with high temperature scanning electron microscopy (SEM). Some partially crystallized glasses sealed fractured during heating at ~810°C as shown in Figure 4. Viscous flow was also monitored via dilatometer samples fabricated by glass powders heated for 500 h at 850°C to create a monolithic bar. Dilatometer measurements indicate dilatometric softening points near 650°C. This indicates flow of GBS2 glasses even after ~40% crystallization.

Conclusions and Future Directions

Non-alkali GBS1 glasses are candidates for viscous sealing SOFC stacks with OTs near 700 to 750°C. GBS2 glasses are candidates for viscous sealing over the entire OT range of 650 to 850°C. The GBS2 glasses exhibit compatibility with aluminized SS interconnects and 8YSZ electrolytes at 850°C. Effects of electric potentials across the sealants at operating temperatures

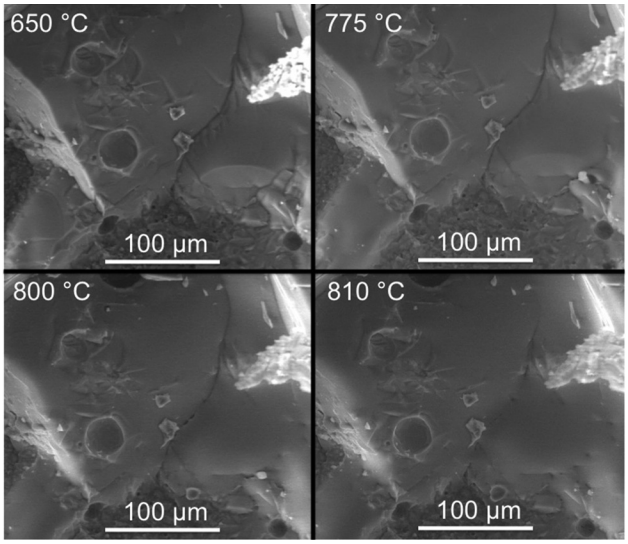

FIGURE 4. In situ high temperature SEM micrographs of a partially crystallized GBS2 glass frit. Each micrograph was taken at the temperature listed in the top left of each image, respectively. A fracture through the bulk partially crystallized glass begins healing around 800°C and is nearly completely healed at 810°C.

are currently being investigated. Interactions of wet atmospheres are also being investigated at operating temperatures.

Special Recognitions & Awards/Patents Issued

1. M.O. Naylor, J.E. Shelby, S.T. Misture, "A Glass Compositional Range Developed to Form a Seal Between Metallic and/or Ceramic Solid Oxide Fuel Cell Components," Provisional Patent filed 2011.

FY 2011 Publications/Presentations

1. M.O. Naylor, J.E. Shelby, and S.T. Misture, "Interactions of Viscous Glass Sealants with Solid Oxide Fuel Cell Components," Presented at the International Conference on Advanced Ceramics and Composites Meeting, Daytona Beach, Florida, 2011.

2. M.O. Naylor, J.E. Shelby, and S.T. Misture, "Interactions of Viscous Glass Sealants with SOFC Stack Components," Presented at the American Ceramic Society Glass and Optical Materials Division Meeting, Savannah, Georgia, 2011.

References

1. S.C. Singhal and K. Kendall, *High Temperature Solid Oxide Fuel Cells: Fundamentals, Design, and Applications;* pp. xvi, 405 p. Elsevier, Oxford; New York, 2003.

2. Z. Yang, J.W. Stevenson, and K.D. Meinhardt, "Chemical Interactions of Barium-Calcium-Aluminosilicate-Based Sealing Glasses with Oxidation Resistant Alloys," *Solid State Ionics,* **160** [3-4] 213-25 (2003).

3. M. Brochu, B.D. Gauntt, R. Shah, G. Miyake, and R.E. Loehman, "Comparison between Barium and Strontium-Glass Composites for Sealing Sofcs," *Journal of the European Ceramic Society,* **26** [15] 3307-13 (2006).

4. A. Flugel, M.D. Dolan, A.K. Varshneya, Y. Zheng, N. Coleman, M. Hall, D. Earl, and S.T. Misture, "Development of an Improved Devitrifiable Fuel Cell Sealing Glass," *Journal of the Electrochemical Society,* **154** [6] B601-B8 (2007).

III.D.2 Glass Composite to Coated Interconnect Seals for Long-Term Chemical Stability

Niladri Dasgupta (Primary Contact),
Bruce Butler, Erinn Sorge
Materials & Systems Research, Inc.
5395 West 700 South
Salt Lake City, UT 84104
Phone: (801) 530-4987 Ext.17; Fax: (801) 530-4820
E-mail: ndasgupta@msrihome.com

DOE Project Manager: Joseph Stoffa
Phone: (304) 285-0285
E-mail: Joseph.Stoffa@netl.doe.gov

Contract Number: ER85202

Start Date: June 30, 2008
End Date: August 13, 2011

Fiscal Year (FY) 2011 Objectives

- Complete long-term (3,000 hours) evaluation of thermal, chemical and mechanical stability of glass-MgO sealing compositions.
- Evaluate mechanical properties of selected glass-MgO compositions.
- Carry-out helium leak tests on gaskets fabricated from selected glass-MgO compositions and Ba-Ca-Al-B silicate (BCAS) glass.
- Evaluate the performance of a stack that incorporates select glass-MgO sealing gaskets and metallic interconnects with Nb-$LaCrO_3$ coating applied on the sealing area.

FY 2011 Accomplishments

- The selected glass-MgO compositions-3 and -5 demonstrated adequate phase stability after holding at 800°C for 2,500 hours.
- Composition-5 demonstrated very stable coefficient of thermal expansion (CTE) after holding at 800°C for 2,500 hours. Composition-3 showed some decrease in CTE, although it was much less than that for BCAS glass.
- Excellent bonding was demonstrated by microscopy at the sealing glass/8 mol% yttria-stabilized zirconia (8YSZ) and sealing glass/coated Crofer interface after holding at 800°C for 3,000 hours.
- The helium leak testing apparatus was upgraded to incorporate automated data acquisition, more accurate pressure sensing and faster heating.
- Helium leak tests were performed using bigger tape-cast glass-MgO gaskets at 800°C and it was demonstrated that in the short-term (less than 1,000 hours) gaskets fabricated from compositon-3 and composition-5 have similar or better sealing ability than BCAS glass.
- Satisfactory sealing performance was demonstrated for a three cell stack tested at MSRI that used sealing gaskets fabricated from compositon-5 and Nb-doped $LaCrO_3$ coating on the sealing area of the stainless steel interconnects.

Introduction

Solid oxide fuel cells (SOFCs) operate in the temperature range 650 to 850°C and typically function under an oxygen chemical potential gradient that develops across the electrolyte. A hermetic seal which prevents the intermingling of the cathode and anode side gases is a critical requirement for planar SOFCs as any leakage leads to reduced system performance, lower power-generation efficiency, poor fuel utilization [1,2] and accelerated degradation of the stack [2]. One popular approach for such seals is to use rigid bonded, specially tailored glass or glass ceramic compositions. The primary challenges in developing such seals are: 1) maintaining proper viscosity in the glass; 2) matching the thermal expansion of the material with that of the primary cell components and stabilizing it as a function of time and temperature; and 3) controlling their reactivity with metal components. An example of state-of-the-art sealing glass is a BCAS glass developed by the Pacific Northwest National Laboratory [3,4] which has a very good CTE match with other SOFC components after short-term crystallization. However the CTE reduces significantly after ageing at 750°C after 1,000 hours. The glass also reacts in contact with common metallic interconnects which results in the weakening of the seal joint. Recent attempts to remove these impediments by design of the glass composition [5,6] have met with limited success. Loehman [7] demonstrated that the flow, adhesion, thermal expansion and reactivity of borate glasses can be controlled by the selective addition of oxide nanoparticles. Similar results were reported by Nielsen et al. [8] for sodium aluminosilicate glasses using nano-MgO filler.

The Phase I effort generally showed the beneficial effects of incorporating MgO in the base BCAS glass

composition. While the maximum benefits in terms of long-term stability were derived in compositions with a threshold amount of MgO, most of the experiments were performed with lower levels of MgO in the glass because of its better fluidity. The first task of the Phase II effort was therefore to make suitable modifications to the base glass composition in order to accommodate larger amounts of MgO in the glass and still maintain a lower viscosity. Accordingly, during the first year of the Phase II effort, two glass-MgO compositions were selected for long-term evaluation of thermal expansion and phase development. Both showed stable thermal expansion and phase composition after 1,000 hours at 800°C. The overall objective during the second year was to obtain similar information after 3,000 hours at 800°C. The compositions were also to be tested for helium leak at 800°C with and without thermal cycling. Finally they were to be incorporated into SOFC stacks in the form of tape-cast gaskets, the stacks run for over 1,000 hours with intermediate thermal cycling and their performance documented. The current report summarizes the results obtained during the second year of the Phase II project as on the date of reporting.

Approach

The overall approach for this project was to select a base-glass which is widely known to be compatible with standard SOFC materials and conditions and to eliminate some of its glaring deficiencies by: 1) adding suitable amounts of nano-MgO; and 2) applying an appropriate protective coating to the area of the metallic interconnect in contact with the glass seal to reduce chemical reaction. It was concluded after the Phase I effort that the addition of a threshold quantity of nano-MgO ensures that a unique phase mix is formed in the crystalline glass that imparts durational stability to the thermal expansion coefficient. The approach in the first year of the Phase II investigation was to suitably modify the base-glass composition so as to ensure that the addition of the required amount of nano-MgO does not adversely affect the wettability and flowabilty of the glass. The other approach was to improve the doped lanthanum chromite protective interconnect coating developed in Phase I by modifying the spray parameters, introducing an infiltration step to reduce porosity and firing the coating in a reducing atmosphere to prevent oxide formation. The approach in the second year of the Phase II work was to complete the long-term (3,000-hour) tests on the two selected compositions and the BCAS glass for comparison. Helium leak tests accompanied by thermal cycling were to be performed at 800°C on the two selected glasses and the BCAS glass. Based on the combined results of all the tests one composition was to be further selected for stack tests. Short and long stack tests were to be performed using gaskets fabricated from the selected glass-MgO composition. The stacks were to be tested for their open circuit voltage, overall performance characteristics at various fuel utilizations and also tested for cross leakage by gas chromatography. The effect of thermal cycling was to be investigated and the performance after 1,000 hours of operation was to be examined. The data obtained was to be compared with a stack using BCAS glass gaskets.

Results

Bars and discs of selected glass-MgO compositions-3 and -5 along with the BCAS glass were held at 800°C for 3,000 hours. The discs were then used for phase analysis by X-ray diffraction (XRD) while the bars were used for determining the CTE. Figure 1 shows the XRD pattern for composition-5 after heat treatment at 800°C for 500, 1,000 and 2,500 hours. The presence of crystalline phases A (squares-wine) and B (circles-magenta) is clearly seen. Comparing the XRD traces for the three durations, it is apparent that the two phases are stable and they dominate the phase spectrum even after 3,000 hours. Table 1 is a comparison of the CTE values for BCAS glass, composition-3 and

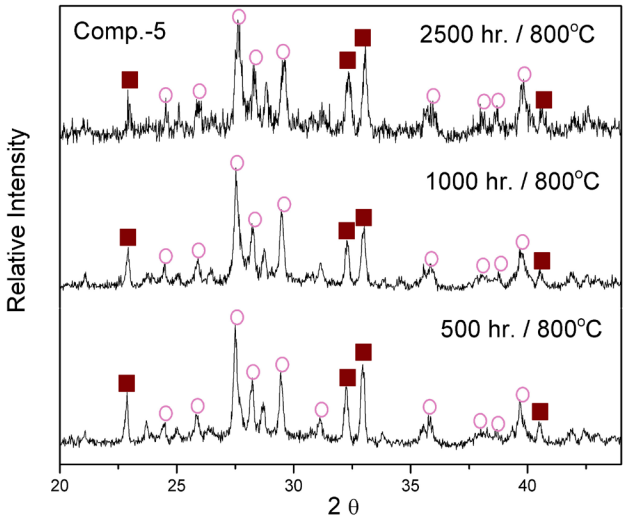

FIGURE 1. XRD Patterns for Glass-MgO Composition-5 Held at 800°C for 500, 1,500 and 2,500 Hours

TABLE 1. A Comparison of the CTE Values of BCAS Glass, Composition-3 and Composition-5 Heated at 800°C for Different Durations

Duration at 800°C (Hours)	BCAS Glass	Comp.-3	Comp.-5
0.5	11.1 x 10^{-6}/°C	11.8 x 10^{-6}/°C	11.8 x 10^{-6}/°C
1500	10.0 x 10^{-6}/°C	12.0 x 10^{-6}/°C	12.0 x 10^{-6}/°C
2500	9.79 x 10^{-6}/°C	11.2 x 10^{-6}/°C	12.0 x 10^{-6}/°C

composition-5 heated at 800°C for 0.5, 1,500 and 2,500 hours, respectively. The CTE of the BCAS glass is seen to reduce by 11.8% when it is held for 2,500 hours at 800°C. This is one of the primary drawbacks for this glass and is known to happen because of the progressive crystallization of monoclinic celsian which has a CTE of 2.3 x 10^{-6}/°C. The CTE for composition-3 actually increases marginally after 1,000 hours of heat treatment and then decreases to 11.2 x 10^{-6}/°C after 2,500 hours of heat treatment. The overall decrease after 2,500 hours is 5.3%. For composition-5 there is actually an increase of 1.7% in the CTE after heating for 1,500 hours and then it remains stable when heated for 2,500 hours. Since the final value is within the desired range of (12-12.5) x 10^{-6}/°C, this may actually result in better sealing properties over longer durations of operation.

The condition of the uncoated and coated metal/glass interface and the bonding of the glass to this interface and the 8YSZ interface is of particular interest. Figure 2 shows a scanning electron microscope (SEM) micrograph of a test specimen where glass-MgO composition-5 is sandwiched between an anode supported SOFC (with the 8YSZ electrolyte in contact with the glass) and a perovskite coated Crofer-22 foil heat treated at 800°C for 3,000 hours. There is obviously significant crystallization of the glass but the 8YSZ/glass as well as the glass/perovskite interface look well bonded. Energy dispersive analysis by X-rays has indicated that there is some oxidation of the metal surface behind the coating and this is expected. The coating has however largely prevented contact between the oxide scale and the glass and thereby avoided

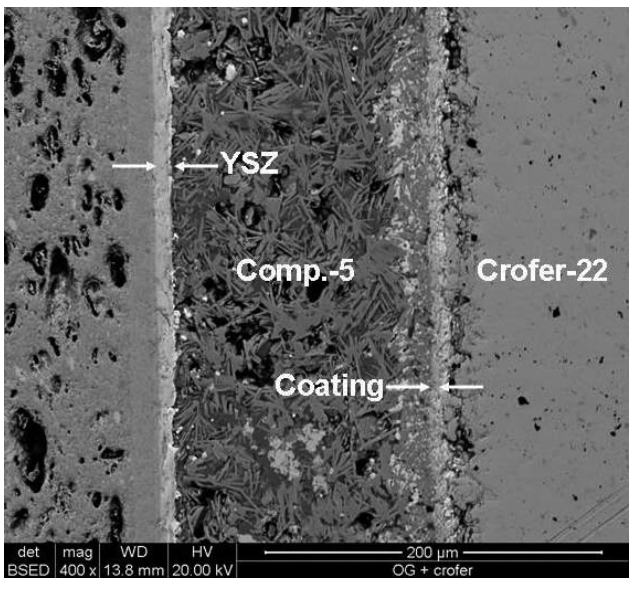

FIGURE 2. SEM Micrograph of Sectional View of a SOFC Cell_Glass-MgO_Crofer-22 (Doped $LaCrO_3$ Coated) Sandwich Heated at 800°C for 3,000 Hours

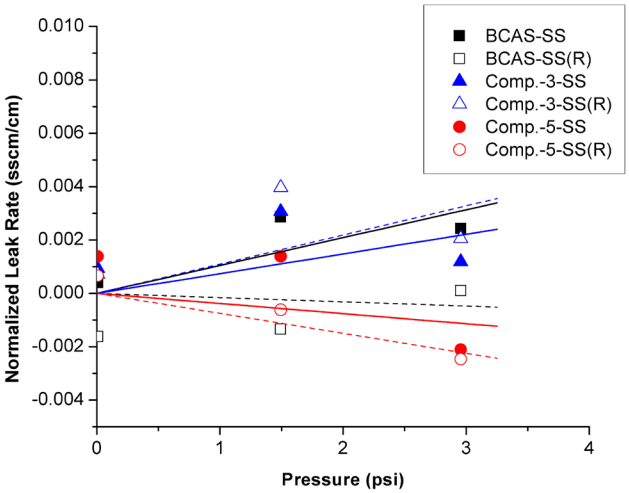

FIGURE 3. Leak Rate versus Pressure Graphs for Sealing Gaskets of BCAS Glass, Compostion-3 and Composition-5

delamination of the interface even after 3,000 hours in air at 800°C.

Leak tests were conducted at 800°C to ascertain helium leak rates at glass-MgO/YSZ, glass-MgO/$LaCrO_3$ and glass-MgO/metal interfaces with thermal cycling. The results for the leak tests on tape-cast gaskets of composition-3, composition-5 and BCAS glass to metal (SS430) are shown in Figure 3. The filled symbols denote the first heating cycle while the corresponding open symbols denote the data points for the second heating cycle after cooling down to room temperature. The lines are best fit lines where the broken lines indicate reheating. BCAS glass is known to provide hermetic sealing with stainless steels at 800°C for shorter durations. The data suggests that all three glasses show minimal leakage with pressure and are comparable in their sealing abilities in the short-term. Thermal cycling does not result in any significant deterioration of the seal. It is however expected that beyond 1,000 hours at 800°C, composition-5 will retain the best sealing ability.

MSRI also assembled a three-cell stack using gaskets of glass-MgO composition-5. Conditioning included binder burnout at 580°C and a temperature excursion to 880°C; stack operation was at 800°C. The stack was not operated at high power output conditions (was not operated near discharge capacity), but rather under a range of fuel and air utilizations to determine stack sensitivity to reductions of fuel and/or oxidant levels. Figure 4 shows resultant polarization curves. Values show minimal curve deviation with increasing fuel and air utilization, indicating satisfactory sealing performance.

Conclusions and Future Directions

The results indicate that glass-MgO composition-5 has the most stable crystalline phases and thermal

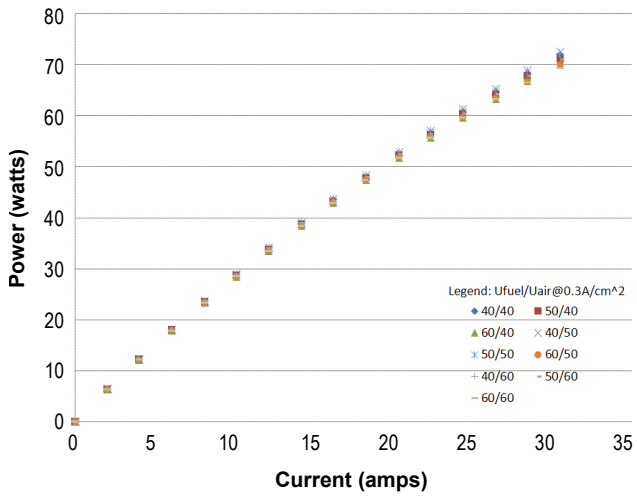

FIGURE 4. Polarization Curves for MSRI Three-Cell Stack Sealed Using Glass Composition-5

expansion coefficients over prolonged durations at 800°C. It also forms clean and stable seal interfaces with the SOFC electrolyte (8YSZ) and Crofer-22 metal foil coated with doped lanthanum chromite. Helium leak tests on glass/stainless steel seal interfaces suggest that compositions-3 and -5 display short-term sealing characteristics that are at par with or better than that of BCAS glass at 800°C. One may reasonably assume that the better stability of the CTE for the above glass-MgO compositions, particularly compositon-5 will impart superior leak resistance over longer durations when compared with BCAS glass. Data obtained from a three-cell stack (sealed with gaskets made from composition-5) tested at MSRI that uses Nb-doped $LaCrO_3$ coating on the sealing area of the stainless steel interconnects indicates satisfactory sealing performance.

Two more short stacks will be evaluated for performance over 1,000 or more hours of operation. One of these will use sealing gaskets made of composition-5 glass and the other will use gaskets of BCAS glass. The results will be compared below and above thousand hours of operation. The seal to coated metal interface will be examined microscopically after the stacks have been dismantled.

FY 2011 Publications/Presentations

1. N. Dasgupta, B. Butler, and E. Sorge, "Effect of MgO Addition on Crystalline Phase Formation and Thermal Expansion of a Barium Aluminosilicate Solid Oxide Fuel Cell Glass Ceramic Sealant," Poster presented at the 11th Annual SECA Workshop, Pittsburgh, Pennsylvania, July 27–29, 2010.

2. N. Dasgupta, B. Butler, and E. Sorge, "Effect of MgO Addition on Crystalline Phase Formation and Thermal Expansion of a Barium Aluminosilicate Solid Oxide Fuel Cell Glass Ceramic Sealant," Oral presentation at the 35th International Conference and Exposition on Advanced Ceramics and Composites (ICACC), Daytona Beach, Florida, January 23–28, 2011.

References

1. T. Iwata and Y. Enami, "Analysis of Fuel Utilization Performance of Round Substrates, Planar Solid Oxide Fuel Cells," J. Electrochem. Soc., 145 (1998) 931.

2. J. Hartvigsen et al., Ceram. Trans., 65 (1996) 279.

3. Z. Yang, J.W. Stevenson, and K.D. Meinhardt, "Chemical Interactions of Barium-Calcium-Aluminosilicate-Based Sealing Glasses with Oxidation Resistant Alloys," Solid State Ionics, 160 (2003) 213-225.

4. K.D. Meinhardt, J.D. Vienna, T.R. Armstrong, and L.R. Pederson, "Glass-Ceramic Material and Method of Making," U.S. Patent No. 6,430,966 (2002).

5. R.K. Brow and D.S. Reis, "Designing Sealing Glasses for Solid Oxide Fuel Cells," ASM Materials Solutions Conference and Exposition, Columbus, Ohio, October 18–20, 2004.

6. R.N. Singh, "Sealing Technology for Solid Oxide Fuel Cells," Int. J. Appl. Ceram. Technol., 4 (2007) 134-144.

7. R. Loehman, "Development of High Performance Seals for Solid Oxide Fuel Cells," SECA Core Technology Program Review, Albany, New York, October 1, 2003.

8. K.A. Nielsen, M. Solvang, S.B.L. Nielsen, A.R. Dinesan, D. Beeaff, and P.H. Larsen, "Glass Composite Seals for SOFC Application," J. Eur. Cer. Soc., 27 (2007) 1817-1822.

III.D.3 Innovative Self-Healing Seals for Solid Oxide Fuel Cells (SOFCs)

Professor Raj N. Singh
University of Cincinnati
Department of Chemical and Materials Engineering
Cincinnati, OH 45221-0012
Phone: (513) 556-5172; Fax: (513) 556-3773
E-mail: Raj.Singh@uc.edu

DOE Project Manager: Joseph Stoffa
Phone: (304) 285-0285
E-mail: Joseph.Stoffa@netl.doe.gov

Contract Number: FE0001390

Start Date: October 1, 2009
End Date: March 31, 2011

Fiscal Year (FY) 2011 Objectives

- Develop self-healing glass composites containing fillers as seals for SOFCs.
- Down-select appropriate filler materials suitable for making glass-composites.
- Determine stability of the most promising self-healing composite glass.
- Complete Phase I and propose work for Phase II.

FY 2011 Accomplishments

- Self-healing glass composites were fabricated using alumina, magnesia, and zirconia fillers. Thermomechanical behaviors of the glass-composites were measured between 25-800°C.
- Alumina and MgO fillers reacted with the glass and found to be unsuitable as fillers. Yttria-stabilized zirconia (YSZ) was stable and a more promising filler material. Stability of the glass-YSZ filler composites was determined by annealing samples up to 1,000 hours in fuel and air environments. Stability of the glass-YSZ composite was demonstrated for 1,000 hours.
- All the objectives of the Phase I project were accomplished.
- Phase II project started based on accomplishments of Phase I.
- These results provide great promise towards meeting the Solid State Energy Conversion Alliance (SECA) goals of seals for SOFC.

Introduction

A functioning SOFC requires seals that prevent electrode leakage and internal gas manifold leakage if internal gas manifolds are utilized. The seals must prevent the mixing of fuel and oxidant streams as well as prevent reactant escape to the surrounding environment. The seal material must be electrically isolating and be mechanically and chemically stable in contact with interfacing cell components in humid dual reducing and oxidizing conditions. Particular importance is the ability to seal between metallic and ceramic components with differing coefficients of thermal expansion (CTE), and do so while exposed to temperature transients over a range from room temperature up to SOFC operating temperature (≈800ºC). This project is developing innovative self-healing sealing concepts for both short- and long-term functionality of SOFCs, addressing the aforementioned issues.

Approach

A novel in situ self-healing sealing glass concept was further advanced in the current Phase I funding cycle of the SECA program to demonstrate in situ self-repair capability of the glass seals. Seal tests performed earlier displayed excellent seal performance including in situ self-repair of cracked/leaking seals. The self-healing concept requires glasses with low viscosity at the SOFC operating temperature of 800°C but this requirement may lead to excessive flow of the glass under load in areas forming the seal. To address this challenge, a modification to glass properties such as creep via addition of particulate fillers is proposed and pursued in the current project. The underlying idea is that non-reactive ceramic particulate filler is expected to form glass-ceramic composite and increase the glass transition/glass softening temperatures and seal viscosity thereby increasing the creep resistance of the glass-composite seals under load. In addition, the incorporation of an appropriate filler can affect the CTE of the glass-ceramic thereby providing additional flexibility for developing sealing glasses with the optimum expansion mismatch among materials forming the seal thereby reducing mismatch stresses and improving seal reliability. This report summarizes progress made towards advancing this concept.

Results

A filler phase is required for sealing glasses as a part of this activity. The filler phase should be oxidation resistant at 800°C, strong, and have expansion behavior

close to the sealing glass. Three types of fillers – Al_2O_3, YSZ, and MgO – were selected and used for the initial screening effort in the project because these ceramics have expansions close to or higher than the glass and are electrical insulators. Al_2O_3 and YSZ have expansions slightly smaller than the glass and MgO has a higher value than the glass. Samples of glass-composites containing 30% by weight of Al_2O_3, YSZ, or MgO powders were fabricated using tape casting, lamination, and sintering to make dense glass-ceramic composites. The composites were then characterized for CTE between 25-800°C and crystallization by X-ray diffraction. These results suggested that the best filler phase for further studies is YSZ because MgO reacted with the glass and Al_2O_3 produced a low CTE. The data from glass-alumina composite also suggested reaction of alumina with the glass leading to formation of aluminum silicate. From these results YSZ was down-selected for further studies. Composites of glass-YSZ containing 10-30% YSZ were prepared for further characterization, CTE measurements, and stability at 800°C as a function of time upon exposure in air and humid fuel environments for times up to 1,000 hours.

The CTE of glass-YSZ composites was measured after processing. The glass transition and softening behaviors also showed a significant change because of the addition of YSZ. Both parameters increased upon YSZ addition. In particular the softening temperature increased from ~560°C to 750°C with 30% YSZ addition. This is very promising because YSZ addition should provide superior load-carrying capability for the glass-composite seal. The CTE decreased from 10.4 to 9.3 ppm upon addition of 30% YSZ to the glass. An optimum level of YSZ in a glass can be determined from sealing ability and the overall requirement of resistance to deformation of the composite seal under load.

Based on these findings a glass-30% YSZ composite was selected for assessing its stability at high temperature of 800°C. This glass-YSZ composite was placed on an YSZ plate and annealed in air and in moist fuel environments for 1,000 hours at 800°C to demonstrate stability. In addition, crystallization behavior upon annealing was evaluated by X-ray diffraction along with the CTE data.

Figure 1 shows the effect of annealing at 800°C in air on the CTE of glass-YSZ composite in the as-sintered state and after 1,000 hours of annealing. There is an insignificant change to the expansion behavior and glass transition/softening temperatures indicating stability. A similar sample was annealed at 800°C in moist fuel environment to assess stability. Figure 2 shows data for samples annealed in moist fuel at 800°C for 1,000 hours. It also shows insignificant change to the expansion behavior and glass transition/softening temperatures indicating excellent stability.

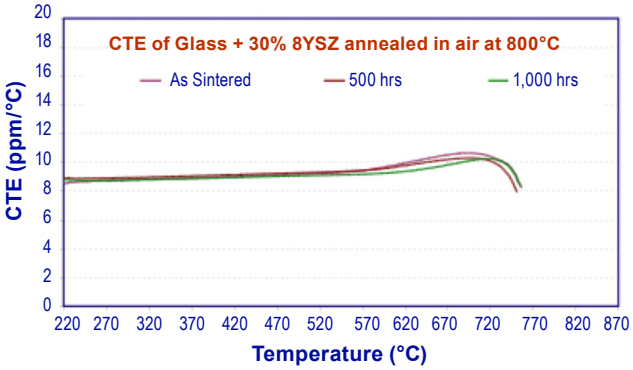

FIGURE 1. Effect of Annealing in Air at 800°C on the Coefficient of Thermal Expansion of Glass-30% YSZ Composite

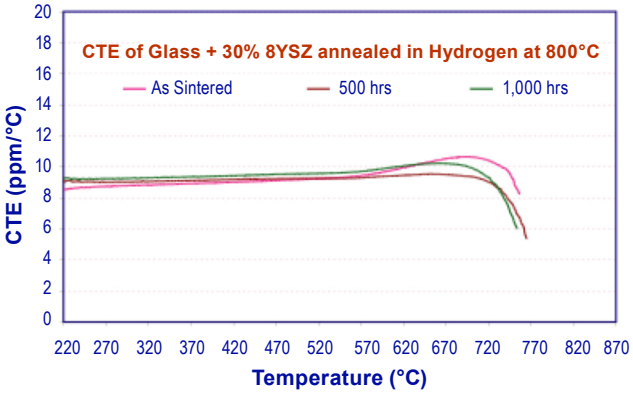

FIGURE 2. Effect of Annealing in Fuel (Ar-4% H_2-6% H_2O) Environment at 800°C on the Coefficient of Thermal Expansion of Glass-30% YSZ Composite

Figure 3 shows the X-ray diffraction patterns from glass-YSZ composite in the as-sintered state and after annealing for 1,000 hours. No other crystalline peaks except for YSZ are evident from the X-ray data indicating stability of the YSZ filler against reaction with the glass up to 1,000 hours of exposure.

These results indicated stability of the glass-YSZ composite in both air and fuel environments for 1,000 hours at 800°C. The results on stability of self-healing glass-YSZ composite based on CTE and X-ray diffraction suggest that the glass-YSZ composite should also be stable against reaction with YSZ electrolyte membrane at 800°C over an extended time period. In this study, stability of the glass-YSZ composite was also investigated by placing a glass-30% YSZ composite on a dense YSZ membrane and then fabricating a glass-composite/YSZ seal by sintering the sample at 800°C for 2 hours. Then the sample was cooled to room temperature, annealed in air and fuel environments for 1,000 hours, sectioned, and polished to reveal the glass-composite/YSZ interface for examination

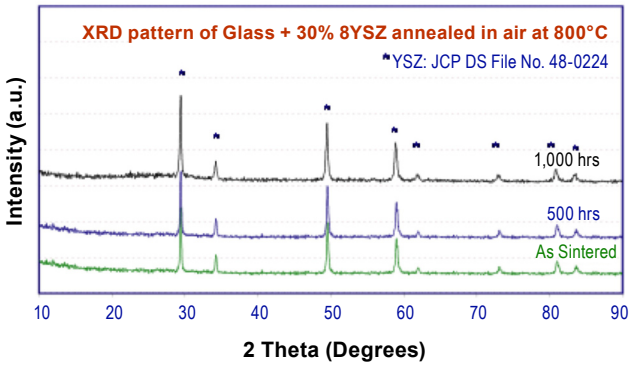

FIGURE 3. X-ray Diffraction from Glass-YSZ Composite in the As Fabricated State and after Annealing in Air at 800°C for 1,000 Hours

by scanning electron microscopy (SEM). The results showed an interface between glass-YSZ composite and YSZ substrate without any reaction between the glass-composite and YSZ substrate indicating stability in contact with a dense YSZ membrane. Energy dispersive X-ray spectroscopy analysis of the interface did not show any evidence of interdiffusion of elements into each other thereby further confirming the stability of the glass-composite in contact with the electrolyte.

While a significant progress is demonstrated by the results of Phase I of the project, there remains a healthy skepticism on whether glass-YSZ composite seals displaying self-healing response have sufficient long-term durability and life to meet the SECA goals of 40,000 hours. The stability of the sealing materials were determined in fuel and air at 800°C for 1,000 hours but the longer-term durability over thousands of hours require further development and testing. Consequently, the primary objectives of Phase II project are to: 1) further develop the self-healing glass-YSZ composites with long-term durability through testing in air and fuel environments; and 2) characterize long-term stability of the glass-YSZ composites through ex situ SEM and X-ray diffraction analyses. The proposed project will utilize successful approaches developed in Phase I on materials selection, property measurements, environmental stability considerations, and analytical characterization for Phase II work.

Conclusions and Future Directions

- The self-healing glasses with fillers were fabricated and studied. Composites with alumina and magnesia fillers showed reactivity with the glass and inappropriate CTE for making seals for SOFC.
- Glass-composites with zirconia filler showed good expansion matching and stability against reaction during processing. This system was down-selected for further testing.
- Glass-zirconia composites demonstrated stability for 1,000 hours upon annealing in air and fuel environments at 800°C.
- Plans are to further pursue long-term stability of the self-healing glass-composites at 800°C in SOCF testing environment as a part of Phase II project.

FY 2011 Publications/Presentations

1. Program Quarterly Reports between October (2009) – March (2011).

2. Phase-I Annual Reports (July, 2010 and 2011).

3. Phase I Progress Report (December 2010).

III. SECA CORE RESEARCH & DEVELOPMENT

E. Cross-Cutting Materials, Testing, and Manufacturing

III.E.1 Testing and Evaluation of Solid Oxide Fuel Cells in Extreme Conditions

A. Alan Burke (Primary Contact),
Louis G. Carreiro
Naval Undersea Warfare Center (NUWC),
Division Newport
1176 Howell Street, Bldg. 1302/1
Newport, RI 02841
Phone: (401) 832-6675; Fax: (401) 832-6202
E-mail: Adrian.Burke@navy.mil

DOE Project Manager: Maria Reidpath
Phone: (304) 285-4140
E-mail: Maria.Reidpath@netl.doe.gov

Subcontractor:
Delphi Corporation, Troy, MI

Collaborator:
NASA Lyndon B. Johnson Space Center/EP3,
Houston, TX

Contract Number: NT43247

Start Date: January 1, 2011
End Date: December 31, 2011

Fiscal Year (FY) 2011 Objectives

- Demonstrate successful cold start-up of Delphi fuel processor using air/methane burner.
- Use hot, steam-rich anode exhaust from solid oxide fuel cell (SOFC) stack to drive (heat) steam reforming in Delphi's Gen 8T fuel processor.
- Demonstrate steady steam reforming of S-8 (synthetic diesel fuel from Syntroleum), JP-10, and methane fuels to simulate half the proposed anode recycle loop for an undersea vehicle SOFC power system.
- Demonstrate pure oxygen-blown catalytic partial oxidation (CPOX) reformer in conjunction with SOFC stack for National Aeronautics and Space Administration (NASA)-specific missions.

FY 2011 Accomplishments

- Established basis for proposing methane as a fuel for unmanned, underwater vehicles (UUVs) launched from surface ships. The usage of methane as opposed to gasoline or diesel-type fuels could also be extended to other military platforms such as auxiliary power units and small vehicles. This could expedite the usage of highly efficient SOFC-based platforms in advanced military settings as well as meet energy security and conservation goals mandated by U.S. Navy leadership.
- Demonstrated adequate steam reforming of JP-10, S-8, and methane fuel streams using a Delphi Gen 8T reformer. Concluded that methane-based systems offer the best prospect of successfully testing first-generation SOFC-powered, undersea vehicles.
- Demonstrated pure oxygen-blown CPOX reformer and integration with a 30-cell Delphi Gen 3.2 SOFC stack showed a reactant-based specific energy of 4,900 kJ/kg for a NASA-specific application. With ~90% methane utilization, an efficiency of 45% was attained based upon the lower heating value (LHV) of methane fed into the CPOX reformer.

Introduction

A refined analysis of fuel options was conducted, based upon prototyped hardware for a SOFC-powered undersea vehicle. Sulfur-free fuels such as S-8 and JP-10 were contrasted against methane. With waste heat being at a premium in such a highly efficient system (>70%), it has been determined that steam reforming of liquid fuels will likely require an additional burner or CPOX reforming, which in turn decreases system efficiency and energy metrics. Using LNG (liquefied natural gas) as the fuel maximizes the hydrogen-to-carbon ratio, thus decreasing the amount of oxygen storage and carbon dioxide sorbent required on board. In addition to these energy gains, the greatest advantage of using methane might be that waste heat can directly be used for steam reforming both in the stack and throughout the CO_2 sorbent bed. A gaseous fuel feed should be more resilient towards carbon deposition, power transients, and flow disruptions.

In addition to providing UUV-specific advantages, a wider adoption of natural gas/methane usage would aid in meeting energy security and conservation goals established by U.S. Navy leadership. Versus diesel or gasoline, methane has a lower carbon footprint and can more easily be synthesized from renewable resources. Natural gas or other light hydrocarbon fuels would also open the door to SOFC and other advanced energy solutions that offer higher efficiency than standard diesel or gasoline generators. As shown in this work, SOFC systems utilizing methane and pure oxygen can also extend to space applications that interest NASA.

Approach

For UUV-related tests, a Delphi Gen 3.2 SOFC stack was integrated with a Delphi Gen 8T fuel processor. The aim was to utilize the latent heat in the anode exhaust to drive the steam reforming of S-8 and JP-10 liquid fuels as well as gaseous methane fuel. The combustor channel was also used to ensure proper reformer operating temperature, but this is not likely to be feasible for an actual UUV power system due to the limited oxygen supply. The steam reformer replenishes the anode reformate and results in an anode recycle loop that is continuous and highly efficient. In a fully operational system, reformate is directed back into the SOFC stack via a high temperature recycle blower (see previous reports and papers for the full system layout). Carbon dioxide sequestration in a high temperature scrubber was not employed in these tests.

In NASA-related testing, a Delphi Gen 3.2 SOFC stack was integrated with a Delphi CPOX fuel processor and tested. The goals were: 1) to demonstrate CPOX reformation of methane using pure oxygen instead of air; and 2) to use the CPOX reformate in an SOFC stack to achieve high efficiency. This test was a baseline study for NASA, which is considering single-pass SOFC systems for space applications that utilize methane and pure oxygen as reactants.

Results

An SOFC stack was integrated with a steam reformer that was placed downstream of the stack and hot anode exhaust gas was used in an attempt to heat the reformer to its minimum operating temperature of 600°C *without using the combustor*. The stack was unable to provide sufficient heat to the reformer at an acceptable rate so it was decided to let the stack run overnight in order ascertain the maximum temperature the reformer could achieve. Unfortunately, the reformer inlet temperature never exceeded 400°C (which is too low to initiate liquid fuel reforming). Subsequent tests focused on isolated fuel processor testing to steam reform JP-10 and S-8 liquid fuels. To heat the reformer, methane gas was combusted with air in the combustor channel of the fuel processor. While Delphi generally uses a heat exchanger tied into the combustor outlet for diesel fuel vaporization, this option was not available. Instead, superheated steam was used to vaporize the S-8 or JP-10 feed at the reformer inlet. During the steam reforming operation, the fuel processor performed quite well with the combustor turned on. Hydrocarbon slippage ensued when the reformer outlet temperature dropped below 500°C. Reformer efficiency is based upon the LHV of fuel outlet versus the LHV of fuel into the reformer plus methane to the combustor. In some cases the efficiency exceeds 1.0 because the calculation did account for the superheated steam energy content which partially drove the steam reformer. This hot steam would be provided by the SOFC exhaust in an actual UUV system. Atomic mass balances were calculated to +/- 5% accuracy, with error attributed to gas chromatograph (GC) measurement accuracy, minor fuel impurity/degradation, and slight carbon deposition/coking.

Tests were also performed on steam reforming of methane gas with results shown in Table 1. The "H_2 Balance" column in Table 1 refers to the calculated outlet versus controlled inlet mass flow ratio for hydrogen. Ideally, this value should be one if all species are measured and controlled accurately. In this study, roughly 40-50% of the methane was reformed while producing a favorable recycle stream composition for the SOFC stack. However, the energy contribution from

TABLE 1. Reformer performance on steam reforming of methane fuel (CH_4). The SOFC stack was fed with 20 sL/min H_2, 4 sL/min CO_2, and 4.8 g/min steam. Stack current was held at 45 amps. The reformer bypass temperature (T) refers to annular flow space in the combustor flow path.

CH_4 feed, g/min	Steam feed, g/min	Dry reformer exhaust, L/min	S/C at reformer outlet	Reformer bypass T, °C	Dry mol% CH_4 in outlet	Reformer efficiency, %	H_2 balance
0.00	4.8	13.98	4.41	454	2.43	57.9	1.07
0.00	4.8	13.26	4.44	440	3.38	56.7	1.06
0.00	4.8	12.58	4.51	411	4.70	62.7	1.05
1.00	4.8	17.13	3.19	427	2.49	62.7	1.02
1.00	4.8	15.38	3.40	432	5.92	64.0	1.03
1.00	4.8	15.48	3.41	431	6.69	73.7	1.04
2.00	4.8	19.17	2.60	420	5.51	68.8	1.02
2.00	4.8	19.70	2.56	438	4.60	73.2	1.01
3.00	4.8	21.78	2.12	448	7.46	71.8	1.01
3.00	4.8	21.09	2.15	450	7.80	73.0	1.00
3.00	4.8	21.23	2.17	450	8.37	57.9	1.02

the methane burner reached 1.33 kW, which approached the limits for the combined CO_2 scrubber and SOFC stack thermal output. Thermal integration of SOFC stack and CO_2 scrubber to drive methane reforming will be critical to achieve system efficiency and high energy storage metrics for a UUV. While a burner for continual supply of 1.3 kW will not be available, addition of a smaller scale burner could be advantageous, especially if it can be used to ensure a waste stream that is entirely converted to water and CO_2 (so that the anode recycle loop can be vented for water collection without losing fuel value).

In the NASA-related tests, the CPOX was initiated after the SOFC temperature exceeded 700°C. During CPOX start-up, the CPOX exhaust was diverted from the SOFC stack until stable reformate was produced, as determined by reformer operating temperature (>590°C). Pure hydrogen gas was fed to the SOFC stack during CPOX start-up and flow stabilization. Once steady reformate was being produced, the CPOX outlet was diverted back to the SOFC and the hydrogen flow was turned off. Due to the low steam-to-carbon ratio (S/C) in the CPOX reformate and its potential for carbon deposition, the stack only briefly remained at open circuit. Current was ramped at roughly 2 amps every minute to achieve the steady-state performance summarized in Table 2. In this case, the stack temperatures and CPOX outlet temperature needed to be monitored to ensure acceptable SOFC thermal gradients and proper reformate production, respectively. The core stack temperature was kept below 850°C, and the furnace set point was decreased to aid in cooling the stack at high current excursions.

The peak efficiency was near 45%, which was achieved while drawing 50 amps. However, cells 1, 3, 5 and 13 suffered from fuel starvation at this current. Reducing the current by only one amp to 49 amps restored stable voltages. For NASA's application,

TABLE 2. Peak Performance Demonstration

	Peak Performance	Notes
Steady-State Feeds into CPOX Reactor	CH_4 Flow: 5.1 SLPM N_2 Flow: 0 SLPM O_2 Flow: 3.3 SLPM O/C = 1.30	Fuel flow slightly increased from steady-state to meet original O/C target
SOFC Stack with Cathode Feed of 5.5 SLPM Pure O_2	46 Amps 85% CH_4 Utilization 86% O_2 Utilization ~ 0.88 V/cell 1210 Watts ~ 43% $CH_{4,\ LHV}$	Stack was also pushed to 50 amps to achieve ~90% fuel utilization & 45% efficiency, but cells 1,3,5, and 13 suffered from fuel starvation
SOFC Exhaust	2.4 SLPM H_2 (16%) 8.4 SLPM H_2O (50.5%) 4.1 SLPM CO_2 (27%) 1.0 SLPM CO (6.5%)	Mass balance >95%

SLPM - standard liters per minute

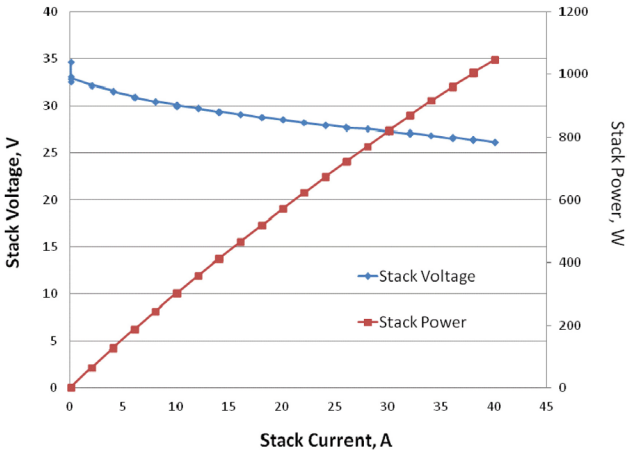

FIGURE 1. IV plot for stack performance using CPOX reformer and pure oxygen. Anode inlet feeds to the CPOX reformer were 3.3 L/min O_2 and 4.9 L/min CH_4. Cathode inlet feed was 5.5 L/min O_2.

45% efficiency with 90% fuel utilization results in a theoretical reactant specific energy of:
45% * 802 kJ/mol_{CH4} / (16 g/mol_{CH4} + 64 g_{O2}/mol_{CH4}) = 4500 kJ/kg (= 1250 W-hr/kg).

A gradual increase in current was used to generate the current-voltage (IV) plot shown in Figure 1. The fuel and oxygen feeds were held constant during this IV plot.

Conclusions and Future Directions

For the UUV application, heating the steam reformer solely by hot anode exhaust gas appears to be a non-starter for liquid hydrocarbon-fueled systems. Oxygen conservation in the UUV system design is also a concern and it appears that at least some level of CPOX operation or supplemental burner will be required to drive the steam reforming process for liquid fuels. In addition to reforming-specific heating issues, vaporization of the liquid fuel feed into the reformer remains a concern, especially during start-up. JP-10, essentially a single component compound, would favor better vaporization control because of its single boiling point as compared to standard diesel or S-8 fuel. However, some coking appears unavoidable, and initial vaporization during start-up will likely require battery-driven heaters or some combustion process that is vented instead of being directed into the SOFC stack. An alternative is to use methane, which would lower amount of CO_2 generated and help ensure that no significant coking within the SOFC stack occurs during power level transients or fuel flow instabilities. Additionally, methane could be reformed either by internal SOFC reforming or by catalyst dispersed over the scrubber section. This would allow reforming to occur wherever temperature and species concentrations are appropriate instead of having to direct heat to specific locations for fuel vaporization and reforming, as

is the case with liquid fuels. Testing in 2011 will focus on full system demonstrations using methane as the fuel.

Targeted metrics were achieved, showing that efficiency approaching 45% with fuel and oxygen utilizations near 90% is possible. However, uncertainties still remain regarding optimized CPOX design and operation using pure oxygen. An optimized, pure-O_2 CPOX design is also of interest to the Navy and could be valuable for system start-up.

Special Recognitions & Awards/Patents Issued

1. Division Newport Annual Award for Excellence in the Area of Basic and Applied Research

FY 2011 Publications/Presentations

1. "Analysis of Fuel Options for SOFC-based Power Systems in Undersea Vehicles," Presentation and Paper, 219th Electrochemical Society Meeting & Twelfth International Symposium on Solid Oxide Fuel Cells (SOFC –XII), Montreal, Quebec, Canada, May 1–6, 2011.

III.E.2 Manufacturing Analysis of SOFC Interconnect Coating Processes

Matthew M. Seabaugh (Primary Contact), Michael J. Day, Sergio Ibanez, Kellie Chenault, Lora Thrun, Neil Kidner, and Scott L. Swartz
NexTech Materials, Ltd.
404 Enterprise Drive
Lewis Center, OH 43035
Phone: (614) 842-6606; Fax: (614) 842-6607
E-mail: m.seabaugh@nextechmaterials.com

DOE Project Manager: Briggs White
Phone: (304) 285-5437
E-mail: Briggs.White@netl.doe.gov

Contract Number: SC0001208

Start Date: May 12, 2010
End Date: May 2011

Fiscal Year (FY) 2011 Objectives

- Develop and production-validate cost models for aerosol spray deposition (ASD) coatings to address the range of metallic interconnect (IC) production volumes (1,000 – 100,000 parts/month) anticipated as the solid oxide fuel cell (SOFC) market evolves.
- Develop customer-specific cost curves (5-year forecasts).
- Identify manufacturing strategies to reduce volume manufacturing costs.
- Demonstrate ASD-coated IC performance to reinforce the value proposition for Solid State Energy Conversion Alliance (SECA) teams.
- Identify key coated IC failure mechanisms and develop lifetime predictive models.
- Create and validate accelerated testing protocols to simulate 40,000-hour service.
- Develop a refined firing condition to maintain a high quality protective coating while preventing resistive scale formation on any area of the IC left uncoated.

FY 2011 Accomplishments

- Refined cost and manufacturing models to encompass volumes from prototyping through pilot-scale production and full volume production.
- Created metallic IC SOFC market forecast and demand curves at various stages of commercialization (immediate, intermediate and long-term) defined.
- Defined key process limits and lifetime stability tests in progress (>1,500 hours operation at 800°C in both single and dual-atmosphere configurations).
- Tailored firing processes to prevent the formation of a deleterious resistive scale on any uncoated areas of the IC.
- Identified key failure mechanisms and acceleration factors for metallic ICs. Predictive lifetime models successfully applied to long-term stability tests.
- Integrated coating technology into SOFC stacks from three to five cell short stacks up to 1 kW stacks on concurrent Department of Defense and commercial demonstration efforts. More than 40 stacks have been built using the coating technology.

Introduction

The adoption of oxidation resistant, high-temperature alloys as alternatives to traditional ceramic interconnect materials for intermediate temperature SOFC provides a path for DOE SECA teams to meet these aggressive cost targets for SOFC stacks. The IC cost has been targeted at approximately 20% of SOFC stack cost.

Chromia-forming ferritic stainless steels are a leading metallic IC candidate due to their protective chromia scale, low cost and thermal expansion compatibility with other stack components. Engineered alloy formulations such as Crofer 22APU and AL SS441-HP have further improved oxidation resistance through the formation of dual-phase native scales. However, to meet SECA lifetime performance targets low cost, protective coatings for the metallic systems and stack components will likely be necessary. Current coating technologies cost tens to hundreds of dollars per part, making clear the need for a manufacturing assessment and optimization of interconnect coating processes.

Approach

Phase I assessed the viability of five competing coating technologies. The analysis identified ASD as a commercially viable (<$2/part at 400 MW annual stack production volumes), high value method to apply protective coatings to metallic interconnects.

Work during FY 2011 has built upon the Phase I results, with emphasis on driving the technology towards commercialization. Cost modeling/product planning has continued to be refined, with barriers to volume production identified. The technical focus has been on addressing specific challenges that impede successful adoption of coated metallic IC and application-scale performance validation.

Results

The manufacturing cost models analyses developed in Phase I continue to be refined to address the range of production volumes anticipated as the SOFC market evolves, from prototyping through pilot-scale production and full volume production. An example of one such cost model curve developed in coordination with a commercial customer is shown in Figure 1. The three regimes of production correspond to Stage I: Prototyping (1-1,000 parts/month), Stage II: Outsourced coating runs (1,000-100,000 parts/month), and Stage III: Continuous Component Coating (>100,000 parts/month). Manufacturing strategies within each of these regimes have been identified to reduce volume manufacturing costs.

For many SOFC applications it is undesirable to coat the entire IC. The firing conditions used in Phase I were not sufficient to prevent the formation of a thick, resistive chromia scale on any uncoated regions of the IC including the anode side of the IC. As a result, these regions are resistive and pose issues for integration into SOFC stacks. Additional processing, either using a protective layer to mask uncoated areas or post-treatment to remove the scale would be required. A better approach is to prevent chromium oxide from forming by tailoring the firing cycle. A proprietary firing process has been developed capable of achieving high quality $(Mn,Co)_3O_4$ (MCO) spinel coatings with acceptable electrical performance while preventing the formation of chromia on any area left uncoated.

To demonstrate the effectiveness of the new firing process, MCO coatings deposited by ASD on a range of ferritic steel substrates (both sheet and powder metallurgy substrates) and fired with the new firing process have been electrically tested in both single and dual-atmosphere configurations. The coatings have demonstrated very good initial electrical performance and long-term stability (>1,500 hours). A representative area-specific resistance (ASR) versus time plot is shown in Figure 2 for MCO-coated AL SS441 tested in humidified air at 800°C.

By correlating electrical ASR behavior with microstructural evolution within the coating and scale during high temperature oxidation, predictive lifetime models based on the mechanical and electrical degradation of the coating have been developed. These oxidation-based models have been continuously validated against the long-term stability experiments. Figure 3 shows the long-term ASR behavior of two MCO-coated samples tested in humidified air at 800°C. ASR versus √time for both samples have a linear dependence indicating that growth process is diffusion controlled and can be modeled with parabolic oxidation kinetics. For both samples the predicted ASR at 40,000 hours is less than 50 $m\Omega.cm^2$.

Understanding the underlying mechanisms that control coating behavior has allowed acceleration factors to be identified. In parallel to electrical tests, a series of oxidation weight-gain experiments under both nominal (800°C) and accelerated (900°C) conditions has been started to support the oxidation-based degradation models. Preliminary data is shown in Figure 4 for MCO-coated and uncoated AL SS441 substrates. The MCO-coated samples show significantly improved oxidation resistance. The accelerated test condition of 900°C results in a significant increase in oxidation, greatly speeding up the time for process validation. Figure 5 shows MCO-coated versus uncoated AL SS441 substrates after 200 hours in air at 900°C. The uncoated

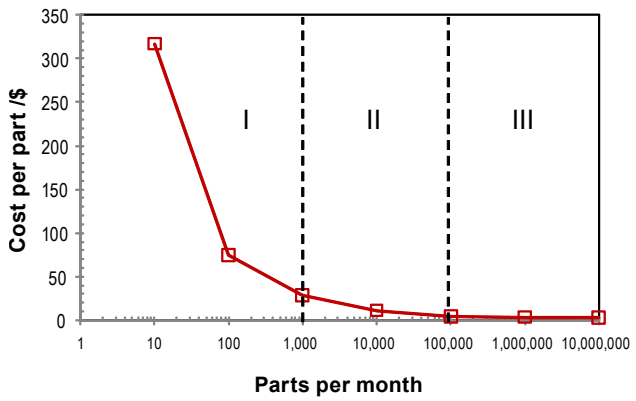

FIGURE 1. Anticipated Cost Curve for ASD Coated Metallic ICs of Active Areas <400 cm^2

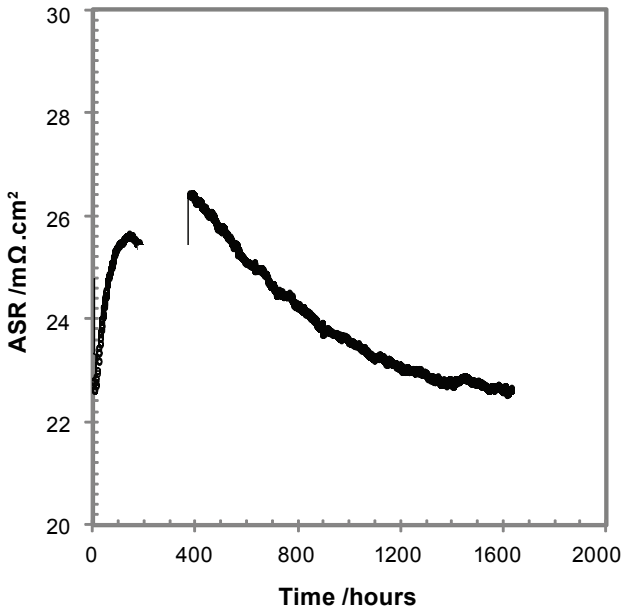

FIGURE 2. Long-Term ASR Trend for 10 μm MCO-Coated AL SS441 Sample Tested in Humidified Air at 800°C

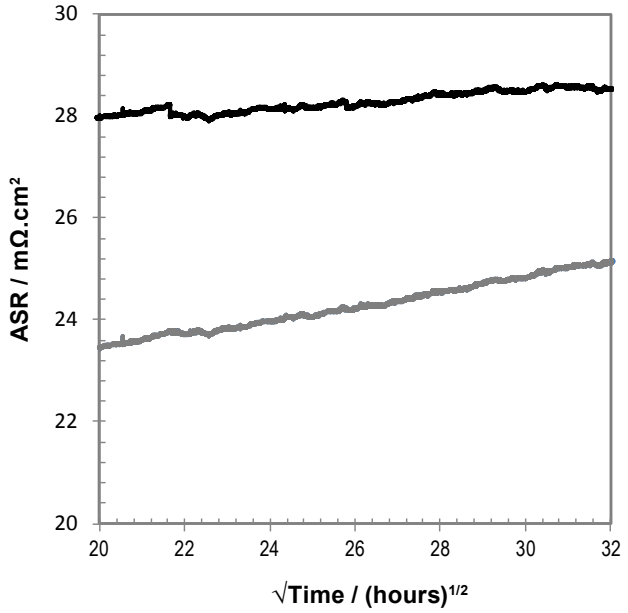

FIGURE 3. Long-Term ASR Behavior of Two MCO-Coated Samples Described with a Diffusion-Limited Oxidation-Based Model

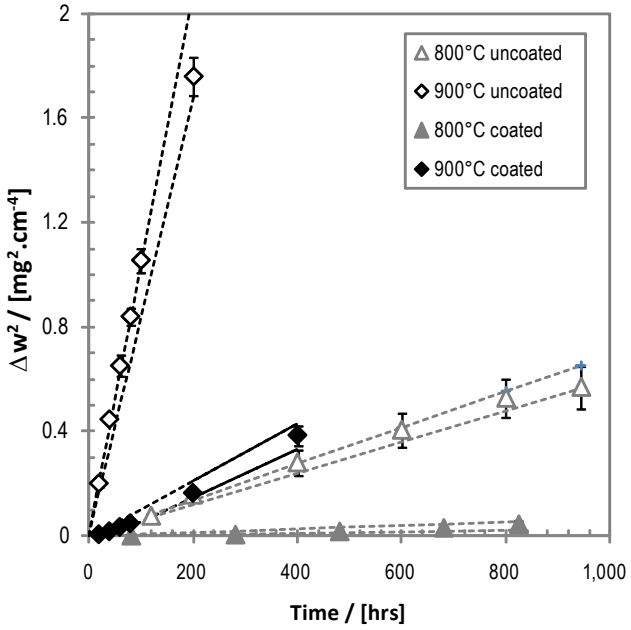

FIGURE 4. Oxidation Weight Gain of AL SS441 with and without 10 μm MCO Coating as a Function of Exposure Time at 800°C and 900°C in Air

sample shows significant spallation, whereas the coated sample displays no indication of spallation.

Conclusions and Future Directions

Production validated cost models for ASD coatings at various production volumes have been developed

FIGURE 5. Coated and Uncoated AL SS441 Substrates after Accelerated Oxidation at 900°C for 200 Hours in Air

that meet SECA cost targets. The effectiveness of ASD coatings have been demonstrated through long-term electrical testing in both single- and dual-atmosphere configurations and parallel oxidation weight gain experiments. Accelerated testing protocols are allowing expeditious experimental validation of oxidation kinetics and prediction of coating lifetime.

Future work will focus on addressing technical hurdles to reinforce the value proposition of the ASD coating approach for SECA teams, for example, masking components to selectively apply multiple coatings to components. Another objective is to extend the coating approach beyond planar ICs to include current collector meshes and non-line of sight surface features such as holes and trenches.

Continuous improvement in coating quality and performance through optimization of the MCO powder, suspension formulation and spray/firing conditions will be coupled with an emphasis to identify and drive process optimization for high volume manufacturing.

FY 2011 Publications/Presentations

1. M. Seabaugh et al., "Oxide Coatings for Metallic SOFC Interconnects," 8th International Symposium on Solid Oxide Fuel Cells (SOFC): Materials, Science, and Technology, Daytona, Florida, January 27, 2011.

2. M. Seabaugh et al., "Protective Oxide Coatings for Metallic SOFC Interconnects," 219th ECS Meeting, Montreal, Quebec, Canada, May 6, 2011.

III.E.3 Manufacturing System Design Analysis of SOFC Stacks

Lora B. Thrun (Primary Contact),
Scott L. Swartz, Michael J. Day
NexTech Materials, Ltd.
404 Enterprise Drive
Lewis Center, OH 43035
Phone: (614) 842-6606; Fax: (614) 842-6607
E-mail: l.thrun@nextechmaterials.com

DOE Project Manager: Briggs White
Phone: (304) 285-5437
E-mail: Briggs.White@netl.doe.gov

Subcontractors:
Xigent Automation Systems, Lewis Center, OH
buyCASTINGS.com, Miamisburg, OH

Contract Number: SC0004845

Start Date: July 19, 2010
End Date: March 19, 2011

Fiscal Year (FY) 2011 Objectives

- Complete roadmap for manufacturing of solid oxide fuel cell (SOFC) stacks at 500 MW gross volume to meet Solid State Energy Conversion Alliance (SECA) $175/kW manufactured stack cost target.
  - Determine top four opportunities to reduce stack cost and manufacturing risk including a timeline for implementation.
  - Rank cost reduction tasks on basis of technical risk, cost reduction and investment.
  - Identify manufacturing scale-up campaigns required to support manufacturing level.
- Complete analysis of commercial manufacturing of planar SOFC stacks, with 500 cm^2 active area cells, 20 kW module design and metallic interconnects. The analysis will include:
  - Cost projections of component and stack manufacture at the 500 MW gross volume.
  - Specified materials, processes and equipment, with automation to proportional to labor.
  - Make vs. buy strategies for components, including quality control/quality assurance for production/procurement.
  - Plant layout and logistics (materials, outsourced components and services, and overhead).
- Determine the most cost-effective and low risk approaches for component manufacturing to meet SECA $175/kW manufactured stack cost target.

FY 2011 Accomplishments

- A detailed process-driven assessment of manufacturing costs of 20 kW-scale planar SOFC stacks was performed at an annual manufacturing volume of 500 MW.
- Cell cost models were established for both NexTech's electrolyte-supported *FlexCell* and anode-supported cells, using SECA provided raw material costs. Using these models, cell manufacturing costs were forecasted to be in the range of $28 to $30 per kW at the 500 MW/year-scale.
- A stack assembly process, and corresponding facilities layout, was defined and all equipment identified in order to determine accurate cost contributions to the stack manufacturing process.
- A comprehensive cost model was established for NexTech's 20 kW-scale SOFC stack, forecasting a total stack manufacturing cost of $166 per kW, validating SECA's cost target of $175/kW at high volume production scale.

Introduction

SOFCs present an opportunity to significantly enhance the efficiency of energy generation from fossil and renewable fuels. Demonstration systems have been fielded for power output ranging from tens of watts to hundreds of kilowatts. SOFC systems offer exceptional value propositions for combined heat and power at the small scale (<25 kW) and integrated power generation using gas and steam turbine bottom-cycling in large distributed and central power applications. SOFC technology also is being actively developed for military applications, based on the potential for step-function improvements in both efficiency and reliability of power systems operating on military logistic fuels.

For SOFCs to be successfully commercialized, the path to volume production must be clearly understood, the cost obstacles identified and overcome. Demonstration systems have been built using laboratory and pilot-scale manufacturing processes unsuited to large-scale manufacturing. These approaches allow critical demonstrations and performance assessments, but they are too expensive for production. Manufacturers, end users and other stakeholders have been cognizant of the gap between pilot and volume production from the outset of SOFC development. Perhaps the clearest example of this vision is the primary economic focus of DOE's SECA Program, in which clear benchmarks for SOFC stack, system, and operating costs were established in January

2002 [1], and subsequently revised in 2007 to the current targets of $175/kW for the stack and $700/kW for the system [2] (see Figure 1). To this aim, NexTech Materials initiated this Phase I Small Business Innovation Research project to provide a bottoms-up analysis of manufacturing cost of a planar SOFC stack, providing the perspective of a manufacturer of SOFC materials and components and developer of SOFC stacks.

Approach

In this analysis, NexTech pursued a bottoms-up approach to establishing a comprehensive manufacturing system design and cost analysis for SOFC stacks at an annual manufacturing scale of 500 MW. To ensure completeness of the analysis, NexTech based this cost analysis on its own 20 kW-scale SOFC stack design, thus incorporating all components in its analysis including: cells, seals, interconnects, current collectors, end plates, assembly operations, and quality control.

Working with subcontractor, buyCASTINGS.com, the team analyzed the lowest cost methods for fabricating endplates, currently a high cost contributor to the total stack manufacturing cost. Working with subcontractor, Xigent Automation Systems, manufacturing equipment was identified for high volume stack assembly to enable accurate costing stack manufacturing.

Results

A detailed process-driven assessment of manufacturing costs of 20 kW-scale planar SOFC stacks was performed at an annual manufacturing volume of 500 MW. Leveraging existing cell and stack component cost models, high volume process and component design investigations, and analysis support from collaborative partners, NexTech developed a manufacturing system design and cost analysis for its SOFC stack. First, a cell cost model was established for both NexTech's electrolyte-supported *FlexCell* and anode-supported cells. Manufacturing costs of other stack components (endplates, coated interconnects, current collectors, and seals) were then determined, with endplate analysis activities led by investment casting experts buyCASTINGS.com.

Working with automation experts, Xigent Automation Systems, stack components, processes, and labor requirements were evaluated to determine appropriate levels of automation and process control methods. Particular attention was given to handling requirements of individual stack materials to ensure component integrity and quality throughout the assembly process. From these inputs, a stack assembly process was defined and all equipment identified in order to determine accurate cost contributions to the stack manufacturing process. A facilities layout was then created for the stack assembly operation, showing all unit operations and material transport systems between stations. Finally utilizing its manufacturing system design and cost analysis process, NexTech established a comprehensive cost model for its 20 kW–scale SOFC stack, forecasting a total stack manufacturing cost of $166/kW, validating SECA's cost target of $175/kW at high volume production scale.

Phase	I	II	III
Power Rating	3-10 kW	3-10 kW	3-10 kW
System Cost (*)	$800/kW	$600/kW	$400/kW
Efficiency			
Mobile	25-45%	30-50%	30-50%
Stationary	35-55%	40-60%	40-60%
Steady-State Test			
Test Hours	1,500	1,500	1,500
Availability	80%	85%	95%
Degradation (per 500 hours)	≤2%	≤1%	≤0.1%
Transient Test			
Number of Thermal Cycles	10	50	100
Total Power Degradation	≤1%	≤0.5%	≤0.1%

(*) $400/kW was set as the system factory cost goal in 2002; this goal was adjusted to $700/kW in 2007 (to account for inflation).

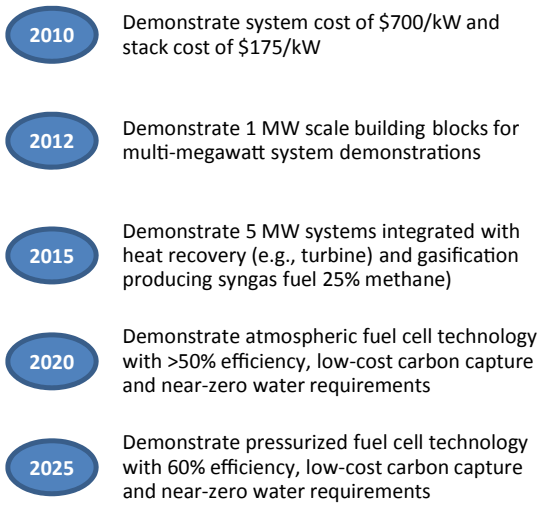

FIGURE 1. SECA 2010 Goals, Demonstrating a Consistent Focus on Manufacturing Cost Reduction [1-3]

Conclusions and Future Directions

NexTech's analysis validated the feasibility of achieving SECA's SOFC stack cost targets at high volume manufacturing, based on current stack design parameters and currently available manufacturing processes and equipment approaches. Future work would involve targeted efforts to further reduce stack manufacturing cost, with specific focus on endplate manufacturing and cell cost reduction.

FY 2011 Publications/Presentations

1. Final project report submission: Manufacturing System Design Analysis of SOFC Stacks.

References

1. http://www.netl.doe.gov/technologies/coalpower/fuelcells/publications/Wayne%20SOFCVII%20Japan%202001.pdf

2. http://www.netl.doe.gov/technologies/coalpower/fuelcells/pdf/SECA%20Brochure%2001_27_09.pdf

3. http://www.netl.doe.gov/technologies/coalpower/fuelcells/publications/2010_10_19_FC%20Seminar_SD%20Vora.pdf

III.E.4 Reliability and Durability of Materials and Components for Solid Oxide Fuel Cells

Edgar Lara-Curzio (Primary Contact), Amit Shyam, Rosa Trejo, Dana McClurg, Melanie Kirkham, Dieter Isheim[1]
Oak Ridge National Laboratory
1 Bethel Valley Rd.
Oak Ridge, TN 37831-6062
Phone: (865) 574-1749; Fax: (865) 574-4913
E-mail: laracurzioe@ornl.gov
[1]Northwestern University, Evanston, IL

DOE Project Manager: Patcharin Burke
Phone: (412) 386-7378
E-mail: Patcharin.Burke@netl.doe.gov

Contract Number: FEAA066

Start Date: August 1, 2001
End Date: September 30, 2011

Fiscal Year (FY) 2011 Objectives

- Support the Solid State Energy Conversion Alliance (SECA) industrial teams in the development of reliable and durable solid oxide fuel cells (SOFCs).
- Identify and utilize test techniques to determine the physical and mechanical properties of SOFC component materials and the interfaces between them.
- Characterize candidate glasses developed for SOFC seal applications.
- Develop economically viable sealing materials and concepts.

FY 2011 Accomplishments

- Successfully characterized the microstructural changes in two candidate glasses for SOFC sealing application after 10,000 hours aging at 800°C in air and a gas mixture of H_2O+H_2+N_2.
- Determined the effect of aging time at 800°C in air and steam+H_2+N_2 environments on the glass transition temperature of two candidate glasses for SOFC sealing applications.
- Supported the SECA industrial teams in the characterization of potential glass seal materials.

Introduction

Planar SOFC stacks consist of alternating fuel and air chambers, which are sealed from each other and connected to fuel and air delivery manifolds, respectively. Seals must have low electrical conductivity, be chemically and mechanically stable in SOFC operating environments, and demonstrate chemical compatibility with the cell and interconnect materials. Fuel leakage should be less than one percent averaged over the seal area and the seal material must be capable of a service life of more than 40,000 hours and dozens of thermal cycles. In addition to the above factors, manufacturability and cost of the sealing material are critical factors in meeting the SECA program goals.

In previous reports the basic physical and mechanical properties of SCN-1 glass, a barium alkali silicate glass that is being considered for SOFC sealing applications, were reported [1-2]. During FY 2011, Oak Ridge National Laboratory (ORNL) continued investigating how the microstructure and properties of SCN-1 evolve when exposed to SOFC-relevant environments. Another commercially available barium alkali silicate glass (G6) was also studied during FY 2011. In particular, test specimens that had been exposed for 10,000 hours to air and a gas mixture of steam+N_2+H_2 at 800°C were characterized. The effect of time of exposure on the glass transition temperature of the two glasses was also determined.

During FY 2011, the physical and mechanical properties of G6 glass were investigated. In particular, values of elastic modulus, thermal expansion, viscosity and wetting behavior were obtained as a function of temperature. During the reporting period work also continued to assess the precision of analysis techniques to determine the chemical composition of glasses and work continued in the development of various advanced engineering sealing concepts. To demonstrate the feasibility of such sealing concepts, a test facility was developed to subject such seals to dual environments (air/gas mixtures of H_2+N_2+H_2O).

Approach

A box furnace and a tubular furnace with environmental control capability were used for aging studies of SCN-1 and G6 glasses in air and in a gas mixture of H_2O+H_2+N_2. Aging tests were carried out at 800°C and interrupted periodically to remove test

specimens for microstructural characterization. Test specimens consisted of glass beads sintered onto alumina or 8 mol% yttria stabilized zirconia (8YSZ) plate substrates. A suite of microstructural characterization techniques, including scanning electron microscopy, energy dispersive spectroscopy, and X-ray diffraction (XRD), were applied to determine the phase composition of the glass, and any chemical reactions between the substrate and the glass. Thermal expansion, glass transition temperature and viscosity were determined by thermomechanical analysis. The wetting behavior of G6 glass on the two different substrates was determined in real time using digital photography. An image analysis-based methodology[1] was developed and applied to quantify pore size distributions and other microstructural features, such as crystalline precipitates.

The atom probe was used to determine the chemical composition of the two glasses and the results were compared to those obtained in FY 2010 using inductively coupled plasma – mass spectroscopy, inductively coupled plasma – atomic emission spectroscope, and neutron activation analysis.

Results

SOFC seals must exhibit thermal expansion behavior that is compatible with other components of the stack. The thermal expansion behavior of G6 was determined using a thermomechanical analyzer. The test specimen, which consisted of a rectangular parallelepiped with nominal dimensions of 3 mm × 3 mm × 5 mm, was heated and cooled at a constant rate of 5°C/min between 25 and 600°C. A constant compressive load was maintained over the test specimen during the test.

Figure 1 shows the thermal expansion behavior of G6. This behavior is comparable to that of SCN-1. The thermal expansion of G6 exhibits a slight temperature dependence, which could be expressed as:

$$\alpha(T) = 7.25 \times 10^{-6} + (6.67 \times 10^{-9})\ T\ (°C^{-1})$$

for temperatures between 100°C and 400°C. These values are in the range of thermal expansion values reported for barium silicate glasses [3-4] and are comparable to that of 8YSZ, which increases slightly with temperature from 8.5 x10^{-6} °C^{-1} at 100°C to 10.5 x 10^{-6} °C^{-1} at 950°C [5]. The thermal expansion behavior of G6 is also close to that of ferritic stainless steels, which are being considered for metallic interconnects for planar SOFCs [6-7]. Matching the thermal expansion of the glass seals to those of the metallic interconnects and electrolyte is important to minimize residual stresses during cooling at temperatures below the glass transition temperature of the glass seal. From the thermal expansion tests, it was also possible to determine the glass transition

[1] ImageJ®, National Institute of Health

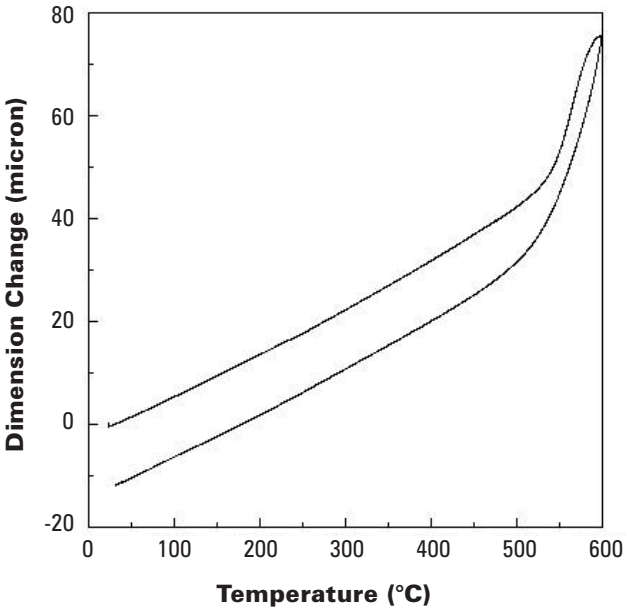

FIGURE 1. Thermal expansion behavior of G6 using a thermomechanical analyzer at a heating/cooling rate of 5°C/min. The initial length of the test specimen was 9.965 mm.

temperature according to ASTM E1545[2], which was found to be 505°C. It was found that for aging times up to 10,000 hrs, in air and a gas mixture of H_2+N_2+H_2O at 800°C the glass transition temperature exhibits a very slight increase with temperature for SCN-1 but remains constant for G6. Figure 2 shows the effect of aging time in the aforementioned environments on the glass transition temperature of SCN-1 and G6 glasses. This is an important finding because it indicates that these glasses will preserve their ability to flow and heal cracks even after very long-term exposure to these environments.

The viscosity of G6 was determined using a thermomechanical analyzer at a heating rate of 1°C/min and a constant compressive load of 0.1 N. It was found that the temperature-dependent viscosity could be expressed using the Vogel-Fulcher-Tamman (VFT) relation:

$$Log_{10}(\eta) = -3.126 + \frac{3917.5}{T - 295.45}$$

where η is viscosity and T is absolute temperature. Overall, both SCN-1 and G6 exhibit viscosity values in the range of 4x10^5 to 3x10^9 Pa s, which is a desirable range for SOFC applications [4].

During the reporting period, the evolution of the microstructure and phase composition of G6 and SCN-1 glasses was characterized. Figure 3 shows a collection of scanning electron micrographs of the cross sections of

[2] Standard Test Method for Assignment of the Glass Transition Temperature by Thermomechanical Analysis

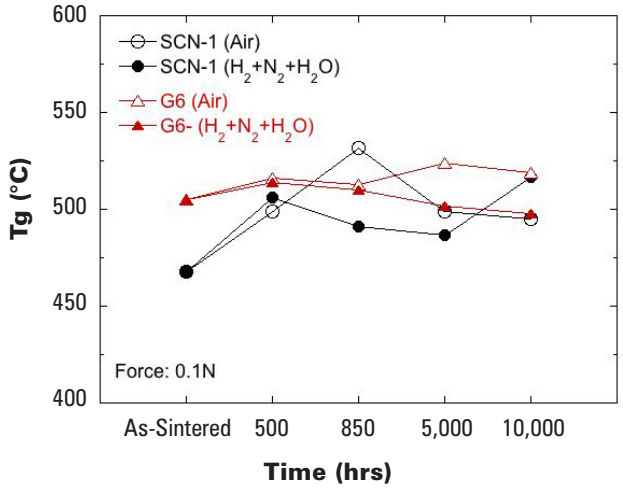

FIGURE 2. Effect of Aging Time on the Glass Transition Temperature of SCN-1 and G6 Glasses

SCN-1 and G6 glass test specimens on 8YSZ substrates as a function of time of exposure in air and H_2O+H_2+N_2 at 800°C. A quantitative analysis of porosity revealed that the total porosity of sintered SCN-1 is 17% while the porosity in G6 was 3.5%. The value of porosity appears to be constant but in the case of SCN-1 glass, pores coarsen with time of exposure. At the time this report was being prepared, models were under development to describe and explain pore coarsening in SCN-1. Complementary studies using XRD revealed the precipitation of $KAlSi_3O_8$ and BaO in SCN-1 glass sintered onto a zirconia substrate after exposure to H_2O+H_2+N_2 at 800°C. In the case of G6 glass sintered onto both alumina and 8YSZ, crystalline precipitates of $MgCaSi_2O_6$ and $CaSiO_3$ are clearly identified after 10,000 hours of aging time in air. Analysis of test specimens of G6 sintered onto Al_2O_3 revealed the precipitation of $MgAl_2O_4$ and $KAlSi_3O_8$ after aging in a gas mixture of H_2O+N_2+H_2. Cristobalite appeared on the surface of SCN-1 glass after 9,000 hours aging in air.

The elastic modulus of SCN-1 and G6 glasses is plotted in Figure 4 as a function of temperature. The Young's modulus of SCN-1 was found to decrease from 51.9 GPa at room temperature to 49.8 GPa at 400°C while its Poisson's ratio remained nearly constant at 0.22. Attempts to determine values of the elastic constants of SCN-1 above 400°C were unsuccessful because of the broadening of the spectra peaks. Data were collected during cooling and the values obtained during heating and cooling were found to be equivalent. The Young's modulus of G6 was found to decrease from 72.8 GPa at 25°C to 59.2 GPa at 600°C. These values are comparable to other values mid range of values for alkali-alkaline-earth silicates [8]. However, there is a large discrepancy between the values of these two glasses considering that their chemical composition is comparable.

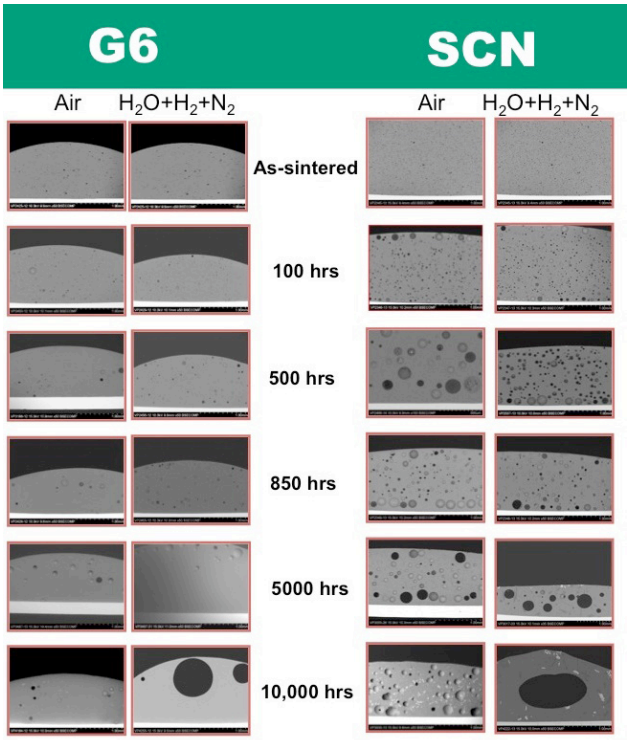

FIGURE 3. Collection of Scanning Electron Micrographs of the Cross Sections of SCN-1 and G6 Glass Test Specimens on 8YSZ Substrates as a Function of Time of Exposure at 800°C in Air and H_2O+H_2+N_2

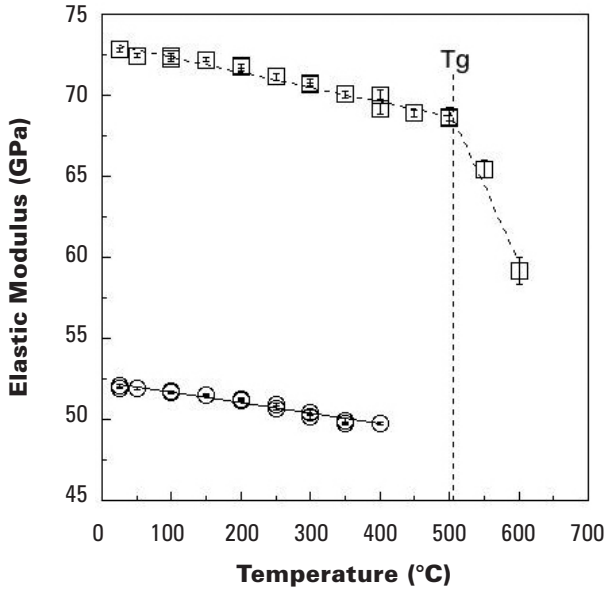

FIGURE 4. Young's modulus of G6 and SCN-1 determined as a function of temperature using a resonant ultrasound spectrometer. Squares correspond to G6. Circles correspond to SCN-1.

Using the Makishima-Mackenzie model [9], the Young's modulus of glasses with the composition of SCN-1 and G6 were found to be 70.2 GPa and 71.8 GPa, respectively. While the value predicted for G6 with the Makishima-Mackenzie model is within 1.3% of the value determined by resonant ultrasound spectroscopy, there is a large discrepancy between the value predicted for SCN-1 and that determined experimentally. However, by accounting for 18% porosity and using the rule of mixtures, the predicted modulus for SCN-1 is 57 GPa, which is within 10% of the value determined experimentally by resonant ultrasound spectroscopy.

When this project was initiated, attempts were made to quantify the volatilization, if any, of certain elements in barium alkali silicate glasses using a thermogravimetric analyzer coupled with a mass spectrometer. However, these measurements did not have enough precision. During FY 2011 work continued to evaluate test techniques to determine the chemical composition of SCN-1 and G6 glasses. In particular, the composition of these glasses was determined using the atom probe. Figure 5 shows a reconstruction of a volume of 70 x 70 x 109 nm^3 containing 3,997,448 atoms. The analysis of these reconstructions provides an accurate compositional analysis of the glass. Similar tests are being performed at the time of the preparation of this report for test specimens that had been subjected to aging in air and a gas mixture of $H_2O+H_2+N_2$ at 800°C.

Conclusions and Future Directions

Characterization of the cross section of glass specimens of SCN-1 and G6 that have been exposed to air and $H_2O+H_2+N_2$ environments at 800°C for 10,000 hours was completed. The results of their microstructural characterization and phase stability indicate that SCN-1 and G6 glasses are stable under SOFC operating conditions for long exposure times, although pore coarsening in SCN-1 was excessive. Sets of test specimens continue being exposed to both air and $H_2O+H_2+N_2$ with the objective of achieving exposure times in excess of 20,000 hours. The physical and mechanical properties of G6 glass were also evaluated as a function of aging time.

Future work will be focused on studying microstructural changes in these glasses when subjected to dual environments and to demonstrate the feasibility of engineered glass sealing concepts.

FY 2011 Publications/Presentations

1. Quarterly Report for 1st quarter fiscal year 2011, January 2011.

2. Quarterly Report for 2nd quarter fiscal year 2011, April 2011.

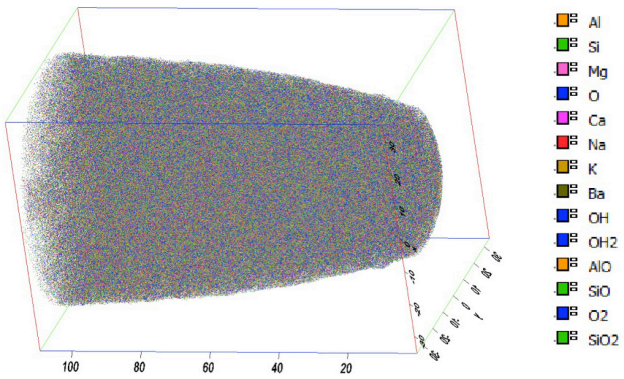

FIGURE 5. Reconstruction of a Volume of 70 x 70 x 109 nm^3 Containing 3,997,448 Atoms of SCN-1 Glass in the As-Sintered Condition Obtained with an Atom Probe

References

1. ORNL SECA Annual Report for fiscal year 2010, December 2010.

2. "Characterization of a Barium Silicate Glass," ORNL Technical Report TM-SECA-02-09.

3. P. Geasee, T. Schwickert, U. Diekmann, and R. Conradt, in: J.G. Heinrich, F. Aldinger (Eds.), Ceramic Materials and Components for Engines, Wiley-VCH Verlag GmbH, Weinheim, Germany, 2001, pp. 57–62.

4. J.W. Fergus, "Sealants for Solid Oxide Fuel Cells," *Journal of Power Sources* **147** (2005) 46–57.

5. M. Radovic, E. Lara-Curzio, R. Trejo, H. Wang, and W.D. Porter, "Thermo-Physical Properties of Ni-YSZ as a Function of Temperature and Porosity," *Ceramic Engineering and Science Proceedings* **27**, Issue 4 (2006) 79-85.

6. Allegheny Ludlum, Technical Data, Stainless Steel 441HP™ Alloy, ThyssenKrupp VDM GmbH (2005).

7. Crofer® 22 APU, Material Data Sheet No. 4046, May 2010 Edition.

8. T. Rouxel, "Elastic Properties and Short-to Medium-Range Order in Glasses," *J. Am. Ceram. Soc.* **90** [10] (2007) 3019-3039.

9. A. Makishima and J.D. Mackenzie, "Direct Calculation of Young's Modulus of Glass," *Journal of Non-Crystalline Solids* **12** (1973) 35-45.

III.E.5 Development and Implementation of Stack Fixture Tests

Yeong-Shyung "Matt" Chou (Primary Contact), Edwin C. Thomsen, Jung-Pyung Choi, William E. Voldrich, Jared Templeton, and Jeff Stevenson
Pacific Northwest National Laboratory
K2-44, P.O. Box 999
Richland, WA 99354
Phone: (509) 375-2527; Fax: (509) 375-2186
E-mail: yeong-shyung.chou@pnl.gov

DOE Project Manager: Briggs White
Phone: (304) 285-5437
E-mail: Briggs.White@netl.doe.gov

Contract Number: FWP40552

Start Date: October 1, 2010
End Date: September 30, 2011

Fiscal Year (FY) 2011 Objectives

- Develop a solid oxide fuel cell (SOFC) stack test fixture for use by Pacific Northwest National Laboratory (PNNL) and other Solid State Energy Conversion Alliance (SECA) Core Technology Program (CTP) participants.
- Implement the test fixture in evaluation/validation of new materials, processes, and design concepts developed by PNNL and other SECA CTP participants.

FY 2011 Accomplishments

- Developed 2nd generation stack test fixture on behalf of SECA CTP.
- Successfully assembled two 3-cell stacks for long-term (~6,000 h) evaluation/validation of Ce-modified Mn-Co spinel-coated AISI 441 interconnects.
- Successfully demonstrated brazing approach for fabrication of 3rd generation stack test fixture interconnects in single-cell testing.

Introduction

PNNL and other SECA CTP participants use a wide range of materials characterization techniques (X-ray diffraction [XRD], scanning electron microscopy [SEM], energy dispersive spectroscopy [EDS], transmission electron microscopy [TEM], X-ray photoelectron spectroscopy [XPS], thermal gravimetric analysis [TGA], differential scanning calorimetry [DSC], particle size analysis [PSA], electrical conductivity, single- and dual-atmosphere oxidation, etc.) and sub-stack multiple component tests (e.g., "button" cell testing, area-specific resistance [ASR] testing of interconnect/cathode contact/cathode structures, and leak testing of cell/seal/interconnect structures) to evaluate the performance of newly developed materials, fabrication processes, and design concepts. In recent years, PNNL has developed and implemented a "stack" test fixture intended to evaluate/validate cell and stack component performance under realistic stack conditions. It is anticipated that results from these stack fixture tests will help to bridge the gap between typical CTP tests and the full-scale cells and stacks under development by the SECA industrial teams, and thus facilitate technology transfer from the CTP to those teams.

Approach

In FY 2011, PNNL continued the implementation of the 2nd generation stack test fixture in evaluation/validation of new materials, processes, and design concepts developed by PNNL and other SECA CTP participants. The 2nd generation stack test fixture, which was utilized not only for single-cell testing, but also for multiple cell stack testing, allows for the simultaneous testing of cell-to-frame and stack perimeter seals, anode and cathode contact materials, interconnect materials (including coatings), and cell constituents (cathode, electrolyte, anode). To facilitate cell consistency, commercial NiO/yttria-stabilized zirconia (YSZ)-supported YSZ cells were used which had overall dimensions of 50 mm x 50 mm with an active area of 40 mm x 40 mm. The other components of the stack test fixture (cell frames, anode and cathode plates, contact pastes, and seals) were fabricated at PNNL. The stack fixtures were assembled and then sealed and tested in test stands consisting of a furnace, heat exchangers, gas handling system with mass flow controllers, and electrical characterization units. The electrochemical performance of the cells was measured under isothermal and/or thermal cyclic conditions. Once the tests were complete, the fixtures were disassembled and their components were analyzed by appropriate characterization techniques, such as optical and electron microscopy, EDS, XRD, XPS, etc. Results from the tests were compared to results obtained from testing of individual components and sub-stack structures to assess intrinsic stability and inter-component reactions, and their effects on performance under stack operating conditions.

Results

Figure 1 shows the computer-aided design drawings of the 3-cell Gen2 stack fixture, which was developed through an iterative process, with results from previous fixture tests helping to identify design changes required to optimize fixture performance. The 2nd generation fixture uses AISI441 sheet stock of 0.133" thickness for interconnect plates and 0.040" thickness for cell frame plates. For a typical 3-cell stack fixture test, three cell frames and four interconnect plates are used, along with mica-based seals separating each cell and interconnect plate. As mentioned above, a commercial cell of NiO/YSZ-supported thin YSZ electrolyte with Sr-doped lanthanum manganite (LSM)/YSZ cathode was used for all tests. The commercial cell has an NiO/YSZ anode support of 465-555 μm thick, an active NiO/YSZ anode of 4-10 μm, a dense YSZ electrolyte of 4-6 μm, and a double layer LSM/YSZ-LSM cathode of 30-60 μm. The cells were first sealed onto an aluminized cell frame plate at 950°C/2 h in air using refractory sealing glass. Three cells in frames were then assembled with Ce-(Mn,Co) spinel coated interconnect plates, and sealed with hybrid mica and composite sealing glass as perimeter seals. On each cell frame plate, Pt or Ni wire was spot welded for voltage sensing. Four Inconel 600 rods were also attached to the interconnect plates for current leads. Contact pastes containing NiO and LSM were applied to the anode and cathode, respectively, prior to stack assembly. The assembly was slowly heated to the final sealing temperature of 930°C in slowly flowing air. After sealing at 930°C for 2 h, the stack was cooled to 800°C and a fuel of 5% H_2/N_2 with 3% H_2O was introduced into the fuel channel. Both the fuel and air flow rates were then gradually increased to reach an open circuit voltage (OCV) of about 0.7-0.8 V, after which time the dilute 5% H_2 was switched to a mixed fuel with H_2:N_2 =1:1, and flow rates were increased again. After the OCV was stabilized, the electrochemical performance measurements for each cell were then conducted.

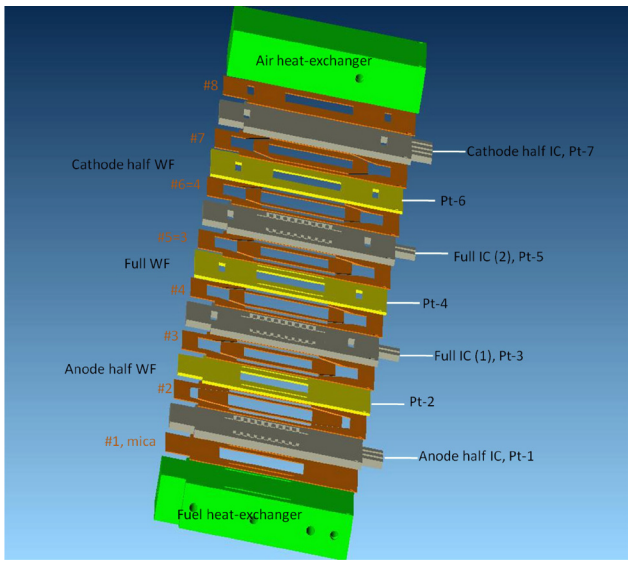

FIGURE 1. Schematic View of 2nd Generation Stack Test Fixture in 3-Cell Configuration (WF = window frame; IC = interconnect)

For FY 2011, a major task was to evaluate/validate the stability of Ce-modified Mn-Co spinel-coated AISI 441 interconnects in the SOFC environment. The Mn-Co spinel coating was developed as a conductive and protective air-side coating for ferritic stainless steel interconnects. Modification with Ce was found to improve the oxide scale adhesion in stand-alone small coupon tests, so this material set was selected for evaluation in a real SOFC environment in a 3-cell stack configuration. Two 3-cell tests (designated #4 and #5) containing Ce-modified Mn-Co spinel-coated AISI 441 interconnects were assembled and tested. The target time for these long-term tests was set at 6,000 h. At the time of the writing of this report, stack #4 had reached 4,500 h, while stack #5 had reached 3,800 h. For these stack tests, the cells were operated in constant current mode at 800°C, with the voltage across each cell being recorded versus time. Every ~500 h, the tests were interrupted to collect impedance and current-voltage (I-V) sweep data for each cell. The constant current was set for a total current of 5 A (or 313 mA/cm^2), based on initial I-V sweep and power density data, as shown in Figure 2(A) and 2(B) for each cell, respectively. The top and middle cells had a maximum power density greater than 300 mW/cm^2. The bottom cell had a lower power density of ~225 mW/cm^2. It was suspected that gas flow was not uniform among the three cells and that the bottom cell may have received a reduced gas supply, since the I-V sweep showed deviation from linearity at higher currents (Figure 2(A)). The initial OCVs of the three cells were 1.084 V, 1.064 V, and 1.080 V for the bottom, middle, and top cell, respectively. The theoretical OCV for a fuel of H_2:N_2=1:1 and a few percent of moisture versus air at 800°C is 1.070 V, so the measured OCVs suggested no cell fracture or major leaks. The higher than theoretical values may be attributed to temperature fluctuation or lower than expected water content in the fuel. Figure 3 shows the electrochemical performance stability of the three cells in stack test #4 at 800°C. It is evident the top cell had the best stability, with minimum degradation compared to the other two cells. Using voltage data at t=130 h (0.819 V) and 4,500 h (0.764 V), the calculated degradation rate for the top cell was ~1.5%/1,000 h. The middle and bottom cells had a higher degradation rate of ~11%/1,000 h and ~10%/1,000 h, respectively. From OCV measurement at every 500 h, it appeared that the middle cell suffered a major leak between 1,983 h and 2,483 h, causing the OCV to drop substantially from 1.059 V to 1.019 V (Table 1); the OCV continued to decrease over time to 0.824 V (4,499 h). The top

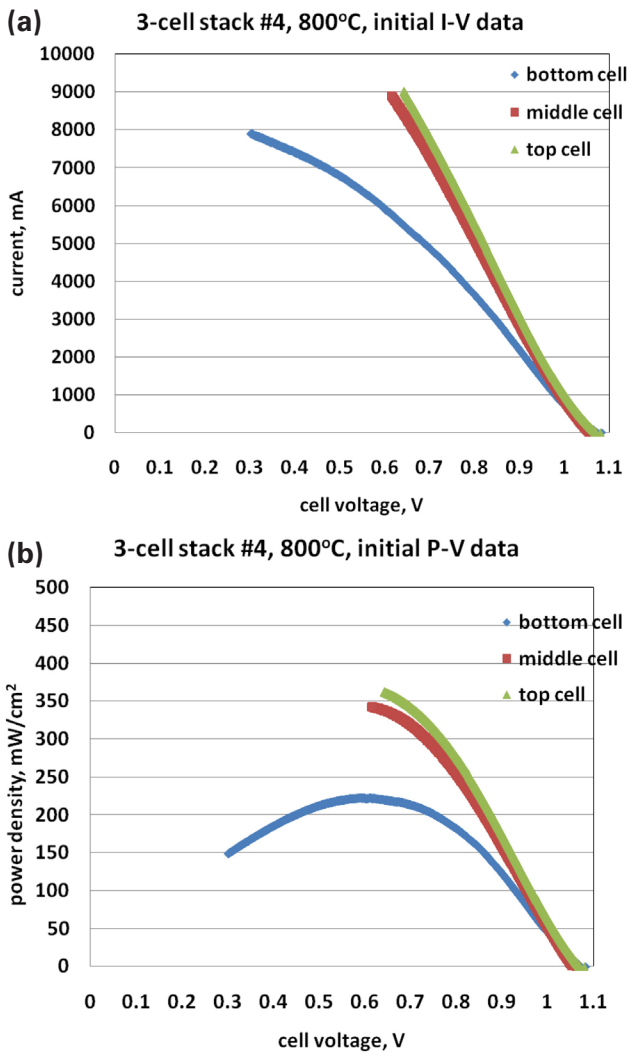

FIGURE 2. Initial Electrochemical Performance Data of Each Cell in Stack Test #4 at 800°C: (A) I-V Sweep, and (B) Power Density versus Voltage

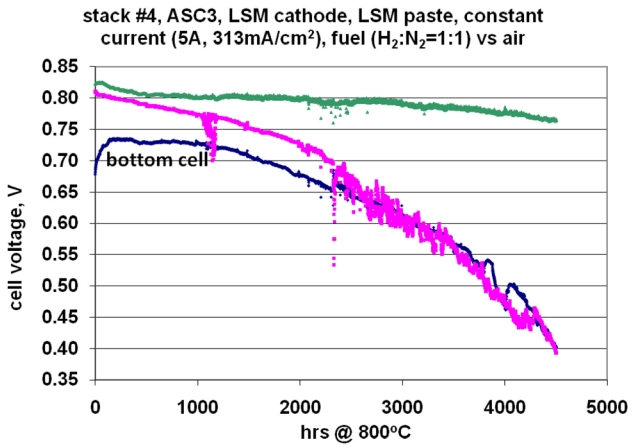

FIGURE 3. Long-Term Stability 3-Cell Stack Test #4 with Ce-Modified Mn-Co Spinel-Coated AISI 441 Interconnects under Constant Current Conditions at 800°C

TABLE 1. Open Circuit Voltages of Test #4 as a Function of Time

hour	bottom	middle	top
0	1.080	1.063	1.084
500	1.057	1.045	1.056
983	1.084	1.066	1.083
1,403	1.094	1.072	1.087
1,983	1.084	1.059	1.084
2,483	1.075	1.019	1.070
2,990	1.086	0.978	1.080
3,495	1.075	0.967	1.088
3,997	0.966	0.900	1.087
4,499	0.929	0.824	1.082

cell appeared to be well-sealed without a significant decrease in OCV over the entire test period. The bottom cell appeared to be intact for the first 3,500 h, but also apparently suffered a major leak after that, with OCV dropping to 0.966 V. It will not be possible to determine the exact cause for the drastic reduction in OCVs until the stacks are disassembled for post-mortem analysis. Nonetheless, it is believed the dimensional control is very critical, in that the current fixture design does not have compliance on the cathode side, while the anode side is somewhat compliant due to the presence of embedded Ni mesh. The cell impedance data were also recorded every 500 h, as shown in Figure 4(A), 4(B), and 4(C) for the top, middle, and bottom cell, respectively. Clearly, the top cell showed the best stability, with a minimal increase in both the ohmic and polarization impedance components (Figure 4(A)). For the middle and bottom cells, the impedance increased substantially over the time, consistent with the voltage versus time data (Figure 3).

Similar results were observed in a duplicate 3-cell stack fixture test (#5, Figure 5). The top and bottom cells showed very stable electrochemical performance with low degradation up to 2,500 h, at which time the air supply to the stack was unexpectedly shut down. Using cell voltages at t=50 h and 2,554 h, the calculated cell degradation for the top cell and the bottom cell was ~0%/1,000 h and 0.67%/1,000 h, respectively, indicating the desired stability of the Ce-modified (Mn,Co)-spinel coating. The unexpected loss of air exposed the cathode side to the reducing fuel gas since, based on OCV measurements, the middle cell appeared to have a leak. This resulted in a sudden drop in electrochemical performance, possibly due to reduction of the cathode or the spinel coating. Nonetheless, the top and bottom cells exhibited partial recovery and stability once the air flow was resumed. The middle cell, on the contrary, continued to exhibit severe degradation.

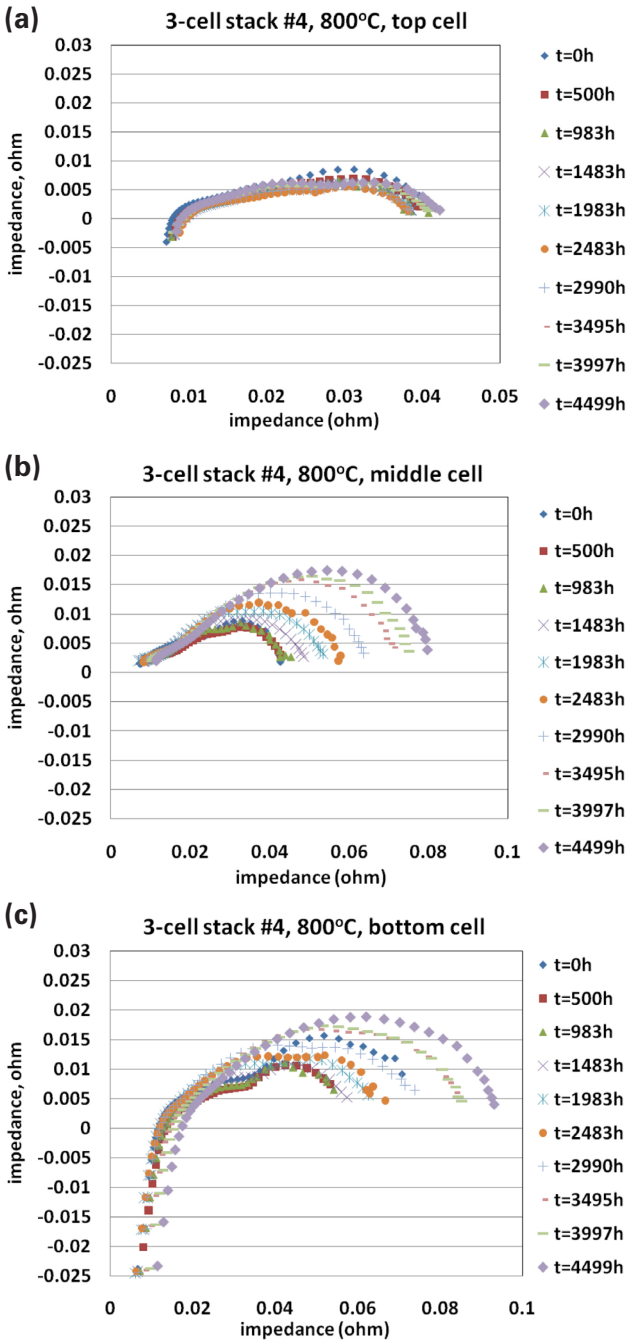

FIGURE 4. Impedance of Each Cell for 3-Cell Stack Test #4, (A) Top Cell, (B) Middle Cell, and (C) Bottom Cell

In FY 2011, a redesign of the 2nd generation stack test fixture was also initiated. The objective of this "3rd generation" design was to reduce weight/mass by using thinner AISI441 stock (0.040" and 0.020") for better stress distributions, to allow for cathode contact reinforcement/modification for thermal cycle stability, and to allow for better flow channel design for gas distribution to achieve high utilization. This design will also significantly reduce machining time and cost.

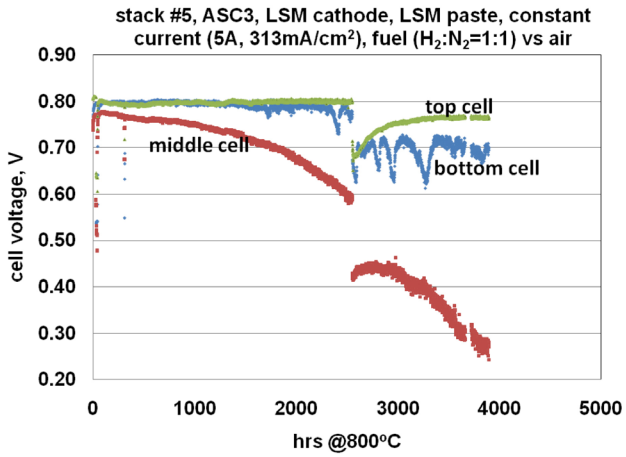

FIGURE 5. Long-Term Stability 3-Cell Stack Test #5 with Ce-Modified Mn-Co Spinel-Coated AISI 441 Interconnects under Constant Current Conditions at 800°C

Initial trials involving brazing of 0.040" and 0.020" sheets to replace the 0.133" thick machined interconnect plates were conducted at various brazing temperatures (1,020, 1,060, and 1,100°C in vacuum). Results showed hermetic brazing can be obtained by brazing at 1,060 and 1,100°C; however, the metal surface showed large particle/nodule formation. The surface particles contained an appreciable amount of Si; the source of the Si has not been identified yet. The presence of nodules on the surface affected the subsequent aluminization process and resulted in a rougher surface as compared to as-machined thick metal parts after aluminization. Nonetheless, a single-cell test (#62) was conducted using the brazed hermetic parts and the other standard cell materials. The electrochemical data (not shown) including impedance spectrum, I-V sweep, power density, and stability were similar to previous Gen2 tests. These results suggest the validity of the brazing approach, although further optimization to minimize the nodule deposition, improve long-term electrical stability in air, and improve gas distribution remains to be performed.

Conclusions and Future Directions

The 2nd generation stack test fixture was utilized in single and 3-cell configurations at 800°C. Two 3-cell short stacks were tested to evaluate the long-term stability of Ce-modified Mn-Co spinel-coated AISI 441 interconnects. The results of these two tests indicate that the Ce-modified (Mn,Co)-spinel coating was stable at 800°C for at least 4,500 h (tests were still in progress at the time of report preparation). Modification for the test fixture to reduce machining time and interconnect mass was also performed. An initial test with brazed thin AISI 441 sheets in a single-cell configuration was successful, exhibiting electrochemical performance data

consistent with previous 2nd generation tests. Future directions will include candidate SOFC materials and processes validation, optimization of the weight/mass reduction process, dimensional control to minimize damage to cell-to-frame seals, and better stress/gas distribution.

FY 2011 Publications/Presentations

1. Y-S. Chou, E.C. Thomsen, J-P Choi, W.E. Voldrich, and J.W. Stevenson, "Short Stack Test Fixture Development at Pacific Northwest National Laboratory," MS&T 2010 Conference & Exhibition, Houston, Texas, October 17–21, 2010.

2. Y-S. Chou, E.C. Thomsen, J-P Choi, J.W. Stevenson, W.E. Voldrich, and J.F. Bonnett, "Standard SOFC Test Fixture Development and Materials Evaluation at Pacific Northwest National Laboratory," 2010 Fuel Cell Seminar, San Antonio, Texas, October 18–22, 2010.

3. Y-S. Chou, J.W. Stevenson, and J-P Choi, "Evaluation of a Single Cell and Candidate Materials with High Water Content Hydrogen in a Generic Solid Oxide Fuel Cell Stack Test Fixture, Part I: Test Fixture and Electrochemical Performance," Int'l J. Appl. Ceram. Tech., 8, 23 (2011).

III. SECA CORE RESEARCH & DEVELOPMENT

F. Fuel Processing

III.F.1 Oxide-Based Reforming Catalyst Evaluation and Development

Dushyant Shekhawat (Primary Contact),
David A. Berry, Daniel J. Haynes,
Mark W. Smith[1]
U.S. Department of Energy
National Energy Technology Laboratory
3610 Collins Ferry Road
Morgantown, WV 26507-0880
Phone: (304) 285-4634; Fax: (304) 285-0903
E-mail: Dushyant.Shekhawat@netl.doe.gov
[1]URS Corporation
3610 Collins Ferry Rd.
Morgantown, WV 26507-0880

Contract Number: 07-220611

Start Date: October 1, 2010
End Date: September 30, 2011

Fiscal Year (FY) 2011 Objectives

- Apply fundamental understanding of fuel reforming and deactivation mechanisms into design of alternative catalyst systems for long-term, stable hydrogen-rich synthesis gas production for commercially representative fuel cell applications (e.g., diesel auxiliary power units).
- Develop a synthesis method that produces a pyrochlore-based catalyst in significant quantities with a comparable performance to the catalyst produced using the modified-Pechini method.
- Evaluate graded catalyst bed approach in order to reduce the amount of expensive noble-metal catalyst needed for reforming diesel fuel.
- Perform diesel reforming studies with the optimized pyrochlore-based catalyst deposited onto a structured catalyst such as a monolith.

FY 2011 Accomplishments

- Prepared several pyrochlore-based catalyst powders; performed catalyst characterization using Brunauer-Emmett-Teller (BET), inductively coupled plasma (ICP), temperature-programmed oxidation (TPO), temperature-programmed reduction (TPR), X-ray diffraction (XRD), X-ray photoelectron spectroscopy (XPS), transmission electron microscopy (TEM), and scanning electron microscopy (SEM)/energy dispersive spectroscopy (EDS); and evaluated activity and selectivity under oxidative steam reforming (OSR) and catalytic partial oxidation (CPOX) conditions.
- Synthesized pyrochlore material using several methods and compared the performance of these materials to the powder prepared by the Pechini method.
- Evaluated different graded bed configurations to evaluate the optimal graded bed compositions.
- Evaluated several monoliths coated with different pyrochlore materials.
- Submitted a patent application for method for designing reforming catalyst systems.
- Published a book on fuel processing for fuel cell applications.

Introduction

The U.S. Department of Energy is sponsoring the development of high temperature fuel cell power systems based on solid oxide technology through its Solid State Energy Conversion Alliance (SECA) program. Diesel-fueled auxiliary power units are an important market segment for solid oxide fuel cell systems. The most promising route to hydrogen production from middle distillate fuels is catalytic reforming. The catalyst used in the fuel processor is a critical component of this system and must be able to provide a clean, tailored synthesis gas to the fuel cell stack for long-term operation.

For the past several years, the National Energy Technology Laboratory (NETL) has been developing reforming catalyst based on the pyrochlore crystal structure to produce synthesis gas from diesel fuel to power a solid oxide fuel cell [1-4]. These oxide catalysts are of interest primarily due to their refractory nature and their stability in high temperature, reducing and oxidative environments. They also have the ability to "atomically-disperse" the active metal catalyst within an oxide framework that separates it from deposited metal catalysts which are more prone to sintering at high temperature due to less control of particle size or "next nearest neighbor interactions". A series of pyrochlores with different formulations were prepared and evaluated for diesel reforming. Recently, one of the pyrochlore-based formulations demonstrated 1,000 hrs of successful diesel reforming [5,6]. Now, the goal is to apply the optimized pyrochlore catalyst used in the 1,000-hr test onto a structured material to produce a commercially representative form such as a monolith, foam, pellet, etc. Furthermore, a scalable catalyst synthesis method has to be established to produce a larger batch of the powdered catalyst for further external catalyst performance validation and eventually for commercialization.
The synthesized catalyst material as well as the coated structure need to be further characterized (TPR, XRD,

XPS, TEM, SEM/EDS, surface acidity/basicity, etc.) to relate the material properties to the performance of the material.

Approach

100-Hour Diesel Reforming with Pyrochlore Supported on Monolith: A long-term (100-hour) reforming experiment using a locally obtained low sulfur diesel fuel was conducted on a monolith after preliminary testing on earlier versions deemed the catalyst synthesis method and coating procedures were optimized for composition, loadings of zirconia-doped ceria (ZDC) and catalyst, and dispersion of catalyst. The monolith is comprised of a base square channel alumina framework (400 cubic channels per square inch), which is coated with an oxygen conducting ZDC layer onto which the proprietary NETL derived pyrochlore catalyst is deposited; the monolith coating was done by NexTech Materials (Ohio). Specifications for the diesel fuel are shown in Table 1. Reaction conditions for the monolith run are given in Table 2.

TABLE 1. Properties of Diesel Fuel Used for the Study

Composition of Diesel Fuel	$C_{14.6}H_{27.7}$
Sulfur Concentration	11.6 ppmw
Paraffins	38.5 wt%
Naphthenes	42.0 wt%
Aromatics Monoaromatics Diaromatics Triaromatics and greater	19.5 wt% 15.7 wt% 3.6 wt% 0.3 wt%

TABLE 2. OSR Reaction Conditions

Pre-Heat (°C)	375
Reactor (°C)	900
Weight hourly space velocity (WHSV) ($scc/g_{cat}/hr$)	20,000
Steam to Carbon Ratio (S/C)	0.5
Oxygen to Carbon Ratio (O/C)	1.0

Grade-Bed Tests: Initial studies of the graded catalyst bed approach for the reforming of hydrocarbon fuels to produce synthesis gas were reported in the FY 2010 Office of Fossil Energy Fuel Cell Program Annual Report [7]. The purpose of that study was to reduce the amount of expensive noble-metal catalyst needed for reforming diesel fuel. A 1,000-hr OSR experiment was successfully conducted previously on pump diesel with a Rh-substituted pyrochlore catalyst on an oxygen-conducting support developed at NETL [5,6]. It was proposed that a catalyst substituted with a less expensive reforming metal (i.e., Ni, Ru) could be placed in a portion of the catalyst bed to reduce cost while still producing an acceptable level of performance. Specifically, the study examined various catalyst bed configurations using a Ni-substituted barium hexaaluminate (BNHA) catalyst and a Rh-substituted pyrochlore (Rh1-PC; 1 wt% Rh in the pyrochlore) in powder form. The major conclusion of the study was that the amount of Rh-based catalyst can indeed be reduced by substituting less expensive catalysts in sections of the bed that are less likely to deactivate them. The study identified that the bottom region of the catalyst bed is the most likely place that non-noble metal catalysts will deactivate. This study is a continuation of that project that will ultimately lead to a graded commercial catalyst configuration (i.e., monolith).

The reasoning behind the graded bed approach has to do with the indirect mechanism widely reported for the CPOX and OSR of hydrocarbons in a fixed bed reactor [8-10]. In the indirect mechanism the formation of the products takes place in two separate regions, or zones, of the reactor. First, a portion of the fuel reacts with oxygen to form combustion products (water and carbon dioxide). This is followed by steam reforming and CO_2 reforming reactions with the remaining fuel in the second region of the bed. Further, as a result of the indirect mechanism where the first step is exothermic and the second is endothermic, there are significant differences in the reaction conditions in the beginning and end sections of the catalyst bed. It was suggested that additional formulations be examined, and that the bed could be divided into potentially three different catalyst compositions to optimize the performance based on the indirect mechanism, as well as the large temperature gradients along the bed.

Two new substituted pyrochlore catalysts were tested in various graded bed configurations. As with the first study, the two compositions were selected with a significant enough difference in performance to study the benefit of different combinations and configurations of the catalyst bed. The catalysts were Ni and Ru-substituted pyrochlore catalysts (Ni3-PC (3 wt% Ni) and Ru1-PC (1 wt% Ru) with the same formula as the Rh-substituted pyrochlore from the previous study. The two catalysts were configured in several different ways. The simplest tests consisted of dividing the bed in half and putting one composition on top and the other on the bottom, and then testing the reverse. Another configuration considered the reactor to consist of three regions, still using two different compositions.

The reactions studies conducted were CPOX of n-tetradecane (TD), a diesel surrogate, and were carried out in a laboratory-scale, fixed-bed reactor, described elsewhere [11]. 50 ppmw sulfur as dibenzothiophene (DBT), and 5 wt% aromatic species, 1-methyl-naphthalene (MN), were added to TD during a 2-hr portion of the tests. TPO was performed after each test to determine the total carbon formed in the catalyst

bed during testing. Reaction conditions are summarized in Table 3.

TABLE 3. Operating Conditions for Graded Catalyst Bed Tests

O/C Ratio	1.1
Temperature (°C)	900
Flow Rate (sccm)	400
WHSV (sccm/g_{cat}/hr)	25,000
Step 1	1 hr TD only
Step 2	2-hr TD + 5 wt% MN + 50 ppm DBT
Step 3	2-hr TD only

Results

100-Hour Diesel Reforming with Pyrochlore Supported on Monolith: Results from the long-term study are shown in Figure 1. The composition of gaseous products formed was near that predicted by equilibrium for the entire time on stream. Carbon balance during the experiment was roughly 100± 10%, and no other hydrocarbons higher than CH_4 were observed. It should be noted that the experiment was interrupted briefly, for about 2 hrs, because of a rupture disc failure. However, safety interlock systems in place prevented the monolith from exposure to air, which minimized the possible regeneration of the catalyst during this time. No degradation in synthesis gas yields was observed over the course of the experiment, suggesting the monolith would be stable and active for not only the entire 100 hrs, but likely for much longer testing period.

Grade-Bed Tests: The H_2 production of several catalyst bed configurations is presented in Figure 2. The two graded bed configurations with the Ni3-PC in the inlet (top) section of the bed yielded the best overall performance. These configurations were better than both single-composition beds, indicating a synergistic effect between the two compositions. The data also suggest that the conditions in the bottom section of the reactor deactivate the Ni-PC more rapidly than the Ru3-PC. This is likely due to lower temperatures in this section caused by endothermic reforming reactions. At lower temperatures Ni-sulfides are more stable, which can lead to poisoning.

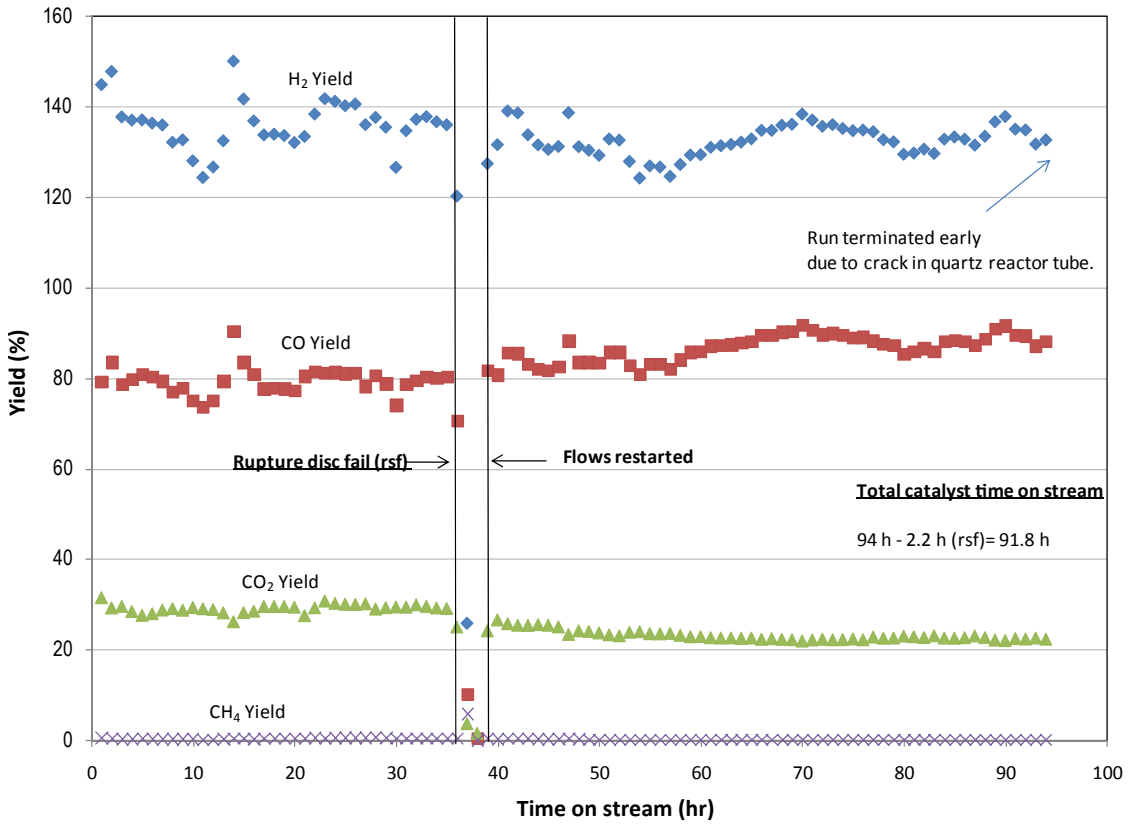

FIGURE 1. Synthesis gas yields produced during long term (~100 h) reforming study on monolith containing Rh-based pyrochlore catalyst. Conditions for experiment were O/C= 1.0, S/C=0.5, 900°C, and weight hourly space velocity = 20,000 scc/g_{cat}/hr.

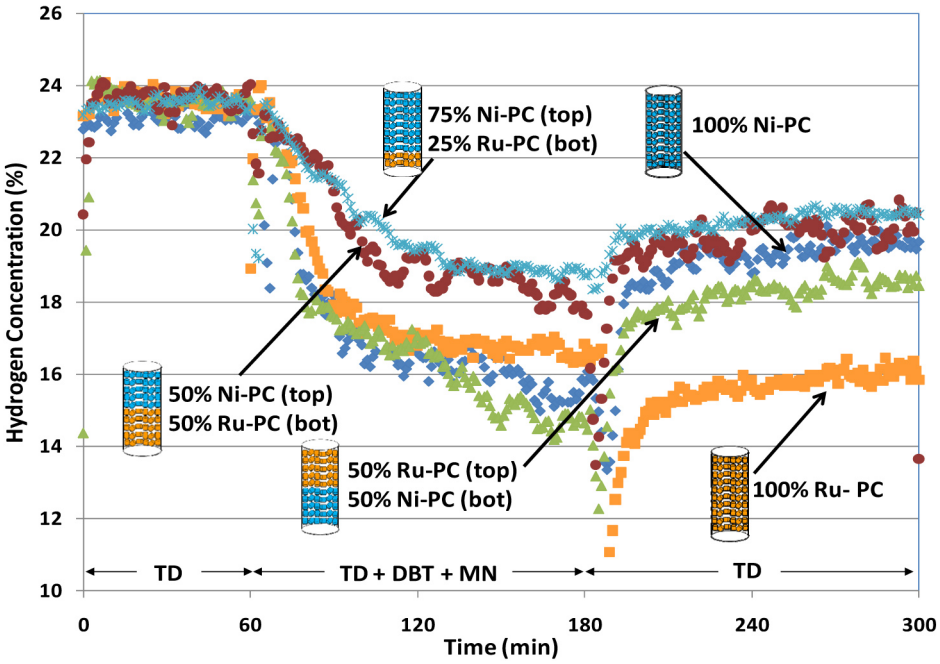

FIGURE 2. Performance of graded catalyst bed configurations in the CPOX of *n*-tetradecane (TD) with addition of aromatic and sulfur species: WHSV = 25,000 scc/g_{cat}/hr, 900°C, 0.23 MPa, O/C = 1.1.

The amount of carbon formed during each test is presented in Table 4. The predicted carbon for the graded beds was calculated from the carbon formed in the single-composition beds using the following equation:

$$\text{Total Carbon Predicted} = \text{Weight}_{Cat1} \times \text{Total Carbon}_{Cat1} + \text{Weight}_{Cat2} \times \text{Total Carbon}_{Cat2}$$

TABLE 4. Total Carbon Formed in Graded Catalyst Beds during CPOX Testing

Top (%) / Bottom (%)	Total Carbon (g)	Predicted* Carbon (g)
100% Ni-PC	1.12	--
100% Ru-PC	0.59	--
50% Ru-PC/ 50% Ni-PC	0.75	0.86
50% Ni-PC/ 50% Ru-PC	0.82	0.86
75% Ni-PC/ 25% Ru-PC	0.72	0.99
*Calculated from Total Carbon measured for 100%Ni-PC and Ru-PC		

The configuration with Ni3-PC in the top 75% of the bed and Ru1-PC in the bottom 25% yielded the highest hydrogen production as well as the most significant reduction in carbon formation compared to the predicted amount.

Fuel Processing Book: NETL researchers have edited a book, Fuel Cells: Technologies for Fuel Processing. The book, published by Elsevier in April 2011, is available in hardcover and a Kindle version. Several of the chapter authors are affiliated with NETL while others are well-known global contributors from industry, academia, government research laboratories, and foreign institutes. Despite the increasing technical and commercial importance of fuel cells, few books have addressed the critical subject of fuel reforming technology in a comprehensive fashion. This book provides an overview of the most important aspects of fuel reforming to the generally interested reader, researcher, technologist, teacher, student, or engineer. The topics covered include all aspects of fuel reforming: fundamental chemistry, modes of reforming, catalysts types, catalyst deactivation, fuel desulfurization, reaction engineering, thermodynamics, heat and mass transfer, system design, and recent research and development. This book will serve as an excellent self-instruction book for those new to fuel cells or as a comprehensive resource for experts in the area of fuel processing. The material is presented in such a way that it can also serve as a reference for graduate level courses, fuel cell developers, and fuel cell researchers.

Conclusions and Future Directions

Complete hydrocarbon conversion and near equilibrium syngas yields with no signs of catalyst degradation (olefin formation, pressure buildup, etc.) were observed during diesel reforming over pyrochlore supported on monolith for 100 hours. This short-term testing has confirmed adequate initial performance of the monolithic-based catalyst system. NETL plans to further

the development and demonstrate catalyst viability through long-term (>1,000 hr) testing.

NETL-developed Ni, Ru, and Rh-substituted pyrochlore catalysts separately, and combined in the graded catalyst bed approach, have exhibited excellent hydrocarbon reforming performance. Remaining tests will be long-term studies of a graded monolith using up to three different pyrochlore compositions. It will also utilize an oxygen-conducting interlayer with the same composition as the 1,000-hr catalyst support formulation. This will represent a commercially representative product comprised of a deposited catalyst/support system with multiple compositions active for different reforming reactions and conditions within a hydrocarbon reforming reactor.

Special Recognitions & Awards/Patents Issued

1. Published a book: D. Shekhawat, J.J. Spivey, and D.A. Berry, Fuel Cells: Technologies for Fuel Processing, Elsevier, Amsterdam, April 2011.

2. Filed a patent: D.A. Berry, D. Shekhawat, M.W. Smith, and D.J. Haynes, "Method for Designing a Reforming and/or Combustion Catalysts System," February 17, 2011.

3. Organized a symposium: NETL organized American Institute of Chemical Engineers Conference Symposium, *2011 Spring National Meeting – Topical 2: Advanced Fossil Energy Utilization.*

FY 2011 Publications/Presentations

1. D. Shekhawat, D.A. Berry, and J.J. Spivey, "Introduction to Fuel Processing," in: Fuel Cells: Technologies for Fuel Processing, Chapter 1, p. 1-10, Elsevier, Amsterdam (2011).

2. D. Shekhawat, "Nonconventional Reforming Methods," in: Fuel Cells: Technologies for Fuel Processing, Chapter 9, p. 261-283, Elsevier, Amsterdam (2011).

3. D. Haynes and D. Shekhawat, "Oxidative Steam Reforming," in: Fuel Cells: Technologies for Fuel Processing, Chapter 6, p. 129-190, Elsevier, Amsterdam (2011).

4. M.W. Smith and D. Shekhawat, "Catalytic Partial Oxidation," in: Fuel Cells: Technologies for Fuel Processing, Chapter 5, p. 73-128, Elsevier, Amsterdam (2011).

5. M.W. Smith, D.A. Berry, D. Shekhawat, D.J. Haynes, J.J. Spivey, and D.L. Floyd, "Effect of Catalyst Configuration on the Partial Oxidation of Hydrocarbons: Graded Bed Approach," *22nd North American Meeting*, North American Catalysis Society, Detroit, Michigan, June 7, 2011.

6. M.W. Smith, D.A. Berry, D. Shekhawat, D.J. Haynes, C.N. Wildfire, and E.M. Sabolsky, "Effect of Oxide Catalyst Surface Coverage in the Presence of Oxygen-conducting Supports for CPOX," *241st National Meeting and Exposition*, American Chemical Society, Anaheim, California, March 28, 2011.

7. M.W. Smith, D.A. Berry, D. Shekhawat, D.J. Haynes, and J.J. Spivey, "Development of a Structured Graded Catalyst System for the Catalytic Partial Oxidation of Hydrocarbons," *2011 Spring National Meeting*, American Institute of Chemical Engineers, Chicago, Illinois, March 16, 2011.

8. S. Guar, D.J. Haynes, J.J. Spivey, "Rh, Ni, and Ca Substituted Pyrochlore Catalysts for Dry Reforming of Methane," Applied Catalysis A: General, 403: p. 142-151, 2011.

References

1. D.J. Haynes, et al., "Catalytic Partial Oxidation of n-Tetradecane Using Rh and Sr Substituted Pyrochlores: Effects of Sulfur," Catalysis Today, 2009. **145**(1-2): p. 121-126.

2. D.J. Haynes, et al., "Catalytic Partial Oxidation of n-Tetradecane Using Pyrochlores: Effect of Rh and Sr Substitution," Catalysis Today, 2008. **136**(3-4): p. 206-213.

3. D.J. Haynes, et al., "Catalytic Partial Oxidation of a Diesel Surrogate Fuel Using an Ru-Substituted Pyrochlore," Catalysis Today, 2010. **155**(1-2): p. 84-91.

4. D.J. Haynes, et al., "Reducing the Deactivation of Ni-Metal during the Catalytic Partial Oxidation of a Surrogate Diesel Fuel Mixture," Catalysis Today, 2010. **154**(3-4): p. 210-216.

5. D.J. Haynes, D.A. Berry, D. Shekhawat, M.W. Smith, and J.J. Spivey, "Long Term Reforming of Commercial Diesel Fuel Using a Layered Pyrochlore Catalyst," in *Spring National Meeting*. 2010, American Chemical Society: San Francisco, California.

6. M.W. Smith, D.A. Berry, D. Shekhawat, D.J. Haynes, and J.J. Spivey, "Catalytic Material Development for a SOFC Reforming System: Application of an Oxidative Steam Reforming Catalyst to a Monolithic Reactor," in *8th International Fuel Cell Science, Engineering and Technology Conference*. 2010, American Society of Mechanical Engineers: Brooklyn, New York.

7. D. Shekhawat, D.A. Berry, D.J. Haynes, and M.W. Smith, "Oxide-Based Reforming Catalyst Evaluation and Development," in 2010 Office of Fossil Energy Fuel Cell Program Annual Report, DOE/NETL-2010-1439, October 2010.

8. A.P.E. York, T. Xiao, M.L.H. Green, and J.B. Claridge, "Methane Oxyforming for Synthesis Gas Production," Catalysis Reviews, 2007. **49**(4): p. 511-560.

9. R. Horn, et al., "Syngas by Catalytic Partial Oxidation of Methane on Rhodium: Mechanistic Conclusions from Spatially Resolved Measurements and Numerical Simulations," Journal of Catalysis, 2006. **242**(1): p. 92-102.

10. M. Prettre, C. Eichner, and M. Perrin, Trans. Faraday Soc., 1946. **43**: p. 335.

11. D. Shekhawat, et al., "Catalytic Partial Oxidation of n-Tetradecane in the Presence of Sulfur or Polynuclear Aromatics: Effects of Support and Metal," Applied Catalysis A: General, 2006. **311**: p. 8-16.

III.F.2 High-Methane Molten Catalytic Coal Gasifier for SOFC Power Plants

Nicholas Siefert (Primary Contact),
Dushyant Shekhawat
U.S. Department of Energy
National Energy Technology Laboratory
626 Cochrans Mill Road
Pittsburgh, PA 15236-0940
Phone: (412) 386-4404; Fax: (412) 386-6004
E-mail: Nicholas.Siefert@netl.doe.gov

Contract Number: 07-220611

Start Date: October 1, 2010
End Date: September 30, 2011

Fiscal Year (FY) 2011 Objectives

- Determine the kinetics of molten catalytic gasification of coal for a range of different alkali salt compositions, reactor temperatures, and reactor pressures.
- Evaluate the effects of alkali salt type and composition, temperature, and pressure on the methane composition in the syngas derived from molten catalytic gasification of coal.
- Optimize the process parameters in order to maximize the methane content in syngas.
- Initiate exergy analysis study to determine the overall process efficiency of integrating a molten catalytic gasifier with a solid oxide fuel cell (SOFC).

FY 2011 Accomplishments

- Submitted patent application for generating a methane and hydrogen rich syngas via coal gasification with molten alkali hydroxides."
- Completed experiments on the molten catalytic reactor that study the effect of pressure and temperature:
  - Measured both steam-coal gasification rates and methane compositions.
  - Highest weighted average methane composition was 18% (while also producing ~2.5% ethane).
- Initiated experiments on the molten catalytic reactor that study the effect of steam-to-coal ratio and catalyst-to-coal ratio.
- Published and presented experimental results from molten catalytic reactor.
- Published and presented results from exergy analysis of integrating catalytic gasification with pressurized SOFCs.

Introduction

In the United States (U.S.) today, coal power plants supply approximately 50% of the demand for electricity [1]. Nearly all of these coal power plants combust coal with air to provide the heat required to generate electricity in a Rankine vapor power cycle. This combustion process creates acid gases (NO_x, SO_x, and weakly CO_2), greenhouse gases (CO_2, etc.), entrained particulates, and heavy metal species. Emissions of strong acid gases and particulates are currently regulated in the U.S. and the emission of greenhouses gases may soon be regulated. Current methods for capturing CO_2, NO_x, SO_x, heavy metals species, and particulates from pulverized coal combustion (PCC) power plants cause decreased overall net energy efficiency and increased capital costs. The combination of these two effects causes the cost of electricity to increase compared with an unregulated coal power plant [2]. The goal of future research on coal use should focus on generating electricity from coal with minimal air emissions as well as minimal water consumption in concert with decreasing the cost of electricity. As such, the U.S. Department of Energy Office of Fossil Energy (DOE/FE) has set a 2015 Energy Goal of 60% electricity generation with greater than 90% capture and sequestration of greenhouse gases [3]. DOE/FE has also set a 2015 Energy Goal of multi-product capability, which includes co-generation of fuel/chemicals from a power plant during times of low electricity demand [3].

It appears that one of the ways to achieve both of these goals in an economically viable power plant is to integrate a catalytic coal gasifier with a SOFC [4-8]. Figure 1 shows the system efficiency of various coal-based power plant designs that capture and compress >90% of the greenhouse gases generated at the power plant. In Figure 1, the IGFC (integrated gasification fuel cell) represents entrained-flow gasification followed by a 0.1 MPa SOFC stack. Four cases of catalytic gasification are compared in Figure 1: a) 0.1 MPa stack and no anode recycle to gasifier; b) 1.8 MPa stack with no anode recycle; c) 0.1 MPa stack with anode recycle back to the gasifier; and d) 4.0 MPa stack with anode recycle back to the gasifier. Of the systems shown above, only the case that includes both anode recycle to the catalytic gasifier and pressurized operation of the fuel cell stack can reach the DOE/FE 2015 Energy Goal of at least 60% overall system efficiencies. One way of achieving an overall system efficiency of 60% is the following process: a) the coal gasifier produces a syngas with a methane composition of roughly 25% on a dry volume

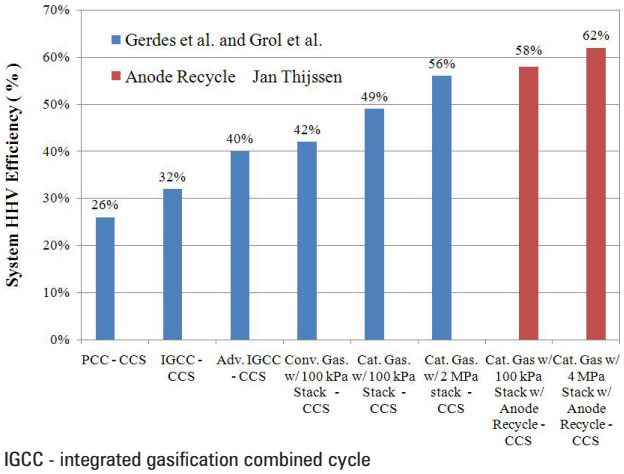

IGCC - integrated gasification combined cycle
CCS - carbon capture and sequestration

FIGURE 1. System efficiency for various configurations with carbon capture and compression to 15 MPa. Of the four catalytic gasification cases, two cases include recycling the anode tail gas back to the gasifier and two cases include oxy-combustion of the anode tail gas. The IGCC and IGFC cases use conventional entrained-flow gasifiers.

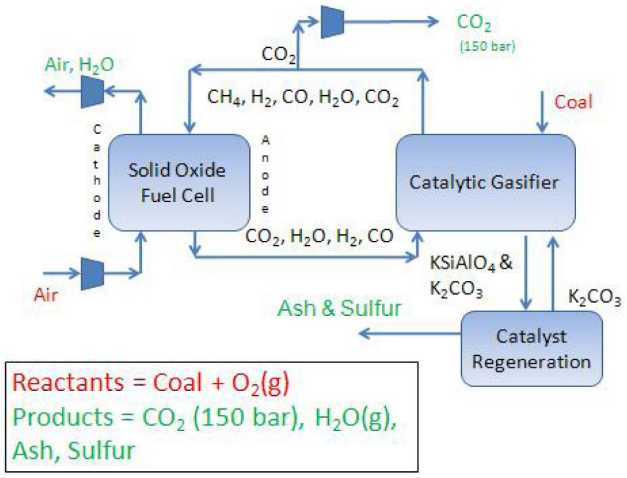

FIGURE 2. Molten catalytic gasification of coal integrated with an SOFC for an overall system efficiency near 60% and >90% capture of carbon dioxide. CO_2 is captured pre-SOFC and the anode tail gas is recycled back to the catalytic gasifier.

basis, b) the methane-rich syngas is sent to a SOFC, and c) the off-gases from the SOFC are recycled back to coal gasifier (Figure 2). The overall generation of work (electricity) in the process described here (~60%) is larger than conventional IGFC processes (~42%) where significant amounts of exergy destruction, i.e., entropy production, occur in entrained-flow, high-temperature coal gasification and in cooling a SOFC when the fuel is rich in hydrogen and low in methane. Some of the problems remaining before the "60% efficient/ multi-product capable" process described above could be commercialized include scaling up each individual sub-system and reducing the cost of fresh catalyst or catalyst recovery.

Approach

The goal of this research is to expand the operating range of molten salt gasifiers, compared with previous research by Esso Research & Engineering, Kellogg and Rockwell International in the 1970s [9-13] and compared with more recent work from Matsunami et al. [14], Jin et al. [15], and Kamo et al. [16]. This has been done by lowering the temperature of the reactor by using eutectic (mixed) alkali salts and by lowering the pressure so as to improve integration with SOFCs that operate at or just above atmospheric pressures. Our goal is to operate a molten catalytic gasifier at pressures near 2 MPa. This pressure was chosen as a balance between increased methane production at higher pressures and increased costs of associated turbines (to let down the pressure) and compressors (to compress the anode off-gas back to the pressure of the catalytic gasifier).

From a thermodynamic point of view, in order to operate at lower pressure and achieve at least 20% composition of methane in the syngas, the temperature of the reactor must be lowered. However, in order to maintain a molten bed and comparable kinetics, the use of 100% potassium carbonate must be replaced with the use of eutectic alkali salt mixtures (sodium, potassium, and lithium carbonates). The eutectic alkali salt mixture has a lower melting temperature, allowing the catalyst to be active at lower temperatures than pure potassium carbonate [15].

Potassium carbonate/hydroxide was found to catalyze both the steam-carbon reaction ($C+H_2O \leftrightarrow CO+H_2$) and the methanation reaction ($CO + H_2 \leftrightarrow \frac{1}{2}CH_4 + \frac{1}{2}CO_2$) [17-18], whereas sodium carbonate/hydroxide was found to only catalyze the steam-carbon reaction. Figure 3 is a qualitative energy diagram showing the two-step process for generating methane from carbon. It is expected that mixtures of sodium, potassium, and lithium carbonates should have the capability to catalyze the methanation reaction when there is a sizable portion of potassium in the mixture (>20%), and this will be one of main areas of experimental research because, to the best of our knowledge, there is no previous published literature on using molten carbonate eutectic mixtures for generating high methane content syngas.

In order to measure the kinetics of molten catalytic gasification of coal and to measure the methane composition in the syngas, a molten catalytic reactor was constructed along with associated equipment required for operation of the reactor. The reactor system and associated equipment are shown in Figure 4. The equipment consists of pressure vessel with a ceramic crucible at the bottom holding the catalyst and coal.

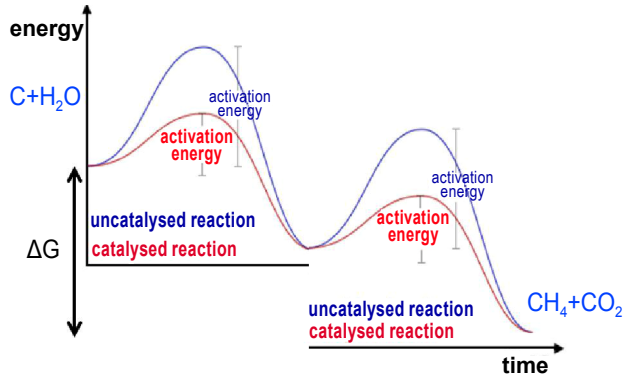

FIGURE 3. Gibbs free energy diagram vs. the reaction coordinate for the reaction of carbon and steam to methane and carbon dioxide at relative low temperature and high pressure (qualitative).

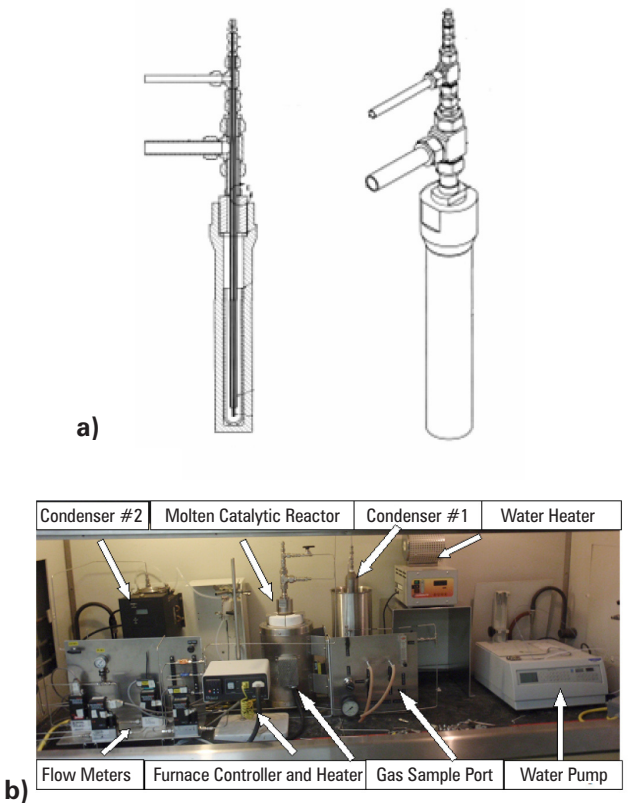

FIGURE 4. Molten catalytic reactor a) design and b) laboratory experiment. Steam and coal react in a bed of molten alkali salts. The reactor is designed for a maximum pressure of 2.5 MPa and temperature of 900°C.

A tube carrying steam is placed inside of the ceramic crucible, so that steam has to pass through a molten bed of coal and catalyst. The syngas exits the reactor and liquids are condensed before going through a pressure transducer. After this, liquids are condensed again in a second condenser held at a lower temperature. After this, the syngas goes to a Pfeifer OmniStar mass spectrometer. Alternatively, the syngas can be sampled just before the pressure transducer in order to check mass spectrometer results with gas chromatography. All experiments were semi-continuous, meaning that there was a set amount of coal and catalyst loaded into the reactor and then there was a continuous flow of steam into the reactor. So, by the end of the run, the coal is consumed and the main gas species in the pre-quenched syngas is just the water being continuously added. In future research, we plan to conduct experiments in which the water, coal, and catalyst are added into the reactor on a continuous basis. For our current experiments, the composition of unconverted water in the syngas was not measured because there were two liquid condensers before the mass spectrometer. The flow rate of syngas was determined by adding in a known amount of argon (10 sccm) throughout the experiment. For all experiments presented here, we used Pittsburgh #8 coal (100 mesh). In some experiments, fresh coal was used while in others devolatilzed coal was used. Devolatization of coal was performed at 700°C for 4 hours in an argon atmosphere. After devolatilization, the coal was ground down to approximately 20 mesh. The devolitalized coal was then mixed with the catalyst and devolitalized a second time before the experiment began. This devolitalization process was used in order to determine steam-carbon gasification reaction rates and to quantify the non-volatile methane production.

For all experiments, the coal and the catalyst was added dry such that there was a 1:1 ratio between carbon in the coal and alkali. Since equal amounts of Li, Na, and K were used, this means the ratio of elements on a mol-basis was C:Li:Na:K = 3:1:1:1. The elemental analysis of the coal by dry-wt% was C=83.2%, H=5.3%, O=8.8%, S=2.2%, and ash=9.2%. On an ash-free, dry mol-basis, this is: 54% C, 41% H, 4.3% O, and 0.5% S. The elemental analysis did not include a nitrogen balance. The ratio of hydrogen to carbon was 0.76. For the devolatized coal, we used a proximate analysis to determine the carbon remaining in the coal.

Results

Figure 5 shows the exhaust gas flow rate from gasification of 5 g of Pittsburgh #8 coal (100 mesh), 2.7 g of LiOH, 4.6 g of NaOH, and 6.4 g of KOH at 900°C and 2.1 MPa (300 psig). There is ~50 minutes delay in data collection because of the time required to pressurize and heat the vessel from pure argon at ambient conditions to 2.1 MPa (300 psig) and 900°C. After the first data point, there was an overall decrease in the total flow rate of syngas as time increased because the amount of coal in the reactor was slowly consumed. The methane and ethane composition decreased rapidly for two reasons: 1) the amount of coal was decreasing with time, and 2) the amount of steam available to reform the methane-ethane increased with time.

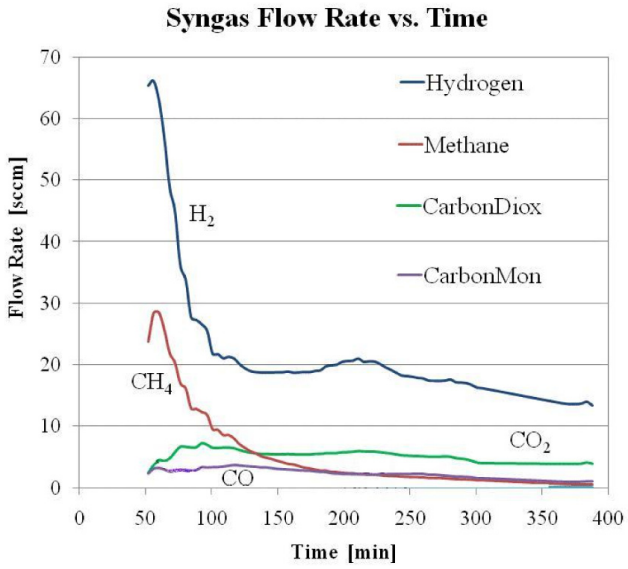

FIGURE 5. Flow rate of the syngas components from a coal-catalyst-steam experiment at 900°C and 2.1 MPa. Coal = 5 g of fresh Pittsburgh #8. Catalyst = 2.7 g of LiOH, 4.6 g of NaOH, and 6.4 g of KOH. Water flow rate = 0.05 mL/min.

Figure 6 shows the difference in reaction rates for coal with or without catalyst when the reactor pressure and temperature are the same: 2.1 MPa and 700°C. There is an obvious increase in the reaction rates with catalyst, as seen by the significant increase in the production of hydrogen and methane when catalysts are included with the coal. Figure 7 shows the production-averaged, syngas composition from the molten catalytic gasifier as a function of temperature of the reactor when the pressure was held constant at 2.1 MPa. Production-averaged means that the total amount of species X produced during the experiment divided by the total amount of syngas during the experiment. The highest average methane composition achieved so far was 18% while at the same time producing 2.5% ethane. This gives an equivalent amount of methane of 23%, which is consistent with the objectives of this project. The optimal methane composition was obtained at 800°C and 2.1 MPa.

The amount of CO_2 and CO, as well as H_2S and C_6H_6, increased with increasing temperatures, whereas the methane and ethane composition were largely independent of temperature. The reason why the methane and ethane composition do not decrease with increasing temperature, as one would initially expect from thermodynamic arguments, is that, at higher temperatures, there is less steam available to reform the methane and ethane into CO and H_2 because of the higher kinetic rates of steam-coal gasification. So, Le Chatelier's principle would predict less methane and ethane at higher temperature, but Le Chatelier's principle would also predict more methane and ethane

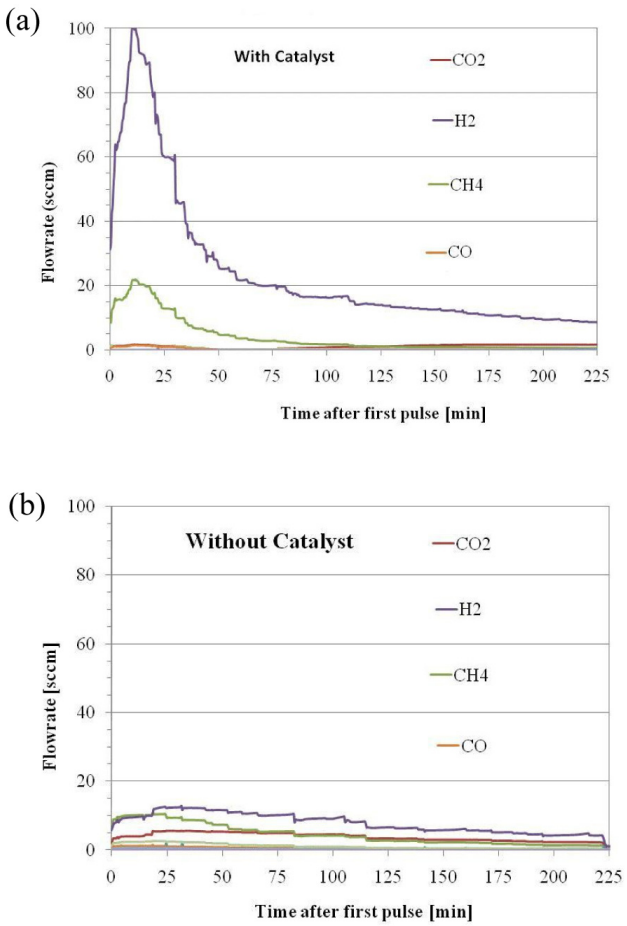

FIGURE 6. Flow rate of the syngas components from experiment at 700°C and 2.1 MPa using 5 g of fresh Pittsburgh #8. Water flow rate of 0.05 mL/min, (a) with catalyst [2.7 LiOH, 4.6 NaOH, 6.4 KOH] and (b) without catalyst.

as the steam is consumed. The two effects cancel with each other, which is why there is very little change in the methane and ethane composition as we increase the temperature in the reactor. From the difference in the kinetic rates versus temperature we were able to estimate an activation barrier for catalyzed steam-coal gasification of 58.7 kJ/mol.

Figure 8 shows the syngas composition, as well as the kinetic rates of steam-coal gasification, as a function of pressure of the vessel when the temperature was held constant at 700°C. As expected there was an increase in the methane composition as the pressure was increased. In this set of experiments we pyrolyzed the coal before use in the reactor because we wanted to rule out any change in the amount of pyrolysis gases as a function of pressure. So, we can confirm prior thermodynamic simulations in HSC Chemistry 7.0 [19] that predict larger amounts of methane at higher pressures. Interestingly, increased pressure had a positive effect on the reaction rates. This suggests that the reactions are not surface

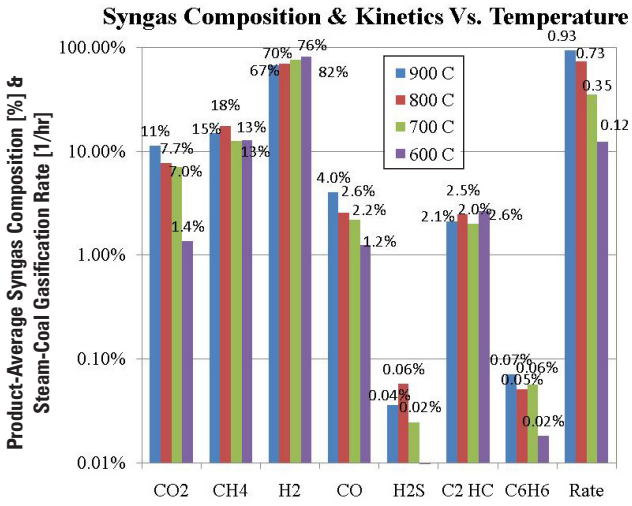

FIGURE 7. Production-averaged, dry syngas composition from the molten catalytic gasification of fresh Pittsburgh #8 coal (100 mesh) as a function of temperature of the reactor. 2.1 MPa, water flow rate = 0.05 mL/min, coal = 5 g, catalyst = 2.7 g of LiOH, 4.5 g of NaOH, 6.3 g of KOH. Note: C_2HC = ethane plus ethylene.

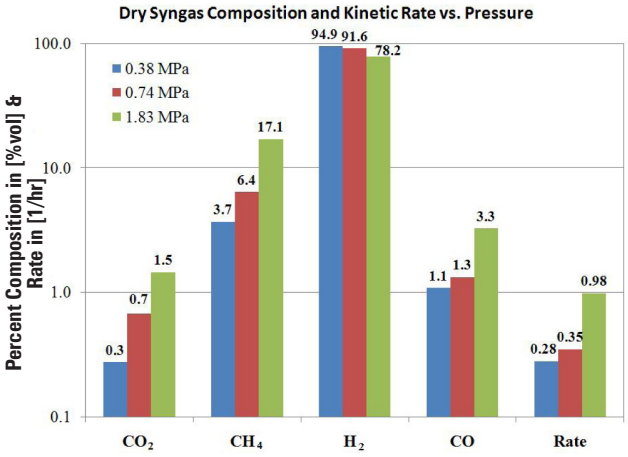

FIGURE 8. Syngas composition and kinetic rate from the molten catalytic gasification of pre-devolatized Pittsburgh #8 coal (20 mesh) as a function of pressure of the reactor. Water flow rate = 0.05 mL/min; 700°C; 3.6 g of pre-devol coal; 2.3 g of LiOH, 3.9 g of NaOH, and 5.5 g of KOH.

limited, but rather diffusion limited. This most likely means that the rates would be increased by forced mixing of the molten bed during the experiment, which we could not do in these experiments.

Conclusions and Future Directions

NETL has successfully measured the kinetics of catalytic coal gasification using molten alkali hydroxide salts and has measured the composition of methane in the syngas. To date, we have studied the effect of pressure and temperature, and have initiated experiments studying the effect of steam-to-coal ratio and catalyst-to-coal ratio. We have achieved an average composition of methane plus ethane greater than our initial goal of 20 mol% (dry). In future, we will continue studying the effect of steam-to-coal ratio and catalyst-to-coal ratio, as well as studying the effect of varying the composition of the molten catalysts. In addition, we will be converting our exergy analysis into an economic analysis of SOFC-based power plants fueled by either fluidized or molten catalytic reactors. Details of the exergy analysis can be found in Siefert et al. [8].

FY 2011 Publications/Presentations

1. N. Siefert and S. Litster, "Exergy & Economic Analysis of Catalytic Coal Gasifiers Coupled with Solid Oxide Fuel Cells," ASME Fuel Cell Science, Engineering & Technology Conference, Washington, D.C., August 2011.

2. N. Siefert, D. Shekhawat, T. McQuain, J. Ferrell, S. Litster, and D. Berry, "Molten Catalytic Coal Gasification for Methane Rich Syngas," 28th Annual Pittsburgh Coal Conference, Pittsburgh, Pennsylvania, September 2011.

References

1. U.S. Department of Energy, Energy Information Administration, International Energy Outlook 2006, DOE/EIA-0484 (2006).

2. E.S. Rubin, C. Chen, and A.B. Rao, 2007, "Cost and Performance of Fossil Fuel Power Plants with CO_2 Capture and Storage," Energ Policy, 35(9), pp. 4444-4454.

3. W.A. Surdoval, 2008, "Clean Economic Energy in a Carbon Challenged World," Presentation at 2008 International Pittsburgh Coal Conference, September 30, 2008.

4. M. Li, A.D. Rao, J. Brouwer, and G.S. Samuelsen, 2010, "Design of Highly Efficient Coal-Based Integrated Gasification Fuel Cell Power Plants," J Power Sources, 195(17), pp. 5707-5718.

5. J. Thijssen, 2009, "IGFC with Catalytic Hydro-Gasification Using Anode Exhaust," Presentation at NETL, July 13, 2009.

6. K. Gerdes, E. Grol, D. Keairns, and R. Newby, 2009, "Integrated Gasification Fuel Cell Performance and Cost Assessment," DOE/NETL-2009/1361.

7. E. Grol and J. Wimer, 2009, "Systems Analysis of an Integrated Gasification Fuel Cell Combined Cycle," DOE/NETL - 40/080609.

8. N. Siefert and S. Litster, 2011, "Exergy & Economic Analysis of Catalytic Coal Gasifiers Coupled with Solid Oxide Fuel Cells," ASME Fuel Cell Science, Engineering & Technology Conference, Washington, DC, August 2011.

9. R.L. Hirsch, J.E. Gallagher, R.R. Lessard, and R.D. Wesselhoft, 1982, "Catalytic Coal-Gasification - an Emerging Technology," Science, 215(4529), pp. 121-127.

10. C.A. Trilling, 1977, "Mass and Heat Balance for Coal-Gasification by Atomics Internationals Molten-Salt Gasification Process," Abstr Pap Am Chem S, 173(Mar20), pp. 17-17.

11. A.E. Cover, W.C. Schreine, and G.T. Skaperda, 1973, "Coal Gasification - Kelloggs Coal Gasification Process," Chem Eng Prog, 69(3), pp. 31-36.

12. C.A. Kumar, L.D. Fraley, and S.E. Handman, 1975, "Combined Power Cycle Using Low BTU Gas Produced from Kellogg Molten-Salt Coal Gasification Process," Abstr Pap Am Chem S, 170(Aug24), pp. 39-39.

13. C.L. Aldridge and D. Buben, 1972, "Production of Methane Rich Gases," U.S. Patent #3,689,240, assigned to Esso Research and Engineering Co., September 5, 1972.

14. J. Matsunami, S. Yoshida, Y. Oku, O. Yokota, Y. Tamaura, and M. Kitamura, 2000, "Coal Gasification with CO_2 in Molten Salt for Solar Thermal/Chemical Energy Conversion," Energy, 25(1), pp. 71-79.

15. G. Jin, H. Iwaki, N. Arai, and K. Kitagawa, 2005, "Study on the Gasification of Wastepaper/Carbon Dioxide Catalyzed by Molten Carbonate Salts," Energy, 30(7), pp. 1192-1203.

16. T. Kamo, K. Takaoka, J. Otomo, and H. Takahashi, "Production of Hydrogen by Steam Gasification of Dehydrochlorinated Poly(vinyl chloride) or Activated Carbon in the Presence of Various Alkali Compounds," J Mater Cycles Waste Manag (2006) 8:109–115.

17. A. Sheth, Y.D. Yeboah, A. Godavarty, Y. Xu, and P.K. Agrawal, 2003, "Catalytic Gasification of Coal Using Eutectic Salts: Reaction Kinetics with Binary and Ternary Eutectic Catalysts," Fuel, 82(3), pp. 305-317.

18. N.C. Nahas, 1983, "Exxon Catalytic Coal-Gasification Process - Fundamentals to Flowsheets," Fuel, 62(2), pp. 239-241.

19. HSC Cemistry 7.0, Outotec Solutions, http://www.outotec.com/.

III.F.3 Solid Oxide Fuel Cells Operating on Alternative and Renewable Fuels

Chunshan Song (P.I. and Primary Contact),
Serguei Lvov (co-P.I.), Xiaoxing Wang,
Mamoru Fujii, Jing Xiao,
Cigdem Sentorun-Shalaby, Chao Xie,
Emanuela Peduzzi, Xiaoliang Ma,
Mark LaBarbera, Sanchit Khurana,
Mark Fedkin, David Johnson
The Pennsylvania State University (PSU)
EMS Energy Institute and Department of Energy and Mineral Engineering
C211 CUL
University Park, PA 16802
Phone: (814) 863-4466; Fax: (814) 865-3573
E-mail: csong@psu.edu

DOE Project Manager: Joseph Stoffa
Phone: (304) 285-0285
E-mail: Joseph.Stoffa@netl.doe.gov

Contract Number: NT0004396

Start Date: October 1, 2010
End Date: August 31, 2012

Fiscal Year (FY) 2011 Objectives

- Develop new fuel processing approaches for using selected alternative and renewable fuels – anaerobic digester gas (ADG) and commercial diesel fuel, in solid oxide fuel cell (SOFC) power generation systems.
- Develop and evaluate effective sorbents for ADG cleanup.
- Improve the performance of the Ni-based and metal oxide-based adsorbents for adsorptive desulfurization (ADS) of ultra-low sulfur diesel (ULSD).
- Develop Ni-based catalysts for steam reforming of commercial diesel fuel with fundamental understanding of the sulfur tolerance and carbon resistance of the developed catalysts via various characterization techniques.

FY 2011 Key Accomplishments

- A novel molecular basket sorbent (MBS) that is able to remove both CO_2 and H_2S has been developed for ADG cleanup. The MBS was prepared by loading 50 wt% of polyethylenimine (PEI) on SBA-15, and evaluated in the in the flow adsorption system at 25 and 75°C using a simulated ADG gas.
- Mixed metal oxide-based adsorbents have been explored in this project for ADG cleanup and a highly efficient Cu-Ti-Ce-O adsorbent has been developed. A series of Ti-Ce-O-based adsorbents have been prepared and explored for ADG cleanup.
- Supported Ni adsorbents were found highly effective for sulfur removal from ULSD. The supported Ni adsorbents prepared by a impregnation method with ultrasonic aid showed great performance for ADS of ULSD with a breakthrough capacity higher than 75 g-F/g-A. It was found that the best Ni loading on MCM-48 is 20 wt%.
- The effects of Ti-Ce loading and support on the performance of mesoporous silica supported Ti-Ce-O adsorbent for adsorptive desulfurization of ULSD have been studied and clarified. Through the comparison, of the adsorption performance of the 15 wt% CeO_2/MCM-48, 15 TiO_2/MCM-48 and 15 wt% $Ti_{0.9}Ce_{0.1}O_2$/MCM-48, we found that Ce and Ti oxides have a strong synergetic effect on the performance of the Ti-Ce-O/MCM-48 adsorbent.
- A new iron modified Ni catalysts with and without K modification were prepared and studied for steam reforming of a commercial diesel. It was found that the 10Ni-5Fe/Al showed better activity than both 10Ni/Al and 10Ni5Co/Al.
- A combined steam reforming, nickel-yttria stabilized zirconia (Ni-YSZ) anode SOFC test system has been developed and tested for a period of 200+ hours running on a simulated anaerobic digester gas and reformed commercial diesel.
- Electrochemical impedance spectroscopy (EIS) and equivalent circuit modeling have been used to track the degradation of SOFC performance operating on anaerobic digester gas over a period of 200+ hours.
- Effects of SOFC poisoning by H_2S impurities in ADG fuel were evaluated using EIS.
- In this period, the work has generated four journal articles and three presentations at national/international conferences.

Introduction

The EMS Energy Institute at PSU focuses on the development of fuel processors for both ADG and commercial diesel fuels for integration with SOFC power generation systems, and is responsible for the development of the sorbents and reforming catalysts formulations. As scheduled, during this annual report period, our major work focused on: 1) preparation and

evaluation of novel sorbents including MBS and mixed metal oxides adsorbents for ADG cleanup; 2) improving the adsorption performance of mesoporous molecular sieve supported Ni adsorbents and mixed Ti-Ce-O-based adsorbents for adsorptive desulfurization of ULSD; 3) evaluation and characterization of Ni-based catalysts for steam reforming of commercial diesel fuel; and 4) the continued operation of a Ni-YSZ single cell SOFC on both a model anaerobic digester gas and also a commercial diesel reformate.

Originally this project included a subcontract to Siemens Energy Inc, to provide SOFC ring cell samples to PSU for testing. However, an economic downturn led to the elimination of the Siemens Stationary Fuel Cell Division within the company. Unfortunately, this led to the Siemens subcontract with PSU ending on September 23, 2010.

Approach

To achieve the FY 2011 objectives, the following approaches have been applied:

1. For ADG cleanup, novel MBSs have been prepared by loading PEI to mesoporous molecular sieve, SBA-15 with different PEI loadings. Considering the removal of H_2S alone, mixed Ti-Ce metal oxide-based adsorbents have also been explored and studied.
2. For ADS of ULSD, mesoporous molecular sieves supported Ni sorbents and a series of Ti-Ce-O-based adsorbents have prepared and evaluated for deep removal of sulfur from ULSD.
3. For steam reforming of commercial diesel fuel, the catalyst development has been focused on non-noble metal, Ni-based catalysts by the addition of iron and potassium.
4. The SOFC system for single cell operation utilized NextCell SOFC buttons consisting of a 50 µm porous Ni-YSZ anode supported by a 150 µm dense 8% YSZ membrane, countered by a 50 µm porous lanthanum strontium manganite cathode. Each test was carried out at 900°C. Air was fed to cathode. Humidified fuels were supplied at 50 sccm. The SOFC operation was controlled by the Arbin fuel cell station connected with the Solartron EIS system for electrochemical characterization.

Results

Development of ADG Fuel Processor Concept (Novel)

Copper-incorporated Ti-Ce-O adsorbent with the molar ratio of 1:9:1 for Cu:Ti:Ce, has been prepared as the same procedure for the preparation of Ti-Ce-O by a co-precipitation method. The obtained H_2S breakthrough curve is presented in Figure 1. For comparison, those from Ti-Ce-O adsorbent, SulfurTrap R7 and SulfaTreat are also presented. The current result shows that the Cu-Ti-Ce-O adsorbent is more promising for ADG cleanup.

Deep Desulfurization of ULSD

The effects of Ti-Ce loading and support on the performance of mesoporous silica supported Ti-Ce-O adsorbent for adsorptive desulfurization of ULSD have been studied and clarified. Through the comparison, of the adsorption performance of the 15 wt% CeO_2/MCM-48, 15 TiO_2/MCM-48 and 15 wt% $Ti_{0.9}Ce_{0.1}O_2$/MCM-48, we found that Ce and Ti oxides have a strong synergetic effect on the performance of the Ti-Ce-O/MCM-48 adsorbent. Different mesoporous silicas including EH-5, SBA-15, MCM-41 and MCM-48 supported mixed metal oxide adsorbents have been studied for ADS of ULSD at room temperature. MCM-48 showed the best among the studied supports. It was found that both the surface area and the pore structure of the support influence the adsorption performance of the supported Ti-Ce-O adsorbents. In addition, adding an activated carbon column as the guard-bed can significant improve the adsorption performance of supported Ti-Ce-O adsorbents.

Catalyst Development for Steam Reforming of Commercial Diesel

A new iron-modified Ni catalysts with and without K modification were prepared and studied for steam reforming of a commercial diesel. It was found that the

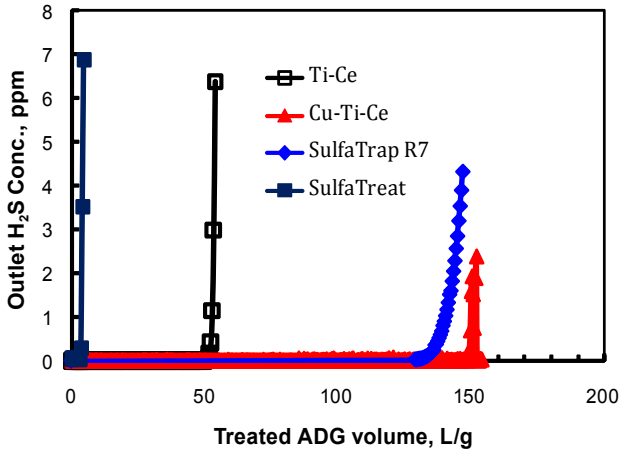

FIGURE 1. H_2S Breakthrough Curves over Cu-Ti-Ce-O, Ti-Ce-O, SulfaTrap R7 and SulfaTreat Adsorbents at Room Temperature. Conditions: ADG, 200 ppmv H_2S-10 v% N_2-40 v% CO_2-50 v% CH_4; Volume of Adsorbent Bed, 2 ml; Pressure, 1 atm.; Flow-rate, 50 ml/min (gas hourly space velocity, 1,500 h^{-1}).

10Ni-5Fe/Al showed better activity than both 10Ni/Al and 10Ni5Co/Al. The addition of iron can promote the resistance to both carbon deposition and sulfur poisoning. With the addition of K, the catalytic performance of Ni-Fe catalyst can further improved. The prepared Ni-based catalysts were characterized by sulfur and Carbon X-ray absorption near edge structure (XANES), and X-ray photoelectron spectroscopy, respectively. The characterization results indicate that the presence of Fe may hinder sulfur adsorption on reforming catalysts, thus improving the sulfur tolerance of the Ni-Fe catalyst. The addition of K can enhance the gasification of deposit carbon and therefore reduce the carbon accumulation on the 10Ni-5Fe-5K/Al reforming catalyst.

Ni-YSZ Solid Oxide Fuel Cell Testing Results

EIS and equivalent circuit modeling have been used to track the degradation of SOFC performance operating on anaerobic digester gas over a period of 200+ hours. Various amounts of H_2S (50-200 ppm) were introduced to the anaerobic digester gas fuel fed to the system anode. The Ni-YSZ anode SOFC showed a strong sensitivity to H_2S, which caused a nearly immediate decrease in power density of 50-60%. The poisoning of the anode was shown to be partially but not completely reversible with the removal of H_2S from the fuel.

Conclusions and Future Directions

Within this period, the following conclusions can be drawn:

1. A novel MBS sorbent for ADG cleanup has been prepared by loading 50 wt% of PEI on SBA-15, and evaluated in the in the flow adsorption system at 25 and 75°C using a simulated ADG gas containing 200 ppmv H_2S-10 v% N_2-40 v% CO_2-50 v% CH_4. It was found that the prepared sorbent can remove both CO_2 and H_2S from the gas at 25 and 75°C.
2. Ti-Ce mixed oxide adsorbents have been developed in this project for ADG cleanup. The Cu-Ti-Ce-O adsorbent exhibited very good performance for ADG cleanup. It can treat about 150 L-ADG/g before H_2S broke through. The corresponding adsorption capacity is 41.7 mg-H_2S/g, better than the best commercial adsorbent, SulfaTrap R7, tested in this project, which can treat about 139 L-ADG/g with an adsorption capacity of 39.1 mg-H_2S/g.
3. Supported Ni adsorbents prepared by ultrasonic aid method showed great performance for adsorptive desulfurization of ULSD with a breakthrough capacity higher than 75 g-F/g-A. It was found that loading 20 wt% of Ni on MCM-48 can prepare the best sorbent. The breakthrough capacity of 2.1 mg-S/g-sorb at sulfur level of 1 ppmw can be reached, which is higher than that of the best Ni-based sorbent reported in the literature by a factor of more than 2.
4. Through the comparison of the adsorption performance of the 15 wt% CeO_2/MCM-48, 15 TiO_2/MCM-48 and 15 wt% $Ti_{0.9}Ce_{0.1}O_2$/MCM-48, we found that Ce and Ti oxides have a strong synergetic effect on the performance of the Ti-Ce-O/MCM-48 adsorbent, which will be further studied in the continuous work. Adding an activated carbon column as the guard bed can significant improve the adsorption performance of supported Ti-Ce mixed oxide adsorbents.
5. Different mesoporous silica including EH-5, SBA-15, MCM-41 and MCM-48 supported mixed metal oxide adsorbents have been prepared and applied for ADS of ULSD at room temperature. MCM-48 supported adsorbent showed the best adsorption performance among the studied supports. It was found that both the surface area and the pore structure of the mesoporous silica support influence the adsorption performance of the supported mixed metal oxide adsorbents.
6. A new iron-modified Ni catalysts with and without K modification were prepared and studied for steam reforming of a commercial diesel. It was found that the 10Ni-5Fe/Al showed better activity and reforming performance than both 10Ni/Al and 10Ni5Co/Al. The addition of iron can promote the resistance to both carbon deposition and sulfur poisoning. With the addition of K, the catalytic performance of Ni-Fe catalyst can further improved.
7. The prepared Ni-based catalysts were characterized by X-ray diffraction and Carbon XANES, respectively. The results show that the presence of K in the Ni-based catalysts may be able to promote the formation of carbonate species, which can benefit the gasification process and thus reduce the carbon deposition. The XANES results indicate that the presence of Fe may hinder sulfur adsorption on reforming catalysts, thus improve sulfur tolerance of Ni-Fe catalyst. While the addition of K can enhance the gasification of deposit carbon and therefore reduce the carbon accumulation on the 10Ni-5Fe-5K/Al reforming catalyst.

Special Recognitions & Awards/Patents Issued

1. The P.I. of this project, Chunshan Song, received the 2010 Henry H. Storch Award in Fuel Chemistry from American Chemical Society, was selected as recipient for the Distinguished Researcher Award in Petroleum Chemistry from American Chemical Society in 2011, was named Distinguished Professor of Fuel Science at the Pennsylvania State University in 2010, and received the Faculty Scholar Medal for Outstanding Achievements in Engineering from the Pennsylvania State University in 2011.

FY 2011 Publications/Presentations

1. Cigdem Sentorun-Shalaby, Shyamal Kumar Saha, Xiaoliang Ma, and Chunshan Song, "Mesoporous-Molecular-Sieve-Supported Nickel Sorbents for Adsorptive Desulfurization of Commercial Ultra-Low-Sulfur Diesel Fuel," *Applied Catalysis B – Environmental* 101(3-4) 2011, 718-726.

2. Chao Xie, Yongsheng Chen, Yan Li, Xiaoxing Wang, and Chunshan Song, "Influence of Sulfur on the Carbon Deposition in Steam Reforming of Liquid Hydrocarbons over CeO_2-Al_2O_3 Supported Ni and Rh Catalysts," *Applied Catalysis A – General* 394 (1-2) 2011, 32-40.

3. Chao Xie, Yongsheng Chen, Yan Li, Xiaoxing Wang, and Chunshan Song, "Sulfur Poisoning of CeO_2-Al_2O_3-Supported Mono- and Bi-Metallic Ni and Rh Catalysts in Steam Reforming of Liquid Hydrocarbons at Low and High Temperatures," *Applied Catalysis A – General* 390 (1-2) 2010, 210-218.

4. Xiaoxing Wang, Shuqi Zhao, Xiaoliang Ma, and Chunshan Song, "Carbon Dioxide Sorption over Molecular Basket Sorbents: a Detailed TPD Study," 22nd North American Catalysis Society meeting, Detroit, Michigan, June 2–10, 2011.

5. Chao Xie, Yongsheng Chen, Xiaoxing Wang, and Chunshan Song, "Influence of Sulfur on Carbon Deposition in Steam Reforming of Liquid Hydrocarbons," 22nd North American Catalysis Society meeting, Detroit, Michigan, June 2–10, 2011.

6. Xiaoxing Wang, Xie Chao, Mark Labarbera, Mark Fedkin, Serguei Lvov, and Chunshan Song, "Steam Reforming of Liquid Hydrocarbon Fuels with On-Line Solid Oxide Fuel Cell Test," 241st ACS National Meeting, Anaheim, California, March 27–31, 2011.

7. M. LaBarbera, M. Fedkin, X. Wang, X. Chao, C. Song, and S. Lvov, "Solid Oxide Fuel Cell Fueled by Diesel Reformate and Anaerobic Digester Gas," *ECS Transactions* 35 (1) 2011, 2867-2872.

8. Jiahua Guo, Chao Xie, Kyungtae Lee, Neng Guo, Jeffrey T. Miller, Michael J. Janik, and Chunshan Song, "Improving the Carbon Resistance of Ni-Based Steam Reforming Catalyst by Alloying with Rh: A Computational Study Coupled with Reforming Experiments and EXAFS Characterization," *ACS Catalysis* 1 (6) 2011, 574–582.

III.F.4 Novel Water-Neutral Diesel Fuel Processor and Sulfur Trap

Subir Roychoudhury (Primary Contact), Christian Junaedi, Jeff Weissman and Dennis Walsh
Precision Combustion, Inc. (PCI)
410 Sackett Point Rd.
North Haven, CT 06473
Phone: (203) 287-3700 ext. 267; Fax: (203) 287-3710
E-mail: sroychoudhury@precision-combustion.com

DOE Project Manager: Joseph Stoffa
Phone: (304) 285-0285
E-mail: Joseph.Stoffa@netl.doe.gov

Contract Number: ER84674

Start Date: August 15, 2008
End Date: February 14, 2012

Fiscal Year (FY) 2011 Objectives

- Further develop and optimize the low pressure drop fuel injector/nozzle to permit stable steady-state operation, cold start-up, and 5:1 turndown ratio. Map autothermal reformer (ATR) performance and perform durability test with the low pressure drop nozzle and show coking avoidance with complete fuel conversion to C1 products and ~85% reforming efficiency while operating the reformer with low water usage.
- Compare different catalyst options and evaluate their performance to determine the optimal catalyst for reforming application to meet commercially viable auxiliary power unit (APU) system targets.
- Through the Phase II Supplemental effort (awarded in 2010), further develop and demonstrate the benefits of Rh-pyrochlore catalysts for diesel reforming, gearing towards commercialization and high-volume reforming applications.
- Advance PCI's reformer development towards specific value-added fuels and operating conditions as well as towards supporting designs for a variety of fuel cell stack opportunities.
- Demonstrate operation of fuel processor system integrated with a solid oxide fuel cell (SOFC).

FY 2011 Accomplishments

In the third budget period of this Phase II project, the reformer operation under water neutral condition via direct anode recycle and condensation approaches was further applied and optimized. The low pressure nozzle was further developed, optimized, and tested for turndown and cold-start capability. Additionally, PCI has successfully scaled up the preparation method for the National Energy Technology Laboratory's (NETL's) rhodium-pyrochlore catalyst and performed multiple tests to determine the applicability of this material for practical, cost-effective diesel fuel ATR operation. Finally, preliminary testing of PCI's fuel reformer using biodiesels was performed to evaluate fuel flexibility of the reformer system.

- **Evaluated and optimized water neutral reformer operation via both direct anode recycle and condensation approaches:** Performance mapping of a Microlith®-based fuel reformer has been completed with Tier II diesel to evaluate and optimize operating conditions using anode recycle approach for water recovery and water neutrality. Stable reformer operation was demonstrated with low water usage while avoiding coke formation and sulfur poisoning. An alternative approach to water neutral operation by using a condenser was also demonstrated. Tests were performed to validate the maximum achievable water recovery from anode exhaust at different ambient/cooling air conditions and to compare experimental results with the predicted values. Test results indicated that a sufficient amount of water can be recovered to permit fuel reformer operation under a water neutral condition.
- **Further developed, optimized, and tested low pressure drop nozzle:** Tests were performed to evaluate turndown capability of the low pressure nozzle by evaluating the performance of the fuel reformer. A durability test was performed for 50 hours to evaluate the reactor performance and stability during operation with Tier II diesel under a water neutral condition. Results from the 50-hour test showed stable catalyst temperature profile and product composition with very low nozzle pressure drop (further improved over the program objective) and capability of cold-start.
- **Developed coating technique for an alternative catalyst and performed diesel ATR reforming:** PCI has successfully scaled up the preparation method for NETL's rhodium-pyrochlore catalyst and performed multiple tests to determine the applicability of this material for practical, cost-effective diesel fuel ATR operation. A washcoat formulation was specifically developed to coat an alternative catalyst on the Microlith® substrate for fuel reforming. Results from catalyst testing to date demonstrated potential for a low-cost, efficient reformer that can accomplish complete fuel conversion and high reforming efficiency for reformation of diesel fuel.

- **Demonstrated fuel flexible reformer system:** Testing of PCI's fuel reformer unit with different fuels, including biodiesel (B50 blend), camelina oil, synthetic fuels, and sulfur containing military jet fuels has been performed. Stable reformer performance was obtained from all these tests, which demonstrates fuel flexibility of the reformer system. More tests will be performed using other biodiesel blends, such as B99 and B75, to further evaluate the performance of the fuel reformer.

Introduction

Fuel cell technology for auxiliary power or hybrid vehicle range extension offers the potential for major contributions towards long-term U.S. Department of Energy (DOE) objectives of clean energy, efficiency, and independence. Yet fuel cell technology faces daunting entry barriers, notably including high unit costs amidst low sales volume as well as the absence of a hydrogen fueling infrastructure. Thus, reforming of liquid fuels to produce hydrogen for fuel cell stacks is a practical approach for operating fuel cells due to the high energy density and the infrastructure availability. However, key barriers for the Solid State Energy Conversion Alliance (SECA) industrial teams are the lack of a compact and economical diesel fuel processor capable of operating with long-term stability under a water neutral condition (i.e., very low steam-to-carbon ratios) while being resistant to coke formation and sulfur poisoning. Fuel preparation for these reformers also remains problematic primarily due to the lack of good mixing at low air-pressure drop and resultant reactor non-uniformities leading to coke formation, among other things.

PCI is developing ultra-compact and sulfur-tolerant Microlith® fuel processor technology to reform conventional fuels such as diesel, gasoline, distillate fuels, and liquid biofuels to the sulfur-free, hydrogen-rich fuels required by fuel cells. By avoiding the need for a hydrogen fueling infrastructure, PCI's technology offers a major step advance towards a vital, self-sustaining American fuel cell industry. Through DOE Small Business Innovation Research (SBIR) Phase II and Phase II Supplemental (awarded in 2010), PCI has demonstrated this technology, along with improved catalyst effectiveness, demonstrated water neutral operation, fuel flexibility, and substantially improved fuel injection pressure drop without performance loss, reducing parasitic losses of the overall system. The resulting fuel processor enables fuel cell use of wide range of fuels including medium sulfur JP-8, ultra-low sulfur diesel (ULSD)/medium sulfur diesel, and biodiesels. This system and balance-of-plant simplification will allow for cost optimization to meet commercially viable targets for the entire APU fuel cell system.

Approach

Reformer operation under water neutral or waterless condition by avoiding the need for external water addition is a significant requirement for practical portable systems. Moreover, lower water usage can lead to faster start-up times, as less water needs to be vaporized at start-up. The reduction/elimination of water usage, however, can result in higher peak temperatures within the reactor/catalyst bed and can increase the production of higher hydrocarbons, particularly olefins, in the reformate stream. The former can compromise catalyst durability while the latter increases the likelihood of coking in the fuel cell stacks. It is important, therefore, to demonstrate long-term reformer operation at water neutral condition using feasible water recovery approaches without catalyst degradation and coke formation.

The proposed concept being developed in this project builds upon PCI's Microlith® reforming technology which employs a mesh-based, short-contact-time catalyst as an integrated component of a novel reformer system involving fuel injector, reactor, steam generator, and sulfur trap. PCI's existing 5 kW_{th} system size is approximately 5 liters and weighs about 5 kg. This reactor starts up in partial oxidation mode and then transitions to ATR mode upon introduction of steam, operating at low steam-to-carbon ratios. It uses a limited amount of water that can be recovered from the system exhaust, either via a direct recycle approach or a condenser approach, while performing efficient fuel reformation without performance degradation and coke formation. Since the reformer is operated at very low steam-to-carbon ratios, sulfur compounds are readily adsorbed in a downstream desulfurizer bed. Appropriate thermal integration of the reformer, fuel cells, water recovery unit, and other balance-of-plant components in the APU system is also necessary to maximize the overall system efficiency and has been explored using ASPEN process simulation software.

Results

Key results from the third budget period of this Phase II project include: (i) the successful demonstration of a low pressure nozzle for fuel processor operation under water neutral conditions; (ii) the development of an alternative catalyst and demonstration of the applicability of this material for practical, cost-effective diesel fuel reformer operation; and (iii) the evaluation of fuel flexibility of PCI's reformer system.

Development of a Low Pressure Drop Fuel Injector

A critical challenge for on-board fuel reforming is the use of low air pressure drop nozzles which permit uniform mixing of fuel, air and steam prior to entering the reactor. While lower pressure drop

reduces parasitic losses of the overall APU system, it generally compromises mixture quality, resulting in higher peak temperatures due to local unmixedness and higher propensity for catalyst deactivation due to sintering and coke formation. In this Phase II effort, PCI has successfully developed a novel low pressure nozzle with cold-start and turndown capability. This result is significant because it reduces parasitic power requirements while providing uniform flow and consistent performance over wide operating range.

Tests were performed to continue the validation of the low pressure nozzle by evaluating the performance of the fuel reformer. Operational window and performance mapping were developed to determine the optimum operating conditions of the low pressure ATR unit that demonstrate coking avoidance with complete fuel conversion to C1 products (i.e., CO, CO_2, and CH_4) and ~85% reforming efficiency while operating the reformer under water neutral conditions. Here, the reforming efficiency is calculated based on the ratio of the lower heating values (LHVs) of H_2 and CO in the reformate stream to the LHV of feed fuel. To date, the durability of the nozzle has been demonstrated for at least 100 hours by integrating it with an ATR fuel processor and operating it with Tier II diesel and sulfur containing distillate fuel for 50 hours each. Results from these 50-hour tests showed stable catalyst temperature profile and product composition with very low nozzle pressure drop (further improved over the project objective).

Development of an Alternative Catalyst for Water Neutral Diesel Reformation

With fuel processor technology drawing substantial commercial interest, fuel processor costs in manufacture need to be substantially reduced to help fuel cells achieve economic viability compared to alternatives such as internal combustion gensets. The use of expensive precious metal catalysts in the reformer and fuel cell system mainly determines the high cost of this technology. Thus, it is key to develop a highly selective, sulfur tolerant multifunctional reforming catalyst for reformation of diesel and logistics fuels at low cost.

During FY 2010, the feasibility of integrating the NETL catalyst on PCI's Microlith® reactor to perform ATR operation with diesel and logistic fuels was demonstrated. A washcoat formulation and coating technique was specifically developed to coat the alternative catalyst on the Microlith® substrate.

PCI has successfully prepared both the 2 wt% and 5 wt% Rh-pyrochlore materials. Conventional powder X-ray diffraction (XRD) of this material determined the presence of pyrochlore diffraction intensities. Some of this PCI-synthesized Rh-pyrochlore was tested at NETL on their small-scale rapid-aging diesel fuel catalytic partial oxidation apparatus. Good reforming performance, equivalent to NETL-synthesized material, was obtained, with deactivation behavior similar to that of the NETL's Rh-pyrochlore material.

Washcoating the Rh-pyrochlore material directly onto the Microlith® substrate using our conventional coating methods was not particularly successful. In order to obtain good coating adhesion on the Microlith® substrate, the washcoat must be stable and easily applied, and the resulting coating must have a high degree of adhesion and be sufficiently abrasion resistant to withstand routine handling and multiple thermal cycles. Prepared pyrochlore material proved difficult to suspend in an aqueous slurry. Nevertheless, an approach was identified that worked best and resulted in acceptable adhesion.

For our initial proof-of-concept study, the Microlith® substrate was coated directly with the Rh-pyrochlore and the resulting sample was tested in PCI's ATR reactor using low-sulfur JP-5 (resembles Tier II diesel, but with lower aromatics content) from 3.5 to 5 kWth input (based on fuel energy content). Table 1 shows the results from this Rh-pyrochlore/Microlith® catalyst test along with the results from similar tests using PCI's conventional catalyst for comparison. Even though the Rh-pyrochlore test had much less active metal, as compared to the PCI's base catalyst, performance for JP-5 autothermal reforming was acceptable, approaching that of the conventional catalyst; but product hydrocarbon content was not acceptable. Thus, there is a need to understand the underlying structural features of this material responsible for the catalytic activity so as to enable pathways towards improving Rh-pyrochlore coating protocol on the Microlith substrate and catalyst performance.

Further development effort to optimize coating of the Rh-pyrochlore on the Microlith® substrate is currently ongoing at PCI. To date, four catalyst iterations and testing have been performed, with notable improvement in conversion, reforming efficiency, and formation of coke precursor (i.e., ethane, ethylene, propane, propylene), as shown in Table 2. The latest catalyst iteration resulted in near complete fuel conversion to C1 products (i.e., CO, CO_2, and CH_4) and 79% reforming efficiency with 200 ppm_v of total higher hydrocarbons level in the reformate stream. Even though the performance of the Rh-pyrochlore coated on the Microlith® substrate has shown significant improvement, it is still below the targeted values of 85% reforming efficiency and <50 ppm_V higher hydrocarbons (i.e., $>C_1$) in the reformate stream. We expect to achieve these target values with further catalyst optimization effort to be continued in 2011.

TABLE 1. Comparison of PCI's Synthesized 2 wt% Rh-Pyrochlore and PCI's Rh-based Conventional Catalyst for ATR Testing with Low-Sulfur JP-5

	PCI's synthesized 2 wt% Rh-pyrochlore	PCI Rh-based conventional catalyst
Relative Rh content in reactor (normalized value)	0.03	1
H_2O/C in feed	1.3	0.9
O (from air)/C in feed	1.0	1.0
Average operating temperature (°C)	880	860
Reforming efficiency (LHV product H_2+CO) /LHV feed fuel	74%	80%
Product CH_4 content	0.31%	0.06%
Product detectable non-CH_4 hydrocarbons	1,460 ppm	0

TABLE 2. Performance Results, Including Fuel Conversion to C1 Products, Reforming Efficiency, and Higher Hydrocarbons Level in the Reformate Stream, for Each Iteration from Rh-Pyrochlore Catalyst Development

Iteration #	Conv. to C1s (%)	Efficiency (%)	C2s (ppm_v)	C3s (ppm_v)
1	94.1	73.9	1,175	260
2	97.1	75.5	1,100	290
3	~100	79.3	634	64
4	~100	78.8	198	0
(Target)	100	85	0	0

Fuel Processor Tests with Biodiesels

In order to demonstrate the fuel flexibility of PCI's reformer system, tests were performed using B50 biodiesel and camelina oil. A B50 biodiesel blend was obtained by blending B99 biodiesel with Tier II diesel in 50:50 ratio by weight. Tests were performed under autothermal reforming and catalytic partial oxidation conditions. In both tests, the reactor was successfully started up and stable catalyst performance was demonstrated. The test with B50 biodiesel was performed under autothermal reforming condition, and the reactor produced a reformate stream consisting of 30 mole% H_2 and 15 mole% CO (dry basis), with less than 50 ppm_v (dry basis) of total higher hydrocarbons. Preliminary tests, therefore, showed potential for highly efficient biodiesel reforming to syngas, and more tests will be performed to develop performance maps and to optimize the operating conditions for reformation of biodiesel fuels.

Conclusions and Future Directions

PCI has successfully demonstrated efficient, durable, fuel flexible autothermal reforming operation under water neutral condition. Both direct anode recycle approach and condensation approach for recovering exhaust water were demonstrated during diesel autothermal reforming operation. The operating conditions of the proposed water recovery approaches have been optimized and the reactor performance has been characterized and evaluated.

PCI has also developed and tested a novel low pressure nozzle prototype that operates with Tier II diesel (at 5 kW_{th} operation), and is capable of cold start. Thus, the parasitic losses related to the operation of the fuel processor unit were minimized by utilizing this low pressure nozzle for the introduction of fuel, air, and steam to the catalyst in the reformer unit. The low pressure nozzle was further developed, optimized, and tested for turndown and cold-start capability. The durability of the nozzle has also been demonstrated for over 100 hours by integrating it with an ATR fuel processor and operating it with Tier II diesel and sulfur containing distillate fuel. This result is significant because it permits reduction in parasitic power requirements of the APU system while providing uniform flow and reliable performance over a wide operating range.

Additionally, alternative catalysts were evaluated in order to develop a highly selective, sulfur tolerant multifunctional reforming catalyst for reformation of logistics fuels at low cost. Results from preliminary catalyst testing demonstrated potential for a reduced-cost, highly efficient reformer system that can accomplish complete fuel conversion and >80% reforming efficiency for reformation of diesel fuel. Further catalyst development and tests are ongoing to characterize and optimize reformer performance and durability. Finally, preliminary testing of PCI's fuel reformer using biodiesels and other fuels was successfully performed to demonstrate the fuel flexibility of the reformer system.

In summary, PCI has demonstrated a novel fuel reformer technology, along with improved catalyst effectiveness, demonstrated water neutral operation, and substantially improved fuel injection pressure drop without performance loss, reducing parasitic losses of the overall system. The resulting fuel processor enables fuel cell use of widely available conventional fuels including ULSD/medium sulfur diesels and medium sulfur logistic fuels.

FY 2011 Publications/Presentations

1. 2011 North American Catalysis Society in Detroit, Michigan.

2. 2011 DOE SECA Meeting in Pittsburgh, Pennsylvania.

3. Abstract accepted for 2011 Fuel Cell Seminar in Orlando, Florida.

III. SECA CORE RESEARCH & DEVELOPMENT

G. Modeling and Simulation

III.G.1 NETL RUA Cathode Modeling R&D

Kirk Gerdes
U.S. Department of Energy
National Energy Technology Laboratory (NETL) - Regional University Alliance (RUA)
3610 Collins Ferry Rd.
Morgantown, WV 26507
Phone: (304) 285-4342; Fax: (304) 285-4469
E-mail: Kirk.Gerdes@netl.doe.gov

Contract Number: 10-220621 6923
(NETL RUA Cathode Modeling R&D)

Start Date: October 1, 2010
End Date: September 30, 2011

Fiscal Year (FY) 2011 Objectives

- Improve the cathode oxygen reduction reaction (ORR) model to incorporate surface over-potential effects created between electrode surface and bulk into the calculation formalism for single phase solid oxide fuel cell (SOFC) cathode. Transfer improved ORR model to parallel three-dimensional (3-D) multi-physics cathode potential distribution modeling effort and assist in integration.
- Complete a focused ion beam (FIB)-scanning electron microscope (SEM) reconstruction of commercial baseline cells of interest to cathode modeling teams.
- Generate a working 3-D (axisymmetric) cathode model using empirical input from experiments and spectroscopic reconstructions. Describe average and local properties of a conventional cathode reconstructed using raw data from SEM images.
- Develop an initial phase-field model incorporating complex and temporally evolving SOFC cathode microstructures, electronic and ionic transport through a microstructure, and presence of inhomogeneous stress and electric fields.
- Generate public report on the key conclusions from the work.

FY 2011 Accomplishments

- Generated an improved oxygen reduction reaction model that incorporates descriptions of a surface charge layer induced by adsorption of surface gas molecules. Provided improved model to parallel 3-D multi-physics and microstructural evolution modeling projects.
- Completed FIB-SEM evaluation and 3-D reconstructions of real cathode microstructures for industrially relevant cells. Provided digital reconstructions to parallel modeling activities describing the cathode performance and long-term cathode evolution.
- Completed generation of a 3-D multi-physics model describing cathode operations using real 3-D cathode microstructure. Configured model to report relevant performance parameters including localized overpotential and local active species concentrations.
- Developed initial phase field model describing the evolution of cathode microstructure over industrially relevant time periods.
- Reported detailed technical results of cathode modeling development efforts in two published reports and four conference presentations.

Introduction

An SOFC is a device which generates electrical energy by exchanging oxygen ions between an oxygen containing process stream such as air and a process stream containing an oxidizeable material such as hydrogen. The SOFC cathode facilitates the reduction of oxygen to an ionic form in preparation for transport across the impermeable electrolyte membrane. The electrochemical oxygen reduction process is sensitive to the material composition and physical structure of the cathode, and the ORR efficiency can be impacted by chemistry and structure.

Although much effort has been devoted to explicit descriptions of the ORR on the cathode surface, a generally accurate model correlating cathode performance directly to microstructure has never been successfully generated. Indeed, questions remain about the identity of even the relevant processes that oxygen undergoes as it transfers from the bulk gas to the cathode. Mathematical descriptions of the fundamental transport processes and real 3-D microstructure are required to inform more comprehensive models investigating the multi-scale physics of operation and describing the long-term evolution of the cathode microstructure. The symbiotic nature of individual modeling efforts on these discrete topics must be clearly appreciated in order to generate the ultimate product: a comprehensive mathematical tool that can assist pre-screening of cathode materials and microstructures by predicting performance and long-term microstructural evolution.

The projects described here each focus on maturation of a component model to support development of the final comprehensive model. Two projects investigate

fundamental cathode structure and reaction processes to supply information to two additional projects developing higher-order models that describe cathode operation and microstructural evolution. In the first fundamental effort, the details of the ORR on the lanthanum strontium manganite (LSM)-based cathode system are described and a one-dimensional (1-D) reaction model is generated. In the second fundamental effort, an advanced spectroscopic technique is coupled to cutting-edge visualization software to produce detailed 3-D maps of the microstructure of real SOFC cathodes. Results from the fundamental modeling efforts are passed to a 3-D multi-physics model predicting chemical, thermal, and electrical potential distributions throughout the cathode. The results are used to predict dynamic and steady state performance. These performance results along with the fundamental data are also passed to a cathode evolution model based on phase field principles. This model can predict the microstructure after thousands of hours of operation, which is particularly relevant to SOFC developers.

Approach

During FY 2010, a 1-D model was developed to simulate the parallel-pathway controlled ORR within a mixed ionic electronic conductor electrode by incorporating multi-step charge-transfer mechanisms into the electrode kinetics of the computational model. During FY 2011, the model has been refined to improve its quality, physical accuracy, and functionality. The formulation of the governing equations and the boundary conditions have been modified and potential rate limiting steps and kinetic transitions are evaluated between two phase boundary (2PB) control and three phase boundary (3PB) control. Electrode microstructural and compositional features are incorporated to improve agreement between model representations and the actual electrode activity. Features targeted for improved model/physical agreement include surface diffusion paths, presence of surface charge, and multiple ionic transport paths. Finally, efforts are exerted to enhance computation efficiency by optimization of the source program and utilization of more powerful computation tools.

It is well known that the microstructural characteristics of electrodes in SOFCs strongly influence the overall device performance. Recently, 3-D reconstruction techniques have been developed to assess quantitatively the microscale phase distributions and crystallography of electrodes in typical commercially-available SOFCs. Methods to quantitatively describe the microstructure at a large enough scale to assess likely degradation locations and at a fine enough scale to characterize nanoparticle distributions are required. In FY 2011, a metrology protocol is developed to characterize infiltrated cathode microstructures, which is essential in establishing structure-property relationships. Initially FIB sample preparation is used in conjunction with SEM-based microstructural characterization to determine the essential structural characteristics of infiltrated cathodes. X-rays, secondary electrons, back-scattered electrons, and transmitted electrons can be used to image and identify phases and reconstruct microstructures. Using these tools, the microscale and nanoscale phase distributions will be determined in separate steps on industrially relevant cathodes.

Information derived from the first two fundamental activities is then used to support generation of a detailed, multi-dimensional, multi-scale, and dynamic continuum model of SOFC cathodes. The proposed model incorporates the effects of cathode microstructural properties on the local transport phenomena and electrochemistry inside the cathode. The model predicts distributions of local thermodynamic values, over-potentials, Faradaic currents, and parameters relevant to cathode performance. The model produces dynamic simulations and can generate virtual impedance measurements. The virtual impedance model permits parametric evaluations that provide detailed information on causes of observed overall impedance of the electrode, which is then used to accurately decipher experimental impedance data. The 3-D dynamic model is used in conjunction with experiments to correlate cathode performance and microstructural properties, and to explore strategies for improving cathode performance and durability.

Fundamental performance data and results from the dynamic continuum model are then made available to a model predicting the temporal evolution of microstructures in different operating states and the effect of evolving cathode microstructure on the electronic and ionic transport. For this purpose, the phase-field approach is employed, which has emerged as one of the most powerful methods for modeling transport phenomena and complex microstructural evolution. The effect of 3-D static microstructure features in SOFC cathodes on properties and cell performances obtained from phase-field simulations is compared with those obtained by parallel tasks. The focus of this effort is on developing the capability to predict the temporal microstructure evolution and the relevant local parameter variations of a cathode driven by inhomogeneous electric, stress, and chemical potential fields. The activity contributes to the microstructural optimization of SOFC performances and to the understanding of long-term baseline cell degradation.

Results

Throughout FY 2011, substantial results have been generated by the cathode modeling projects. The oxygen reduction reaction model has been modified

and tested to show important performance features of the competing reaction pathways. Figure 1 depicts a schematic of the parallel pathways of the oxygen reduction reaction. The cartoon at the top describes the process by which oxygen is adsorbed to the solid material surface, dissociates to become a charged surface species, and proceeds either to the 3PB via a surface path, or to the 2PB via a bulk path. The figure at the bottom shows the results of the computational model, and indicates that dominating control of the reaction mechanism changes as a function of the operating condition. As the cell is driven to produce more power, the cathode begins to supply less oxygen through the surface path and more oxygen through the bulk path. Such phenomenological behavior must be characterized, as there are implications to efforts for enhancing cathode materials and structure as well as impacts to the postulated modes of cathode degradation.

Detailed 3-D microstructural reconstructions have been generated by FIB-SEM and application of advanced visualization software. Figure 2 shows reconstructed 3-D portions of an LSM cathode typical of an SOFC. The top image shows only the reconstructed porous phase, and provides a detailed view from which interfacial areas, triple phase boundary length, tortuosity, and other relevant parameters may be calculated. The bottom image depicts all phases of a reconstructed 3-D region of the cathode at the cathode/electrolyte interface. In this image, the yttria-stabilized zirconia (YSZ) phase (green) is shown as wholly dense in the electrolyte region, as a segregated constituent in the 10 μm thick cathode active layer, and is absent from the cathode current collecting region. The LSM phase (red) is shown distributed evenly throughout the cathode active layer and current collecting regions. The pore phase (yellow) constitutes a large fraction of the current collecting region, a smaller portion of the cathode interlayer region, and is not present in the dense electrolyte region. Digitized versions of this visual representation are supplied to support parallel modeling efforts.

The multi-physics continuum model is generated using parameters developed in the ORR modeling effort, and is informed with parameters from the digitized 3-D reconstructions. Figure 3 demonstrates the incorporation of microstructural information in the performance

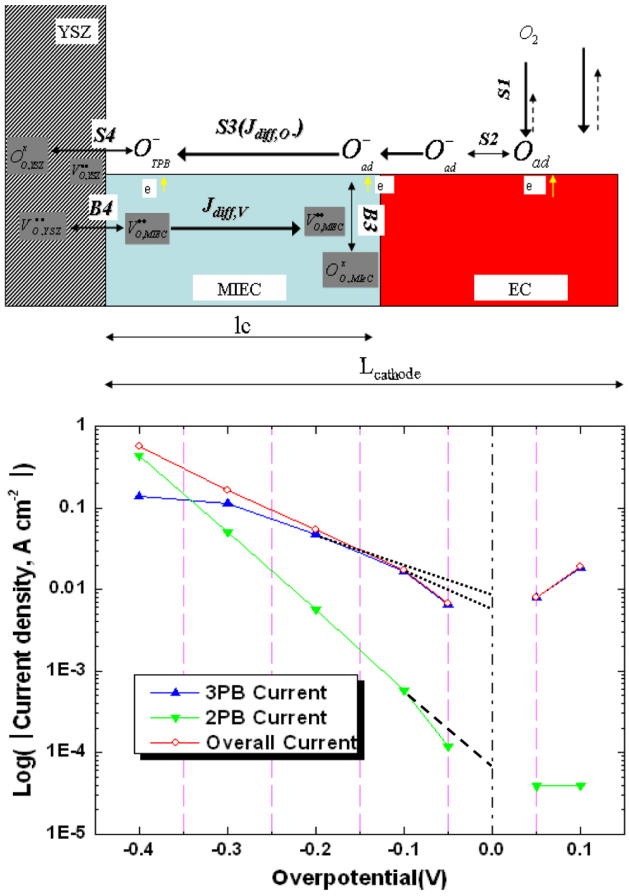

FIGURE 1. (Top) Schematic depiction of the ORR as a parallel process between surface and bulk states. (Bottom) Model results indicating that above a certain overpotential threshold, the dominating reaction pathway changes from 3PB reaction to the 2PB reaction. Such predictions impact cathode designs.

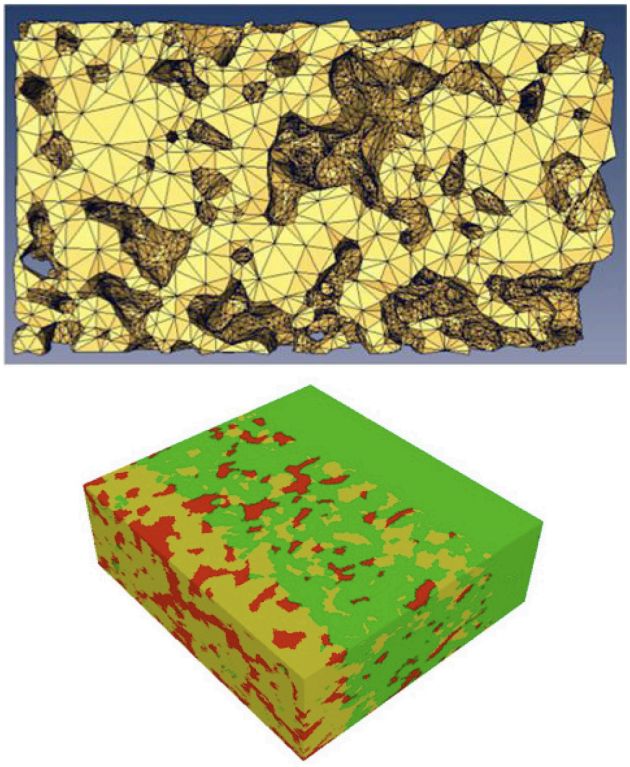

FIGURE 2. (Top) Reconstructed pore volume of a commercially available LSM cathode. The total sampled volume of 54 mm^3 has dimensions of 5.65 mm^3 x 3.15 mm^3 x 3 mm^3 (60-50 nm slices). (Bottom) The technique can also determine solid phase volume fractions and depict distributions and interfaces. The phases shown are YSZ (green), LSM (red) and pore (yellow).

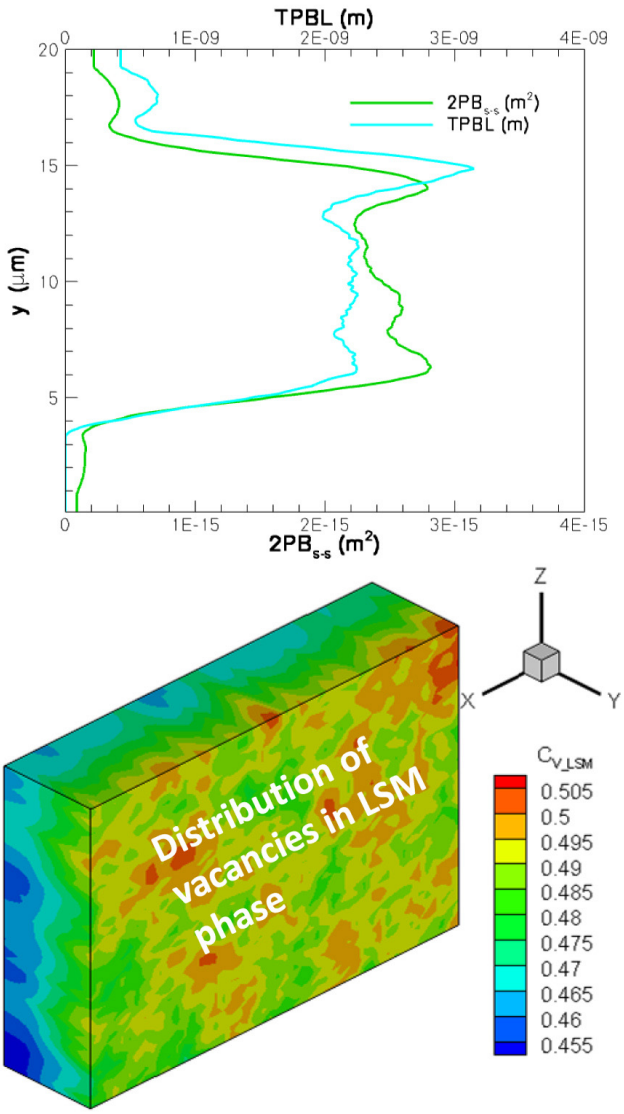

FIGURE 3. (Top) Evaluations of the real 3-D microstructure can be digitized to quantify the distributions of physical and microstructural properties. (Bottom) The digitized microstructural information is used to describe the physical performance on the cathode in a 3-D multi-physics model. Here the vacancy distribution in the LSM phase is shown in 3-D.

predicting physics models. The top figure is an example of digitized data that is incorporated, in this case a description of the relative presence of 2PB areas and 3PB interfacial lengths. The microstructural information permits direct evaluation of local structure, and also facilitates inspection of the physical gradients associated with the microstructural features. The bottom image describes performance metrics of the cathode that are potentially correlated to microstructural features. Here the distribution of vacancies throughout the cathode is determined. Such parameters can be examined to guide cathode improvement efforts, or performance can be

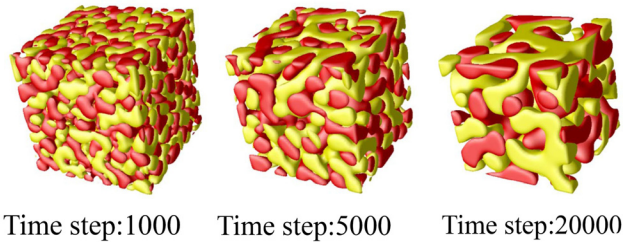

FIGURE 4. Depiction of the evolution of microstructure for an arbitrary time step given assumptions for the interactions between phases and a starting microstructure.

catalogued in a parametric analysis to determine the sensitivity to variations in the operating conditions.

Information from each of the previously described models is required to support development of a model that predicts cathode microstructural evolution as a function of thermodynamic and kinetic drivers and starting microstructure. Figure 4 shows the temporal evolution of cathode microstructure of an arbitrary three-phase system consisting of two solid phases and a single porous phase. The left most figure shows the evolution of the microstructure from time zero (not depicted) to some arbitrary time 1,000 steps away from zero. The middle figure shows the evolution of the structure from time step 1,000 to time step 5,000. The rightmost figure shows the 'final' microstructure at some value 20,000 time steps from the beginning of the process. Continued phase coarsening is observed throughout the process, even as the total mass and volume fraction of each phase is conserved. Resulting structural information at a given time step can be returned to the 3-D multi-physics continuum model to update the physical performance predictions. Information can be passed back and forth between the two models as desired. As the models become more mature, degradation processes can be examined to discern between steady and cascading processes.

Conclusions and Future Directions

The cathode modeling effort has provided a critical framework to research predicting long-term performance and microstructural evolution in the SOFC cathode. The research combines information from fundamental performance modeling and investigation of the cathode microstructure with higher-order multi-physics models to produce a consistent, informed evaluation of the cathode performance. In particular, the ORR mechanism investigation has quantified the extent of competition between reaction pathways within the cathode. Such information is useful to efforts to mitigate cathode degradation as well as investigation of methods for enhancing cathode performance. The 3-D microstructural reconstructions have produced

compelling images which can be probed with advanced visualization software to observe previously unattainable microstructural details. Leveraging of this information informs higher order models with directly measured parameters instead of theoretically determined parameters, which ultimately enhances the predictive accuracy of the models.

The multi-physics models describing performance and microstructural evolution of the cathode system are rapidly maturing and have generated important predictions of cathode operation. In particular, the 3-D dynamic continuum model has shown distributions of performance properties and evaluations of the local states throughout the cathode. The core phase field model has also been fully constituted and preliminary predictions of temporal changes in microstructure have been generated. The model awaits input from other basic parameter evaluation efforts to fully describe the constituent phases and their interrelationship, but will soon predict the evolution of a real LSM cathode microstructure for comparison to long term tests.

Future efforts in cathode modeling will focus on permutation of the ORR model to extend its applicability to other widely used cathode constituent materials such as lanthanum strontium cobaltite ferrite. The model will also begin to consider the presence of cathode infiltrate materials applied to enhance the cathode performance. FIB/SEM efforts will focus on resolving the cathode to the finest scale possible, without compromising the ability to sample large cathode volumes. The dynamic 3-D performance model will be tuned to more exactly match experimental data and leveraged for a detailed parametric analysis of cathode performance. The model will also be updated to account for the impacts of cathode infiltrate materials. The microstructural evolution model will be compared to data collected in long-term tests and ultimately integrated into a computational tool facilitating accelerated prototyping of advanced SOFC cathodes.

FY 2011 Publications/Presentations

1. X. Liu and Y. Li, "An Improved Method to Increase the Predictive Accuracy of the ECR Technique."

2. X. Liu and Y. Li, "Oxygen Transport Properties of $La_{0.6}Sr_{0.4}Co_{0.2}Fe_{0.8}O_{3-\delta}$," ICACC'11, Daytona Beach, Florida, January 23–28, 2011.

3. X. Liu and Y. Li, "SDC Infiltrated LSM Cathodes Based on Yttria-Stabilized Zirconia Electrolytes for Intermediate Temperature SOFC," MS&T, Houston, Texas, October 17–20, 2010.

4. X. Liu and Y. Li, "Oxygen Transport Investigation on Infiltrated SOFC Cathode," MS&T 11, Columbus, Ohio, October 16–20, 2011.

5. I. Celik and R. Pakalapati, "A Micro-scale Model for Oxygen Reduction on LSM-YSZ Cathode," Twelfth Symposium on SOFC (SOFC-XII), Montreal, Quebec, Canada (2011).

6. L.Q. Chen and Q. Li, "Phase-Field Modeling of Three-Phase SOFC Electrode Microstructures," MS&T 11, Columbus, Ohio, October 16–20, 2011.

7. L.Q. Chen and Q. Li, "Phase-Field Modeling of Microstructure Evolution and Electrochemical Transport in SOFC Cathodes," MRS, Boston, Massachusetts, November 28, 2011.

III.G.2 SOFC Modeling and Simulation Tools

Moe A. Khaleel (Primary Contact), Xin Sun, Elizabeth V. Stephens, Kurt P. Recknagle, Emily M. Ryan, Brian J. Koeppel, and Kevin Lai
Pacific Northwest National Laboratory
902 Battelle Blvd.
Richland, WA 99352
Phone: (509) 375-2438; Fax: (509) 375-4392
E-mail: moe.khaleel@pnnl.gov

DOE Project Manager: Briggs White
Phone: (304) 375-2438
E-mail: Briggs.White@netl.doe.gov

Contract Number: FWP40552

Start Date: October 1, 2010
End Date: September 30, 2011

Fiscal Year (FY) 2011 Objectives

- Develop and validate multi-physics (MP) modeling tools to simulate solid oxide fuel cell (SOFC) stack performance.
- Utilize computational techniques for the optimization of modular SOFC stack and system designs with mitigation of performance degradation.
- Disseminate/transfer modeling tools to Solid State Energy Conversion Alliance (SECA) industry teams and Core Technology Program (CTP) members.

FY 2011 Accomplishments

- Enhanced the Pacific Northwest National Laboratory (PNNL)-developed modeling tool SOFC-MP 2D with significantly improved algorithm and software. A new version of the two-dimensional (2D) SOFC-MP modeling code with demonstration models was released along with a user manual with demonstration cases.
- Developed and validated a multi-dimensional distributed electrochemistry (DEC) modeling tool that includes the electrode microstructures and solves the charge transfer, electric potential, and gas species distributions within the cell electrodes to examine factors affecting cell performance.
- Developed a constitutive model for cathode contact material to evaluate the sensitivity of contact material densification to material type, initial parameters, processing history, and geometry. Densification of the cathode contact layers in a five-cell stack was simulated followed by predictions of the stresses during electrochemical operation and after shutdown.
- Incorporated process-induced glass seal volume shrinkage on stress predictions of the PNNL leak test set-up in the developed continuum level model for self-healing glass seals.
- Investigated self-healing mechanisms/driving forces for self-healing glass seal.
- Demonstrated the effects of mechanical surface modification on life improvement of coated, 441 stainless-steel interconnect materials.

Introduction

In order to efficiently develop and optimize planar SOFC stacks to meet technical performance targets, it is desirable to perform numerical experiments on the effects of geometry, material properties, operational parameters, and thermal-mechanical loading. The computations with representative baseline designs, validated by experimental data, have been used to develop better understanding of the stack behavior while avoiding costly and time-consuming experiments. In order to model the coupled physics associated with an SOFC stack, the simulation tool SOFC-MP was developed. This modeling tool combines the versatility of a commercial MP code and a validated electrochemistry calculation routine to predict the gas flow distributions, current distribution, temperature field, and power output for stack-level simulations. The fundamental building blocks of the modeling and simulation tools are electrochemical models, heat and mass transfer simulations, computational mechanics, and experimental data.

The modeling tools are used to evaluate challenging issues anticipated for cell scale up. A systematic methodology was developed for quantifying the thermal and electrical performance improvements available with pressurized operation. For SOFC cathode contact materials and stack development, a sintering model was developed to explore/optimize the load distribution within the stack as a function of cathode contact densification and strength. The modeling tools developed were also used in studying current material development and degradation challenges. The mechanical durability of the surface scale present on metallic interconnects was evaluated for its ability to resist scale growth-induced spallation, and glass sealants were evaluated to understand geometry stability and structural integrity.

Approach

The following technical approach has been taken in the modeling task to meet program goals:

- Maintain, enhance, and provide guidance for the integrated modeling tools developed under the SECA CTP for evaluating fuel cell stack design concepts by the industry teams.
- Explore scale up related topics such as enhanced cooling and performance boosting strategies.
- Investigate the effects of materials degradation on cell performance and life.
- Investigate the effects of cell geometric design, material property distributions, and operating conditions on SOFC reliability.
- Perform material experiments for property data essential to constitutive and numerical model development.

Results

Enhancement and Performance Improvement of Modeling Tools

Numerical experiments to study the effects of geometry, material properties, operational parameters, and thermal-mechanical loading on SOFC performance have long been used to supplement the physical experiments used in testing, development, and optimization of SOFC stacks. Such computations with representative baseline designs, validated by experimental data, have provided better understanding of the stack behavior while reducing the number of these costly and time-consuming experiments. The simulation tool SOFC-MP (both in two and three dimensions) was developed to model the coupled physics associated with an SOFC stack. This modeling tool combines the versatility of a commercial MP code and a validated electrochemistry calculation routine to predict the gas flow distributions, current distribution, temperature field, and power output for stack-level simulations.

- The PNNL-developed SOFC-MP modeling tool was greatly enhanced during the past year. The focus of the modeling effort has been to increase the utility of the models for wider usage within the SECA and SOFC community by making the SOFC-MP software completely independent of commercial software. In FY 2011, a new 2D software version was released, a user manual with demonstration cases was created, and a parametric study of the effects of different design parameters on stack temperature uniformity was performed to demonstrate the utility of the model.

A Distributed Electrochemistry Modeling Tool for Simulating SOFC Performance and Degradation

Improving the durability of the SOFC, especially when consuming coal gas or alternative fuels such as land-fill gas or anaerobic digester gas, is essential to making SOFCs practical for stationary and distributed power generation. In general, SOFC performance and durability is adversely affected by reactions that cause unwanted changes to the electrode microstructures such as grain coarsening, cracking, nickel leaching, clogging of pores, and the formation of secondary phases and insulating layers. The DEC modeling tool is being developed to investigate the electrochemistry within the electrodes and electrolyte of the SOFC and to help quantify the effects of these unwanted reactions. The DEC model calculates the current-voltage (I-V) performance of the cell based on the fuel cell MP and characteristics of the electrode microstructure, such as particle size, pore size, electrolyte- and electrode-phase volume fractions, and triple-phase-boundary length. The DEC model is able to consider varying microstructural properties through the electrodes. The model has been validated with experimental button cell data and has been used to consider the changes in fuel cell performance with changes in local conditions and properties within the electrodes.

- In FY 2011, the DEC modeling tool was expanded to include multi-dimensional fuel cell geometries and was validated for simulating actual cell performance. The model was validated by accurately simulating the I-V performance of an experimental button cell that was operated on hydrogen fuel with various dilution ratios of nitrogen and helium. The modeled performance matched the data well with good replication of peak power and limiting current density values. Work on the modeling tool will continue with the focus shifting to the development of sub-models describing the effects of secondary reactions on the electrode microstructures and overall cell performance.

Modeling of Cathode Contact Degradation

Planar SOFC stack performance requires reliable uniform contact to carry the electrical current between the series-connected cells. On the cathode side, the contact layer must survive the oxidizing environment to maintain a durable bond between the ceramic electrode and the metallic interconnect. Since the contact layer may be the final fabrication step completed in situ during the stack assembly process, heat treatment temperatures are limited when a metallic interconnect is used to prevent unacceptable oxide scale growth. Densification and other similar material behaviors during stack fabrication have not typically been included in thermal-stress analyses of SOFCs, but they do create an initial

stress state. An understanding of these densification effects on the load distribution and stresses in the stack during assembly is necessary to quantify the mechanical reliability of the contact layer. Numerical modeling can be used to evaluate these contact layer residual stresses in addition to the typical thermal-mechanical stresses at the operating temperature. The results of these modeling analyses will help stack designers reduce high stresses in the stack so that structural failures are prevented and high stack mechanical reliability is achieved to meet program technical targets.

- In FY 2011, the three-dimensional (3D) continuum densification model was applied to study contact layer behavior for a realistic SOFC stack cell geometry. The model results showed that the continuum sintering model is suitable for modeling densification in stacks and that good densification for candidate contact materials (lanthanum strontium manganite with 3 mol% CuO and $BaCuO_2$, lanthanum strontium cobalt ferrite with 3 mol% CuO, and lanthanum nickel ferrite with 3 mol% Bi_2O_3) is possible for temperatures less than 1,000°C when sintering aids are used. Smaller initial grain size was beneficial for improving the final cathode contact density in the stack, but the densification of the layer was non-uniform due to the stiffness of the cell design.

Computational Investigation of Performance of Self-Healing Glass Seals used in SOFC Stacks

A self-healing glass seal has the potential of restoring its mechanical properties upon reheating to SOFC stack operating temperature, even when it has experienced some cooling induced damage/cracking at room temperature. Such a self-healing feature is desirable for achieving high-seal reliability during thermal cycling. On the other hand, self-healing glass is also characterized by its low mechanical stiffness and high creep rate at the typical operating temperature of SOFCs. Therefore, geometry stability and structural integrity of the glass seal system becomes critical to its successful application in SOFCs. It is crucial to be able to predict the effects of sealing system design and their structural stability under long term stack operating conditions, and to guide the design and optimization of a sealing system with a self-healing glass and appropriate containment mechanisms to achieve the ultimate goal of SOFC seal development.

- In FY 2011, a stack model was developed based on the PNNL leakage test for compliant glass seals. The material model incorporated volumetric changes of glass during processing. The effect of glass volume shrinkage during sintering and interfacial conditions was evaluated. The model predicted the outflow pattern for pure glass seal with different initial glass height (volume) in the leak test setup. The results indicated that more glass prior to sintering (~2.5X of stopper height), will allow the glass to fully fill the gaps between the ceramic stoppers and the positive electrode-electrolyte-negative electrode structure (Figure 1), providing a better integrated sealing system. In addition, emphasis was placed in quantifying the self-healing behaviors of the SCN-1 self-healing glass to better understand the driving force mechanisms for self-healing and the critical conditions which self-healing will occur.

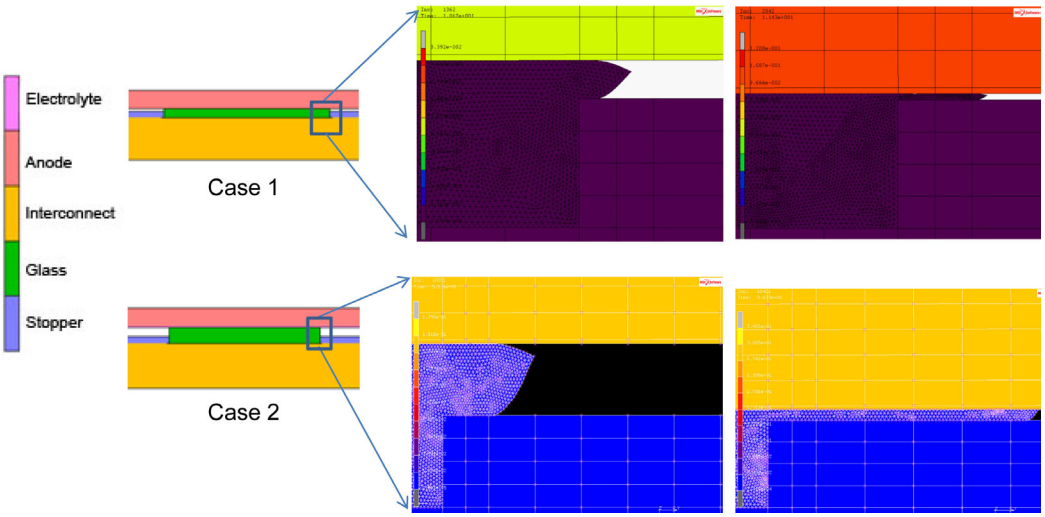

FIGURE 1. Comparison of the predicted results of the glass sealant during sintering where different initial glass heights, 1.5X (case 1) and 2.5X (case 2) of the height of the stoppers, was used before sintering.

Modeling for Interconnect Life Prediction

The interfacial strength between the oxide scale and the substrate is crucial to the reliability and durability of the metallic interconnect (IC) in SOFC operating environments. An integrated experimental/analytical methodology for quantifying the interfacial strength between the oxide scale and the different metallic interconnect candidates has been developed; therefore being able to predict the life of IC candidate materials under typical SOFC operating conditions. This integrated approach can also be used to quantify the effects of different surface finishes, coating layer thicknesses as well as different coating materials such that an optimized coating thickness as well as surface condition for the IC candidates can be developed to satisfy SECA life requirements.

- In FY 2011, investigations continued on improving spallation resistance and reducing the spallation driving force. It was found that the spallation resistance can be improved by increasing the interfacial strength between the oxide scale and substrate and the spallation driving force can be reduced through cooling profile optimization and by reducing the interconnect substrate thickness. New experimental methodologies are being investigated to quantify the interfacial strength of varying surface modified specimens, hence, to predict life of these specimens.

Conclusions and Future Directions

During FY 2011, the modeling tools were improved and expanded with additional capabilities developed to address scale up, strength, and durability issues. Future modeling activities will continue to focus on these issues together with work on reliability, degradation, time-dependent response:

- Continue to enhance and maintain the modeling tools to meet the needs of the SECA program. Continue to promote the usage of the tools by the industry and academic teams.
- Add functionality to 2D SOFC-MP for user definition and control of state variables to simulate pseudo-transient degradation processes or provide structure for multi-scale coupling with electrochemistry models.
- Implement the flexible framework for 3D SOFC-MP analyses to eliminate reliance on a single commercial third party software and test and validate the enhanced 3D model by benchmarking the results with the cases used for validation of the existing 2D model.
- Continue to add improved material models and numerical procedures to the modeling tools for simulation of time-dependent mechanical response and reliability.
- Continue to develop the DEC modeling tool to investigate degradation mechanisms that result in damage to the electrodes and electrochemical performance decay.
- Continue to support development of a robust test cell design.
- Perform additional experimental testing to characterize the densification behaviors of a selected contact material for different initial grain sizes, initial densities, sintering temperatures, and applied stress levels. This will better provide the required parameter inputs for the constitutive contact model.
- Develop temperature dependent constitutive model for self-healing glass incorporating aging/crystallization.
- Use modeling tools to examine varying engineering seal design concepts with glass/stopper sealing systems in a multi-cell stack.
- Continue modeling work on ferritic stainless steel interconnects to meet SECA target on stack life.

FY 2011 Selected Publications/Presentations

1. K.P. Recknagle, E.M. Ryan, and M.A. Khaleel, "Distributed Electrochemistry Modeling Tool for Investigating Solid Oxide Fuel Cell Performance," *Journal of Power Sources*, 2011 (submitted).

2. K. Lai, B.J. Koeppel, K. Choi, K. Recknagle, X. Sun, and M. Khaleel, "A Quasi-Two-Dimensional Electrochemistry Modeling Tool for Planar Solid Oxide Fuel Cell Stacks," *Journal of Power Sources* 196(6):3204-3222, 2011.

3. W. Liu, X. Sun, E. Stephens, and M. Khaleel, "Effect of Substrate Thickness on Oxide Scale Spallation for Solid Oxide Fuel Cells," *Corrosion Science* 53:2406-2412, 2011.

III.G.3 Optimization of Stack Load Path and Contact Materials

Brian J. Koeppel (Primary Contact),
Elizabeth V. Stephens, and Moe A. Khaleel
Pacific Northwest National Laboratory
902 Battelle Blvd.
Richland, WA 99352
Phone: (509) 372-6816; Fax: (509) 375-6736
E-mail: brian.koeppel@pnnl.gov

DOE Project Manager: Briggs White
Phone: (304) 285-5437
E-mail: Briggs.White@netl.doe.gov

Contract Number: FWP40552

Start Date: October 1, 2010
End Date: September 30, 2011

Fiscal Year (FY) 2011 Objectives

- Use numerical modeling to evaluate the sensitivity of contact material densification to material type, initial parameters, processing history, and geometry.
- Simulate densification of contact material layers in a large area multi-cell stack.
- Evaluate the effect of densification on the stack stresses and load path at operating and shutdown conditions.
- Evaluate the effect of initial grain size, stack mechanical preload and thermal expansion coefficient on the densification behavior.

FY 2011 Accomplishments

- Obtained constitutive model parameters for lanthanum strontium manganite (LSM), lanthanum nickel ferrite (LNF), and lanthanum strontium cobalt ferrite (LSCF)-based contact materials with various sintering aids.
- Simulated densification of the cathode contact layers in a five-cell stack followed by predictions of the stresses during electrochemical operation and after shutdown.
- Evaluated the effects of initial grain size, stack mechanical preload and thermal expansion coefficient on final predicted density and stresses in the stack components.
- Achieved maximum relative density of 72% for the baseline stack, but the relative density was not uniform across the cell due to its geometry and stiffness.
- Contact layer stresses were generally lower than the estimated allowable material strength after sintering and during operation, but large regions exceeded the allowable strength after shutdown to room temperature.
- Reduced initial grain size was the most beneficial modification to increase densification, but out-of-plane tensile stresses in the cell and seals also increased.

Introduction

Planar solid oxide fuel cell (SOFC) stack performance requires reliable uniform contact to carry the electrical current between the series-connected cells. On the cathode side, the contact layer must survive the oxidizing environment to maintain a durable bond between the ceramic electrode and the metallic interconnect. Stable, but expensive, noble metals have been used for contact materials; hence, less expensive alternatives are being investigated including ceramics with additions to aid low temperature sintering. Since the contact layer may be the final fabrication step completed in situ during the stack assembly process, heat treatment temperatures are limited when a metallic interconnect is used to prevent unacceptable oxide scale growth. Ceramic contact materials are desirable due to compatibility with the cathode and good oxidation resistance, but densification is generally poor at the expected heat treatment range (<1,000°C) which results in very low mechanical strength. Densification also results in volumetric changes that create additional residual stresses in the stack. Densification and other similar material behaviors during stack fabrication have not typically been included in thermal stress analyses of SOFCs, but they do create an initial stress state. An understanding of these densification effects on the load distribution and stresses in the stack during assembly is necessary to quantify the mechanical reliability of the contact layer. Furthermore, if the structural ability of the contact layer can be improved sufficiently to carry and distribute the thermal mismatch loads between the cell and interconnect, mechanical reliability of the entire cell and seal layers may also be improved. Numerical modeling can be used to evaluate these contact layer residual stresses in addition to the typical thermal-mechanical stresses at the operating temperature. The results of these modeling analyses will help stack designers reduce high stresses in the stack so that structural failures are prevented and high stack mechanical reliability is achieved to meet program technical targets.

Approach

The technical approach taken for this study was to develop the necessary model enhancements for densification analyses and to transfer them to Pacific Northwest National Laboratory's existing SOFC modeling tool set. To capture the mechanical effects of contact material densification, the continuum viscous sintering model [1] was selected to simulate volumetric material changes due to densification in the three-dimensional (3D) stack modeling framework. This phenomenological constitutive model is a general nonlinear-viscous continuum model based on plastic deformation of porous materials. The model computes the inelastic strain rates as a function of grain size, relative density, mechanical properties, stress, and temperature. The model can capture the enhanced sintering behavior that occurs under applied stress and the influence of the mechanical constraint by the material layers being joined.

The constitutive model was implemented in the MSC MARC general purpose finite element analysis code through user-defined subroutines. A five-cell, 25×25 cm, planar cell stack was created and used as the baseline model geometry for the numerical evaluations (Figure 1). The model used a ribbed interconnect where a 400 μm thick contact material layer was placed between the ribs and cathode. The material parameters required for the constitutive model were obtained from screening experiments of candidate contact materials being investigated under the companion materials development effort. The cathode contact material assumed for the stack simulations was LSCF with 3 mol% CuO added as a sintering aid. The baseline case also assumed an initial grain size of 0.4 μm, an initial density of 51%, and a two-hour heat treatment at 930°C. After the heat treatment, the operating temperature distribution was imposed. This predicted temperature distribution was obtained assuming a 97% H_2 fuel, 400 mA/cm^2 current density, 80% fuel utilization, 12% air utilization, 700°C furnace temperature, and 700°C fuel/oxidant inlet temperature. These conditions predicted a thermal field where the temperatures varied from 703°C to 823°C across the stack. The model then reduced the stack temperature to 25°C room temperature to simulate system shutdown. This baseline model was then exercised in parametric studies to evaluate the resulting densification and component stresses due to different grain sizes (0.1-1.0 μm), mechanical preload applied to the stack (0.2-2.0 MPa), and thermal expansion coefficient for the contact material (95-105% of the nominal value). Mechanical testing of the selected contact material has not been performed, so an allowable tensile strength of 15 MPa was assumed for the contact layer based on prior testing of similar materials.

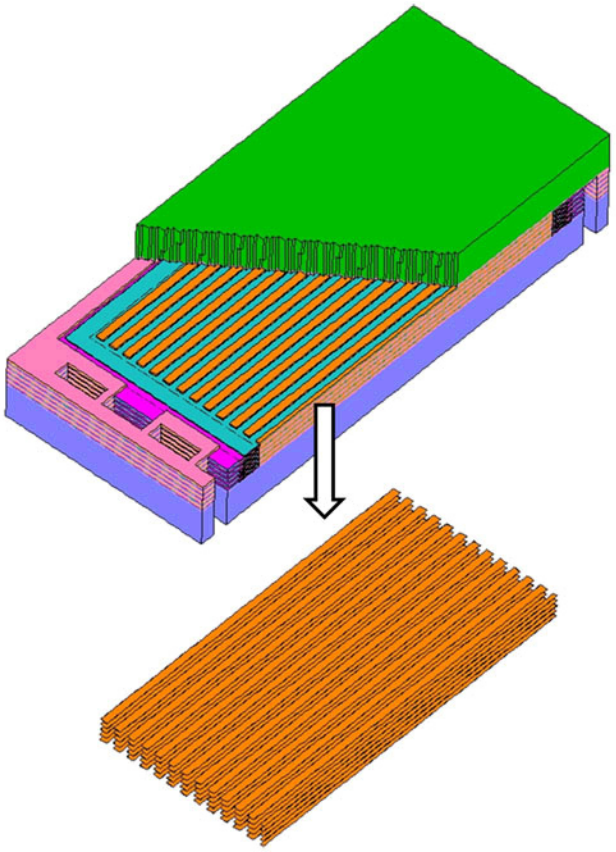

FIGURE 1. Symmetric Half-Cell Geometry of the 5-Cell, 25×25 cm, Stack and the Corresponding Contact Material Locations

Results

Contact Material Selection

The contact material development effort used dilatometric testing under a constant heating rate to screen candidate materials. The strain data from this simple test was used to estimate key parameters of the densification model for different materials. The densification model was then used to evaluate the free sintering response of the materials. The predicted relative densities for LSM with 3 mol% CuO and $BaCuO_2$, LSCF with 3 mol% CuO, and LNF with 3 mol% Bi_2O_3 after freely sintering at various temperatures for a two hour heat treatment are shown in Figure 2. The materials generally could not achieve full density in this temperature range. The LSM-based material showed the highest densification above 925°C, but it exhibited the lowest densification below 875°C. The LSCF-based material exhibited the highest densification up to 925°C. The heat treatment temperature range for devitrification of glass-ceramic sealants is estimated to be in the 800-950°C range. Therefore, the LSCF-based material was chosen for the baseline stack simulations such that a combined heat

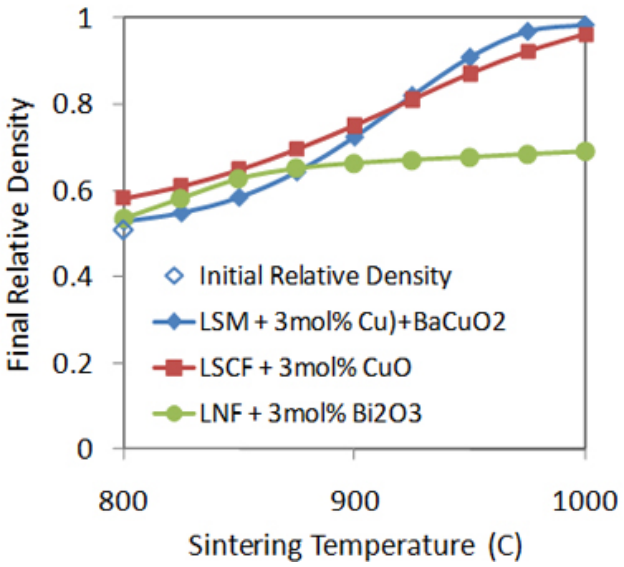

FIGURE 2. Predicted Final Relative Density as a Function of Sintering Temperature for LSM with 3 mol% CuO+$BaCuO_2$, LNF with 3 mol% Bi_2O_3, and LSCF with 3 mol% CuO after 2-Hour Heat Treatment

treatment for formation of both the seal and contact layer may be possible.

Stack Results

The final relative density of the contact layer for the baseline case is shown in Figure 3. The maximum relative density was only 72% and occurred at the center of the cell. The relative density varied greatly with the smallest relative density of 52% near the corners of the cell. The center of the cell is more flexible to accommodate the volumetric shrinkage of the contact layer, while little densification occurred at the cell corners due to the stiff support frame which prevented out-of-plane displacement. This developed tensile stresses in the contact layer which halted further densification. Therefore, the overall stack design will be vitally important to ensure the formation of strong contact across the entire cell. Only small variations in relative density were observed between the various cells in the stack.

Assuming that the tensile allowable strength of the contact material is 15 MPa, the contact stresses after sintering were acceptable with only small regions at the end of the ribs exceeding the allowable (Figure 4). The operating temperature distribution was then applied to simulate the thermal expansion effects of the cell. The stresses were still acceptable along most of the rib, but the high stress at the ends of the rib increased slightly (Figure 5). This could result in local delamination of the contact layer, but the stack would still be expected to electrochemically operate reasonably well with only the

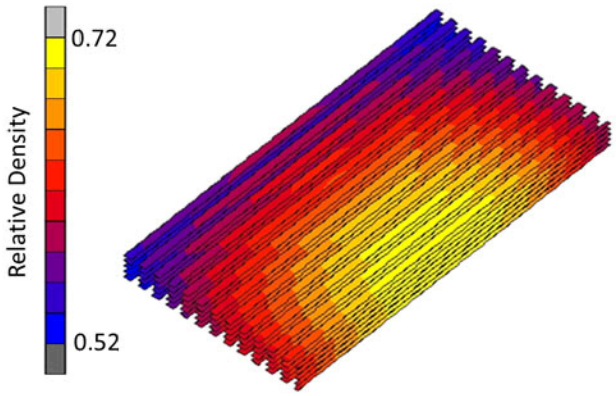

FIGURE 3. Contour of the Final Relative Density for the LSCF-Based Contact Layer after 2-Hour Heat Treatment at 930°C

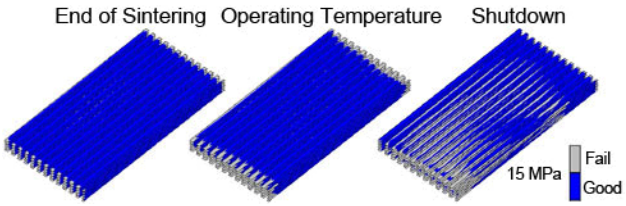

FIGURE 4. Contour of the Contact Layer Tensile Stresses (blue is below the allowable tensile stress)

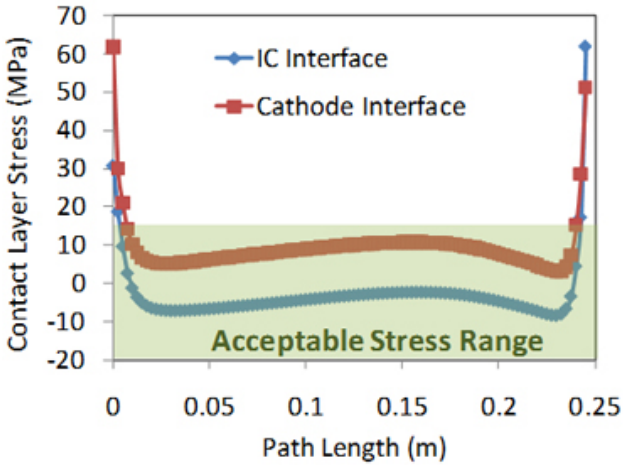

FIGURE 5. Profile of the Maximum Principal Stress in the Contact Layer along an Interconnect Rib

small contact loss here. Upon shutdown, large regions of the contact layer exceeded the allowable stress. This would most likely result in significant performance degradation and the stack would not be able to acceptably tolerate planned or unplanned thermal cycling.

Effect of Initial Grain Size

Smaller grain sizes have higher curvatures which increase the driving force to reduce surface energy and increase the sintering rate. The effect of initial grain size on the final density in the stack was evaluated. With the smallest 0.1 μm grain size, the maximum relative density at the center of the cell was increased considerably up to 98%. The density variation across the cells was improved slightly, but corner densities still remained at only 60%. The maximum density with the larger 1.0 μm grain size was only 59% showing very little densification.

The improved densification with smaller grain sizes generally did not affect the contact layer stresses. For a grain size of 0.2 μm, the operating temperature stresses were very similar and shutdown stresses were only slightly higher. For a grain size of 0.1 μm, much larger regions of the contact layer exceeded the allowable stress at both operation and shutdown. The enhanced densification also created higher peak stresses in the cell at operation and shutdown as well as in the cell seal at shutdown (Figure 6). The cell designer may want to avoid the rapid increase in stress near full densification.

Effect of Stack Mechanical Preload

The sintering rate can be increased by application of a remote compressive stress that supplements the inherent sintering stress. Preload values of 2X and 10X the nominal value of 0.2 MPa were applied to the baseline stack model. The maximum density increased only slightly to 74% and 82%, respectively. The preload must be on the order of the inherent sintering stress, which is around 2 MPa for this example, to have a significant effect. Such high preloads will be very difficult to apply uniformly on actual large area stacks. Therefore, the stack preload primarily serves to ensure that the planar layers remain in contact while sintering rather than increasing the actual rate of densification.

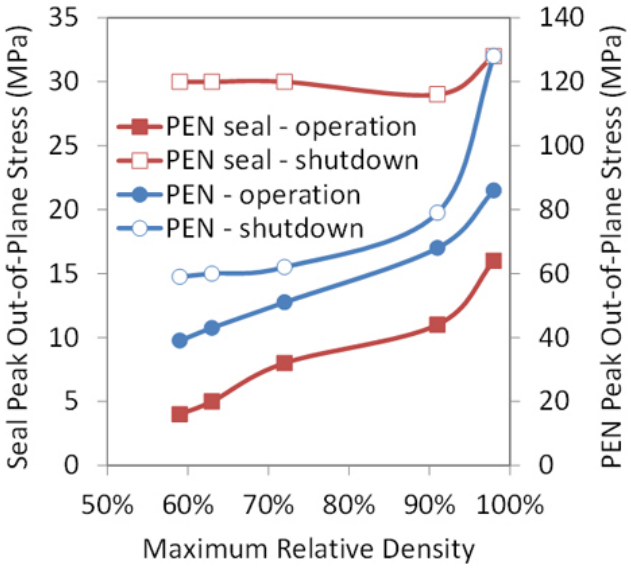

FIGURE 6. Effect of Densification on the Maximum Tensile Stresses in the Cell and Cell Seal

Effect of Thermal Expansion Coefficient

The thermal expansion coefficient (TEC) is usually matched between the various layers in the cell to avoid mismatches of thermal strain. The effect of different thermal expansion on the contact layer formation was evaluated. For contact material with TEC values of 95-105% of the nominal value, there was little influence on the maximum densification achieved or the stresses at the operating temperature due to the small temperature difference from the stress-free condition. Upon shutdown, the stresses in the contact layer were improved somewhat for the lower TEC values. The contact layer does not shrink as much upon shutdown, thereby, inducing more compression to reduce the high tensile stresses. Therefore, material modifications to manipulate the contact layer TEC could be possible to improve stresses for a particular design.

Conclusions and Future Directions

During this year, the 3D continuum densification model was applied to study contact layer behavior for a realistic SOFC stack geometry. The model results showed that:

- The continuum sintering model is suitable for modeling densification in stacks.
- Good densification of candidate contact materials is possible for temperatures less than 1,000°C if sintering aids are used.
- Densification of the contact layer was less than 100% for the proposed heat treatment, and significant density variations were predicted due to the stiffness of the cell support frame.
- Contact layer stresses above the estimated allowable strength occurred only at the rib ends during stack operation, but larger regions of high stress occurred after shutdown.
- Reduced initial grain size increased the densification rate without significant impact on contact layer stresses at operation and shutdown, but cell and seal peak stresses increased.
- Mechanical preload applied to the stack was too high before it significantly improved the densification rate.
- Smaller TEC values for the contact layer slightly improved stresses at shutdown.

The design of the contact layer depends strongly on the material properties as well as the stack design.

Additional experimental testing should be done to well characterize the densification behaviors of a selected contact material for different initial grain sizes, initial densities, sintering temperatures, and applied stress levels. This will better provide the required parameter inputs for the constitutive model than the initial screening tests. Further testing of the resulting strength at high and low temperatures is also required to better evaluate reliability of the contact layer for operation and thermal cycling conditions. Then additional modeling can be done to provide better guidelines for formation of reliable contact layers.

FY 2011 Publications/Presentations

1. B.J. Koeppel, W. Liu, E.V. Stephens, and M.A. Khaleel, "Numerical Modeling of Cathode Contact Material Densification," 35th International Conference and Exposition on Advanced Ceramics and Composites, Daytona Beach, Florida, January 23–28, 2011.

References

1. E.U. Olevsky, "Theory of Sintering: From Discrete to Continuum," *Materials Science and Engineering* **R23**, 41-100 (1998).

III.G.4 SOFC Multi-Physics (SOFC-MP) Modeling and Simulation Tools

Brian J. Koeppel, Kevin Lai (Primary Contact), and Moe A. Khaleel
Pacific Northwest National Laboratory
902 Battelle Blvd.
Richland, WA 99352
Phone: (509) 372-6461; Fax: (509) 372-4720
E-mail: kevin.lai@pnnl.gov

DOE Project Manager: Briggs White
Phone: (304) 285-5437
E-mail: Briggs.White@netl.doe.gov

Contract Number: FWP40552

Start Date: October 1, 2010
End Date: September 30, 2011

Fiscal Year (FY) 2011 Objectives

- Develop, validate, and distribute the multi-physics modeling tool SOFC-MP to simulate solid oxide fuel cell (SOFC) stack performance.
- Demonstrate usage of the two-dimensional (2D) SOFC-MP modeling tool and provide user documentation.
- Establish a flexible framework for the SOFC-MP code using open source software tools that eliminates the existing need for expensive third party commercial software.
- Support industry teams usage of the SOFC-MP tool for SOFC development.

FY 2011 Accomplishments

- Released a new version of the 2D SOFC-MP modeling code with demonstration models.
- Created a user manual for 2D SOFC-MP with demonstration cases.
- Performed parametric studies using 2D SOFC-MP to evaluate different approaches for minimizing thermal gradients in tall stacks.
- Created a roadmap to develop an improved framework for the three-dimensional (3D) SOFC-MP including a new pre-processing graphical user interface (GUI), translators to interface with common finite element analysis (FEA) solvers, and a post-processing viewer using ParaView.
- Continued to promote and support the use of SOFC-MP and Mentat-FC software packages with Solid State Energy Conversion Alliance (SECA) industry teams and Core Technology Program (CTP) members for modeling and development of SOFC stacks.

Introduction

Numerical experiments to study the effects of geometry, material properties, operational parameters, and thermal-mechanical loading on SOFC performance have long been used to supplement the physical experiments used in testing, development, and optimization of SOFC stacks. Such computations with representative baseline designs, validated by experimental data, have provided better understanding of the stack behavior while reducing the number of these costly and time-consuming experiments. The simulation tool SOFC-MP was developed to model the coupled physics associated with an SOFC stack. This modeling tool combines the versatility of a commercial multi-physics code and a validated electrochemistry calculation routine to predict the gas flow distributions, current distribution, temperature field, and power output for stack-level simulations. The fundamental building blocks of the modeling and simulation tools are electrochemical models, heat and mass transfer simulations, structural mechanics, and experimental data. The tool is available both as a 2D version which is used to rapidly predict performance of tall symmetric stacks and as a 3D version to predict performance of fully-detailed realistic cell and stack geometries. The tool can be used standalone for stack engineering analysis to study operating conditions and the effects on power output, utilizations, temperatures, and temperature gradients. The 3D tool can also be coupled with a commercial FEA code such as MSC MARC to evaluate structural integrity based on thermal-mechanical stresses from the predicted temperature field.

Approach

In the past year, the focus of the modeling effort has been to increase the utility of the models for wider usage within the SECA and SOFC community. A primary restriction to use is the current close integration with MSC MARC finite element software and the MSC Mentat pre/post-processing GUI. End users must obtain and license these commercial software packages to use the 3D SOFC-MP version. This is not desirable due not only to cost but also the reality that the modelers for a team usually have a preferred alternate modeling platform. Therefore, making the SOFC-MP software completely independent of the commercial software

used will make it fully distributable for wider usage. The different tasks pursued over the last year to achieve this goal include the following:

1. **Develop a post-processor for 2D SOFC-MP.** The 2D model allows the user to quickly simulate many different cases. A spreadsheet currently using Excel (not freely distributable but very common) is used to automatically import the model results for instant visualization of the important performance metrics and distributions. This helps to make the software easier to use for new users.
2. **Document the 2D SOFC-MP.** Use of the keyword driven 2D version requires some knowledge of the input file format and parameter names. A user manual to guide the user in how to install the software, build a model input file, run the solution, and evaluate the results will be very beneficial. The documentation provides full description of these tasks and includes several demonstration cases as tutorials.
3. **Demonstrate the utility of 2D SOFC-MP.** The utility of the code is demonstrated through parametric studies and documented in a conference paper.
4. **Develop a new framework for 3D SOFC-MP.** A new solution procedure for SOFC-MP which doesn't rely on the commercial MARC finite element code will be developed.
5. **Continue to improve the SOFC-MP packages.** Continual improvements on capability and usability will be pursued to make the code more useful.
6. **Aid the industry teams.** Maintain, enhance, and provide guidance for the integrated modeling tools developed under the SECA CTP for evaluating fuel cell stack design concepts by the industry teams.

Results

User Manual for 2D SOFC-MP Published

To aid the fuel cell designers and modelers, a user manual for the 2D SOFC-MP version was created. The manual contains all of the practical knowledge required to use the code. It includes:

- Installation and setup instructions for Windows-based and Linux-based machines.
- Overview of the data required for model pre-processing.
- Full descriptions of the keywords for model input.
- The procedure for job submission and solution monitoring.
- Instructions for use of the post-processing spreadsheet.
- Description of several benchmark and demonstration cases with results.
- Demonstration of the code usage for a parametric study.

By working through this manual, users should be proficient in running their own analysis jobs using 2D SOFC-MP.

Official Release Compact Disc (CD) for 2D SOFC-MP Tool Created

"SOFC-MP 2D: Modeling Tool for Solid Oxide Fuel Cell Stacks" official release CD is made available for all SECA participants or other interested parties. The CD includes installation files for the executable and necessary library files, other utilities, example models, and user documentation which includes the "User manual for 2D SOFC-MP" mentioned above.

2D SOFC-MP Used to Evaluate Stack Thermal Fields

The 2D SOFC-MP model was used to evaluate the effect of different modifications to stack geometry or operation on stack temperature uniformity. The baseline model for the examples consisted of a 96-cell stack, 625 cm^2 active area, wet H_2 fuel, 65% fuel utilization, 15% air utilization, 0.5 A/cm^2 average current density, and 750°C furnace environment. The effect of different flow orientation, fuel composition, methane reforming rate, fuel exhaust recycling percentage, cell aspect ratio, interconnect thickness, and heat spreader plates was investigated. The influence of these parameters on the stack maximum temperature, stack temperature difference, and cell temperature difference was tabulated. For example, the results for the co- and counter-flow baseline cases with H_2 and CH_4 fuels are shown in Figure 1. Generally, the co-flow geometry and the fuel composition with CH_4 exhibited lower temperature differences. In Figure 2, the results of varying the interconnect thickness from 0.5-1.5 mm are shown. The maximum stack temperature, stack temperature difference, and cell temperature difference all decreased nearly linearly with increased interconnect thickness. The greater thickness provides larger heat conduction across the planar cell which tends to smooth the temperature profile. The importance of the interconnect on the thermal field and its role in stack thermal management is thereby demonstrated. The full results of these parametric studies were documented in a conference paper.

Flexible Framework for 3D SOFC-MP Initiated

The existing 3D SOFC-MP software package is tightly integrated with the MSC MARC general purpose FEA code and its pre/post-processing GUI called Mentat-FC. While this tool fully integrates the model creation, electrochemical solution, thermal-

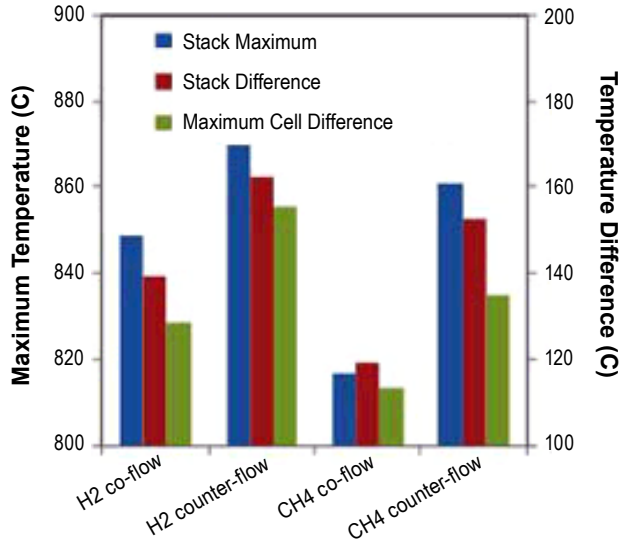

FIGURE 1. Effect of Flow Orientation and Fuel Type on Temperature Uniformity of a Tall Stack

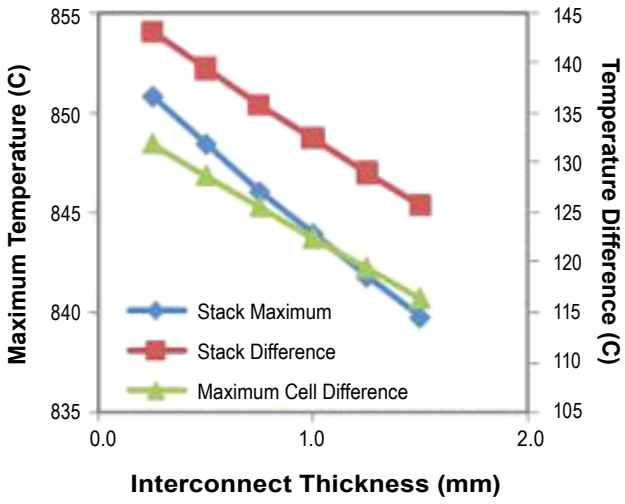

FIGURE 2. Effect of Interconnect Thickness on Temperature Uniformity of a Tall Stack

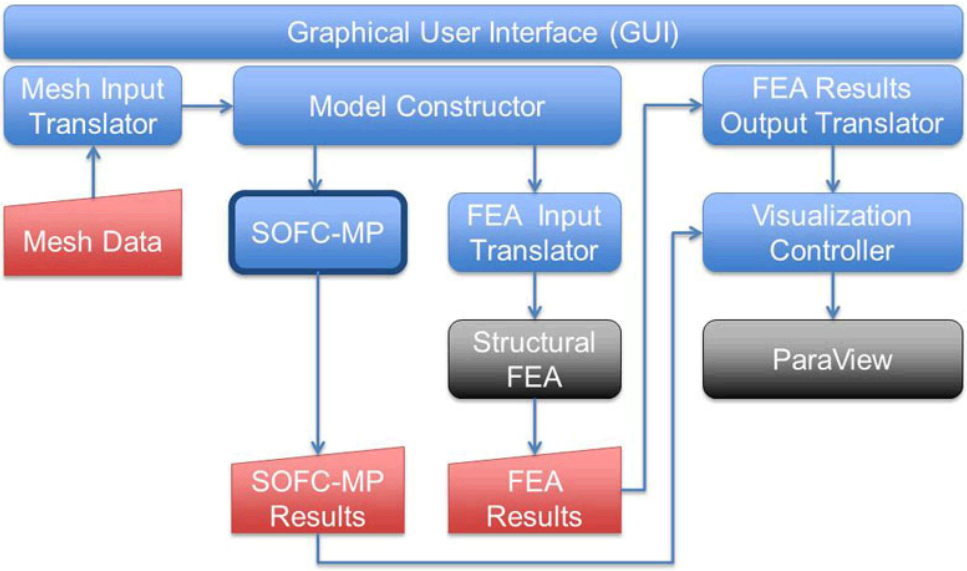

FIGURE 3. Proposed Framework for the SOFC-MP Tool to Increase Its Flexibility

mechanical solution, and results visualization, it is inherently tied to usage with the MARC code. This often makes it less attractive to customers who have a different preferred finite element code for their structural modeling. To make the core SOFC-MP multi-physics solver more accessible to the industry teams, a plan was made for transitioning the multi-physics solver to a general framework which does not rely on additional commercial software and licensing costs.

A new framework was proposed as shown in Figure 3. Similar to the existing procedure, the analysis would be driven by a single GUI that operates the pre-processing, solution, and post-processing phases of an analysis. The pre-processing phase would initially consist of updated mesh translators that read the node and element data for the cell component geometry from the user-defined mesh. The GUI would then lead the user through model creation to define material properties, boundary conditions, operating conditions, etc. The completed model would then be submitted to SOFC-MP for the solution of the flow-thermal-electrochemical solution. The GUI would also create the model for the thermal-structural solution, which

would then be output in the required format for the finite element code being used by the designer (e.g., MARC, ANSYS, ABAQUS, etc.). Upon completion of the thermal field calculation, the structural job would be submitted. Upon job completion, results from both solutions will be output and formatted for visualization. The visualization controller would guide the user in reviewing all of the relevant results within an open-source viewer such as ParaView. The benefit of this new arrangement is that it is more flexible for the cell designers to use the finite element software tools that they are already familiar with.

Conclusions and Future Directions

During FY 2011, the 2D SOFC-MP modeling tool was greatly improved and made more accessible for use of the industry teams:

- A new software version was released.
- A user manual with demonstration cases was created.
- A parametric study of the effects of different design parameters on stack temperature uniformity was performed to demonstrate the utility of the model.

Future modeling activities will continue to focus on computational improvements, capability enhancements, and model validation. The specific tasks are listed as follows:

- Implement the flexible framework for 3D SOFC-MP analyses to eliminate reliance on a single commercial third party software.
- Test and validate the enhanced 3D model by benchmarking the results with the cases used for validation of the existing 2D model.
- Continue to improve the SOFC-MP modeling tool to meet the needs of the SECA program and continue to promote the usage of the tool by industry and academic teams.

FY 2011 Selected Publications/Presentations

1. K. Lai, B.J. Koeppel, K. Choi, K. Recknagle, X. Sun, and M. Khaleel. 2011. "A Quasi-Two-Dimensional Electrochemistry Modeling Tool for Planar Solid Oxide Fuel Cell Stacks," Journal of Power Sources, 196(6) pp. 3204-3222.

2. K. Lai, B.J. Koeppel, and M.A. Khaleel. 2010. "A Two-Dimensional Electrochemistry Modeling Tool for Planar Solid Oxide Fuel Cell Stacks," presented at the ASME 2010 International Mechanical Engineering Congress & Exposition, Vancouver, British Columbia, Canada, November 14–17.

3. B.J. Koeppel, K. Lai, and M. Khaleel. 2011. "Effect of Geometry and Operating Parameters on Simulated SOFC Stack Temperature Uniformity," to be presented at the 9th Fuel Cell Science, Engineering and Technology Conference (ESFuelCell2011), Washington, D.C. , August 7–10, 2011.

4. E.M. Ryan, X. Sun, B.J. Koeppel, K. Lai, K.P. Recknagle, and M.A. Khaleel. 2011. "Modeling Electrochemical Performance and Degradation in High Temperature Electrochemical Devices," presented at the Beyond Li Symposium, Richland, Washington, June 7–9, 2011.

5. B.J. Koeppel, K. Lai, and M.A. Khaleel. 2011. "SOFC-MP 2D User Manual," PNNL-20433.

6. K. Lai, B.J. Koeppel, M.A. Khaleel. 2011. "SOFC-MP 2D: Modeling Tool for Solid Oxide Fuel Cell Stacks," PNNL-SA-80665.

III.G.5 A Distributed Electrochemistry Modeling Tool for Simulating SOFC Performance and Degradation

Kurtis P. Recknagle (Primary Contact), Emily M. Ryan, and Moe A. Khaleel
Pacific Northwest National Laboratory
902 Battelle Blvd.
Richland, WA 99352
Phone: (509) 372-4840; Fax: (509) 375-3865
E-mail: kurt.recknagle@pnnl.gov

DOE Project Manager: Briggs White
Phone: (304) 285-5437
E-mail: Briggs.White@netl.doe.gov

Contract Number: FWP40552

Start Date: October 1, 2010
End Date: September 30, 2011

Fiscal Year (FY) 2011 Objectives

- Develop a multi-dimensional cell-level distributed electrochemistry (DEC) modeling tool that can simulate solid oxide fuel cell (SOFC) performance by solving the coupled and spatially varying multi-physics that occur within the membrane electrode assembly (MEA).
- Extend the DEC modeling tools to include the capability to simulate graded electrode microstructures.
- Validate the model for an SOFC operating on various fuel gas compositions.
- Investigate the effect of electrode microstructure on the electrochemical performance.

FY 2011 Accomplishments

- Developed a continuum cell-level DEC model that describes the electrode microstructure and solves the distributed electrochemistry through the MEA in multiple dimensions.
- Validated the DEC modeling tool by simulating an experimental button cell for a range of operating conditions.
- Performed an optimization exercise based on anode microstructure to demonstrate the DEC model capabilities and its sensitivity to structural changes.

Introduction

The SOFC is an excellent candidate for stationary and distributed power generation due to the high power density and flexibility to run on coal gas and alternative fuel sources such as landfill gas and pipeline natural gas. To be viable for this application the cost per kW and cell longevity of SOFCs must be further improved. Experimental efforts are ongoing to improve the initial performance and durability of SOFCs through the use of novel materials and microstructural designs. Experimental design and testing of SOFCs is a complex, time consuming process. Computational modeling, which is able to simulate the multi-physics occurring within a SOFC, can be used to inform and guide experimental efforts and help to reduce the amount of experimental testing necessary for new designs and materials. The distributed electrochemistry model, which has been developed under this work, is capable of investigating the electrochemistry and local conditions with the SOFC MEA based on the local microstructure and multi-physics. The DEC model can calculate the global current-voltage (I-V) performance of the cell as determined by the spatially varying local conditions through the thickness of the electrodes and electrolyte. The simulation tool is able to investigate the electrochemical performance based on characteristics of the electrode microstructure, such as particle size, pore size, electrolyte and electrode phase volume fractions, and triple phase boundary (TPB) length. It can also investigate performance as affected by fuel and oxidant gas flow distributions and other environmental/experimental conditions such as temperature and fuel gas composition. The long-term objective for the DEC modeling tool is to investigate factors that cause electrode degradation and the decay of SOFC performance which decrease longevity.

Approach

The DEC model is a three-dimensional multi-physics model which solves for the reactive transport of gas species, ion transport, current density and electric potential. The model is based on a commercial computational fluid dynamics code (STAR-CD) and employs a user-defined module to solve the distributed electrochemistry and provide source terms for the gas species and electric potential. In the anode and cathode, the charge transfer is solved using a modified Butler-Volmer formulation which is based on the rate

limiting step for the electrochemical reactions within each electrode [1]. The DEC model includes all three phases of the composite electrodes (gas, electrolyte phase, electrode phase), and the TPBs throughout the full thickness of the electrodes. This allows the model to solve for the electrochemistry throughout the electrodes without defining a set reactive zone; the coupled multi-physics solution, not a specific layer dimension, determines the extent of the reactions into the electrodes. The DEC model can also handle spatially varying microstructural properties and compositions within the electrodes. For example, the model allows for electrode layers with unique structural properties, such as porosity or particle size.

In the work presented here, the composite anode electrode phase material is nickel (Ni) and the electrolyte phase material is yttria-stabilized zirconia (YSZ). The electrolyte layer is comprised of fully dense YSZ. In the composite cathode, the electrode phase material is strontium-doped lanthanum manganese oxide (LSM) and the electrolyte phase is YSZ.

A schematic of the computational domain used for the simulation results presented in this report is given in Figure 1. The model geometry represents the test section of a button cell testing apparatus [3]. A two-dimensional axisymmetric model geometry was created to represent the test section (see dashed line in Figure 1). The model domain includes the fuel flow region from the fuel feed tube to the anode, and the air flow region above the cathode surface. Within the MEA, the anode is separated into two layers with separate property definitions to investigate the performance of a graded anode. The base layer is 17 microns thick, and the support layer makes up the remaining 1,100 µm of the anode thickness.

Results

Model Validation

Jiang and Virkar [3] performed tests to examine the relationship between SOFC performance and gas transport in porous anodes. To validate the DEC model, simulations were performed to replicate the H_2-He and H_2-N_2 cases over the full range of dilution ratios they tested. The structural parameters used in the DEC model for all validation cases are summarized in Table 1. For the calculations the DEC model settings were made such that the performance matched at one experimental fuel composition. All other simulations were made with no changes to the model except for the fuel compositions and operating voltages. Without including all the details of these validation cases, which are part of the subject of a journal article submitted for publication [4], the simulation results for the N_2-H_2 cases from that work are

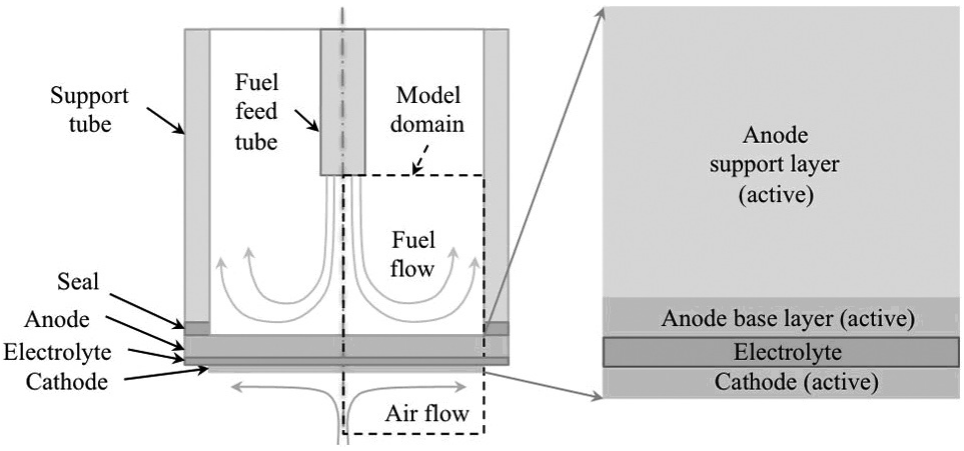

FIGURE 1. Schematic View of the Experimental Testing Section and Computational Domain Used for the DEC Model Simulation Results

TABLE 1. Structural Parameters Used for All Validation Cases

	Thickness, micron	Volume fraction			Particle radius, micron		Pore radius, micron	Tortuosity factor
		YSZ	Pores	Ni/LSM	YSZ	Ni/LSM		
Anode	1,100	0.274	0.35	0.376	0.5	0.5	0.5/0.8	2.5
Electrolyte	10	1.0	0.0	0.0	-	-	-	-
Cathode	30	0.315	0.35	0.335	0.5	0.5	0.5	2.5

plotted in Figure 2. In the figure, the symbols represent the experimental data and the modeled performance is shown by the solid and dashed curves. The performance predicted by the DEC model matched the data very well for operating voltages up to about 0.9 V for all N_2 dilutions. The maximum difference between predicted and experimental peak power was 12%, and the maximum difference between predicted and measured limiting current density was 11% including all N_2 dilution cases. Results of the validation test cases indicate that the DEC model accurately predicts the gas diffusion effects of the anode-supported SOFC. The accuracy of the DEC model predictions over the range of fuel compositions considered suggests the DEC modeling tool is suitable for calculating peak power and current density for operating voltages up to ~0.9 V for simple fueling cases.

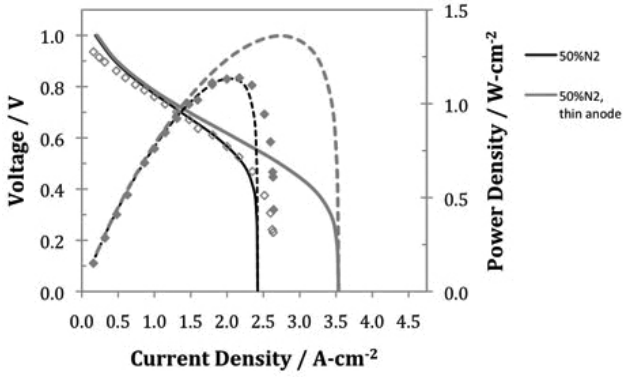

FIGURE 3. Modeled performance for "thin" (0.55 mm) anode (gray curves) compared to model validation case (black curves) and experimental data (symbols) for a button cell with 1.1 mm thick anode. All cases operating on 50% N_2 50% H_2 fuel at 800°C.

Anode Optimization Exercise

The DEC model can be used to consider the structural and compositional design of the electrodes. To demonstrate this capability, an optimization study was performed in the anode. The optimization study used five separate steps to systematically increase the performance of the anode. For the optimization case the 50% N_2 validation case (operating at 0.8 V and 800°C) was used as the baseline of performance (Step 1) and anode modifications are made cumulatively to improve the performance. The first optimization step (Step 2) is to decrease the thickness of the anode by 50% from 1,100 μm to 550 μm. Figure 3 shows the resulting I-V performance of the "thin" 550 μm anode case (gray curves) compared to the "50% N_2" case (black curves) and the experimental data (symbols) for that case are included in the figure for reference. After Step 2, the current density increased at 0.8 V from 0.862 to 0.914 A/cm^2 and the gas diffusion limitations of the thicker anode have been substantially decreased as indicated by the limiting current density, which increased from about 2.4 to 3.5 A/cm^2. Of note also is the substantially increased peak power due to the thinner anode.

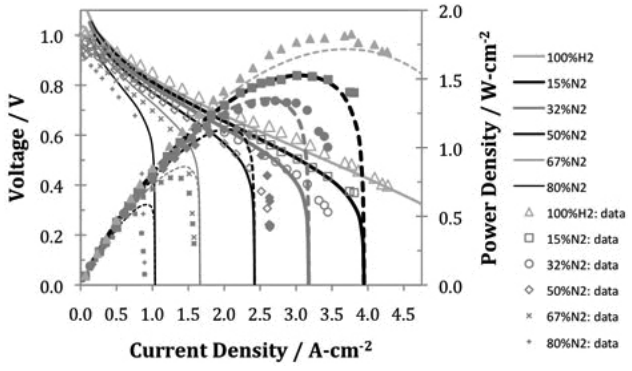

FIGURE 2. Comparison of the DEC model simulation results with experimental N_2-H_2 button cell data [3]. Symbols represent the experimental data, and the DEC modeled performance is shown by the solid and dashed curves.

Step 3 of the optimization enhances the performance (of the 550 μm anode case) by increasing the average pore radius and porosity in the anode support layer to further decrease gas transport limitations within the anode. Assuming the optimal particle size and associated pore size in the base layer will be small to maximize the TPB length, the pore size is increased only in the support layer, from 0.8 μm to 2.0 μm. Also, the porosity in the support layer is increased from 0.35 to 0.45. These changes applied to the support layer increased the current density to 0.935 at 0.8 V.

In Step 4, the ionic conductivity in the anode base layer is increased by 90%. This is done by increasing the YSZ fraction (from 0.274 to 0.35). The porosity within the base layer was simultaneously decreased from 0.35 to 0.30 such that the Ni fraction could remain relatively high at 0.35 equal to the YSZ fraction. The additional result of these changes in the fractions of the three phases was an increase of 23% in TPB length. The increased ionic conductivity and TPB result in a considerable increase of the current density at 0.8 Volts to a value of 1.162 A/cm^2.

Step 5, the final optimization step for this exercise, is to decrease the average YSZ and Ni particle radii in the anode base layer from 0.5 to 0.3 μm, and increase the porosity from 0.30 back to 0.35 while maintaining equal fractions of the solid phases at 0.325. The physics affected by these changes are a three-fold increase in TPB, a slight decrease in the ionic conductivity compared to the previous case, and a return to the better gas transport associated with the more open porosity. The effect on the performance is substantial, with the current density now at 1.401 A/cm^2. This step and the steps preceding it are summarized in Table 2.

TABLE 2. Microstructural Parameter Changes Applied for Anode Optimization Cases

Step	Structural parameters changed	Physics effected compared to baseline	Current density, A/cm^2 at 0.8 V
1	Baseline (1,100 mm anode)	Baseline physics	0.862
2	+ Model anode thickness decreased to 550 mm	Increased gas transport	0.914
3	+ Increase porosity and pore size in anode support layer (from 0.35 to 0.45, and 0.8 mm to 2.0 mm)	Increased gas transport	0.935
4	+ Increase YSZ fraction in anode base layer (from 0.274 to 0.35, porosity decreased from 0.35 of 0.30)	90% increase in ionic conductivity, 23% increase in TPB, and decreased gas transport in base layer	1.162
5	+ Decrease particle radius of YSZ and Ni from 0.5 to 0.3 mm, increase porosity back to 0.35 (slight decrease in YSZ and Ni compared to Step 4)	70% increase in ionic conductivity, 300% increase in TPB, and return to gas transport in base layer as in case 3	1.401

The Faradaic current density distributions in the anode resulting from the local charge transfer for the above steps 1, 2, 4, and 5 are shown in Figure 4. Step 3 is not shown because its current density is very similar to both Steps 1 and 2. Note that in Figure 4 the Faradaic current density is larger for the higher case numbers coinciding with the higher global (I-V) current density numbers summarized in Table 2. The Faradaic current density distributions show the effects of microstructural changes made in the optimization exercise. The baseline (Step 1) is the lowest performing case and has the smallest current density. Step 2 overlays Step 1 except near the electrolyte layer where the current is higher. These two cases feature very similar structural properties in both the base and support layers and have very smoothly decreasing current density values that are diminishingly small, but non-zero for about 30 microns into the anode. Steps 4 and 5 have current density distributions shaped differently than the other cases. Step 4 has a maximum value slightly less than Step 2, but the volume of the current is larger for a greater distance into the anode with a slightly faster rate of decrease in the anode beyond the 17 micron thick base layer; while Step 5 has by far the largest maximum current density. The current density of Step 5 decreases smoothly through the base layer then decreases sharply within the courser, more porous support layer where the TPB density and ionic conductivity are smaller.

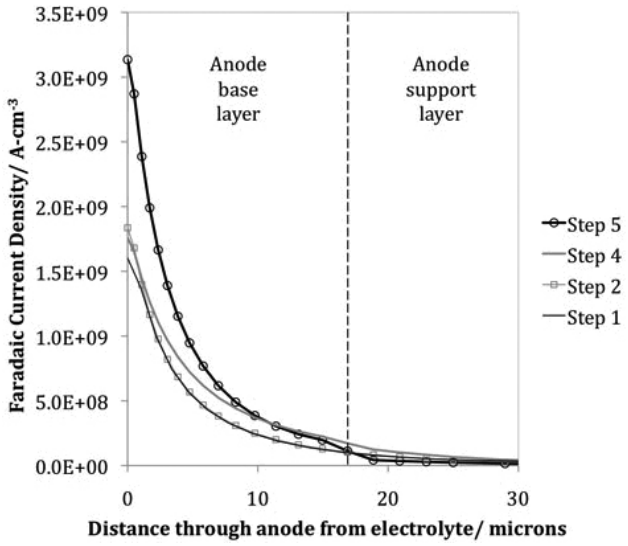

FIGURE 4. Faradaic Current Density Distributions in the Anode for the Optimization Steps 1, 2, 4, and 5

Conclusions and Future Directions

During FY 2011, the DEC modeling tool was developed to simulate realistic SOFC performance. The DEC model calculates the global performance of the SOFC based on the local conditions and multi-physics within the MEA. The model is able to accurately reproduce experimental data at various operating voltages and gas compositions. An effective properties approach is used to model the SOFC electrodes, which allows the porous microstructure to be included in the model via effective parameters based on the structural properties of the electrodes. The DEC model results presented here included:

- Validation of the DEC model against experimental button cell data. The validation cases demonstrate the suitably of the DEC modeling tool to represent the performance and gas transfer limitations of anode supported SOFCs by successfully matching experimental data for a fuel cell operating on various fuel gas compositions.
- An anode optimization exercise, which demonstrates the sensitivity of the DEC model to the electrode microstructure. Changes to microstructural properties that affect the gas transport, ion transport, TPB length, and the distributed charge transfer through layered or graded electrodes were shown to have the greatest effect on SOFC performance.

Further development of the DEC model is needed to investigate degradation mechanisms that result in damage to the electrodes and electrochemical performance decay. The validation and demonstration

of the DEC model has laid the framework for considering the degradation and long-term performance of SOFCs. The DEC model can now be expanded to look at degradation and performance problems of interest to the Solid State Energy Conversion Alliance industrial team members. Such problems might include: examining the conditions within the anode in the event of fuel supply interruption and the evolution of events leading up to Ni oxidation, or sulfur from a diesel fuel reformer poisoning of the anode in an auxiliary power supply unit on board a tractor-trailer.

FY 2011 Publications/Presentations

1. K.P. Recknagle, E.M. Ryan, and M.A. Khaleel, "Numerical Modeling of the Distributed Electrochemistry and Performance of Solid Oxide Fuel Cells," ASME 2011 International Mechanical Engineering Congress & Exposition, Denver, Colorado, November 2011.

2. K.P. Recknagle, E.M. Ryan, and M.A. Khaleel, "Distributed Electrochemistry Modeling Tool for Investigating Solid Oxide Fuel Cell Performance," Power Sources, 2011.

3. E.M. Ryan, K.P. Recknagle, and M.A. Khaleel, "Modeling the Electrochemistry of an SOFC through the Electrodes and Electrolyte," ECS Trans., vol. 35, issue 1, 2011.

References

1. H. Zhu and R.J. Kee, "Modeling Distributed Charge-Transfer Processes in SOFC Membrane Electrode Assemblies," Journal of The Electrochemical Society, 2008. 155(7): p. B715-B729.

2. W.G. Bessler, S. Gewies, and M. Vogler, "A New Framework for Physically Based Modeling of Solid Oxide Fuel Cells," Electrochemica Acta, 2007. 53(1): p. 1782-1800.

3. Y. Jiang and A.V. Virkar, "Fuel Composition and Diluent Effect on Gas Transport and Performance of Anode-Supported SOFCs," Journal of The Electrochemical Society, 2003. 150(7): p. A942-A951.

4. K.P. Recknagle, E.M. Ryan, and M.A. Khaleel, "Distributed Electrochemistry Modeling Tool for Investigating Initial and Long-Term Solid Oxide Fuel Cell Performance," Power Sources, 2011.

III.G.6 Rolls-Royce SOFC Model Development

Greg Rush
Rolls-Royce Fuel Cell Systems (U.S.) Inc.
6065 Strip Ave. NW
North Canton, OH 44720
Phone: (330) 491-4831; Fax: (330) 491-4808
E-mail: greg.rush@rrfcs.com

DOE Project Manager: Patcharin Burke
Phone: (412) 386-7378
E-mail: Patcharin.Burke@netl.doe.gov

Subcontractor:
Dr. Ben Haberman
Toronto, Canada

Contract Number: FE0000773

Start Date: August 1, 2009
End Date: September 30, 2011

Fiscal Year (FY) 2011 Objectives

- Enhance multi-physics code (MPC) to install and configure the following Rolls-Royce Fuel Cell Systems (RRFCS) solid oxide fuel cell (SOFC) models:
  - Integrated current flow and electrochemistry
  - Empirical and kinetic fuel cell degradation
  - Plug fluid flow
  - Heat transfer by convection, conduction and radiation
  - Turbulent fluid flow
- Establish three-dimensional models of a five-cell test piece, a complete substrate (tube structure on which anode and cathode layers are printed) and a bundle.
- Validate three-dimensional models against RRFCS experimental data and complete validation of two-dimensional models that were developed in FY 2010.
- Validate fuel cell degradation models against available experimental data.
- Establish external supercomputing capability for running large simulations.
- Interface with lifetime and reliability modeling project (not included in this contract) to supply required variables from substrate and bundle models.
- Interface with larger-scale lower resolution model (RRFCS code development separate from this contract) to obtain boundary conditions for in situ bundle operation within a block.
- Develop new model applications to demonstrate MPC predictive capabilities to RRFCS team.

FY 2011 Accomplishments

- Completion of MPC enhancements as set out in project objectives.
- Successful development and running of three-dimensional models of five-cell and substrate.
- Validation of three-dimensional five-cell and substrates model against experimental data and completion of validation work for two-dimensional models that were developed in FY 2010.
- Development of empirical degradation models from five-cell test results obtained from over 6,000 hours of operation (experiments are ongoing).
- Set up of agreement with a supercomputer center to run large models using MPC installed on their machines. Substrate models have been run successfully at the supercomputer center.
- Model of substrate test rig built to demonstrate MPC predictive capabilities and support the design process.
- Further MPC code enhancements developed to fully automate meshing and geometry operations.

Introduction

The objective of this project is for RRFCS to develop a multi-physics SOFC computer code for performance calculations of the RRFCS fuel cell structure to support fuel cell product design and development. This work consolidates years of RRFCS investment and research throughout the world as part of its business objective to develop an SOFC product for stationary power generation.

The focus of activity during the first year of the project (FY 2010) was the downselect of a suitable commercially available multi-physics computer code, STAR-CCM+ (from CD-adapco) and the commencement of the code enhancement and model verification/validation work required to develop and test the MPC. The second project year (FY 2011) is focused on the extension of the MPC from small scale models to substrate and bundle models, and the development of degradation models to enable the prediction of fuel cell durability.

Approach

The MPC development project has been split into two work streams: code enhancement, and model verification and validation. A code enhancement methodology has been implemented whereby the MPC comprises three distinct elements:

- STAR-CCM+ the downselected commercially available computational fluid dynamics simulation tool.
- An Excel (from Microsoft) spreadsheet where all model data is stored.
- A set of Java (from Oracle) macros to perform all model operations.

This approach has been used to fully automate the process of installing all model features required to perform an SOFC simulation. The starting point is the model geometry (a computer-aided fuel cell drawing that has been imported into STAR-CCM+). The MPC automatically configures the mesh, installs existing STAR-CCM+ models, installs the code enhancements required for new models, runs the simulation and post-processes the results.

The model verification and validation program has run concurrently with the code enhancement program and has involved building and testing SOFC models on a variety of scales including: one-dimensional single cell models, two dimensional five-cell models and three-dimensional models of five-cells, substrates and bundles. The validation process involves several steps including comparisons with experimental data and predictions from other models.

Results

The MPC code enhancements for FY 2011 are complete and all model settings are input via an Excel spreadsheet. This spreadsheet consolidates all model settings into a single form and facilitates the quick checking and sharing of model data without requiring a STAR-CCM+ license. The desired models for a particular application are installed using Java macros and Figure 1 shows an example of the output generated within STAR-CCM+ during this process.

Figure 1 shows the extensive feedback the macros provide to the user to highlight any errors or problems encountered during the model installation process.

The model verification and validation program for FY 2011 has successfully validated three-dimensional models of five-cells and substrates and two-dimensional models of five-cells. Bundle model construction is in progress and the substrate models are also being extended to model the complete substrate test apparatus. Figure 2 shows a plot of predicted hydrogen mole-fraction within a three-dimensional five-cell model.

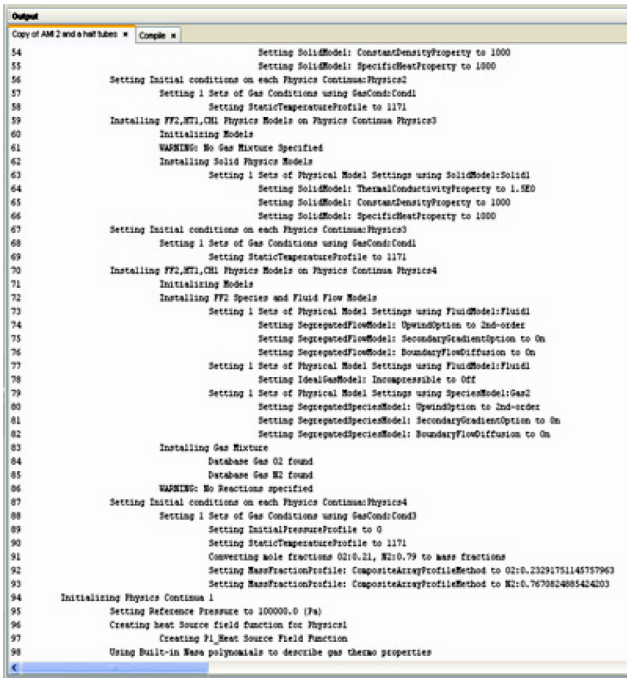

FIGURE 1. Output Generated by Java Macro in STAR-CCM+

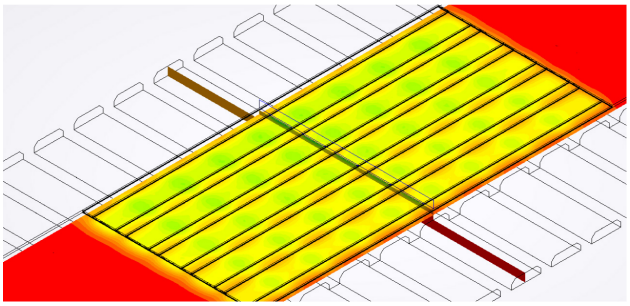

FIGURE 2. Predicted Hydrogen Mole Fraction within a Five-Cell Model

Figure 2 shows that the MPC is able to predict how substrate geometry influences hydrogen mole fraction in the five anodes; a lower mole fraction is seen in anode regions that are not directly above fuel channels where the flow path through the substrate is longer. The MPC is also able to predict how these variances in mole fraction are manifested in the electrochemical reaction rates. Figure 3 shows the current density distribution in the electrolyte and illustrates how sensitive the reaction rates are to hydrogen mole fraction.

Figures 2 and 3 illustrate the detailed output generated by the MPC and its capabilities as a design analysis tool.

Model predictions are commonly validated against experiment current voltage measurements and Figure 4 shows an example plot which illustrates the influence of cell temperature on predicted and measured performance.

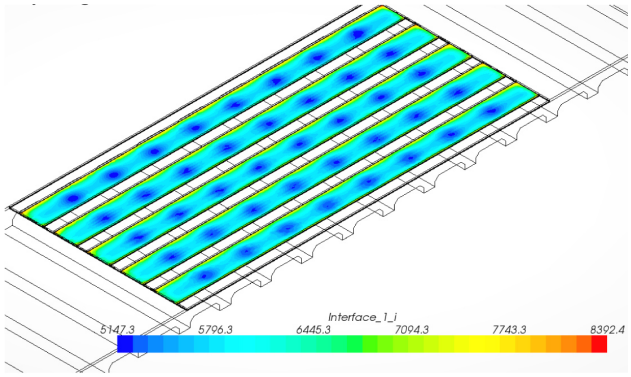

FIGURE 3. Calculated Current Density Distribution within the Electrolyte of Each Cell

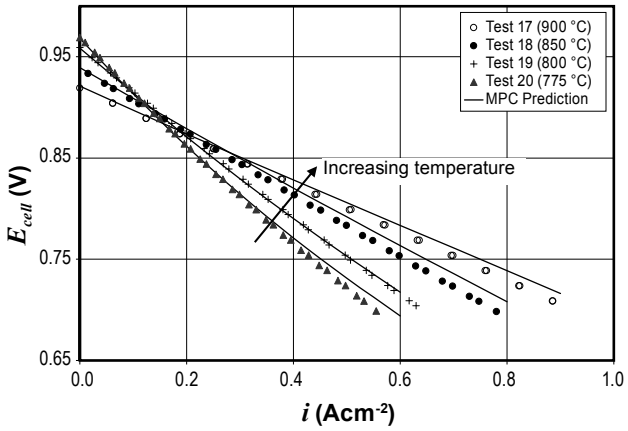

FIGURE 4. Measured and Predicted Cell Performance over a Range of Temperatures

Conclusions and Future Directions

The aim of this project is for RRFCS to develop a multi-physics SOFC computer code for performance calculations of the RRFCS fuel cell structure to support fuel cell product design and development. The MPC is based in the STAR-CCM+ (CD-adapco) computational fluid dynamics software package and MPC development is organized into concurrent code enhancement and model verification/validation work programs.

A code enhancement methodology has been implemented to fully automate all aspects of model generation and to consolidate all model input into a single Excel file. This work has progressed on schedule and the MPC is now capable of performing simulations of the coupled heat and mass transfer, chemical, electrochemical, current flow and porous flow processes that occur in SOFCs.

The model verification/validation work program is progressing on schedule and MPC models of five-cells and substrates have been successfully validated in FY 2011. The substrate model is now being extended to the bundle scale. The MPC is being applied to applications outside of validation activities and a model of the substrate test apparatus has been built to support future design work.

This project has proceeded on schedule and under budget and a no cost project extension will be requested to incorporate model developments that were beyond the original project scope and facilitate the testing of the MPC outside of the code development team.

FY 2011 Publications/Presentations

1. Ben Haberman, Carlos Martinez Baca, and Greg Rush, "SOFC Model Development," U.S. Department of Energy, National Energy Technology Laboratory, Strategic Center for Coal's FY11 Fuel Cells Peer Review, February 14–18, 2011.

2. B.A. Haberman, C. Martinez Baca, and T. Ohrn, "IP-SOFC Performance Measurement and Prediction," SOFC XII ECS Meeting, Montreal, Canada, May 4, 2011.

III. SECA CORE RESEARCH & DEVELOPMENT

H. Balance of Plant

III.H.1 Foil Gas Bearing Supported High Temperature Cathode Recycle Blower (Large Size Cathode/Anode Recycle Blower)

Giri Agrawal (Primary Contact), Bill Buckley, Dennis Burr, Sam Rajendran
R&D Dynamics Corporation
49 West Dudley Town Road
Bloomfield, CT 06002
Phone: (860) 726-1204; Fax: (860) 726-1206
E-mail: agragiri@rddynamics.com
Website: www.rddynamics.com

DOE Project Manager: Robin Ames
Phone: (304) 285-0978
E-mail: Robin.Ames@netl.doe.gov

Contract Number: ER85020

Start Date: June 30, 2008
End Date: August 13, 2011

Fiscal Year (FY) 2011 Objectives

Develop a high temperature capable (up to 850°C), energy efficient, reliable, maintenance-free, oil-free and low-cost cathode and anode recycle blower for large megawatt-size solid oxide fuel cell (SOFC) power plants.

FY 2011 Accomplishments

The following are the accomplishments during current FY 2011 Phase II research and development of the foil gas bearing supported high temperature cathode recycle blower, also called the large size cathode/anode recycle blower (LC/ARB):

- A prototype blower unit and two sets of rotating assemblies for ambient temperature testing and high temperature testing were manufactured.
- The motor end of the prototype unit was assembled separately and successfully tested with a cooling fan load.
- The cooling fan performance was tested and aerodynamic data analysis was completed.
- The full prototype unit (coupled configuration) was assembled and tested successfully up to design speed and full motor power at ambient temperature conditions.
- A work plan for testing the blower at high temperature operation (up to 850°C) was developed to demonstrate the high temperature capability of the blower for Solid State Energy Conversion Alliance (SECA) members.

Introduction

Fossil fuels are projected to remain the mainstay of energy consumption well into the 21st century. As the nation strives to reduce its reliance on imported energy sources, the United States (U.S.) Department of Energy's (DOE's) Office of Fossil Energy supports research and development to help ensure that new technologies and methodologies will be in place to promote the efficient and environmentally sound use of the U.S.'s abundant fossil fuels.

The SECA cost reduction goal is to develop and design a SOFC capable of manufacture at $400/kW in the near future. Concurrently, SECA coal-based systems will scale and integrate SECA SOFC technology for delivery to 5 MWe plant in the near future. Development of large (greater than 100 MWe) SOFC power blocks will enable affordable, efficient and environmentally friendly electrical power from coal.

SOFC-based power block configurations for coal-fueled central generation applications could benefit from recycling a portion of the high temperature (e.g., 800-850°C) cathode air and anode gas effluent back in to the system in order to improve the overall plant efficiency. System studies have indicated that a recycle ratio of (40-50%) would be desirable. Key requirements for the cathode and anode recycle blower are:

- Reliability at high temperature (up to 850°C)
- Contamination free operation (no oil or grease)
- Energy efficiency
- Scalability of design
- Maintenance
- Low cost
- Lower noise

In discussion with SECA members, additional technical requirements are also identified as listed below:

- Hermeticity
- Corrosion-free operation
- No metal outgassing
- No sulphur leak into fuel stream
- No free silica leak into fuel stream
- No heavy metal leak into fuel stream
- Purge gas undesirable

Currently, there is no blower available to meet these challenges; hence, an innovative blower technology is needed.

Approach

- A nominal specification was chosen for the blower design in discussion with SECA members.
- During current Phase II research and development a detailed design of the blower was completed and detailed drawings were prepared for manufacturing.
- The blower was manufactured, assembled and tested at ambient temperature conditions and successfully demonstrated the following key technical aspects of the blower design:
  - Mechanical integrity
  - Rotordynamic stability
  - Cooling fan performance
  - Motor performance
- A work plan for testing the blower at high temperature operation (up to 850°C) during a Phase II project extension was developed to demonstrate the high temperature capability of the blower for SECA members.

Results

The LC/ARB is an innovative hermetically sealed high temperature design where the hot end of the machine is separated thermally from the motor end. Figure 1 shows the isometric view of the blower. The hot fan side takes in the recycle gas and raises the pressure using an axial fan. The hot end and motor end has separate sets of journal and thrust bearings, hence they can act independent thermally and rotordynamically. The blower was designed meeting all the stringent technical requirements as an ARB and can be easily adapted as a cathode recycle blower. Hence it has dual use. The rotating assembly of the blower is supported on high reliability foil gas bearings. The blower is driven by a permanent magnet motor and controlled by a sensorless controller. The blower design has the following features:

- High temperature capable (up to 850°C)
- Highly reliable
- Highly energy efficient
- Low life cycle cost
- Oil free
- Maintenance free
- Long design life (>40,000 hrs)
- Low noise (<70 dBa)
- Scalable
- Turn down ratio up to 5:1

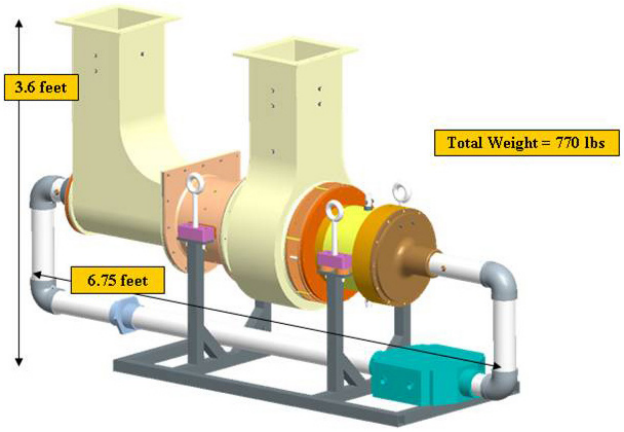

FIGURE 1. Isometric View of the Blower

Technical Specification

The blower was designed for the following nominal specification chosen from discussions with SECA members:

Molecular Weight	28.31
Specific Heat Ratio	1.22
Inlet Pressure	15.31 psia
Outlet Pressure	15.77 psia
Pressure Rise	12" of water
Inlet Temperature	825°C
Flow	185 lbm/min
Input Voltage	480 Vac

Technical Summary of Design

Technical summary of the blower design is listed as follows:

Rotor Type	Axial
Motor Type	Permanent Magnet
Controller Type	Sensorless
Specific Speed	800
Speed	26,520 rpm
Tip Diameter	8.8 inches
Hub Diameter	4.5 inches
Isentropic Power	12.77 kW
Cooling Fan Power	3 kW
Total Input Power	21.2 kW
Overall Efficiency	60%

Detailed Design and Analysis

The following detailed design and analysis work was performed:

- Material selection
- Cooling scheme design
- Heat transfer analysis
- Heat exchanger design
- Seal design
- Bearing design
- Coupling design
- Stress analysis
- Rotordynamic analysis
- Thrust load analysis
- Motor design and analysis
- Controller design and analysis

Computer-Aided Design Modeling and Detailed Drawings

Several optimizing iterations of the design were performed and solid models were created using Pro/ENGINEER. Detailed drawings of the machine were completed considering all detailed analysis results, assembly aspects and manufacturing methods.

Manufacturing and Assembly

A prototype unit blower was manufactured and assembled for testing. The blower key components such as rotating assembly and bearings were manufactured in-house and sheet metal ducts and housings were manufactured at vendor shops. Two sets of rotating assemblies were manufactured one for ambient temperature testing and another for high temperature testing. The high temperature testing rotor was coated with ceramics for blade life and thermal insulation.

Motoring Test and Cooling Fan Performance

The motor assembly of the machine was assembled separately and run with cooling fan load to ensure motor performance. The motor rig is shown in Figure 2. During the motor test the cooling fan performance was also tested and the aerodynamic data was analyzed. The cooling fan performance is shown in Figure 3.

Fully Coupled Machine Testing

The blower was fully assembled and ambient temperature testing of the blower was completed. Figure 4 shows the fully coupled blower.

The LC/ARB is designed to operate at 850°C inlet gas temperature. Testing at ambient conditions required blade heights to be cut down to match motor power.

FIGURE 2. Motor Test Rig

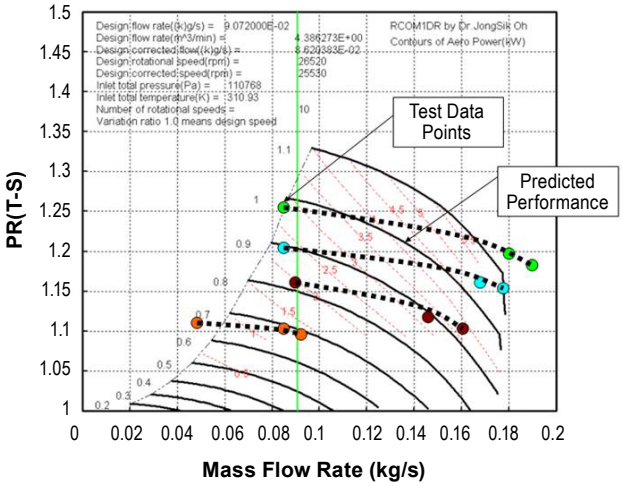

FIGURE 3. Cooling Fan Performance Map

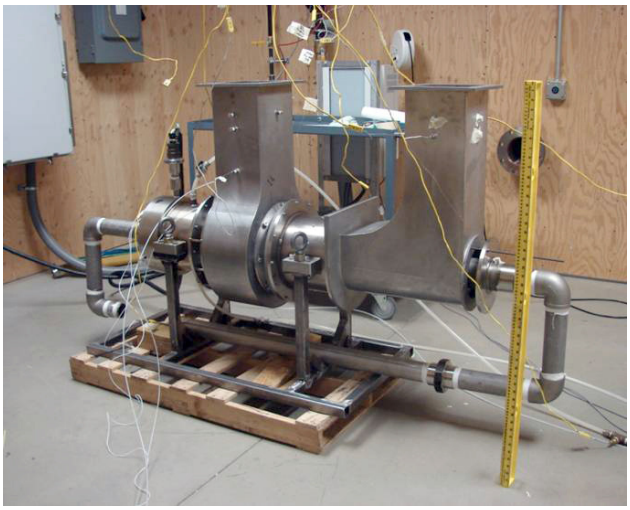

FIGURE 4. Fully Coupled Machine

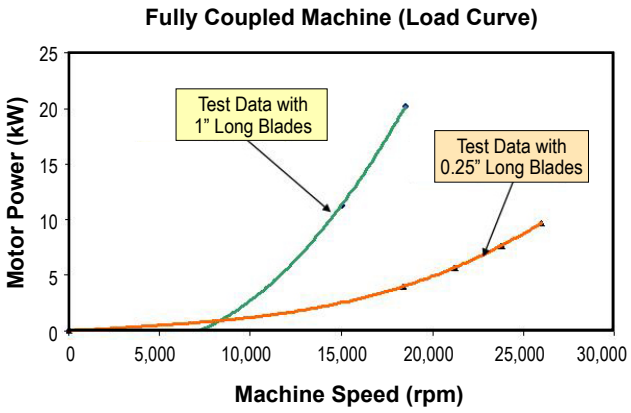

FIGURE 5. Fully Coupled Machine Test Data

Initial testing was done with 1" long blades and the motor reached its max torque at 18,400 rpm. The 1" long blade test proved motor performance at max torque. The blade was further cut down to 0.25" which enabled the blower to operate at design speed (26,520 rpm). The load curve data collected during ambient testing is shown in Figure 5.

Phase II Success

R&D Dynamics made significant progress and achieved success during the current FY 2011 Phase II research and development.

- A hermetically sealed high temperature capable (up to 850°C), oil-free, maintenance-free and highly efficient dual use LC/ARB was designed, manufactured and successfully tested at ambient temperature conditions.
- The ambient testing of the LC/ARB demonstrated mechanical integrity, rotordynamic stability, cooling fan performance and motor performance of the blower.

Conclusions and Future Directions

The LC/ARB being developed under this project is the largest size high temperature foil gas bearing supported recycle blower ever manufactured and tested. The machine spans 6.75 feet across by 3.6 feet tall and weighs 770 lbs. During various stages of Phase II development R&D Dynamics faced challenging technical problems. R&D Dynamics was able to resolve all of the challenges and successfully test the LC/ARB.

The FY 2011 Phase II funding period accomplishments were highly successful in demonstrating the LC/ARB at ambient temperature conditions. However, the LC/ARB needs to be tested at high temperature conditions up to 850°C to meet SECA goals in demonstrating megawatt-size SOFC systems. The following are the remaining efforts in demonstrating the blower at high temperature conditions:

- High temperature heater design for closed-loop testing at 850°C.
- High temperature test rig design including component selection such as flow control valves, flow meters, temperature sensors, pressure sensors and other instrumentations.
- High temperature test rig fabrication and setup.
- Mechanical integrity testing at 850°C inlet gas temperature.
- Performance testing, leak testing and seal integrity testing.
- Design improvements, improved design manufacturing and testing for final demonstration to SECA members.

The remaining efforts are within the original scope of work proposed for the Phase II research, and R&D Dynamics is planning to perform these tasks during a Phase II project extension.

Special Recognitions & Awards/Patents Issued

A provisional patent was filed in July 2010 and a full patent called "Mechanically Coupled Turbomachinery Configurations and Cooling Methods for Hermetically Sealed High Temperature Operation" is being prepared for filing in July 2011.

FY 2011 Publications/Presentations

1. WEBEX "Project Review Presentation" December 14, 2010, DOE.

III.H.2 Post-SOFC Residual Fuel Oxidizer for CO_2 Capture

Jeannine Elliott (Primary Contact),
Robert Copeland, Gokhan Alptekin
TDA Research, Inc.
12345 West 52nd Ave.
Wheat Ridge, CO 80027
Phone: (303) 261-1142; Fax: (303) 261-1130
E-mail: jelliott@tda.com

DOE Project Manager: Joseph Stoffa
Phone: (304) 285-0285
E-mail: Joseph.Stoffa@netl.doe.gov

Subcontractor:
FuelCell Energy, Danbury, CT

Contract Number: SC0004380

Start Date: July 19, 2010
End Date: March 18, 2011

Fiscal Year (FY) 2011 Objectives

The overall objective of the Phase I research was to demonstrate the merit of a sorbent-based fuel oxidizer for the anode exhaust of solid oxide fuel cells (SOFCs). The key feature of the system is the metal oxide sorbent which is used to oxidize the fuel, allowing us to keep the CO_2 from being diluted with the nitrogen during combustion. Therefore, the main objective was to develop a high-capacity, long life sorbent, and demonstrate its performance. A second major part of our work in this Phase I Small Business Innovation Research project was the system analysis to determine the most efficient way to integrate the anode oxidizer into an integrated gasification fuel cell (IGFC), and calculate the economics of this approach. The specific research objectives supporting the overall objective are as follows:

- Identify the optimum metal oxide sorbent composition with the high oxygen absorption capacity (>3 wt%).
- Characterize the best sorbent compositions in terms of crush strength and chemical stability at high temperatures (800°C).
- Evaluate the best sorbent in a laboratory-scale test system. Identify the effect of pressure, space velocity, and temperature on the oxygen absorption capacity.
- Carry out system design and determine the best way to integrate TDA's system with the SOFC power island.
- Evaluate economic benefits of the proposed system, including its effect on efficiency and capital costs of the power island.

FY 2011 Accomplishments

During Phase I, TDA prepared and screened many different sorbent formulations, focusing on their O_2 absorption capacity, regenerability and ability to rapidly oxidize H_2 and CO. Sorbent testing experiments were conducted by thermogravimetric analysis (TGA) and in a laboratory testing apparatus under simulated anode exhaust and cathode exhaust gas conditions. Based upon the experimental results, a preliminary design of the system was carried out with our partner, FuelCell Energy (FCE), to assess how the technology best integrates into an IGFC system. FCE included our system in their existing ChemCad model developed under the U.S. Department of Energy (DOE) Solid State Energy Conversion Alliance (SECA) program, and optimized the system integration to maximize the plant efficiency. The benefits offered by this system were compared to a baseline oxy-combustion anode fuel oxidizer.

The key conclusions of the Phase I research are as follows:

- The new sorbent had excellent oxygen capacity (5.9 wt% dynamic loading) and rapidly cycles under the anode and cathode exhaust conditions at the temperature range of interest.
- The sorbent has a low cost of $5-8/lb.
- The sorbent reaction rates are fast and the fuel oxidation process can be run at high space velocities (4,000 hr^{-1}).
- The sorbent showed it could reduce the residual anode fuel rapidly to very low levels. The CO concentration was oxidized down to 10 ppmv levels and hydrogen concentration was reduced to less than 80 ppmv. This means the process will be extremely effective at completely oxidizing the residual fuel which allows us to utilize all energy remaining in the anode-off gas and maximize the efficiency of the plant.
- TDA's fuel oxidizer increases the net system efficiency (based on coal higher heating value [HHV]). The system efficiency when integrated with TDA's anode exhaust fuel oxidizer is 59.25% compared to 58.50% with the SECA baseline oxycombustion fuel oxidizer (exclusive of CO_2 compression) at normal operating conditions. At peak power operation the efficiency is 54.64% (compared to 53.93%). This analysis was done using the methodologies and guidelines of the SECA program.

- The system can also be configured to reduce the capital cost of the power island by 6% (at equal or greater efficiency). The factory power island cost with TDA's fuel oxidizer is $350/kW versus $372 for baseline SECA system with oxy-burner.
- TDA's system will reduce the cost of CO_2 capture on an IGFC plant. It decreases the levelized cost of electricity (LCOE) by 1.4% compared to oxy-combustor. When our process is integrated with high efficiency catalytic coal gasification/SOFC system the LCOE is estimated at only 6.4 cents/kWh including CO_2 capture, compression and storage.

Introduction

Power generation systems based on coal gasification and SOFCs are an attractive alternative for coal-fueled electricity production. Gasification is a clean cost effective means of producing a gaseous fuel from coal (which is inexpensive and plentiful). SOFC systems have the advantage of higher system efficiencies up to (40 to 60%) and lower oxides of nitrogen emissions than conventional pulverized coal power plants. Further, they are particularly amenable to CO_2 capture because the air and fuel streams are kept separate in the fuel cell. If a SOFC is combined with CO_2 capture, it promises to be a clean way to produce electricity while capturing greenhouse gases. To realize this goal, technologies are needed to effectively capture CO_2 from the fuel anode exhaust gas. The fuel cell anode gas contains CO_2, H_2O, and up to 10% H_2. By oxidizing the hydrogen and condensing the resulting water the CO_2 in this stream could be isolated. The goal of this project was to develop an efficient and cost-effective technology to oxidize the residual fuel in the anode exhaust of SOFCs and thereby enable CO_2 capture.

Approach

Our system works by oxidizing the residual fuel in the fuel cell anode exhaust gas so that only H_2O and CO_2 are left; after this, the CO_2 is readily isolated.

TDA's anode fuel oxidizer technology uses a metal oxide sorbent to burn the residual fuel in the anode off-gas. This process is a type of chemical looping combustion, where a metal oxide sorbent is oxidized (picks up oxygen) by the hot, slightly oxygen depleted air exiting the cathode section of the fuel cell (Figure 1). The sorbent is then contacted with the anode exhaust. The sorbent is reduced and gives up its oxygen while oxidizing the fuel exhaust gases to CO_2 and H_2O. The system does not introduce nitrogen into the gas steam, oxygen is drawn into the fuel gas by the reducing potential power of the anode off-gas and the CO_2 product is not contaminated with excess oxygen. Thus, with a sorbent-based process the fuel is oxidized without requiring an air separation unit.

In Phase I of the project, TDA demonstrated the technical and economic feasibility of using a metal oxide oxygen sorbent to burn residual fuel in the anode exhaust stream without diluting it with nitrogen or adding traces of oxygen gas. TDA prepared and screened many different sorbent formulations, focusing on their O_2 absorption capacity, regenerability and ability to rapidly oxidize H_2 and CO. TDA identified a metal oxide formula that is inexpensive, thermally stable at the desired operating temperatures, and most importantly, has the reducing power to oxidize the fuel down to only 37 ppm. The reaction in the oxidizer (where the fuel is oxidized and the metal [M] is reduced) is:

$$MO + H_2 = M + H_2O.$$

The reaction in the regenerator where the sorbent is oxidized is:

$$MO + O_2 = MO.$$

The metal oxide sorbent was prepared using TDA's proprietary techniques to create a durable, long cyclic life sorbent.

Results

The Phase I project included both experimental testing and system and economic analyses. The first

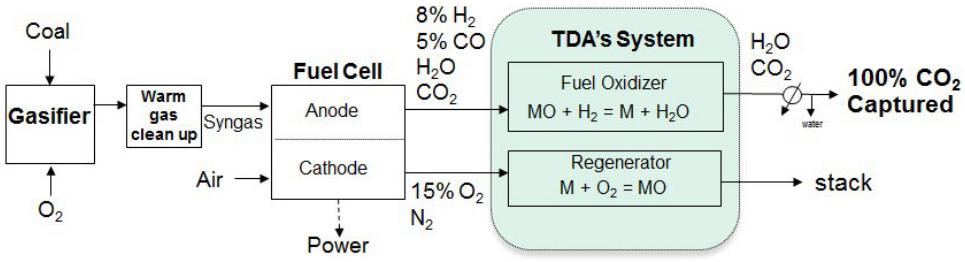

FIGURE 1. TDA Fuel Oxidizer Process for CO_2 Capture on IGFC

part of this project was focused on developing a suitable metal oxide sorbent and demonstrating that it has the required performance. This work was done first by screening materials in thermogravimetric testing and then in a fixed bed. The second part of the work was done in conjunction with FCE (under subcontract) to carry out a detailed engineering and economic analysis to determine the merit of the proposed fuel oxidizer in terms of plant performance and cost.

The regenerable fuel oxidation sorbent was evaluated by TGA in an analyzer and then in a fixed bed testing apparatus under simulated anode exhaust and cathode exhaust gas conditions. These tests showed that the sorbent had high capacity (~6 wt% dynamic oxygen loading), fast reaction rates and could completely reduce all the fuel in anode exhaust stream down to ppm levels at high space velocities (4,000 hr^{-1}). The sorbent was also tested for over 50 cycles under simulated conditions and had good chemical stability (Figure 2). Further, the sorbent is able to oxidize the fuel without releasing excess oxygen in order to meet pipeline requirements. The O_2 specification for pipeline CO_2 is <10 ppm.

Fixed bed tests were performed in an automated testing apparatus (Figure 3). The apparatus was built at TDA for the specific purpose of measuring the activity of sorbents and catalysts. The testing apparatus is fully automated with online gas analyzer to monitor the outlet composition. The fuel oxidation bed and sorbent regeneration bed were simulated in a single 300 cc reactor bed by alternating the inlet gas compositions.

In our first tests breakthrough curves of oxygen and fuel (H_2) were measured as we cycled the sorbent. The anode exhaust feed was simulated as 13% H_2, 47% H_2O, and the balance N_2. CO/CO_2 was not included in this test because it interfered with the H_2 analyzer output and all the residual fuel was modeled as H_2. The cathode exhaust gas will be depleted in O_2 with concentration ranging between 13% and 17%. Initial tests were run at 1,600 hr^{-1} (Figure 4). The results show the sorbent had about a 10 wt% loading. Outlet gases were measured on a dry basis but are presented on a wet basis in terms of H_2 composition in order to be consistent with the anode off-gas feed compositions which are also on a wet basis. Figure 4 shows that the hydrogen is completely consumed down to the detectible limit of the online hydrogen analyzer (<0.1%). During this step the sorbent is giving up oxygen. The fuel oxidation is very fast, goes to completion and then (since this is a batch reactor) eventually breaks through. This is exactly what is desired for this application. It can also be seen in Figure 4, how H_2O is forming as the H_2 is reacting with the oxygen given off the sorbent. When H_2 breaks through the $\%H_2O$ in the outlet drops simultaneously.

Addition tests evaluated the sorbent and higher space velocities. Figure 5 shows the laboratory test results with a simulated anode exhaust gas (8% H_2, 5% CO, 47% H_2O, and 40% CO_2) at 4,000 hr^{-1}. CO and H_2 were monitored in the outlet during the fuel oxidization step. In this test a non-dispersive infrared online CO analyzer was used which could detect CO down to ppm levels and the hydrogen content was monitored with gas chromatography (GC). The CO level (shown in purple) was reduced to 10 ppm and the H_2 level was reduced to below the detection limit of the GC analyzer (<0.1%). It is expected that the hydrogen oxidizes along with CO at similar rates; our TGA work showed the H_2 was reduced to below 80 ppm.

Based upon the experimental results, TDA carried out a preliminary design of the system with our partner, FuelCell Energy (FCE), to assess how the technology best integrates into an IGFC system. FCE included our system in their existing ChemCad model

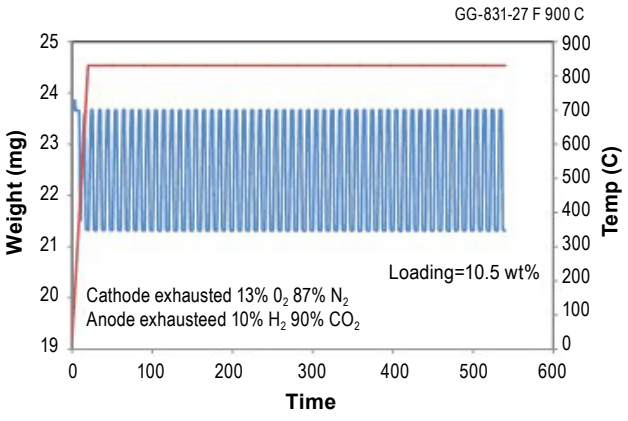

FIGURE 2. Cyclic testing in TGA shows chemical stability over multiple cycles. Anode gas off-gas simulated as 10% H_2, 90% CO_2; cathode off-gas simulated with 13% O_2, 87% N_2.

FIGURE 3. Automated Sorbent Testing Apparatus

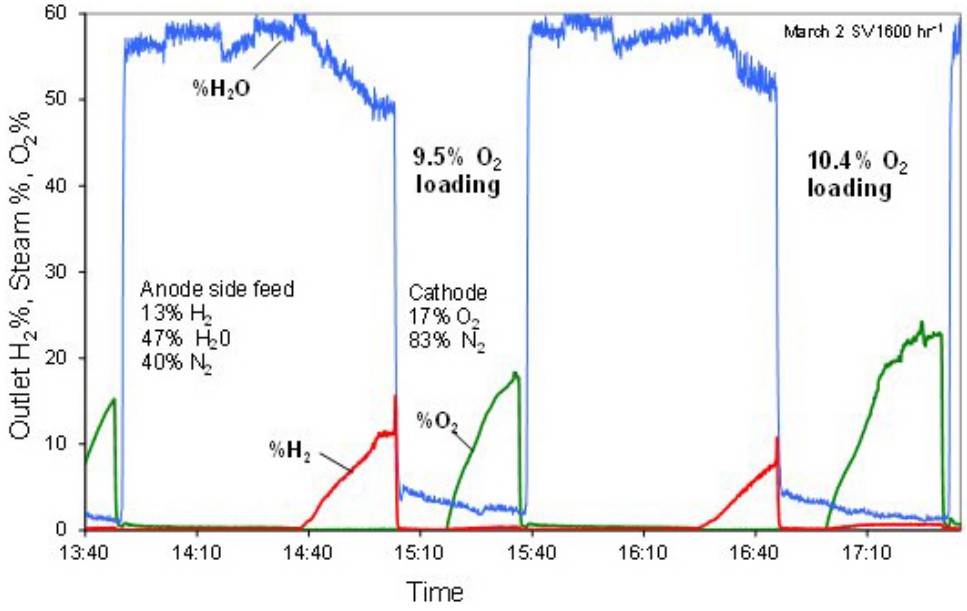

FIGURE 4. Fixed Bed Reactor Experiments Cycling at 1,600 hr^{-1} under Simulated Anode and Cathode Exhaust

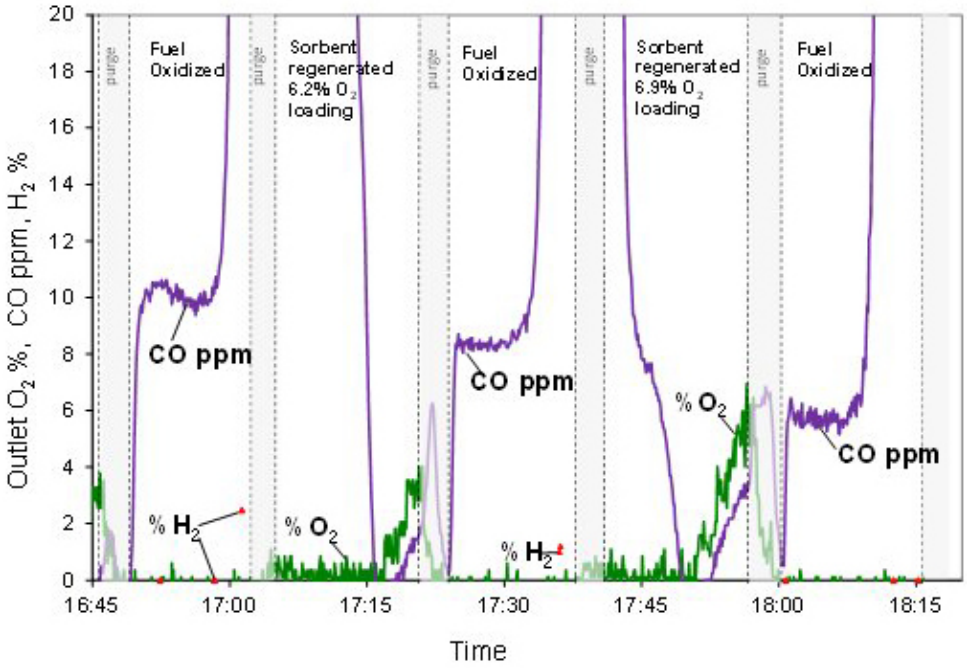

FIGURE 5. Fixed bed reactor experiment with simulated anode exhaust feed with 8% H_2 and 5% CO, 47% H_20, 40% CO_2, 2% N_2 and cathode exhaust feed of 13% O_2 and 83% N_2. Space velocity is 4,000 hr^{-1} in fuel oxidation and 2,000 hr^{-1} in sorbent regeneration. The test shows complete oxidation of CO and H_2.

developed under the SECA program and optimized the overall system to maximize the plant efficiency. TDA and FCE compared the benefits offered by this system with a baseline oxy-combustion anode fuel oxidizer using the same methodologies and guidelines DOE SECA program. This work showed that an IGFC plant (680 MW) with this new sorbent-based fuel oxidizer can be designed with a ~1% higher net plant efficiency (based on coal HHV). The system efficiency when integrated with TDA's anode exhaust

fuel oxidizer is 59.25% compared to 58.50% with the SECA baseline oxycombustion fuel oxidizer (exclusive of CO_2 compression) at normal operating conditions. The factory power island cost with TDA's fuel oxidizer was also 6% lower at $350/kW versus $372 for baseline SECA system with oxy-burner. This is 23% below DOE's SECA program goal of $400/kW.

Capturing CO_2 on an IGFC plant has the potential to be an extremely cost-effective way to reduce greenhouses gases at stationary power generation plants. Our Phase I estimate of the LCOE on an IGFC plant with TDA's fuel oxidizer integrated with FCE's power island is only 6.4 cent/kWh, including CO_2 capture and sequestration. This is extremely attractive, as a supercritical pulverized coal plant without CO_2 capture has a LCOE of 6.3 cent/kWh [1].

Conclusions and Future Directions

It is clearly worth investing in technologies for CO_2 capture on IGFC because these systems can keep the cost of electricity low while significantly reducing greenhouse gas emissions. The Phase I project results showed the technical merit of TDA's sorbent fuel oxidized approach through experimental studies. Further, system studies showed it has the potential to capture CO_2 at a significantly lower cost than the competing oxy-burner technology.

The following work is planned for the Phase II project to fully demonstrate the fuel oxidizer technology that will enable cost effective CO_2 capture on coal.

- The sorbent formulation will be optimized. In particular, experiments will demonstrate the sorbent has the ability to oxidize the residual fuel in the anode exhaust down to low levels over many cycles. The best sorbent formulation evaluated in an extended multiple-cycle (1,000-cycle) test to demonstrate the long-term performance and durability of the sorbent.
- We will scale up the sorbent using techniques representative of commercial manufacturing methodology to produce 10 kg batches of sorbent in our pilot plant for use in a larger scale demonstration unit.
- The system and cost analysis on this process developed in Phase I will be updated in collaboration with FCE to optimize integration of TDA's anode fuel oxidizer within the SOFC system to maximize efficiency and capital costs for the lowest levelized cost of energy.
- To demonstrate the fuel oxidation process as it will be commercialized, the sorbent will be tested in a two circulating bed system where the sorbent moves between the fuel oxidizer and regeneration beds. This unit will demonstrate the continuous oxidation of fuel to water and CO_2 in the oxidizer bed.
- Based on the experimental results, the detailed system design and economic analysis will be updated with FCE. The engineering system analysis will be refined to optimize the integration for the lowest power generation cost. A detailed engineering analysis will be conducted to design and size all of the hardware for TDA's new fuel oxidizer. Lastly, a +/- 30% cost analysis model will be developed to determine the levelized cost of energy and cost of CO_2 capture with TDA's system in comparison to competing technologies.

References

1. Phil DiPietro, "The Impact of Advanced Syngas Conversion Technologies on the Cost of Electricity from Gasification-based Power Generation Platforms," DOE/NETL-402/061308, June 2008.

IV. INNOVATIVE CONCEPTS

IV.1 Liquid Tin Anode Direct Coal Fuel Cell

Dr. Thomas Tao
CellTech Power, LLC
131 Flanders Road
Westborough, MA 01581
Phone: (508) 898-2223 x34; Fax: (508) 898-2690
E-mail: Tao@celltechpower.com

DOE Project Manager: Joseph Stoffa
Phone: (304) 285-0285
E-mail: Joseph.Stoffa@netl.doe.gov

Contract Number: NT0004111

Start Date: April 1, 2010
End Date: September 30, 2011

Fiscal Year (FY) 2011 Objectives

- Conduct testing of bench-scale electrochemical testing of Liquid Tin Anode (LTA) devices operating on coal in a tin bath reactor.
- Determine how coal contaminants partition between the liquid tin and coal ash in an operating LTA solid oxide fuel cell (SOFC). In other words: where do the coal contaminants go?
- Analyze the impact of coal ash on LTA components and operation. Evaluate the fuel properties for a range of coals representing the majority of United States coal use. Select coal or coal blends with contamination and other properties that will provide the best baseline for testing activities.

FY 2011 Accomplishments

- Direct coal experimental apparatus with continuous coal feeder was completed.
- Two initial tests of direct coal conversion on a tin bath using Illinois #6 coal were conducted.

Introduction

ElectroChemical Looping (ECL) using the LTA-SOFC produces direct current electrical power in an electrochemical reaction powered by coal or other common fuels. For utility-scale applications the fuel oxidation step is carried out in a separate tin-coal reactor (TCR) as shown in Figure 1. The liquid tin "loops" between the fuel cell and the tin reactor, shuttling all of the oxygen used to convert the coal. The net effect is that power is produced directly and efficiently from coal or biomass without burning and with inherent separation/rejection of nitrogen. To verify this concept, flowsheets were analyzed under another project to evaluate efficiency and cost. Oxides of nitrogen (NOx) are not formed because nitrogen does not participate in the reactions and sulfur emissions can be cleaned up using conventional technology. CO_2 can be captured in a pure stream from the ECL system in the tin reactor. CO_2 emissions and ash production are lower than other alternatives because less coal is used per kWh produced. Coal can incorporate a number of elements which are potentially harmful to the fuel cell.

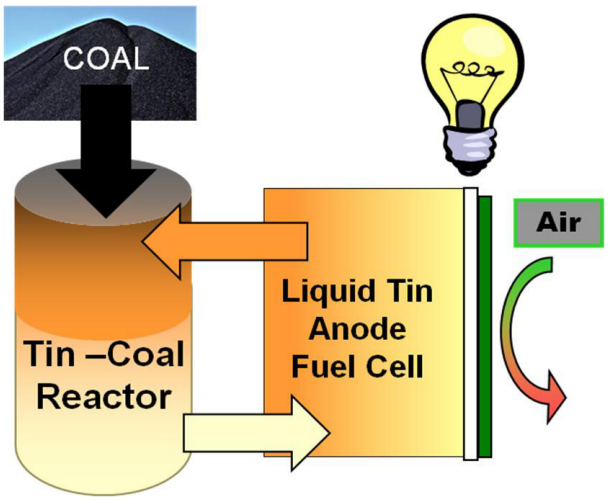

FIGURE 1. The Two Major Elements of the ECL Flowsheet Are the Tin-Coal Reactor which Processes the Coal and the Liquid Tin Anode Fuel Cell which Produces Power

In Phase 1 of this project, initial testing of coal oxidation by tin oxide was conducted. The results of this testing demonstrated that the tin can act as a purifier, rejecting some harmful contaminants (Nb, V, Mo, Cr, etc.) before they reach the fuel cell under certain conditions. To demonstrate the harmful impact of potential coal contaminants a preliminary spiking testing was conducted in an actual cell containing five elements (Nb, V, Mo, Cr and As for a total of 1,600 ppm) during Phase I. The spiked cell had a measurable decay rate of 3% per 100 hours. This initial result demonstrates the technical feasibility of an LTA direct coal power plant. The result from the spiking test will provide a target for comparison with future tin/coal experiments.

Approach

Coal impurities and ash and their impact on fuel cells can be a show-stopper for any direct coal conversion fuel cell. A mitigation strategy to

understand and deal with coal contaminants and ash is of paramount importance. As a result, the objective of this project is to develop an LTA cell technology which can be used to evaluate cell durability in a coal environment. The method of identifying durability issues is through testing of single cell test articles. In order to complete the testing, three areas of importance will be addressed. The first is the design and construction of a test apparatus and test articles that will contain a tin bath of reasonable size, up to 1 kg, the fuel cell and current collection in order to conduct the direct coal experiments. The second is to test the performance of the direct coal fuel cell under various conditions to determine the behavior of ash and impurities likely to be present in coal and their interaction with the tin bath and fuel cell materials. The third area consists of post-mortem analysis of the fuel cell article and tin bath to measure the quantity and form of the ash and unused carbon, contamination levels in the tin and contamination levels at the electrolyte surface.

Molten tin has been demonstrated as being a potential media for separating, reducing or eliminating coal impurities under certain conditions similar to the tin-coal reactor. These previous tin chemistry studies have been narrowly focused, short in duration and have not systematically evaluated the equilibrium of tin-contaminants at conditions which are expected in the TCR. In this project the primary focus is the coal ash – which is hypothesized to exist in a layer above the tin bath – and its physical separation with molten tin in an operating fuel cell. The coal source selected for the direct coal experiments is Illinois #6 seam (Harris Seam) coal obtained from the Penn State Coal Sample Bank and Database as sample DECS-24.

Results

- Figure 2 shows the direct coal test apparatus. A bath of liquid tin is contained in an aluminum oxide vessel. The Gen 3.1 cell electrolyte assembly is submerged into the tin and covered with another aluminum oxide tube above the tin to separate any air from the tin bath environment. Coal is dropped onto the tin surface near the center of the tube and opposite the exhaust tube. Other tubes include a vibrating stir rod and an input for a cover gas.
- The results of 24-hour continuous testing are shown in Table 1.
- Figure 3 shows a plot of power output (watts) under various current load vs. time. Illinois #6 coal was delivered and dropped onto the molten tin surface through a coal feeder while electricity was produced. The initial current-voltage (I-V) curve was obtained by incremental step increase in current load. Then the LTA-SOFC was operated at constant current for a while, and current load was adjusted either increased or decreased to maintain a stable power output. Some agitation was needed during the run. Preliminary analysis of the test article showed that ash and unreacted coal had gravimetrically separated on top of the tin as expected.
- The interaction of coal with the tin can be seen in Figure 4a, showing coal residue on the coal feed side and relatively clean tin on the electrochemical side. The electrolyte half cell was removed during the cooling operation. After the coal/coal ash was removed, the surface of the tin bath can be seen (Figure 4b). There is evidence of the white ash on

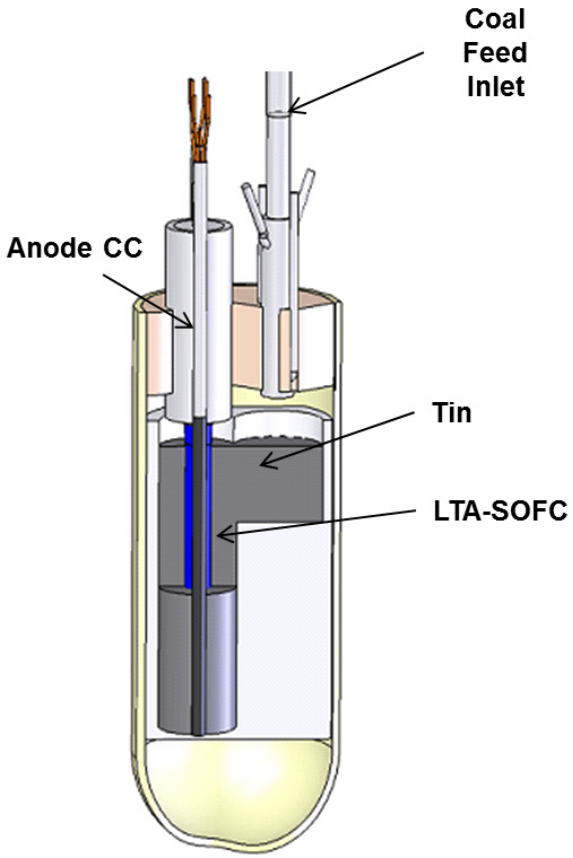

FIGURE 2. Direct Coal Tin Bath Test Apparatus

TABLE 1. Results from 24-hour Continuous Testing

Average Power	0.97	Watts
Total Runtime at Load	58.8	hours
Total Coal Input (Illinois #6)	20.4	grams
Average Coal Feeding Rate	18.4	mg/min
LHV Illinois #6	28454	J/g

LHV – lower heating value

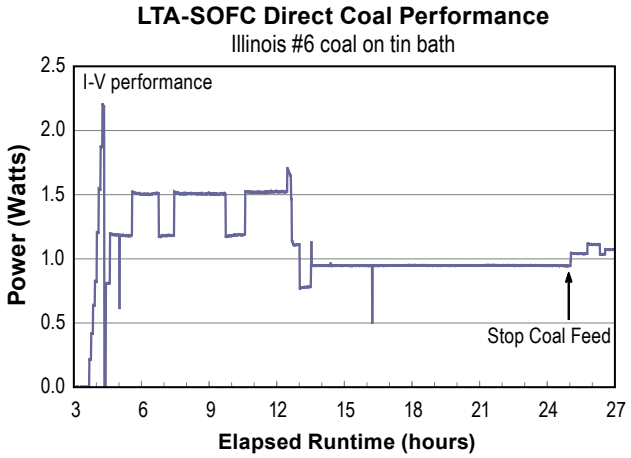

FIGURE 3. Power Output of an LTA-SOFC Cell vs. Time at Various Current Load Using Illinois #6 Coal

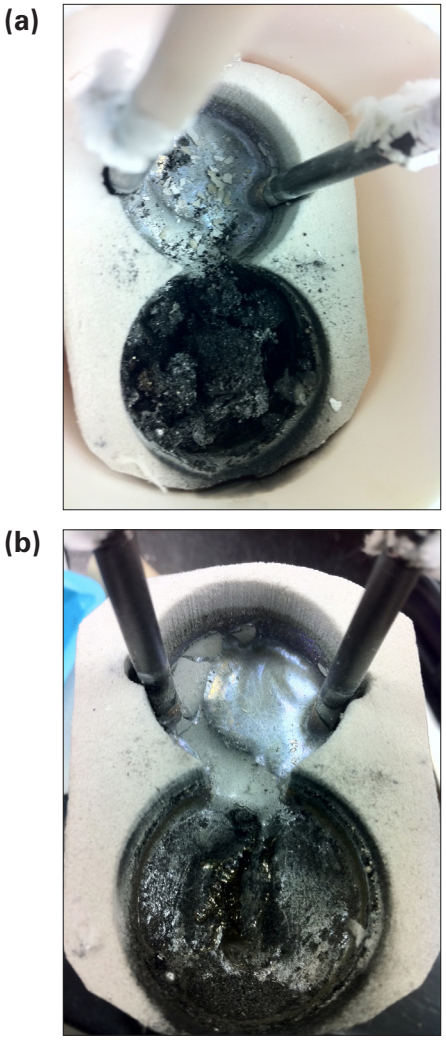

FIGURE 4. Tin/Coal Bath after Test with Residual Coal/Ash (top, a) and Ash Removed (b)

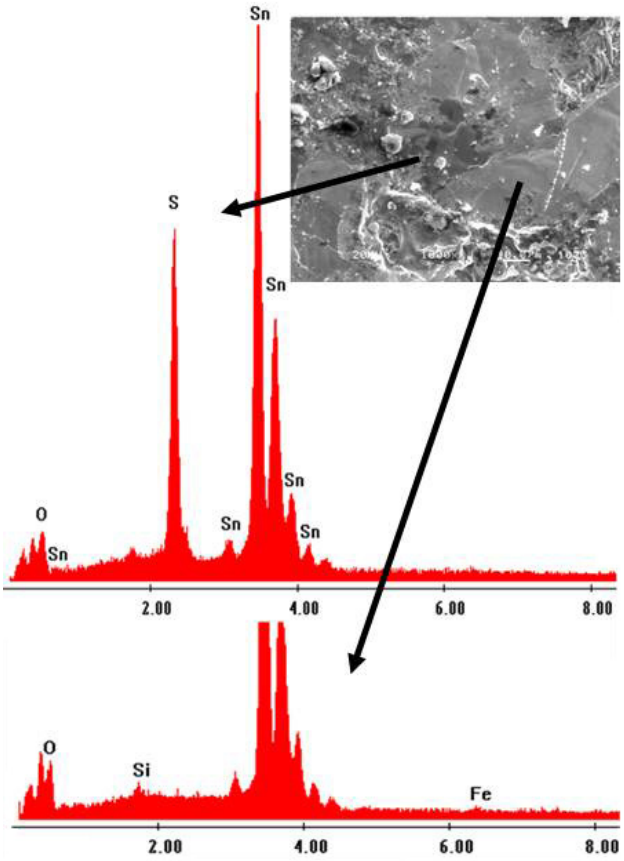

FIGURE 5. EDS Elemental Analysis of Tin Surface Showing Regions of SnS and Pure Tin

the surface. Analysis of the tin surface by energy dispersive spectroscopy (EDS) is shown in Figure 5. There are darker regions which show the presence of sulfur along with lighter regions that are pure tin. There was no evidence of coal contaminants in the bulk tin.

Conclusions and Future Directions

- The activities during this time period have demonstrated the feasibility of direct coal conversion in an LTA-SOFC in a laboratory-scale prototype.
- The prototype appears to have achieved adequate gravimetric separation of reaction products (ash and exhaust gas) from the tin anode. This provides additional proof-of-concept validation for the use of LTA-SOFC in a direct coal environment.
- Future work will include additional testing of the single cell direct coal prototype and more detailed post mortem analysis for the anode following testing on coal.

FY 2011 Publications/Presentations

1. SECA – 2010
2. Fuel Cell Seminar – 2010
3. SOFCXII – 2011

References

1. CellTech Power presentation at Fuel Cell Seminar 2010

IV.2 Liquid Tin Anode Direct Coal Fuel Cell

Dr. Thomas Tao
CellTech Power, LLC
131 Flanders Road
Westborough, MA 01581
Phone: (508) 898-2223 x34; Fax: (508) 898-2690
E-mail: Tao@celltechpower.com

DOE Project Manager: Joseph Stoffa
Phone: (304) 285-0285
E-mail: Joseph.Stoffa@netl.doe.gov

Contract Number: ER85006

Start Date: August 14, 2009
End Date: August 14, 2011

Fiscal Year (FY) 2011 Objectives

- Determine long-term cell performance and material stability impact for tin spiked with each coal contaminate element within their solubility limits.
- Analyze and evaluate experimental data/results, and continue to carry out remaining project.

FY 2011 Accomplishments

- Completed tin contaminant solubility testing with all metallic elements and non-metallic elements including the halogen species.
- Conducted study of coal contaminant cell material impact by spiking individual metallic and non-metallic elements into tin anode of laboratory-scale cells for 100 hour testing.

Introduction

ElectroChemical Looping (ECL) using the Liquid Tin Anode Solid Oxide Fuel Cell (LTA-SOFC) produces direct current electrical power in an electrochemical reaction powered by coal or other common fuels. For utility-scale applications the fuel oxidation step is carried out in a separate Tin-Coal Reactor (TCR) as shown in Figure 1. The liquid tin "loops" between the fuel cell and the tin reactor, shuttling all of the oxygen used to convert the coal. The net effect is that power is produced directly and efficiently from coal or biomass without burning and with inherent separation/rejection of nitrogen. In Phase 1 of this Small Business Innovation Research (SBIR), flowsheets for this concept were created and analyzed to evaluate efficiency and cost. Oxides of nitrogen (NOx) are not formed because nitrogen does not participate in the reactions and sulfur emissions can be cleaned up using conventional technology. CO_2 can be captured in a pure stream from the ECL system in the tin reactor. CO_2 emissions and ash production are lower than other alternatives because less coal is used per kWh produced. Coal can incorporate a number of elements which are potentially harmful to the fuel cell. Laboratory testing of tin/coal reactions has demonstrated that the tin coal reactor can act as a purifier, rejecting some harmful contaminants before they reach the fuel cell under certain conditions. This is a key positive finding demonstrating technical feasibility of LTA direct coal power plant.

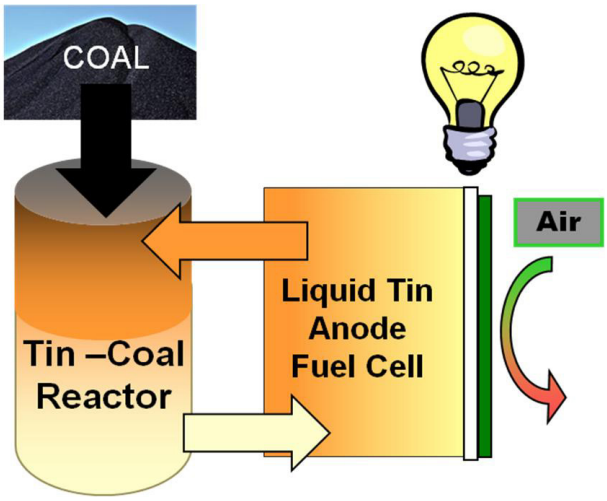

FIGURE 1. The Two Major Elements of the ECL Flowsheet Are the Tin-Coal Reactor which Processes the Coal and the Liquid Tin Anode Fuel Cell which Produces Power

Approach

Coal impurities and their impact on fuel cells can be a show-stopper for any direct coal conversion fuel cell. A mitigation strategy to understand and deal with coal contaminants is of paramount importance. As a result, the objective of this project is to develop an LTA cell technology which addresses the key issue of cell durability in a coal environment. The method of identifying durability issues is through simulated testing of single cell test articles. In order to complete the testing, three areas of importance will be addressed. The first is the implementation of a dedicated test stand (Figure 2) which can reliably maintain test conditions over the duration of testing from 100 to 1,000 hours. The stand will simulate TCR conditions for at least 1,000 hours. The second is to understand the behavior of impurities likely to be present in coal

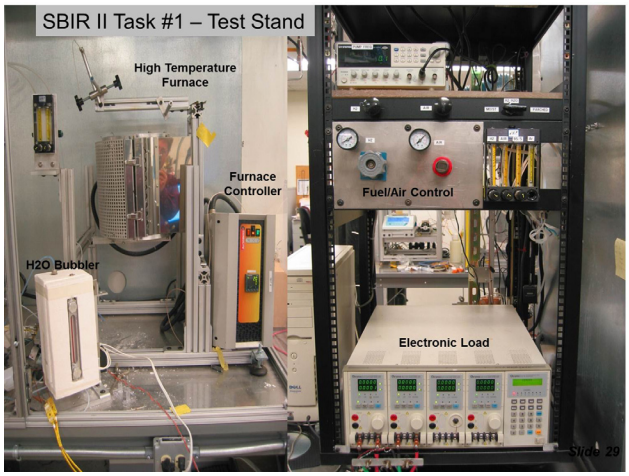

FIGURE 2. CellTech DOE Coal Test Stand

and their interaction with tin, in order to establish the spiking levels of contaminants of interest. This impurity solubility data will be obtained by specific tin/contaminant testing and analysis. The third area consists of simulated single fuel cell testing with single elements spiked into the tin. The simulated cell testing will identify specific contaminants which cause accelerated performance degradation and allow evaluation of degradation mechanisms. Finally, the experimental data/results of solubility, cell performance and subsequent analysis of degradation mechanisms will be used to propose future mitigation strategies including selection/optimization of materials, components and process to ensure long-term stable direct coal conversion in liquid tin.

Molten tin has been demonstrated as being a potential media for separating, reducing or eliminating coal impurities under certain conditions similar to the TCR. These previous tin chemistry studies have been narrowly focused, short in duration and have not systematically evaluated the equilibrium of tin contaminants at conditions which are expected in the TCR. In prior projects, CellTech has identified and modeled 10 metallic elements (V, Nb, W, Cr, Mo, Mn, As, Ta, U and Se) in coal that have the potential to be the most harmful to the ytrria-stabilized zirconia electrolyte. Additional non-metallic elements of F, Cl, Br, I, S, Si and P will be evaluated in this project also. Individual elements will be spiked into tin under an environment simulating the TCR exit. Analysis of the bulk tin will be completed to determine the solubility of the contaminate element. The results from this experiment with each element will be used to set the contamination levels for the simulated cell test. Preliminary contaminate testing in actual cells containing a number of contaminants (five elements, Nb, V, Mo, Cr and As to 1,600 ppm) in a single test had been conducted in Phase I at a measurable decay rate of 3% per 100 hours. In this project each element or contaminant will be tested individually to determine cell performance and degradation if any.

Results

- The solubility of coal contaminants was completed by spiking individual metallic and non-metallic elements in tin and subjecting the material to a simulated TCR environment that is 1% H_2O in hydrogen for 5 hours. Ten metallic (V, Nb, W, Cr, Mo, Mn, As, Ta, U and Se) and seven non-metallic elements (Cl, Si, S, Br, I, P and F) were spiked. Figure 3 shows the surface and the cross-section of four tin samples from left to right spiked with chlorine (Cl) as sodium chloride, sulfur (S) as tin sulfide, phosphorous (P) as tin phosphide and silicon (Si). The completed contaminant solubility results are shown in Table 1. The halogen elements were not measured by inductively charged plasma-optical emission spectroscopy (ICP-OES). However, the element phosphorous shows a larger than expected value, roughly 1/3 of the initial spiked value. The ICP-OES results included the dissolved and the entrained (trapped particles for example) – that the maximum solubility of each spiked element shall not be greater than data listed in Table 1.
- Performance testing of cells with spiked elements was completed with nine elements plus a pure hydrogen baseline. The curves in Figure 4 compare the initial current-voltage (I-V) curves for these 10 cells, with only Mn showing abnormal initial behavior. Figure 5 shows the performance of the 10 cells at 4.8 amps for 100 hours (Mn was loaded only to 1.25 A). As expected various degree of degradations were observed.
- Completed a 1,000-hour cell longevity test at 2 amps using hydrogen with tin showing a 1.1% per 1,000 hr voltage degradation. By comparison, at

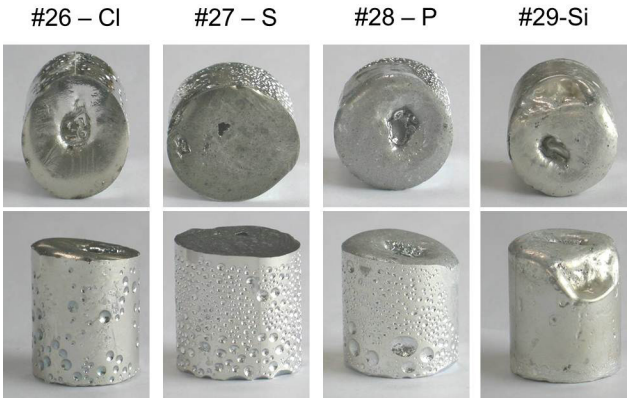

FIGURE 3. Coal Contaminate Element Solubility in Tin Samples Showing Tin Morphology for Different Contaminant Spiking

TABLE 1. Spiked Element Level Found in Tin Glow Discharge Mass Spectrometry (GDMS)

Spiked Element	Initial amount (ppm wt)	ICP-OES Results (ppm wt)	Pure Sn GDMS results (ppm wt)
Cr	4000	1,098	2.7
V	4000	10	<0.001
Mo	4000	9	<0.01
Nb	4000	115	<0.005
As	4000	2,535	1
Mn	4000	2,405	0.2
W	4000	60	<0.01
Ta	4000	8	<5
Se	4000	44.7	<0.01
Cl	4000	n/a	<0.01
S	4000	<8	0.07
P	4000	203	0.08
Si	4000	<5	<0.01
Br	4000	n/a	<0.05
I	4000	n/a	<0.05

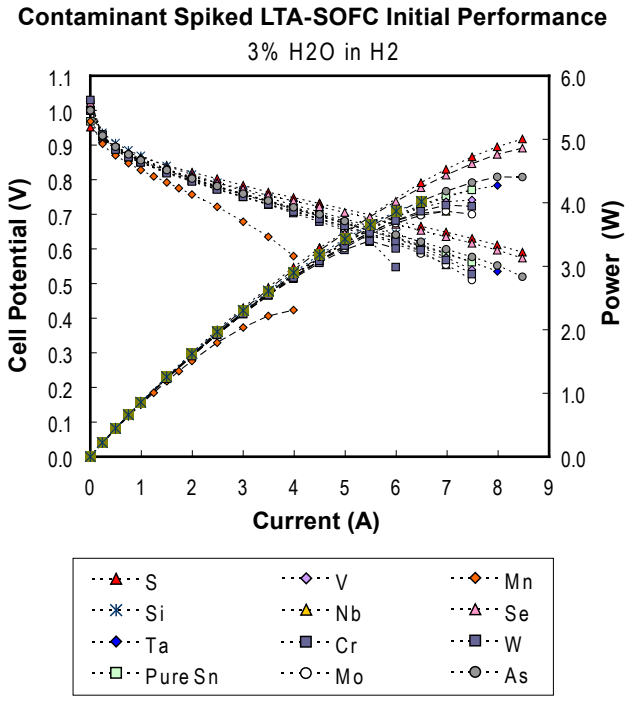

FIGURE 4. Initial I-V Curve for Nine Cells Spiked with Contaminants Compared with Hydrogen Baseline

4.8 amps the degradation rate was at one order of magnitude higher, about 10% per 1,000 hr.

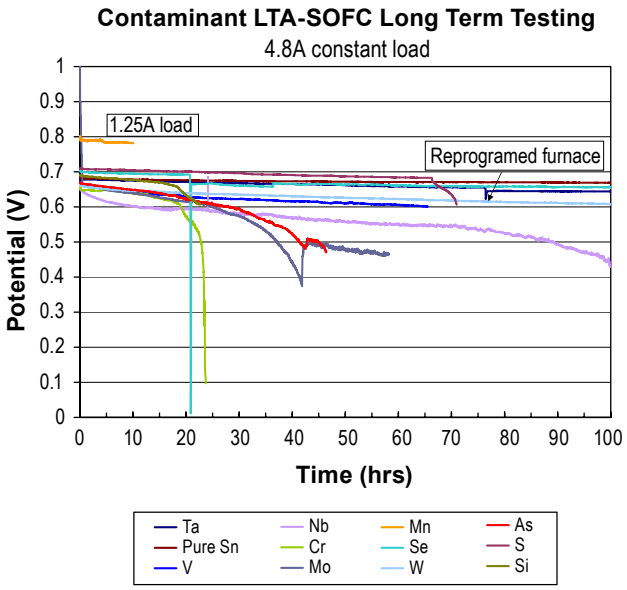

FIGURE 5. Voltage Traces for 100-Hour Initial Durability Testing of Nine Cells Spiked with Contaminants Compared with Hydrogen Baseline

Conclusions and Future Directions

- The previous (2009) Annual Report had summarized a study of direct oxidation of coal with tin oxide to form tin. No detectable harmful elements (V, Nb, W, Cr, Mo, Mn, Ta, U and Se) were founded in tin indicating the technical feasibility of direct coal conversion in an LTA-SOFC.
- Liquid tin has been found to be capable of separating out some key harmful elements under simulated TCR conditions of 1% H_2O in H_2–forming oxides thus separated from bulk tin. These data seem to support a technical pathway to enable the isolation of coal contaminants and perhaps coal ash and slag in the TCR. The 1% H_2O condition represents the lowest oxygen state in the tin, represented by 1.1 V. It is expected that under operation, the oxygen content in the tin would approach 0.8 V condition represented by 85% H_2O in H_2.
- The electrochemical testing of cells with spiked elements at the maximum possible solubility show that for those most harmful elements there was some cell degradation as expected. In the remaining project, correlation of their concentration in coal will be derived, post-mortem chemical analysis will be performed, and future mitigation strategies will be presented.

FY 2011 Publications/Presentations

1. SECA - 2010
2. Fuel Cell Seminar - 2010

References

1. CellTech Power presentation at Fuel Cell Seminar 2010

IV.3 Liquid Tin Anode Direct Coal Fuel Cell

Dr. Thomas Tao
CellTech Power, LLC
131 Flanders Road
Westborough, MA 01581
Phone: (508) 898-2223 x34; Fax: (508) 898-2690
E-mail: Tao@celltechpower.com

DOE Project Manager: Joseph Stoffa
Phone: (304) 285-0285
E-mail: Joseph.Stoffa@netl.doe.gov

Contract Number: SC0004582

Start Date: June 19, 2010
End Date: March 18, 2011

Fiscal Year (FY) 2011 Objectives

- Evaluate the technical merit and feasibility of incorporating a liquid tin anode in situ gasification cell into a Direct Coal powerplant using United States Illinois #6 coal by addressing high sulfur content (5 wt%), chlorine (0.12 wt%) and medium ash fusion characteristics.
- Test Liquid Tin Anode Solid Oxide Fuel Cell (LTA-SOFC) cells using a simulated gas stream of H_2S in H_2 whose concentration was comparable with and exceeding the total sulfur content in Illinois #6 coal.

FY 2011 Accomplishments

- Developed a simulated gas stream for high sulfur testing with 3.6 wt% H_2S in H_2.
- Tested four Gen 3.1 cells.
  - Two cells at 2,134 ppmv (3.6 wt% H_2S in H_2) for 20 hours.
  - Two cells at 36,900 ppmv (50 wt% H_2S) for limited duration.
- Operation on high sulfur fuel at 60% max power (3 watts).
  - No short-term impact on electrochemical performance for 3.6 wt% H_2S.
- Dissection and evaluation of the structural integrity of cell components and seals revealed:
  - No apparent damage was found to any of ceramic cell component for the short-term exposure of 20 hours. This includes the anode current collector (ACC), electrolyte, cap, porous separator and holder. The ACC was not cracked and ACC at alumina tube joint looked good.
  - High temperature adhesive/glue used to seal the anode chamber and to seal the anode current collector was damaged and became permeable to H_2S.
- Scanning electron microscopy/energy dispersive spectroscopy (SEM/EDS) evaluation determined the following:
  - Sulfur and tin peaks in EDS analysis of black spikes and ball specimens found after testing on 3.6 wt% H_2S in H_2 indicate these are tin sulfite.
  - SEM/EDS of anode current collector showing that H_2S penetrated through the high temperature adhesive and reacted with metal core forming metal sulfide.
  - Demonstrated feasibility of a direct coal conversion in an "In situ Gasification" LTA-SOFC.

Introduction

Coal will continue to play a vital role for power generation in the U.S. Improving the generation efficiency of existing and future fuels will increase their economic viability and improve their environmental impact, but efficient generation options are limited, particularly for applications where carbon capture and sequestration is desired. The direct conversion of fuel to energy in a fuel cell can be highly efficient, particularly if cleaning and gasification steps can be eliminated. The LTA-SOFC shows promise as a direct coal power conversion device.

Operation of the LTA-SOFC has been proposed in two very different configurations. In other projects, CellTech is evaluating a concept called ElectroChemical Looping (ECL) where coal is directly fed to the oxidized liquid tin in a tin-coal reactor and reduced tin is circulated to fuel cell stack to produce power. This concept shows significant promise for high efficiency. Since coal will be in intimate contact with molten tin, the key risk area for ECL is the potential impact to the fuel cell from those refractive and less volatile impurities in coal, if dissolved in tin. A second concept called "In situ Gasification" allows the anode products (water and CO_2) to gasify the solid fuel in a zone immediately adjacent to the anode but separated by a porous media. Since only gas phase constituents interact with the tin anode, technical risk areas will be volatile coal impurities existing in gas phase and their impact on LTA-SOFC.

Approach

Figure 1a shows a schematic configuration of an LTA-SOFC gasification cell. The molten tin anode is contained between the electrolyte and a porous refractory ceramic separator - there is no direct coal-tin contact. Unlike a conventional Ni anode-based SOFC, the molten tin anode has exceptional tolerance toward carbon, sulfur and other volatile coal impurities, making direct coal conversion through in situ gasification a feasible approach. The cathode and electrolyte utilize conventional materials, benefiting from the vast amount of SOFC materials research being conducted by DOE and other organizations worldwide. The porous ceramic matrix shown in Figure 1a is used in smaller systems to manage the tin-fuel interface. Figure 1b shows a SEM cross-section of an LTA-SOFC gasification cell, showing the location of the various chemical and electrochemical reactions when coal is used as fuel. Notice in the Figure 1b, coal is simplified as CxHy or C. Inside the anode chamber at the 1,000°C operating temperature, simultaneous pyrolysis, and shift

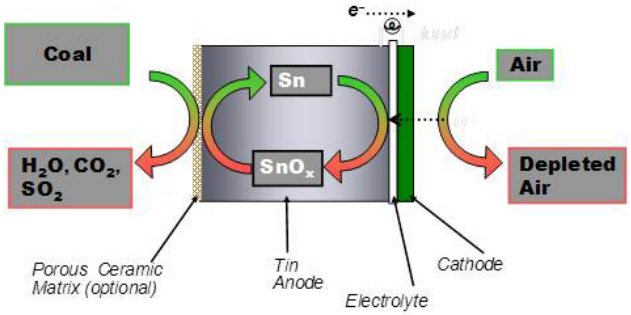

FIGURE 1A. A Schematic of the LTA-SOFC Process Illustrating How Coal Drives the Tin Redox Cycle

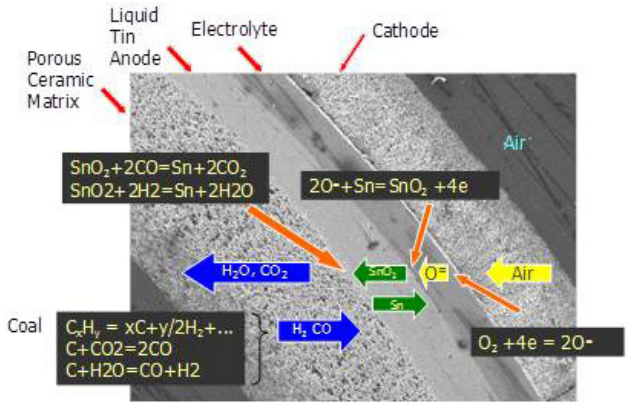

FIGURE 1B. Chemical and Electrochemical Processes Shown on a Cross-Section of an LTA-SOFC Cell with a Porous Ceramic Separator

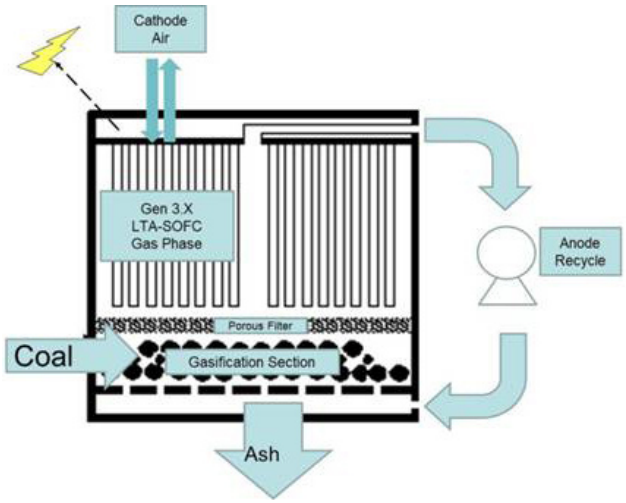

FIGURE 2. Concept of "In Situ Gasification" Direct Coal Conversion in an LTA-SOFC

reactions occur, generating gaseous fuel molecules such as hydrogen, CO and small hydrocarbons which can be readily transported through the porous separator. Figure 2 shows a conceptual drawing of how the in situ gasification approach could work. The technical approach included testing an LTA-SOFC cell using a simulated gas stream of H_2S in H_2 whose concentration was comparable with and exceeding the total sulfur content in Illinois #6 coal.

Results

In Phase I CellTech successfully completed all four technical tasks as summarized in Table 1.

Conclusions and Future Directions

- Demonstrated 3.6 wt% H_2S in H_2 as fuel in Gen 3.1 LTA-SOFC cells leading to the feasibility of direct coal conversion using Illinois #6 high sulfur coal in the operational mode of in situ gasification.
- Cell components were not affected by the high sulfur content.
- A logical next step is to demonstrate operation with high sulfur carbonaceous fuel in the LTA-SOFC. The following steps will demonstrate high sulfur operation under realistic small scale conditions:
  - Develop LTA cell technology which continues to addresses the key issue of LTA cell operation on sulfur and carbonaceous components that are contained in coal.
  - Conduct continuous testing of high sulfur carbonaceous fuels with LTA-SOFC in situ gasifier cells.

TABLE 1. Summary of Technical Tasks

Phase I Tasks	Key Accomplishments/Issues
Experimental Validation-Operation on simulated gas stream	Developed a simulated gas stream for high sulfur testing. Tested four Gen 3.1 cells (Figure 3) • Two cells at 2,134 ppmv (3.6 wt% H_2S in H_2) for 20 hours • Two cells at 36,900 ppmv (50 wt % H_2S) for limited duration
Test Data Analysis (electrochemical)	Baseline operation on hydrogen was normal for Gen 3.1 cells. Operation on high sulfur fuel at 60% max power (3 watts) as shown in Figure 4. • No short-term impact on electrochemical performance for 3.6 wt% as shown in Figure 5.
Test Article Analysis (physical)	Dissection and evaluation of the structural integrity of cell components and seals revealed: • No apparent damage was found to any of ceramic cell component for the short-term exposure of 20 hours. This includes the ACC, electrolyte, cap, porous separator and holder. The ACC was not cracked and ACC at alumina tube joint looked good. • High temperature adhesive/glue used to seal the anode chamber and to seal the anode current collector was 100%damaged and became permissible to H_2S. SEM/EDS evaluation determined the following: • Sulfur and tin peaks in EDS analysis of black spikes and ball specimens found after testing on 3.6 wt% H_2S in H_2 indicate these are tin sulfite. • SEM/EDS of anode current collector showing that H_2S penetrated through the hi-temp adhesive and reacted with metal core forming metal sulfide.
Identification of Technical Issues and Program Planning	• Volatility of tin sulfite must be managed. • Sealants and current collector components may be susceptible to H_2S attack but major fuel cell components did not suffer damage during short-term testing at 3.6 wt% H_2S. • 50 wt% H_2S in H_2 caused tin leakage probably indicating a change in surface tension.

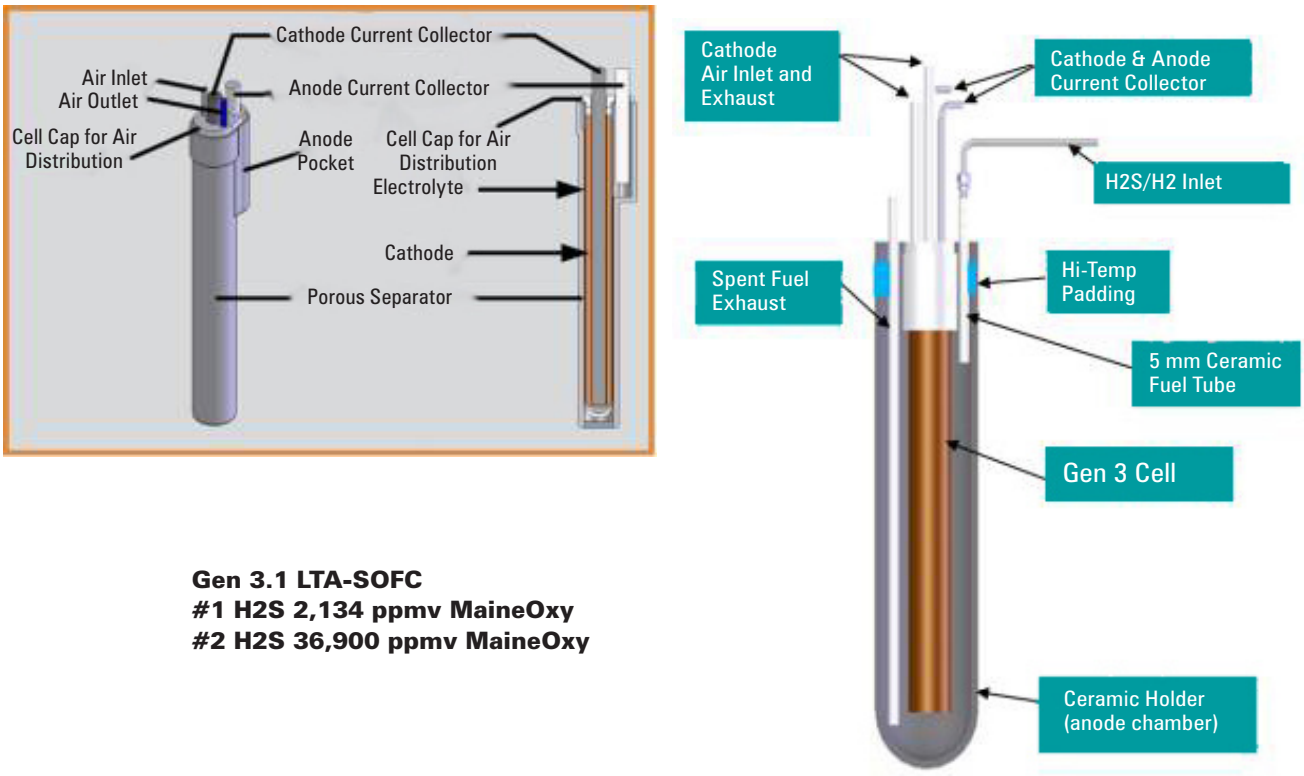

FIGURE 3. Single Cell H_2S Spiking Tests Were Conducted in a Standard Test Set-Up

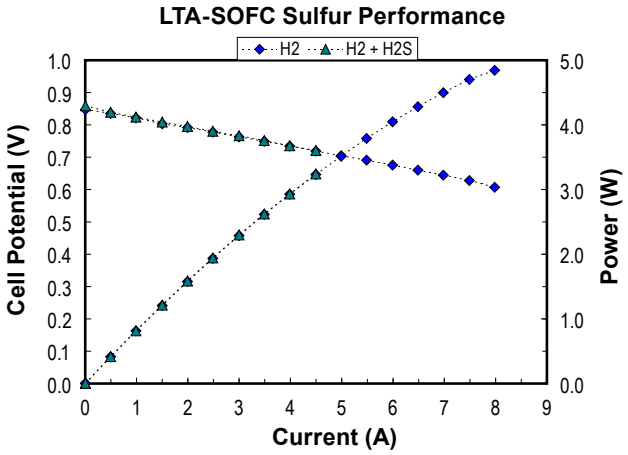

FIGURE 4. Polarization and power curves for Gen 3.1 cells (I-V curves) using hydrogen as a baseline (diamonds) and 2,134 ppmv H_2S in H_2 (3.6 wt% H_2S) (triangles). Flow rate 300 cc/min - a complete overlap.

- Scale up effort from single cell to multi-cell stack assemblies to further verify LTA-SOFC operation on high sulfur carbonaceous fuels derived from coal-based fuels.
- Testing of LTA-SOFC on pure sulfur in an inert carrier gas, which to CellTech's knowledge has never been attempted before in an SOFC.

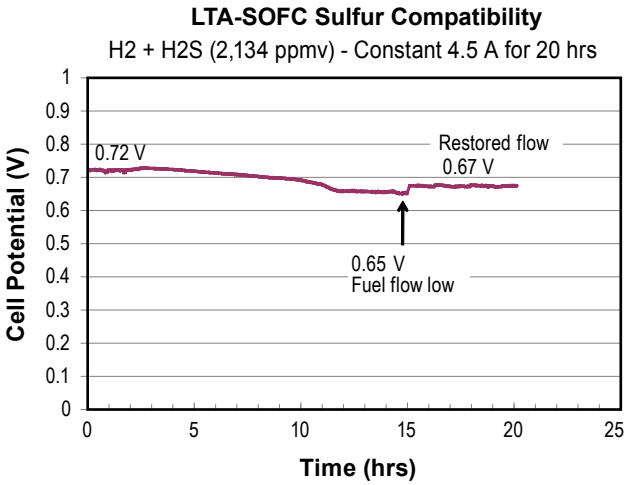

FIGURE 5. Cell voltage at constant current load operating on 2,134 ppmv H_2S in H_2 (3.6 wt% H_2S). In the last 5 hours, no degradation was observed. Test condition was constant load at 4.5 amps.

FY 2011 Publications/Presentations

1. SECA - 2010
2. Fuel Cell Seminar - 2010

References

1. CellTech Power presentation at Fuel Cell Seminar 2010.

IV.4 Performance Degradation of LSCF Cathodes

Matthew Alinger
GE Global Research
1 Research Circle, MB277
Niskayuna, NY 12309
Phone: (518) 387-5124; Fax: (518) 387-5403
E-mail: alinger@ge.com

DOE Project Manager: Joseph Stoffa
Phone: (304) 285-0285
E-mail: Joseph.Stoffa@netl.doe.gov

Subcontractors:
- Rensselaer Polytechnic Institute, Troy, NY
- NexTech Materials, Lewis Center, OH

Contract Number: NT0004109

Start Date: October 1, 2008
End Date: December 30, 2011

Fiscal Year (FY) 2011 Objectives

- Develop a mechanistic understanding of degradation mechanisms associated with microstructural sintering and coarsening during operation.
- Identify and validate degradation mitigation solution for microstructural sintering and coarsening during cell operation.
- Develop and demonstrate low-cost thermal spray manufacturing capabilities for metal supported fuel cells.
- Develop a conceptual design and cost estimate of a 100 kW solid oxide fuel cell (SOFC) system.

FY 2011 Accomplishments

- Identified electrode structural evolution during operation as performance degradation mechanism.
- Implemented and tested an integrated thermal spray manufacturing system for SOFCs.
- Identified anode roughness as a key criteria to enable hermetic electrolytes.
- Developed thermal spray process conditions for a smooth fuel electrode (anode), to enable a dense electrolyte on a metallic support.

Introduction

Through research and development efforts conducted within the U.S. Department of Energy's (DOE) Solid State Energy Conversion Alliance (SECA) fuel cell program, considerable progress has been made towards the realization of current SOFC stack cost goals. However, performance degradation of high-performance SOFC cathodes, in particular $La_{1-x}Sr_xCo_{1-y}Fe_yO_{3-\delta}$ (LSCF), remains a technical barrier to the commercial viability of SOFC technology. The objective of this project is to identify the dominant degradation mechanisms, and to develop and implement cost-effective mitigation strategies to retain high electrochemical performance in LSCF-based cathodes over the operational lifetime of an SOFC stack (>40,000 hours). The project goal is to reduce power density degradation rates to less than 1% per 1,000 hours, while maintaining high initial power densities (>0.75 W/cm^2).

Approach

The LSCF-based cathode degradation mechanisms will be identified and evaluated using the state-of-the-art SOFC characterization laboratory at the GE Global Research Center, Niskayuna, New York. The approach relies on the electrochemical testing of SOFCs under realistic operating conditions. However, given the complexity of SOFCs, off-line laboratory testing including sintering studies, contact resistance, and diffusion couples will be leveraged to isolate and understand specific mechanisms under representative conditions. The structural and chemical degradation components will be identified using advanced characterization techniques such as high-resolution transmission electron microscopy, scanning electron microscopy, and high-angular resolution synchrotron X-ray diffraction.

As the contact integrity of critical interfaces has been recently identified as a major degradation mechanism, alternative cell manufacturing approaches will also be evaluated. In particular, approaches will be evaluated for improved barrier layers to provide enhanced cathode interfacial strength. In addition, interconnect chromium barrier coatings will be evaluated and optimized, with a focus on $(Mn,Co)_3O_4$, for thin and dense coatings to mitigate the well-known chromium poisoning degradation mechanism. Combined, these results will enable the development

of structure-property-performance correlations. These will be used to guide the identification and development of cost-effective solutions to reduce the degradation of high-performance LSCF-based SOFCs.

In addition, low-cost thermal spray manufacturing approaches will be developed and evaluated with respect to cost-effectiveness as well as cell performance.

Results

Cathode side degradation mechanisms comprise contributions of various ohmic (e.g., oxide scale growth and interaction/reaction layers between the metal interconnect and cathode) and non-ohmic (destruction of catalytically active sites and diffusion pathways for oxygen reduction within the cathode) mechanisms. A summary of potential mechanisms is presented in Figure 1. A combination of electrochemical cell testing and electrical contact resistance experiments has been employed to simulate the configuration and conditions of operating SOFCs. A quantitative comparison of the results from the experiments, in conjunction with existing models, will furnish an understanding of the degradation processes that contribute to the performance degradation of LSCF-based SOFCs.

Using an embedded voltage lead in the cathode bond layer allows for the simultaneous measurement of interconnect contact resistance and electrochemical performance as shown schematically in Figure 2. Two current collector materials were used; a gold mesh as an inert baseline, and ferritic steel representative of a commercial cell. As shown in Figure 3, for gold current collector samples, the contact resistance was very stable and did not increase, as expected. However, for the coated steel interconnected samples, the interconnect contact area specific resistance (ASR) increased about 4.8 mΩ-cm^2/khr, in agreement with standard contact resistance measurements. This data is the critical degradation component of the operating fuel cell and can be used to develop long-term performance models to support the low degradation targets of the SECA program.

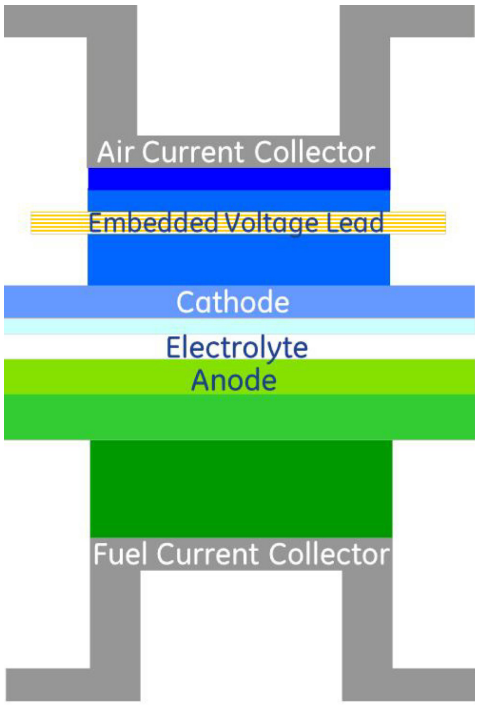

FIGURE 2. Button Cell Configuration of the Ferritic Steel and Gold Interconnected SOFCs with Embedded Gold Cathode Interconnect to Measure Location-Specific Degradation

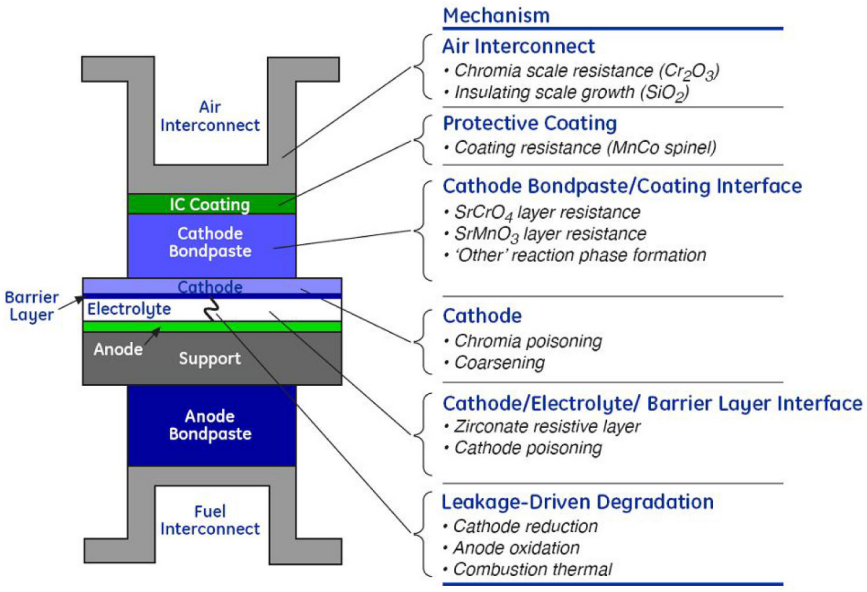

FIGURE 1. Schematic of an SOFC Highlighting Potential Degradation Mechanisms

A key barrier to the commercialization of SOFCs is the high capital cost involved with developing a manufacturing infrastructure for fabricating sufficient quantities of the multilayered cells for demonstration units. In addition, to accommodate low initial rates of market adoption, low-cost manufacturing is imperative to establishing a commercially viable fuel cell technology business. Recent progress in thermal spray technology at GE is very promising for dramatically reducing low-volume

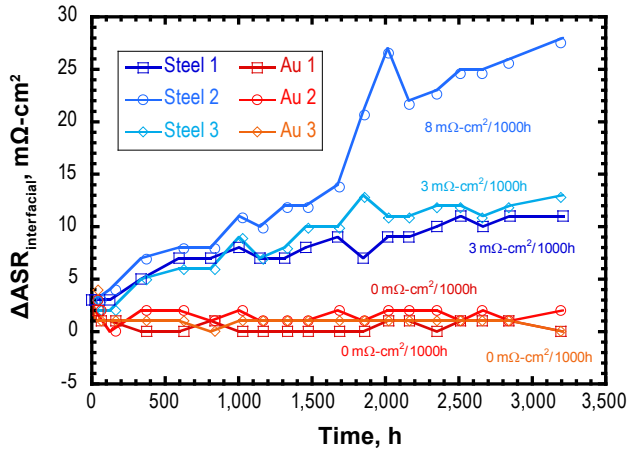

FIGURE 3. Evolution of the Ohmic Interfacial Current Collector-Cathode Contact Resistance (ASR) for Gold Current Collectors (Red) and Ferritic Steel Current Collectors (Blue)

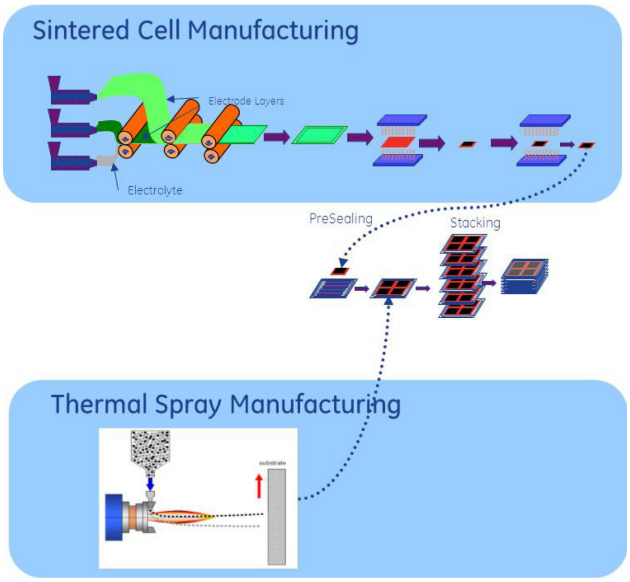

FIGURE 4. SOFC Manufacturing Process Map Comparing a Traditional Sintering Approach with Thermal Spray

manufacturing costs. Thermal spray processing offers a new, lean manufacturing paradigm for the production of planar SOFCs (see Figure 4).

In addition to significantly diminished initial capital costs, four additional advantages of thermal spray manufacturing include:

1. Integrated electrolyte-to-metal seal that is formed during thermal spray deposition, eliminating the need for the traditional post-fabrication glass sealing methods used for sintered cells.
2. The thermal spray manufacturing process is scalable to a large cell area that reduces part count, and is a modular process that allows flexibility in accommodating production volume and design changes that is critical for demonstration/prototype units. Larger cell sizes are directly related to a decreased part count, and thereby play a major role in reducing the stack cost through reduced materials and labor.
3. Thermal spray manufacturing could also be tailored to the production of graded properties of cell components.
4. A successful thermal spray manufacturing process could be implemented through existing thermal spray supply chains with only a minimal investment in additional equipment. This approach enables the commercial introduction of prototype units and low-volume production as the technology finds market acceptance with significantly reduced capital risk.

Recent efforts have been devoted to the development of a suitable substrate and thermal spray process parameters for the fuel side electrode (anode). Experimental results suggest that surface topography is key to developing proper anode support for a hermetic electrolyte. Anode roughness is a key indicator of the surface quality. Full coverage of the porous metal support by the anode material is also expected to be required for adequate cell performance. Therefore, development activities focusing on developing a thermal sprayed smooth and continuous anode layer onto a porous substrate were carried out. Preliminary results show that deposition of a continuous anode onto a porous support is possible, however, characterization of the anodes reveals that the surface roughness is driven by the topological growth of the surface roughness of the substrate during the anode deposition process. This roughness is detrimental to the development of a hermetic electrolyte and needs to be eliminated by developing appropriate deposition parameters. Work was performed which led to development of thermal spray parameters suitable for deposition of smooth anodes on porous metal supports, as shown in Figure 5, which shows topography of the anode surface when sprayed with optimized conditions. Furthermore, a minimum thickness for full foam coverage with a smooth anode was established.

Conclusions and Future Directions

The inherent stability and high electrochemical performance entitlement of LSCF cathode-based SOFCs has been demonstrated. The high performance of this material system plays a major role in decreasing the cost per kilowatt of SOFCs. However, a reliable solution to the degradation behavior requires a more detailed understanding of the kinetics of the dominant mechanisms and requires additional investigation.

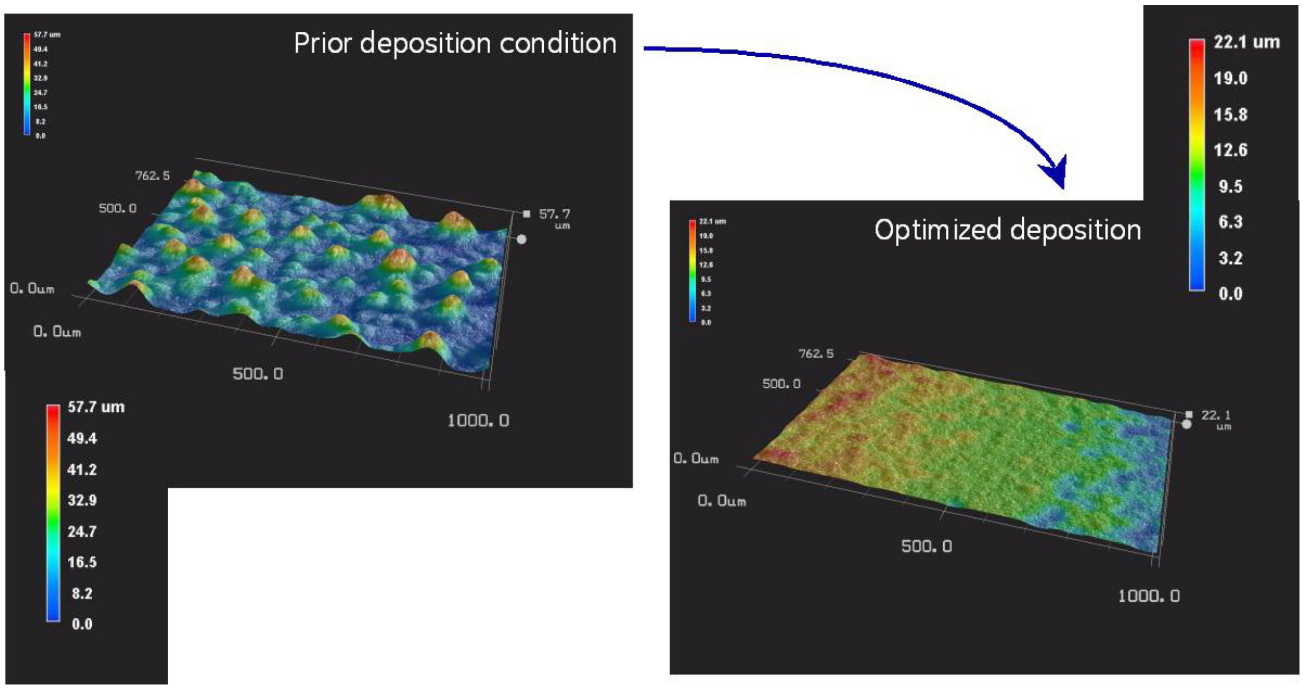

FIGURE 5. Surface Topographic Images of the Effect of Optimized Thermal Spray Deposition to Ensure Full Coverage and Smooth Anode on a Porous Metal Support

Ultimately, a degradation mitigation solution for high performance (>0.75 W/cm^2) SOFCs with ferritic steel interconnects, having a repeatable performance degradation of <1%/1,000 h, will be demonstrated.

Thermal spray manufacturing offers a new, lean manufacturing paradigm for the production of planar SOFCs. Continued development of substrate design and thermal spray conditions will ultimately lead to the required innovation to overcome the commercialization barrier for solid SOFCs with the ability to meet SECA cost targets at much lower production volumes.

FY 2011 Publications/Presentations

1. Quarterly Report for 4th calendar quarter 2010, January 30, 2010.

2. Quarterly Report for 1st calendar quarter 2011, April 30, 2011.

3. V. Dheeradhada, H. Cao, and M.J. Alinger, "Oxidation of Ferritic Stainless Steel Interconnects: Thermodynamic and Kinetic Assessment," Journal of Power Sources, 196 (2011) 1975-1982.

4. M.J. Alinger, "Degradation of LSCF Cathodes," 11th Annual SECA Workshop, Pittsburgh, Pennsylvania, 2010.

IV.5 NETL RUA LMA SOFC R&D

Kirk Gerdes
U.S. Department of Energy
National Energy Technology Laboratory (NETL) –
Regional University Alliance (RUA)
3610 Collins Ferry Rd.
Morgantown, WV 26507
Phone: (304) 285-4342; Fax: (304) 285-4469
E-mail: Kirk.Gerdes@netl.doe.gov

Contract Number: 10-220621 6923
(NETL RUA LMA SOFC R&D)

Start Date: October 1, 2010
End Date: September 30, 2011

Fiscal Year (FY) 2011 Objectives

- Using a liquid metal anode solid oxide fuel cell (LMA SOFC), measure the oxygen diffusion coefficient for at least two tin alloy compositions and for at least two temperatures.
- Determine the electrochemical performance for at least one LMA operated at three temperature conditions on hydrogen and coal fuel. Report the differences observed in impedance measurements using equivalent circuits.
- Generate an ab initio model that can predict the state of oxygen in a liquid tin anode (LTA) SOFC. Report the adopted computational methodology and initial results regarding the estimation of oxygen diffusivity in liquid tin.
- Complete chemical analysis on reaction product distribution from LMA SOFC coal contaminant tests (metal/slag/electrolyte). Report results of testing.
- Complete a report based on microstructural analysis that provides sufficient evidence to affirmatively identify partitioning of trace contaminant material between LMA phases (metal/slag/electrolyte) and that identifies the distribution of trace material in terms of penetration depth.

FY 2011 Accomplishments

- Completed LMA SOFC tests to determine oxygen diffusion coefficient for base metal and two alloys, each operated at three temperatures.
- Developed an experimental system to evaluate electrochemical performance of an LMA SOFC test apparatus using electrochemical impedance spectroscopy (EIS) to understand the behavior of the cell. First EIS tests were performed at three temperatures.
- Established an ab initio model describing the oxygen/tin system using the VASP package, and generated a report describing the computational methodology and primary results.
- Completed chemical analysis and spectroscopic analysis of tin in LMA SOFC system and reported results of testing.
- Completed microstructural analysis of LMA SOFC to evaluate contaminant partitioning using transmission electron microscopy (TEM) analysis. Interfaces are especially examined.

Introduction

In 2009, electricity consumers in the United States were supplied with 69% of their electricity from fossil fuels, with 45% of the total electric power generated from coal fuel alone. Sustained, economically feasible production of electric power will require continued consumption of substantial amounts of coal, with biomass fuel resources expected to also increase their contribution to power production over the coming decade. Improving the electricity generation efficiency using coal and biomass fuel extends the lifetime of coal and biomass reserves and reduces the amount of carbon dioxide and other pollutants produced per kilowatt of electricity (relative to lower efficiency processes). High efficiency production from coal and biomass is possible in power plant designs that include fuel cell technology.

Most fuel cell systems leveraging coal and biomass as a fuel source require gasification of the material to produce synthesis gas, which significantly increases system cost and complexity. By replacing the traditional ceramic fuel electrode of a typical high temperature SOFC with an LMA such as tin, pulverized coal and carbonaceous fuels like plastics and biomass can be fed directly into the fuel cell and their chemical energy converted to electricity. Direct utilization of the coal and biomass facilitates decreased cost and complexity of the total system, features which serve to offset the lower power density of this novel unit relative to traditional SOFC. This project investigates the basic performance features of an LMA SOFC to produce fundamental data that will be useful for designing commercially significant systems.

Approach

In order to properly model and understand the performance of an LMA SOFC, careful measurements of the transport and reaction kinetics of the anode are needed. A series of standard electrochemical tests

including chronoamperometry, chronopotentiometry, and EIS are used to measure the oxygen diffusion coefficient through the liquid metal, the oxygen content within the liquid metal, and the interfacial polarization resistance at the liquid metal/fuel interface. To increase oxygen transport through the liquid metal, different liquid metal alloys of tin are tested for oxygen diffusion rate and surface reaction kinetics. Selection of liquid metal alloys is based on thermodynamic calculation of the oxygen solubility limit within the metal. Kinetic parameters experimentally determined for the metal alloys are incorporated into a one-dimensional model of the LMA SOFC system to judge the magnitude of power density increases possible from adjusting the composition and geometry of the LMA.

Recent advances in the EIS methodology can be applied to explore and analyze the behavior of individual electrodes and components of electrochemical systems. EIS methodology provides direct information on the behavior of SOFC electrodes, reaction kinetics and ionic conductivity in SOFC components that are generating electrical power. EIS data are also used to monitor SOFC degradation. These tools are applied to develop accurate and detailed equivalent electrical circuit models of the LMA SOFC, which are used to evaluate fundamental performance differences associated with operating current, fuel type, and anode composition. Evaluation is also possible for electrochemical performance of a coal-fuelled LMA SOFC.

Computational methods may also be used to produce quantitative evaluation of oxygen transport. First the oxygen state within the liquid metal must be determined, whether it exists as an oxide or sub-oxide of the metal, or in some 'dissolved' form. Knowledge of the stable oxygen forms is critical since the form influences the precise mechanism of oxygen transport and the interconversion between different states of similar energy. Accordingly, different tin oxide species including tin monoxide (SnO) and tin dioxide (SnO_2) in liquid tin will be studied at the level of density functional theory (DFT). DFT is ideal for studying systems where bond breaking and formation events are likely to occur in the condensed phase. A specific DFT methodology is first chosen and validated, and then DFT-based molecular dynamics simulations of SnO and SnO_2 in liquid tin are performed at a simulated temperature of 800°C. Subsequent work focuses on the computation of diffusion coefficients for oxygen in liquid tin. Validation of the computational result is made based on the measured rate of oxygen diffusion experimentally determined in parallel work.

Knowledge of the impact of trace metal materials contained in coal on the LMA SOFC electrochemical operation must also be characterized. Direct testing of contaminant partitioning in LMA SOFC systems was conducted using representative Eastern and Western coals. Partitioning of contaminant materials within the cell between soluble, insoluble, and cell component phases will be investigated. To overcome the limitations in analytical sensitivity to trace materials, the reactants are spiked with specific contaminants of interest to facilitate examination of the partitioning behavior. Metal-soluble contaminants reacting with the yttrium-stabilized zirconium (YSZ) electrolyte material will be examined by analyzing the YSZ crucibles with optical microscopy and/or scanning electron microscopy (SEM)/TEM to determine surface alteration and depth of penetration. The comprehensive microstructure information obtained by high-resolution techniques will facilitate the correlation between the anode electrocatalysis, microstructure, and chemistry degradation mechanisms attributable to various contaminants.

Results

Research is completed to evaluate the basic performance of the LMA SOFC, to computationally predict the state of oxygen in the liquid tin system, and to determine the impact of trace materials on cell structure and chemistry. Experimental efforts are first conducted on the liquid tin and liquid metal alloy systems to evaluate basic performance. Figure 1 depicts a schematic of the LMA test system. The tin is contained in a crucible made of the fuel cell electrolyte material, which has a cathode painted on the bottom. Gaseous or solid fuel is fed through an interior tube oriented co-axially with the outer tube. One current collecting electrode is attached to the painted cathode and one electrode is submerged inside the tin. The electrodes are connected externally to instrumentation that can probe the current/voltage/power characteristics and perform EIS experiments on the cell. Limited translation of probes is possible, and allows spatial resolution of liquid tin bath conditions to ensure that key assumptions in the transport models are satisfied during the experiments.

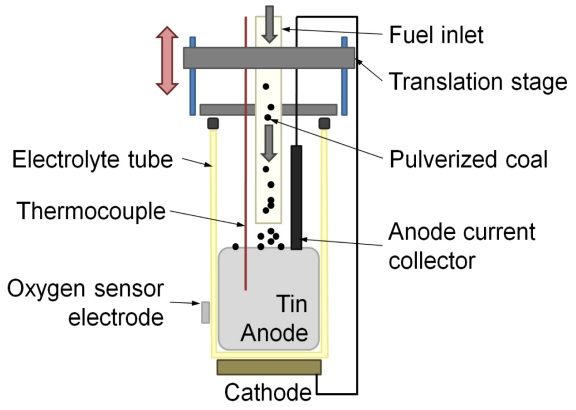

FIGURE 1. Schematic of the LMA SOFC system. Gaseous, pulverized coal, or biomass fuels are added through a central tube directly to the anode where the reactions take place.

Data collected on the system are analyzed to determine oxygen diffusion rates and evaluate electrochemical kinetic performance. Figure 2 shows typical performance data collected for the LMA SOFC system. The graph on top depicts the current relaxation upon application of a precise potential gradient across the cell. The figure shows that the steady-state current following relaxation is a function of temperature, with greater steady-state currents observed at relatively higher temperatures. Fitting of the relaxation data to an electrochemical diffusion model reveals the magnitude of the oxygen diffusion, which is on the order of 10^{-4} cm^2/sec at the highest temperatures. The graph on the bottom shows impedance plots determined for an LTA operated at three temperatures. The data collected are fitted with equivalent circuit models to predict the relative importance of various reaction steps. In the sample tested, the observed low frequency behavior implies that a substantial diffusion limitation is present, which may correspond to slow transport of active species through the liquid tin.

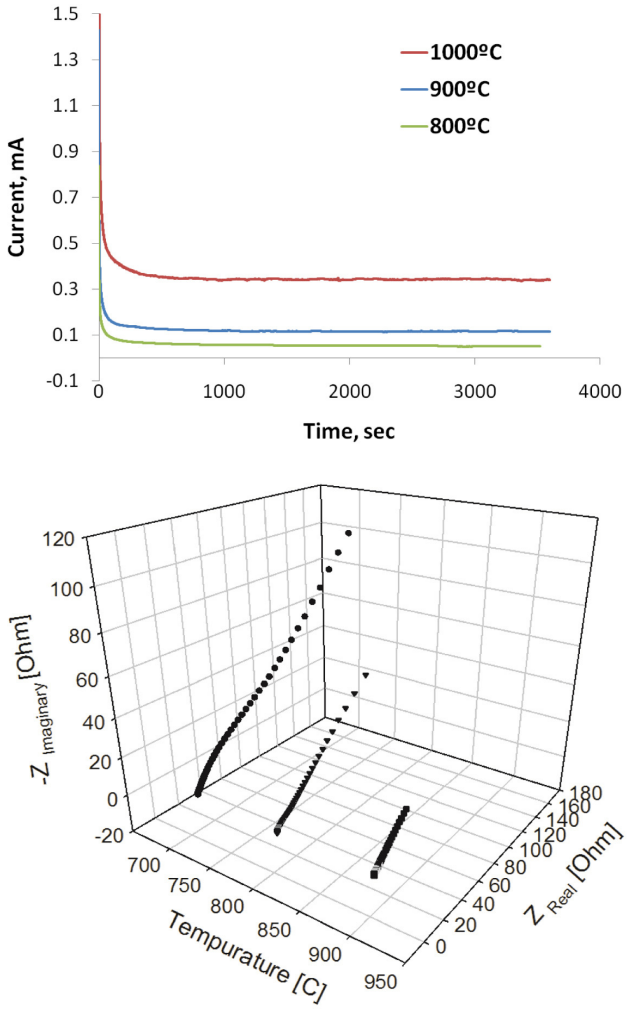

FIGURE 2. (Top) Depiction of typical data collected during oxygen diffusion measurements. Analysis of the data shows increasing oxygen diffusion as temperature increases. (Bottom) Typical impedance plots generated at different operating temperatures. The plots indicate that cell resistances decrease as temperature increases, as expected.

Computational chemistry is used to generate predictions of the state and transport of oxygen in the LMA SOFC system. The predictions can be used in the formation of reaction mechanism hypotheses, and also to screen potential anode metals and constituent alloys. Figure 3 shows an example of some computational predictions for ground state energies generated for the tin-oxygen system. Accurate ground state predictions are achieved by proper selection of computational parameters, including pseudo potentials and electron interaction (or exchange-correlation) functionals. Ground state energies (or, more precisely, energies or enthalpies of formation) for the tin-oxygen system are known experimentally, therefore the computational results can be compared to known values to ensure that the description of the ground states is accurate. Prediction of the proper ground states implies that the proper modeling assumptions have been made in formation of computational chemistry problem. The information depicted is used in subsequent calculations to computationally predict the diffusion of oxygen in the liquid tin system, and the results can be verified by comparison to the parallel experiments described.

In addition to knowledge of the oxygen state, proper design and operation of the LMA SOFC system requires knowledge of the impact of trace materials contained in coal on the cell operation. Figure 4 depicts microscopic images of critical reaction interfaces within the LMA SOFC system. In the image at left, the interface between the liquid tin and the carbonaceous solid fuel is investigated by SEM to identify formation of unwanted phases. Both tin oxide and tin-sulfur phases are found in a very narrow region at the interface. The presence of the material may hinder oxygen transport, diminish the efficiency of the fuel reactions, increase the difficulty of undesirable phase removal from LMA, or simply increase the total ohmic resistance in the cell. The image at the right shows TEM micrographs of the interface between the carbonaceous fuel and the YSZ. Many trace metal oxides are located at this region, which implies that many of the unwanted trace materials will form an oxide slag that can be removed through careful processing.

Conclusions and Future Directions

The LMA SOFC system has been thoroughly characterized in a series of efforts ranging from basic performance testing and computations to applied analysis of operation and trace material partitioning. Research methods have been optimized to accurately determine the oxygen diffusion coefficient using a standard test system, and have provided reliable and

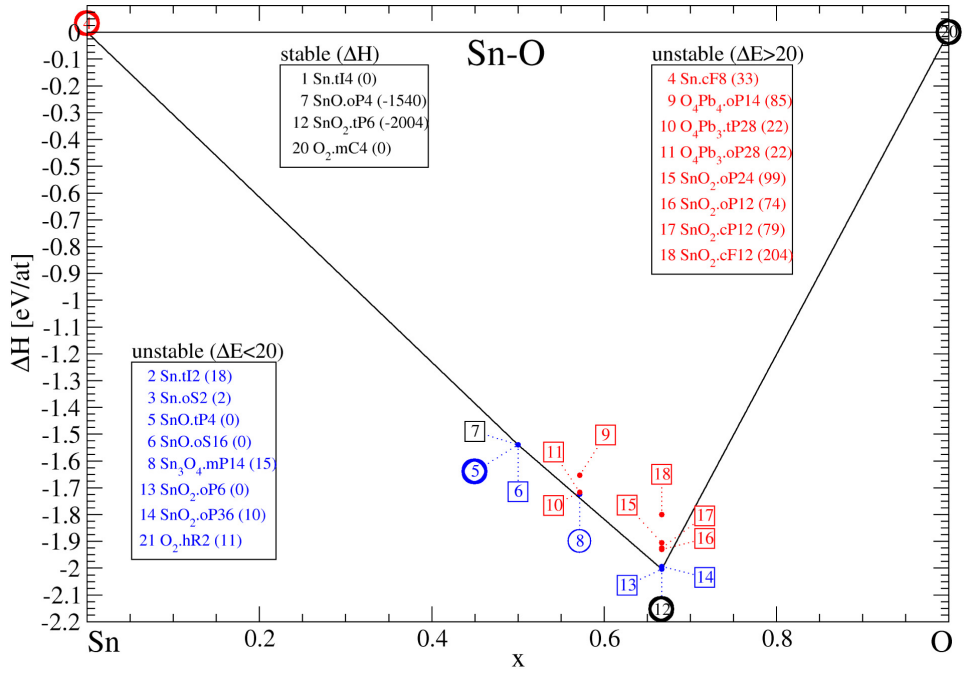

FIGURE 3. Depiction of the ground state predictions generated by ab initio computations. Proper predictions are critically dependent upon assumption of proper pseudo-potentials and exchange-correlation functionals, and have been verified for accuracy in the present work.

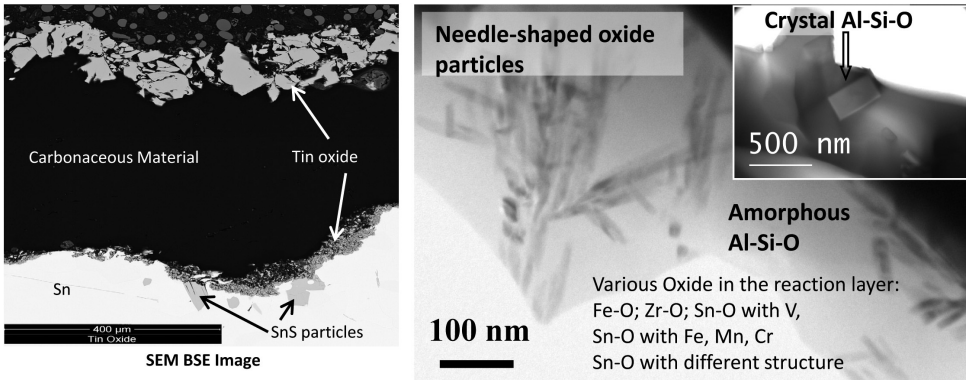

FIGURE 4. (Left) SEM image of the interface between a tin anode and a carbonaceous solid fuel. Tin oxide and tin-sulfur species are detected at the interface. (Right) TEM image of regions at the carbon-YSZ interface. Many trace metals are found in the oxide scale generated at the surface of the tin bath.

quantitative results. Efforts have been completed to probe evaluation of reaction kinetics using electrochemical impedance spectroscopy and the data have been used to generate equivalent circuit models that provide insight into the factors limiting system performance. Computational methods have been developed that accurately predict the core properties of the oxygen-tin system, and which will provide evaluations of the oxygen diffusivity. Experiments have been completed that evaluate the partitioning of trace material contained in coal to the various active components within the cell. Advanced microscopy has been applied to observe critical interfaces within the coal-fueled system, and regions of intensified trace material concentration have been identified.

Future efforts will focus on further development of advanced alloys that will ultimately be deployed to commercial LMA SOFC systems. Alloy performance will be tested to assure high activity and responsive kinetics for a variety of solid fuels, and may be adjusted according to the computational chemistry

predictions. Trace material partitioning and electrode deactivation will be examined in direct tests for the most promising alloys. Materials may be added to the tin system to facilitate formation of slag phases that may be more easily removed from the cell, thereby preventing deleterious interaction with the LMA SOFC components.

FY 2011 Publications/Presentations

1. H. Abernathy et al., "Basic Properties of a Liquid Tin Anode Solid Oxide Fuel Cell," Journal of Power Sources 196(10) 4564-4572, 2011.

2. S. Lvov et al., "Electrochemical Characterization of Liquid Metal Anode Solid Oxide Fuel Cell," Presentation at 220th ECS Meeting, Boston, Massachusetts, October 9–14, 2011.

3. M. LaBarbera, M.V. Fedkin, and S.N. Lvov, "Liquid Tin-Lead Anode Solid Oxide Fuel Cell Fueled by Coal," ECS Transactions, 35(1) 2725-2734, 2011.

4. Gao et al., "First-Principles Prediction of Oxygen States and Transportation in Liquid Tin Anode SOFC," MS&T 11, Columbus, Ohio, October 16–20, 2011.

5. H. Abernathy et al. "Impact of Impurities and Alloying Metals on the Performance of Liquid Metal Anode Solid Oxide Fuel Cells," Materials Science & Technology 2010, Houston, Texas, October 2010.

6. H. Abernathy et al., "Material Selection and System Design for Liquid Metal Anode Solid Oxide Fuel Cells (LA-SOFCs)," Materials Research Society Fall 2010 Meeting, Boston, Massachusetts, November 2010.

IV.6 Validation of Novel Planar Cell Design for MW-Scale SOFC Power Systems

Michael J. Day, Ph.D. (Primary Contact), Kellie Chenault, Lora Thrun, and Scott Swartz
NexTech Materials, Ltd.
404 Enterprise Drive
Lewis Center, OH 43035
Phone: (614) 842-6606; Fax: (614) 842-6607
E-mail: m.day@nextechmaterials.com

DOE Project Manager: Briggs White
Phone: (304) 285-5437
E-mail: Briggs.White@netl.doe.gov

Subcontractor:
Professor Mark Walter
The Ohio State University, Columbus, OH

Contract Number: NT0004113

Start Date: October 1, 2008
End Date: September 30, 2011

Fiscal Year (FY) 2011 Objectives

The overall goal of this project is to validate the performance, robustness, cost and scalability of a novel electrolyte-supported planar cell design, termed the FlexCell, for use in coal-based solid oxide fuel cell (SOFC) power systems. Specific objectives of work in FY 2011 include:

- Demonstrate scalability of the FlexCell design by fabricating ytrria-stabilized zirconia (YSZ)-based FlexCells having a total cell area of at least 500 cm^2. *This objective was met by fabricating a minimum of 20 large-area cells and achieving a production yield of greater than 80 percent.*
- Demonstrate that high performance can be achieved in large-area FlexCells. *This objective was met by performing single-cell SOFC tests on large-area FlexCells and achieving a power density of more than 300 mW/cm^2 at 800°C (0.7 volts and 70 percent fuel utilization).*
- Demonstrate stable performance of YSZ-based FlexCells operating with syngas that is typical of gasified coal after syngas cleanup operations. *This objective will be met by achieving a steady-state degradation rate of less than 1% per 1,000 hours over 500 hours of single-cell testing.*
- Demonstrate potential of achieving stack manufacturing cost of less than $100/kW using FlexCells. This objective was met by performing a comprehensive manufacturing and cost analysis and confirming that cell costs will be less than $50/kW at full-scale production (250 MW/year).

FY 2011 Accomplishments

- Based on the results of this project, all SOFC stack fabrication and testing work at NexTech was transitioned to YSZ-based FlexCells. To date in the project, NexTech successfully fabricated more than 700 YSZ-based FlexCells of varying sizes (from 100 cm^2 to 540 cm^2 in total area).
- A robust ISO-9001:2008 certified quality control system was implemented at NexTech for FlexCell manufacturing, which led to the achievement of the targeted production yields and continuous process improvements.
- NexTech established capability and methodology for single-cell testing of large-area FlexCells and confirmed targeted performance levels (>400 mW/cm^2, 800°C, U_F = 70 percent).
- NexTech updated its manufacturing cost analysis, confirming that full-scale production costs (at the 250 MW scale) of FlexCells will be less than $50/kW, and identifying paths to reduce costs to less than $40 per kilowatt.

Introduction

This Solid State Energy Conversion Alliance (SECA) Core Technology project is aimed at advancing planar solid oxide fuel cell technology for coal-based, megawatt-scale power generation systems. It is anticipated that such systems will be comprised of a multitude of SOFC stack modules to achieve targeted power outputs. In order to increase the power output per stack module (and reduce the number of modules in the system), planar SOFC cells with large areas will be required. NexTech Materials has established a novel electrolyte-supported planar cell design, termed the FlexCell, which offers intrinsic scalability to large areas, as well as other important performance attributes. The FlexCell is based on a patent-pending, electrolyte-supported planar membrane. As shown in Figure 1, the FlexCell is a two-layer structure comprising a thin electrolyte membrane layer that is mechanically supported by a "honeycomb" mesh layer of electrolyte material. With the FlexCell, 60 to 70 percent of the electrolyte membrane within the active area is thin (less than 40 microns), and the periphery of the cell is dense.

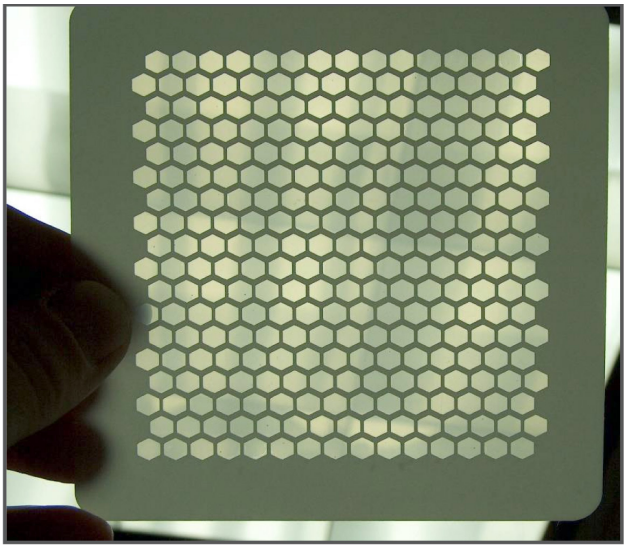

FIGURE 1. Example of a FlexCell Membrane

NexTech established its FlexCell membrane design using scandium-stabilized zirconia (ScSZ) as the electrolyte material. Although ScSZ offers an excellent combination of high oxygen ion conductivity and high mechanical strength, its cost is expected to be prohibitive for large-scale power generation systems. Thus, the focus of work on this project is on fabrication and testing of FlexCell membranes made with lower-cost YSZ as the electrolyte material. Phase I of this project, completed in March of 2010, focused on validating manufacturability and performance capabilities of YSZ-based FlexCells under conditions expected for coal-based SOFC systems. Specific tasks included fabrication of 100-cm^2 area FlexCells, testing of these FlexCells under application-specific conditions, finite element analysis of mechanical robustness of FlexCell membranes, and manufacturing cost analysis. Work in Phase II is aimed at fabrication and testing of large-area FlexCells (nominally 500 cm^2), and validation of the cost model established in Phase I.

Approach

Partially stabilized YSZ electrolyte compositions are being used to fabricate FlexCells in this project. Although ionic conductivity of partially stabilized compositions (3 to 6 mol% Y_2O_3) is lower than that of fully stabilized compositions (8 to 10 mol% YSZ), partially stabilized compositions have significantly higher mechanical strength. The optimal YSZ composition is a trade-off between these two endpoints. Commercially sourced YSZ powder was used to prepare green tape, from which FlexCell membranes are prepared using NexTech's standard procedures. NexTech's proprietary anode and cathode layers then were applied in separate deposition/sintering steps, with the anode applied to the support (corrugated) face of the FlexCell membrane and the cathode applied to the non-corrugated face. Successfully fabricated FlexCells were subjected to SOFC performance testing following NexTech's existing single-cell testing methods. Manufacturing cost analyses were performed using standard chemical engineering principles with raw materials cost guidance provided by SECA.

Results

A considerable amount of compositional and process development work was conducted with the aims of improving sintered density of YSZ-based FlexCell membranes, reducing defect density, and improving electrochemical performance. This work led to the successful fabrication of FlexCells with 476 cm^2 total area (see Figure 2). NexTech also has fabricated FlexCells with 320 cm^2 and 540 cm^2 areas for use in stacks being fabricated and tested at NexTech (see Figure 3).

Single-cell SOFC testing was performed on a large-area YSZ-based FlexCell, with data presented in Figure 5. The testing manifolds and the set-up of this test are shown in Figure 4. Tests were conducted with the furnace temperature set at 800ºC, with diluted hydrogen as fuel (50% H_2, 50% N_2). In one such test, the fuel flow rate was set at 4.0 lpm (2.0 lpm H_2) and the air flow rate was set at 16 lpm. Under these conditions, the open circuit voltage was 1.246 volts. Current then was stepped up at a rate of 2.5 amps per minute to generate a pole curve. As shown in Figure 5, 135 watts was obtained at a potential of 0.69 volts. This corresponded to a current density of 0.602 A/cm^2,

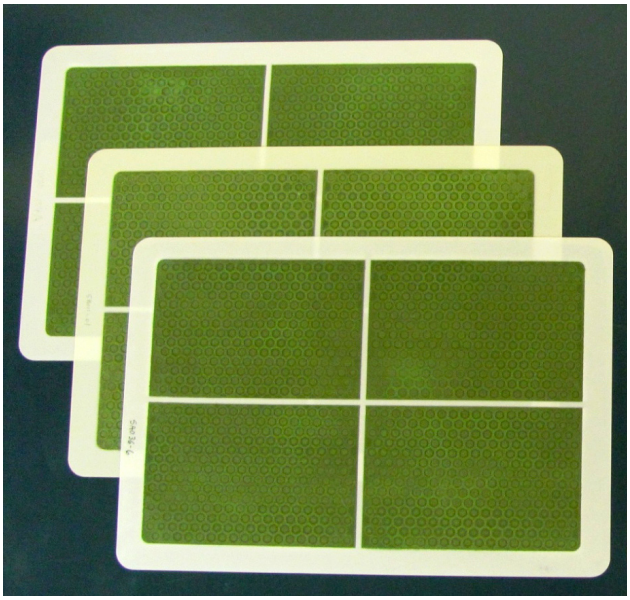

FIGURE 2. Examples of FlexCells Made with 476 cm^2 Area (left) and 330 cm^2 Area (right)

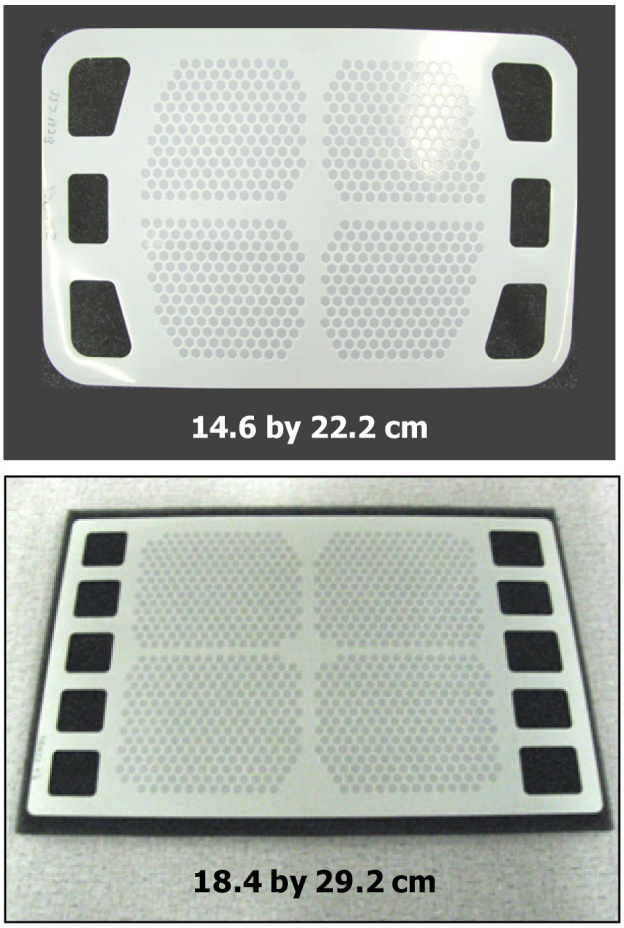

FIGURE 3. YSZ-Based FlexCell Membranes for NexTech's Stacks: 1-2 kW Scale Stack Platform (top) and 5-10 kW Scale Stack Platform (bottom)

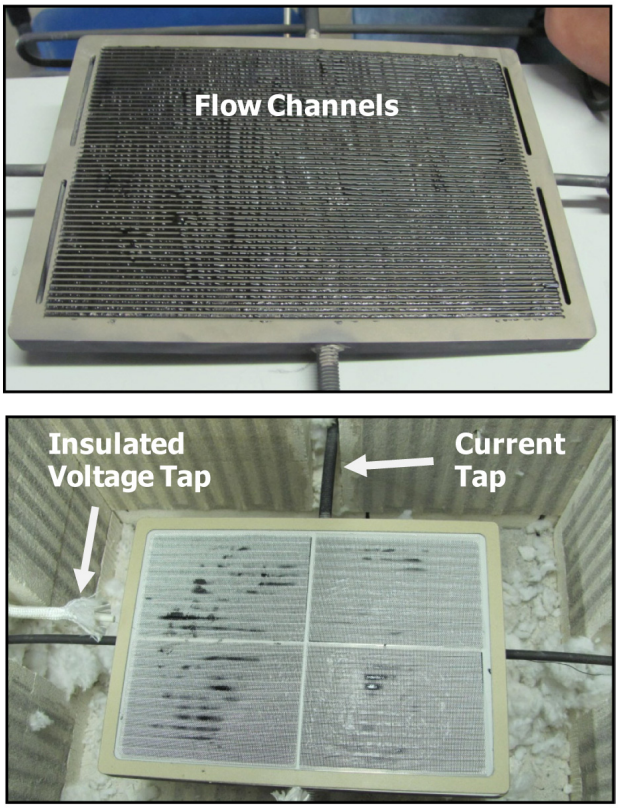

FIGURE 4. Cathode Manifold with Flow Channels and Contact Paste Applied (top); Cell Loaded in Test Stand with Current and Voltage Taps for Testing (bottom)

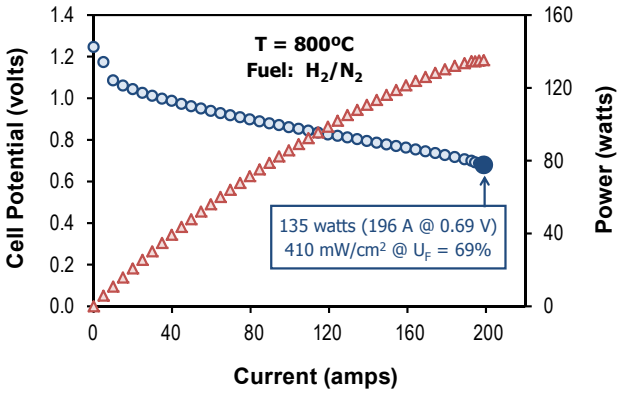

FiGURE 5. Pole Curve Obtained on Large-Area YSZ-Based FlexCell at 800°C (fuel flow was 2.0 lpm H_2 and 2.0 lpm N_2, air flow was 16 lpm)

power density of 409 mW/cm^2 and fuel utilization of approximately 70 percent.

In Phase I, a manufacturing cost analysis was completed for large-area FlexCells at the 250 MW/year volume level. This analysis was updated based on the results of the Phase II project and additional insights gained at NexTech since the original analysis was completed. The process flow diagram for the FlexCell manufacturing process is shown in Figure 6. A seven-day, three-shift operation was assumed to maximize capacity of the highly automated manufacturing equipment. Gas-fired tunnel kilns were assumed for sintering electrolyte substrates, while electrically heated tunnel kilns were assumed for annealing of electrodes. The capital equipment cost needed for the full-scale (250 MW) FlexCell production facility was determined through vendor quotes for each manufacturing operation. Raw material costs for the full-scale production plant were based on SECA-provided estimates, vendor quotations, and large-scale production estimates. Based on these assumptions and a complete accounting for costs associated with building and operating the production facility, a manufactured cost estimate of $51 per kW was estimated (see Table 1). Several approaches were identified to provide a path toward reduction of manufacturing cost to the $40/kW level.

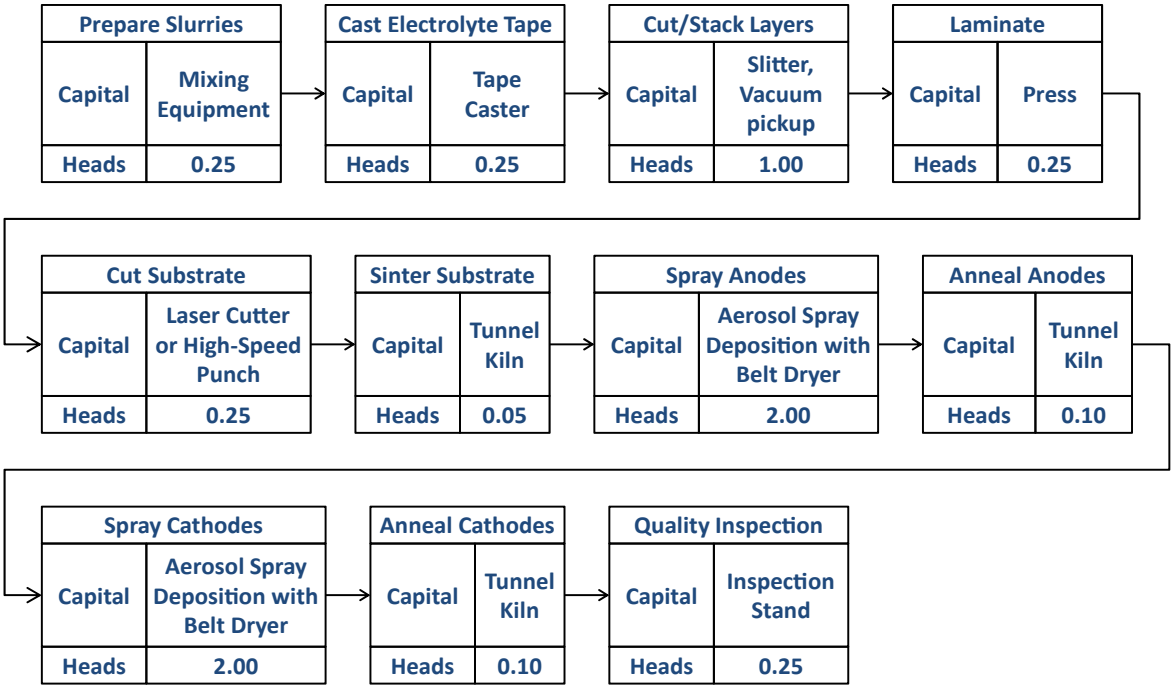

FIGURE 6. Process Flow Diagram, Including Capital Equipment and Labor Requirements for FlexCell Manufacturing

TABLE 1. Breakdown of FlexCell Production Costs at 250 MW/Year Scale

Cost Category	Yearly Cost	Cost Per Cell	Cost Per kW
Raw Materials	$5,617,891	$2.75	$22.47
Depreciation	$2,063,502	$1.01	$8.25
Operating Labor	$1,833,930	$0.90	$7.34
Utilities	$1,300,558	$0.64	$5.20
Operating Supplies	$1,123,578	$0.55	$4.49
Local Taxes	$550,267	$0.27	$2.20
Maintenance & Repairs	$112,358	$0.06	$0.45
Insurance	$220,107	$0.11	$0.88
Total	**$12,822,191**	**$6.29**	**$51.29**

Conclusions and Future Directions

To date in this project, NexTech has successfully demonstrated the fabrication of FlexCell membranes made with yttrium-stabilized zirconia as the electrolyte material. Electrochemical testing has confirmed that SOFC performance of YSZ-based FlexCells is essentially the same as that achieved with FlexCells made with ScSZ electrolyte material at 800°C. The fabrication of YSZ-based cells was successfully scaled up to 540-cm^2 areas, and single-cell testing of large-area FlexCells has confirmed that performance is scalable with cell size. Additional work remaining on the project includes the following:

1. Continued fabrication and testing of large-area FlexCells (>300 cm^2 active area), and evaluating performance with simulated coal gas as fuel.
2. Long-term testing on simulated coal gas with the goal of demonstrating stable performance over a minimum of 500 hours of testing.

FY 2011 Publications/Presentations

1. Quarterly Status Report #7 (July 31, 2010).

2. Quarterly Status Report #8 (October 30, 2010).

3. Quarterly Status Report #9 (January 31, 2011).

4. Quarterly Status Report #10 (April 30, 2011).

5. Topical Report on Manufacturing Cost Analysis for YSZ-Based *FlexCells* (April 30, 2011).

6. Presentation at SECA Core Technology Workshop (July 27, 2010).

7. Interim Review Meeting Presentation (December 15, 2010).

8. Interim Review Meeting Presentation (June 10, 2011).

9. Presentation at FY 2011 Fuel Cells Peer Review (February 15, 2011).

IV.7 Improved Flowfield Structures for Direct Methanol Fuel Cells

Bogdan Gurau, Corey Grice, Eugene Smotkin, John Staser (Primary Contact)
NuVant Systems, Inc.
Purdue Technology Center of NW Indiana
9800 Connecticut Drive
Crown Point, IN 46307
Phone: (781) 697-8623; Fax: (219) 644-3682
E-mail: j.staser@nuvant.com

DOE Project Manager: Maria Reidpath
Phone: (304) 285-4140
E-mail: Maria.Reidpath@netl.doe.gov

Contract Number: FE0000982

Start Date: August 1, 2009
End Date: July 31, 2011

Fiscal Year (FY) 2011 Objectives

- Produce computational fluid dynamic (CFD) models of various flowfield geometries and material porosities using FLUENT software package.
- Fabricate porous plates according to modeling results.
- Maximum fuel energy density by optimizing membrane electrode assembly (MEA) structure and operating scheme.
- Perform extended life tests of optimized MEAs.
- Construct one or more short stacks consisting of three to four cells.
- Optimize the short stack(s) in terms of operating parameters.

FY 2011 Accomplishments

- FLUENT modeling of the integrated flowfield diffusion layer (IFDL) structure was performed and determined that a square-grid flowfield on both sides of the porous plate would provide the most uniform flow distribution.
- IFDL plates were successfully fabricated from porous graphite using a table-top endmill machine.
- Direct methanol fuel cell (DMFC) single cells were evaluated using the porous graphite IFDL plates and resulted in gross fuel energy densities of over 781 Wh/L with fuel utilizations of over 79%.
- Single cells have been operated using the IFDL method for over 80 hours with no significant decrease in power output.
- A short stack has been constructed consisting of two cells and initial performance testing has begun.

Introduction

Direct liquid fuel oxidation fuel cells hold great promise for portable power sources and even intermediate power sources (low hundreds of watts) because the fuels have high energy density. One of the fuels with high energy density is methanol (which can be synthesized from gasified coal), so the DMFC is perfectly suitable for the above mentioned applications. Currently, state-of-the-art DMFCs have acceptable degradation rates but the excessive crossover of the fuel diminishes greatly the ability to harvest the energy contained in the fuel. The crossover impediment can be mitigated by the use of diluted fuel but this decreases heavily the gross fuel energy density (GFED), which is the energy produced per unit of fuel solution (the largest volume component for a long-term power system), and brings about a complex and bulky balance of plant, which impacts the final energy and power density of the system. If the DMFCs are going to be successful in coming years an alternative approach, which enables the use of concentrated fuel, will have to be devised.

Approach

NuVant Systems, Inc. will tackle the problem of methanol crossover by employing highly porous structures at the DMFC anode which will allow for controlled delivery of highly concentrated or neat methanol to the anode side. The methanol delivery to the anode side will be adjusted in concert with the back-diffusion of water from the cathode side such that diluted methanol will be created in situ at the anode. In this way crossover will be minimized and high GFED will be achieved. The secret to success is the tightly controlled structure of the porous material and the fuel delivery mode. The pore diameter and total porosity play a very important role on how (and how much of) the highly concentrated methanol arrives at the anode. Various hydrophilic and/or hydrophobic treatments of the porous substrate impact the way methanol distributes over the entire geometric area of the electrode. Also, these treatments impact the way reaction products are being exhausted. In order to best build these porous structures, a thorough understanding of flow and diffusion through porous media is required. By employing CFD modeling NuVant will study various porosities, various geometries and various flowfields which will enable optimal delivery of methanol to the reaction site. Based on the optimal design of these structures NuVant will build a short DMFC stack that will deliver high GFED and high power density.

Results

Prior to fabricating any fuel cell hardware associated with the IFDL cell operating concept, CFD modeling using the FLUENT software program was conducted to confirm the effectiveness of the flowfield designs to be incorporated into the porous graphite plate. The initial concept of the flowfield was to have a web-like configuration for the fuel (methanol) side of the plate. A continuous stream of fuel would be injected into the center of this flowfield and would radiate outward to the extremities of the plate (see Figure 1). Since the velocity of the fuel radiating outward would be much greater than the rate of permeation of fuel through the thickness of the porous plate, it was anticipated that this configuration would allow for relatively uniform lateral distribution of fuel across the plate which would lead to even fuel availability on the opposite side of the plate (contacting the anode electrode of the MEA). This MEA side of the porous plate was intended to have a square pin grid as a flowfield which would enable CO_2, a byproduct of methanol oxidation, to be easily removed from the anode electrode (see Figure 2). The Fluent modeling revealed the web-like flow was too restrictive to allow the fuel to diffuse across the plate laterally and thus caused regions of fuel depletion on the MEA-side of the porous plate. The web-like flowfield was then replaced by a square-grid flowfield (similar to the MEA side, but offset such that the square pins did not overlap). This configuration was predicted to allow a more uniform flow distribution across the fuel side of the plate and eliminated regions of fuel depletion on the MEA-side. Once the design had been verified, the plate was fabricated successfully using a Roland MDX-540 endmill from porous graphite material.

The porous graphite IFDL plates were inserted into single cell assemblies made from gold-coated brass endplates which would accommodate a 25 cm^2 DMFC

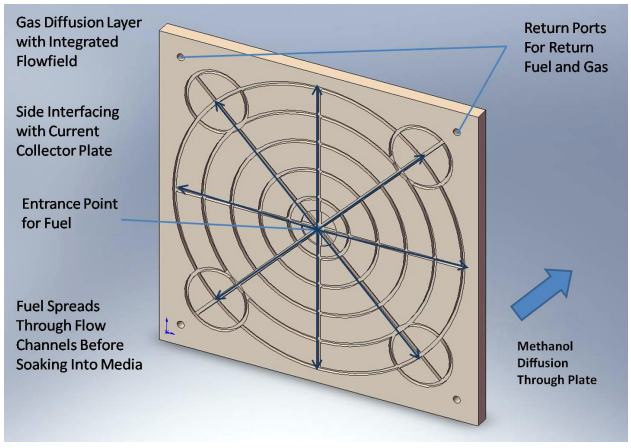

FIGURE 1. Fuel Side Flow Design for Porous IFDL Plate

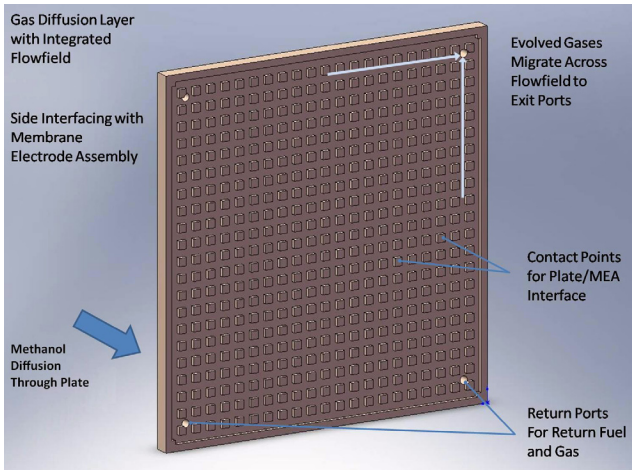

FIGURE 2. MEA Side Flowfield Design for Porous IFDL Plate

MEA. One of the plates would hold the IFDL plate and serve as the electrical connection for the anode (see Figure 3). The opposing endplate contained a serpentine flowfield for air delivery and electrical connection to the cathode. This configuration was then examined by manipulation of several operating parameters such as cell temperature, fuel flow rate, method of fuel delivery (continuous flow or discrete doses), fuel concentration, and air flow rate. Thus far we have been able to achieve up to 781 Wh/L of GFED at a utilization of 79.4%. While this means that approximately 20% of the methanol fuel is being lost due to crossover to the cathode side (where it reacts with O_2 in the air to create heat and not electrical energy), the high degree of fuel energy density means the system can provide significant power on a volumetric basis – thus reducing the size requirements of a commercialized power system. Work is continuing to attempt to maximize the energy density, with a goal of 1,000 Wh/L in the near future. These cells have been operated up to 80 hours continuously without significant loss of power output, but longer experiments are planned (several 100s of hours) to confirm the stability of the IFDL arrangement.

After successful operation of a single cell using the IFDL concept, the next logical step was to create a "stack" consisting of multiple cells electrically connected in series. This arrangement results in a higher voltage than a single cell operating at the same current which translates into a greater power output. A commercial power system would entail at least 10 or more cells to supply meaningful current and voltage, depending on the intended application. A small stack, consisting of only two cells for now, has been constructed although performance testing and evaluation has only just begun (see Figure 4).

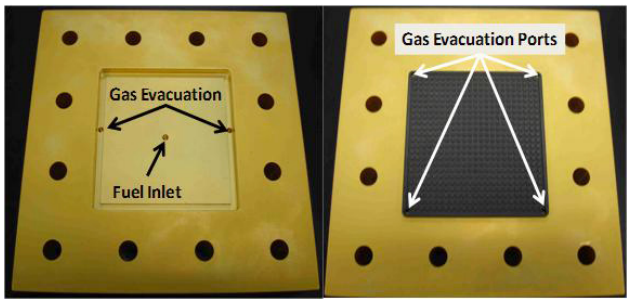

FIGURE 3. Photograph of Anode Endplate for Porous IFDL Plate

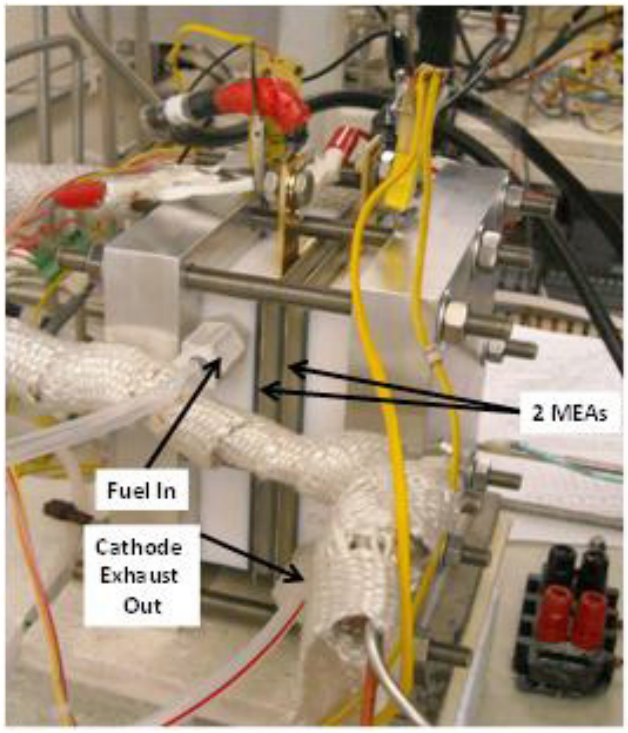

FIGURE 4. Photograph of Two-Cell Stack with Fluid and Electrical Connections

Conclusions and Future Directions

The IFDL porous plate concept, guided by computational modeling efforts, was successfully demonstrated using a single cell DMFC. Gross fuel energy densities have been demonstrated as high as 781 Wh/L with fuel utilizations up to 79.4% with cells that have operated up to 80 hours in duration. Work is continuing to attempt to improve this value to 1,000 Wh/L or greater without significant losses in fuel utilization while achieving operating times of at least several 100s of hours. This concept is now being tested in a laboratory grade fuel cell stack to confirm performance levels and evaluate cell-to-cell variation. Experiments may also be performed to evaluate the applicability of the IFDL concept to other fuel species (ethanol, formic acid, etc.) and using other fuel cell materials (alkaline electrolyte membranes, non-noble metal catalysts, etc.) Future work, beyond the scope of this project, would entail decreasing the size and complexity of this system such that commercialization would be enabled.

FY 2011 Publications/Presentations

1. B. Gurau, C. Grice, M. Taslim, and M. Abedi, "Direct Methanol Fuel Cell Operating with Concentrated Methanol," Poster at the NETL 11th Annual SECA Workshop, Pittsburgh, Pennsylvania, July 27–29, 2010.

IV.8 Small Scale SOFC Demonstration Using Bio-Based and Fossil Fuels

Michael Petrik (Primary Contact),
Robert C. Ruhl, and Christopher Milliken
Technology Management, Inc. (TMI)
9718 Lake Shore Boulevard
Cleveland, OH 44108
Phone: (440) 995-9500; Fax: (440) 720-4527
E-mail: mpetrik@anywherenergy.com

DOE Project Manager: Maria Reidpath
Phone: (304) 285-4140
E-mail: Maria.Reidpath@netl.doe.gov

Contract Number: FE0005132

Start Date: October 1, 2010
End Date: September 30, 2011

Fiscal Year (FY) 2011 Objectives

- Identify potential end-user demonstration sites and obtain user permission and cooperation for final selections.
- Complete fuel cell system designs for procurement.
- Complete system fabrication, installation at end-user site, and testing to show system operational lower heating value efficiency greater than 30%.
- Identify long-term risks associated with commercialization and prepare a preliminary product/market roll out plan.

FY 2011 Accomplishments

- Selected two end-user sites for demonstration of the TMI solid oxide fuel cell (SOFC) system on multiple bio-based and conventional fuels.
- Completed the system design (Figure 1) and initiated procurement and fabrication of the demonstration system.

Introduction

TMI is working to develop and demonstrate a residential-scale prototype fuel cell system that will provided the basis for a new paradigm power production and integration to utility Smart Grids - Massively Distributed Generation. These small scale systems would operate 24/7, producing electric power for on-site use and grid export with the option for recovered heat for cogeneration thereby transforming today's residential power grid. Small on-site generation provides a critical missing component to the Smart Grid equation – intelligent on-site power generation that can adapt to user loads, including electric and plug-in hybrid vehicles. The systems would operate on both conventional and renewable biofuels, providing cost effective, uninterruptible whole-house power with major environmental and reliability advantages. The critical component to point-of-use distributed power generation is the unique TMI SOFC integrated module, which would operate on whichever fuel is used for an adjacent furnace. Most residential systems would use multiple 1 kW modules to provide continuous 24/7 to all of the electric power needs, including power to charge plug-in hybrid and electric vehicles, and hot water needs of the home plus a significant fraction of its space heating. Excess power would be available to be exported to the grid whenever necessary or economically prudent, thus providing the equivalent of massively distributed power storage. During grid outages, the system would

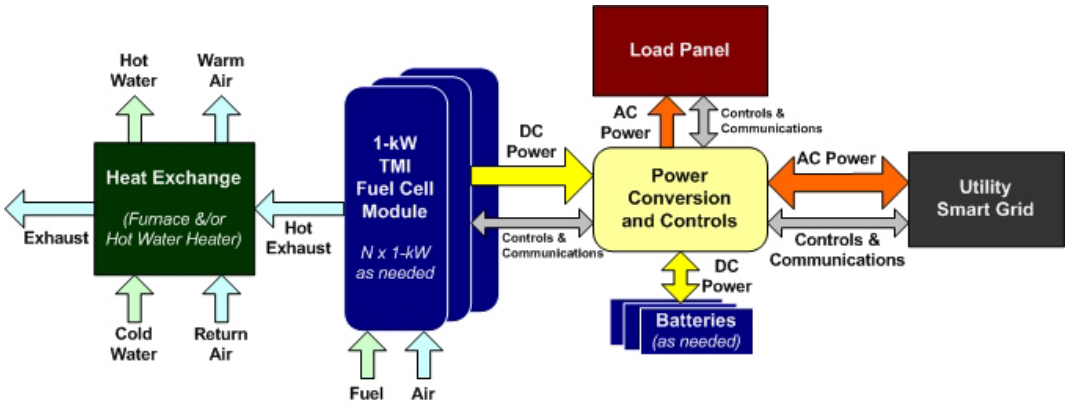

FIGURE 1. Residential Fuel Cell-Grid Interconnection System Schematic

continue to provide uninterruptible power for unlimited times, with a battery bank supplying surge power needs.

Relative to the primary mission of the DOE Fuel Cell Program, the TMI SOFC system is potentially a 'drop-in' distributed generation subsystem that can be grid-independent and/or grid-connected which operates on fossil fuels as well as on various bio-based fuels, with zero water consumption and no air pollutants. The TMI fuel cell system is at the engineering system prototype stage in the 1-5 kW scale, and may contribute improvements to fabrication and operation on a proffered biofuel. Expected outcomes would be positive economic and technical metrics which can establish early market demands for the system and feedback for TMI product developers. There are few practical alternatives for ordinary consumers to obtain all *their home electric energy from zero carbon biofuels*. This feature, while attractive to environmentally conscious consumers, will not build broad product adoption until there are credible performance metrics and a clear value proposition for the consumer. In addition, given the poor track record of many fuel cell system developers, solid performance metrics will benefit the entire industry and re-engage traditional venture capital investment, which has drifted away.

Approach

Two key areas will be addressed under this project. First, economic and technical metrics describing fuel cell system operation must be captured and evaluated in a realistic environment. TMI is proposing to manufacture two 1-kW modular fuel cell systems populated with stacks for installation at a pre-qualified demonstration site. Results will be compared with alternative technologies such as reciprocating engine-based generators. Second, the fuel cell system performance will be compared with other small scale fuel cell systems. TMI will modify existing designs to integrate the system with batteries and add power conditioning and controls to allow direct tie-in to the grid. In both cases, performance will include operation on traditional fuels found in a typical farm or residence as well as a liquid biofuel.

Results

Technical results are limited because the testing is scheduled for the final quarter of FY 2011. To date, two project milestones have been completed:

- Site selection activities were completed. Two sites, a primary site (Figure 2, Patterson Fruit Farm, Chesterland, Ohio) and a secondary site (Figure 3, Gates Mills Environmental Education Center, Gates Mills, Ohio) were selected, evaluated, and confirmed for the demonstrations. Final site preparation will begin in the first half of 2011 while the system design and fabrication tasks are completed.
- System engineering and designs have been completed. Purchase orders for the major fabricated components (hot subassembly and frame) were released in April 2011.

FIGURE 2. Demonstration Site #1: Patterson's Fruit Farm, Chesterland, Ohio

FIGURE 3. Demonstration Site #2: Gates Mills Environmental Education Center, Gates Mills, Ohio

Conclusions and Future Directions

As of this early point in the project, strong support has been found from potential end-users for a small fuel cell system for distributed energy generation from biofuels or conventional fuels. Demonstration of the technology later in the project is expected to provide the necessary early user and engineering feedback required for continued commercial advancement.

Future work includes:

- Completion of fabrication and assembly of the 1-kW systems,
- siting of the systems, and
- demonstration of operation on multiple fuels for 30 to 90 days at the end user site.

IV.9 Techno-Economic Analysis of Scalable Coal-Based Fuel Cells

Steven S.C. Chuang (Primary Contact),
Felipe Guzman, Tritti Siengchum,
Jelvehnaz Mirzababaei, Azadeh Rismanchian,
and Brian Mohrman
The University of Akron
Department of Chemical and Biomolecular Engineering
230 E. Buchtel Commons
Akron, OH 44325-3906
Phone: (330) 972-6993; Fax: (330) 972-5856
E-mail: schuang@uakron.edu

DOE Project Manager: Maria Reidpath
Phone: (304) 285-4140
E-mail: Maria.Reidpath@netl.doe.gov

Contract Number: FE0000528

Start Date: September 1, 2009
End Date: August 31, 2013

Fiscal Year (FY) 2011 Objectives

The goal of this project is to demonstrate the technical and economic feasibility of building a kW-scale pilot plant coal-based fuel cell with participation by industries. This project will address initial development, scaling, and manufacturing of the core technology. Objectives for 2011 include the following:

- Develop anode materials that exhibit high activity for the direct electrochemical oxidation of carbon/hydrocarbons and resistance to deactivation due to contaminants present in coal.
- Develop a scalable, reproducible, and cost-effective approach for the fabrication of fuel cells that possess sufficient mechanical strength and meet the target demonstration performance of 100 mA/cm^2 at 0.4 V.
- Design a coal injection and flyash withdraw system.
- Identify suitable sealant materials for the continuous operation of the coal-based fuel cell.
- Simulate the performance of a coal-based fuel cell.

FY 2011 Accomplishments

- Synthesized and characterized a Cu-Ni/YSZ (yttria-stabilized zirconia) anode that exhibits high catalytic activity for electrochemical oxidation of carbon and hydrocarbons, and resistance to deactivation.
- Developed a tape casting formulation that allows fabricating highly active fuel cells with variable anode porosity and high mechanical strength.
- Identified and tested suitable ceramic and glass-ceramic sealant materials for the operation of a coal-based fuel cell with leakage rates as low as 0.17 sccm/cm, matching the performance of compression seals designed for operation in H_2 and other gas fuels.
- Simulated the performance of a steady-state coal-based fuel cell during steady-state operation, completing the mass and energy balances as well as calculating fuel cell energy efficiency.

Introduction

The direct use of coal in a solid oxide fuel cell (coal-based fuel cell) is an innovative concept for electric power generation. The coal-based fuel cell could offer significant advantages: 1) minimization of oxides of nitrogen (NOx) emissions due to its operating temperature range of 700-1,000°C; 2) high overall efficiency because of the direct conversion of coal to CO_2; 3) production of a nearly pure (>99%) CO_2 exhaust stream for the direct CO_2 sequestration; and 4) low investment and maintenance costs due to the simplicity of the power generation process. This project is expected to develop a scalable coal fuel cell manufacturing process through testing and simulation, demonstrating the feasibility of building a large-scale coal fuel cell power plant. The success of this project will further attract industrial investment for the commercialization of this technology for applications ranging from small-scale battery replacement to megawatt-scale power generation. Ultimate success of this technology will reduce the nation's dependence on foreign oil, reduce pollution and CO_2 emission, and increase power generation efficiency above 50 percent, meeting the U.S. Department of Energy clean coal technology performance targets.

Approach

A set of experiments were designed to address the development of: 1) anode materials that increase the carbon-surface reaction/conversion, and resists deactivation by coal contaminants; 2) a technology for the large-scale manufacturing of coal-based fuel cells; and 3) suitable materials for sealing the fuel cell assembly. A Cu-Ni/YSZ anode catalyst was synthesized and characterized for chemical composition, crystalline structure, morphology/microstructure, and electrochemical performance in carbon and hydrocarbon fuels. Tape casting formulations containing fuel cell materials (i.e., NiO and YSZ), organic additives,

and different concentrations of pore formers were designed and tested. Fuel cells fabricated according to this procedure were characterized using X-ray fluorescence (XRF), scanning electron microscopy, and electrochemical impedance spectroscopy. Potential sealant materials (i.e., ceramic cements and glass-ceramic composites) were evaluated by attaching fuel cells to a low cost steel frame, monitoring the composition of exhaust gases during steady-state operation at 750°C as well as during thermal cycling.

Results

A Cu-Ni/YSZ anode catalyst was prepared by depositing a layer of reduced copper (i.e., Cu^0) over a Ni/YSZ anode electrode fabricated by tape casting technique. Cu was deposited on the surface of the Ni/YSZ anode by the electroless deposition method, which involves activating the Ni/YSZ anode surface with a $SnCl_2$ solution, adding a Pd precursor, and introducing the electroless plating solution containing the Cu salt at 70°C, a complexing agent and formic acid. Electrochemical characterization results revealed the Cu-Ni/YSZ possess high activity towards electrochemical oxidation of hydrocarbons and higher resistance to poisoning due to coking compared to traditional Ni/YSZ anodes. Figure 1 shows the voltage-current polarization curves of a Ni/YSZ and Cu-Ni/YSZ anode fuel cell tested in H_2 and CH_4 for more than 120 h.

Fuel cells comprising porous anode electrodes were successfully fabricated by the tape casting approach. Slips containing YSZ (TZ-8Y Tosoh), nickel oxide, and a pore former agent were used to prepare (40-65 vol%) porous anode electrodes. The preparation of the slips involved: 1) mixing the powders in a solution of organic solvents; 2) ball-milling the resulting mixture at 60 rpm; 3) adding a dispersant, binder, plasticizer and additional solvent; and 4) ball-milling for 20 h. The slips were casted by a motorized moving doctor blade on top of a stationary Mylar film, and dried at room temperature for 2 days. The porous anode tapes were laminated/co-casted to an interlayer and electrolyte layers, and fired at 1,400°C to produce button fuel cells. The distribution of Ni and YSZ in the porous Ni/YSZ anode tapes was characterized by XRF mapping. The apparent porosity was determined according to the Archimedes method by measuring the cell's dry and suspended weights in distilled water. Figure 2 shows an optical microscope image and XRF mapping of the cross-section of a porous fuel cell fabricated by the tape casting approach. The XRF mapping evidences the formation of well-dispersed and interconnected Ni and YSZ microstructure. Addition of a pore former resulted in anode electrodes containing open and interconnected pores as well as close pores. The performance of the fuel cell fabricated according to the described procedure met

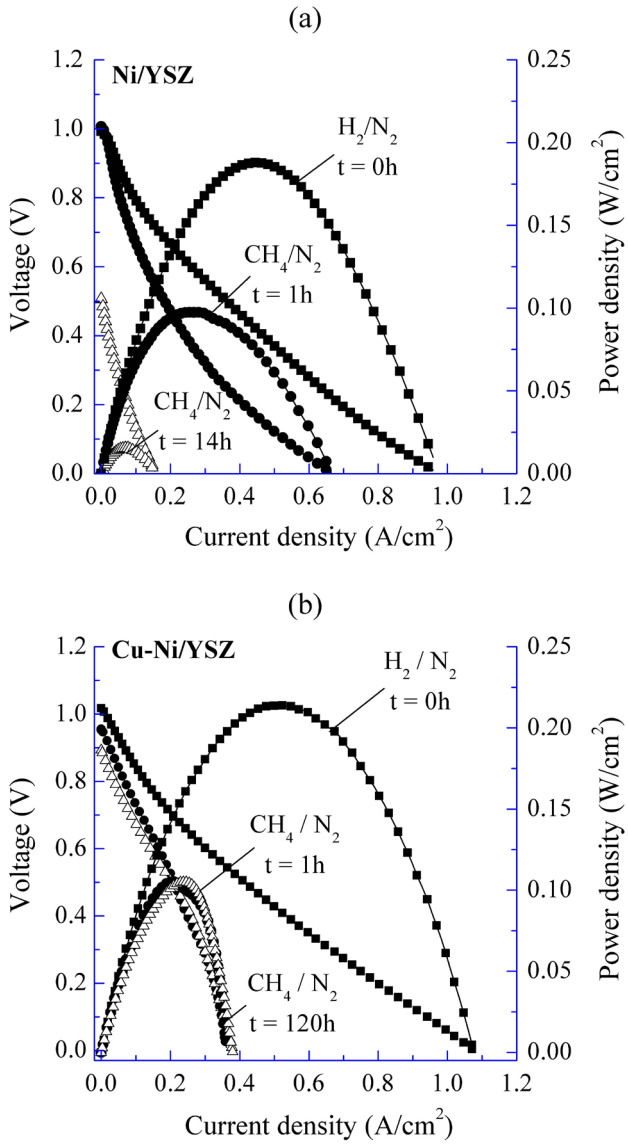

FIGURE 1. Voltage-Current Polarization Curves Recorded during Steady-State Testing of (a) Ni-YSZ and (b) a Cu-Ni/YSZ Anode Fuel Cell in H_2 and CH_4 Fuel (200 sccm, 50% vol.) at 750°C

the target performance, as evidenced by electrochemical characterization results.

Ceramic cements, and glass-ceramic seals were investigated as potential materials for the coal-based fuel cell. The sealant materials were tested during steady-state operation at 800°C and thermal cycling, by attaching bottom cells to a steel tubular fuel cell housing device. Figure 3 shows an image of the ceramic cements, and glass-ceramic seals prior to testing on a steel fuel cell housing. The performance of the seals was compared to that of alternative compressive phlogopite mica seals ($KMg_3(AlSi_3O_{10})(OH)_2$) designed for gaseous fuels such as H_2. Table 1 presents key physical

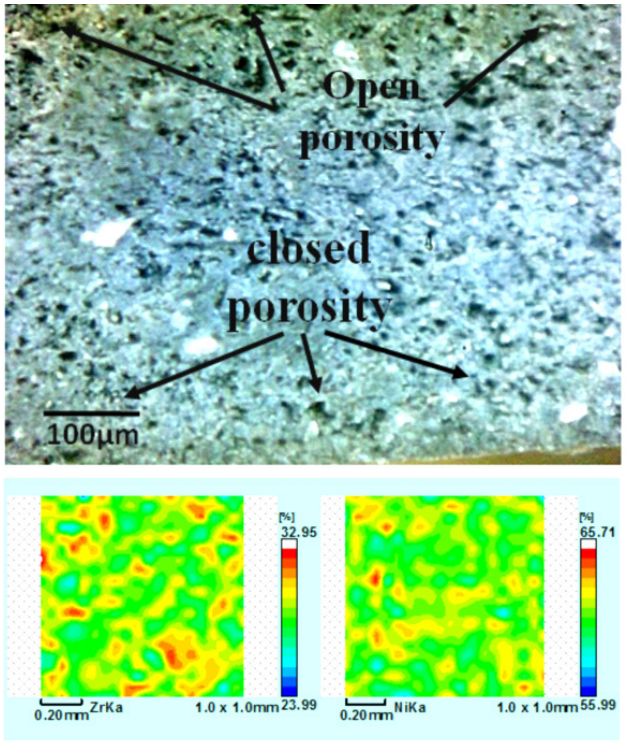

Ni	Zr	Y	Hf	Fe
68%	16.8%	3.65%	0.41%	0.06%

FIGURE 2. Optical Microscope Image and XRF Mapping of the Cross Section of a Porous Ni/YSZ Anode Fabricated by the Tape Casting Approach

properties of the seals investigated and leakage rates measured by mass spectrometry and gas chromatography analysis of the fuel cell exhaust gases. Results from these studies indicate the use of ceramic cements could facilitate the fabrication of fuel cell systems capable of achieving leakage rates as low as those reported for mica compressive seals [1].

TABLE 1. Ceramic Cement and Glass-Ceramic Sealants for the Fuel Cell

Sealant material	CTE ($x10^{-6}$ °C-1)	Composition	Curing Temp (°C)	Leak rate* (sccm/cm)
Phlogopite Mica	6.9	$KMg_3(AlSi_3O_{10})(OH)_2$	-	0.1-0.5
Ceramic cement A	4.5	Al_2O_3	30	0.17
Ceramic cement B	12.6	MgO	105	3.1
Glass-ceramic seal A	10.6	N/A	830	1.4
Glass-ceramic seal B	11.0	N/A	930	-

* Leakage rates measured at 800°C.

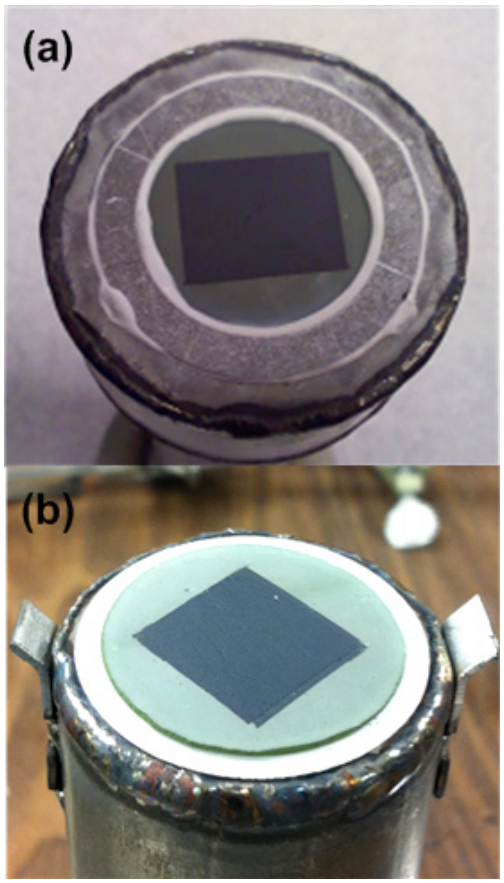

FIGURE 3. (a) Ceramic Cement A and (b) Glass-Ceramic Seal A Prior to Testing on a Steel Fuel Cell Housing

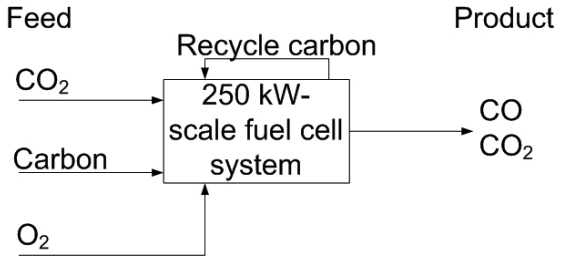

FIGURE 4. Block Flow Diagram of a Simulated 250 kW-Scale Fuel Cell System

The steady-state operation of the 250 kW-scale fuel cell system was simulated by calculating the equilibrium flow rate of the product species in the product stream. The equilibrium flow rate of the specie *i* is the product of the volumetric flow rate and the concentration of species *i*, which was calculated considering molar volume of ideal gas and the mole fraction (y_i). The mole fraction of the gaseous products was obtained through the total Gibbs energy minimization method, which is commonly used for simultaneous multi-reaction systems [2]. Figure 4 shows the block flow diagram

TABLE 2. Simulation Results from Steady-State Operation of a 250 kW Coal-Based Fuel Cell

Current density (A/cm^2)	Fuel cell area (m^2)	Feed			Product (mol/hr)		Heat generate (kW)	Efficiency (%)
		CO_2 (L/min)	O_2 (L/min)	Carbon (lb/hr)	CO_2 (L/min)	CO (L/min)		
0.05	862	100	1,635	196	347	2,776	276	41.6
0.10	657	100	2,497	296	520	4,153	430	27.5

of the 250 kW-scale fuel cell system. The components considered on the anode of the fuel cell system were CO_2 stream (100 L/min), CO, carbon and O_2 transferred from the cathode. The CO_2 stream was used as a carrier gas. The carbon that was not consumed in the fuel cell system was recycled to the anode compartment. The amount of O_2 transferred from the cathode for each individual fuel cell was determined from the current density according to Faraday's law. The simulation of the fuel cell stack was performed assuming a single cell performance obtained experimentally at: 1) an operating voltage of 0.58 V and a corresponding current density of 0.05 A/cm^2, and 2) an operating voltage of 0.38 V and a current density of 0.10 A/cm^2. Table 2 shows the results of the simulation. Operating the fuel cell at 0.05 A/cm^2, and 0.10 A/cm^2 requires the total area of the fuel cells of 862 m^2 and 657 m^2, respectively to achieve 250 kW. Despite the higher fuel cell area, operation at 0.05 A/cm^2 yields higher overall efficiency than that at 0.10 A/cm^2. The low efficiency of the operation at 0.10 A/cm^2 was caused by the high amount of heat generated from the electrochemical oxidation of carbon.

Conclusions and Future Directions

Results from these experimental studies provide experimental evidence supporting the feasibility of developing a coal-based fuel cell manufacturing technology. Milestones achieved during fiscal year 2011 demonstrated that: 1) anode materials exhibiting high catalytic activity and resistance to poisoning due to contaminants can be synthesized by the electroless plating method; 2) high performance fuel cells comprising (40-65 vol%) porous electrodes can be successfully fabricated by tape casting; and 3) ceramic cement sealants can be successfully used in the coal-based fuel cell, resulting in leakage rates comparable to those obtained for compressive seals used for H_2 and gas fuel cells. Simulation of the 250 kW fuel cell unit suggests that operation of the fuel cell at low current density results in higher efficiency than that at high current density.

Future studies will focus on:

- Design of a coal injection and flyash withdraw system: The removal of flyash from the anode chamber of the fuel cell is one of the most challenging tasks in developing a coal-based fuel cell stack. This system will enable the continuous operation of the coal-based fuel cell. Two different prototypes will be built and tested for further modifications.
- Evaluate the durability of the kW fuel cell components including the Cu-Ni/YSZ anode electrode, interconnects and sealant materials.
- Design a 250 kW fuel cell pilot plant.

FY 2011 Publications/Presentations

1. F. Guzman, R. Singh, and S.S.C. Chuang, *Energy & Fuels* **2011**, 25, 2179.

References

1. Y.-S. Chou and J.W. Stevenson, *J. Power Sources* **2003**, 124, (2), 473.

2. J.-H. Koh, B.-S. Kang, H.C. Lim, and Y.-S. Yoo, *Electrochemical and Solid-State Letters* **2001**, 4 (2), A12-A15.

V. Acronyms & Abbreviations

°	Degree
°C	Degree(s) Celsius
°C/min	Degree(s) Celsius per minute
Δ	Change, delta
ΔE	Change in enthalpy
ΔH	Change in heat
ΔW	Change in weight, weight gain
~	Approximately
≈	Equals approximately
>	Greater than
≥	Greater than or equal to
≤	Less than or equal to
<	Less than
±	Plus or minus
+	Plus
-	Minus
@	At
#	Number
%	Percent
®	Registered trademark
μg	Microgram(s)
μg/L	Microgram(s)/liter
μm	Micrometer(s), micron(s)
η	Viscosity
Ω	Ohm(s)
Ω/cm^2	Ohm(s) per square centimeter
$	United States dollars
1-D	One-dimensional
2D	Two-dimensional
2PB	Two phase boundary
3d, 3D, 3-D	Three-dimensional
3PB	Three phase boundary
441	A ferritic stainless steel
8YSZ	Eight mole percent yttria-stabilized zirconia
A	Ampere(s), amp(s)
Å	Angstrom(s)
ABAQUS	A computer modeling code
ABO_3 P	Erovskite type material composed of AO and BO_2 planes of ions
Abstr	Abstract
AC	Alternating current
ACC	Anode current collector
ACS	American Chemical Society
A/cm^2	Amp(s) per square centimeter
ADG	Anaerobic digester gas
ADS	Adsorptive desulfurization
Adv.	Advanced
AFM	Atomic force microscopy
AIChE	American Institute of Chemical Engineers
AISI	American Iron and Steel Institute
AISI 441	A ferritic stainless steel
Al	Aluminum
AL	Alabama
ALD	Atomic layer deposition
Al_2O_3	Alumina, aluminum oxide, sapphire
AL441, AL SS441-HP	A ferritic stainless steel alloy by Allegheny Ludlum
Am	American
Amer.	American
Amp	Ampere
ANL	Argonne National Laboratory
ANL-APS	Argonne National Laboratory Advanced Photon Source
ANSYS	A computer modeling code
Appl.	Applied
APS	Advanced Photon Source
APU	Auxiliary power unit
As	Arsenic
AS	Area specific
ASD	Aerosol spray deposition
AsH_3	Arsine
ASME	American Society of Mechanical Engineers
ASPEN	Modeling software, computer code for process analysis
ASR	Area specific resistance
ASTM	American Society for Testing and Materials
ASU	Air separation unit
ATI	Allegheny Technologies Incorporated
ATI 441HP	A stainless steel alloy
ATI E-BRITE	A stainless steel alloy
atm	Atmosphere(s)
ATR	Autothermal reformer
Au	Gold
a.u.	Arbitrary unit

B50	Fuel blend with 50% biodiesel
B75	Fuel blend with 75% biodiesel
B99	Fuel blend with 99% biodiesel
Ba	Barium
BaO	Barium oxide
Bara, bar_a	Bar absolute
BCAS	Barium-calcium-aluminum-boron silicate
BET	Brunauer-Emmett-Teller
Bi	Bismuth
Bldg.	Building
Blvd.	Boulevard
BNHA	Ni-substituted barium hexaaluminate
BOP	Balance of plant
Br	Bromine
C	Coal
C	Carbon
C	Celsius
C1	A class of hydrocarbons containing a single carbon atom, such as CH_4
Ca	Calcium
CA	California
$CaCrO_4$	Calcium chromate
$CaCr_2O_4$	Calcium chromium oxide
$CaZrO_3$	Calcium zirconium oxide
CBS	Coal-based systems
cc	Cubic centimeter(s)
CCM	Cathode contact material
cc/min	Cubic centimeter(s) per minute
CCS	Carbon capture and sequestration
CD-adapco	A provider of CFD-focused engineering simulation software
Ce	Cerium
Ce-MC	Cerium modified $(Mn,Co)_3O_4$
CeO_2	Ceric oxide
Ceram.	Ceramics
CFD	Computational fluid dynamics
Ch.	Chapter
CH_4	Methane
C_2H_2	Acetylene
C_2H_4	Ethylene
Chem, Chem.	Chemistry
Cl	Chlorine
cm	Centimeter(s)
cm^2	Square centimeter(s)
CMU	Carnegie Mellon University
CO	Carbon monoxide
CO	Colorado
Co	Cobalt
CO_2	Carbon dioxide
Comp.	Composition
COS	Carbonyl sulfide
CPOx, CPOX	Catalytic partial oxidation
Cr	Chromium
CRISMAT	Laboratorie de Cristallographie et Sciences des Materiaux
Cr_2O_3	Chromic oxide, trivalent chromium
CT	Connecticut
CTE	Coefficient of thermal expansion
CTP	Core Technology Program
Cu	Copper
CuO	Copper oxide
CxHy	Coal
c-YSZ	Cubic yttria-stabilized zirconia
D	Degree
dASR	Difference in area specific resistance
DBT	Dibenzothiophene
DC	Direct current
D.C.	District of Columbia
DEC	Distributed electrochemistry
DECS-24	A sample of coal from the Penn State Coal Sample Bank
deg.	Degree
DFT	Density functional theory
DMFC	Direct methanol fuel cell
DOE U.S.	Department of Energy
DOE/FE U.S.	Department of Energy Office of Fossil Energy
DOE-SECA	U.S. Department of Energy's Solid State Energy Conversion Alliance
DOI U.S.	Department of Interior
Dr.	Doctor
DREAM SOFC	A multi-dimensional modeling tool
DS	Desiliconized
DSA	Dimensionally stable anode
dt	Difference in time
ECL	ElectroChemical Looping
ECR	Electrical conductivity relaxation
ECS	The Electrochemical Society
ed.	Edition
EDAX	Energy dispersive X-ray analysis
Eds.	Editors
EDS	Energy dispersive spectroscopy
e.g.	Exempli gratia, for example
EH-5	A high surface fumed silica material

EIS	Electrochemical impedance spectroscopy
EISA	Evaporation-Induced Self Assembly
Electrochem.	Electrochemical
E-MRS	European Materials Research Society
EMS	Earth and Mineral Sciences
EPSCOR	Experimental Program to Stimulate Competitive Research
et al.	et alii, and others
etc.	et cetera, and so on
Eur.	European
eV	Electron volt(s)
EXP	Experimental
F	Fluorine
FARADAYIC	A platform technology for electronic interconnect manufacturing
FC	Fuel cell
FCE	FuelCell Energy, Inc.
Fe	Iron
FE U.S.	Department of Energy Office of Fossil Energy
FEA	Finite element analysis
FIB	Focused ion beam
FIB-SEM	Focused ion beam-scanning electron microscopy
FLUENT	A computer modeling package
FY	Fiscal year
g	Gram(s)
G6	A barium alkali silicate glass
Ga	Gallium
GA	Georgia
GBS1	Gallio-silicate glass series
GBS2	Gallio-silicate glass series
GC	Gas chromatograph
g_{cat}	Gram(s) catalyst
GC-ICP/MS	Gas chromatograph-inductively coupled plasma/mass spectrometer
GDC	Gadolinia-doped ceria
GDMS	Glow discharge mass spectrometry
GE	General Electric
Gen	Generation
Gen2	Second generation
GFED	Gross fuel energy density
g-F/g-A	Gram(s) fuel per gram adsorbent
GLAM	Geballe Laboratory for Advanced Materials
g/m	Gram(s) per minute
GPa	Gigapascal(s)
GT	Gas turbine
g(t)	Normalized conductivity
GUI	Graphical user interface
h	Hour(s)
H	Hydrogen
H_2	Diatomic hydrogen
H52	A ferritic stainless steel alloy
H53	A ferritic stainless steel alloy
H54	A ferritic stainless steel alloy
H55	A ferritic stainless steel alloy
HBE	Higher binding energy
Hg	Mercury
HHV	Higher heating value
H_2O	Water
HR	High resolution
hrs.	Hours
HRSG	Heat recovery steam generation
HRTEM	High resolution transmission electron microscopy
HS	Sulfanyl group
H_2S, H2S	Hydrogen sulfide
H_2Se	Hydrogen selenide
HT	High temperature
I	Current
I	Iodine
IC	Interconnect
ICACC	International Conference and Exhibition on Advanced Ceramics and Composites
ICP	Inductively-coupled plasma
ICP/MS	Inductively-coupled plasma/mass spectrometer
ICP-OES	Inductively-coupled plasma optical emission spectroscopy
i.e.	id est, that is
IGCC	Integrated gasification combined cycle
IGFC	Integrated gasification fuel cell
IL	Illinois
in.	Inch(es)
Inc.	Incorporated
Int.	International
IP-SOFC	Integrated-planar solid oxide fuel cell
IR	Infared
I^2R	Current squared times resistance
ISBN	International Standard Book Number
ISO	International Organization for Standardization
iss.	Issue

IT	Intermediate temperature
IT-SOFC	Intermediate-temperature solid oxide fuel cell
I-V, IV	Current-voltage
J.	Journal
JCPDS	Joint Committee on Power Diffraction Standards
JP-5	Jet Propellant 5, a jet fuel
JP-8	Jet Propellant 8, a jet fuel
JP-10	Jet Propellant 10, a jet fuel
K	Kelvin
K	Potassium
k_{chem}	Chemical surface exchange coefficient
kg	Kilogram(s)
khr	1,000 hours
KOH	Potassium hydroxide
kPa	Kilopascal(s)
kV	Kilovolt(s)
kW	Kilowatt(s)
kWe	Kilowatt(s) electric
kWth, kW_{th}	Kilowatt(s) thermal
L	Liter(s)
La	Lanthanum
$LaCrO_3$	Lanthanum chromite
$LaFeO_3$	Lanthanum ferrite
lb.	Pound(s)
lbs.	Pounds
LBNL	Lawrence Berkeley National Laboratory
LC/ARB	Large size cathode/anode recycle blower
LCOE	Levelized cost of electricity
LDC	Lanthanum doped ceria
LERIX	Lower energy resolution inelastic X-ray scattering
Lett.	Letter
LHV	Lower heating value
Li	Lithium
LiOH	Lithium hydroxide
LLC	Limited Liability Company
LMA	Liquid metal anode
LMA SOFC	Liquid metal anode solid oxide fuel cell
L/min	Liter(s) per minute
LNF	Lanthanum nickel ferrite
LNG	Liquefied natural gas
Log	Logarithm
lpm	Liter(s) per minute
LSC	Lanthanum strontium cobaltite, lanthanum strontium cobalt oxide
LSCF	Lanthanum strontium cobalt ferrite, lanthanum strontium cobalt iron oxide
LSCo	Lanthanum strontium cobalt oxide
LSCuF	Lanthanum strontium copper ferrite, lanthanum strontium copper iron oxide
LSF	Lanthanum strontium ferrite
LSM	Lanthanum strontium manganite, strontium doped lanthanum manganite
LTA	Liquid tin anode
LTA-SOFC	Liquid tin anode solid oxide fuel cell
m	Meter(s)
M	Million
M	Metal
MA	Massachusetts
mA	Milliampere(s)
mA/cm^2	Milliampere(s) per square centimeter
MARC	A computer modeling code
Mat.	Material
Mater.	Material
MBS	Molecular basket sorbent
MC	Manganese cobalt oxide, $(Mn,Co)_3O_4$
MCM-41	Mobil Composition of Matter No. 41
MCM-48	Mobil Composition of Matter No. 48
MCO	Manganese-cobalt spinel, $(MnCo)_3O_4$
MEA	Membrane electrode assembly
Meet.	Meeting
mg	Milligram(s)
Mg	Magnesium
MgO	Magnesium oxide
MI	Michigan
Mill	Millimeter(s)
MIT	Massachusetts Institute of Technology
mL	Milliliter(s)
mL/min	Milliliter(s) per minute
mm	Millimeter(s)
Mn	Manganese
MN	Methylnapthalene
MnCo, Mn-Co	Manganese cobalt
Mn-Co-Cu	Manganese cobalt copper
MnO_3	Manganate
Mo	Molybdenum
mol	Mole(s)
mol%	Mole percent
mΩ	Milli-ohm(s)
$m\Omega \cdot cm^2$	Milli-ohm square centimeter(s)
MP	Mesoporous particles
MP	Multi-physics

MPa	Megapascal(s)
MPC	Multi-physics code
MR	Mill reference
MRS	Materials Research Society
MS	Mail stop
MSC MARC	A fuel cell stack computer model
MSRI	Materials and Systems Research, Inc.
MS&T	Materials Science and Technology
MT	Montana
mTorr	Millitorr(s)
MTS	Mechanical tensile stress
mV	Millivolt(s)
MW	Megawatt(s)
mW	Milliwatt(s)
mW/cm^2	Milliwatt(s) per square centimeter
MWe	Megawatt(s) electric
N	Nitrogen
N_2	Diatomic nitrogen
NaOH	Sodium hydroxide
NASA	National Aeronautics and Space Administration
nA/V	Nanoampere(s) per volt
Nb	Niobium
Nd	Neodymium
$NdGaO_3$	Neodymium gadolinium oxide
NETL	National Energy Technology Laboratory
NGO	Neodymium gadolinium oxide, $NdGaO_3$
Ni	Nickel
Ni-Co	Nickel-cobalt
$NiCo_2$	Nickel cobalt
NiO	Nickel oxide
Ni_3-PC	Nickel-substituted pyrochlore
Ni-YSZ	Nickel-yttria-stabilized zirconia
nm	Nanometer(s)
nm^3	Cubic nanometer(s)
No.	Number
NOC	Normal operating conditions
NOx, NO_x	Oxides of nitrogen
NP	Nanoparticles
NUWC	Naval Undersea Warfare Center
NV	Nevada
NW	Northwest
NY	New York
NYS	New York State
O	Oxygen
O_2	Diatomic oxygen
O/C	Oxygen to carbon ratio
OCV	Open circuit voltage
OH	Ohio
ORNL	Oak Ridge National Laboratory
ORR	Oxygen reduction rate
ORR	Oxygen reduction reaction
OSR	Oxidative steam reforming
OT	Operating temperature
p.	Page
P	Phosphorus
P	Pressure
PA	Pennsylvania
pA	Picoampere(s)
Pa	Pascal(s)
Pap	Paper
PBN	Pyrolytic boron nitride
PCC	Pulverized coal combustion
PCI	Precision Combustion Inc.
PCM	Proof-of-concept module
PEI	Polyethyleneimine
PH_3	Phosphine
Phys.	Physics
P.I.	Principal investigator
PNNL	Pacific Northwest National Laboratory
PO, P.O.	Post office
pO_2, P_{O2}	Partial pressure of oxygen
pp.	Pages
ppb	Part(s) per billion
ppbv	Part(s) per billion by volume
ppm	Part(s) per million
ppmv	Part(s) per million by volume
ppmw	Part(s) per million by weight
Pr	Praseodymium
Proc.	Proceedings
PSCF	Praseodymium-containing perovskite
psi	Pound(s) per square inch
PSM	Praseodymium strontium manganite
PSU	Pennsylvania State University
Pt	Platinum
PVL	Process verification line
S	Siemen(s)
SBA-15	An ordered mesoporous silica material
S/C	Steam to carbon ratio
sccm	Standard cubic centimeter(s) per minute
Sr	Strontium
$SrCrO_4$	Strontium hexavalent chromium

$SrTiO_3$	Strontium titanate
SS	Stainless steel
SS430	A stainless steel alloy
SSC	Strontium samarium cobalt oxide
St.	Saint
St.	Street
STAR-CD	A computational fluid dynamics code
STAR-CCM+	A multi-physics computer code
STM	Scanning tunneling microscopy
STM/STS	Scanning tunneling microscopy/scanning tunneling spectroscopy
STO	Strontium titanate, $SrTiO_3$
STS	Scanning tunneling spectroscopy
STTR	Small Business Technology Transfer
Surf.	Surface
Symp.	Symposium
t	Time
T	Temperature
Ta	Tantalum
TCR	Tin-coal reactor
TD	n-Tetradecane
TDA	TDA Research
TEC	Thermal expansion coefficient
Tech.	Technology
TEM	Transmission electron microscopy
Tg	Glass transition temperature
TGA	Thermogravimetric analysis
Ti	Titanium
Ti-Ce-O	Titanium-cerium-oxygen
TMI	Technology Management, Inc.
TN	Tennessee
TPB	Triple-phase boundary
TPBL	Triple-phase boundary layer
TPR	Temperature-programmed reduction
TR	Temper rolled
Trans.	Transactions
TSC-3	Tape castingñScreen printingñCo-firing
TXRF	Total reflection X-ray fluorescence
t-YSZ	Tetragonal yttria-stabilized zirconia
U	Uranium
U	Utilization
Ua	Air (oxidant) utilization
Uf	Fuel utilization
UHV	Ultra-high vacuum
UK	United Kingdom
ULSD	Ultra-low sulfur diesel
um	Micron, micrometer
UNLV	University of Nevada Las Vegas
U.S.	United States
USD	United States dollar
UT	Utah
UTC	United Technologies Company
UTRC	United Technologies Research Center
UUV	Unmanned undersea vehicle
V	Vanadium
V	Volt(s)
v.	Volume
VA	Virginia
VASP	A computer modeling program
VFT	Vogel-Fulcher-Tamman
Vo	Oxygen vacancy
vol, Vol.	Volume
VPS	Versa Power Systems
W	Tungsten
W	Watt(s)
WA	Washington
WEBEX	Web exchange internet conferencing
WF	Window frame
Wh/L	Watt hour(s) per liter
WHSV	Weight hourly space velocity
wt	Weight
wt%	Weight percent
WV	West Virginia
WVU	West Virginia University
x	Times
XANES	X-ray absorption near edge structure
XAS	X-ray adsorption spectroscopy
XES	X-ray emission spectroscopy
XPS	X-ray photoelectron spectroscopy
XRD	X-ray diffraction
XRR	X-ray reflectivity
Y	Yttrium
YDC	Yttria-doped ceria
Y_2O_3	Yttrium oxide (yttria)
YSZ	Yttria-stabilized zirconia
Z	Impedance
Zr	Zirconium

VI. Primary Contact Index

VII. Organization Index

VIII. Contract Number Index

IX. Index of Previous Projects

Projects Discontinued Since the FY 2010 Annual Report

Contract Number	Performer	Project Topic
ER84394	Eltron Research and Development Inc.	Reformer for Conversion of Diesel Fuel into CO and Hydrogen
ER84590	Acumentrics Corporation	Hybrid Ceramic/Metallic Recuperator for SOFC Generator
ER84595	Ceramatec, Inc.	Proton Conducting Solid Oxide Fuel Cell
ER84616	R&D Dynamics Corporation	Foil-Bearing Supported High-Speed Centrifugal Cathode Air Blower
NT0006343	Treadstone Technologies, Inc.	Investigation of Modified Ni-YSZ-Based Anode for High Impurities Containing Syngas Fuels
NT43042	National Institute of Standards and Technologies	Advanced Power Conditioning System (PCS) Technologies for High-Megawatt Fuel Cell Power Plants
SC0000871	Eltron Research and Development Inc.	Perovskite Adsorbents for Warm-Gas Arsenic and Phosphorus Removal
SC0000872	Eltron Research and Development Inc.	First Principles Identification of New Cathode Electrocatalysts for Fuel Cells
SC0001492	TDA Research, Inc.	Sorbents for Warm Temperature Removal of Arsenic and Phosphorous from Coal-Derived Synthesis Gas
SC0001659	Materials & Systems Research, Inc.	Novel SOFC Anodes with Enhanced Tolerance to Coal Contaminants
SC0002491	Mo-Sci Corporation	High-Temperature Viscous Sealing Glasses for Solid Oxide Fuel Cells

Note: Previous contract number ER86387 (Faraday Technology) is now reported under FE0006165.

Projects Discontinued Since the FY 2009 Annual Report

Contract Number	Performer	Project Topic
41567	Virginia Polytechnic Institute and State University	A Low-Cost Soft-Switched DC-DC Converter for Solid Oxide Fuel Cells
41817	American Society of Mechanical Engineers (ASME)	SOFC Design Basis Development Project
41817	Carnegie Mellon University	TEM Investigations of SOFCs: Stability of LSCF-based Cathodes
41817	University of California	High Efficiency Coal Gasification-Based SOFC Power Plants
42219	Georgia Institute of Technology	Novel Sulfur-Tolerant Anodes for Solid Oxide Fuel Cells
42533	Tennessee Technological University	Novel Composite Materials for SOFC Cathode-Interconnect Contact
42613	Siemens Energy, Inc.	Coal Gas-Fueled SOFC Hybrid Power Systems with CO_2 Separation
42735	Georgia Institute of Technology	Characterization of Atomic and Electronic Structure of Electrochemically Active SOFC Cathode Surfaces
43063	University of Texas at San Antonio	Novel Low Temperature Solid State Fuel Cells
44036	Montana State University	SECA Coal-Based Systems Core Research – Montana State University
84209	Phoenix Analysis & Design Technologies	Anode and Cathode Blower Systems for SOFC
84210	R&D Dynamics Corporation	Foil Gas Bearing Supported High-Speed Centrifugal Anode Gas Recycle Blower

Note: Previous contract number FWP44036 (Pacific Northwest National Laboratory) is now reported under FWP40552. Contract number NT0003893 [Rolls-Royce Fuel Cell Systems (U.S.) Inc.] has been changed to FE0000303.

Projects Discontinued Since the FY 2008 Annual Report

Contract Number	Performer	Project Topic
05690	American Society of Mechanical Engineers	SOFC Design Basis Development Project (project transferred to RDS41817.3130105-036)
08-220692	National Energy Technology Laboratory	Materials Development for the Solid Oxide Fuel Cell Environment
41572	Georgia Institute of Technology	Functionally Graded Cathodes for Solid Oxide Fuel Cells
42221	Missouri University of Science & Technology	Thermochemically Stable Sealing Materials for Solid Oxide Fuel Cells
42223	Tennessee Technological University	Development of Low-Cr Fe-Ni-Based Alloys for Intermediate Temperature SOFC Interconnect Application
42225	Arcomac Surface Engineering, LLC	Oxidation Resistant, Cr Retaining, Electrically Conductive Coatings on Metallic Alloys for SOFC Interconnects
42227	University of Cincinnati	Innovative Seals for Solid Oxide Fuel Cells (SOFCs)
42229	Delavan d.b.a. Goodrich Turbine Fuel Technologies	An Innovative Injection and Mixing System for Diesel Fuel Reforming
42471	Ceramatec, Inc.	Intermediate Temperature Solid Oxide Fuel Cell Development
42516	University of Michigan	Carbon Tolerant Steam Reforming and SOFC Anode Catalysts
42527	Ohio University	Combined Theoretical and Experimental Investigation and Design of H_2S Tolerant Anode for Solid Oxide Fuel Cells
42614	GE Global Research	Solid Oxide Fuel Cell Coal-Based Power Systems
42623	University of Utah	A High Temperature Electrochemical Energy Storage System Based on Sodium Beta Alumina Solid Electrolyte (BASE)
42627	SRI International	Effect of Coal Contaminants on Solid Oxide Fuel Cell System Performance and Service Life
44036	University of Florida	SECA Coal-Based Systems Core Research - University of Florida
49071	Massachusetts Institute of Technology	Local Electronic Structure and Surface Chemistry of SOFC Cathodes
68250	Sandia National Laboratories	Reliable Seals for Solid Oxide Fuel Cells
84662	Aspen Products Group, Inc.	Waterless 5 kWe Diesel Reformer
84663	Ceramatec, Inc.	SOFC Integrated Multi-Mode Diesel Reformer
84673	Lynntech, Inc.	Low Cost, Compact Plasma Fuel Reformer for APUs
84881	NexTech Materials Ltd.	Intermediate Temperature Solid Oxide Fuel Cell Cathode Enhancement through Infiltration Fabrication Techniques

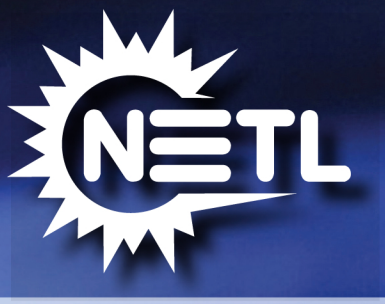

National Energy Technology Laboratory

1450 Queen Avenue SW
Albany, OR 97321-2198
541-967-5892

3610 Collins Ferry Road
P.O. Box 880
Morgantown, WV 26507-0880
304-285-4764

626 Cochrans Mill Road
P.O. Box 10940
Pittsburgh, PA 15236-0940
412-386-4687

Dr. Shailesh D. Vora
Technology Manager, Fuel Cells
412-386-7515
shailesh.vora@netl.doe.gov

Visit the NETL website at:
www.netl.doe.gov

Customer Service:
1-800-553-7681

DOE/NETL-2012-1525 October 2011